

Part II Actions and Material Strength Requirements Section

Chapter 1 General

[Ministerial Ordinance] (Requirements for the Setting of Environmental and Other Conditions)

Article 6

In designing, constructing, and maintaining the facilities subject to the Technical Standards, required items for setting the environmental conditions, usage conditions, and other conditions for the facilities shall be provided by the Public Notice.

[Public Notice] (Setting of Environmental and Other Conditions)

Article 5

The items to be specified in Article 6 of the Ministerial Ordinance for the setting of the conditions surrounding the facilities shall be provided in the subsequent Article through Article 20.

1 General

- (1) This Part (**Part II**) explains the content of the principles of action occurrence; modeling of actions (loading) and resistance applied to the performance verification method and others described in the **Part III**; and the concept of the design condition setting as characteristic values in the performance verification targeting at main actions and materials and others to be considered in the design, construction, or maintenance of facilities subject to the Technical Standards.

2 Fundamental Items

- (1) In designing, constructing, or maintaining the facilities subject to the Technical Standards, the environmental conditions, usage conditions, and other conditions for the facilities concerned (hereinafter the “conditions such as natural conditions”) need to be properly set the design, construction, or maintenance according to the performance required for the facilities concerned, as well as the conditions in which the facilities are subjected to.

Conditions such as natural conditions include following factors: winds, tides, waves, tsunamis, movement of sea water, estuary hydraulics, littoral drift, ground conditions, earth pressure, water pressure, ground settlement, ground motions, soil liquefaction, principal dimensions of design ships, environmental actions, self weights, surcharges, and material strength, etc.

- (2) The setting of conditions such as natural conditions has significant effects on the performance, economic efficiency, etc., of the facilities; hence, it should be carried out carefully.
- (3) Conditions such as natural conditions generally need to be properly set on the basis of the results of sufficiently conducted preliminary surveys and tests (including the utilization of past similar cases, various databases, and others) to ensure the required quality in setting objective conditions. It is desirable to organize the method to reflect the results of surveys, tests, and others in past design and construction activities to plan effective examinations and tests.

3 Other Items

- (1) **Reference (Part II), Chapter 1 Observation, Examination and Test** may be used as a reference. This describes the technical information (how quality and data should be managed, notes on the examination plan, methods to examine and test, utilization of numerical analysis methods, etc.) on how to properly and effectively conduct examinations, tests, and others at setting conditions such as natural conditions.
- (2) **Reference (Part II), Chapter 2 Examinations and Tests after Large Earthquakes and Tsunamis** describes helpful technical information concerning various examinations and tests to expedite recovery design after large-scale disasters, such as the 2011 Great East Japan Earthquake.

Chapter 2 Meteorology and Oceanography

1 Meteorology and Oceanography Items to be Considered for Performance Verification

1.1 General

The following meteorology and oceanography items and effects on the facilities subject to the Technical Standards shall be considered with regard to the performance verification of the facilities.

- ① Atmospheric pressure and its distribution are dominant factors that generate winds and storm surge.
- ② Winds which generate waves and storm surge induce the pressure on the facilities subject to the Technical Standards and moored vessels, and can hamper cargo handling and other port operations. See **2 Winds** for further details.
- ③ The tidal level affects the earth pressure and water pressure, which act on facilities subject to the Technical Standards, and can interfere with cargo handling and other port operations. Furthermore, it affects wave transformation in areas of shallow water. See **Part II, Chapter 2, 3 Tidal Level** for further details.
- ④ Waves exert force on the facilities subject to the Technical Standards and become an important factor which affects the function of the facilities depending on their scales and frequencies. They also cause moored vessels to move and interfere with cargo handling and other port operations. They can also cause the rise of the mean water level, which has effects similar to the tidal level, as mentioned above. See **Part II, Chapter 2, 4 Waves** for further details.
- ⑤ Tsunamis exert forces as waves and fluid on the facilities subject to the Technical Standards and become a factor in the interference with the facilities concerned. It also causes moored ships to move. See **Part II, Chapter 2, 5 Tsunamis** for further details.
- ⑥ Wave forces appear due to the actions of the waves, storm surge, and tsunamis on the facilities subject to the Technical Standards and their scales and properties depend on location, shape, structural type, and other factors of facilities. See **Part II, Chapter 2, 6 Wave Force** for further details.
- ⑦ Water currents affect the sedimentation of the sea bottom sediments and become a factor which interferes the function of facilities subject to the Technical Standards. See **Part II, Chapter 2, 7 Water Currents** for further details.

2 Winds

[Public Notice] (Winds)

Article 6

The characteristics of winds shall be set by the methods provided in the subsequent items corresponding to the single action or combination of two or more actions to be considered in the performance criteria and performance verification:

- (1) The ocean surface winds to be used in the estimation of waves and storm surge shall be appropriately defined in terms of wind velocity, wind direction, etc., on the basis of long-term measured values or estimated values of weather.
- (2) The winds to be used in the calculation of wind pressures shall be appropriately defined in terms of wind velocity and direction corresponding to the return period on the basis of the statistical analysis of the long-term measured values or estimated values of winds or other methods.
- (3) The winds to be used in the calculation of wind energy shall be appropriately defined in terms of the joint frequency distribution of wind velocity and direction for a certain duration of time on the basis of the long-term measured values or estimated values of winds.

[Interpretation]

7. Setting of Natural Conditions and Others

- (1) Requirements for Winds** (Article 6 of the Ministerial Ordinance and the interpretation related to Article 6 of the Public Notice)

The single action or combination of two or more actions indicates a design state. The conditions for winds shall be properly set by the subsequent provisions in accordance with the performance criteria and the design state considered in the performance verification.

① Winds for the estimation of waves and storm surge:

Winds for the estimation of waves and storm surge shall be observed or hindcasted values for 30 years or more as a standard.

② Winds for the calculation of wind pressure:

Winds for the calculation of wind pressure shall be observed or hindcasted values for 30 years or more as a standard.

③ Winds for the calculation of wind energy

Winds for the calculation of wind energy shall be observed or hindcasted values for on the order of three years or more as a standard. A certain period shall be one year as a standard.

2.1 General

- (1)** Wind is one of the most distinctive meteorological phenomena, namely, the phenomenon that the air moves owing to atmospheric pressure differences and heat. The states of the wind blows over the ocean are usually very different from those over land. Wind velocities over the ocean are higher than those over land near the shore.¹⁾ For the performance verification of facilities subject to the Technical Standards, the effects of winds must be appropriately evaluated. At the same time, it is also important to perform verifications from the viewpoint of the effective utilization of wind energy considering that wind is an energy resource that creates clean energy and does not exhaust carbon dioxide.²⁾

(2) Gradient Winds

- ① The velocity of the gradient wind can be expressed as a function of air pressure gradient, radius of curvature of barometric isolines, latitude, and air density, as in **equation (2.1.1)**.

$$V_g = r\omega \sin\phi \left(-1 + \sqrt{1 + \frac{\frac{\partial p}{\partial r}}{\rho_a r \omega^2 \sin^2\phi}} \right) \quad (2.1.1)$$

where

V_g : velocity of gradient wind (m/s)

In the case of an anticyclone, **equation (2.1.1)** provides a negative value; therefore, the absolute value should be taken.

$\partial p/\partial r$: pressure gradient (positive for a cyclone, and negative for an anticyclone) (kg/m²/s²)

r : radius of curvature of barometric isolines (m)

ω : angular velocity of Earth's rotation (1/s) $\omega = 7.27 \times 10^{-5}/s$

ϕ : latitude (°)

ρ_a : density of air (kg/m³)

Before performing the calculation, practical units should first be converted into the MKS units listed above. Note that an air pressure of 1.0 hPa is 100 kg/m/s².

- ② A gradient wind for which the barometric isolines are straight lines (i.e., their radius of curvature in **equation (2.1.1)** is infinite) is called the geostrophic wind. In this case, the wind velocity is expressed as **equation (2.1.2)**.

$$V = \frac{\frac{\partial p}{\partial r}}{2\rho_a \omega \sin\phi} \quad (2.1.2)$$

- ③ The nomograph in **Fig. 2.1.1** is helpful in calculating the velocity of the gradient wind. This assumes that $\rho_a = 1.1$ kg/m³. As a usage example, if the interval (pressure gradient) between contours per 2 hPa at latitude 40° is equivalent to 0.6° in latitude and if the cyclonic curvature radius of contours is equivalent to 6°, the velocity of the gradient wind can be calculated to be approximately 21.5 m/s by connecting points A and B with a straight line, by determining point C where the curvature radius crosses the curve with the curvature radius of 6°, and by reading the scale of the vertical line.
- ④ The actual sea surface wind velocity is generally lower than the value obtained from the gradient wind equation. Moreover, although the direction of a gradient wind is parallel to the barometric isolines in theory, the sea surface wind blows at a certain angle α to the barometric isolines in reality (**Fig. 2.1.2**). In the northern hemisphere, the winds around a cyclone blow in a counterclockwise direction and inwards, whereas the winds around an anticyclone blow in a clockwise direction and outwards. It is known that the relationship between the velocity of gradient winds and that of the actual sea surface wind varies with the latitude. **Table 2.1.1** summarizes this relationship under the average conditions,³⁾ where V_s is the wind velocity at 10 m above the sea surface and V_g is the wind velocity of gradient wind. However, this is just a rough standard. When estimating the sea surface wind, it is necessary to refer to the actually measured values on the shore, and the values reported from ships on the sea, which are written on the meteorological chart, and to properly correct these values if necessary.

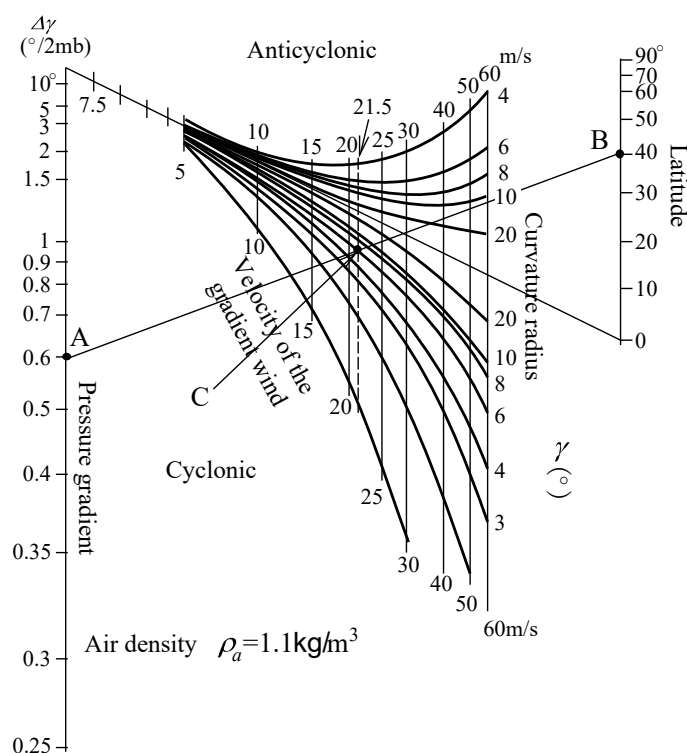


Fig. 2.1.1 Nomograph to Calculate the Gradient Wind

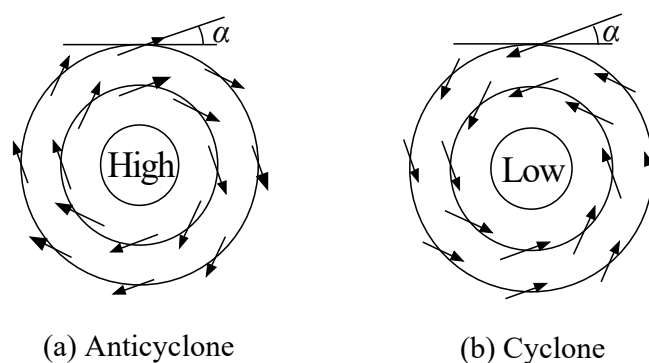


Fig. 2.1.2 Wind Direction for an Anticyclone (High) and a Cyclone (Low)

Table 2.1.1 Relationship between Sea Surface Wind Speed and Gradient Wind Speed

Latitude (°)	10	20	30	40	50
Angle α (°)	24	20	18	17	15
Velocity ratio V_s/V_g	0.51	0.60	0.64	0.67	0.70

(3) Typhoon Winds

In calculations concerning the generation of storm surge or waves due to a typhoon, it is common to assume that the air pressure distribution follows either Fujita's equation (**equation (2.1.3)**)⁴⁾ or Myers' equation (**equation (2.1.4)**)⁵⁾; the constants in the chosen equation are determined on the basis of actual air pressures measured in the region of the typhoons.

Fujita's equation

$$p = p_{\infty} - \frac{\Delta p}{\sqrt{1 + \left(\frac{r}{r_0}\right)^2}} \quad (2.1.3)$$

Myers' equation

$$p = p_c + \Delta p \cdot \exp\left(-\frac{r_0}{r}\right) \quad (2.1.4)$$

where

- p : air pressure at a distance r from the center of typhoon (hPa)
 r : distance from the center of typhoon (km)
 p_c : air pressure at the center of typhoon (hPa)
 r_0 : estimated distance from the center of typhoon to the point where the wind velocity is maximum (km)
 Δp : air pressure drop at the center of typhoon (hPa) $\Delta p = p_\infty - p_c$
 p_∞ : air pressure at $r = \infty$ (hPa); $p_\infty = p_c + \Delta p$

The size of a typhoon varies with time; thus, r_0 and Δp must be determined as functions of time

(4) Meteorological GPV and Mesoscale Meteorological Model

Organizations such as the Japan Meteorological Agency, the European Center for Medium-Range Weather Forecasts, and America's National Center for Environmental Protection, calculate the values of items such as air pressure, wind velocity, wind direction, and water vapor flux on the basis of 3D grid calculation models for meteorological values, and the calculated values at the grid points (GPV: grid point values) are saved. These GPVs may be used instead of wind hindcasting on the basis of **equations (2.1.1) to (2.1.4)**. However, when a grid with large spacing is used for meteorological calculations, the atmospheric pressure and winds may not be satisfactorily reproduced at places where meteorological conditions change drastically with position, such as near the centers of typhoons. Therefore, when GPVs are used, it is preferable to verify the precision by using observational values. Moreover, the meteorological fields may be hindcasted by a numerical model (mesoscale meteorological model; MM5,⁶⁾ WRF,⁷⁾ or others) that sets these meteorological GPV as initial and boundary values. The mesoscale meteorological model enables the hindcasting (downscaling) of the meteorological field with more minute time and spatial resolutions by considering the influence of land (elevation of land and land utilization) in the vicinity of the sea area concerned on the meteorological field. In this case, it is also desirable to verify the precision of the meteorological fields obtained from a local weather model by comparing it with the observed values. Therefore, by using a meteorological field hindcasted from a mesoscale meteorological model, it is expected that the precision of hindcasted waves and storm surge will be improved, particularly in the inner bay area.^{8), 9)}

(5) Wind Energy

If winds are considered the movement of air, then the wind energy that crosses a unit cross-sectional area in unit time is given by **equation (2.1.5)**.¹⁾

Winds for estimating the wind energy shall be appropriately specified with joint statistic distributions for velocity and direction for a fixed time (usually one year) on the basis of observed or hindcasted data for three years or more.

$$P = \frac{1}{2} \rho_a V^3 \quad (2.1.5)$$

where

- P : wind energy per unit cross-sectional area (W/m²)
 ρ_a : air density (kg/m³)
 V : wind velocity (m/s)

In other words, the wind force energy is proportional to the cube of the wind velocity; therefore, a small difference in wind velocity can mean a big difference in energy (power generation). Therefore, during the performance verification of facilities that use wind force energy, it is important to accurately understand how the conditions change with regard to time and space.

In the coastal zone, the wind conditions vary drastically between land and sea. Furthermore, wind velocity shows significant variations owing to land altitude. Over the sea, the changes in wind velocity with altitude are gradual; therefore, it is possible to obtain highly stabilized winds that are appropriate for power generation at relatively low

altitudes. For example, the results of measurements in the vicinity of the Kansai International Airport show that the wind energy over the course of a year at a measurement tower (MT station) placed at a height of 15 m over the ocean were roughly same as those at a land station (C station) with an altitude of 100 m; as the results the wind energy at MT station is approximately five times greater than that at a land station with an altitude of 10 m.¹⁰⁾

Fig. 2.1.3 shows a comparison of wind conditions at each observation point by showing the annual mean wind velocity at coastal wind observation points all over Japan collected and processed by the Nationwide Ocean Wave information network for Ports and HARbourS (NOWPHAS) on the vertical axis and the mean coefficient of variation during the 10-minute observation period on the horizontal axis.²⁾ Here, the mean coefficient of variation is the mean value of the coefficient defined as the value of the standard variation of wind velocity fluctuation divided by the mean wind velocity. The difference between sea and land observation points appears more distinctly than the area difference. It shows that the mean wind velocity at the sea is faster and the variance at the sea in a short period is smaller, comparing corresponding those at the land.

When designing facilities that utilize wind energy, it is important to properly estimate and simulate the production of electric power by considering the temporal and spatial variations of winds and by referring to the design examples of coastal wind power illumination system.^{10)–12)} See Ref.¹³⁾ for the installation of wind power generation facilities utilizing wind energy.

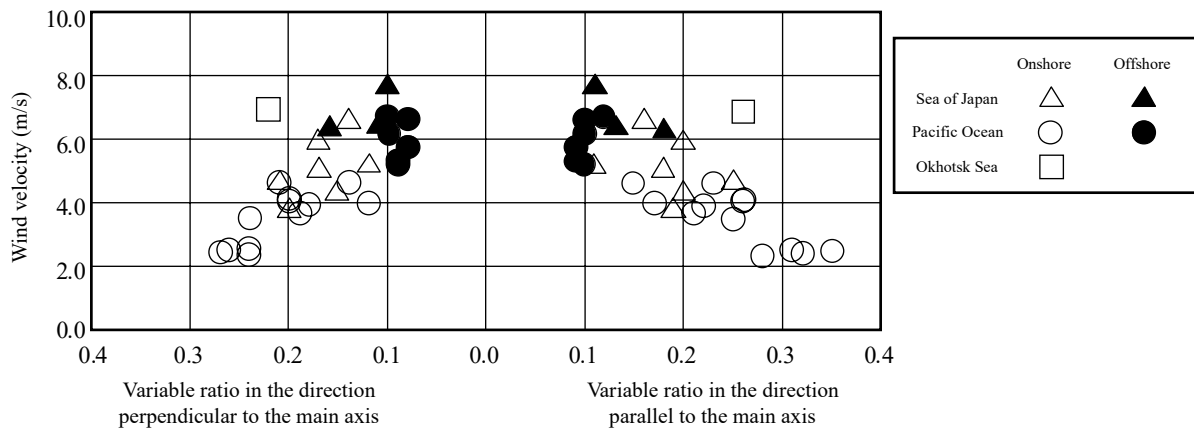


Fig. 2.1.3 Distribution of Mean Wind Velocity and Variable Ratio at Each NOWPHAS Observation Point²⁾

2.2 Characteristic Values of Wind Velocity

(1) Determination of Characteristic Value of Winds

The elements of winds are direction and velocity. The wind direction and velocity are expressed as one of 16 directions, and the mean velocity over 10 minutes, respectively. The velocity of winds that acts directly on facilities subject to the Technical Standards and moored ships is specified in general as a velocity corresponding to a certain period of re-occurrence on the basis of the occurrence probability distribution of wind velocity derived measured or hindcasted long-term values over 30 years. By using the annual maximum 10-minute mean wind velocities over approximately 35 years based on Measurement Technical Data Sheet #34 of the Japan Meteorological Agency¹⁴⁾ and by assuming a double exponential distribution, the expected wind velocities over 5, 10, 20, 50, 100, and 200 years have been calculated at 141 meteorological stations. For the performance verification of facilities, these data can be used as reference values; however, if the location of interest has topographical conditions different from those at the close meteorological stations, it is preferable to take measurements at least for 1 year to determine the effect of the topography.¹⁵⁾

- (2) The wind velocities obtained at the meteorological stations are approximately 10 m above the ground. Therefore, if the height of the target facility is different from the height mentioned above at the estimation of the wind over the sea from the observed values, height correction shall be performed for the wind velocity. The vertical distribution of wind velocity is usually shown on a logarithmic scale; however, for simplicity, an exponential scale is often used for the performance verification of various types of facilities.

$$U_h = U_0 \left(h/h_0 \right)^n \quad (2.2.1)$$

where

U_h : wind velocity at height h (m/s)

U_0 : wind velocity at height h_0 (m/s)

n : index according to the situation, such as roughness degree near the earth's surface

- (3) The exponent n in **equation (2.2.1)** varies with the roughness of the nearby terrain and the stability of the air. In general, it is possible to use a value of $n = 1/10$ to $1/4$ for performance verification when specifying the wind velocity for purposes such as calculating wind pressure, and a value of $n \leq 1/7$ is often used over the ocean. Statistical data for wind velocity is usually the mean wind velocity over 10 minutes; however, depending on the facility, the mean wind velocity over a shorter time period may be required, or the maximum instantaneous wind velocity may be required. In such cases, one should understand the gust factor (the ratio of the maximum instantaneous wind speed to the 10-minute mean wind velocity) and the characteristics of the region, such as the relationship between the main wind velocity and maximum wind velocity.

2.3 Wind Pressure

- (1) Wind pressure shall be appropriately specified by considering items such as structure and location of the facility.

- (2) Wind pressure that acts on sheds, warehouses, and cargo handling equipment shall be specified as follows.

- ① Wind pressure acting on sheds and warehouses shall conform to the **Order for Enforcement of the Building Standards Act** (Cabinet Order No. 246 of 2005) Article 87.
- ② Wind pressure acting on cargo handling equipment shall conform to the **Structural Standard for Cranes** (Health, Labour and Welfare Ministry Public Notice No. 399 of 2003), the **Structural Standard for Mobile Cranes** (Health, Labour and Welfare Ministry Public Notice No. 400 of 2003), or the **Structural Standard for Derrick Cranes** (Ministry of Labour Public Notice No. 120 of 2000). Refer to **Comment of Each Structural Standard for Cranes and Others**.¹⁶⁾ However, cargo handling equipment that is not covered by the same codes is excluded.

(a) Structural Standard for Crane

In Article 9, **Structural Standard for Crane**, it is specified that the wind load shall be calculated as follows:

- 1) The value of the wind load is calculated by using **equation (2.3.1)**:

$$W = qCA \quad (2.3.1)$$

where

W : wind load(N)

q : velocity pressure (N/m²)

C : wind pressure coefficient

A : pressure-receiving area (m²)

- 2) The value of the velocity pressure in **equation (2.3.1)** can be calculated from either **equation (2.3.2)** or **equation (2.3.3)** depending on the condition of the crane. **Equations (2.3.2)** and **(2.3.3)** correspond to wind velocity values of 16 and 55 m/s, respectively.

$$\text{Crane in operation:} \quad q = 83\sqrt[4]{h} \quad (2.3.2)$$

$$\text{Crane stopped:} \quad q = 980\sqrt[4]{h} \quad (2.3.3)$$

where

h : height (m) above the ground of the crane surface that receives the winds

Use 16 m as the value of h if height < 16 m.

- 3) For the value of the wind pressure coefficient it is possible to use the value found in the wind tunnel tests on the surface of the crane that receives the winds or the value given in **Table 2.3.1** for the category of the surface of the crane that receives the winds. A “surface composed of flat surfaces” in **Table 2.3.1** is the surface of a structure with a box-like shape such as a box girder, operator's cab,

machine chamber, or electrical chamber. A “cylindrical surface” includes the surface of a wire rope. The “face area” is the shaded portion in **Fig. 2.3.1**.

Table 2.3.1 Wind Pressure Coefficients for the Wind Load on a Crane

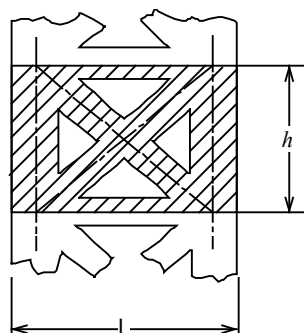
Classification of crane surfaces that receive winds		Value
Surfaces composed with horizontal trusses (Other than horizontal trusses made with steel pipe)	$W_1 < 0.1$	2.0
	$0.1 \leq W_1 < 0.3$	1.8
	$0.3 \leq W_1 < 0.9$	1.6
	$0.9 \leq W_1$	2.0
Surfaces composed of flat surfaces	$W_2 < 5$	1.2
	$5 \leq W_2 < 10$	1.3
	$10 \leq W_2 < 15$	1.4
	$15 \leq W_2 < 25$	1.6
	$25 \leq W_2 < 50$	1.7
	$50 \leq W_2 < 100$	1.8
	$100 \leq W_2$	1.9
Surfaces composed of cylindrical surfaces or horizontal trusses made with steel pipe	$W_3 < 3$	1.2
	$3 \leq W_3$	0.7

Note: In this table, W_1 , W_2 , and W_3 represent the following values:

W_1 : area occupying ratio (the value obtained by dividing the projected area of the surface of the crane that receives the winds by the area of the surface that receives that same winds)

W_2 : the value obtained by dividing the length in the longitudinal direction of the surface of the crane that receives the winds by the width of the surface that receives that same winds

W_3 : the value obtained by multiplying the projected width of the cylinder or steel pipe (unit: m) by the square root of the value shown in 2) for the velocity pressure (unit: N/m²) when the crane stops.



Projected Area

A_r : Area of the shaded portion

Area Occupying Ratio

$$W_1 = \frac{A_r}{lh}$$

Fig. 2.3.1 Projected Area

- 4) The pressure-receiving area in **equation (2.3.1)** shall be the area of the surface of the crane that receives the winds projected onto a surface perpendicular to the direction of the winds (hereinafter “projected area”). When there are two or more surfaces of the crane that receive the winds, the area subject to wind pressure calculation is determined by summarizing the following;
 - i) The projected area of the first surface in the direction of the winds
 - ii) The areas obtained by multiplying the portions of the surface areas of the second and later surfaces in the direction of the winds (hereinafter “second and later surfaces” in this paragraph) that overlap the first surface in the direction of the winds by the reduction factors shown in **Fig. 2.3.2**
 - iii) The projected areas of the portions of the surface areas of the second and later surfaces that do not overlap the first surface in the direction of the winds

In **Fig. 2.3.2**, b , h , ϕ , and η represent the following values:

b : distance between the beams of the crane that receive the winds (see **Fig. 2.3.3**)

h : height of the first beam in the direction of the winds among the beams that receive the winds (see **Fig. 2.3.3**)

- ϕ : the area occupying ratio of the first beam in the direction of the winds among the beams for the surfaces of the crane that receive the winds (For surfaces that are formed of horizontal trusses, ϕ is the value W_1 specified in the note of the table of the previous section; for surfaces formed of flat surfaces or cylindrical surfaces, it is one.)
- η : reduction factor

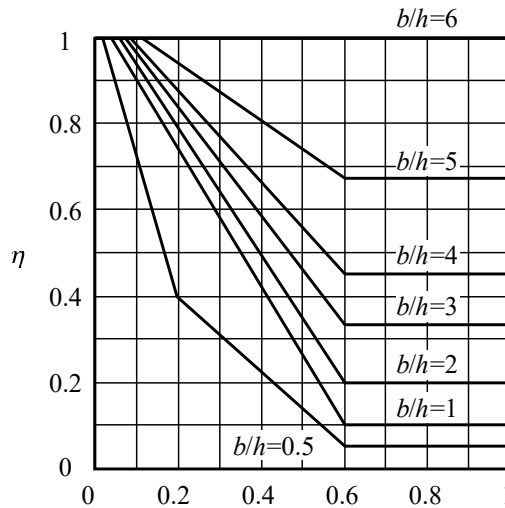
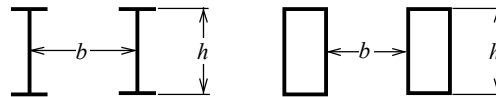


Fig. 2.3.2 Reduction Factors for Projected Areas



(a) Beams of Steel Structure (b) Beams of Box Type Structure

 Fig. 2.3.3 Measurement of b and h

(b) Structural Standards for Mobile Crane

Article 9 of **Structural Standard for Mobile Crane**, specifies that the wind load shall be calculated as follows:

- 1) The value of the wind load can be calculated from **equation (2.3.1)**.
- 2) The velocity pressure can be calculated from **equation (2.3.2)**.
- 3) For the value of the wind pressure coefficient, it is possible to use the value found in the wind tunnel tests of the mobile crane that receives the winds or the value given in **Table 2.3.1** of **Section a) Structural Standard for Crane**. For the value of velocity pressure in W_3 calculation, the value from **equation (2.3.3)** shall be used.
- 4) The pressure-receiving area can be calculated by the method of **4) in Section a) Structural Standard for Crane**.

(c) Structural Standard for Derrick Crane

Article 11, **Structural Standard for Derrick Crane**, specifies that the wind load shall be calculated as follows:

- 1) The value of the wind load can be calculated from **equation (2.3.4)**. In this case the wind velocity is taken to be 50 m/s at the time of storms and 16 m/s at all other times.

$$W = qCA \quad (2.3.4)$$

where

W : wind load(N)

- q : velocity pressure (N/m²)
 C : wind pressure coefficient
 A : pressure-receiving area (m²)

- 2) The wind velocity pressure can be calculated from **equation (2.3.5)**:

$$q = \frac{U^2}{30} \sqrt[4]{h} \quad (2.3.5)$$

where

- q : velocity pressure (N/m²)
 U : wind velocity (m/s)
 h : height (m) of the surface of the crane above the ground
 (Use $h = 15$ m if the height is less than 15 m.)

- 3) For the value of the wind pressure coefficient, it is possible to use the value found in wind tunnel tests or the value given in **Table 2.3.2** for the type of surface and the area occupying ratio of the surface that receives the winds.

Table 2.3.2 Wind Pressure Coefficients for the Wind Load of a Derrick

Classification of the surface that receives the winds	Area occupying ratio	Wind pressure coefficient
Surfaces composed of horizontal lattices or horizontal trusses	$W_1 < 0.1$	2.0
	$0.1 \leq W_1 < 0.3$	1.8
	$0.3 \leq W_1 < 0.9$	1.6
	$0.9 \leq W_1$	2.0
Surfaces of structures composed of flat surfaces	-	1.2
Wire rope surfaces	-	1.2

Note: The value of the area occupying ratio is the value obtained by dividing the projected area of the surface of the crane by the area of the surface that receives the same winds.

- 4) The pressure-receiving area is the wind area projected onto a surface perpendicular to the direction of the winds. When there are two or more surfaces that overlap in the direction of the winds, it shall be calculated as follows;

The area subject to wind pressure calculation is determined by summarizing the following;

- i. In case there are two overlapping surfaces that receive the winds
 - i) The projected area of the first surface in the direction of the winds
 - ii) The 60% areas of the portions of the second surface in the direction of the winds that overlap the first surface
 - iii) The projected areas of the portions of the second surface in the direction of the winds that don't overlap the first surface.
- ii. In case there are three or more surfaces that receive the winds
 - i) The area where three or more surfaces overlap receiving the winds
 - ii) 50% of the projected areas of the portions of the third and later surfaces in the direction of the winds that overlap the front surfaces
 - iii) The projected areas of the portions of the third and later surfaces in the direction of the winds that do not overlap the front surfaces

- (3) The wind pressure that acts upon structures such as highway bridges and elevated highways shall be set as follows:

- ① The wind pressure that acts upon structures such as highway bridges and elevated highways can be specified according to the **Highway Bridge Specifications and Commentary**.¹⁷⁾

- ② In the **Highway Bridge Specifications and Commentary**, the wind load that acts upon a bridge is specified by appropriately considering the location, topography, and ground conditions at the bridge construction, the structural characteristics, and the cross-sectional shape of the bridge.

(a) Steel beams

Table 2.3.3 shows the wind pressure force on a steel beam per 1m long in the bridge axial direction for one span.

Table 2.3.3 Wind Load for Steel Beams (Units: kN/m)

Cross-sectional shape	Wind pressure force
$1B/D < 8$	$\{4.0 - 0.2 (B/D)\} D 6.0$
$8B/D$	$2.4 D 6.0$

where

B = total width of the bridge (m) (see **Fig. 2.3.4**)

D = total height of the bridge (m) (see **Table 2.3.4**)

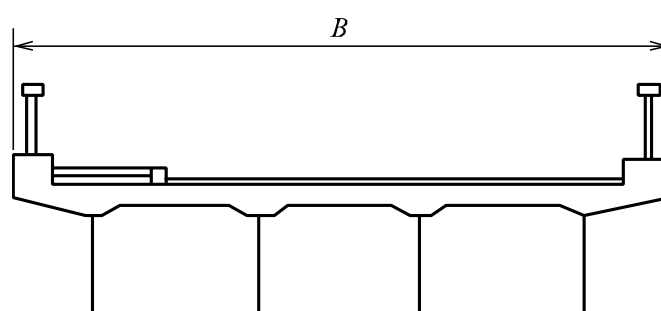


Fig. 2.3.4 Measurement of B

Table 2.3.4 Measurement of D

Bridge guard fence	Wall type rigid guard fence	Other than a wall type rigid guard fence
Measurement of D		

(b) Dual main truss

Table 2.3.5 shows the wind load on a dual main truss per 1 m² of the effective perpendicular projected area on the windward side. For a standard dual **main** truss, it is also possible to use the wind load shown in **Table 2.3.6** per 1 m of length of the arch material on the windward side in the bridge axial direction.

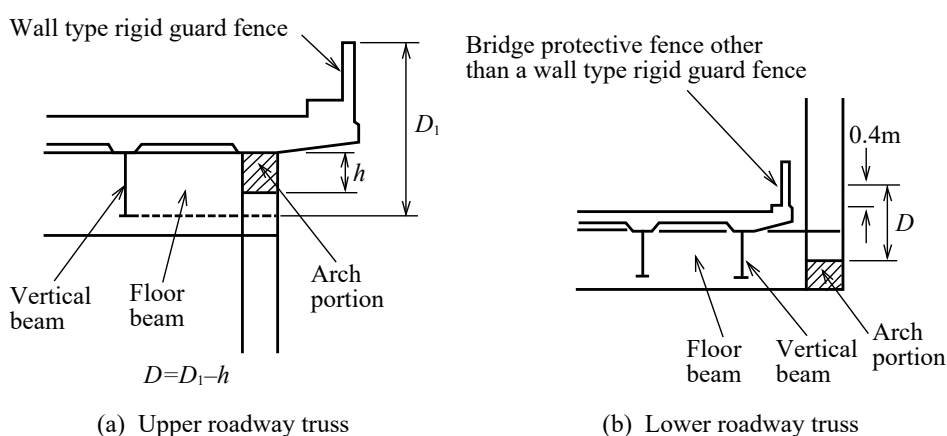
Table 2.3.5 Wind load on a Dual Main Truss (Unit: kN/m²)

Truss	a live load	$1.25 / \sqrt{\phi}$
	no live load	$2.5 / \sqrt{\phi}$
Bridge foundation	a live load	1.5
	no live load	3.0
$0.1 \leq \phi \leq 0.6$ where ϕ = area occupying ratio of the truss (the ratio of the truss projected area to the truss enveloped area)		

Table 2.3.6 Wind load on a Standard Dual Main Truss (Units: kN/m)

Arch material		Wind load
Loaded arch	a live load	$1.5 + 1.5D + 1.25\sqrt{\lambda h} \geq 6.0$
	no live load	$3.0D + 2.5\sqrt{\lambda h} \geq 6.0$
Not loaded arch	a live load	$1.25\sqrt{\lambda h} \geq 3.0$
	no live load	$2.5\sqrt{\lambda h} \geq 3.0$

$7 \leq \lambda/h \leq 40$
 where
 D : total height of the bridge floor (m) (not including the height of the portion that overlaps the arch portion, as seen from the horizontal direction perpendicular to the bridge axis) (see **Fig. 2.3.5**)
 h : height of the arch portion (m)
 λ : main truss height (m) from the center of the lower arch portion to the center of the upper arch portion


Fig. 2.3.5 Measurement of D for a Dual Main Truss

(c) Other types of bridges

Depending on the beam shape, either (a) or (b) shall be applied to obtain the wind load on other types of bridge beams. The wind load on members not described under (a) or (b) is given by the value in **Table 2.3.7** depending on the cross-sectional shape. When there is a live load, the wind load is taken to be 1.5 kN/m for the live load at a position 1.5 m from the bridge's upper surface.

Table 2.3.7 Wind Pressure Force Acting on Bridge Members Other than Steel Beams and Dual Main Trusses (Unit: kN/m²)

Cross-sectional shape of members		Wind load	
		Members on the leeward side	Members on the windward side
Circular shape	a live load	0.75	0.75
	no live load	1.5	1.5
Polygonal shape	a live load	1.5	0.75
	no live load	3.0	1.5

(d) Parallel bridges

When the steel beams are parallel, appropriately correct the wind pressure force in **Table 2.3.3** by considering the effect of the parallel beams.

- (e) The wind load that acts directly on the lower portion of the structure is taken to be a horizontal load that is either perpendicular or parallel to the axial direction of the bridge. It is assumed that it does not act

simultaneously in both directions. The magnitude of the wind load shall be the value shown in **Table 2.3.8** for the effective vertical projected area in the wind direction.

Table 2.3.8 Wind load Acting on the Lower Portion of the Structure (Unit: kN/m²)

Cross-sectional shape of the body		Wind load
Circular or elliptical shape	a live load	0.75
	no live load	1.5
Polygonal shape	a live load	1.5
	no live load	3.0

2.4 Meteorological Observations and Investigations

(1) Overview

Facilities subject to the Technical Standards must be designed to have the required performance with regard to natural phenomena, such as strong winds. Therefore, in the performance verification of the facilities, it is necessary to examine items relevant to that purpose by observing meteorological elements or conducting numerical simulations.

A meteorological investigation includes various methods such as statistical analysis of past data, analysis through numerical simulations, and on-site meteorological observations. Furthermore, it is necessary to formulate a plan by generally considering the following items of ① to ⑥ to determine which methods are desirable: See **Reference (Part II), 2.2 Meteorological Observation and Examination** for details.

- ① Determination of the required meteorological elements
- ② Necessity for real-time on-site meteorological data
- ③ Possibility to obtain meteorological observation data from the past
- ④ Possibility to use observational data from the closest meteorological stations or the AMeDAS observation stations
- ⑤ Necessity for numerical simulations
- ⑥ Necessity for on-site meteorological observations

Based on these investigation results, determine which of the following methods to use in order to specify the natural conditions:

- ① Statistical analysis of past data
- ② Analysis by numerical simulations
- ③ On-site meteorological observations

(2) Meteorological Observations

Meteorological observations aim to measure the atmospheric conditions in physical ways and clarify the structure and mechanism of atmospheric phenomena. It is important as a means to clarify the meteorological conditions of the points concerned. If the situation at the site permits, it is desirable to do fundamental on-site meteorological observation rather than relying on the numerical simulation. Proper meteorological observation equipment shall be selected by setting meteorological items to be considered in the design and performance verification of the facilities subject to the Technical Standards.

Meteorological observation points and points to note for facilities are indicated below:

- ① It is desirable that the observation points are the locations where the observation results obtained there represent the area. Therefore, it is necessary to select a flat and open place for installing instruments and to avoid tall building or topographic valleys, which may affect the observation results.
- ② The names, latitude, longitude, land elevation, altitude above the ground where instruments are installed, and other items of the observation points need to be clarified.

- ③ When observing the precipitation, temperature, and humidity, it is desirable to have the observation field. The observation field shall be flat and open, and turf grass shall be planted on horizontal ground not shaded by buildings and surrounded by airy fence.

The Guides for Meteorological Observation¹⁸⁾ and the Commentary on Statistics of Meteorological Observation¹⁹⁾ published by the Japan Meteorological Agency may be used as a reference for meteorological observation methods, type and structure of instruments, handling method of instruments, processing and statistical methods of observation data, etc.

(3) Meteorological Simulation

As described in **Part II, Chapter 2, 2.1 General (4)**, the meteorological simulation using a numerical model (mesoscale meteorological model) may be conducted to hindcast a meteorological field required for the hindcasting of waves and storm surge, particularly in the inner bay area. On the contrary, the eddies of wind around high buildings in urban areas where many high-rise buildings appear may become a social problem as a smaller-scale meteorological phenomenon. The generating mechanism of these eddies of wind around high buildings is the obstruction of the fast flow in the upper air by the building, and a positive pressure area and negative pressure area appear around the building; therefore, strong wind flows from the positive pressure area to the negative pressure area.²⁰⁾

The same influence may be considered when building facilities subject to the Technical Standards. Therefore, it is desirable to understand the influence that the facilities exert to the meteorological environment beforehand with the meteorological numerical simulation when planning large facilities. k-ε model or large eddy simulation model is available as a simulation model that can consider up to turbulence around the building in such a small scale as eddies of wind around high buildings and is often used for the examination of influence of strong wind around facilities.^{21)–23)}

As described above, it is necessary to use a simulation model that corresponds to the meteorological phenomenon concerned in the meteorological simulation. It is desirable to apply these simulation models to individual verification cases after validating accuracy and reliability with actual observation values.

(4) Obtaining of Weather Prediction and Weather Information

It is desirable to obtain locally predicted information such as wind (strong wind), precipitation, fog (visual range), in addition to generally available weather information to improve construction efficiency and avoid disaster in large-scale port and harbor construction. This type of information²⁴⁾ is instantly available on the Internet and other media.

[References]

- 1) Nagai, T., K. Sugahara, K. Sato and K. Kawaguchi: Characteristic of Japanese Coastal Wind Power based on Long Term Observation, Technical Note of PHRI, No.999, p.59, 2001 (in Japanese)
- 2) Nagai, T: Observed Offshore Wind Characteristics from a View of Energy Utilization, Technical Note of PHRI, No.1034, p.34, 2002 (in Japanese)
- 3) Takahashi, K: Study on quantitative weather forecasting based on extrapolation (Part 1), Study Bulletin No. 13, 1947 (in Japanese)
- 4) Fujita, T: Rep. Met. Lab., Kyushu Inst. Tech., Vol.2, No.1-2, 1952.
- 5) Myers, V.A. and Malkin, W.: Some properties of hurricane wind fields as deduced from trajectories, U.S. Weather Bureau, National Hurricane Research Project, Report 49, 1961.
- 6) Mesoscale and Microscale Meteorology Division National Center for Atmospheric Research: PSU/NCAR Mesoscale Modeling System Tutorial Class Notes and User's Guide MM5:Modeling System Version 3, 2015.
- 7) The National Center for Atmospheric Research: WRF-ARW V3:User's Guide, 2017.
- 8) Kawaguchi, K. and H. Kawai: Estimation of wind and wave during typhoon based on mesoscale model, Technical Note of PARI, No.1169, 19p, 2007 (in Japanese)
- 9) Kawai, H and K. Kawaguchi: Applicability of typhoon bogus and mesoscale model to simulation of storm surge in bays, Report of PARI, Vol.46, No.3, pp.43-86, 2007 (in Japanese)

- 10) Nagai, T., H. Ogawa, A. Nakamura, K. Suzuki and T. Nukada: Characteristics of occurrence of offshore wind energy based on observation data, JSCE Proceedings of Coastal Eng., pp.1306-1310, 2003 (in Japanese)
- 11) Nagai, T, I. Ushiyama, Y. Nemoto, K. Kawanishi, T. Nukada, K. Suzuki and T. Otozu: Examination of field application of lighting system utilizing coastal wind force, Journal of the Japan Society for Marine Survey and Technology Vol. 17 No. 1, JSMST, 2005 (in Japanese)
- 12) Shiraishi, S., K. Shimosako, H. Yoneyama, I. Ushijima, Y. Nishizawa, M. Hosomi, R. Ogawa and T. Nagai: Wind power utilization at port facilities and future view of smart energy system in ports, Journal of Japan Society of Civil Engineers, Ser. B3 (Ocean Engineering), Vol.70, No2, pp.I_121-I_126, 2014 (in Japanese)
- 13) Ministry of Land, Infrastructure, Transport and Tourism Port Authority and Ministry of the Environment Global Environment Bureau: Wind power generation at ports -Manual for symbiosis with port management and operation-, 104p, 2012 (in Japanese)
- 14) Japan Meteorological Agency, Catalogue of annual maximum wind speed (1929-1966) at various places in Japan and the probability of occurrence, Meteorological Agency observation Technical Note No. 34, 1971 (in Japanese)
- 15) JSCE, Civil Engineering Handbook, Giho-do Publications, 1974, pp. 541-544 (in Japanese)
- 16) Industrial Health Division, Industrial Safety and Health Dept., Labour Standards Bureau, Ministry of Health, Labour and Welfare: Commentary of structural standards of various types of cranes (Revision 3), Japan Crane Association, 2015 (in Japanese)
- 17) Japan Road Association: Specifications and commentary of highway bridges, Part I General and Part II Steel Bridge, 2012 (in Japanese)
- 18) Japanese Meteorological Agency: Guides for Meteorological Observation, http://www.jma.go.jp/jma/kishou/known/kansoku_guide/tebiki.pdf, 81p, 2007 (in Japanese)
- 19) Japanese Meteorological Agency: Commentary on Statistics of Meteorological Observation, <http://www.data.jma.go.jp/obd/stats/data/kaisetu/>, 2016 (in Japanese)
- 20) Kiyohide Takeuchi: Wind meteorology, University of Tokyo Press, p.172, 1997 (in Japanese)
- 21) Nagai T., H. Ogawa, A. Nakamura, Y. Suzuki and K. Nukada: Appearance characteristics of coastal wind energy based on observation data, JSCE Proceedings of Coastal Engineering, Vol.50, pp.1306-1310, 2003 (in Japanese)
- 22) Nagai, T, I. Ushiyama, Y. Nemoto, K. Kawanishi, T. Nukada, K. Suzuki and T. Otozu: Examination of field application of lighting system utilizing coastal wind force, Journal of the Japan Society for Marine Survey and Technology Vol. 17 No. 1, JSMST, pp.1-12, 2005 (in Japanese)
- 23) Architectural Institute of Japan: Evaluation and planning of urban wind environment, Maruzen Publishing, p.208, 1993 (in Japanese)
- 24) Eguchi, I., K. Okada, T. Nakata, Y. Uchida, K. Kubota and Y. Utsunomiya : Improvement of the coastal oceanographic and meteorological information system, Journal of Japan Society of Civil Engineers, Ser. B3 (Ocean Engineering), Vol.70, No2, pp.I_61-I_66, 2014 (in Japanese)

3 Tide Level

[Public Notice] (Tidal Level)

Article 7

The tidal level shall be appropriately specified as the water level relative to a datum level for port and harbor management through the statistical analysis of measured values or estimated values and/or others by taking into account the astronomical tides, meteorological tides, wave setup (rise of water level by waves near the shore), and abnormal tidal levels due to tsunamis and others.

[Interpretation]

7. Setting the Environmental Conditions and Other Conditions

(2) Requirements for Tidal Level (Article 6 of the Ministerial Ordinance and the interpretation related to Article 7 of the Public Notice)

① Tide level

When specifying the tide level for the performance verification of the facilities subject to technical standards, appropriately consider how the tide level affects the action of waves and water pressure. Furthermore, when specifying the combination of tide level and waves in the performance verification of the facilities, take as a standard the tide level that would be the most dangerous among the tide levels that have a high likelihood of occurring simultaneously with waves from the viewpoint of the performance verification of such facilities.

② Astronomical tides

With regard to astronomical tides that are considered in the specification of the tide level, take as a standard the specification of chart datum level (C.D.L.), mean sea level (M.S.L.), mean monthly highest water level (H.W.L.), and mean monthly lowest water level (L.W.L.) on the basis of measured values for one year or more.

③ Storm surge

With regard to storm surges that are considered in the specification of the tide level, take as a standard the observation values for 30 years or more, hindcasted values of storm surges caused by the past largest or more typhoons or cyclones, past disaster records, etc. In storm surge hindcasting, wave step-up due to wave breaking near the shore shall be appropriately considered as necessary.

3.1 Astronomical Tides

(1) Definitions^{1) 2) 3)}

Astronomical tides are tides produced by the gravity of the moon and sun and can be viewed as a super-imposition of components known as tidal constituents. The definitions for the representative types of water level are as follows:

① M.S.L.

The average height of the sea level over a certain period is referred to as the M.S.L. for that period. For practical purposes, the M.S.L. is taken to be the average of the water level over one year.

② C.D.L.

The standard water level obtained by subtracting the sum of the amplitudes of the four principal tidal constituents (M_2 , S_2 , K_1 , and O_1) from the M.S.L.. This is used as the standard for water depth in nautical charts.

③ Mean monthly H.W.L.

The average of the monthly H.W.L., where the monthly H.W.L. for a particular month, is defined as the H.W.L. occurring in the period from 2 days before to 4 days after the day of the lunar syzygy (new moon and full moon).

④ **Mean monthly L.W.L.**

The average of the monthly L.W.L., where the monthly L.W.L. for a particular month, is defined as the L.W.L. occurring in the period from 2 days before to 4 days after the day of the lunar syzygy.

⑤ **Mean high water level (M.H.W.L.)**

This is the mean value of all H.W.L.s, including the spring tide and neap tide.

⑥ **Mean low water level (M.L.W.L.)**

This is the mean value of all of low water levels, including the spring tide and the neap tide.

⑦ **Near highest high water level (N.H.H.W.L.)**

The water level obtained by adding the sum of the amplitudes of the four principal tidal constituents (M_2 , S_2 , K_1 , and O_1) to the MSL.

⑧ **High water of ordinary spring tides (H.W.O.S.T.s)**

This is the water level obtained by adding the sum of an amplitude of the tidal constituents M_2 and S_2 to the M.S.L.. The height of the H.W.O.S.T. as measured from the chart datum is known as the spring rise.

⑨ **Low water of ordinary spring tides (L.W.O.S.T.s)**

This is the water level obtained by subtracting the sum of an amplitude of the tidal components M_2 and S_2 from the M.S.L..

⑩ **M.S.L. of Tokyo Bay (T.P.)**

The M.S.L. for Tokyo Bay was determined during the Meiji period from tidal level observations. Since then, T.P. has become the standard for measuring altitude in Japan. The bench mark is located in Nagata-cho, Chiyodaku, Tokyo. Incidentally, T.P. does not correspond to the present day M.S.L. of Tokyo Bay.

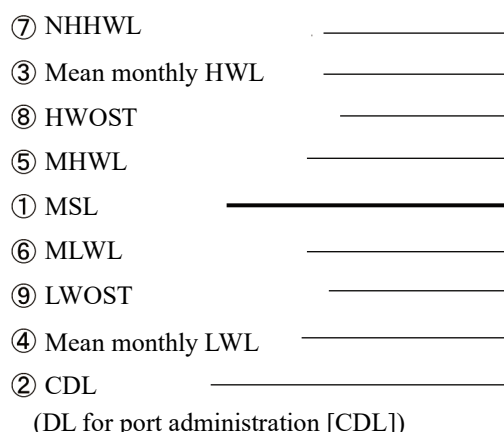
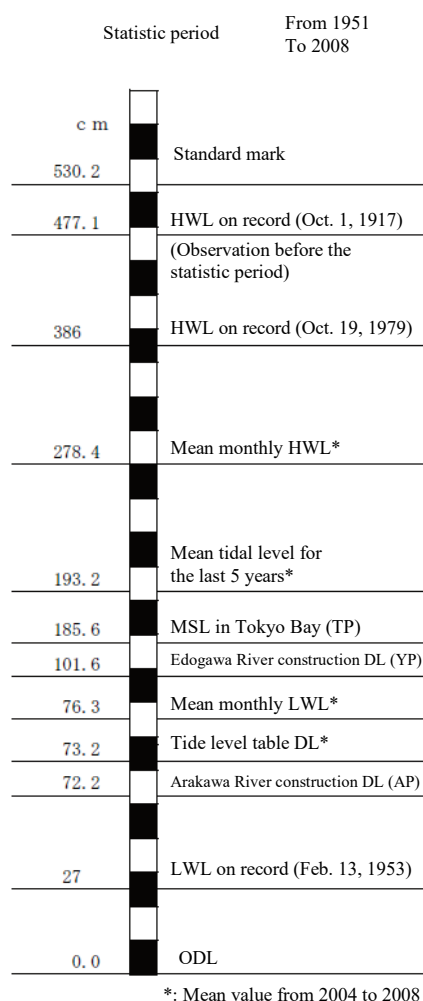


Fig. 3.1.1 Datum Level (DL) of Tidal Levels

There are four principal tidal constituents, namely, the M_2 tide (the principal lunar semidiurnal component of tides, period = 12.421 hours), the S_2 tide (the principal solar semidiurnal component of tides, period = 12.00 hours), the K_1 tide (the luni-solar diurnal component of tides, period = 23.934 hours), and the O_1 tide (the principal lunar diurnal component of tides, period = 25.819 hours). Moreover, Z_0 is defined as the plane with a lower sum of amplitudes of four principal tidal constituents, namely, M_2 , S_2 , K_1 , and O_1 , than the MSL.

Fig. 3.1.2²⁾ shows the relation between tide levels ①, ③, ④, and ⑩ and other regularly used various tide levels at the Tokyo (Harumi) tide observatory as an example. Given that similar D.L. names are used for the D.L.s of tide levels, such as tide level table D.L., observation D.L. (O.D.L.; D.L. may be used as an abbreviation of datum line), C.D.L., DL for port administration (nautical C.D.L.), it is necessary to confirm to the corresponding D.L. of the tide level. The D.L. for port administration shall be the same value as the C.D.L. so that the nautical chart matches the port facilities, but they do not necessarily coincide with the observed value. When a significant difference becomes apparent, it shall be amended through discussions with the Japan Coast Guard. See **Reference (Part II), 2.3 Observation and Examination of Tidal Levels** for details.



Note: YP (Edogawa River construction DL) is -0.84 m from TP (Tokyo MSL) as a reference, AP (Arakawa River construction DL) is -1.134 m.

Fig. 3.1.2 Actual Status Values of Tide Level in the Tokyo (Harumi) Tide Observatory²⁾

(2) Seasonal and Annual Changes in Mean Water Level³⁾

The mean water level for each month varies over the year owing to factors such as the ocean water temperature and atmospheric pressure distribution near the Japanese islands. In many places, the mean water level can vary by ± 5 to 20 cm over the years. Along the Japanese coast, it is typically higher in the summer and lower in the winter.

The annual mean water level is also affected by factors such as the ocean water temperature and atmospheric pressure distribution for that year, and there may be variations of ± 10 cm depending on the ocean region.

(3) Occurrence Probability Distribution of Astronomical Tidal Levels⁴⁾

Astronomical tidal levels have repeated high tides and low tides approximately twice per day and repeated highest tides and lowest tides approximately twice per month. The shape of the occurrence probability distribution of these astronomical tidal levels varies with location, and the tide levels that have the highest probability of occurrence are the tidal levels that are close to the M.S.L.. By contrast, the occurrence probability of high tide levels (e.g., the mean monthly H.W.L.) or low tide levels (e.g., the mean monthly L.W.L.) are small.

3.2 Storm Surge

(1) Definitions

In addition to the astronomical tides caused by the gravity of the moon and sun, the height of the ocean surface can change because of factors such as changes in atmospheric pressure and winds accompanying the passage of low

atmospheric pressure systems (including typhoons, hurricanes, and cyclones) and high atmospheric pressure systems. These meteorological changes of the sea surface are called meteorological tides, and the difference between the measured tidal level and the forecasted astronomic tidal level is called the tidal level anomaly. In particular, among meteorological tides, the rise of tidal level due to the passage of a typhoon or low atmospheric pressure system is called a storm surge.

(2) Causes of Storm Surge

If the atmospheric pressure at the sea surface is lowered by 1 hPa for a sufficiently long time so that the sea surface is in equilibrium with the atmospheric pressure at the sea surface, the ocean surface rises by approximately 1 cm higher than the normal level. If the winds blow at a constant velocity for a long time from the mouth of an internal bay toward the innermost of the bay so that the sea surface rises toward the innermost of the bay and reaches equilibrium, the amount of sea level rise at the furthest point inside the bay is roughly proportional to the square of the wind velocity; furthermore, the amount is also larger when the bay is longer or shallower. During an actual typhoon, the atmospheric pressure, wind velocity, and wind direction on the sea surface changes in a complicated manner at different locations and times.

(3) Past Storm Surges

Table 3.2.1 shows the typical storm surges observed in tide observatories along Japan's shores. Tidal levels of 2 m or more have been observed on the Pacific and East China Sea coasts. The highest tidal level was 3.5 m, which occurred in the Port of Nagoya during the Ise Bay Typhoon in 1959. Furthermore, although it is not included in this table, significant tidal levels were recorded in the Yatsushiro Sea and Kagoshima Bay.^{3), 5)} Moreover, tidal levels in storm surge due to extratropical cyclones, which were higher than those due to typhoons, have been observed in Hokkaido, Tohoku District, and Hokuriku District since 2003.⁶⁾ Therefore, storm surges due to extratropical cyclones shall also be properly considered in these areas.

Even in the same sea area, the tidal level differs place by place and depends on the location of a tide observatory that does not necessarily show the highest tidal level in that sea area. For example, an on-site observation reveals that some shores in the northern Yatsushiro Sea experienced a 3.9 m tidal level by Typhoon #9918 (the 18th typhoon in 1999).⁷⁾ Furthermore, where the coast line significantly changed from the past owing to reclamation and the like, another typhoon with a condition that is identical with a past typhoon provides different tidal levels from the past.

Table 3.2.1 Major Storm Surges with 2 m or Higher Instantaneous Highest Deviation Observed in 1900–2016
(Japan Meteorological Agency,³⁾ revised)

Month/Day/ Year	Location	Highest deviation (m)	Cause	Month/Day/ Year	Location	Highest deviation (m)	Cause
10/1/1917	Tokyo Bay	2.1Ext	Typhoon	9/16/1972	Ise Bay	2.0	Typhoon #7220
7/18/1930	Ariake Sea	2.5Ext	Typhoon	9/27/1991	Ariake Sea	2.7	Typhoon #9119
9/21/1934	Osaka Bay	3.1 Ext	Muroto Typhoon	9/17/1995	Hachijo Is.	3.4	Typhoon #9512
9/1/1938	Tokyo Bay	2.2 Ext	Typhoon	9/22/1996	Hachijo Is.	2.9	Typhoon #9617
9/3/1950	Osaka Bay	2.4	Jane Typhoon	9/24/1999	Suonada Sea	2.1 Ext	Typhoon #9918
8/17/1956	Ariake Sea	2.4 Ext	Typhoon #5609	7/8/2000	Hachijo Is.	2.5	Typhoon #0003
9/26/1959	Ise Bay	3.5	Ise Bay Typhoon	10/1/2002	Hachijo Is.	2.4	Typhoon #0221
9/21/1961	Osaka Bay	2.5	Daini Muroto Typhoon	9/7/2004	Ariake Sea	2.1	Typhoon #0418
9/25/1964	Osaka Bay	2.1 Ext	Typhoon #6420	9/7/2004	Western Setonaikai Sea	2.1	Typhoon #0418
9/10/1965	Eastern Setonaikai Sea	2.2	Typhoon #6523	10/20/2004.	Tosa Bay	2.5	Typhoon #0423
8/21/1970	Tosa Bay	2.4 Est	Typhoon #7010				

No marks: from a document of the tide observatory operated by the Japan Meteorological Agency; Est: Estimated value; Ext: from a document of the tide observatory not controlled by the Japan Meteorological Agency

(4) Empirical Formula to Predict Storm Surge

The tide anomaly due to a typhoon can be roughly estimated from an empirical formula, such as **equation (3.2.1)**.³⁾

$$\zeta = a(p_0 - p) + bW^2 \cos \theta + c \quad (3.2.1)$$

where

ζ : tide anomaly (cm)

p_0 : reference atmospheric pressure (1010 hPa)

p : lowest atmospheric pressure at the target location (hPa)

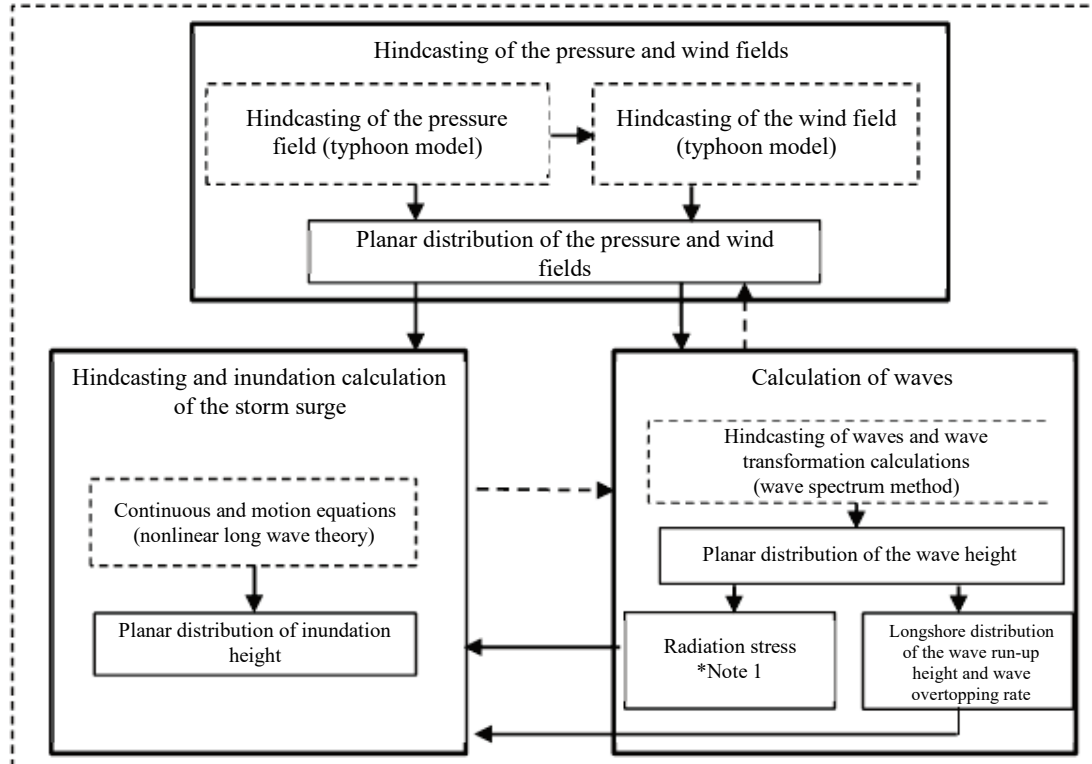
W : maximum value of the mean 10-minute wind velocity at the target location (m/s)

θ : angle between the main wind direction for the bay and that of the maximum wind velocity W

a, b, c : constants determined from past observational results at the target location

(5) Numerical Calculation of Storm Surge

A numerical calculation is conducted to analyze the phenomenon of storm surge in more detail. In this numerical calculation, items such as the atmospheric pressure that acts on the sea surface, the frictional stress on the sea surface due to winds, the frictional stress that acts on the currents at the sea bottom, and the eddy viscosity of the sea water are taken into consideration, and the changes in tidal level and flux at the grid points are calculated at each time step from the time the typhoon approaches until it passes.⁸⁾ The topography is approximated using a grid with a spacing of several hundred meters or finer than that and the water depth is given at each grid point. The distributions of the atmospheric pressure and the wind velocity of the typhoon are calculated from the central (atmospheric) pressure, the radius of the maximum wind velocity, and the forwarding speed of the typhoon. The MASCON model that considers influence of the onshore topography on the wind fields, or the local meteorological model that can reproduce complicated pressure and the wind fields may be applied in the calculations.⁹⁾ Furthermore, numerical models that consider density layers and water discharge from rivers have been developed, as well as models that do not consider storm surge, astronomical tides, and waves as independent phenomena but rather consider them together with their interactions.^{10), 11), 12), 13)} (Fig. 3.2.1) There are various models for the numerical calculation of storm surge; therefore, an appropriate calculation method that sufficiently reproduces storm surges in the target sea region shall be employed.



*Note 1: Radiation stress: required when calculating the tide level and considering the wave setup.

*Note 2: Dotted arrows are limited to cases wherein interactions can be considered such as integrated models.

Fig. 3.2.1 Flow of the Numerical Calculation of Storm Surge Due to a Typhoon⁶⁾

(6) Storm Surge and Astronomical Tides

A storm surge is caused by meteorological disturbances, such as typhoons, whereas astronomical tides are caused mainly by the gravity of the moon and sun. Considering that storm surges and astronomical tides are phenomena with independent causes each other, the time of maximum tide anomaly due to storm surges might overlap either the astronomical high tide or the low tide. In particular, the astronomical tide range is large at internal bays in the Seto Inland Sea and along the coast of the East China Sea; therefore, even if a remarkable tide anomaly occurs, severe damage is unlikely to occur at astronomical low tide. When specifying the design tidal level so that one does not overlook such a superimposition of storm surge and astronomical tide, one should not only consider the tidal level obtained by combining the storm surge with the astronomical tide, but also one should consider the characteristics of the occurrence of tide anomalies due to the storm surge.

(7) Coincidence of Storm Surges and High Waves

A storm surge in an internal bay mainly occurs owing to the suction effect of depression and wind setup effect. The suction effect usually predominates at the bay mouth, and the tide anomaly reaches the maximum value when a typhoon is closest and when the atmospheric pressure has decreased the most. The wind setup effect often predominates at the bay innermost; therefore, the tidal level anomaly is the greatest when the typhoon winds are blowing from the bay mouth toward its innermost. On the contrary, waves are not directly related to the suction effect but develop owing to winds; furthermore, their propagation is affected by the bathymetry in shallow sea areas. Waves are also affected by the surrounding bathymetry and can easily be sheltered by capes or islands. Considering that a storm surge differs from waves, the peak of the tide anomaly and the peak of the waves may not occur simultaneously depending on the track and location of the typhoon within the bay.¹⁴⁾

(8) Rise of Mean Water Level due to Waves Breaking

In the surf zone, regardless of whether the sea level is being drawn up by depression or wind setup effect, the mean water level increases due to wave breaking, and there is a long period of oscillation. As part of this process, the increase in the mean water level is called the wave setup. The amount of increase depends on factors such as the slope of the sea bottom and the steepness of the incident waves. It tends to be larger near the shoreline and may be 10% or more of the significant wave height offshore (see **Part II, Chapter 2, 4.4.8 Rise of Mean Water Level Due to Waves and Surf Beats**). Therefore, at the shore that is directly hit by waves, the absolute increase amount of mean water level is large; this is also an important factor of tide anomaly.

For example, a study of several typhoons revealed that the tidal level observed in the Minami-izu tide observatory cannot be explained by the storm surge numerically calculated by considering only the depression and wind setup; the rise of water level due to wave breaking need to be considered.^{15), 16)} Moreover, it is considered that approximately half of the tidal level in Tosa Bay caused by Typhoon #7010 listed on **Table 3.2.1** was attributable to the rise of mean water level due to wave breaking.¹⁷⁾

For the performance verification of facilities in the surf zone, it is necessary to consider the rise of the mean water level due to wave breaking and oscillation; however, the calculation formulas and diagrams for factors such as wave height in surf zone, wave force, and wave overtopping rate usually include the effect of rise of the mean water level. Therefore, it is not necessary to separately add the amount of rise of mean water level into the design tidal level. However, in areas where reefs form a large increase in water level of 1 meter or more, it is preferable to include the rise of mean water level in the tidal level for the purpose of performance verification in such locations.

3.3 Harbor Resonance

(1) Definition

Harbor resonance is a phenomenon of resonance on the sea surface in a closed or semi-closed water area, bay, or strait. The period of resonance is up to several tens of minutes and differs according to the topography of the water area (depth and size). Generally, the sea level change occurs due to ocean disturbance owing to meteorological disturbance such as typhoons, cyclones, and others or tsunamis resonates with the natural frequency in the bay and becomes harbor resonance.

Harbor resonance is divided into two main types: One occurs within a bay owing to the suction effect of the depression and wind setup effect due to a typhoon. This phenomenon is called seiche, which is characterized by free waves propagating independently in the meteorological field. **Fig. 3.3.1** shows the observed records of tidal level in Tokyo Bay during Typhoon #0115, when remarkable seiche occurred (shown by the triangles [▽]).

The other is the type of oscillation forced in a bay or harbor owing to waves from the outer ocean and their accompanying long-term water level variations and currents. This type of oscillation can cause a large resonance with an oscillation period that is unique for the shape and size of the bay or harbor. In particular, remarkable harbor resonance often occurs in places wherein the shape is long and narrow, such as an artificially excavated port, and wherein the water area is surrounded by facilities with a high reflection coefficient, such as quaywalls,

The period for harbor resonance is usually from several minutes to several tens of minutes, and the amplitude may reach several tens of centimeters. Nagasaki Bay has shown amplitudes of approximately 2 meters. Even though the vertical variational amplitude due to harbor resonance may only be several tens of centimeters, the current velocity in the horizontal direction is large; therefore, this can be a significant problem for ship mooring and cargo handling operations. Component waves with a period of 30 to 300 seconds in the frequency spectrum analyzed from continuously observed records for 20 minutes or more, are defined as long-period waves (for long-period waves, see **Part II, Chapter 2, 4.5, Long-Period Waves**).

Therefore, it is necessary to know the natural frequency period of a port for the performance verification of port facilities. Unoki¹⁸⁾ studied the characteristics of harbor resonance in the major ports of Japan. It is also possible to numerically estimate the amplification factor in a harbor resonance to the incident waves with the period of several minutes to an hour.¹⁹⁾

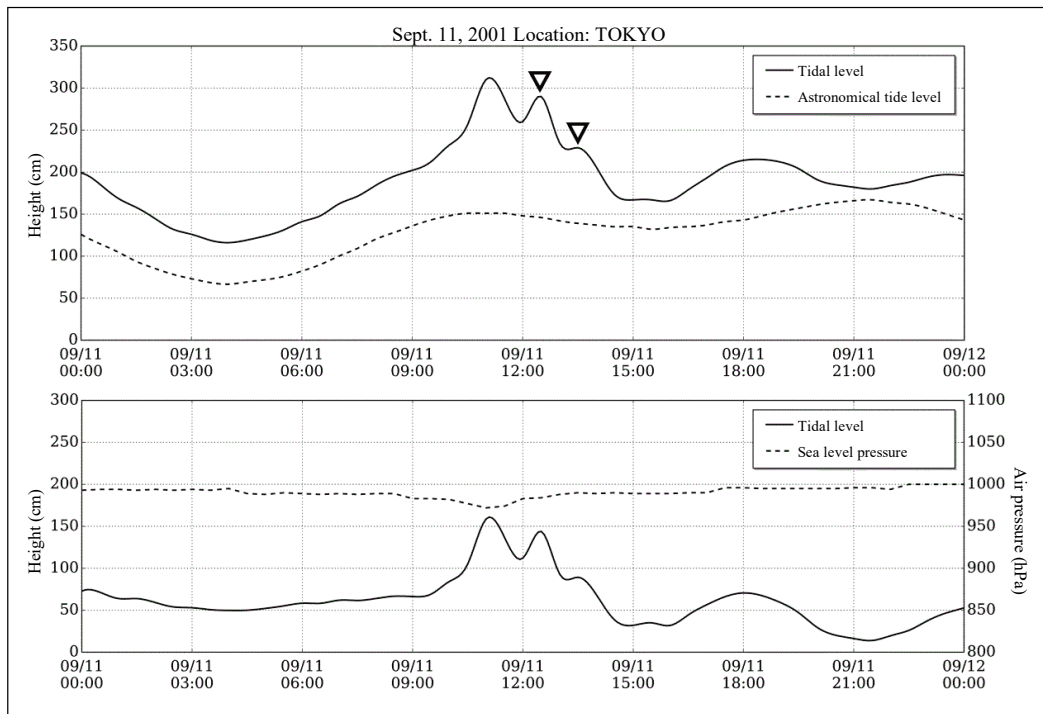


Fig. 3.3.1 Tidal Level Observational Recordings during Typhoon #0115

(2) Harbor Resonance Periods

For harbors that can be modeled in a simple shape, their natural frequency period and amplitude amplification ratio can be found by theoretical calculations. However, the shapes and boundary conditions of actual harbors are extremely complicated; therefore, it is preferable for their natural frequency periods and amplitude amplification ratios to be found by on-site observations or numerical calculations.¹⁹⁾ For reference, formulas for the natural frequency periods in the simplest cases are given as follows:

- ① Rectangular harbor of constant depth (surroundings are closed and no water enters or leaves; **Fig. 3.3.2(a)**):

$$T = \frac{2l}{m\sqrt{gh}} \quad (3.3.1)$$

where

- T : natural frequency period (s)
 l : length of the water surface (the longitudinal direction) (m)
 m : mode of the oscillation (1, 2, 3, ...)
 g : gravitational acceleration (9.8 m/s²)
 h : water depth (m)

- ② Rectangular harbor of constant depth (water can freely enter and leave in one place, and the harbor is narrow and long; **Fig. 3.3.2(b)**):

$$T = \frac{4}{2m+1} \frac{l}{\sqrt{gh}} \quad (3.3.2)$$

The amplitude amplification ratio often takes its maximum when m is zero or one; therefore, in practice, it is acceptable to investigate just this case. In reality, the sea waters within the harbor and in the outer ocean near the harbor entrance oscillate to some extent; therefore, the natural period becomes somewhat longer than that given by **equation (3.3.2)** and becomes closer to the value given by **equation (3.3.3)**²⁰⁾:

$$T = \alpha \frac{4l}{\sqrt{gh}} \quad (3.3.3)$$

where

- l : longitudinal length of a harbor (m)
 α : harbor entrance modification coefficient (**equation (3.3.4)**):

$$\alpha = \left\{ 1 + \frac{2b}{\pi l} \left(\frac{3}{2} - \gamma - \ln \frac{\pi b}{4l} \right) \right\}^{1/2} \quad (3.3.4)$$

where

- π : ratio of the circular constant
 b : width of a harbor (m)
 γ : Euler–Mascheroni constant (= 0.5772)

Table 3.3.1 shows the values of the harbor entrance modification coefficient α for the representative values of b/l , as calculated from **equation (3.3.4)**.

Table 3.3.1 Harbor Entrance Modification Coefficients

b/l	1	1/2	1/3	1/4	1/5	1/10	1/20
α	1.320	1.261	1.217	1.186	1.163	1.105	1.064

- ③ Rectangular harbor of constant depth (water can freely enter and leave in one place, and the harbor entrance is narrow; **Fig. 3.3.2 [c]**):

$$T = \frac{2}{\sqrt{gh \left\{ \left(\frac{m}{l} \right)^2 + \left(\frac{n}{b} \right)^2 \right\}}} \quad (3.3.5)$$

where

- b : width of a harbor (m)

l : length of a harbor (m)

n : number of nodes in the width direction of a harbor ($n = 0, 1, 2, \dots$)

In actual cases, the natural period has a somewhat smaller value than that calculated from **equation (3.3.5)** because of the effect of the harbor entrance.

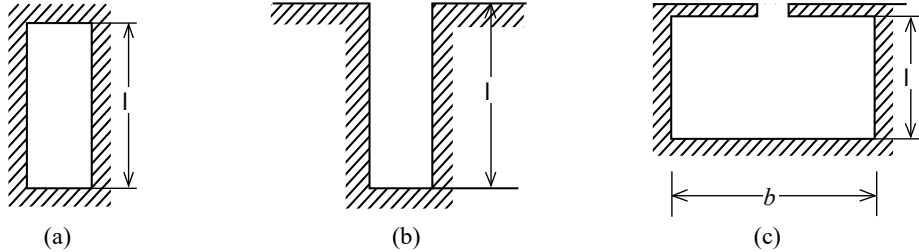


Fig. 3.3.2 Models of Harbor Shapes

(3) Amplitude

The amplitude of harbor resonance is determined by the amplification ratio to the incident long wave. As the period of the incident wave is closer to the natural period of the harbor, the phenomena of harbor resonance become clearer and more severe; therefore, the amplification ratio takes a high value. The large amplification of the resonance causes very strong currents around the narrow harbor entrance. The strong current induces the sea bottom friction, disturbed waves and eddies at the harbor entrance. Consequently, these friction, waves and eddies cause some amount loss of energy. As a result, the amplitude of the harbor resonance does not increase without any limitations. A harbor resonance with small amplitude still forms even if the period of the action is different from the natural period of the harbor.

If the width of the harbor entrance is narrowed to increase the calmness inside the harbor, it may instead make harbor resonance more likely to occur. This phenomenon is called the harbor paradox. When the shape of the harbor is changed, such as by extending the breakwaters, one must be careful not to cause a remarkable harbor resonance.

If the energy loss at the harbor entrance is neglected, the amplitude amplification ratio R at the inside corners of a rectangular harbor can be calculated from the ratio of the length of the harbor to the wavelength by using **Figs. 3.3.3²¹⁾** and **3.3.4²¹⁾**. These figures show that resonance occurs at relatively shorter harbor lengths in a wide port than narrow one. In **Fig. 3.3.4**, the resonance points are roughly the same as the resonance points for a completely closed rectangular shaped lake, as approximated by **equation (3.3.6)**:

$$\frac{l}{L} = \sqrt{m^2 + \left(\frac{2b}{l}\right)^2} \quad m, n=0, 1, 2, \dots \quad (3.3.6)$$

where

L : wave length (m)

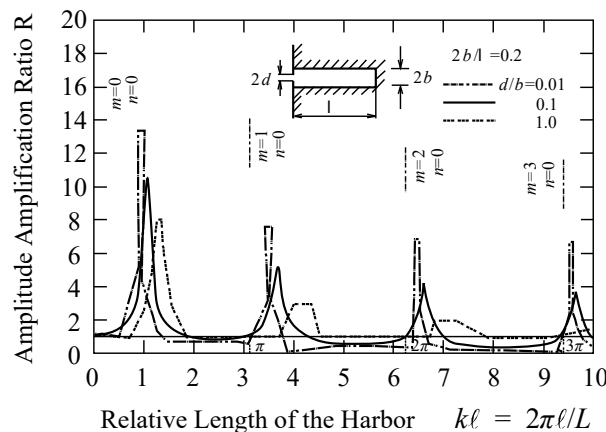


Fig. 3.3.3 Resonance Spectrum for a Long and Narrow Rectangular Harbor²¹⁾

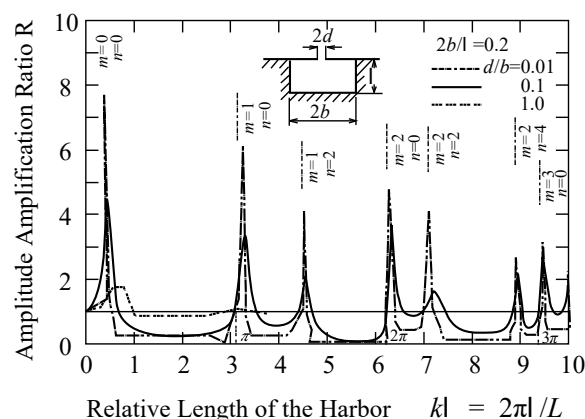


Fig. 3.3.4 Resonance Spectrum for a Wide Rectangular Harbor²¹⁾

(4) Countermeasures against Harbor Resonance

Harbor resonance is the phenomenon whereby long-period waves penetrate into a harbor from the entrance, repeat perfect reflection inside the harbor, and increase their amplitude. To hold down the amplitude of harbor resonance, it is necessary to minimize the reflectance around the inner perimeter of the harbor or alter the shape of the harbor to reduce resonance generation or to increase the energy loss within the harbor. Therefore, it is not advisable to build upright quaywalls around the whole perimeter of a harbor. If a permeable rubble-mound breakwater with a gentle slope is built, wave reflection can be reduced. Furthermore, one can expect a certain energy loss on a sloping breakwater. By installing an inner breakwater close to the position of a node of the harbor resonance, the amplitude of the harbor resonance can be reduced. Regarding the shape of the harbor, it is considered that an irregular shape is better than a geometrically regular shape.

3.4 Abnormal tidal levels

(1) Causes of Abnormal Tidal Levels

In addition to the storm surge caused by typhoons and tsunamis, various other reasons can be given for abnormal tide generation, such as current variations of the Kuroshio current, rise of the ocean water temperature due to the influx of warm water, and the long-term continuation of westward wind-driven currents.²²⁾ Abnormal tidal levels may continue from several days to several months, and in cases such as when the monthly highest tides overlap with a storm surge, water flooding damage can occur.

The analysis of abnormal tidal levels reveals not only abnormally high tidal levels but also abnormally low tidal levels. It is important to clarify their causes for each ocean region.

(2) Effects of Abnormal Tidal Levels

In the performance verification of facilities, an abnormally high tidal level can increase the buoyancy of breakwaters and decrease their stability.²³⁾ Yoshioka et al.²⁴⁾ evaluated the probability distribution of abnormal tide levels at 97 places throughout Japan on the basis of tide observational data (as much as 29 years) and performed a reliability analysis to study the effect on the sliding and overturning stability of breakwaters. Within the scope of their results, the decrease in the safety index due to abnormal tidal levels is small enough to be neglected.

3.5 Long-Term Variation in the Mean Sea Level

(1) Variations in the Mean Sea Level

Both in Japan and abroad the studies on the long-term rise of the mean sea level (M.S.L.) have been conducted separately from the studies on astronomical tidal levels and storm surge in the specification of design tidal levels.

According to the Fifth Assessment Report of the Intergovernmental Panel on Climate Change, it is very likely that the mean yearly rate of global averaged sea level rise was 1.7 mm/year between 1901 and 2010, 2.0 mm/year between 1971 and 2010, and 3.2 mm/year between 1993 and 2010.²⁵⁾

On the contrary, **Fig. 3.5.1** shows the variations in the M.S.L. on Japanese coasts examined by the Japan Meteorological Agency.²⁶⁾ It shows no clear rising trend but the two-decadal variations with a local maximum around 1950 until 1990s. Decadal variations have been observed since the 1990s with a rising trend.

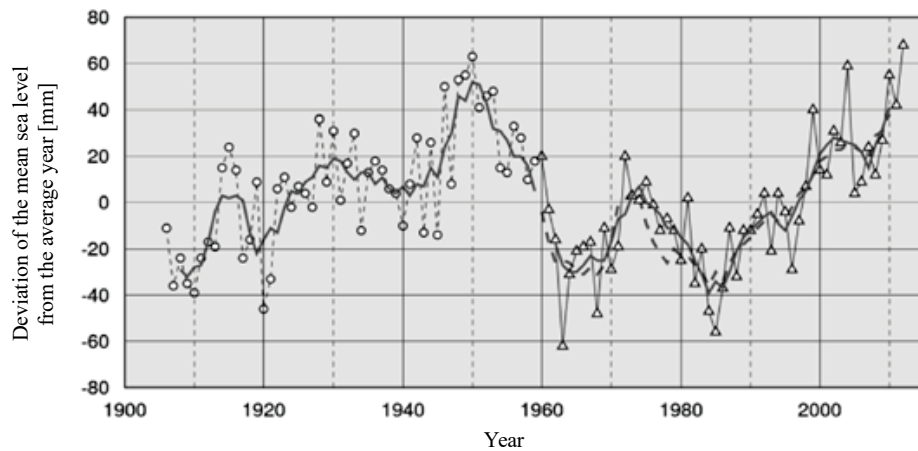


Fig. 3.5.1 Variations in the Mean Sea Level on Japan's Coasts²⁶⁾

Furthermore, interannual variability in the M.S.L. can be examined from the long-term tide records in ports. As shown in **Fig. 3.5.2**, it is estimated that the M.S.L. rose 3.0 mm/year in Kurihama Bay in 53 years, whereas the M.S.L. rose 4.4 mm/year in Karatsu Port in 31 years.²⁷⁾ This variability in the M.S.L. seems to differ on the location of the tide station or the period. In organizing long-term tide records, it is necessary to properly consider the displacement of the ground on which the tide station is built. For example, the ground subsidence at a tide station seems the same as the rise of the M.S.L. Furthermore, the ground height may change before and after an earthquake. See **Part II, Chapter 5, 2 Change in the Crust Caused by Earthquake**. The ground displacement at GNSS-based Continuously Operating Reference Station (CORS) survey may be utilized for the correction of ground displacement at tide station.²⁷⁾

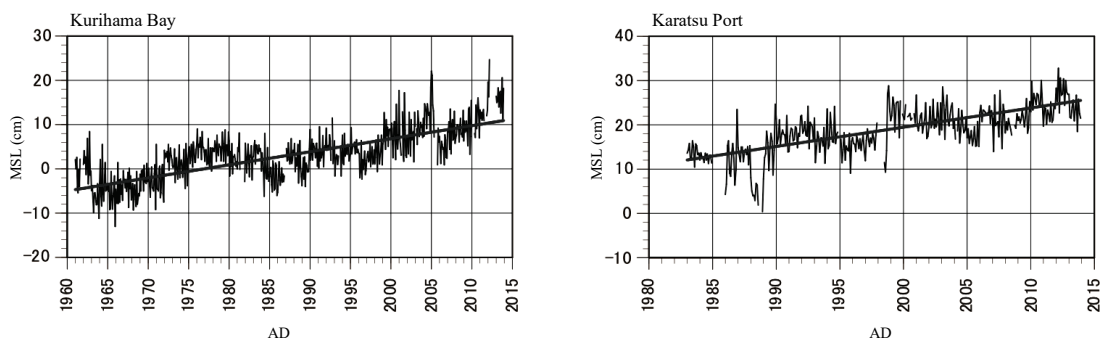


Fig. 3.5.2 Example of Interannual Variability in the MSL in Ports²⁷⁾

(2) Impact of the M.S.L. Rise and Countermeasures

If the M.S.L. rises, the stability of facilities will be lost, and the usage will be restricted owing to inundation or reduced clearance. Furthermore, there will be an impact on the logistics infrastructure.

The countermeasures against the M.S.L. rise include the development and improvement of facilities, modification of land use, and strengthening of disaster prevention systems. It is also necessary to clearly understand the advantages and disadvantages of such countermeasures by taking into account factors such as the social characteristics and natural conditions of the target areas and to combine all countermeasures into adaptable plans.²⁸⁾ In the construction of new facilities or the improvement of existing facilities such as quaywalls, seawalls, roads, and bridges in port areas, it is necessary to consider countermeasures against impacts of climate change in the

construction or renewal stages of facilities so that stepwise adaptation to gradual increases in the impacts can be performed without significant additional costs. It is also necessary to judge the timing of countermeasures on the basis of the result of M.S.L. monitoring and to consider construction plan, design working life, cost-effectiveness, effect on the surrounding environment of these facilities.

3.6 Conditions for Design Tidal Level

(1) Fundamental Concept of Design Tidal Level

A different design tidal level may be used depending on the aim of performance verification even for the facilities used for the same purpose. For example, the design tidal level in protection facilities against storm surge is determined as the tide level wherein wave overtopping becomes highest because the crown height is determined by the amount of wave overtopping. However, a much lower tidal level may become dangerous for the stability of the facilities, and the design tidal level must be determined as such a tidal level. In the performance verification of a breakwater, the tidal levels that make the facility unstable are employed. The highest of these tidal levels is called the planned tidal level.

(2) Design Tidal Level of Protection Facilities against Storm Surge

The design highest tidal level for protection facilities against storm surge shall be determined by using one of the following four methods by considering the occurrence of storm surges.

- ① Use the past highest tidal level or the tidal level by adding some allowance to it.
- ② Use the tide level by adding the past maximum storm surge or the tidal level hindcasted from the model storm surge to the mean monthly highest water level.
- ③ Use the tidal level obtained by determining the occurrence probability curve of the past abnormally high tidal levels and by selecting a tide level that has one or less time of higher tidal levels occurring in a certain return period.
- ④ Economically determine the tidal level by considering the occurrence probability of abnormally high tidal levels, the amount of damage in the hinterland per each tidal level and the construction cost of protection facilities against storm surge.

Each of these methods has the following merits and demerits. Method ① is simplest but requires long-term data. Furthermore, there is no occurrence guarantee of an abnormally high storm surge which exceeds the past highest storm surge level. Method ② is excellent in focusing on the tide level, which is a principal characteristic of a storm surge, but is the same as method ① in that there is no occurrence guarantee for the future. Method ③ is based on the probabilistic concept and clearly shows much occurrence probability exists in the design tidal level. However, reliability and other parameters are doubtful if long-term estimation is made from data covering only a short period of time. Method ④ is reasonable and is the most useful in the context of national economy but requires high technology and labor costs in the estimation of the amount of damage and others.

Methods ① and ② are the most widely adopted. In method ②, the mean monthly highest water level in the typhoon season (July to October) may be adopted instead of the mean monthly highest water level. Normally, the mean monthly highest water level in the typhoon season is higher than the mean monthly highest water level with a difference of 10 cm or more on the Pacific Coast.

Selection among these methods shall be made by comparing each value and considering the observation period, frequency of occurrence, demand and economy of facilities, etc. If the mean monthly highest water level plus the past maximum storm surge is too high to fit the actual plan, the design high water level may be corrected by thoroughly examining the past documents and by considering the frequency of simultaneous occurrence of both events.

In the performance verification of protection facilities against storm surge, it is common to determine the crown height by setting the design high water level as the mean monthly highest water level overlapped by the peak value of storm surge and by considering the worst condition where this design high water level is overlapped by the peak wave height. If the design high water level becomes extremely high under this condition, it is a good idea to examine the design high water level from the frequency of simultaneous occurrence of high tide, peak of storm surge, and peak of wave height.

(3) Tide Level to Set to Accidental Waves

In a shallow water area, the wave height, wave direction, and others are also varied by the tide level. When setting the tide level combined with accidental waves, typhoons or cyclones with adequate strength, size, and route should be assumed under the base on the development limit of typhoons indicated on the records of meteorological disturbance not only in the area concerned but also in the whole of Japan and meteorology irrespective of the past highest high water level or the past maximum tidal level due to storm surges. On the basis of this scenario, hindcast the temporal change in tide level and waves, including storm surges, and examine the condition of tide level and waves that causes the most extensive damage on the port and harbor concerned.^{29) 30) 31) 32)} It is desirable to confirm that the return period of the set tidal level or accidental wave is long enough by the extremal statistics of observation values,³³⁾ the probabilistic typhoon simulation,³⁴⁾ etc.

(4) Simultaneous Occurrence of Storm Surges, Tsunamis, and Harbor Resonance

Both storm surges and tsunamis are rare phenomena and are not generally considered to occur simultaneously. See **Part II, Chapter 2, 5 Tsunamis**.

Harbor resonance is often induced by storm surges or tsunamis. However, harbor resonance is not generally considered to occur simultaneously with storm surges and tsunamis, because the long-period fluctuation of water surface (harbor resonance in the narrow sense) developed, except in storm surges and tsunamis.

(5) Performance Verification of Protective Facilities against Storm Surges, Tsunamis, and Others

Storm surges and tsunamis exceeding the protection objective of the protective facilities against storm surges, tsunamis, and others may occur. To conduct comprehensive disaster prevention countermeasures, including evacuation, if a possible disaster exceeds the design condition on the basis of the generating mechanism of storm surges or tsunamis, it is necessary to set it as the worst case scenario in disaster prevention and to evaluate its protection performance in that case. If damage due to flooding or others is supposed to occur, disaster prevention countermeasures that combine evacuation support countermeasures such as a hazard map also need to be considered. When setting conditions for disaster prevention, it is desirable to calculate the return period (in years) of the disaster.

3.7 Observations and Investigation of Tidal Level**(1) Overview**

Tidal levels are continuously observed as the ocean surface variation, excluding relatively short frequency variations such as waves. Tidal level observations have various purposes, as listed below; therefore, it is preferable for the observations to be done appropriately on the basis of the purpose. The equipment to be installed in tide level observatories (e.g., the tide observation well and tidal level measuring equipment [float type or radio type]), shall be properly selected according to the objective, continuity, and other parameters of the observation. See **Reference (Part II), Chapter 1, 2.3 Observation and Examination of Tide Levels** for details.

① Standard water level

Various datum levels are used for different purposes, such as observation, maintenance, and management of port construction and nautical charts. When observing the tidal level, it is necessary to understand to which datum level the water level should be observed.

② Mean sea level monitoring

Recently, the rise in sea level due to global warming has become a major concern. However, there are great variations in the predictions of the amount of sea level rise; therefore, mean sea level monitoring based on long-term tide level observation is necessary.

③ Understanding tsunamis, storm surge, and long-period waves

When structures along the shore suffer a disaster, the understanding of marine conditions, including tide level records, is the first step in the process of understanding the cause of the disaster and planning recovery measures.

④ Others

The setting of the datum level is also important in the supervision of construction work or environmental monitoring.

(2) Confirmation of Observation Benchmarks

Given that the benchmark (standard mark) of the tide observatory and the benchmark installed near the tide observation booth are subjected to the influence of ground subsidence and others, it is important to properly evaluate the amount of ground subsidence. Therefore, it is desirable to adjust the level to the first-order benchmark of the Geospatial Information Authority of Japan every few years.

The Geospatial Information Authority of Japan periodically surveys the elevation of its first-order benchmarks. If it judges that the ground has risen or subsided excessively, the elevation of the first-order benchmarks is reviewed as survey mean results. The Geospatial Information Authority of Japan makes public the review history of the mean results and the annual survey results of its first-order benchmarks so that everybody can view them.³⁵⁾

(3) Obtaining Documents Related to the Tidal Level Observation

The tidal level is observed by various institutions, such as the national government, which administers ports and harbors, fishery harbors, coasts, and local governments. Among these institutions, the Hydrographic and Oceanographic Department of the Japan Coast Guard and the Japan Meteorological Agency publish the Tidal Table³⁶⁾ and Tide Table,³⁷⁾ respectively, and provide anticipated information on the tidal level calculated by the harmonic analysis at major ports and harbors. Moreover, the Japan Meteorological Agency publicizes the tide level observation records, namely, the “Diagnosis Table and Data on Tide and Sea Level,” on its website.³⁸⁾ Furthermore, the Coastal Movements Data Center of the Geospatial Information Authority of Japan publicizes the monthly and yearly mean tide levels in its registered tidal level observatories on its website; these levels were organized from the data presented by the Ports and Harbours Bureau of the Ministry of Land, Infrastructure, Transport and Tourism, Hokkaido Regional Development Bureau, Okinawa General Bureau, Hydrographic and Oceanographic Department of the Japan Coast Guard, Japan Meteorological Agency, Geospatial Information Authority of Japan, local governments, and others.³⁹⁾

[References]

- 1) Japan Coast Guard: Tide Table, Vol. 1, 1996 (in Japanese)
- 2) Japan Meteorological Agency: Tide Table 2011, 2010 (in Japanese)
- 3) Japan Meteorological Agency: Tide Table 2004, 2003 (in Japanese)
- 4) Study Group of Analysis and utilization of coastal wave observation data,: measurement of tide, Coastal Development Institute of Technology, Coastal development Technical Library. No.13,2002. (in Japanese)
- 5) Takahashi, H. A. Takeda, K. Tanimono Y. Tsuji and I. Isozaki: Prediction and preventive measure of coastal disaster- How to prepare for tsunamis and storm surges, Hakua Publishing, 408p. 1988 (in Japanese)
- 6) Ministry of Agriculture, Forestry and Fisheries and Ministry of Land, Infrastructure, Transport and Tourism: Guide to creating a storm surge flooded area map, p.60, 2015 (in Japanese)
- 7) HIRAISHI, T. K. HIRAYAMA and H. KAWAI: A Study on Wave-Overtopping by Typhoon No. 9918, Technical Note of PHRI, No.972, 2000.12, 19p (in Japanese)
- 8) Shibaki, H., T. Ando, T. Mikami and C. Goto: Development of integrated numerical research system for prevention and estimation of coastal disaster, Jour. JSCE No586/11-42, pp.77-92,1998 (in Japanese)
- 9) Kawai, H and K. Kawaguchi: Applicability of typhoon bougus and mesoscale model to simulation of storm surge in bays, Report of PARI, Vol.46, No.3, pp.43-86, 2007 (in Japanese)
- 10) Yamashita, T., Y. Nakagawa: Simulation of a storm surge in Yatsushiro Sea due to Typhoon No. 9918 by wave-storm surge coupled model considering shear stress of white cap breakers, Proceeding of Coastal Eng. No. 48, pp.291-295, 2001 (in Japanese)
- 11) Takigawa, K.. and M. Tabuchi: Preparation of hazard maps of storm surges and high waves under the most probable occurrence based on tide-wave interaction analysis, probable assumption, Proceeding of Coastal Eng. No. 48, pp. 1366-1370, 2001 (in Japanese)
- 12) Shibaki, H. and A. Watanabe: Study on Multi-level simulation model fore storm surge considering density stratification and wave setup, Journal of the JSCE, No. 719/II pp. 47-61, 2002 (in Japanese)
- 13) Kawai, Y., K. Kawaguxhi and N. Hashimoto: Modeling of wave-storm surge two-way joint hindcasting and case study for Typhoon 9918 hindcasting,, Proceeding of Coastal Eng. No. 50, pp. 296-300, 2003 (in Japanese)

- 14) Kawai, Y., S. Takemura and N. Hara: Characteristics of storm surge-high wave joint occurrence and duration in Tokyo Bay, Proceeding of Coastal Eng. No.49, pp. 241-245, 2002 (in Japanese)
- 15) Konishi, T.: Situations of damages of storm surges and status of the study for forecasting, Oceanographic Society of Japan, Coastal Oceanography Research Vol. 35 No. 2, 1998 (in Japanese)
- 16) Tatsuo KONISHI: A Cause of Storm Surges Generated at the Ports Facing Open Oceans- Effect of Wave Setup-, Sea and sky Vol. 74, No. 2, 1997 (in Japanese)
- 17) Shibaki, H., F. Kato and K. Yamada: Hindcasting of abnormal storm surge in Tosa Bay considering density stratification and wave setup, Proceeding of Coastal Eng. No. 48, pp. 286-290, 2001 (in Japanese)
- 18) Unoki, S: On seiche and long period waves in harbours, Proceeding of 6th conference on coastal Engineering, pp. 1-11, 1959 (in Japanese)
- 19) TAKAYAMA, T. and T. HIRAISHI: Amplification Mechanism of Harbor Oscillation Derived From Field Observation And Numerical Simulation, Technical Note of PHRI No.636, pp.70, 1988 (in Japanese)
- 20) Honda, K., Terada, T., Yoshida, Y. and Ishitani, D.: Secondary undulation of oceanic tides, Jour. Collage of Science, Univ. of Tokyo, Vol.26, 1943
- 21) Goda, Y: Secondary undulation of tide in rectangular and fan-shaped harbour, JSCE 10th conference on Coastal Eng., pp. 53-58, 1963 (in Japanese)
- 22) Shimono T., K. Nakai, H. Nagai, H. Matsumoto, K. Watanabe and M. Isobe: Regional characteristics of abnormal tide levels in coastal areas of Japan, JSCE Proceedings of Coastal Engineering, Vol.51, pp.1221-1225, 2004 (in Japanese)
- 23) Coastal Development Institute of Technology (CDIT): Survey report on Extra-high tide level Fiscal 2002, pp. 86, 2003 (in Japanese)
- 24) Yoshioka, K., T. Nagao, E. Kibe, T. Shimono and H. Matsumoto: Effect of extra-high tide on the external stability of caisson type breakwaters, Technical Note of National Institute for Land and Infrastructure Management, No.241, 2005 (in Japanese)
- 25) IPCC WG1: Fifth Assessment Report Climate Change 2013 (AR5) Summary for Policy-Makers, 2013
- 26) Japanese Meteorological Agency: Marine health checkup table, comprehensive diagnosis table 2nd edition, No2, Monitoring sea level on the coast of Japan 2013, http://www.data.jma.go.jp/kaiyou/shindan/sougou/html_vol2/1_2_vol2.html (in Japanese)
- 27) Naito, R., T. Asai, K. Kawaguchi, T. Inomata, D. Tasumi and K. Narita: Estimation of sea level rise using the tide gauge records in port areas and their characteristics, Technical Note of National Institute for Land and Infrastructure Management, No.855, pp.1-36, 2015 (in Japanese)
- 28) Assemblymen in charge of Environment, Synthetic Science and Technology Conference and, Cabinet Office Director-general for Politics on Science and Technology Condition: Study Report on Climate Change, Synthetic Science and Technology Conference, Global Warming Study Initiative, Frontier of Climate Change Studies, Knowledge and Technology in the Century of Environment, 2002, p. 92, 2003 (in Japanese)
- 29) Takahashi, S., T. Tomita and H. Kawai: Performance design concept applied for storm surge defense, Technical Note of PARI, No.1042, 27p, 2003 (in Japanese)
- 30) Takahashi, S., H. Kawai, T. Hiraishi, K. Oda and T. Takayama: Characteristics of storm surge disaster and worst case scenario in Hurricane Katrina, JSCE Proceedings of Coastal Engineering, Vol.53, pp.411-415, 2006 (in Japanese)
- 31) Ministry of Agriculture, Forestry and Fisheries and Ministry of Land, Infrastructure, Transport and Tourism: Guide to creating a storm surge flooded area map, Ver.1.00, 60p, 2015 (in Japanese)
- 32) Utsunomiya, Y., M. Miyata, T. Takayama, H. Kawai, K. Hirayama, Y. Suzuki, M. Kimizuka and Y. Fukinaga: Estimation and application of the largest class storm surge predicted by scenario typhoons, Journal of Japan Society of Civil Engineers, Ser. B2 (Coastal Engineering), Vol.73, No2, pp.I_247-I_252, 2017 (in Japanese)
- 33) Kawai, H., Y. Goda, N. Kudaka and K. NAKAI: Extreme statistics of storm surge heights around Japan through regional frequency analysis, Journal of Japan Society of Civil Engineers, Ser. B2 (Coastal Engineering), Vol.66, No1, pp.121-125, 2010 (in Japanese)

- 34) Kawai H., N. Hashimoto and K. Matsuura: Estimation of extreme value and duration of storm surge in bays by using stochastic typhoon model, JSCE Proceedings of Coastal Engineering, Vol.54, pp.301-305, 2007 (in Japanese)
- 35) Geospatial Information Authority of Japan: Site for browsing benchmark point results, <http://sokuseikagis1.gsi.go.jp/>. (in Japanese)
- 36) Japan coast guard: 2017 tide table Vol.1 Japan and nearby, Japan hydrographic association, 2016 (in Japanese)
- 37) Japanese Meteorological Agency: Tide table, <http://www.data.jma.go.jp/gmd/kaiyou/db/tide/suisan/index.php> (in Japanese)
- 38) Japanese Meteorological Agency: Diagnostic table and data on tide and sea level, http://www.data.jma.go.jp/gmd/kaiyou/shindan/index_tide.html (in Japanese)
- 39) Coastal movements data center of Geospatial Information Authority of Japan: <http://cais.gsi.go.jp/cmdc/centerindex.html>. (in Japanese)

4 Waves

[Public Notice] (Waves)

Article 8

Characteristics of waves shall be set by the methods provided in the subsequent items corresponding to the single action or combination of two or more actions to be considered in the performance criteria and the performance verification:

- (1) Waves to be employed in the verification of the structural stability of the facilities, the failure of the section of a structural member (excluding failure due to fatigue), and others shall be appropriately defined in terms of the wave height, period, and direction corresponding to the return period through the statistical analysis of the long-term measured values or estimated values or other methods.
- (2) Waves to be employed in the verification of the assurance of the functions of a structural member and the failure of its section due to fatigue shall be appropriately defined in terms of the wave height, period, direction and others of waves having a high frequency of occurrence during the design service life through the statistical analysis of the long-term measured values or estimated values.
- (3) Waves to be employed in the verification of the harbor calmness shall be appropriately defined in terms of the joint frequency distributions of the wave height, period, and direction for a certain duration of time based on the long-term measured values or estimated values.

[Interpretation]

7. Setting of the Natural Conditions

- (3) **Items related to waves** (Article 6 of the Ministerial Ordinance and the interpretation related to Articles 8 and 9 of the Public Notice)

Combined conditions of actions in item (1) or actions in items (2) later indicate a design state. Combined conditions for waves shall be properly set pursuant to the subsequent provisions in accordance with the performance criteria and the design state considered in the performance verification.

① **Waves employed to verify the stability of facilities and to verify the failure of the section of a structural member.**

- a) Return period of variable waves

When setting the waves to be considered in the verification of serviceability for a variable state where dominating action is variable waves, the purpose of the facilities and the performance requirements must be satisfied, and in addition, the return period of the waves is set appropriately by considering suitably the design service life and degree of importance of objective facilities, as well as the natural condition of objective location.

- b) Return period of accidental waves

When setting the waves to be considered in the verification of serviceability for an accidental situation where dominating action is accidental waves, the waves that become most disadvantageous among the waves that can occur in objective marine waters are set appropriately.

- c) Period of observed values or estimated values

A period of 30 years or longer is used as the standard for the long-term observed values or estimated values.

② **Waves employed to verify the assurance of the functions and the failure of sections due to fatigue of the facilities relating to structural members.**

- a) The verification of the assurance of the functions of the facilities relating to structural members refers to the verification of the limit state in which function-related trouble occurs in structural members due to frequently-occurring actions, and in addition, the verification of failure of sections due to fatigue refers to the verification of the limit state in which destruction of a section occurs in a structural member due to repeated action.
- b) The waves to be considered in the verification of the assurance of the functions of the facilities

relating to structural members employ as the standard waves for which the number of times which the waves with a wave height greater than that strike in the design service life is about 10,000 times.

- c) When setting the waves to be considered in the verification of destruction of a section due to fatigue, various conditions such as the natural condition of objective facilities are considered, and the number of times of appearance relating to the wave height and period of the waves that occur during the design service life shall be appropriately set. The standard period of the observed values and estimated values is about 5 years or longer.

③ Waves employed to verify harbor calmness

A period of 5 years or longer is used as the standard period for the long-term observation or estimation. In addition, when setting the waves to be considered in the verification of harbor calmness, long period wave shall be considered appropriately as necessary.

4.1 Setting Wave Conditions

4.1.1 Setting of the Wave Conditions for the Verification of Stability of Facilities and the Safety (Section Failure) of Structural Members

(1) Setting of the variable wave conditions

① General

For the performance verification of port facilities, the wave conditions such as the wave height, period, and direction shall be set appropriately. These wave conditions are preferably set by statistical analysis based on long-term observational data, but in cases where the observation data are inadequate, it is common to supplement the data by wave hindcasting.^{1) 2) 3)}

The waves for the stability verification of the facilities and the safety (section failure) of structural members are generally the probabilistic waves whose return period is 50 years, for facilities whose design service life is 50 years. This is the return period of waves that is generally taken into consideration in conventional design, and conventional design is followed in order to provide continuity of the philosophy of conventional design methods and to avoid confusion in practical design work. However, when the return period is set equal to the design service life, it should be noted that the probability to encounter waves exceeding the design external force⁴⁾ reaches about 63%.

Moreover, the return period needs to be set to three times or more of the design service life in order to suppress the encounter probability on the order of 30%. Owing to this, the return period may be established appropriately by taking into consideration the design service life and degree of importance of objective facilities, as well as the natural conditions of objective location.

The return period of waves should be also set to the swell in order to properly accommodate the swell having longer periods than waves generally considered in the previous design. The swell in this case can be defined as waves having the significant wave period of about more than 8 seconds and the wave steepness less than about 0.025.^{5) 6)}

On the other hand, the design tidal level generally uses the astronomical tidal level that causes the severest actions to the stability of facilities concerned and the ultimate limit state of structural members. However, recent disaster examples show that many such facilities that set the high tidal level as the design tidal level for wave pressure calculation suffer from storm surges.⁷⁾ Therefore, the design tidal level for the calculation of wave pressure may be set to the severest tidal level like the tidal level which adds proper storm surge height to the high tidal level for facilities considering the simultaneous occurrence with waves, as well as the performance verification for wave overtopping.

② Extreme Waves

As far as the abnormal wave characteristics that are employed for the examination of the stability of facilities are concerned, it is preferable to carry out statistical treatment for the peak waves and to express this as the probabilistic wave height. **Reference 8)** is a document concerning design waves based on probabilistic wave height.

③ Statistical Treatment of Extreme Waves

The wave height at abnormal weather that is the object of the design is generally expressed as the probabilistic wave height in respect to the return period for peak waves, from the long-term data i.e., a period of at least 30 years as the standard. Since the number of locations for which it is possible to utilize observational data over the long term is still small, wave hindcasting results are generally used instead.

Peak waves, which are the hindcasting data for probabilistic wave height, refer to waves, in general, significant waves, when the wave height reaches the maximum in the process where the waves develop and attenuate under one certain meteorological disturbance, and it is assumed that the peak waves sampled are statistically independent from each other. To estimate the probabilistic wave height, there are two cases: One is to use the wave data whose peak heights exceed a certain designated value in the subject duration and the other is to use the annual maximum wave data among the peak wave heights observed or hindcasted each year. The ratio of the number of actually used data N against the total number of data N_T is called the data adoption rate $\nu = N / N_T$. As the parent distribution function of the extreme wave heights is unknown in general in either case, the Gumbel distribution, the Weibull distribution, or some other distribution functions is applied. The distribution form most suited to the data distribution is found, and the probabilistic wave height corresponding to the required return period, for example, 50 years or 100 years, is estimated by using the most suited distribution function. The Gumbel distribution is also called the double-exponential distribution, extreme value type I distribution, or type FT-I distribution.

However, if it is clear that a distribution function enough reliable cannot be estimated due to an extremely small number of swell peak wave data, the estimation of the probabilistic wave height for swell can be omitted.

Such estimated values are not absolute, but there are certain confidence intervals. Moreover, the accuracy of such estimated values is dependent more on the reliability of the data than the method of statistical treatment. Therefore, when using actually observed waves observed for 20 min every 2 h, for example, keep in mind that there is a possibility that waves higher than the observed waves may have attacked. On the other hand, in the event that the data for the peak waves is prepared by wave hindcasting, care should be taken of appropriate selection of the hindcasting method and verification of the hindcasted results based on the observed values. The hindcasted value shall be corrected if necessary.

Moreover, the period corresponding to the probabilistic wave height is appropriately estimated through the correlative relation between the wave heights and periods plotted for observed or hindcasted wave data. Furthermore, the following equation ⁹⁾ based on Wilson's wave hindcasting equation can be used for wind waves. The equation estimates the periods of waves with the steepness around 0.04 for small waves and less than 0.03 for large waves. On the coasts of the Sea of Japan and the East China Sea where wind waves are dominant, the wave steepness seems to be on the order of 0.035 to 0.04. ¹⁰⁾

$$T_{1/3} \approx 3.3(H_{1/3})^{0.63} \quad (4.1.1)$$

④ Process in the Statistical Treatment of Extreme Waves

In the statistical treatment, the wave data is sorted in the order of height, and the non-exceedance probability for each wave height value is calculated.

Assuming that the number of data is N , and the number m th wave height from the larger side is $x_{m,N}$, the probability F_m that the wave height does not exceed $x_{m,N}$ is calculated using the following equation:

$$F_m = 1 - \frac{m - \alpha}{N + \beta} \quad (4.1.2)$$

The values for each probability distribution function shown on **Table 4.1.1** are employed for α and β in the above equation. Since Gringorten has calculated the values for the Gumbel distribution ¹¹⁾, it has been set so that the effects of the statistical variance of the data are minimized with the non-exceedance probability F corresponding to the anticipated value of the order statistics x_m . Petruaskas and Aagaard have calculated the values for the Weibull distribution based on the same viewpoint ¹²⁾. Moreover, as N is the number of data for data adoption rate $\nu = 1$ (whole extreme data), the total number of extreme data N_T instead of N should be used for $\nu < 1$ (partial extreme data) to estimate the shape of parent distribution function as precisely as possible.

However, as the accumulated data of the maximum wave height for a long time is still not enough, it is not clearly known what distribution function fits at each longshore location.

Table 4.1.1 Parameters for Non-exceedance Probability Calculation of Extreme Waves

Distribution function	α	β
Gumbel distribution	0.44	0.12
Weibull distribution (k = 0.75)	0.54	0.64
Same as above (k = 0.85)	0.51	0.59
Same as above (k = 1.0)	0.48	0.53
Same as above (k = 1.1)	0.46	0.50
Same as above (k = 1.25)	0.44	0.47
Same as above (k = 1.5)	0.42	0.42
Same as above (k = 2.0)	0.39	0.37

⑤ Proposed Example of Fitted Distribution Functions

- (a) Following Petruaskas and Aagaard, in **Reference 13**), Goda has proposed a method that the function that accords the most data among following eight kinds of functions is selected with the correlation coefficient: the Gumbel distribution in **equation (4.1.3)** and the Weibull distribution in **equation (4.1.4)** wherein k = 0.75, 0.85, 1.0, 1.1, 1.25, 1.5, and 2.0 are applied.

$$F(x) = \exp \left[-\exp \left\{ -\left(\frac{x-B}{A} \right) \right\} \right] \quad (4.1.3)$$

$$F(x) = 1 - \exp \left\{ -\left(\frac{x-B}{A} \right)^k \right\} \quad (4.1.4)$$

Here, the non-exceedance probability F_m is calculated using **equation (4.1.2)**. The values shown in **Table 4.1.1** are adopted for the values of α and β .

Next, from the non-exceedance probability F_m , the standard amount of change y_m is calculated by using **equation (4.1.5)** in the case of the Gumbel distribution and **equation (4.1.6)** in the case of the Weibull distribution, respectively.

$$y_m = -\ln \{ -\ln (F_m) \} \quad (4.1.5)$$

$$y_m = \{ -\ln (1 - F_m) \}^{1/k} \quad (4.1.6)$$

If the data completely accord with **equation (4.1.3)** or **equation (4.1.4)**, a linear relationship exists between x_m and y_m . Therefore, the estimation equation for the probabilistic wave height is calculated by assuming a linear relationship for **equation (4.1.7)** and establishing its coefficients (A, B) by the least squares method.

$$x_m = \hat{A}y_m + \hat{B} \quad (4.1.7)$$

Here, \hat{A}, \hat{B} are the estimated values for the coefficients A and B in **equation (4.1.3)** or **equation (4.1.4)**.

- (b) Moreover, in **Reference 14**), Goda has proposed the following method, which revises the abovementioned procedure.

1) Modification of the fitted distribution function (introduction of extreme value type II)

The extreme value distribution of the type II is given by the following equation. The type II distribution is also called the FT-II distribution or Frechet distribution.

$$F(x) = \exp \left[- \left\{ 1 + (x-B)/kA \right\}^{-k} \right] \quad (4.1.8)$$

Here, the examination has been done in a total of nine ways, one way with the Gumbel distribution in **equation (4.1.3)**, four ways with the Weibull distribution in **equation (4.1.4)** ($k = 0.75, 1.0, 1.4,$ and 2.0), and four ways with the type II distribution in **equation (4.1.8)** ($k = 2.5, 3.33, 5.0,$ and 10.0), as the fitted distribution functions.

In addition, formulation of the following equation is carried out instead of **Table 4.1.1**, for α and β in **equation (4.1.2)**.

In other words, it is set as follows:

In the Gumbel distribution:

$$\alpha = 0.44, \quad \beta = 0.12 \quad (4.1.9)$$

In the Weibull distribution:

$$\begin{aligned} \alpha &= 0.20 + 0.27/\sqrt{k} \\ \beta &= 0.20 + 0.23/\sqrt{k} \end{aligned} \quad (4.1.10)$$

In the type II:

$$\begin{aligned} \alpha &= 0.44 + 0.52/k \\ \beta &= 0.12 - 0.11/k \end{aligned} \quad (4.1.11)$$

Moreover, the standard amount of change is calculated by using **equation (4.1.5)** in the case of the Gumbel distribution, **equation (4.1.6)** in the case of the Weibull distribution without any modification, and the following equation in the case of the type II distribution.

$$y_m = k \{ (-\ln F_m)^{-1/k} - 1 \} \quad (4.1.12)$$

2) Modification of the procedure for selecting the optimal fitted distribution function by introduction of rejection criteria

The estimated probabilistic wave height for a certain return period varies according to adopted fitted distribution function. There are two kinds of criteria of the REC criterion and the DOL criterion to reject unsuitable functions. In practical work the following procedure is adopted in the analysis of extreme values by the least square method: after an unsuitable function has been rejected under either of these criteria, the optimal fitted function is selected according not to the value of the simple correlation, but rather the MIR criterion.

In DOL criterion, the maximum value x_l in the data is made dimensionless with the overall mean value \bar{x} and standard deviation s as shown in the following equation, and if this value ξ is below the 5% value or above the 95% value in the fitted distribution function, that function is rejected as unsuited.

$$\xi = (x_l - \bar{x})/s \quad (4.1.13)$$

The 5% and 95% non-exceedance probability values of fitted distribution function are calculated using the following equation using coefficients a , b , and c set as in **Table 4.1.2** as a function of the data adoption rate v by the distribution function.

$$\xi_P = a + b \ln N + c(\ln N)^2 \quad : P=5\% \text{ and } 95\% \quad (4.1.14)$$

Table 4.1.2 Coefficients of Non-exceedance Probability Values of the Maximum Deviation in Used Data

 (a) 5% Non-exceedance Probability Values $\xi_{5\%}$

Distribution function	Coefficient a	Coefficient b	Coefficient c
Extreme type I distribution	$0.257 + 0.133 \nu^2$	$0.452 - 0.118 \nu^2$	0.032
Weibull distribution ($k = 0.75$)	$0.534 - 0.162 \nu$	$0.277 + 0.095 \nu$	0.065
Sane as above ($k = 1.0$)	0.308	0.423	0.037
Sane as above ($k = 1.4$)	$0.192 + 0.126 \nu^{3/2}$	$0.501 - 0.081 \nu^{3/2}$	0.018
Sane as above ($k = 2.0$)	$0.050 + 0.182 \nu^{3/2}$	$0.592 - 0.139 \nu^{3/2}$	0
Extreme type II distribution ($k = 2.5$)	$1.481 - 0.126 \nu^{1/4}$	$-0.331 - 0.031 \nu^2$	0.192
Sane as above ($k = 3.33$)	1.025	$-0.077 - 0.050 \nu^2$	0.143
Sane as above ($k = 5.0$)	$0.700 + 0.060 \nu^2$	$0.139 - 0.076 \nu^2$	0.100
Sane as above ($k = 10.0$)	$0.424 + 0.088 \nu^2$	$0.329 - 0.094 \nu^2$	0.061

 (b) 95% Non-exceedance Probability Values $\xi_{95\%}$

Distribution function	Coefficient a	Coefficient b	Coefficient c
Extreme type I distribution	$-0.579 + 0.468 \nu$	$1.496 - 0.227 \nu^2$	-0.038
Weibull distribution ($k = 0.75$)	$-0.256 - 0.632 \nu^2$	$1.269 + 0.254 \nu^2$	0.037
Sane as above ($k = 1.0$)	-0.682	1.600	-0.045
Sane as above ($k = 1.4$)	$-0.548 + 0.452 \nu^{1/2}$	$1.521 - 0.184 \nu$	-0.065
Sane as above ($k = 2.0$)	$-0.322 + 0.641 \nu^{1/2}$	$1.414 - 0.326 \nu$	-0.069
Extreme type II distribution ($k = 2.5$)	$4.653 - 1.076 \nu^{1/2}$	$-2.047 + 0.307 \nu^{1/2}$	0.635
Sane as above ($k = 3.33$)	$3.217 - 1.216 \nu^{1/4}$	$-0.903 + 0.294 \nu^{1/4}$	0.427
Sane as above ($k = 5.0$)	$0.599 - 0.038 \nu^2$	$0.518 - 0.045 \nu^2$	0.210
Sane as above ($k = 10.0$)	$-0.371 + 0.171 \nu^2$	$1.283 - 0.133 \nu^2$	0.045

The residual Δr from 1 is calculated using the following equation using the correlation coefficient r between the order statistics x_m and standard amount of change y_m . The REC criterion is used to reject the fitted distribution function as unsuited if Δr exceeds the 95% non-exceedance probability value of the residual of the correlation coefficient in the fitted distribution function.

$$\Delta r = 1 - r \quad (4.1.15)$$

The 95% non-exceedance probability value of the residual of the correlation coefficient of the fitted distribution function is calculated by the following equation for coefficients a , b , and c set on **Table 4.1.3** as a function of the data adoption rate ν by the distribution function.

$$\Delta r_{95\%} = \exp[a + b \ln N + c(\ln N)^2] \quad (4.1.16)$$

Table 4.1.3 Coefficients of the 95% Non-exceedance Probability Values $\Delta r_{95\%}$ of the Residual of Correlation Coefficients

Distribution function	Coefficient a	Coefficient b	Coefficient c
Extreme type I distribution	-1.444	$-0.2733 - 0.0414 \nu^{5/2}$	-0.045
Weibull distribution ($k = 0.75$)	$-1.473 - 0.049 \nu^2$	$-0.2181 + 0.0505 \nu^2$	-0.041
Sane as above ($k = 1.0$)	-1.433	-0.2679	-0.044
Sane as above ($k = 1.4$)	-1.312	$-0.3356 - 0.0449 \nu$	-0.045
Sane as above ($k = 2.0$)	$-1.188 + 0.073 \nu^{1/2}$	$-0.4401 - 0.0846 \nu^{3/2}$	-0.039
Extreme type II distribution ($k = 2.5$)	$-1.122 - 0.037 \nu$	$-0.3298 + 0.0105 \nu^{1/4}$	0.016
Sane as above ($k = 3.33$)	$-1.306 - 0.105 \nu^{3/2}$	$-0.3001 + 0.0404 \nu^{1/2}$	0
Sane as above ($k = 5.0$)	$-1.463 - 0.107 \nu^{3/2}$	$-0.2716 + 0.0517 \nu^{1/4}$	-0.018
Sane as above ($k = 10.0$)	$-1.490 - 0.073 \nu$	$-0.2299 - 0.0099 \nu^{5/2}$	-0.034

The MIR criterion judges the most suitable distribution function which has the minimum ratio of Δr (residual from 1 of the correlation coefficient r between the order statistics x_m and the standard amount of change y_m) to the mean value Δr_{mean} of residual of the correlation coefficient in the fitted distribution function. The mean value of residual of the correlation coefficient in the fitted distribution function is calculated by the following equation for coefficients a , b , and c on **Table 4.1.4** as a function of the data adoption rate ν by the distribution function.

$$\Delta r_{\text{mean}} = \exp[a + b \ln N + c(\ln N)^2] \quad (4.1.17)$$

Table 4.1.4 Coefficient of Residual Mean Values Δr_{mean} of Correlation Coefficients

Distribution function	Coefficient a	Coefficient b	Coefficient c
Extreme type I distribution	$-2.364 + 0.054 \nu^{5/2}$	$-0.2665 - 0.0457 \nu^{5/2}$	-0.044
Weibull distribution ($k = 0.75$)	$-2.435 - 0.168 \nu^{1/2}$	$-0.2083 + 0.1074 \nu^{1/2}$	-0.047
Sane as above ($k = 1.0$)	-2.355	-0.2612	-0.043
Sane as above ($k = 1.4$)	$-2.277 - 0.056 \nu^{1/2}$	$-0.3169 - 0.0499 \nu$	-0.044
Sane as above ($k = 2.0$)	$-2.160 + 0.113 \nu$	$-0.3788 - 0.0979 \nu$	-0.041
Extreme type II distribution ($k = 2.5$)	$-2.470 + 0.015 \nu^{3/2}$	$-0.1530 - 0.0052 \nu^{5/2}$	0
Sane as above ($k = 3.33$)	$-2.462 - 0.009 \nu^2$	$-0.1933 - 0.0037 \nu^{5/2}$	-0.007
Sane as above ($k = 5.0$)	-2.463	$-0.2110 - 0.0131 \nu^{5/2}$	-0.019
Sane as above ($k = 10.0$)	$-2.437 + 0.028 \nu^{5/2}$	$-0.2280 - 0.0300 \nu^{5/2}$	-0.033

⑥ Probabilistic Wave Heights Corresponding to Return Periods

Suppose that the most suitable extreme distribution has been selected by analyzing extreme statistics for N peak waves among abnormal waves in K years. The used peak wave heights occur every $K/N (= 1/(\nu\lambda))$ (λ : mean occurrence rate) years on average. The non-exceedance probability of the wave height x is given by $F(x)$ as the most suitable extreme distribution. One wave height exceeding the height x exists on average among $m (= 1/(1 - F(x)))$ wave heights randomly extracted from this distribution form. It takes $R = m(K/N)$ years on average for m peak waves to occur. Therefore, the non-exceedance probability of wave heights with the return period of R years is given by the equation $F(x) = 1 - (K/N)/R$. For example, if the most suitable extreme distribution is set by 40 peak waves for 30 years, the wave height of the return period of 50-years corresponds to the wave height, of which the non-exceedance probability is $F(x) = 1 - (30/40)/50 = 0.985$. Moreover, the peak

wave height at this time is calculated as $x = F^{-1}(1 - (K/N)/R)$, where F^{-1} is an inverse function of the most suitable fitted distribution function F .

⑦ Challenges in Statistic Processing of Extreme Waves for the Future

Goda et al. further developed the studies described above, published **Reference 15**), and indicated the direction of extreme statistical analysis in the future. That is to say, although the most suitable fitted distribution function has been verified until now by the area of each port and port business, it is not reasonable that the distribution functions discontinuously differ per neighboring points concerned. They think that it is more physically reasonable to select specially designated distribution functions based on the properties of oceanographical phenomena in wider sea area in nature.

Table 4.1.5 showing the verification results on the northeast coast of the Pacific indicates that the Weibull distribution at $k = 1.0$ indicated by G in the table is most likely selected commonly at each observation point.

In order to verify most suitably by the sea area, vast cases at high waves must be verified in future. Although more wave observation data have been accumulated than before, some data are still missing during high waves. On the other hand, the wave observation results and the hindcasting results currently do not necessarily indicate good coincidence, as the precision and reliability of the wave hindcasting results largely depend on the estimated precision of offshore wind and pressure fields. Therefore, how to properly estimate high wave extreme specifications by meteorological disturbance based on wave observation data, including partial missing data, is a big challenge in the future, and the verification is progressing now.

Table 4.1.5 Statistical Analysis Results on All High Wave Extreme Data

Location	N	λ	Conformance/rejection test		H_{100} (m)	
			ABCDE	FGHI	Optimal	Type G
Tomakomai	293	21.47	■▼◆▲	■○○▲	6.39	7.48 ± 0.43
Mutsuogawara	358	16.85	▲◆◆◎▲	▲○■	10.58	10.05 ± 0.53
Hachinohe	431	20.57	◆◆○○◆▲	▲◎▲▲	9.45	9.45 ± 0.44
Miyako	117	11.44	◆◆◆○○	◆◎◆■	6.50	6.50 ± 0.61
Kamaishi	375	24.11	■■▲▲	■◎▲▲	8.30	8.30 ± 0.47
Sendai Shinko	406	27.40	■▼○▲	■◎▲■	7.15	7.15 ± 0.37
Souma	224	18.59	■◆◆○▲	◆◎▲■	7.23	7.23 ± 0.47
Onahama	352	27.48	■▼○◆▲	▼◎▲■	9.67	9.67 ± 0.55
Hitachinaka	426	29.12	■■○◆▲	■◎▲■	8.78	8.78 ± 0.44
Kashima	188	22.60	■▼◆◆	■▼○▲	9.71	9.71 ± 0.70
Habu	409	22.67	■▼○◆▲	◆◎▲■	9.68	9.68 ± 0.44

Note: 1) In Kashima, the type G distribution is at the rejection limit by the DOL criteria but is judged as most suitable by the MIR criteria.

2) The value after ± in type G distribution among the 100-year probabilistic wave height (H_{100}) indicates a standard deviation for an estimated value.

Code	Distribution function	Sign	Conformance/rejection judgment
A	Type FT-II ($k = 2.50$)	◎ ○ ◆ ▲ ▼ ■	The most suitable distribution by the MIR criterion The next most suitable distribution by the MIR criterion Distribution not corresponding to the rejection criterion Distribution rejected by the REC criterion Distribution rejected by the DOL criterion Distribution rejected by both criteria
B	Type FT-II ($k = 3.33$)		
C	Type FT-II ($k = 5.00$)		
D	Type FT-II ($k = 10.00$)		
E	Type FT-I distribution		
F	Weibull distribution ($k = 0.75$)	▼ ■	Distribution rejected by the REC criterion Distribution rejected by the DOL criterion Distribution rejected by both criteria
G	Weibull distribution ($k = 1.00$)		
H	Weibull distribution ($k = 1.40$)		
I	Weibull distribution ($k = 2.00$)		

⑧ Design Waves of Temporary Structures

In the performance verification of temporary structures as well, the design waves are basically set based on the above-described principles. However, since the installation period is limited in the case of temporary structures, it is possible to set the objective return period of the action shorter. If it is a temporary structure whose period is about 2 to 3 years, it is common for the verification to be carried out for action with a return period of about 10 years.

(2) Setting of the Accidental Wave Conditions

Waves as an accidental action are basically set by considering simultaneous occurrence with storm surges (see **Part II, Chapter 2, 3.2 Storm Surges**) as necessary and hindcasting waves (see **Part II, Chapter 2, 4.3 Occurrence, Propagation, and Damping of Waves**) based on assumed disturbance due to typhoons, rapidly developing cyclones and others.¹⁶⁾ In setting the strength, size and route of the assumed disturbance, also consider the extensiveness to social influence due to disaster by storm surges.

(3) Response to Waves Exceeding the Design

Depending on the design service life and degree of importance of target facilities and natural conditions of the point concerned, it is desirable to ensure restorability or safety even for actions exceeding the variable waves used for stability verifications as necessary. For the time being, it is assumed that the performance verification method for toughness is applied. These wave specifications can be set by selecting either variable waves that have relatively longer return period than those used for serviceability verification or waves due to disturbance conforming to the maximum class that sets accidental waves.

4.1.2 Setting of Wave Conditions for the Verification of Serviceability of the Structural Members

- (1) The waves for the verification of the serviceability of the structural members are set appropriately as waves acting during the design service life. For the setting of such waves, a joint frequency distribution table of the wave height and period by wave direction is preferably calculated from wave observation data broken down by month, by season, and annually. In the event that the design service life is 50 years, this may be calculated using the following method.

① Wave data

It is possible to employ the NOWPHAS (Nationwide Ocean Wave Information Network for Ports and Harbors) wave observation data, which are obtained by continuous wave observations in ports throughout Japan. The occurrence frequency statistics by wave height class of the significant waves every 2 hr. or every 20 min. are summarized in the annual Wave Observation Annual Report¹⁷⁾ or Long-Term Statistical Report¹⁸⁾ issued by NOWPHAS. Estimation of the circumstances of occurrence of individual waves within an observation time of 2 hr. or 20 min. is carried out based on the significant wave height values provided once in these 2 hr. or 20 min.

② Estimation of the occurrence circumstances of individual waves

Since the abovementioned wave observation materials concern the occurrence frequency of significant waves, the **occurrence circumstances** of individual waves during the observation period are estimated based on the following hypothesis.

- (a) The occurrence distribution of individual wave height follows a Rayleigh distribution. Assuming that the significant wave height during 2 hr. or 20 min. is constant, it is possible to assume that the distribution of several individual wave heights occurring during the 2 hr. or 20 min. follows a Rayleigh distribution where the significant wave height is equal.
- (b) The number of individual waves during the time differs depending on (their wave period of) each observation; however, since it is extremely difficult to set the number of respective individual waves for each observation for 2 hr. or 20 min., it can be hypothesized that the value obtained by dividing 2 hr. (7,200 seconds) or 20 min. (1200 seconds) by the long-term mean period of objective wave observation point is the number of waves during 2 hr, or 20 min.

③ Frequency distribution of individual waves in the design service life

The number of wave occurrence in the design service life is calculated with the mean period of individual waves during the observation period. The wave for the verification of the serviceability for facilities whose

design service life is 50 years can be set as the wave for which the number of waves with a wave height that or above strike is the order of 10^4 in the total number of the waves in the design service life, counted by the abovementioned method. In the **Design Manual for Prestressed Concrete Structure for Ports and Harbors Facilities**, these waves are the waves for the verification of the serviceability limit state, ¹⁹⁾ based on the provisions of the International PC Association, and this is applied here as well.

4.1.3 Setting of Wave Conditions for the Verification of Harbor Calmness

The ordinary wave properties that are employed for the verification of harbor calmness are generally expressed as a joint frequency distribution table of the wave height and period by wave direction for data broken down by month, by season, and annually from the wave data. In a detailed examination of events in which the effects of the period appear strongly, for example, the operating rate, it is preferable to arrange an occurrence distribution for the equivalent wave height and wave direction for each period band. Conducting an examination of the wave conditions by using observed data serves as the criterion. If the wave observation data are not available, the wave hindcasting results can be utilized. However, in the utilization of the wave hindcasting results, it is preferable to undertake the verification by observed data. It is possible to refer to the manual in **Reference 20)** as regards the setting of the ordinary wave conditions for the verification of harbor calmness.

4.2 Handling of Waves for Design

4.2.1 Setting Method of Waves

(1) Setting procedure of waves

Sea waves are one of the principal actions acting on port facilities. In the performance verification, the offshore waves composing variable action or accidental action shall first be determined in accordance with the function of the facilities. The conditions of the set waves can be expressed by the significant wave height, significant wave period, wave direction, directional spreading of the wave energy, and so on (see **Part II, Chapter 2, 4.2.2 Representation of Waves**). Thereafter, the application of the calculation diagrams, the calculation of wave transformation, or the model experiment shown in **Part II, Chapter 2, 4.4 Wave Transformations** is performed in shallow waters, and the conditions of the waves that act on the facilities shall be determined.

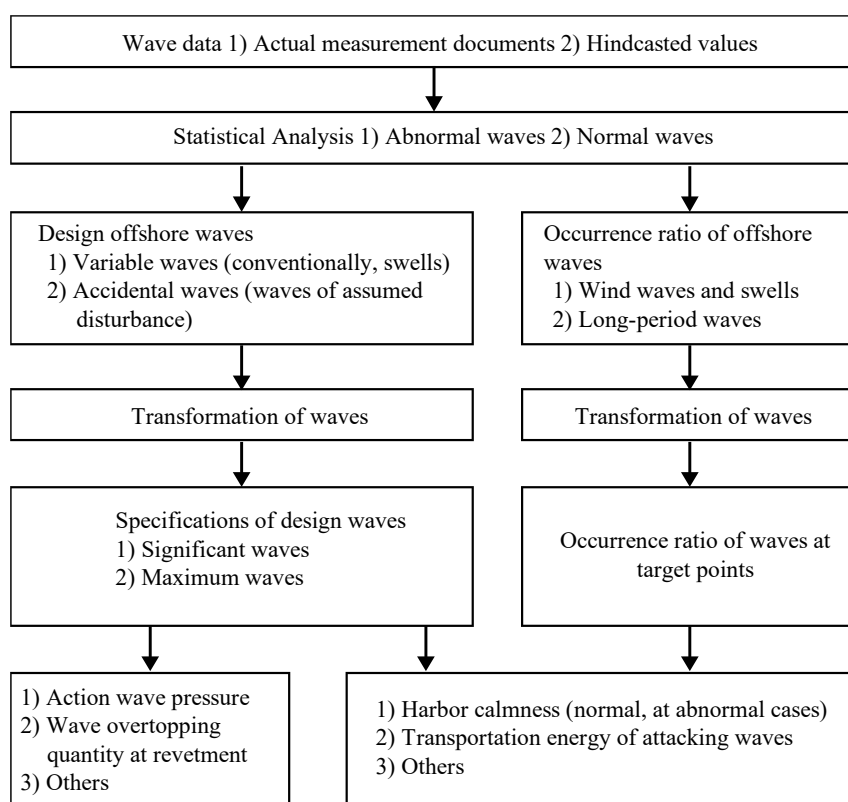


Fig. 4.2.1 Setting Procedure of Waves Used for the Design

(2) Linear dispersion relation of wave

The basic nature of waves generally varies according to the wave height, period (wave length), and water depth. These relations are called dispersion relations of water surface waves. The relation induced by the small amplitude wave theory, which assumes a small wave height as the first approximation, is called the linear dispersion relation and is expressed in the following equation.

$$\sigma^2 = gk \tanh kh \quad (4.2.1)$$

where σ is the angular frequency (1/s), k is the wavenumber (1/m), h is the water depth (m), g is the gravitational acceleration (m/s²). The angular frequency and the wavenumber are also expressed as $\sigma = 2\pi/T$ and $k = 2\pi/L$ using wave period T (s) and wave length L (m), respectively. Furthermore, by substituting and arranging these in **equation (4.2.1)**, the wave celerity C (m/s) is expressed as follows.

$$C = \frac{L}{T} = \sqrt{\frac{gL}{2\pi} \tanh 2\pi \frac{h}{L}} \quad (4.2.2)$$

(3) Offshore Wave (Deepwater Wave) and Shallow Water Wave

The ratio of water depth to wavelength (h/L) may be called relative water depth. In waters where the relative water depth is at least one-half, the waves are hardly affected by the sea bottom and proceed without deforming. However, waves are gradually affected by the sea bottom when they invade waters where the relative water depth is less than one-half. Furthermore, the wave celerity becomes slower, the wavelength shortens, and the wave height also changes. Given this fact, waves in the relative water depth of at least one-half are called deepwater waves, and waves in waters shallower than this are called shallow water waves.

Here, when the relative water depth h/L is on the order of one-half or more, the value of \tanh (hyperbolic tangent) function in **equation (4.2.2)** can be considered almost one. Thus, the length of deepwater waves is calculated by raising both sides of the equality to the second power and by arranging and specifically substituting the length and period of deepwater waves by L_0 and T_0 .

$$L_0 \approx \frac{g}{2\pi} T_0^2 \approx 1.56 T_0^2 \quad (4.2.3)$$

As shown in **equation (4.2.3)**, the length of deepwater waves does not depend on the water depth; therefore, they are called offshore waves.

On the contrary, the length of shallow water waves, the relative water depth h/L of which is on the order of less than one-half, is calculated by **equation (4.2.2)**. As both sides of the equality include the wave length, a convergent calculation is generally required to obtain a solution. Therefore, the length and celerity of waves for a certain water depth and period may be estimated using **Reference (Part III), Chapter 4, 4 Linear Dispersion Relation of Waves**.

The value of the \tanh function in **equation (4.2.2)** is almost equal to the value of the argument $2\pi h/L$ of the function when the relative water depth h/L is on the order of less than one-twenty-fifth. Thus, the following equations are obtained from the relation of both sides of the equality. The wave length can be calculated by multiplying the period.

$$C \approx \sqrt{gh} \quad L = CT \approx T\sqrt{gh} \quad (4.2.4)$$

The shallow water wave in the sea area with a very shallow relative water depth indicating that these approximations are true is specifically called ultrashallow water wave or long wave. For example, a tsunami with a wavelength exceeding 100 km can be considered a long wave even if it propagates in the Pacific Ocean, where the mean water depth is 4 km. The propagation velocity can be estimated by **equation (4.2.4)**.

Moreover, concerning shallow water waves, it is necessary to take into consideration the fact that the shape of the spectrum and the frequency distribution of the wave height differ from the state of offshore waves because of the effects of wave transformation, such as refraction, wave shoaling, and wave breaking due to sea bottom topography.

(4) Wave Transformation in Shallow Waters

The phenomenon wherein the wave height or direction of progressive wave varies owing to the effects of water depth is called wave transformation, which should be taken into consideration in waters where the relative water depth to the wavelength L_0 of offshore waves is shallower than one-half and in waters where waves are affected by shielding due to land and other factors (refer to **Part II, Chapter 2, 4.4 Wave Transformations**). The wave transformation includes phenomena such as refraction, wave shoaling, and wave breaking due to sea bottom topography and diffraction, reflection, and partial penetration due to shielding by island, structures, etc. The calculation of these is performed by using the respective appropriate numerical calculation methods. Considering that these respective phenomena occur by mutually affecting one another, the application of a calculation method that can take all of them into consideration at once is preferable. However, at present, there is no calculation method that can simultaneously consider and perfectly reproduce all of these phenomena regardless of the space scaling in practical use. In principle, the waves that act on the port facilities are appropriate waves that are most disadvantageous for the stability of the structure of the port facilities or the utilization of the port facilities in view of transformations such as refraction, diffraction, wave shoaling, and wave breaking due to the propagation of offshore waves.

(5) Influence of finite amplitude of wave

Waves with heights that cannot be considered small are called finite amplitude waves. The difference from the property of small amplitude waves becomes apparent as the relative water depth decreases in shallow sea areas and wave forms with steep crests and flat troughs. These waves are called nonlinear waves. The influence of the nonlinearity of waves should be taken into consideration for wave shoaling where the wave height increases in shallow water depth as a kind of wave transformation.

Fig. 4.2.2 shows the change in the wave crest elevation of progressive waves obtained by arranging data in the hydraulic model experiment for water depth $h = 100$ to 150 cm. Moreover, **Fig. 4.2.3** was made on the basis of the site wave form records and shows the ratio of the maximum wave crest elevation $(\eta_c)_{\max}$ read for each observation record to the maximum wave height H_{\max} within the record in the $H_{1/3}/h$ relation. Actual wave crest elevation is slightly higher than the value of the model experiment. It is preferable to use the data in **Fig. 4.2.3**, which was obtained from the site records for the area $H_{1/3}/h < 0.5$.

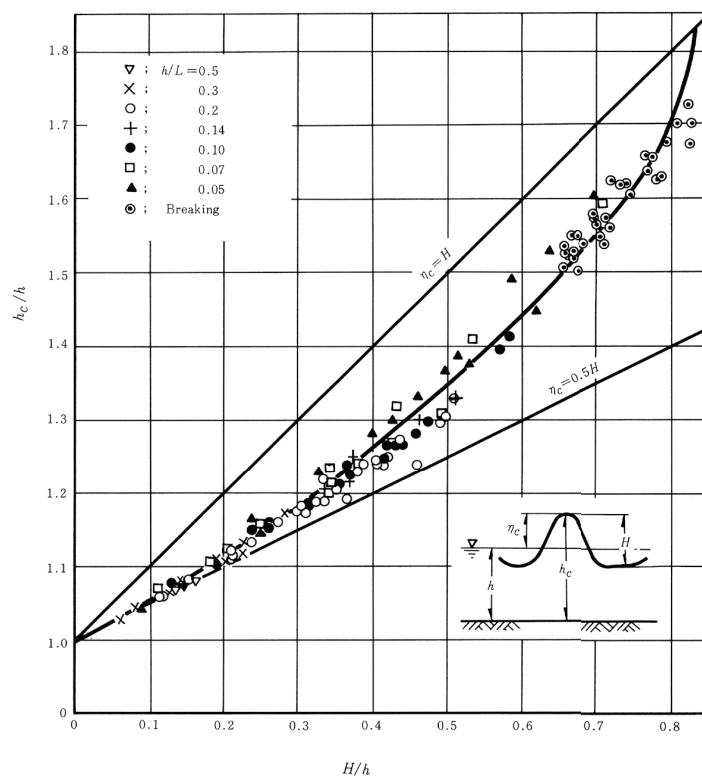


Fig. 4.2.2 Relative Wave Crest Elevation from the Sea Bed ²¹⁾

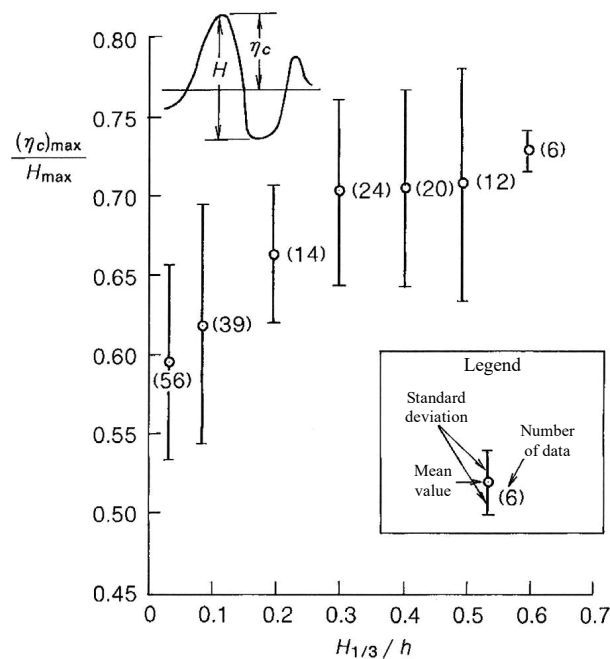


Fig. 4.2.3 Relation between the Maximum Wave Crest Elevation $(\eta_c)_{\max}$ and $H_{1/3}/h$ ²²⁾

On the contrary, this effect can generally and practically be ignored because it is very small in deep sea areas and in shallow sea areas where relative water depth is sufficiently deep.

(6) Return period of offshore waves

Design waves are preferable to provide for the safety verification of the facilities after their completion and during their construction, respectively. When verifying safety during the service life and construction of port facilities, the offshore waves of proper return period must be selected according to the importance of the facilities. For general port facilities, which have a design service life of 50 years, a 50-year return wave may be used. However, although waves acting during construction (when facilities are left for a certain period with unfinished cross sections) need to be properly determined by considering the construction period of facilities and the natural conditions at the point concerned and others, waves on the order of a 10-year return wave may be used for the sake of convenience.

When reviewing design offshore waves as variable waves, it is a good idea to extract the peak wave height of the swell by focusing on period and wave steepness and by considering the return wave height obtained by statistically processing extreme waves as the design offshore waves of the swell as necessary, in addition to making the peak wave height in the past disturbance the peak wave data without any modification (see **Part II, Chapter 2, 4.1.1 (1) Setting of the variable wave conditions**). Moreover, when designing the port facilities that suffered from swell, performance verification shall be conducted together with the wave transformation calculation or model experiment for the design offshore waves of the swell for the design tide level.⁶⁾

(7) Utilization of the wave transformation calculation method

In the performance verification in the sea area where the relative water depth is roughly less than one-half of the offshore wave length, the design wave of facilities shall be calculated from the condition of offshore waves that is generally set by observation or wave hindcasting. When using the wave transformation calculation method, a calculation model should be properly selected according to the topography of the sea area where facilities are installed or on the basis of the importance of facilities.²³⁾ Although a graphic solution method that assumes regular waves as representative waves may be used in the sea area where it can be approximated by parallel bathymetric coast, the energy balance equation method,²⁴⁾ mild-slope equation method,²⁵⁾ and others can be used in the sea area with a complicated topography. Furthermore, a proper numerical calculation method should be used for the calculation in sea areas wherein water depth largely fluctuates or wherein refraction and diffraction occur simultaneously must be taken into consideration. For example, the energy balance equation method²⁶⁾ based on the small amplitude wave theory, which considers diffraction when the nonlinearity of waves can be ignored or handled separately; wave transformation calculation method,²⁷⁾ which uses the weakly nonlinear Boussinesq equation and is capable of simultaneously analyzing the reflection properties of wave-dissipating works when considering wave nonlinearity to some extent; and other methods can be used.

In the reliability design, it is necessary to properly provide the dispersion characteristics of calculation results from the real value by considering the errors in the wave transformation calculation method, referring to **Reference 28**), etc.

(8) Utilization of the model experiment

When the shape of facilities is complicated, when wave transformation or nonlinearity is prominent, or when it is difficult to develop and utilize a proper numerical calculation method, it is preferable to conduct a hydraulic model experiment. In problems concerning waves, the effect of viscosity or surface tension of water is generally small; therefore, the Froude similarity law can be applied to the similarity between model and prototype for both the inertial and gravitational forces acting on the fluid. The Froude similarity law sets the scale reduction of time and velocity to the square root of the scale reduction of length. It is preferable to use a water tank that is 30 m or more wide and is equipped with a multidirectional random wave maker that can reproduce the multidirectional spreading waves in the hydraulic model test basin under consideration of the scale effect of a hydraulic model where the effect of viscosity and surface tension of water becomes relatively larger as the scale becomes smaller.²⁹⁾

(9) Long-period waves and harbor resonance

Long-period waves, which have a water surface fluctuation with a frequency of several tens of seconds or longer, may exert a major effect on the mooring facilities or topography of the sea bottom. It is preferable to examine these waves on the basis of on-site observations and current analytical results if necessary (see **Part II, Chapter 2, 4.5 Long-Period Wave**). Long-period waves in a port not only excite the oscillation of large ships by resonance but also cause the elevation of water surface in front of facilities and increase wave overtopping rate and swash height. Given that they also exert a major effect on the littoral drift movement at the seaside, it is preferable to estimate the effect properly by field measurements. Moreover, the direction of long-period waves is difficult to restrict to one direction only. However, it may be practically possible to select the most dangerous wave direction in the range extending ten and several degrees to both sides of the wave direction which is assumed to be same as that of the wind waves and swells.²⁰⁾

Harbor resonance, which is the natural resonance of harbors and bays, can affect not only moored ships but also the water level of the inner part of the bay; therefore, in the event that clear harbor resonance is found from the current tide records or in the event that the shape of the harbor is widely modified, it is preferable to examine the properties of the resonance with an appropriate numerical calculation method.³⁰⁾ (See **Part II, Chapter 2, 3.3 Harbor Resonance**.)

(10) Other items

A significant change of water depth due to dredging in navigation channels of a port necessitates the consideration of the variation in the navigation channels in the calculation of wave transformation. Considering that the reflection rate of upright wave-absorbing revetments largely changes according to the period of waves, the calculation of waves in a port should properly provide the reflection rate according to the wave period and should be verified using Computational Fluid Dynamics (CFD) method³¹⁾ or model experiment as needed. Ship waves caused by navigating ships become bigger as ships grow larger and faster. The wave height may exceed 1 m. It is preferable to verify the influence of growing up of ship size on surrounding revetments, sand beaches, small fishing boats and small work ships.

In inner seas, such as in Tokyo Bay, the waves generated by strong wind and swells from the ocean become superposed. It is preferable to consider the effect of waves generated in the bay on the design wave by proper wave hindcasting or observation and to verify the effect of swells from the ocean and the increase of the swells in the bay.

At actual installation of facilities in shallow waters, transverse wave actions due to multidirectional spreading, wave amplification due to flows,³²⁾ effects of reflected waves, and so on must be considered in many cases. A more reasonable design can be achieved by considering these matters as a whole in the initial planning stage. The handling of waves during construction shall also be kept in mind.

(11) Concept of waves for the verification of stability in facilities

Acting waves need to be determined by keeping the following in mind in the performance verification of facilities:

- ① Random waves shall be used in principle.
- ② Offshore waves shall be determined by proper observation or wave hindcasting.
- ③ Offshore waves shall be set as probabilistic waves by considering the return period.
- ④ Wave transformation shall be calculated by considering the topography of target points.

- ⑤ Use a proper numerical calculation model for the estimation of design waves.
 - (a) Relatively deep sea area linear calculation model
 - (b) Shallow and topographically complicated sea area nonlinearity shall be preferably considered.
 - (c) Wave breaking or reflected waves occurs significantly hydraulic model experiment is preferable
- ⑥ The tidal level that causes the severest action is basically employed as the design tidal level.
- ⑦ The stability of facilities during construction shall also be fully examined.
- ⑧ The return period of design waves during construction shall be properly set by considering the construction period.
- ⑨ Interaction between waves and flows shall be considered if the stream flow has a strong influence.

4.2.2 Representation of Waves

(1) Definition of Waves

The waves in the oceans are treated as random waves in principle and are set appropriately on the basis of past observation data and latest findings as far as possible. **Fig. 4.2.4** shows the definition of waves. Each wave is defined by the zero up-crossing method. Here, the height from the trough to the peak of the defined one wave is the wave height H , the spatial length is the wavelength L , and the wave propagation speed is the wave celerity C . The wave period T is defined as the time between two sequent zero-up crossing points in the time series of wave profiles observed at a fixed point. **Reference 33)** can be used as a reference for the specifics on the basic nature of waves.

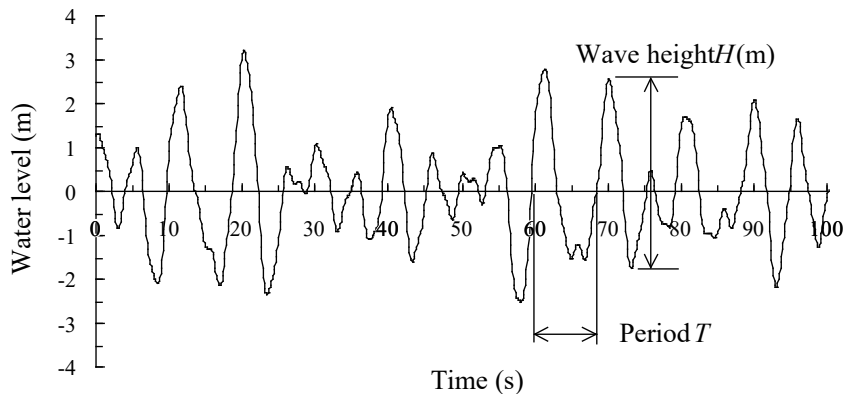


Fig. 4.2.4 Definition of Waves

(2) Waves Represented in Performance Verification

Considering that the wave height of random waves varies depending on time, representative waves shall be employed in the performance verification. Significant wave is normally employed as representative wave. For the representative wave, the waves in the record are counted and selected in descending order of wave height from the highest wave, until one -third of the total number of waves is reached. The height and period of the significant wave are calculated as the means of their heights and periods and denoted as $H_{1/3}$ and $T_{1/3}$. The mean wave as a representative wave is calculated as the wave with mean height and period of all waves in the record. The highest wave refers to the wave having the height and period of the highest individual wave in the record. The height and period of the highest wave are denoted as H_{\max} and T_{\max} . The highest wave shall be employed for the stability verification of a breakwater.

On the assumption that wave energy is concentrated in the extremely narrow band of a certain frequency, the occurrence frequency of the wave heights included in a group of offshore waves follows the Rayleigh distribution, which is expressed in the following equation.

$$p(H/\bar{H}) = \frac{\pi}{2} \frac{H}{\bar{H}} \exp \left\{ -\frac{\pi}{4} \left(\frac{H}{\bar{H}} \right)^2 \right\} \quad (4.2.5)$$

where H denotes the height of the mean wave in the wave group. In the meantime, the period of actual sea waves fluctuates in a certain range; therefore, the wave height distribution tends to offset slightly from the Rayleigh distribution. However, it is known that the Rayleigh distribution consequently provides a very good approximate expression for the height distribution of individual waves defined in the zero up-crossing method.

In the event that the occurrence frequency of wave heights follows the Rayleigh distribution, the following relationship is derived between the heights of individual representative waves.

$$\left. \begin{aligned} H_{1/10} &= 1.27H_{1/3} \\ H_{1/3} &= 1.60\bar{H} \end{aligned} \right\} \quad (4.2.6)$$

Here, $H_{1/10}$ is called the highest one-tenth wave height and is calculated using the highest one-tenth, similar to the calculation method for significant wave height.

Moreover, the mode and mean $H_{\max}/H_{1/3}$, and the highest wave height $(H_{\max})_{\mu}$, where μ denotes the value of the exceedance probability, are respectively given by the following equations, where the number of waves N_0 in the wave group is used as a parameter and γ is the Euler constant (0.5772...).

$$(H_{\max}/H_{1/3})_{\text{mode}} \approx 0.706\sqrt{\ln N_0} \quad (4.2.7)$$

$$(H_{\max}/H_{1/3})_{\text{mean}} \approx 0.706\left\{\sqrt{\ln N_0} + \gamma / \left(2\sqrt{\ln N_0}\right)\right\} \quad (4.2.8)$$

$$(H_{\max})_{\mu}/H_{1/3} \approx 0.706\sqrt{\ln[N_0/\ln\{1/(1-\mu)\}]} \quad (4.2.9)$$

The following equation is commonly employed as the relation between H_{\max} and $H_{1/3}$. They are selected by considering the duration of waves subjected to design, i.e., the number of waves, reliability of the design wave estimation, accuracy of calculation methods, and importance and behavioral properties at the fracture limitation of structures. The relation $H_{\max}=1.8H_{1/3}$ is often used in designing composite breakwaters.³⁴⁾

$$H_{\max} = (1.6 \sim 2.0)H_{1/3} \quad (4.2.10)$$

On the contrary, given that the period distribution is based on the correlation characteristic between the wave height and the period, there is no general form of the period distribution like the Rayleigh distribution for wave height. However, the following equation is true as an average relation among many observation records.

$$T_{\max} \approx T_{1/3} = (1.1 \sim 1.3)\bar{T} \quad (4.2.11)$$

The ratio to $T_{1/3}$ varies to some extent according to the form of the frequency spectrum.

(3) Introduction of Random Waves

It is preferable in principle that random waves are employed in the performance verification. It is possible to consider random waves to be the superposition of regular waves with various periods, and the respective regular waves are called component waves. It is the frequency spectrum of a wave that indicates the degree of the energy of the component waves, and a spectrum shape corresponding to the properties of ocean should be employed in the performance verification. On Japan's seacoast, the Bretschneider–Mitsuyasu-type spectrum based on the observation data at the peak period $T_p \approx 1.05T_{1/3}$ or the modified Bretschneider–Mitsuyasu-type spectrum based on the relation $T_p \approx 1.13T_{1/3}$ obtained from the subsequent observation document is commonly employed.³⁵⁾

The Bretschneider–Mitsuyasu spectrum shape is expressed by the following equation:

$$S(f) = 0.257H_{1/3}^2 T_{1/3}^{-4} f^{-5} \exp\left\{-1.03(T_{1/3}f)^{-4}\right\} \quad (4.2.12)$$

where

$S(f)$: frequency spectrum of the wave

$H_{1/3}$: significant wave height

$T_{1/3}$: significant wave period

f : frequency

The modified Bretschneider–Mitsuyasu-type spectrum shape is expressed by the following equation:

$$S(f) = 0.205 H_{1/3}^2 T_{1/3}^{-4} f^{-5} \exp\{-0.75(T_{1/3} f)^{-4}\} \quad (4.2.13)$$

However, in inner bay areas, such as Tokyo Bay, the peak of the spectrum often becomes pointed; therefore, it is preferable to introduce a spectrum shape of the JONSWAP type³⁶⁾ on the basis of observations to the greatest extent possible and to employ a spectrum that can reflect appropriately the observation results.

The spectrum shape of the JONSWAP type is shown by the following equations. Here, the peak enhancement factor γ takes a value between one and seven (3.3 in average), and the peak of the spectrum becomes steeper as the γ value increases. When $\gamma = 1$, **equation (4.2.14)** coincides with **equation (4.2.13)**.

$$S(f) = \beta_J H_{1/3}^2 T_p^{-4} f^{-5} \exp\{-1.25(T_p f)^{-4}\} \times \gamma^{\exp\left[-0.5\{(T_p f - 1)/\sigma\}^2\right]} \quad (4.2.14)$$

$$\beta_J \approx \frac{0.0624}{0.230 + 0.0336\gamma - 0.185(1.9 + \gamma)^{-1}} [1.094 - 0.01915 \ln \gamma] \quad (4.2.15)$$

$$T_p \approx T_{1/3} / \{1 - 0.132(\gamma + 0.2)^{-0.559}\} \quad (4.2.16)$$

$$\sigma \approx \begin{cases} 0.07 : f \leq f_p \\ 0.09 : f > f_p \end{cases} \quad (4.2.17)$$

where f_p is the peak frequency.

The representative wave height H_{m0} for these spectra is calculated as follows. If the wave spectra are concentrated within a narrow range of frequency band and if the wave height follows the Rayleigh distribution, H_{m0} equals to $H_{1/3}$ defined in the zero up-crossing method.

$$H_{m0} = 4.004 \sqrt{m_0} \quad m_0 = \int_0^\infty S(f) df \quad (4.2.18)$$

where m_0 is the total energy of waves.

Moreover, according to the statistic theory of random waves, the mean period T_{02} in the zero up-crossing method is calculated by the following equation.

$$T_{02} = \sqrt{m_0/m_2} \quad m_2 = \int_0^\infty f^2 S(f) df \quad (4.2.19)$$

Furthermore, the mean period T_{01} is also used under the condition where the spectrum width is sufficiently small.

$$T_{01} = m_0/m_1 \quad m_1 = \int_0^\infty f S(f) df \quad (4.2.20)$$

On the contrary, such cases are significantly increasing recently, particularly in Europe, that the representative period $T_{m-1,0}$ is hardly affected by the high-frequency component of spectrum and is almost equal to the significant wave period $T_{1/3}$ defined by the zero up-crossing method.

$$T_{m-1,0} = m_{-1}/m_0 \quad m_{-1} = \int_0^\infty f^{-1} S(f) df \quad (4.2.21)$$

(4) Double-peaked spectrum

When two types of wave group having different dominant periods, such as wind waves and swells, are superimposed, double-peaked spectrum with peaks near each period may be observed. In such a case, the significant wave height used for the calculation of wave force may be obtained by energy synthesis (see **Part II, Chapter 2, 4.4.4 Reflection of Waves**), and the significant wave period $T_{1/3}$ may be calculated by the following equation.³⁷⁾

$$T_{1/3} = k \sqrt{\frac{(H_{1/3})_I^2 + (H_{1/3})_{II}^2}{\frac{(H_{1/3})_I^2}{(T_{1/3})_I^2} + \frac{(H_{1/3})_{II}^2}{(T_{1/3})_{II}^2}}} \quad (4.2.22)$$

where

$$k = 1.0 + \alpha(R_H/\mu)^{-0.121A \ln(R_H/\mu)} \quad (4.2.23)$$

$$\alpha = 0.08(\ln R_T)^2 - 0.15 \ln R_T \quad (4.2.24)$$

$$\mu = \begin{cases} 0.632 + 0.144 \ln R_T & ; 0.1 \leq R_T \leq 0.8 \\ 0.6 & ; 0.8 \leq R_T < 1.0 \end{cases} \quad (4.2.25)$$

$$A = \begin{cases} 13.97 + 4.33 \ln R_T & ; 0.1 \leq R_T \leq 0.4 \\ 10.0 & ; 0.4 \leq R_T < 1.0 \end{cases} \quad (4.2.26)$$

$$R_H = (H_{1/3})_I / (H_{1/3})_{II} \quad (4.2.27)$$

$$R_T = (T_{1/3})_I / (T_{1/3})_{II} \quad (4.2.28)$$

$(H_{1/3})_I, (H_{1/3})_{II}$: significant wave height (m) of wave groups I and II before superimposition

$(T_{1/3})_I, (T_{1/3})_{II}$: significant wave period (s) of wave groups I and II before superimposition

Wave group I has a shorter period.

(5) Introduction of the multidirectionality of Waves

In shallow waters, the wave height of the component waves becomes orthogonal to the shoreline owing to refraction effects, and the nature of the waves becomes closer to unidirectional random waves. Accordingly, a case in which the ratio of the water depth to the wavelength of offshore waves (h/L_0) becomes 0.1 or smaller is used as the benchmark; the waves in waters shallower than this may be approximated as waves that behave like unidirectional random waves and the approximation is limited to cases wherein the waves are employed as the variable action. In deeper waters, the character as multidirectional random waves whose component energy advances in various directions becomes stronger, and it is preferable to treat the waves as multidirectional random waves. Furthermore, given that the multidirectionality of the waves has a major effect in the stability at the head of a breakwater and the performance verification of floating facilities, the multidirectionality of the waves in waters should be examined beforehand with appropriate observation data. The wave direction has a major effect on the results in the calculation of the degree of calmness; thus, the waves are calculated as multidirectional random waves.

A directional wave spectrum is employed as an index for showing the multidirectionality of waves. The directional wave spectrum is the product of the abovementioned frequency spectrum $S(f)$ and the directional spreading function $G(f, \theta)$ and is expressed as $S(f, \theta) = S(f)G(f, \theta)$. The following Mitsuyasu-type directional spreading function is commonly employed in most cases as the directional spreading function.

$$G(f; \theta) = G_0 \cos^{2S} \left(\frac{\theta - \theta_0}{2} \right) \quad \int_{-\pi}^{\pi} G(f; \theta) d\theta = 1 \quad (4.2.29)$$

where θ_0 signifies the principal wave direction. G_0 and S are expressed by the following equations, respectively.

$$G_0 = \left[\int_{\theta_{\min}}^{\theta_{\max}} \cos^{2S} \left(\frac{\theta - \theta_0}{2} \right) d\theta \right]^{-1} \quad (4.2.30)$$

$$S = \begin{cases} S_{\max} (f/f_p)^5 & : f \leq f_p \\ S_{\max} (f/f_p)^{-2.5} & : f > f_p \end{cases} \quad (4.2.31)$$

Fig. 4.2.5 shows the distribution shape of the Mitsuyasu directional spreading function. The symbols of f , f_p , and l in the figure respectively denote the frequency, the peak frequency of the frequency spectrum, and the parameter in the function of $G(f, \theta) = G_0 \cos^{2l}(\theta - \theta_0)$ which is employed as the directional spreading function instead of **equation (4.2.29)**. The parameter of the directional wave function S_{max} is the directional spreading parameter introduced by Goda and Suzuki,³⁸⁾ and the following numerical values can generally be used.

Wind waves	$S_{max} = 10$
Swell with a short attenuation distance	$S_{max} = 25$
Swell with a long attenuation distance	$S_{max} = 75$

However, the variance of the directional spreading parameter is large on-site. When the directional wave spectrum is observed on-site, these values should be used as a reference.

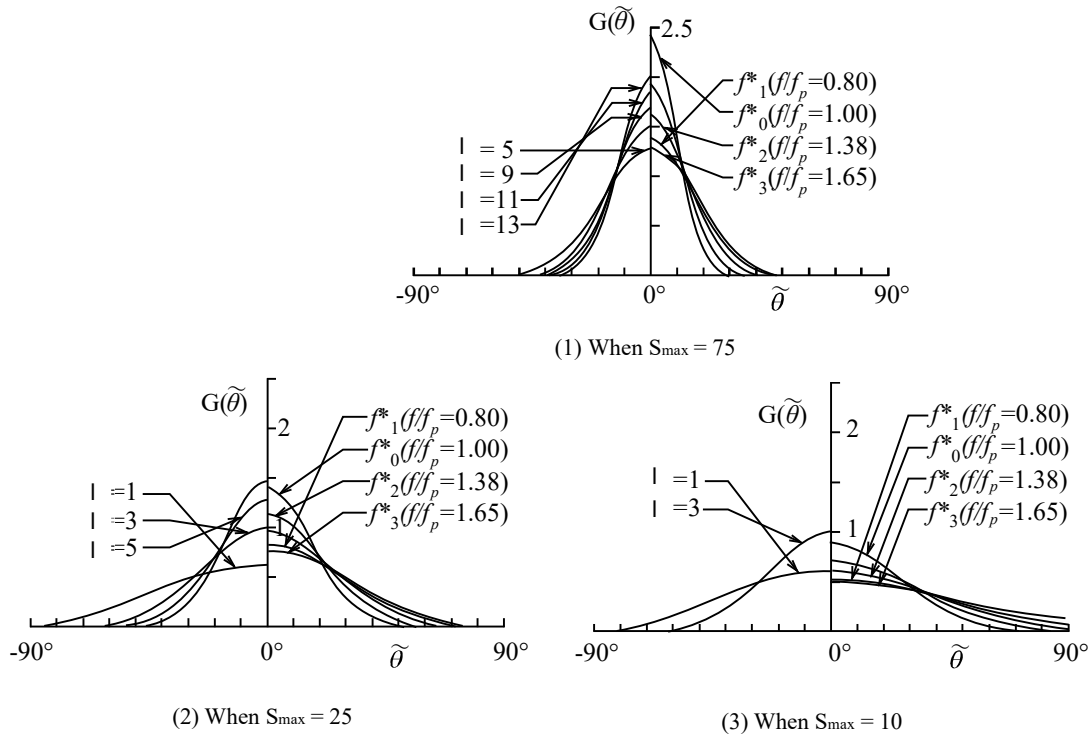


Fig. 4.2.5 Distribution Shape of the Mitsuyasu-Type Directional Spreading Function

The characteristics of the directional wave spectrum can also be expressed from the viewpoint of how the wave energy is distributed as a whole to each direction. To this end, the following curve $P_E(\theta)$ of the cumulative energy ratio shall be defined.

$$P_E(\theta) = \frac{1}{m_0} \int_{-\pi/2}^{\theta} \int_0^{\infty} S(f; \theta) df d\theta \quad m_0 = \int_0^{\infty} \int_{-\pi/2}^{\pi/2} S(f; \theta) d\theta df \quad (4.2.32)$$

Here, the range of component wave direction is set to $[-\pi/2, \pi/2]$ because the components in the direction opposite to the principal one are commonly ignored in the calculation for the design.

Fig. 4.2.6 shows the cumulative curve of the wave energy obtained by using **equation (4.2.12)** as the frequency spectrum, **equation (4.2.29)** as the directional function, and **equation (4.2.31)** as the directional spreading parameter. The SWOP in the figure shows the cumulative curve of energy based on the directional function obtained from the stereo picture of the sea surface taken from two planes in the latter half of 1950s.

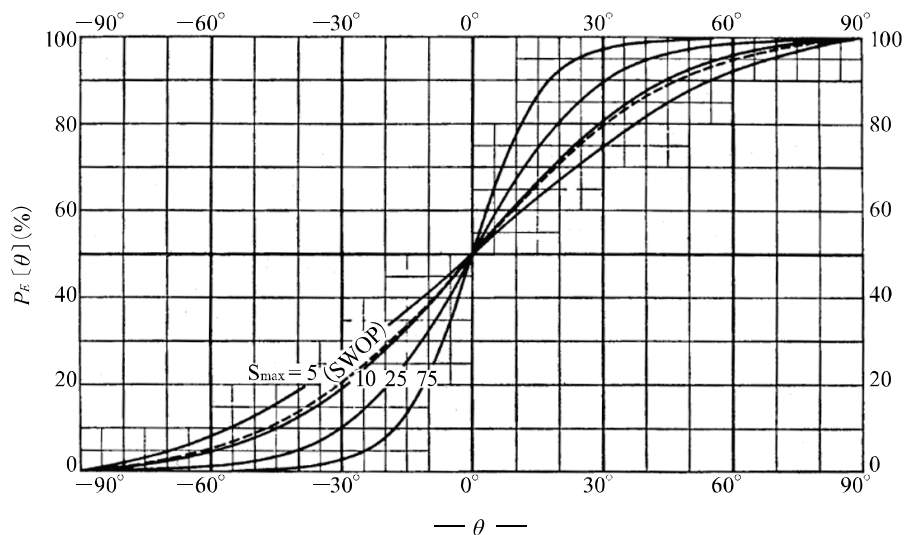


Fig. 4.2.6 Cumulative Curve of the Wave Energy

The directional spreading parameter S_{\max} of offshore waves that expresses the directional spreading of wave energy varies depending on the wave steepness, and it can be estimated with **Fig. 4.2.7** in the event of inadequate observation data. Furthermore, in shallow waters, the value of directional spreading parameter varies depending on the sea bottom topography; therefore, it is preferable to estimate the parameter by a calculation of wave transformation. However, in cases wherein the coastline is close to linear with a simple topography and wherein the water depth contour is deemed parallel to the shoreline, the changes in S_{\max} may be estimated by the diagram in **Fig. 4.2.8**.

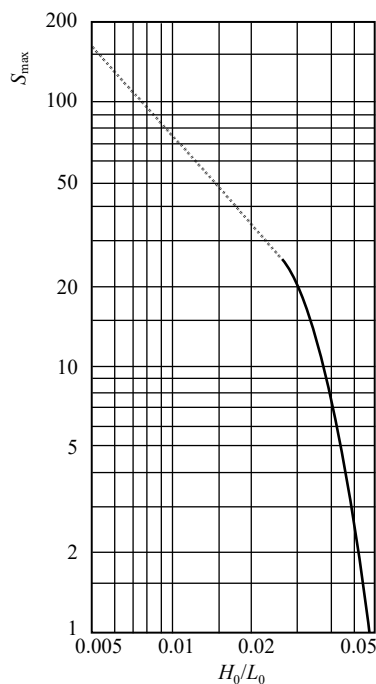


Fig. 4.2.7 Changes in S_{\max} Due to Wave Shape Steepness

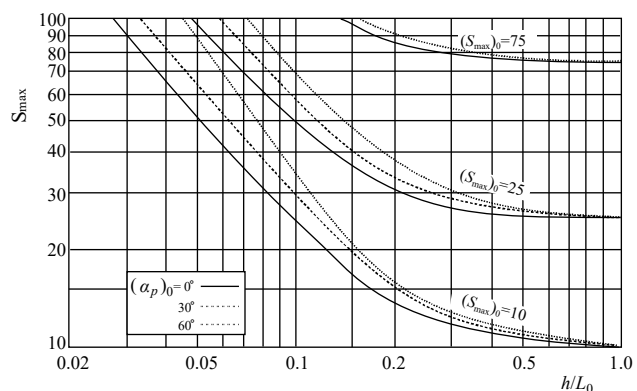


Fig. 4.2.8 Changes in S_{\max} Due to Water Depth

(6) Wave direction

The wave direction is an important parameter for determining the direction of the forces acting on the facilities. It is preferable to determine the principal wave direction to the greatest extent possible by observing the directional wave spectrum or the flow speed of two components.³⁹⁾ In the principal wave direction the crests in the wave train are distributed most densely, and the principal direction is considered an angle where the peak in the directional wave spectrum appears. However, when the swells from outside the bay and the wind waves that occur inside the

bay overlap each other, bidirectional waves that have two peaks for the directional spreading function appear frequently.⁴⁰⁾ In these cases, even if the principal wave direction is determined, it is seldom that this principal wave direction represents the direction in which the energy of the wave proceeds. Therefore, one should examine special measures, such as carrying out the performance verification of the facilities at the most dangerous wave direction, carrying out the performance verification for the respective wave directions, and setting the facilities to be stable for both.

4.3 Generation, Propagation and Attenuation of Waves

(1) Summary of the Wave Hindcasting Method

Wave hindcasting estimates the temporal and spatial changes in wind direction and wind velocity of the prescribed water area from the topographical and meteorological data and estimates the waves under the wind field. There are various methods for wave hindcasting based on the wind field data of the prescribed water area. In general, these methods can be divided roughly into the significant wave method and the spectrum method, which is the mainstream method at present.

(2) Wave Hindcasting by the Significant Wave Method

The modern wave hindcasting method that was first developed in the world treats the series of phenomena known as the generation, development, propagation, and attenuation of waves collectively and estimates the wave height $H_{1/3}$ (m) and period $T_{1/3}$ (s) with wind velocity U_{10} (m/s) value at 10 m above the sea surface, wind duration t (s), and fetch length F (m) as parameters. Its forerunner is the SMB method, which was proposed by Sverdrup and Munk⁴¹⁾ in the 1940s and was revised by Bretschneider.^{42), 43)} Currently, the further improved Wilson IV formula⁴⁴⁾ is generally employed:

$$gH_{1/3}/U_{10}^2 = 0.30 \left[1 - \left\{ 1 + 0.004 (gF/U_{10}^2)^{1/2} \right\}^{-2} \right] \quad (4.3.1)$$

$$gT_{1/3}/(2\pi U_{10}) = 1.37 \left[1 - \left\{ 1 + 0.008 (gF/U_{10}^2)^{1/3} \right\}^{-5} \right] \quad (4.3.2)$$

where

$H_{1/3}$: significant wave height (m)

$T_{1/3}$: significant wave period (s)

U_{10} : wind velocity at 10 m above the sea surface (m/s)

F : fetch (m)

g : gravitational acceleration (m/s²)

Fig. 4.3.1 illustrates these relational expressions (the unit of the fetch F is expressed by meter units in **equations (4.3.1) and (4.3.2)**, and it is expressed by kilometer units in **Fig. 4.3.1**). However, these relational expressions are for cases wherein the wind is continuously blowing constantly for an adequately long time; after the wind starts blowing, it does not reach this wave height or period. Waves generated at the upper extremity of the fetch propagate with growth and arrive at the fetch distance F (m) after the required time. The required time is called the minimum duration t_{\min} (s) and is expressed by the following equation.

$$t_{\min} = \int_0^F \frac{1}{C_g(x)} dx \quad (4.3.3)$$

where

t_{\min} : minimum duration (s)

$C_g(x)$: group velocity of the waves (m/s)

Furthermore, it is possible to make a rough estimate by using the following equation.⁹⁾

$$t_{\min}' = 1.0 F'^{0.73} U_{10}^{-0.46} \quad (4.3.4)$$

where

t_{\min}' : minimum duration (hr)

F' : fetch (km)

It is necessary to pay attention to the fact that the units of the symbols are different between **equations (4.3.3) and (4.3.4)**. When the wind duration is shorter than the minimum duration, the waves are in the state of full development and their magnitude is determined by the wind duration. On the other hand, when the wind duration is longer than the minimum one, the waves are in the process of developing with time and their magnitude depends on the fetch length. Therefore, in cases wherein the fetch and the duration are simultaneously provided, we must adopt the smaller wave of the two waves calculated by the wind duration and the fetch length.

The SMB method fundamentally applies to uniform wind field. However, in the event that the wind speed changes gradually, the waves can be hindcasted by using the equi-energy line (the line showing $H_{1/3}^2 T_{1/3}^2 = \text{const}$).

In the event that the width is shorter than the fetch in a lake or bay or in the event that the fetch is determined by the opposite shore distance and varies widely to the minute fluctuations of the wind direction, **equations (4.3.1) and (4.3.2)** provide a wave height or period larger than real. In such cases, it is better to employ the effective fetch⁴⁵⁾ provided by the following formula.

$$F_{\text{eff}} = \sum F_i \cos^2 \theta_i / \sum \cos \theta_i \quad (4.3.5)$$

where,

F_{eff} : effective fetch (km)

F_i : opposite shore distance in the i th direction from the hindcasting point of the wave (km)

θ_i : angle between the direction of the opposite shore distance F_i and the principal wind direction, $-45^\circ \leq \theta_i \leq 45^\circ$

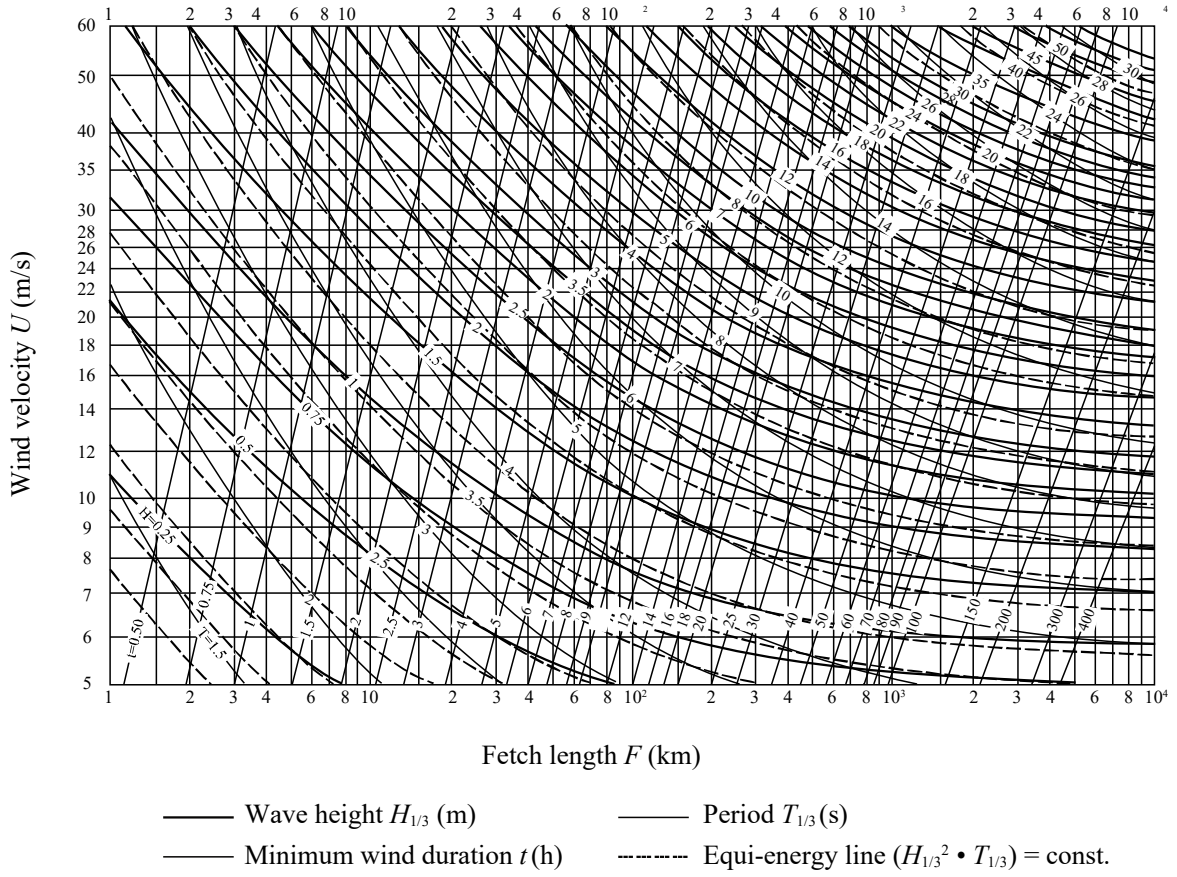


Fig. 4.3.1 Wind Hindcasting Diagram

Moreover, Mitsuyasu⁴⁶⁾ proposed the following equations for the wave hindcasting by assuming the finite fetch.

$$gH_{1/3}/U_{10}^2 = 2.15 \times 10^{-3} (gF/U_{10}^2)^{0.504} \quad (4.3.6)$$

$$gT_{1/3}/(2\pi U_{10}) = 5.07 \times 10^{-2} (gF/U_{10}^2)^{0.330} \quad (4.3.7)$$

where

$H_{1/3}$: significant wave height (m)

$T_{1/3}$: significant wave period (s)

U_{10} : wind velocity at 10 m above the sea surface (m/s)

F : fetch (m)

g : gravitational acceleration (m/s^2)

In the SMB method, when the wind field significantly varies like a typhoon or extra tropical cyclone, it is difficult to provide suitably the values for wind velocity U_{10} , fetch F , or wind duration t . As the methods that solve this problem, Wilson's graphical calculation method,⁴⁷⁾ and the methods of Ijima⁴⁸⁾ and Horikawa,⁴⁹⁾ which solve Wilson's equation numerically, are commonly employed.

As shown in **equations (4.3.1) and (4.3.2)**, the significant wave method is nothing more than a formula that links empirically the development of wind waves with the basic parameters and is not a formula that is constructed in line with the mechanisms of generation and development of waves. Owing to this nature, it leaves a number of vague points, such as how to handle cases wherein the wind gradually deflects, as well as the transition from wind waves to swells and the method for composing wind waves and swells. Furthermore, there is also the problem that the wave direction obtained by hindcasting agrees with the wind direction at the final step of calculation. However,

under the condition that the wind field is simple in the sea and the effects of swells can be ignored, it is a practical estimation method that is simpler than the spectral method and has a short calculation time.

For swells that propagate away from the generation and development areas of wind waves, the Bretschneider equation⁵⁰⁾ was proposed on the basis of simple theoretical considerations and various empirical knowledge.

$$\frac{(H_{1/3})_D}{(H_{1/3})_F} = \left[\frac{k_1 F_{\min}}{k_1 F_{\min} + D} \right]^{\frac{1}{2}} \quad (4.3.8)$$

$$\frac{(T_{1/3})_D}{(T_{1/3})_F} = \left[k_2 + (1 - k_2) \frac{(H_{1/3})_D}{(H_{1/3})_F} \right]^{\frac{1}{2}} \quad (4.3.9)$$

where

$(H_{1/3})_F$: significant wave height at the terminus of the fetch (m)

$(T_{1/3})_F$: significant wave period at the terminus of the fetch (s)

$(H_{1/3})_D$: wave height of a swell (m)

$(T_{1/3})_D$: wave period of a swell (s)

F_{\min} : minimum fetch that generates the wave (km)

D : attenuation distance of waves, i.e., distance between the end of wind area and the arrival position of swells (km)

Constant : $k_1 \doteq 0.4$, $k_2 \doteq 2.0$

Furthermore, the propagation time t of a swell is given by the following equation.

$$t = \frac{4\pi D}{g(T_{1/3})_D} \quad (4.3.10)$$

where

t : propagation time of swells (s)

D : attenuation distance of waves, i.e., distance between the end of wind area and the arrival position of swells (km)

$(T_{1/3})_D$: wave period of swells (s)

G : gravitational acceleration (m/s²)

A wave hindcasting method for shallow water area has also been proposed.⁵¹⁾

(3) Wave Hindcasting by the Spectral Method

In general, the following formula is employed for wave hindcasting by the spectral method.

$$\frac{\partial E(\omega, \theta)}{\partial t} + C_g \nabla E(\omega, \theta) = S_{net}(\omega, \theta) \quad (4.3.11)$$

Here, C_g is the group velocity, the first term at the left stands for the local temporal change in wave spectral density $E(\omega, \theta)$, and the second term stands for the changes due to the transmission effect of the wave spectral density. Furthermore, $S_{net}(\omega, \theta)$ on the right side is the term expressing the total amount of change in energy related to the change of the wave spectral components and is provided by the following formula:

$$S_{net} = S_{in} + S_{n\ell} + S_{ds} \quad (4.3.12)$$

Here, S_{in} is the energy transmitted from the wind to the waves. S_{nl} is the gain and loss of the energy that occurs between the four component waves with different wave numbers and is called the transport of wave energy by nonlinear interactions (hereinafter “nonlinear transport of wave energy”). The nonlinear interactions due to these four waves cause the shape of the directional wave spectrum to vary, with the total sum of energy that the waves have constant. S_{ds} stands for the effects where the energy of the waves dissipates owing to white-cap breaking waves or the internal viscosity of seawater.

Models based on the spectral method are classified into the disjointed propagation (DP) model, the coupled hybrid (CH) model and the coupled disjointed (CD) model, depending on how the nonlinear transport of wave energy term S_{nl} is treated. In the DP model, the nonlinear transport of wave energy term is not introduced directly, and the respective frequency and directional components are not coupled to each other. In the CH model, the nonlinear interactions between component waves are parameterized and introduced. In the CD model, the nonlinear interactions are introduced directly in one form or another.

On the contrary, the models are also classified by the period when they were developed. The DP model, which was developed from the 1960s to the beginning of the 1970s, is the first-generation model. The CH model and CD model, which were developed from the 1970s to the 1980s, are second-generation models, and the CD model, which was developed from the latter half of the 1980s to the present and handles the nonlinear interactions with a higher accuracy, is a third-generation model. In the third-generation model, the degree of flexibility of the scheme of the nonlinear transport of wave energy term is high, and it is possible to hindcast with good accuracy even in cases of waves wherein bidirectional waves, wind waves, and swells are all present.

The wave hindcasting model of the Japan Meteorological Agency started from MRI, ⁵²⁾ which is a first-generation model, and was developed into MRI-II⁵³⁾ and MRI-II new,⁵⁴⁾ which are second-generation models. MRI-III,⁵⁵⁾ which is a third-generation model, is currently being employed. In addition to these, the Inoue model⁵⁶⁾ and the Yamaguchi-Tsuchiya model⁵⁷⁾ are known as a first-generation model, and the Tohoku model⁵⁸⁾ is known as a second-generation model, and the WAM⁵⁹⁾ is known as a third-generation model. Furthermore, in the first-generation models, a one-point method⁶⁰⁾ wherein the waves at one spot are calculated along the wave ray of each component wave that arrives at one spot has been developed.

(4) First-generation model: MRI Model⁵²⁾

The MRI model, developed in 1973, was employed for the numerical wave forecast service of the Japan Meteorological Agency for approximately a decade from 1977.

In the MRI model, the linear and exponential developments of wind waves due to wind are taken into consideration as well as the physical mechanisms of energy dissipation due to the effects of breaking waves, internal friction and headwinds. The effects of nonlinear transport of wave energy S_{nl} are not considered formally, but the effects are expressed indirectly by employing the wave development equation⁵⁶⁾, which does not separate the nonlinear transport of wave energy S_{nl} from the transport of wave energy S_{in} from the wind to the wave.

The total amount of change in energy S_{net} is divided into cases of tailwinds and headwinds and is expressed as follows.

$$\begin{aligned}
 S_{net} &= (A + BE) \left\{ 1 - (E/E_{PM})^2 \right\} \Gamma(\theta - \theta_w) & : E \leq E_{PM}, \quad |\theta - \theta_w| < \pi/2 \\
 S_{net} &= -D f^4 E & : E > E_{PM}, \quad |\theta - \theta_w| < \pi/2 \\
 S_{net} &= -\left\{ B \Gamma(\theta - \theta_w) + D f^4 \right\} E & : |\theta - \theta_w| > \pi/2
 \end{aligned} \tag{4.3.13}$$

Here, f is the frequency, θ is the wave direction, θ_w is the wind direction, and $E = E(f, \theta)$ is the directional wave spectrum. E_{PM} is the Pierson–Moskowitz spectrum and is employed as the standard form of a saturated spectrum. Furthermore, $\Gamma(\theta - \theta_w)$ is the directional wave function that is proportionate to $\cos^2 \theta$, A and B are the linear and exponential development rates⁵⁶⁾ of wind waves per unit time, and D is the coefficient of internal friction (eddy viscosity).

In a DP model including the MRI model, the spectrum shape of the waves is expressed to gradually approximate a saturated spectrum by multiplying the term of the form $\{1 - (E/E_{PM})^2\}$, and $-(E/E_{PM})^2$ expresses the formal energy dissipation. Furthermore, in the DP model, the calculation time is short, and it has practical accuracy with respect to wave height; therefore, it is employed currently as a wave model that can be used simply and conveniently.

(5) Third-generation model: WAM Model⁵⁹⁾

The WAM model is a representative third-generation wave hindcasting model that directly calculates the nonlinear interactions of four wave resonance, by the discrete interaction approximation⁶¹⁾ of S. Hasselmann and K. Hasselmann.

In the model of the spectral method, the transport of wave energy from wind to wave is generally provided by the following.

$$S_{in} = A + BE \quad (4.3.14)$$

Here, A corresponds to the Phillips resonance mechanism, and BE corresponds to the Miles instability mechanism. The Phillips resonance mechanism is a mechanism wherein the random pressure fluctuations of wind that blows over a still water surface and the component waves that have a spatial scale and phase velocity that matches the former cause resonance; owing to the phenomena, a wave is generated. On the contrary, the Miles instability mechanism is a mechanism wherein the airflow on the water surface is disturbed and becomes unstable owing to the unevenness of the water surface due to waves, and energy is efficiently transmitted from wind to waves owing to this phenomenon. In the WAM model, the following equation, from which the items related to the Phillips resonance mechanism are omitted, is adopted:

$$S_{in} = BE \quad (4.3.15)$$

However, in this method, if the initial value of the wave spectrum energy is assumed zero, no waves are generated; therefore, it is possible to provide a spectrum calculated from the fetch length and initial velocity as the initial value.

In the WAM model cycle 4, Janssen's quasilinear theory^{62), 63)} was incorporated in the calculation equation for the transport of wave energy term from wind to waves. Owing to this, even in the event that the conditions of the offshore winds are identical, it is possible to perform calculations that are closer to reality such that the amount of wave energy transported from wind is greater for waves with a younger age.

In the energy dissipation term of the WAM model, the effects of white-cap breaking waves and sea bottom friction have been taken into consideration.

In the nonlinear transport term of wave energy of the WAM model, the nonlinear interactions of the four wave resonance have been taken into account. Nonlinear interactions are a phenomenon wherein the component waves making up the spectrum exchange the energy that they respectively have. Although no change is imparted directly to the total energy of the wave, effects appear on the amount of energy transport from wind to waves and on the amount of energy dissipation due to the fact that the spectral shape changes. Thereafter, the nonlinear transport of wave energy of four wave resonance is expressed by the following equation.⁶⁴⁾

$$S_{nl} = \omega_4 \int_{-\infty}^{\infty} \int_{-\infty}^{\infty} \int_{-\infty}^{\infty} Q(k_1, k_2, k_3, k_4) \delta(k_1 + k_2 - k_3 - k_4) \delta(\omega_1 + \omega_2 - \omega_3 - \omega_4) \\ \times \{n_1 n_2 (n_3 + n_4) - n_3 n_4 (n_1 + n_2)\} dk_1 dk_2 dk_3 \quad (4.3.16)$$

Here, $n(k) = E(k)/\omega$ stands for the wave action density, $Q()$ is the joint function of the spectrum components, δ is the delta function, k is the wave number vector, and the subscripts are the four wave components. The delta function expresses the resonance conditions, and nonlinear interactions occur among the component waves that satisfy the following relations:

$$k_1 + k_2 = k_a = k_3 + k_4, \quad \omega_1 + \omega_2 = \omega_a = \omega_3 + \omega_4 \quad (4.3.17)$$

However, the combinations of the resonance that satisfies these relations exist infinitely. Owing to this, an immense burden is involved in calculating all of these combinations; thus, in the actual model, one representative combination is chosen, and S_{nl} is approximated.

Third-generation wave hindcasting models other than WAM include SWAN⁶⁵⁾ and Wave Watch III.⁶⁶⁾ SWAN is based on WAM, and is expanded so that topographical breaking waves and wave setup can be considered. This model is employed for wave hindcasting in shallow waters. Furthermore, Wave Watch III has been improved by the recent upgrade⁶⁷⁾ to increase the accuracy of the hindcasting for periods and swells.

Although wave hindcasting using the wave spectrum method basically uses a third-generation wave hindcasting model, it is preferable to select the wave hindcasting model which shows good results in the comparison with the observed waves.

4.4 Wave Transformations

In general, the waves for designing port facilities shall be appropriately set as waves that are most unfavorable in terms of structure stability or usage of port facilities. In this consideration, appropriate attention shall be given to wave transformations during the wave propagation from the deep water to the shore, including refraction, diffraction, shoaling, breaking, and others. In the calculation of wave transformations the waves should be regarded as multidirectional random waves, and the wave transformations have to be calculated after assigning the offshore waves with an appropriate directional wave spectrum⁶⁸⁾. However, when determining the rough wave height of the action, an approximate solution may be calculated using regular wave with the representative wave height and period (e.g., $H_{1/3}$ and $T_{1/3}$) of random waves.

Fig. 4.4.1 shows the outline of wave transformations near ports and shores, together with the structure of this chapter.

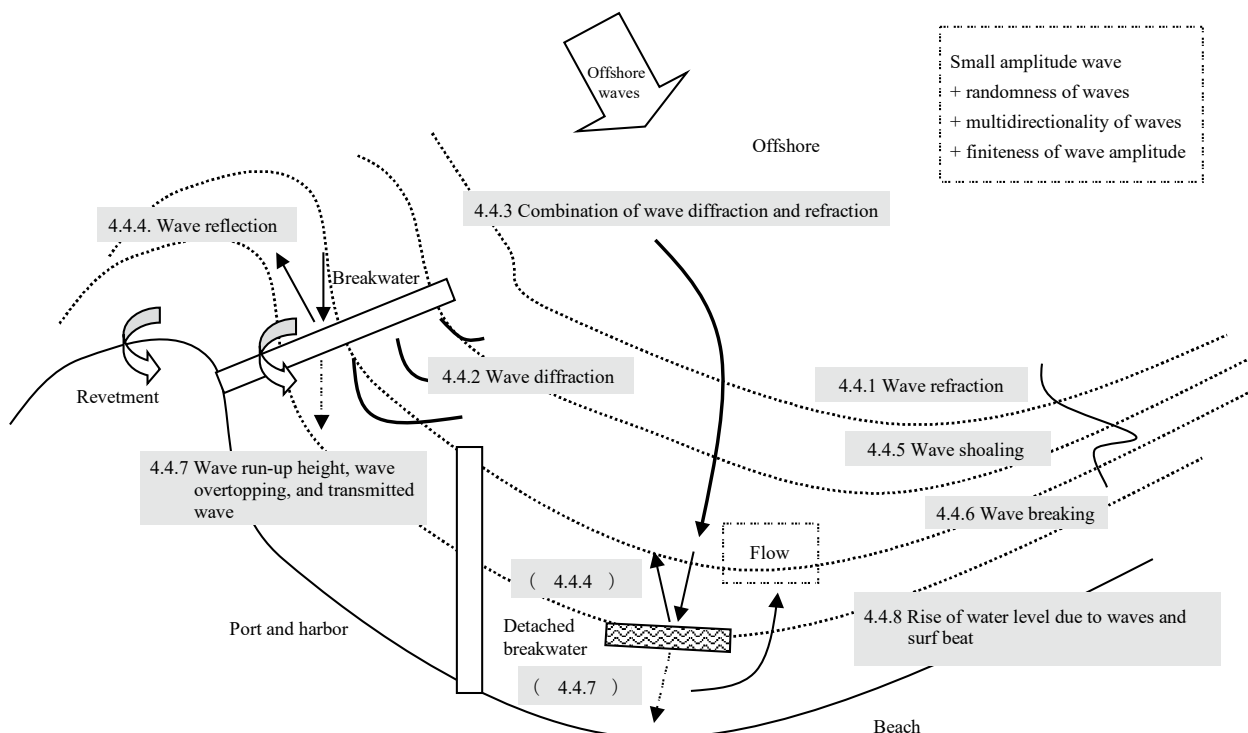


Fig. 4.4.1 Wave Transformations near Ports and Shores

4.4.1 Wave Refraction

- (1) In shallow waters, the changes in wave celerity that depend on place accompanying the changes in water depth cause the wave refraction phenomenon. Therefore, the changes in wave height and wave direction due to refraction must be considered.
- (2) Refraction is a phenomenon whereby the waves change their travel direction as the water depth becomes shallower. The travel direction generally changes perpendicular to the contour line in shallow sea areas. This is the phenomenon that must be verified in the performance verification of facilities when the wave height changes at the same time. For a beach that can be considered a simple one with a parallel contour line, the calculation results of regular wave refraction using the specifications of representative waves may be used as an approximate value. In principle, the effect of refraction in shallow sea areas is calculated by the numerical calculation.
- (3) **Wave refraction calculation of regular waves⁶⁹⁾**

Figs. 4.4.2 and 4.4.3 show the refraction coefficient and refraction angle, which can be calculated from the wave refraction of regular waves, such as refraction drawing.

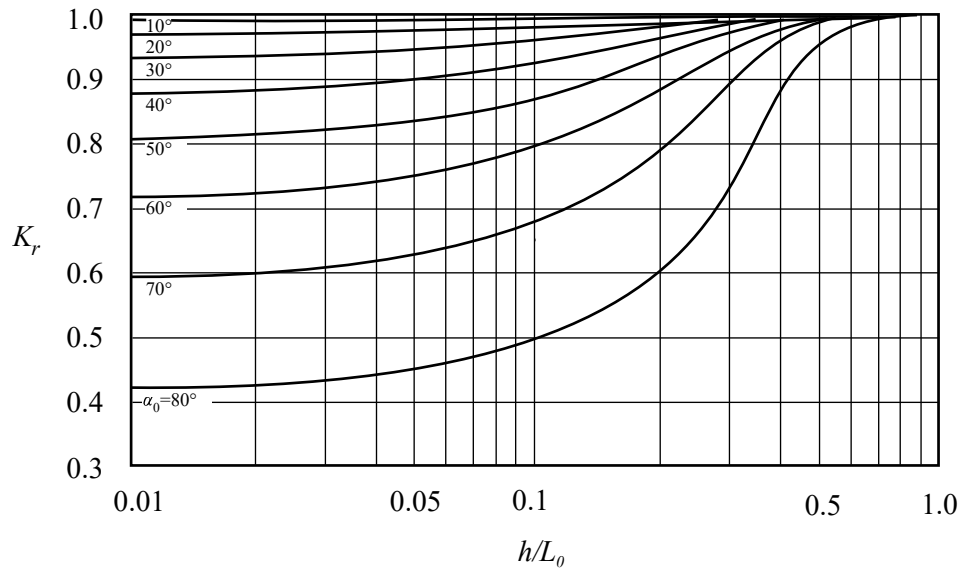


Fig. 4.4.2 Wave Refraction Coefficient of Regular Waves at a Coast with Straight, Parallel Contour Lines

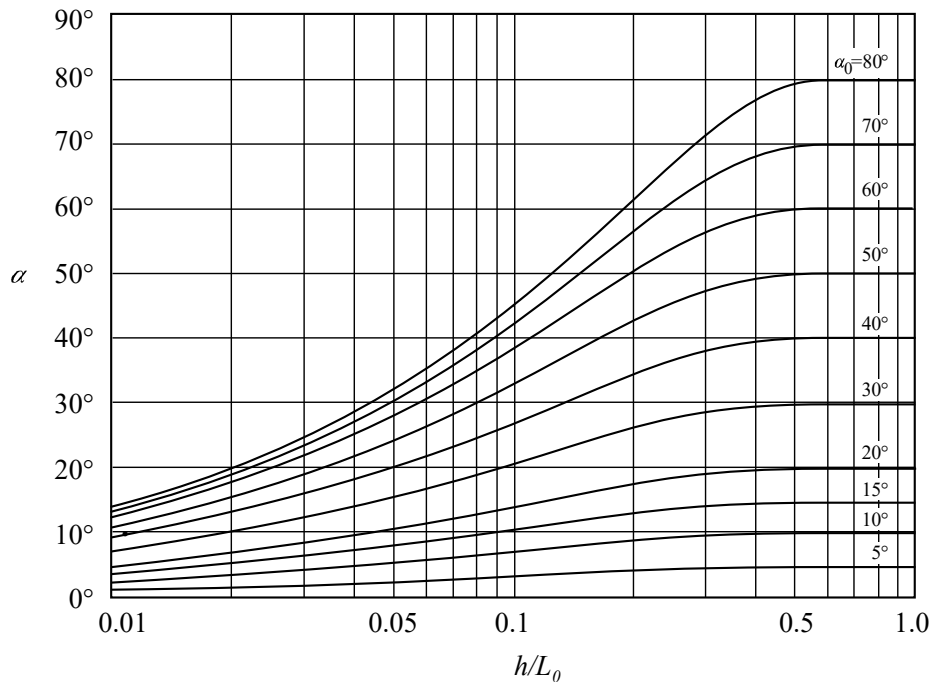


Fig. 4.4.3 Variation Diagram of Regular Wave Directions at a Coast with Straight, Parallel Contour Lines

(4) Refraction Calculation for Random Waves

① Calculation methods

The calculation method for refraction analysis for random waves includes the following: ① the component wave method,⁷⁰⁾ wherein the directional wave spectrum is divided into an appropriate number of component waves, a refraction calculation is performed for each component wave, and the wave refraction coefficient for the random wave is evaluated by making a weighted average of the component wave energies; ② methods in which the wave energy balance equation²⁴⁾ or the mild-slope equation²⁵⁾ for a wave is solved using a computer with finite difference schemes. Similar to the component wave method, the energy balance equation is derived by assuming that wave energy does not pass across wave rays and flow in/out. This means that the technique is basically the same in both cases. However, in the energy balance equation method, the refraction within a small

section is calculated, i.e., the wave refraction coefficient does not become infinite even at a point in which two regular wave rays may converge. On the contrary, the mild-slope equation method for a wave is strictly analytical, but it is difficult to apply it to a large region. When determining the wave refraction coefficient for random waves, it is acceptable to use the component wave method, which involves the linear superposition of wave refraction coefficients for regular waves and is simple and convenient. However, when the intersections of wave rays occur during a refraction calculation for a component wave, the energy balance equation method may be used for practical purposes with the exception of a case wherein the degree of intersection is large.

② Effects of diffraction

When deepwater waves have been diffracted by an island or a headland, the wave spectrum becomes generally different from a standard form that has been assumed initially. Therefore, it is necessary to use the spectral form after diffraction when performing the refraction calculation.

③ Diagrams of the wave refraction coefficient and angle for random waves at a coast with straight, parallel depth contours³⁸⁾

Figs 4.4.4 and 4.4.5 show the wave refraction coefficient K_r and the principal wave direction $(\alpha_p)_0$, respectively, for random waves at a coast with straight, parallel depth contours, with the principal direction of the deepwater waves $(\alpha_p)_0$ as the parameter. The direction $(\alpha_p)_0$ is expressed as the angle between the wave direction and the line normal to the boundary of the offshore sea. S_{\max} is the maximum value of the parameter that expresses the degree of directional spreading of wave energy. (See **Part II, Chapter 2, 4.2.2 Representation of Waves**)

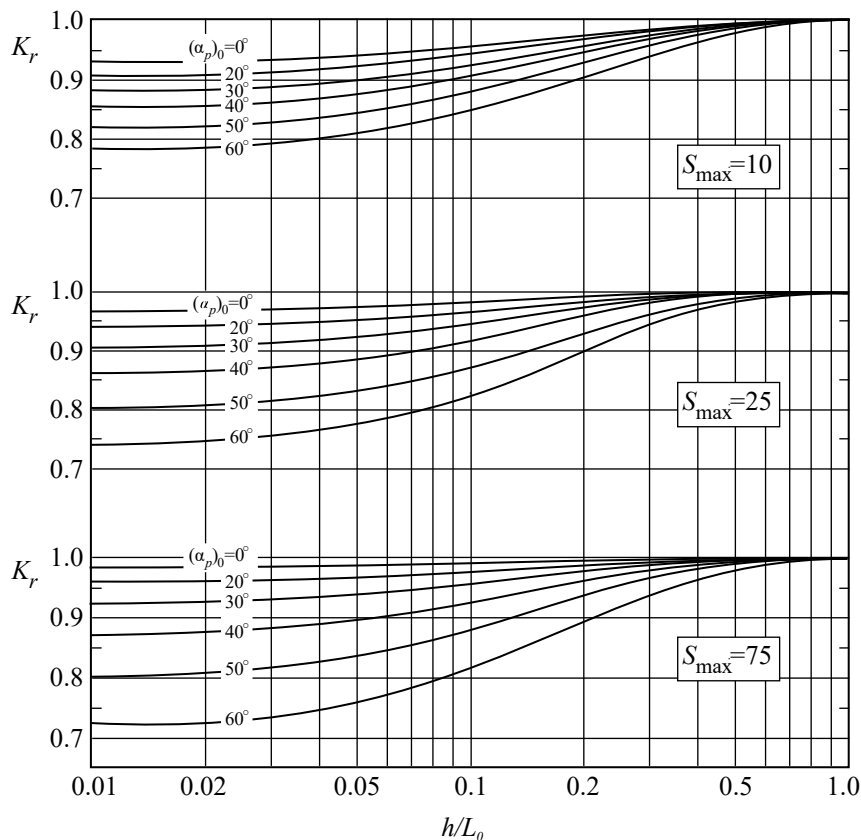


Fig. 4.4.4 Wave Refraction Coefficient of Random Waves at a Coast with Straight, Parallel Depth Contours

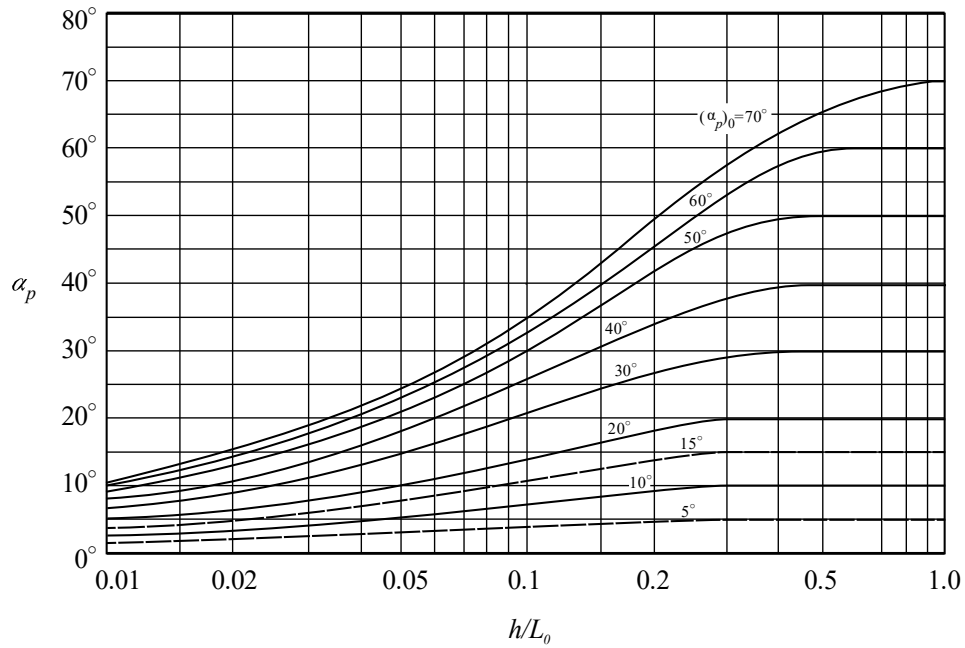


Fig. 4.4.5 Change Due to Refraction in the Principal Direction α_p of Random Waves at a Coast with Straight, Parallel Depth Contours

(5) Energy Balance Equation

The energy balance equation calculates the changes of the spectrum of random waves due to refraction and wave shoaling in the shallow waters and calculates the wave height change in shallow waters. **Equation (4.4.1)** shows the basic form of the energy balance equation.

$$\frac{\partial}{\partial x}(Sv_x) + \frac{\partial}{\partial y}(Sv_y) + \frac{\partial}{\partial \theta}(Sv_\theta) = 0 \quad (4.4.1)$$

$$v_x = C_g \cos \theta$$

$$v_y = C_g \sin \theta$$

$$v_\theta = \frac{C_g}{C} \left(\sin \theta \frac{\partial C}{\partial x} - \cos \theta \frac{\partial C}{\partial y} \right) \quad (4.4.2)$$

Here, S is the directional spectrum of the wave, C is the wave celerity, C_g is the group velocity of the waves, and θ is the wave angle that is measured counterclockwise from the positive direction of the x axis. **Equation (4.4.1)** can be solved from offshore to the direction of the waves. In **equation (4.4.1)**, the right term is zero, and the total energy of the wave being propagated is not considered to vary. Takayama et al.²⁴⁾ focused on the change in energy flux in the surf zone and added the energy loss due to wave breaking expressed in $-\varepsilon'_b S$ to the right side (where ε'_b is the dissipation factor of lost energy in a unit time due to wave breaking) to make improvements so that the effects of horizontally expanded wave breaking can be treated. Although it is not strict, it enabled the effects of reflected waves to be calculated. Therefore, the linear wave transformation due to a phenomenon other than diffraction can be calculated.

Fig. 4.4.6 shows an example of improved calculation by the energy balance equation.

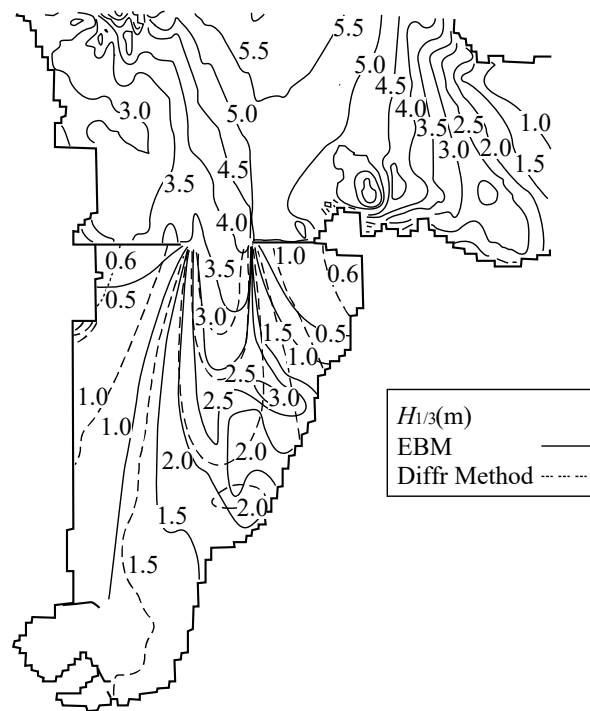


Fig. 4.4.6 Example of Calculation of the Wave Height Distribution by the Energy Balance Equation

In the figure, the solid line is the wave height distribution based on the energy balance equation, and the broken line is the wave height distribution calculated by taking into consideration only the diffraction inside the harbor. The energy balance equation is also applied to wave fields wherein the effects of refraction and diffraction are large. Considering that the shielding effect of structures to the directional dispersion of random waves are dominant compared with the invasion of wave energy due to diffraction, it is possible to examine the wave height inside a harbor that is shielded by a breakwater, excluding the area immediately behind it. The energy balance equation method,²⁶⁾ which considers that diffraction has been improved in the accuracy of the calculation of wave height distribution directly behind the breakwaters.

- (6) At places wherein the water depth is 0.5 times less than the offshore wave height, the nature as a flow is more prominent than the nature as a wave; thus, the refraction calculation employed for computing the wave height and refraction coefficient is applied to the range where the water depth is 0.5 times deeper than the offshore wave height.

4.4.2 Wave Diffraction

- (1) The wave height in regions where waves are anticipated to be greatly affected by the diffraction phenomenon caused by obstacles such as breakwaters or islands, needs to be calculated using an appropriate method.
- (2) Diffraction is a phenomenon that waves invade into a water area sheltered by breakwaters or other obstacles. Since this phenomenon is important when determining the wave height in a harbor, the irregularity of waves should be considered in a diffraction calculation. For a harbor within which the water depth is assumed uniform, the diffraction diagrams for random waves with regard to a semi-infinite length breakwater or straight breakwaters with one opening are prepared. On the contrary, the cases that the regular wave diffraction diagram can be applied approximately to on-site waves are restricted to the diffraction of swells of which wave steepness are small (on the order of $H_0/L_0 \leq 0.005$) with the aligned wave crest line.

(3) Diffraction Calculation of Regular Waves

The change in wave heights due to diffraction can be calculated using the Sommerfeld solution in the velocity potential theory. **Reference (Part III), Chapter 4, 1. Wave Diffraction Diagram** shows the regular wave diffraction diagram by a semi-infinite breakwater and straight breakwaters with one opening.

(4) Diffraction Calculation of Random Waves**① Types of Calculation Methods**

Although the wave diffraction calculation of random waves in harbors with relatively simple shapes can be performed by applying diffraction diagrams, it is generally conducted by numerical computation within a complex shape of harbor. The diffraction calculation methods include Takayama's method,⁷¹⁾ which involves the linear superposition of analytical solutions for detached breakwaters, and calculation methods that use the Green functions.⁷²⁾ On the other hand, when the width of an island or the width of the entrance of a bay is at least ten times the wave length of the incident waves, the estimate by the directional spreading method⁷³⁾ using the amount of wave energy that arrives directly at the point of interest behind the island or in the bay can be approximately used.⁷⁴⁾ However, if the point of interest is just behind an island or headland, the effects of diffracted waves will be large; therefore, this method cannot be applied.

② Effect of Refraction

Diffraction diagrams and diffraction calculation methods assume that the water depth within the harbor is uniform. If there are large variations in water depth within the harbor, the errors will become large; in this case, it is preferable to examine the wave height in the harbor by either hydraulic model tests or numerical calculation methods that also take the effect of refraction into account.

③ Diffraction Diagram

The random wave diffraction diagram of a semi-infinite breakwater and straight breakwaters with one opening is shown in **Reference (Part III), Chapter 4, 1. Wave Diffraction Diagram**. $S_{\max} = 10$ corresponds to the wind waves, $S_{\max} = 25$ corresponds to the swells in the initial damping, and $S_{\max} = 75$ corresponds to swell-like waves. However, in shallow water areas, the change in S_{\max} due to refraction needs to be considered.

④ Treatment of obliquely incident waves

When waves are obliquely incident to breakwaters with opening, it is preferable to obtain the diffraction diagram by using a numerical calculation. When this is not possible or when the diffraction diagram is only required as a rough guideline, the following approximate method may be used instead. In the case of semi-infinite breakwaters, approximate values can be obtained by rotating the diffraction diagram for perpendicular incident waves to the principal direction of waves.

(a) Determining the axis of the diffracted wave

When waves are obliquely incident to breakwaters with opening, the direction θ' of the axis of the diffracted waves (see **Fig. 4.4.7**) varies slightly from the direction of incidence θ . **Tables 4.4.1 (a) to (c)** list the direction of the axis of the diffracted waves as a function of the breakwater opening width ratio B/L and the direction of incident waves. These tables are used to obtain the direction θ' of the axis of the waves after diffraction, and the virtual opening width ratio B'/L corresponding to θ' is obtained from **equation (4.4.3)**:

$$B'/L = (B/L)\sin \theta' \quad (4.4.3)$$

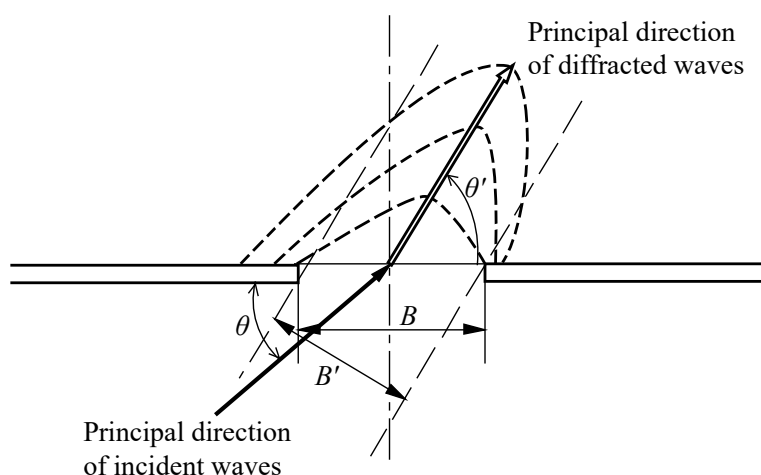


Fig. 4.4.7 Virtual Opening Width B' and Angle of Axis of Wave after Diffraction θ'

Table 4.4.1 Angle of Axis of Random Wave (θ') (The angle in parentheses is the angle of deflection relative to the angle of incidence.)

(a) $S_{\max} = 10$

B/L	Angle between breakwater and wave direction θ			
	15 °	30 °	45 °	60 °
1.0	53 ° (38 °)	58 ° (28 °)	65 ° (20 °)	71 ° (11 °)
2.0	46 ° (31 °)	53 ° (23 °)	62 ° (17 °)	70 ° (10 °)
4.0	41 ° (26 °)	49 ° (19 °)	60 ° (15 °)	70 ° (10 °)

(b) $S_{\max} = 25$

B/L	Angle between breakwater and wave direction θ			
	15 °	30 °	45 °	60 °
1.0	49 ° (34 °)	52 ° (22 °)	61 ° (16 °)	70 ° (10 °)
2.0	41 ° (26 °)	47 ° (17 °)	57 ° (12 °)	67 ° (7 °)
4.0	36 ° (21 °)	42 ° (12 °)	54 ° (9 °)	65 ° (5 °)

(c) $S_{\max} = 75$

B/L	Angle between breakwater and wave direction θ			
	15 °	30 °	45 °	60 °
1.0	41 ° (26 °)	45 ° (15 °)	55 ° (10 °)	66 ° (6 °)
2.0	36 ° (21 °)	41 ° (11 °)	52 ° (7 °)	64 ° (4 °)
4.0	30 ° (15 °)	36 ° (6 °)	49 ° (4 °)	62 ° (2 °)

(b) Fitting of a diffraction diagram

Among the diffraction diagrams of normal incidence (see **Reference (Part III), Chapter 4, 1 Wave Diffraction Diagram**), the diffraction diagram that has a ratio of an opening width B to a wave length L nearly equal to the breakwater opening width virtual ratio is selected. This diffraction diagram is next rotated until the direction of incident waves matches the direction of the axis of the diffracted waves as determined from **Table 4.4.1**. The diffraction diagram is then copied and taken to be the diffraction diagram for obliquely incident waves. The errors in this approximate method are the largest around the opening in the breakwaters; in terms of the diffraction coefficient, the maximum error with the approximate method may amount to around 0.1.

⑤ Notes on the diffraction calculation

- (a) If there is no diffraction diagram with the equal open width ratio B/L , it is common to use a diffraction diagram with an approximate value or to interpolate from two diffraction diagrams with approximate values.
- (b) Given that the wave diffraction is more affected by the change in wave direction than by the change in period, diffraction by island or others, which is larger than the wave length, can be calculated by the directional spreading method by considering only the directional spread of wave energy.⁵⁹⁾
- (c) When the water depth changes significantly in the wave sheltered area, the wave refraction also needs to be considered with an appropriate method.
- (d) It needs to be noted that the period of significant waves of diffracted random waves is different from the period before diffraction.
- (e) When diffracted waves are reflected by quay walls and similar structures, the effect of reflection needs to be calculated by the superposition method for wave diffraction analysis⁷⁵⁾ or other proper methods.
- (f) The broken waves may enter the port entrance in a storm with a significantly high wave height. Furthermore, in this case, the wave height in the port may be calculated by using a diffraction diagram. However, when the directional spreading of wave energy becomes concentrated when waves are broken, a high directional spreading parameter S_{\max} of 75 or more or a regular wave diffraction diagram needs to be used.

⑥ Studies by hydraulic model tests

Owing to improvements of multidirectional random wave generators, it is easy to reproduce waves that have directional spreading in the laboratory nowadays, i.e., diffraction model tests can be performed relatively easily. When performing a model test, an opening in the harbor model is established within the effective wave generating zone, and the wave height is simultaneously measured at a number of points within the harbor. The diffraction coefficient is obtained by dividing the significant wave height in the harbor by the averaged significant wave height for at least two observation points at the harbor entrance.

4.4.3 Combination of Diffraction and Refraction (Equivalent Deepwater Wave Height)

- (1) When performing diffraction calculations for waves in waters where the water depth varies greatly, wave refraction must also be considered.
- (2) When the water depth within a harbor is more-or-less uniform by dredging, which is often seen in large harbors, the refraction of waves after diffraction can be ignored. To determine the wave height in the harbor in this case, it is acceptable to first perform a calculation by considering only refraction, wave shoaling, and breaking from the offshore wave hindcasting point to the harbor entrance. Thereafter, a diffraction calculation for the area within the harbor is performed by taking the incident wave height to be equal to the estimated wave height at the harbor entrance. In this case, the wave height H at a point of interest within the harbor is expressed using the following equation:

$$H = K_d K_r K_s H_0 \quad (4.4.4)$$

where

K_d : diffraction coefficient at the point of interest

K_r : refraction coefficient at the point of interest

K_s : shoaling coefficient at the point of interest (see **Part II, Chapter 2, 4.4.5 Wave Shoaling**)

H_0 : deepwater wave height

The energy balance equation method or the improved energy balance equation method,²⁴⁾ in which a term representing dissipation due to wave breaking is added, is appropriate as the calculation method for refraction analysis for the ocean. The harbor calmness calculation method of Takayama⁷¹⁾, wherein diffraction solutions for detached breakwaters are superimposed to obtain the change in the wave height of random waves within the harbor

due to diffraction and reflection, can be used for the diffraction calculation for the area within the harbor provided that there are no complex topographic variations within the harbor.

In **equation (4.4.4)**, the assumed wave height by multiplying K_r and K_d by H_0 is used as the equivalent deepwater wave height H_0' and is calculated with the following equation.

$$H_0' = K_r K_d H_0 \quad (4.4.5)$$

The equivalent deepwater wave height is the assumed offshore wave used for the performance verification on the results obtained from 2D water tank experiments. The wave height H_0' is obtained by multiplying the effects of refraction and diffraction calculated in advance by H_0 . By using wave height H_0' , it is possible to make use of the calculation diagrams shown in **Part II, Chapter 2, 4.4.5 Wave Shoaling, 4.4.6 Wave Breaking, and 4.4.7 Wave Run-up Height, Wave Overtopping, and Transmitted Waves.**

- (3) When there are large variations of water depth even in the area sheltered by breakwaters often seen in the case with relatively small harbors and coastal areas, it is necessary to simultaneously consider both diffraction and refraction within the harbor. If wave reflection is ignored and if only the approximate change in wave height is examined, it is possible to perform refraction and diffraction calculations separately; thereafter, the change in wave height can be estimated by multiplying together the refraction and diffraction coefficients obtained.

Calculation methods that allow the simultaneous consideration of the refraction and diffraction of random waves include the energy balance equation, which considers diffraction²⁶⁾; a method that uses time-dependent mild-slope equations for wave⁷⁶⁾; a method in which the Boussinesq equation is solved using the finite difference method;⁷⁷⁾ and the multicomponent coupling method of Nadaoka et al.⁷⁸⁾ There are also references in which other calculation methods are explained.⁷⁹⁾ The wave transformation calculation model using the Boussinesq equation has been modified, and NOWT-PARI (Nonlinear wave transformation model by Port and Airport Research Institute) has been proposed as one of the models that can be used at ports.²⁷⁾ Modified versions that allow the simultaneous consideration of run-up and seawall wave overtopping in shallow waters have also been proposed.⁸⁰⁾ Designers should use appropriate numerical calculation methods by taking into consideration water area characteristics and the application limit of the program.

4.4.4 Wave Reflection

(1) General

- ① In the performance verification of port facilities, examination shall be performed on the effects of reflected waves from neighboring structures on the facilities in question and on the effects of wave reflection from the facilities in question on neighboring areas.
- ② It is necessary to take note of the fact that the waves reflected from port facilities can exercise a large influence on the navigation of ships and cargo handling. For example, the waves reflected from breakwaters can cause disturbances in navigation water ways, and multiple-reflected waves from quay walls can cause agitations inside harbors.

③ Composition of Reflected Waves and Incident Waves

When incident waves and waves reflected from a number of reflective boundaries coexist, the wave height H_s can be calculated using **equation (4.4.6)**. Here, a train of incident waves and those of reflected waves from reflective boundaries are termed "wave groups."

$$H_s = \sqrt{H_1^2 + H_2^2 + \dots + H_n^2} \quad (4.4.6)$$

where

H_s : significant wave height when all of the wave groups are taken together

H_1, H_2, \dots, H_n : significant wave heights of individual wave groups

However, if the wave action varies with the wave direction, the differences in the wave directions of various wave groups must be considered. The calculated wave height is valid for places that are approximately more than 0.7 wavelengths away from a reflecting boundary. In a range within 0.7 wavelengths from the reflecting

boundary, the remaining restraint condition for the phases of incident waves and reflected waves significantly changes the wave height.

Regarding the diffraction or refraction of waves, for which wave direction is an important factor, the significant wave height of each wave group is determined separately by performing the calculation necessary for that wave group when the wave directions are different among various wave groups. Thereafter, the composite wave height is calculated by putting these significant wave heights into **equation (4.4.6)**. Here, the composite period may be obtained by applying **equation (4.2.22)**. An acceptable alternative is to determine the spectrum for each wave group, add these spectra together to calculate the spectral form when the wave groups coexist, and then perform diffraction or refraction calculations by using this spectrum.

④ Methods for Calculating the Effects of Reflected Waves

The calculation methods for investigating the extent of the effects of waves reflected from a structure include the calculation method of wave height distribution around an island⁸¹⁾ and a simple method by means of diffraction diagrams.

(a) Calculation method of wave height distribution around an island⁸¹⁾

In this calculation method, the theoretical solution that shows the wave transformation around a single convex corner is separated into three terms, namely, the incident, reflected, and scattered waves. The term for the scattered waves is progressively expanded to obtain an approximate equation so that the method can be applied to a case where there are a number of convex corners.

When there are a number of convex corners, it is assumed as a precondition that the lengths of the sides between convex corners are at least five times the wavelength of the incident waves so that the convex corners do not interfere with each other. It is necessary to pay attention to the fact that errors may become large if the sides are shorter than this.

Considering that another assumption is made such that the water depth is uniform, the refraction of reflected waves cannot be calculated. In general, it is sufficient for practical purposes if the lengths of the sides between convex corners are at least three times the wavelength of the incident waves. This calculation method can also be applied to the reflection of random waves by superposing component waves. Although the wave diffraction problems can also be analyzed with this calculation method, there will be large errors if it is applied to the diffraction of waves by thin structures, such as breakwaters.

(b) Simple method by means of diffraction diagrams

The example shown in **Fig. 4.4.8** is explained as follows. The wave height at point A on the front face of a detached breakwater is estimated when waves are incident on the detached breakwater at an angle α .

Instead of the detached breakwater, it is assumed that there are virtual breakwaters with opening (dashed lines in **Fig. 4.4.8**). Thereafter, one considers the situation whereby waves are incident on the virtual opening from both the wave direction of the incident waves and the direction symmetrical to this with respect to the detached breakwater (i.e., the direction shown by the dotted arrow in **Fig. 4.4.8**) and draws the diffraction diagram for the opening (dotted lines in **Fig. 4.4.8**). The range of influence of the reflected waves is represented by means of the diffraction diagram for the virtual breakwaters with opening. Accordingly, supposing that the diffraction coefficient at point A is read off as being 0.68, the wave height ratio with respect to the incident waves at point A is obtained by combining the value of 0.68 with a value of 1.0 representing the incident waves; given that the energies are added, the wave height ratio becomes $\sqrt{1 + 0.68^2} = 1.21$. However, it should be noted that this value of 1.21 represents the mean value of the wave height ratio around point A. It is not preferable to use this method for points within 0.7 wavelengths away from the detached breakwater because the errors due to a phase coupling effect will be large.

For the case of wave reflection by a semi-infinite breakwater, the virtual breakwater also becomes a semi-infinite breakwater in the opposite direction; thus, the diffraction diagram for a semi-infinite breakwater is used. When the reflection coefficient of the front surface of the breakwater is less than 1.0 (e.g., owing to wave-dissipating work), the diffraction coefficient should be multiplied by the reflection coefficient before being used. For example, if the reflection coefficient of the detached breakwater is 0.4 in the previous example, the wave height ratio at point A becomes $\sqrt{1 + (0.4 \times 0.68)^2} = 1.04$.

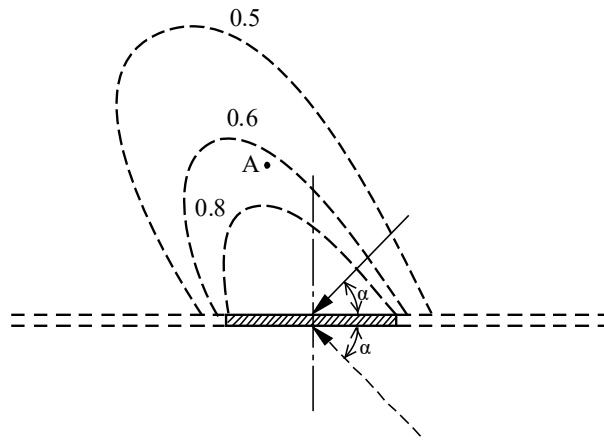


Fig. 4.4.8 Sketch Showing the Effect of Reflected Waves

(2) Estimation of Reflection Coefficient

- ① Reflection coefficients need to be determined appropriately on the basis of the results of field observations, hydraulic model tests, and past data.
- ② **Approximate Values for Reflection Coefficient**⁽⁸²⁾

It is preferable to calculate the value of a reflection coefficient by field observations. However, when it is difficult to perform observation or when the structure in question has not yet been constructed, it is possible to estimate reflection coefficient by referring to the results of hydraulic model tests. In this case, it is preferable to use random waves as test waves. The following is a list of approximate values for the wave reflection coefficients of several types of structures.

Upright wall	: 0.7–1.0 (0.7 is for the case of a low crown with much wave overtopping)
Submerged upright breakwater	: 0.5–0.7
Rubble mound slope	: 0.3–0.6
Deformed wave-dissipating blocks	: 0.3–0.5
Upright wave-dissipating structure	: 0.3–0.8
Natural beach	: 0.05–0.2

With the exception of the upright wall, the lower limits in the above ranges of reflection coefficient correspond to the case of steep waves and the upper limits to waves with low steepness. However, it should be noted that with the upright wave-dissipating structure, the wave reflection coefficient varies with the wavelength, and the shapes and dimensions of the structure. Furthermore, the reflection coefficients of swells with a period longer than 10 seconds or long period waves with a period of several tens of seconds become higher than the abovementioned values in the case of wave energy dissipating blocks or upright wave-dissipating structures. In recent years, there have been reports about calculation methods that incorporate a function that can reproduce the nature wherein the reflection characteristics of waves vary in accordance with the thickness and the porosity of the wave-dissipating layer in nonlinear wave transformation model, which can calculate a wave form temporally and spatially.⁽⁸³⁾ See **Part II, Chapter 2, 4.5 Long Period Waves** for the wave reflection coefficient of long period waves.

③ Calculation Method of Reflection Coefficient

(a) Model experiment

It is best to obtain the reflection coefficient of facilities from the field wave height measurement. However, given that the field measurement is expensive and time consuming, the reflection coefficient of typical facilities may be determined by model experiments. The reflection coefficient of regular waves from the model or the edge of a water tank can be obtained by Healy's method which uses wave height records

obtained by moving a wave gauge or by Goda–Suzuki's analysis method for separation of incident and reflected waves⁸⁴⁾ using wave gauge records of a pair of stationary wave gauges. Furthermore, the latter method is mainly used for random waves.⁸⁵⁾

(b) Field measurement

The reflection coefficient measurement method in experimental flumes is difficult to apply to field measurement. However, Goda–Suzuki's analysis method for separation of incident and reflected waves may be applied if the wave direction is relatively stable in shallow sea area and is considered perpendicular to facilities. The estimation of the reflection coefficient by measuring the directional wave spectrum is possible if the waves acting on offshore breakwaters, etc. cannot be considered single directional waves.⁸⁶⁾

(3) Transformation of Waves at Concave Corners, near the Heads of Breakwaters, and around Detached Breakwaters

- ① Around the concave corners of structures, near the heads of breakwaters, and around detached breakwaters, the wave height becomes larger than the normal value of standing waves owing to the effects of diffraction and reflection. This increase in wave height shall be examined thoroughly. Moreover, the irregularity of waves shall be considered in the analysis.

② Influence of Wave Irregularity

When the wave height distribution near the concave corner, the head of a breakwater, or around a detached breakwater is calculated for regular waves, a distributional form with large undulations is obtained. However, when wave irregularity is incorporated into the calculation, the undulated form of the distribution becomes smoothed out, excluding the region within one wavelength of a concave corner, and the peak value of the wave height becomes decreases. Therefore, a calculation using regular waves overestimates the increase in wave height.

③ Graphs for Calculating Wave Height Distribution around a Concave Corner

Fig. 4.4.9 shows the wave height distributions for random waves near a concave corner. This figure exhibits the form of the distribution of the maximum value of the wave height, as obtained from numerical calculations for each principal wave direction. It has been assumed that waves are completely reflected by the breakwater. In the diagram, K_d is the ratio of the wave height at the front of the main breakwater to the incident wave height. The random waves used in the calculation has a spectral form with $S_{\max} = 75$, which implies a narrow directional spreading. The long dash-dotted line in each graph shows the distribution of the maximum value of the wave height at each point, as obtained using an approximate calculation. l_1 is the length of the main breakwater, l_2 is the length of the wing breakwater, and β is the angle between the main breakwater and the wing breakwater. This figure may be used to calculate the wave height distribution near a concave corner. When it is not easy to use the calculation program, the approximate calculation method (a simple method with diffraction diagrams) may be used.

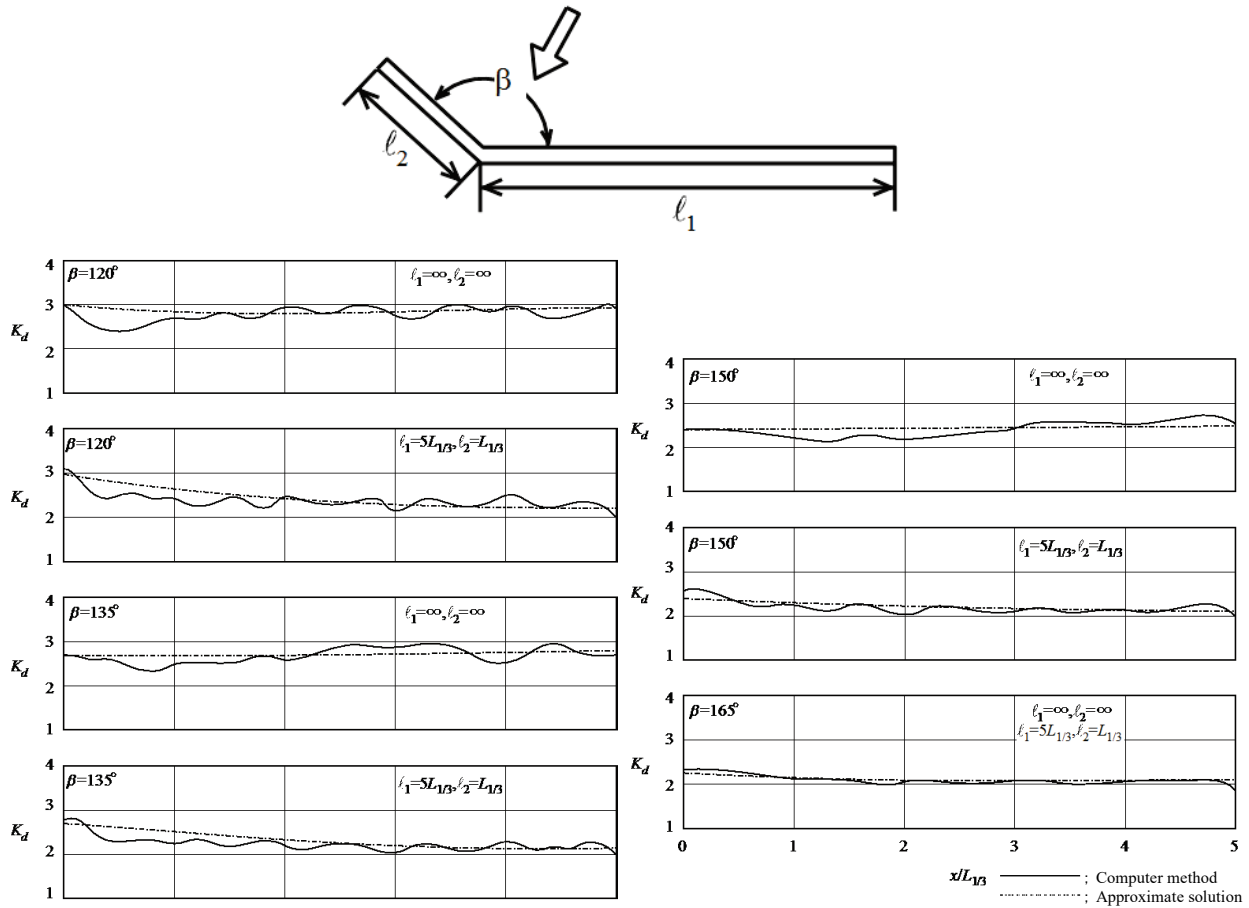


Fig. 4.4.9 Distribution of the Maximum Value of the Wave Height around Concave Corner⁸⁷⁾

④ Wave Height–Reducing Effects of Wave-Dissipating Work

When a wave-dissipating work is installed to reduce the increase in wave height around a concave corner and if the wave-dissipating work is such that the reflection coefficient of the breakwater becomes no more than 0.4, it is quite acceptable to ignore the increase in wave height due to the presence of a concave corner. However, this is only the case when the wave-dissipating work extends along the whole of the wing breakwater. If the wing breakwater is long, one cannot expect the wave-dissipating work to be very effective unless it is installed along the entire length of the breakwater because the effect of waves reflected from the wing breakwater extend even to places that are at a considerable distance away from the concave corner. The same can be said for the influence of the main breakwater on the wing breakwater.

⑤ Increase in Wave Height at the Head of a Breakwater

Near the head of a semi-infinite breakwater or those of breakwaters with opening, specifically within a distance of one wavelength from the head, the waves diffracted by breakwaters cause local wave height increase over the normal standing wave heights. Given that the wave height distribution has an undulating form even at the back of a breakwater, it is necessary to pay attention to the fact that the difference in water level between the inside and outside of the breakwater causes a large wave force. **Fig. 4.4.10** shows an example of the results of a calculation of the ratio of the wave force to that of a standing wave near the head of a breakwater.

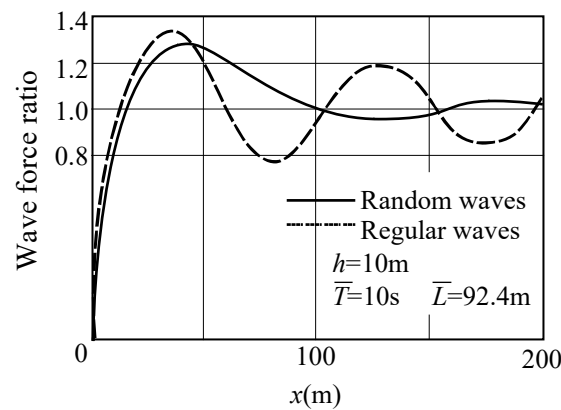


Fig. 4.4.10 Wave Force Distribution along a Semi-infinite Breakwater⁸⁸⁾

⑥ Increase in Wave Height around Detached Breakwater

Along a detached breakwater, waves with a height greater than that of normal standing waves are produced, and the wave height distribution takes an undulating form even at the back of the breakwater because of the effect of wave diffraction at the two ends of the breakwater. The wave force also becomes large owing to the difference between the water levels in the front and back sides of the breakwater. In particular, it is necessary to pay attention to the fact that, with a detached breakwater, the place where the maximum wave force is generated can shift significantly with the wave direction and with the ratio of the breakwater length to the wavelength.

Fig. 4.4.11 shows an example of the calculation results of the wave force distribution along a detached breakwater for unidirectional random waves. In this calculation, the wave direction for which the largest wave force occurs is $\alpha = 30^\circ$ of obliquely incident with a relatively shallow angle.

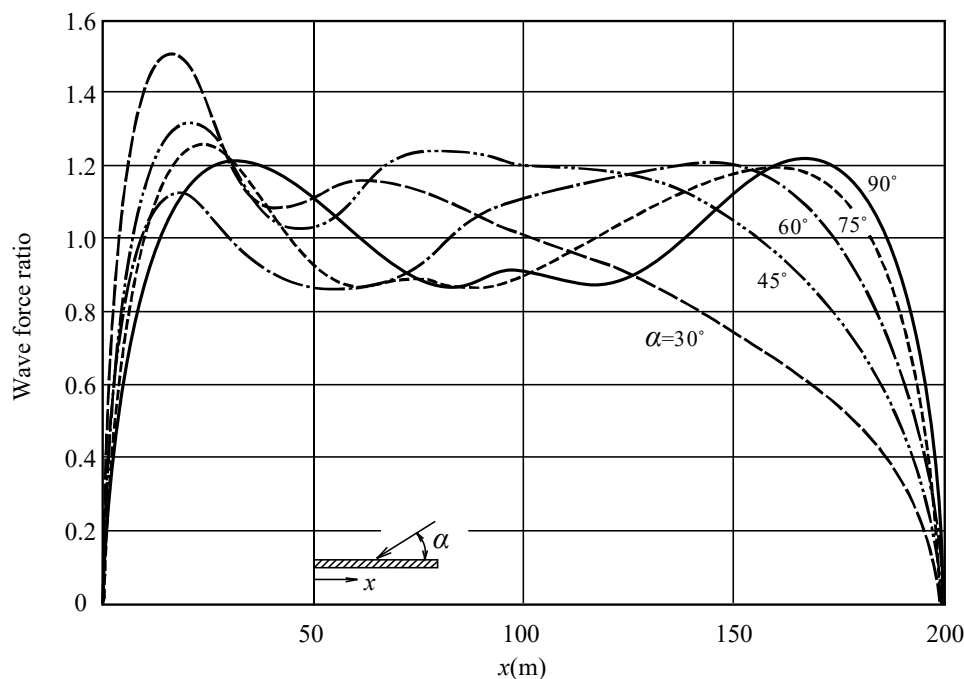


Fig. 4.4.11 Wave Force Distribution along a Detached Breakwater⁸⁹⁾

4.4.5 Wave Shoaling

- (1) When waves propagate in shallow waters, shoaling shall be considered, in addition to refraction and diffraction. In general, the nonlinearity of waves shall be considered when calculating the shoaling coefficient.

- (2) Shoaling is one of the important factors that lead to the changing of wave height in coastal water areas. It exemplifies the fact that the wave height in shallow waters is also governed by the water depth and the wave period. **Fig. 4.4.12** was drawn on the basis of the nonlinear long wave theory of Shuto⁹⁰⁾. It includes the linearized solution by the small amplitude wave theory and enables the estimation of the shoaling coefficient from deep to shallow waters.

In the diagram, K_s is the shoaling coefficient, H_0' is the equivalent deepwater wave height, H is the wave height at water depth h , and L_0 is the wavelength in the deep water.

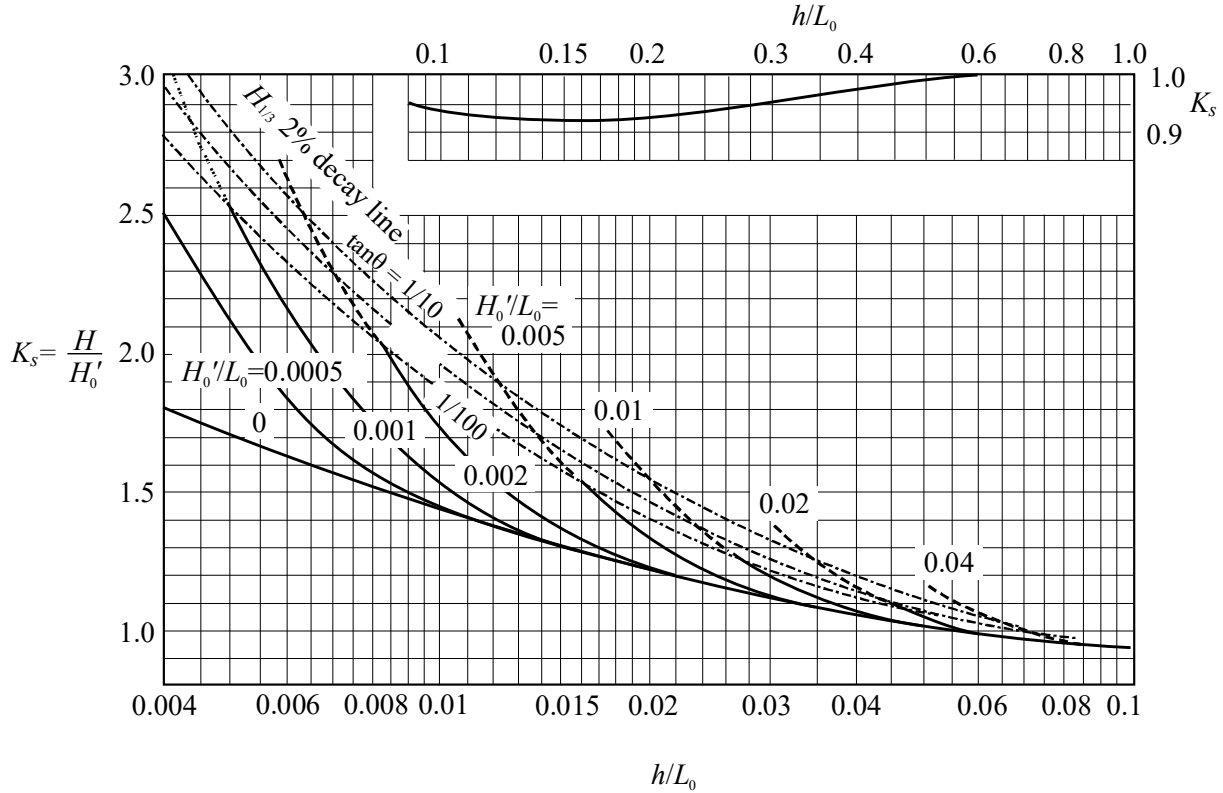


Fig. 4.4.12 Diagram for Evaluation of Shoaling Coefficient

4.4.6 Wave Breaking

- (1) At places where the water depth is shallower than three times the equivalent deepwater wave height, the changing of the wave height due to wave breaking needs to be considered. It is standard to consider the irregularity of waves when calculating the change in the wave height due to wave breaking.
- (2) After the height of waves has increased owing to shoaling, waves break at a certain water depth, and the wave height decreases rapidly. This phenomenon is called wave breaking. It is an important factor to be considered when determining the wave conditions exerting on coastal structures. For regular waves, the place at which waves break is always the same: this is referred to as the "wave breaking point." For random waves, the location of wave breaking depends on the height and period of individual waves, and wave breaking occurs over a certain distance (i.e., the "Surf Zone").
- (3) Limiting Breaking Wave Height for Regular Waves

Fig. 4.4.13 shows the limiting breaking wave height⁹¹⁾ for regular waves. This figure can be used to calculate the limiting breaking wave height in hydraulic model tests by using regular waves. The curves in the diagram can be approximated with **equation (4.4.7)**:

$$\frac{H_b}{L_0} = 0.17 \left[1 - \exp \left\{ -1.5 \frac{\pi h}{L_0} \left(1 + 15 \tan^{4/3} \theta \right) \right\} \right] \quad (4.4.7)$$

Where $\tan \theta$ denotes the seabed slope.

However, given that this approximation tends to give slightly higher breaking wave height at places where the seabed slope is steep, Goda⁹²⁾ reduced the constant concerning $\tan\theta$ from 15 to 11 and modified it as follows. This modification provides an up to 11% less breaker index value H_b/h_b when the seabed slope is 1/10, but it is restricted to 2% when the seabed slope is 1/50.

$$\frac{H_b}{L_0} = 0.17 \left[1 - \exp \left\{ -1.5 \frac{\pi h}{L_0} \left(1 + 11 \tan^{4/3} \theta \right) \right\} \right] \quad (4.4.8)$$

Fig. 4.4.13 shows the limiting wave height at the point of first wave breaking. At places where the water is shallow, the water depth increases owing to the wave setup caused by wave breaking (see **Part II, Chapter 2, 4.4.8 (1) Rise of Mean Water Level Due to Waves**). When estimating the limiting wave height in the surf zone, it is necessary to consider this increase in water level.

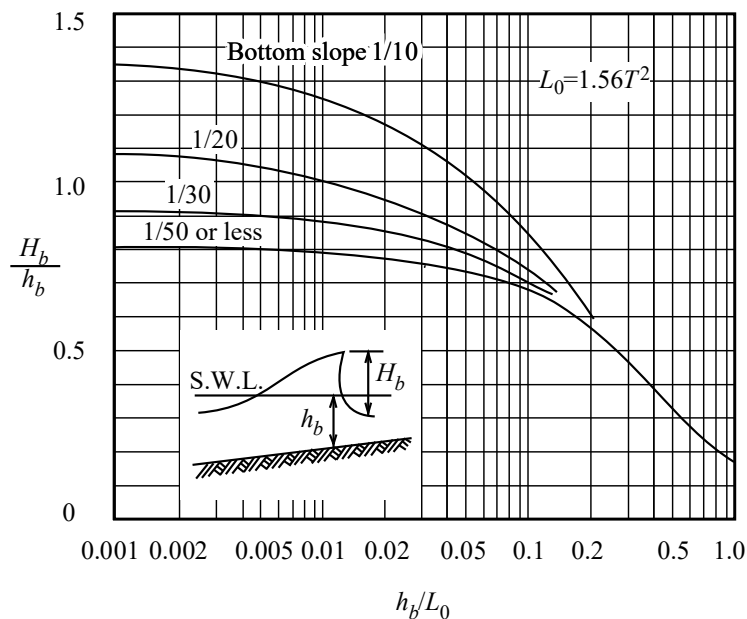


Fig. 4.4.13 Limiting Breaking Wave Height for Regular Waves⁹¹⁾

(4) Change in Wave Height due to Wave Breaking

The change in wave height due to wave breaking may be determined using **Figs. 4.4.14 (a)–(e)** or **Figs. 4.4.15 (a)–(e)**. These figures show the change of the wave height which Goda⁹³⁾ calculated by his theoretical model of random wave breaking. For the region to the right of the dash-dotted line on each diagram, the change of wave height is calculated using the shoaling coefficient (see **Part II, Chapter 2, 4.4.5 Wave Shoaling**). For the region to the left of this dash-dotted line, the change of wave height due to wave breaking dominates; therefore, the wave height must be determined using this diagram. For the seabed slope, it is appropriate to use the mean seabed slope over the region where the water depth to equivalent deepwater wave height ratio h/H_0' is in the range of 1.5 to 2.5.

Although the breaker index used in Goda's theoretical wave breaking model⁹³⁾ was modified to **equation (4.4.8)**, **Reference 94)** indicates that this does not necessitate the modifications of **Figs. 4.4.14 (a) to (e)** and **Figs. 4.4.15 (a) to (e)**.

(5) Scope of Application of Graphs of Wave Height Change

At places where the water depth is shallower than approximately one-half of the equivalent deepwater wave height, a major portion of wave energy is converted to the energy of flows rather than to that of water level changes. Therefore, when calculating the wave force acting on a structure in very shallow water, it is preferable to use the wave height at the location where the water depth is one-half of the equivalent deepwater wave height if the facilities in question are highly important. However, it is necessary to estimate the wave force acting on facilities constructed on land areas from the shoreline with another proposed equation.⁹⁵⁾

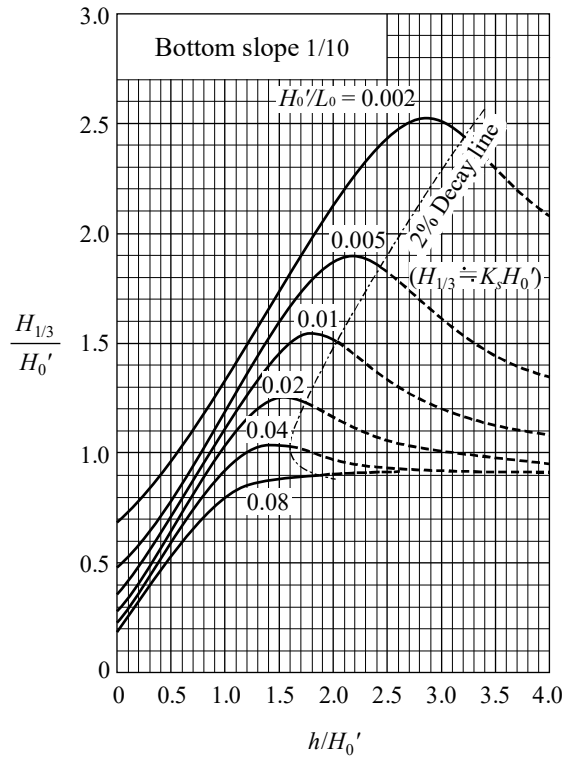


Fig. 4.4.14 (a) Diagram of Significant Wave Height in the Surf Zone for Seabed Slope of 1/10

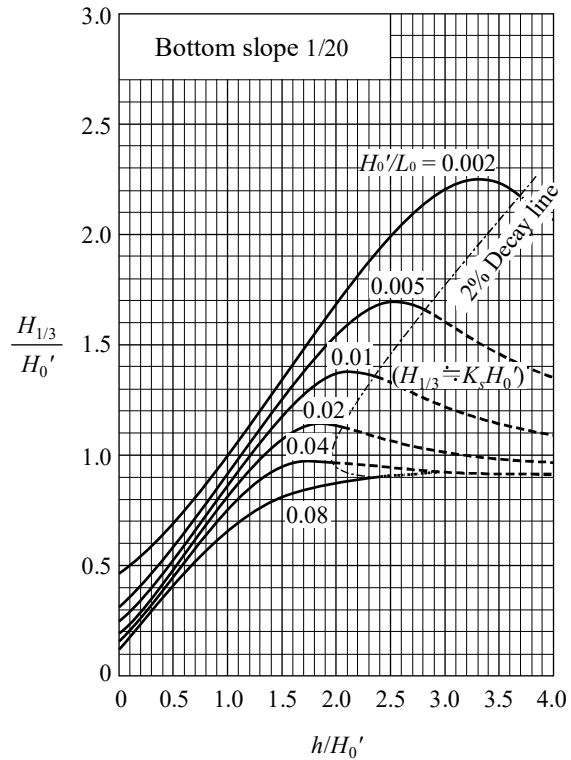


Fig. 4.4.14 (b) Diagram of Significant Wave Height in the Surf Zone for Seabed Slope of 1/20

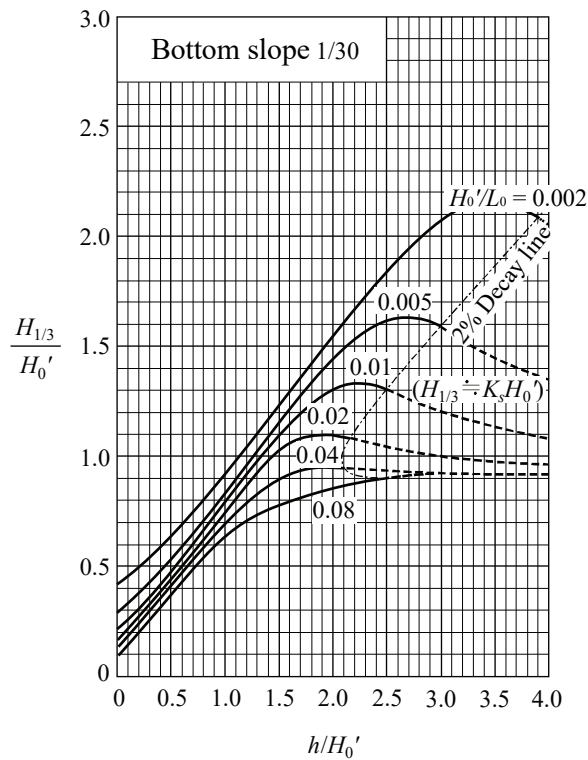


Fig. 4.4.14 (c) Diagram of Significant Wave Height in the Surf Zone for Seabed Slope of 1/30

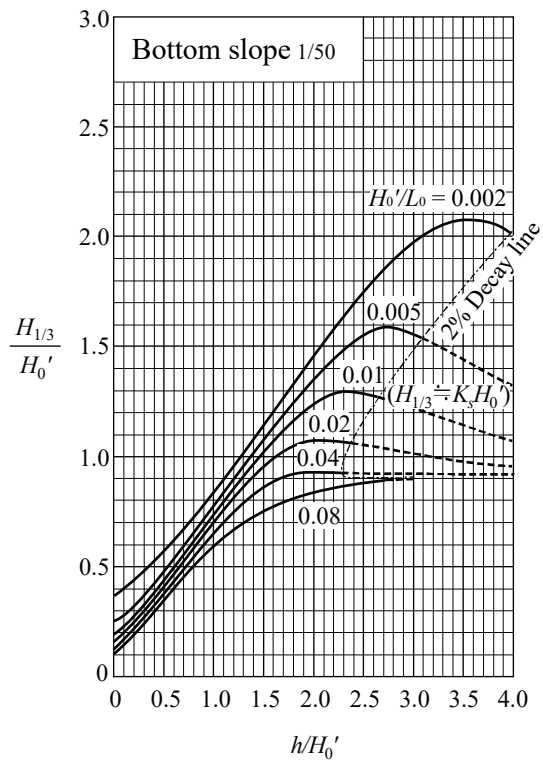


Fig. 4.4.14 (d) Diagram of Significant Wave Height in the Surf Zone for Seabed Slope of 1/50

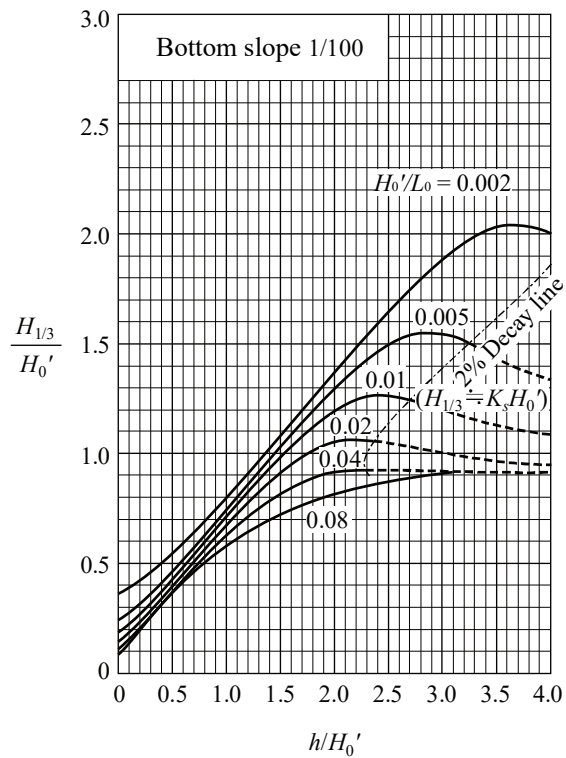


Fig. 4.4.14 (e) Diagram of Significant Wave Height in the Surf Zone for Seabed Slope of 1/100

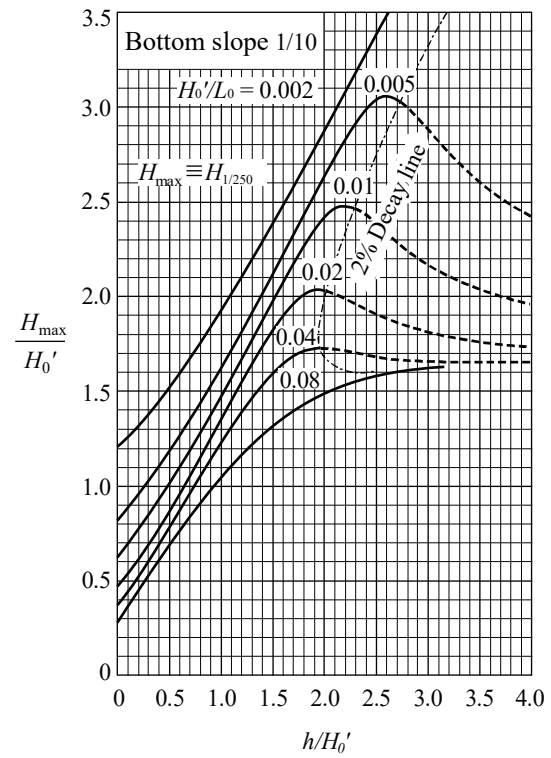


Fig. 4.4.15 (a) Diagram of Highest Wave Height in the Surf Zone for Seabed Slope of 1/10

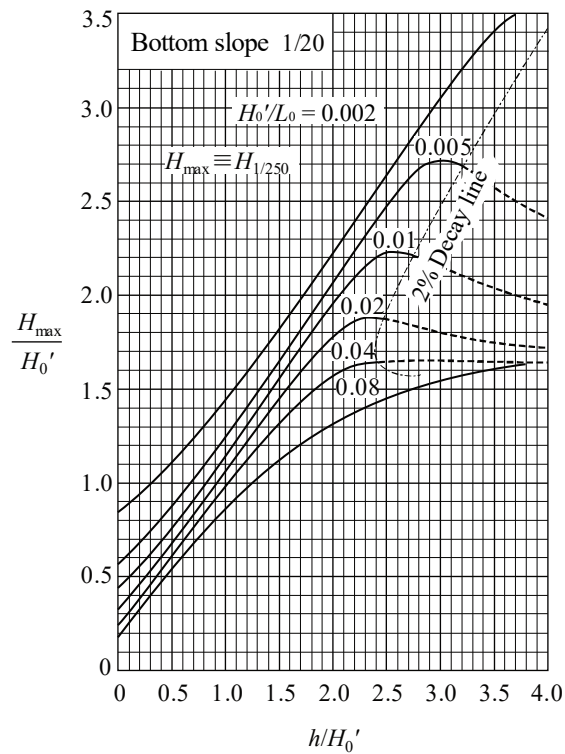


Fig. 4.4.15 (b) Diagram of Highest Wave Height in the Surf Zone for Seabed Slope of 1/20

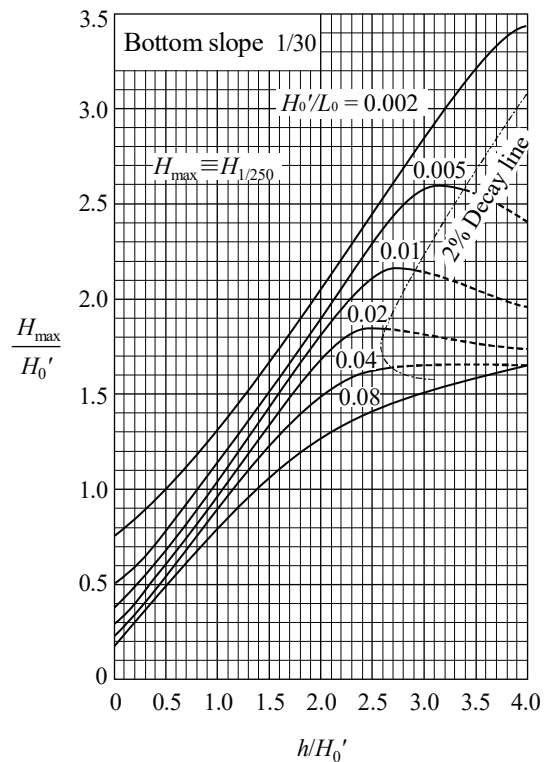


Fig. 4.4.15 (c) Diagram of Highest Wave Height in the Surf Zone for Seabed Slope of 1/30

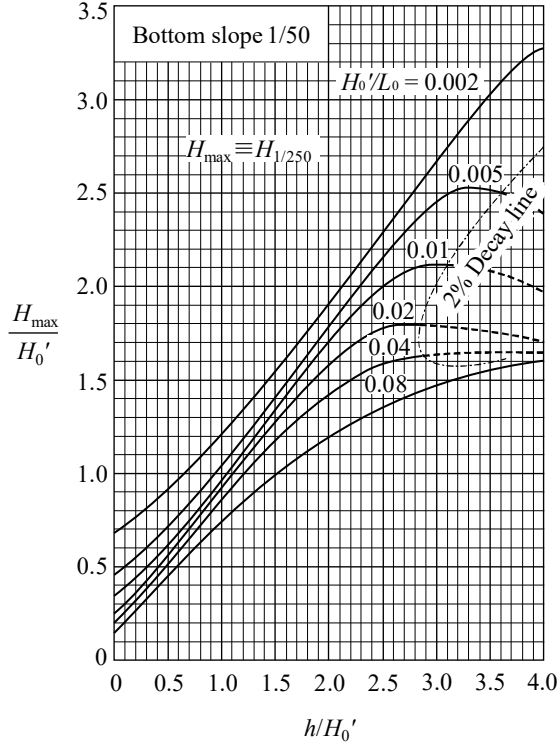


Fig. 4.4.15 (d) Diagram of Highest Wave Height in the Surf Zone for Seabed Slope of 1/50

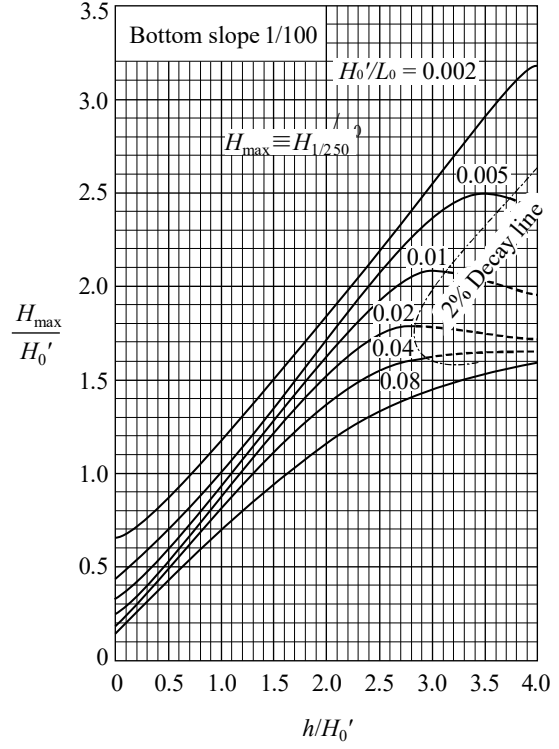


Fig. 4.4.15 (e) Diagram of Highest Wave Height in the Surf Zone for Seabed Slope of 1/100

(6) Approximate Calculation Formulas for Breaking Wave Height

The calculation of wave height changes based on a theoretical model for wave breaking generally requires the use of a computer. However, the wave breaking phenomenon is strongly affected by the individual wave height distribution of random waves and the condition of seabed topography. Therefore, considering the variability of the phenomenon and the overall accuracy, it is acceptable to calculate wave height changes by using the following simple formula in the case of a beach with constant seabed slope of approximately 1/10 to 1/75.⁹³⁾

The shoaling coefficient K_s is determined using **Fig. 4.4.12**, the operators $\min\{ \}$ and $\max\{ \}$ express the minimum and maximum value within the braces, respectively, and $\tan\theta$ is the seabed slope.

$$H_{1/3} = \begin{cases} K_s H_0' & (h/L_0 \geq 0.2) \\ \min\{(\beta_0 H_0' + \beta_1 h), \beta_{\max} H_0', K_s H_0'\} & (h/L_0 < 0.2) \end{cases} \quad (4.4.9)$$

where

$$\begin{aligned} \beta_0 &= 0.028(H_0'/L_0)^{-0.38} \exp[20 \tan^{1.5} \theta] \\ \beta_1 &= 0.52 \exp[4.2 \tan \theta] \\ \beta_{\max} &= \max\{0.92, 0.32(H_0'/L_0)^{-0.29} \exp[2.4 \tan \theta]\} \end{aligned} \quad (4.4.10)$$

Similarly, an approximate calculation formula for the highest wave height H_{\max} is given as follows:

$$H_{\max} = \begin{cases} 1.8 K_s H_0' & (h/L_0 \geq 0.2) \\ \min\{(\beta_0 H_0' + \beta_1 h), \beta_{\max} H_0', 1.8 K_s H_0'\} & (h/L_0 < 0.2) \end{cases} \quad (4.4.11)$$

where

$$\begin{aligned}\beta_0 &= 0.052(H_0'/L_0)^{-0.38} \exp[20 \tan^{1.5} \theta] \\ \beta_1 &= 0.63 \exp[3.8 \tan \theta] \\ \beta_{\max} &= \max\{1.65, 0.53(H_0'/L_0)^{-0.29} \exp[2.4 \tan \theta]\}\end{aligned}\quad (4.4.12)$$

(7) Diagram for Calculating Breaking Wave Height⁹³⁾

If the maximum value $(H_{1/3})_{\text{peak}}$ of the significant wave height in the surf zone is taken as a representative of the breaking wave height, the breaker index curve becomes to be shown in **Fig. 4.4.16**. If the water depth $(h_{1/3})_{\text{peak}}$ at which the significant wave height is a maximum is taken as representative of the breaker depth, the diagram for calculating the breaker depth becomes to be shown in **Fig. 4.4.17**.

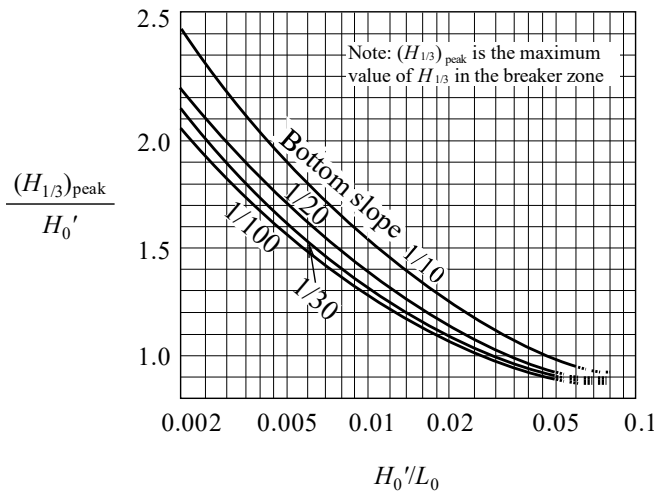


Fig. 4.4.16 Diagram of Maximum Value of the Significant Wave Height in the Surf Zone

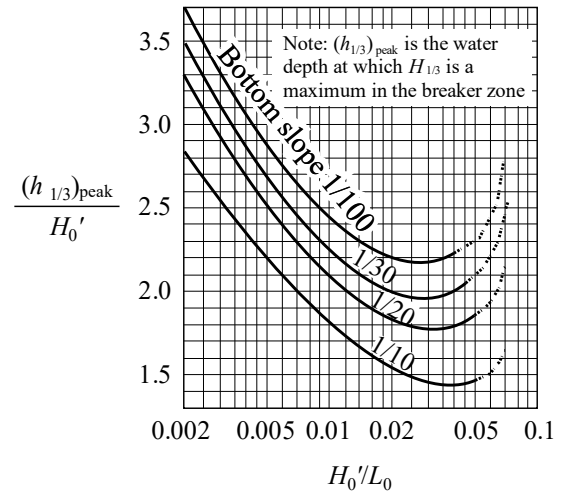


Fig. 4.4.17 Diagram of Water Depth at which the Maximum Value of the Significant Wave Height Occurs

(8) Change in Wave Height at Reef Coasts

At reef coasts where shallow water and a flat sea bottom continue over a long distance, the change in wave height cannot be calculated directly by using **Figs. 4.4.14 (a)–(e)** and **4.4.15 (a)–(e)**. Instead, the following empirical equation⁹⁶⁾ may be used:

$$\frac{H_x}{H_0'} = B \exp\left\{-A\left(\frac{x}{H_0'}\right)\right\} + \alpha \frac{h + \bar{\eta}_\infty}{H_0'} \quad (4.4.13)$$

where

H_0' : equivalent deepwater wave height

H_x : significant wave height at a distance x from the tip of the reef

h : water depth over the reef

$\bar{\eta}_\infty$: increase in the mean water level at a place sufficiently distant from the tip of the reef

Coefficients A and α are 0.05 and 0.33, respectively, according to the results of hydraulic model tests. However, it is advisable to use the following values that have been obtained from the data of field observations.⁹⁷⁾

$$\left. \begin{aligned} A &= 0.089 \frac{H_0'}{h + \bar{\eta}_\infty} + 0.015 \\ \alpha &= \begin{cases} 0.20 & (4m > H_0' \geq 2m) \\ 0.33 & (H_0' \geq 4m) \end{cases} \end{aligned} \right\} \quad (4.4.14)$$

For coefficient B , using the diagram corresponds to the seabed slope at the front of the reef from **Figs. 4.4.14 (a)–(e)**, the significant wave height $H_{1/3}$ at water depth h is $H_{x=0}$. B is obtained as follows:

$$B = \frac{H_{x=0}}{H_0'} - \alpha \frac{h + \bar{\eta}_\infty}{H_0'} \quad (4.4.15)$$

The term $(h + \bar{\eta}_\infty)/H_0'$ is given by

$$\frac{h + \bar{\eta}_\infty}{H_0'} = \sqrt{\frac{C_0}{1 + \frac{3}{8}\beta\alpha^2}} \quad (4.4.16)$$

Where $\beta = 0.56$.

From the continuity of the mean water level at the tip of the reef ($x = 0$), C_0 is given by

$$C_0 = \left(\frac{\bar{\eta}_{x=0} + h}{H_0'} \right)^2 + \frac{3}{8}\beta \left(\frac{H_{x=0}}{H_0'} \right)^2 \quad (4.4.17)$$

The term $\bar{\eta}_{x=0}$ represents the rise of mean water level at water depth h , which is controlled by the seabed slope in front of the reef. However, there are major localized variations in reef topography on actual coastlines. Wave height may increase behind circular reefs owing to the concentration due to the wave refraction; therefore, it is preferable to conduct model experiments by using multidirectional random waves wherever possible.²⁹⁾ See **Part II, Chapter 2, 4.4.8 Rise of Mean Water Level Due to Waves and Surf Beats** for more information on the concept of increased mean water level. The calculation method in the above has been derived under the assumption that the water depth h over the reef is small and that waves break over the reef. Therefore, it is not possible to apply the method when the water is deep and when wave breaking does not occur.

Considering the limiting breaking wave height criterion of a solitary wave, the highest wave height $H_{\max,x}$ at the distance x from the tip of the reef may be obtained as follows.

$$H_{\max,x} = \min \{ 0.78(h + \bar{\eta}_x), 1.8H_x \} \quad (4.4.18)$$

where $\min\{a,b\}$ is the smaller value of a or b , and $\bar{\eta}_x$ is the rise in the mean water level at the distance x and is given by the following equation:

$$\frac{\bar{\eta}_x + h}{H_0'} = \sqrt{C_0 - \frac{3}{8}\beta \left(\frac{H_x}{H_0'} \right)^2} \quad (4.4.19)$$

(9) Handling of wave breaking transformation in complicated seabed topography

In a topography where seabed slope abruptly changes, such as the bar trough topography, and water depth intricately changes, such as the actual coral reef, reef zone, and so on, the changes of wave height and their planar distribution can be obtained by using a numerical calculation model, which can directly calculate the wave breaking transformation of random waves. Goda⁹⁸⁾ proposed a phase-averaged type graded-wave breaking model that changes the wave breaking limit specified by water depth per the wave height of individual waves and indicated that a planar wave height distribution around an artificial reef can be calculated in a relatively short period. On the contrary, the Boussinesq model of time development type,⁹⁹⁾ which considers the wave height damping process by wave breaking, can calculate phenomena such as the rise of mean water level by waves and surf beat together with the planar wave breaking transformation on the complicated seabed topography.¹⁰⁰⁾

4.4.7 Wave Run-up Height, Wave Overtopping and Transmitted Waves

(1) Wave run-up height

- ① Wave run-up needs to be calculated appropriately by taking into account the configuration and location of the seawall and the sea bottom topography.
- ② The phenomenon of wave run-up is dependent upon a whole variety of factors, such as wave characteristics, configuration and location of the seawall, and sea bottom topography; therefore, the run-up height varies in a complex way. Therefore, when the seawall and sea bottom are complex in form, it is preferable to confirm wave run-up heights by performing hydraulic model tests. It is important to consider that calculation diagrams or equations for regular waves proposed on the basis of the results of past research for restricted conditions are the mean values in experiments indicating significant dispersion. Moreover, it must be noted that the frequency of random waves exceeding the crown height set against the regular wave run-up height is high, and approximately half of the waves exceed this crown height in extreme cases even without considering the dispersion in experimental values. The report¹⁰¹⁾ indicates that the run-up height of regular wave with the significant wave height corresponds to $R_{50\%}$ (i.e., the value averaged the wave run-up height with 50% of the number of incident waves) of random waves if the performance of the structural crown height is verified by using significant waves. When conducting the performance verification of sloping revetments, it is preferable to set the crown elevation of the revetment to be higher than the run-up height for regular waves. Therefore, the crown height of seawall, revetment, or others should not only be determined by wave run-up height but also by wave overtopping quantity (see **Part II, Chapter 2, 4.4.7 (2) Wave Overtopping Quantity**) should be considered. It is preferable to determine the ultimate crown height and the revetment form to prevent the wave overtopping quantity from exceeding the threshold value.
- ③ The results presented by Mase¹⁰²⁾ are simple, and the scope of application is wide for the wave run-up height of random waves to a uniform slope.

$$\frac{R_x}{H_0'} = a\xi^b, \quad \frac{1}{30} \leq \tan \beta < \frac{1}{5} \quad \text{and} \quad 0.007 \leq \frac{H_0}{L_0} \quad (4.4.20)$$

Here, x , a , and b stand for the coefficients of the statistical values and calculated values of the wave run-up height and are provided as follows.

Table 4.4.2 Coefficients of equation (4.4.20)

R_x	R_{\max}	$R_{2\%}$	$R_{1/10}$	$R_{1/3}$	\bar{R}
a	2.32	1.86	1.70	1.38	0.88
b	0.77	0.71	0.71	0.70	0.69

Here, R_{\max} is the maximum value of the wave run-up height. $R_{2\%}$ is the value at which the wave run-up height calculated in an experiment exceeds 2%. $R_{1/10}$, $R_{1/3}$, and \bar{R} are the 1/10 maximum wave run-up height, 1/3 maximum wave run-up height, and mean value, respectively, which can be calculated by the same method as the case in which random waves are statistically analyzed. ξ is called the surf similarity parameter and is defined as $\xi = \tan \theta / \sqrt{H_0' / L_0}$, where $\tan \theta$ is the seabed slope, and H_0' / L_0 is the wave steepness of offshore waves.

It is possible to employ the following equation, which has been verified to accord well with experimental results, for the 1/3 maximum wave run-up height.¹⁰³⁾

$$\begin{aligned} R_{1/3} / H_s &= 0.25 + 1.1\xi & (0 < \xi \leq 2.2) \\ R_{1/3} / H_s &= 3.0 - 0.15\xi & (2.2 < \xi \leq 9.0) \\ R_{1/3} / H_s &= 1.65 & (9.0 < \xi) \end{aligned} \quad (4.4.21)$$

- ④ For the wave run-up height of random waves of a rubble slope, the equation of Van der Meer-Stam¹⁰⁴⁾ can be used.

$$\frac{R_x}{H_s} = a \xi_m \quad (\xi_m \leq 1.5)$$

$$\frac{R_x}{H_s} = b \xi_m^c \quad (\xi_m > 1.5)$$
(4.4.22)

Here, the coefficient is shown in the following table. Furthermore, in $\xi_m = \tan \theta / \sqrt{2\pi H_s / g T_m^2}$, H_s is the significant wave height at the water depth at the foot of a seawall (water depth at the foot of a slope), and T_m is the mean wave period.

Table 4.4.3 Coefficients of equation (4.4.22)

R_x	R_{\max}	$R_{2\%}$	$R_{1/10}$	$R_{1/3}$	\bar{R}
a	1.12	0.96	0.77	0.72	0.47
b	1.34	1.17	0.94	0.88	0.60
c	0.55	0.46	0.42	0.41	0.34
d	2.58	1.97	1.45	1.35	0.82

The following equation is proposed for the wave run-up height of a slope that has permeability.

$$\frac{R_x}{H_s} = d$$
(4.4.23)

- ⑤ In the case of complex cross sections, the virtual slope method of Saville¹⁰⁵⁾ and the modified virtual slope method of Nakamura¹⁰⁶⁾ may be used for regular waves.

A "complex cross section" refers to the case where the sea bottom topography and the configuration and location of the seawall are shown in **Fig. 4.4.18**, where S.W.L. (Sea Water Level) denotes the still-water level.

- (a) When the cross section can be considered complex, the run-up height of the seawall is obtained as follows (refer to **Fig. 4.4.18**).
- 1) Wave breaking point B is determined from the offshore wave characteristics.
 - 2) Thereafter, the wave run-up height R (maximum run-up height from the S.W.L.) is assumed, and point A is set at the maximum run-up point. Points A and B are joined by a straight line, and the gradient of this line yields the virtual gradient $\cot \alpha$.
 - 3) The wave run-up height for this virtual gradient is calculated using **Fig. 4.4.19**, and the calculated height is compared with the initially assumed run-up height. If the two do not agree, a new run-up height (i.e., virtual gradient) is assumed, and the estimations are repeated. This iterative process is repeated until convergence is achieved.
 - 4) The value obtained is taken as the run-up height for the complex cross section in question.

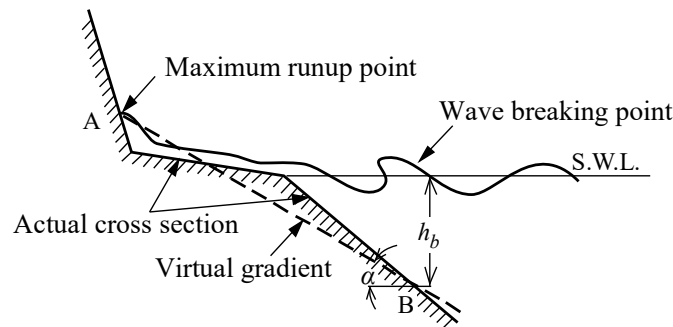


Fig. 4.4.18 Complex Cross Section and Virtual Gradient

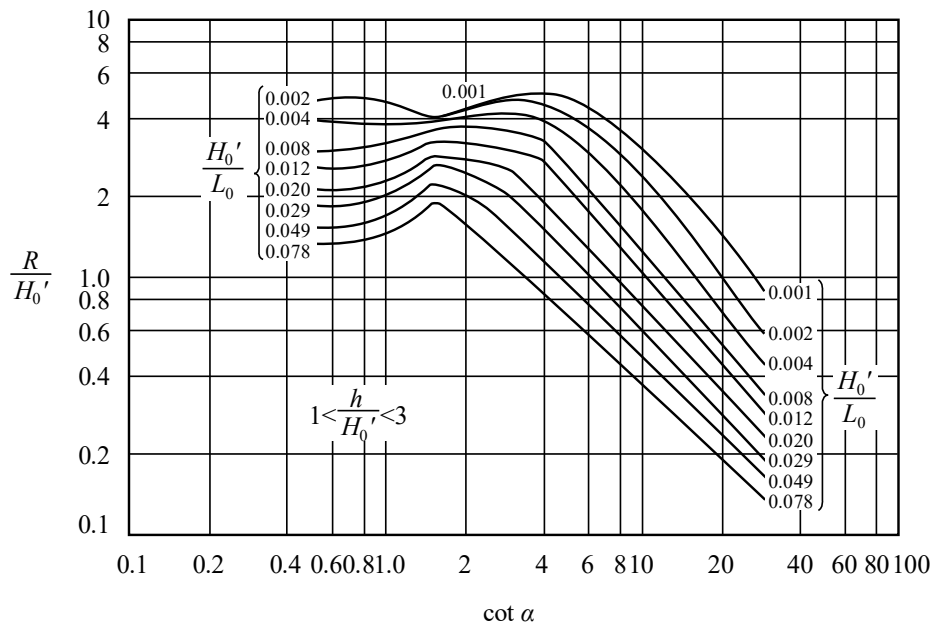


Fig. 4.4.19 Run-up Height on a Slope

- (b) When the results obtained from this method are compared with the actual experimental results for a complex cross section, it is generally found that there is a good agreement between the two, with the error usually being not more than 10%. However, if the seabed slope is too gentle, the agreement between the two becomes poor; therefore, this method should only be used when the seabed slope is steeper than 1/30.
- (c) Fig. 4.4.20 shows the experimental results¹⁰⁷⁾ obtained for a seabed slope of 1/70. This figure provides a useful reference when estimating the wave run-up height for a complex cross section with a gentle seabed slope.

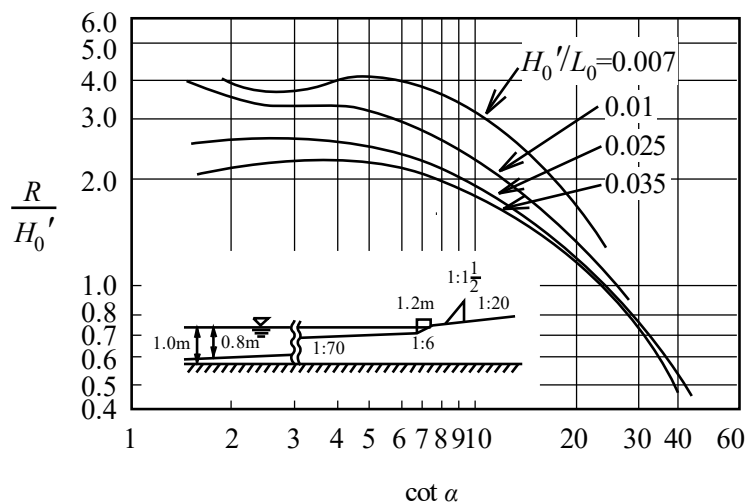


Fig. 4.4.20 Run-Up Height on Seawall Located Closer to Land than Wave Breaking Point

On the contrary, the wave run-up height of random waves for a complex cross section can be calculated with the following equation,¹⁰¹⁾ which was proposed by arranging the experimental data following the concept of modified virtual slope method¹⁰⁶⁾ in the range satisfying $0 < \xi' < 6.0$, $0.009 < H_0'/L_0 < 0.06$ and $-0.37 < h_t/H_0' < 0.53$.

$$\begin{aligned}
 R_{2\%}/H_0' &= 2.99 - 2.73 \exp(-0.57\xi') \\
 R_{1/10}/H_0' &= 2.72 - 2.56 \exp(-0.58\xi') \quad \text{where} \quad \xi' = \frac{\tan \alpha}{\sqrt{H_0'/L_0}} \\
 R_{1/3}/H_0' &= 2.17 - 2.18 \exp(-0.70\xi')
 \end{aligned} \tag{4.4.24}$$

Here, $\tan \alpha$ is the virtual slope ($\tan \alpha = 0.5 (h_b + R)^2/A$) determined by area A of the actual cross section between two points, namely, wave run-up height R and breaker depth h_b ; h_t is the water depth at the foot of a slope. Moreover, **Fig. 4.4.17** can be used in the calculation of the breaker depth used for the setting of wave breaking points in the range of $1/30 < \tan \theta < 1/10$ ($\tan \theta$ is the seabed slope) and $0.02 < H_0'/L_0 < 0.05$.

⑥ Oblique Wave Incidence¹⁰⁸⁾

Fig. 4.4.21 shows the relationship between the incident angle coefficient K_β and the angle β . Here, β is the angle between the wave crest line of the incident waves and the face line of the seawall, and the incident angle coefficient K_β is the ratio of the run-up height for angle β to the run-up height when the waves are normally incident (i.e., when $\beta = 0$). This figure can be used to estimate the effect of wave incident angle on the run-up height in case of regular waves.

⑦ Effects of Wave-dissipating Work

The wave run-up height can be significantly reduced when the front of a seawall is completely covered with wave-dissipating blocks. **Fig. 4.4.22** shows an example for regular waves. However, the effect of the blocks varies greatly according to the way in which they are laid. Therefore, in general, it is preferable to determine the run-up height by means of hydraulic model tests.

⑧ Use of Super Roller Flume for Computer Aided Design of Maritime Structure

It is possible to use CADMAS-SURF, which is also used for wave-resistant design and the like, to perform a numerical simulation in calculating the run-up height on a slope. The calculation method and its applicability for the run-up height of regular waves on a uniform slope³¹⁾ or an arbitrary slope¹⁰⁹⁾ has been identified by the study group on the application of CADMAS-SURF in wave-resistant design. Here, the special grid size for differential simulation should be determined carefully because it directly affects the accuracy of the calculation and the computation time, which have a trade-off relationship¹¹⁰⁾. Moreover, Sakuraba et al.¹¹¹⁾ proposed a numerical calculation method that uses unstructured spatial grid and examined its applicability.

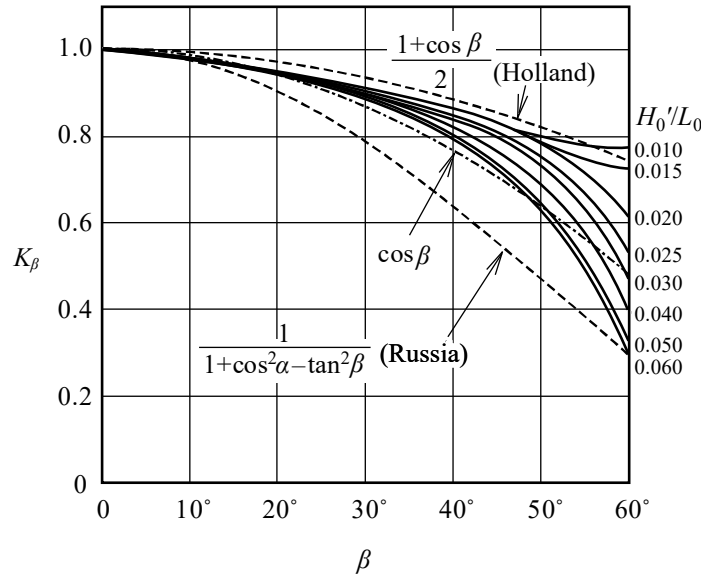


Fig. 4.4.21 Relationship between Wave Incident Angle and Run-Up Height
(Solid Lines: Experimental Values by Public Works Research Institute, Ministry of Construction)

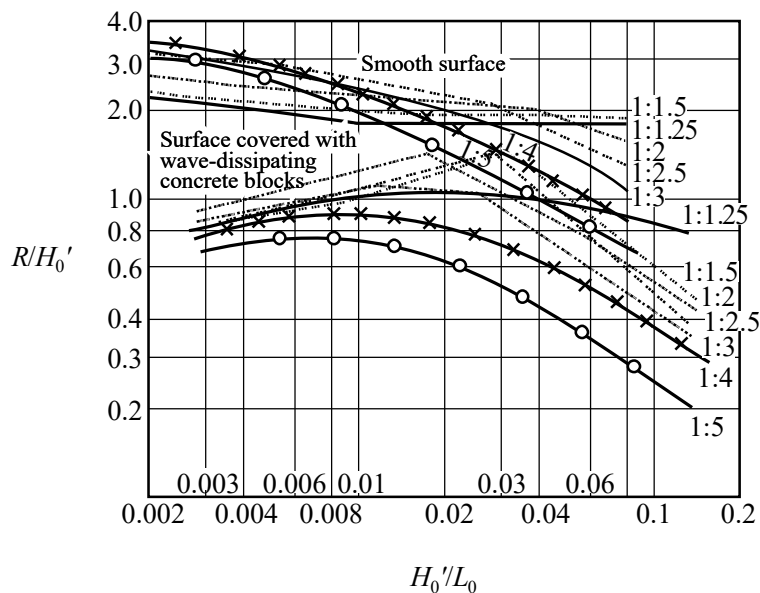


Fig. 4.4.22 Reduction in Wave Run-up Height Due to Wave-dissipating Work²⁰⁸⁾

(2) Wave Overtopping Quantity

- ① The "wave overtopping quantity" is the total volume of overtopped water. The "wave overtopping rate" is the average volume of water overtopping in a unit time; it is obtained by dividing the wave overtopping quantity by the time duration of measurement. The wave overtopping quantity and wave overtopping rate are generally expressed per unit width.
- ② For structures for which the wave overtopping quantity is an important performance verification factor, the wave overtopping quantity must be calculated by considering the irregularity of waves using hydraulic model tests or by using data from hydraulic model tests performed in the past. If the front sea bottom topography is complex, the revetment wave overtopping rate may be estimated¹¹²⁾ by using the equivalent deepwater wave height which is calculated by estimating the wave transformation to obtain the progressive wave height at the front surface of the revetment. In the wave transformation calculation by using the Boussinesq model, the reproduction of the inundation process behind the revetment was also tried¹¹³⁾ by calculating the planar distribution and its temporal variation of the wave overtopping rate by using the overflow formula. Moreover, the wave overtopping rate can be calculated for the revetment of slightly complicated cross-sectional shape by using CADMAS-SURF (the Super Roller Flume for Computer Aided Design of Maritime Structure)¹¹⁴⁾, although its application range is restricted to the vicinity of revetments from the viewpoint of calculation capacity. However, it is preferable to conduct sufficient calibration for calculation model, spatial grid setting, and so on, e.g., examination of the accuracy of calculation in advance by performing reproduction calculation against the results of experiments in this case.
- ③ If the wave overtopping quantity is large, not only will there be damage to the seawall body itself but also damage by flooding to the roads, houses, and/or port facilities behind the levee or seawall even though the levee or seawall is intended to protect them. There is further a risk of drowning or injury to users of water frontage amenity-oriented facilities. When verifying performance, it is necessary to set the wave overtopping rate so that it is equal to or less than the permissible wave overtopping rate that has been determined in line with the characteristics of structures and the situation with regard to their usage. Furthermore, when estimating the wave overtopping quantity by means of experiments, it is preferable to consider changes in tidal water level, i.e., to perform experiments for different water levels.
- ④ **Estimation diagram of wave overtopping rate¹¹⁵⁾**

For an upright or wave-dissipating type seawall that has a simple form (i.e., does not have a toe protection mound or a crown parapet), the wave overtopping rate may be estimated using Figs. 4.4.23 to 4.4.26. These diagrams have been drawn on the basis of experiments employing random waves. From the results of a comparison between the experiments and field observations, it is thought that the accuracy of the curves giving the wave overtopping rate is within the range listed in Table 4.4.4. The wave overtopping rate for the

wave-dissipating type seawall has been obtained under the condition that the upper armor layer at the crown consists of two rows of wave-dissipating concrete blocks.

Table 4.4.4 Estimated Range for the Actual Wave Overtopping Rate relative to the Estimated Value

$q/\sqrt{2g(H_0')^3}$	Upright seawall	Wave-dissipating type seawall
10^{-2}	0.7–1.5 times	0.5–2 times
10^{-3}	0.4–2 times	0.2–3 times
10^{-4}	0.2–3 times	0.1–5 times
10^{-5}	0.1–5 times	0.05–10 times

Note that when obtaining rough estimates for the wave overtopping rate for random waves using **Figs. 4.4.23 to 4.4.26**, the following should be considered:

- If the actual values of the seabed slope and the deepwater wave steepness do not match any of the values on the diagram, the diagram for which the values most closely match should be used or interpolation should be performed.
- The wave-dissipating concrete blocks in the figures are made up of two layers of tetrapods (upper armor layer at the crown consists of two rows). Even if the same kind of wave-dissipating concrete block is used, if there are differences in the crown width, in the placing way, or in the form of the toe, then there is a risk that the actual wave overtopping rate may considerably differ from the value obtained by the diagrams, as the different wave-dissipating block is used.
- If the number of rows of concrete blocks at the crown is increased, the wave overtopping quantity tends to decrease¹¹⁶⁾.
- When there are difficulties in applying the diagrams for estimating the wave overtopping rate, the approximate equation of Takayama et al.¹¹⁷⁾ may be used.

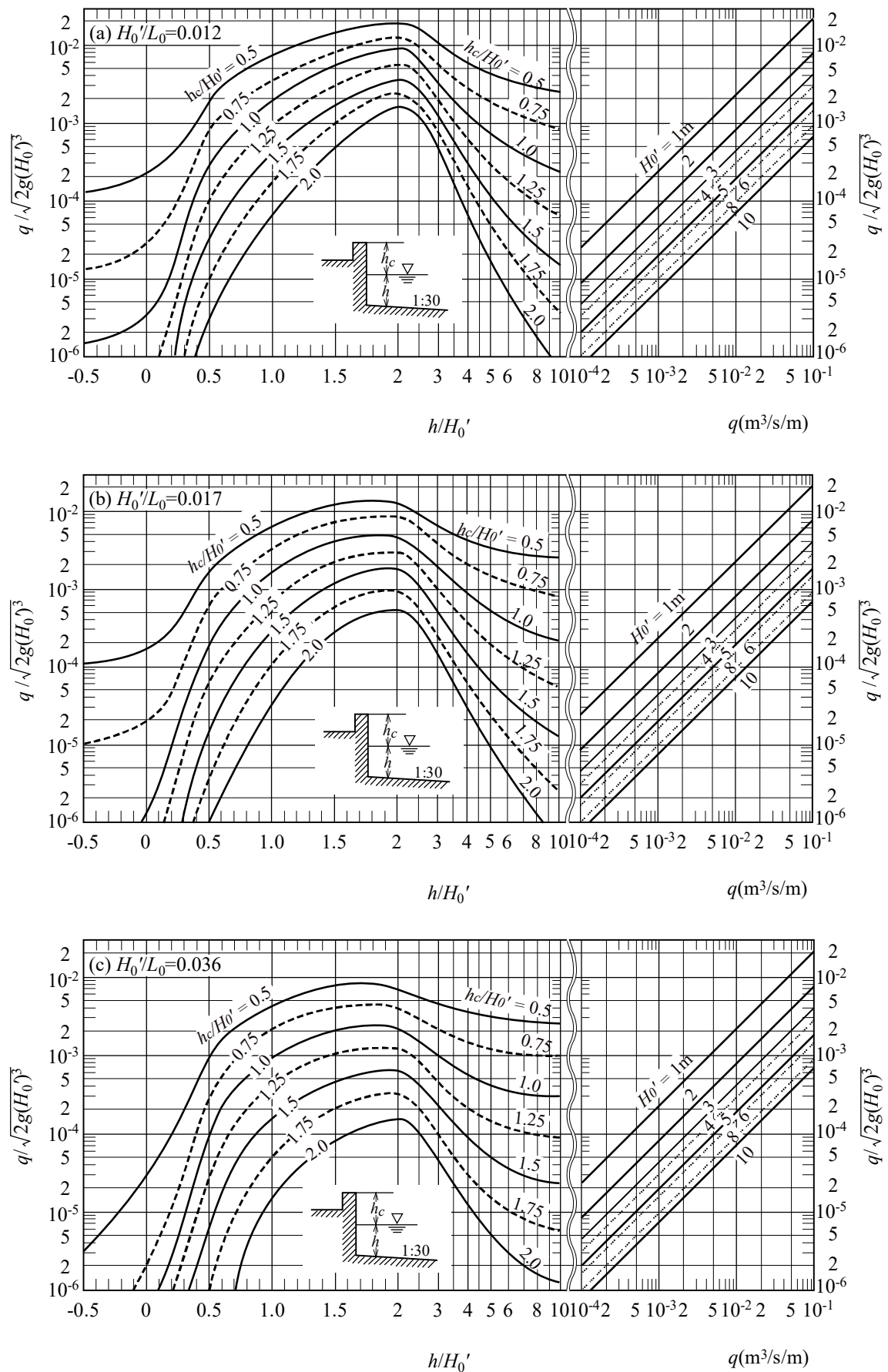


Fig. 4.4.23 Diagrams for Estimating Wave Overtopping Rate for Upright Seawall (Seabed Slope 1/30)

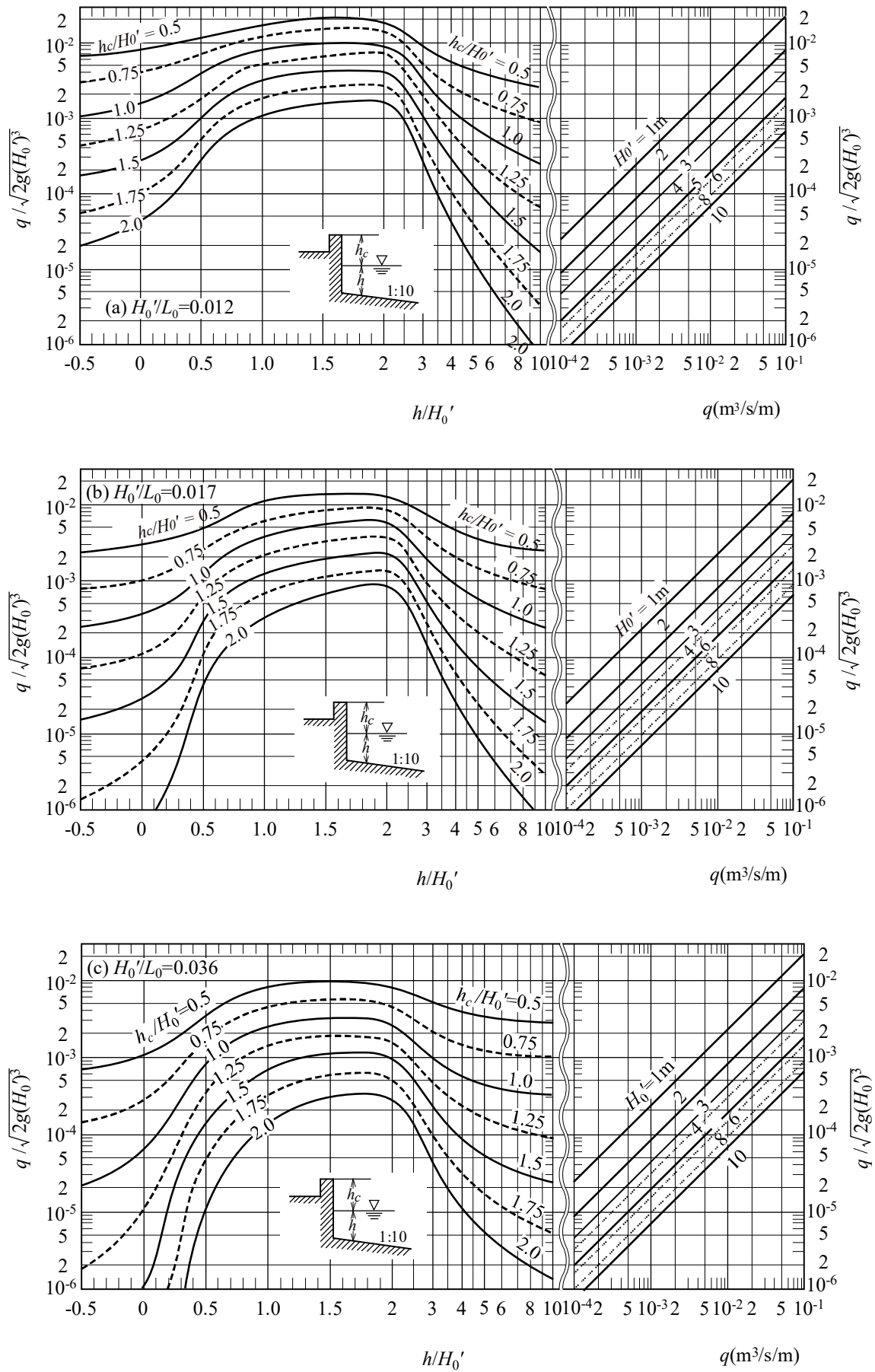


Fig. 4.4.24 Diagrams for Estimating Wave Overtopping Rate for Upright Seawall (Seabed Slope 1/10)

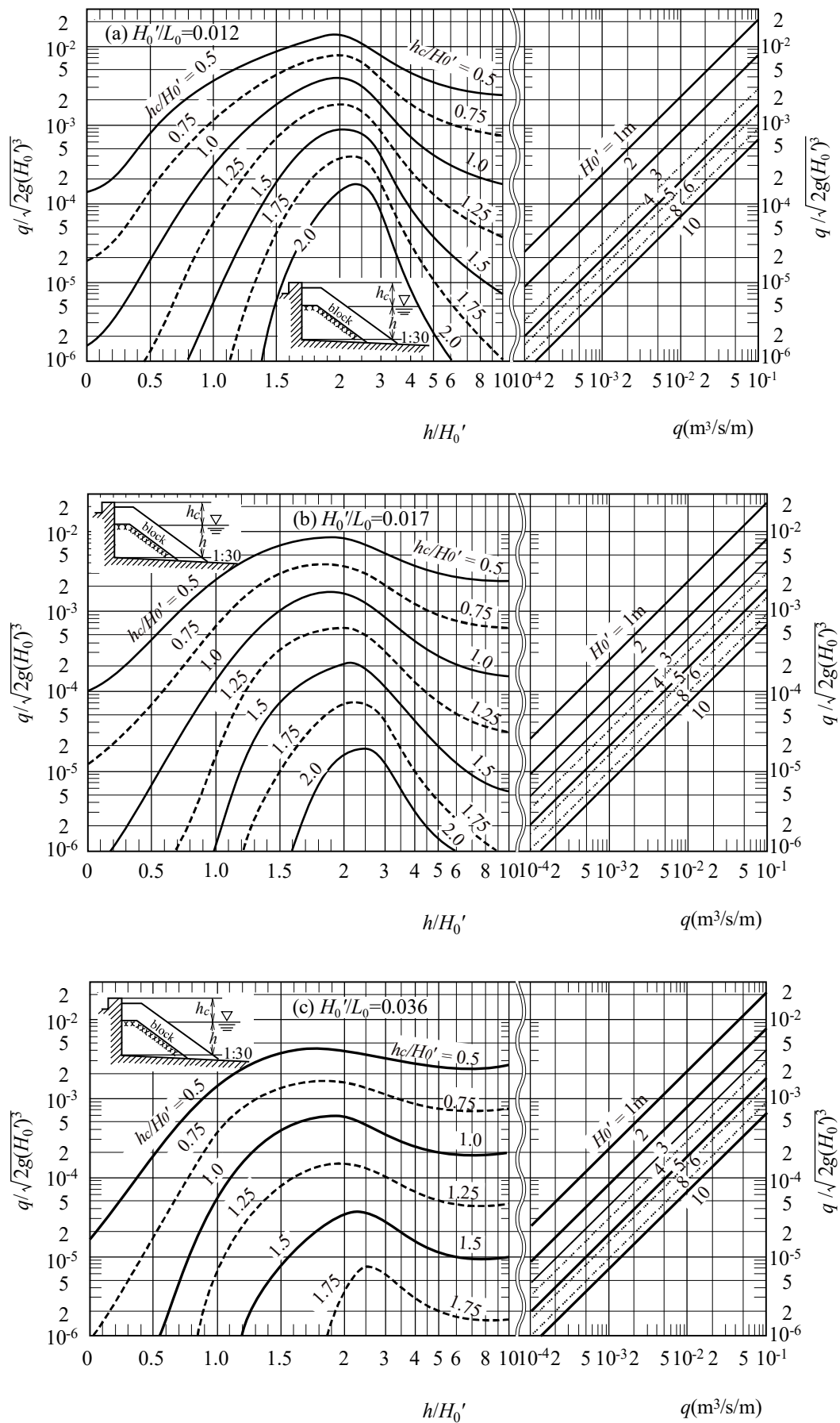


Fig. 4.4.25 Diagrams for Estimating Wave Overtopping Rate for Wave-dissipating Type Seawall (Seabed Slope 1/30)

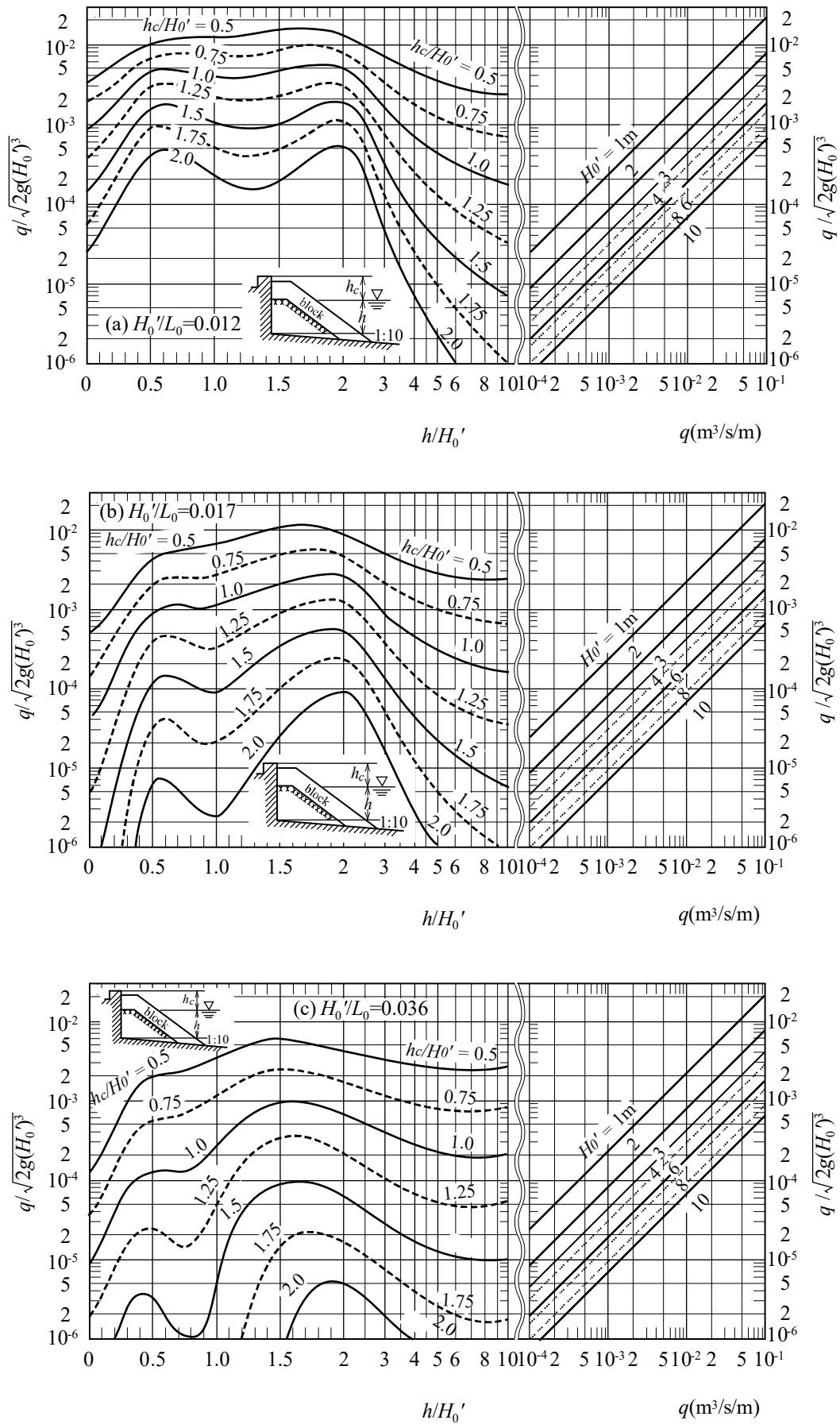


Fig. 4.4.26 Diagrams for Estimating Wave Overtopping Rate for Wave-dissipating Type Seawall (Seabed Slope 1/10)

⑤ Equivalent Crown Height Coefficient

The equivalent crown height coefficient can be used as a guideline when setting the wave overtopping rate for a seawall upon which wave-dissipating concrete blocks are laid or for a wave-dissipating type seawall with vertical slits. The equivalent crown height coefficient is the ratio of the height of the seawall in question to the height of an imaginary upright seawall that results in the same wave overtopping quantity, where the conditions in terms of waves and the sea bottom topography are taken to be the same for the both cases. If the equivalent crown height coefficient is less than 1.0, the crown of the seawall under study can be lowered below that of an upright seawall and still provide the same wave overtopping quantity; in other words, the seawall under study has a form that is effective in reducing the wave overtopping rate. Below are the reference values for the equivalent crown height coefficient β for typical types of seawalls.

Wave-dissipating block-type seawall ¹¹⁷⁾	:	$\beta = 0.9-0.7$
Vertical-slit type wave-dissipating seawall ¹¹⁷⁾	:	$\beta = 0.6$
Parapet retreating type seawall ¹¹⁶⁾	:	$\beta = 1.0-0.5$
Stepped seawall ¹¹⁶⁾	:	$\beta = 1.7-1.0$
When the waves are obliquely incident ^{118) 119)}	:	$\beta = \begin{cases} 1 - \sin^2 \theta & \theta \leq 30^\circ \\ 1 - \sin^2 30^\circ = 0.75 & \theta > 30^\circ \end{cases}$

(θ is the angle of incidence of the waves; it is 0° when the waves are incident perpendicular to the seawall face line)

⑥ Wave Overtopping Quantity on the Revetments Installed on Reefs

On a long reef topography, waves propagating on the reef are newly reproduced after the waves that broke at the tip of the reef were sufficiently damped. The wave overtopping rate over revetments on the reef where these waves act may be calculated by using the diagrams for estimating the wave overtopping rate ¹¹⁵⁾ or the approximate calculation for wave overtopping rate¹¹⁷⁾ against the design tidal level by considering the risen mean water level owing to waves and surf beat (see **Part II, Chapter 2, 4.4.8 Rise of Mean Water Level due to Waves and Surf Beats**). Here, the equivalent deepwater wave height is conveniently calculated by dividing the front wave height (see **Part II, Chapter 2, 4.4.6 (8) Change in Wave Height at Reef Coasts in this chapter**) of the revetment above the reef by the shoaling coefficient considering that the wave reproduction point as offshore. However, if the shape of the reef is not uniform in the direction of shore, it is preferable to calculate the wave transformation by using the Boussinesq model in order to consider the refraction and diffraction at the reef cliff, deviation of water level on the reef, and the planar distribution of surf beat¹¹²⁾.

⑦ Wave Overtopping Quantity of Sloping Revetments

The calculation diagram made by Tamada et al.¹²⁰⁾ can be used to calculate the wave overtopping rate at a sloping revetment that has a waterside slope of 30% (1:3) or more. For 30% slope, 50% slope, and 70% slope, this calculation diagram comprises four combinations: seabed slope of 1/10 and 1/30 and offshore wave steepness of 0.017 and 0.036. The wave overtopping rate of 30% slope revetments tends to be larger than the upright revetments, but it is smaller than the upright revetments in 50% slope revetments for the wind waves of wave steepness 0.036. The wave overtopping rate of 70% slope revetments is smaller than the upright revetments in every case. The wave overtopping rate decreases as the waterside slope becomes mild because the wave run-up height is proportional to the gradient of a slope (see **Part II, Chapter 2, 4.4.7 (1) Wave run-up height in this chapter**).

⑧ Relations between the Wave Run-up Height and the Wave Overtopping Quantity

Tamada et al.¹²¹⁾ and Mase et al.¹²²⁾ proposed a wave overtopping rate calculation equation to link the wave run-up and wave overtopping and named it IFORM. The wave overtopping rate for complex cross-sectional seawalls and revetments near the shoreline (including onshore part) can be calculated using the following equation by considering the random wave run-up height.

$$\frac{q}{\sqrt{gH_0'^3}} = \begin{cases} C \left[0.018 \left(\frac{R_{\max}}{H_0'} \right)^{1.5} \left\{ 1 - \left(\frac{R_c}{H_0'} \right) / \left(\frac{R_{\max}}{H_0'} \right) \right\}^{6.240} \right] & \text{for } 0 \leq R_c \leq R_{\max} \\ 0 & \text{for } R_{\max} \leq R_c \end{cases} \quad (4.4.25)$$

Here, R_c is the crown height of seawalls and revetments, and R_{\max} is the 99% probable maximum wave run-up height. Moreover, R_{\max} is expressed as $R_{\max} = 1.54R_{2\%}$ by using the $R_{2\%}$ calculated by **equation (4.4.24)** when the number of run-up waves is $N = 100$. Moreover, C is a parameter that is concerned with the waterside slope $\cot \gamma$ of a revetment (for example, $\cot \gamma = 2$ denotes a 20% slope revetment) and is given by the following equation.

$$\begin{cases} C = 0.25 \cot \gamma + 0.5 & \text{for } 0 \leq \cot \gamma < 2 \\ C = 1 & \text{for } \cot \gamma \geq 2 \end{cases} \quad (4.4.26)$$

Tamada et al.¹²³⁾ verified the applicability of IFORM by using a CLASH data set¹²⁴⁾ that aggregates the wave overtopping quantity experimental data all over the world, and found that the estimation accuracy of the wave overtopping rate is ensured by IFORM for sloping revetments and upright revetments when the ratio of water depth at the foot of a seawall (water depth at the foot of a slope) h_t to the wave heights h_t/H_0' is less than 3.0 and when the seabed slope $\tan \theta > 1/100$. Consequently, they reported that IFORM covers the installation conditions of many seashore revetments in Japan.

The CLASH dataset was referred to in the EurOtop Wave Overtopping Quantity Evaluation Manual¹²⁵⁾ published in July 2007 by the cooperation of England, Holland, and Germany and greatly contributes to the description of the wave overtopping rate estimation equation for sloping revetments and upright revetments. However, these estimation equations parameterize the significant wave height in front of the seawall, which is different from the wave overtopping rate calculation method in Japan that uses the equivalent deepwater wave height. On the contrary, Goda¹²⁶⁾ extracted and analyzed the wave overtopping quantity data for upright revetments and impermeable smooth slopes among the CLASH data sets and proposed a wave overtopping rate estimation equation, which can treat the wave overtopping quantity of upright revetments, sloping revetments, and wave-absorbing revetments uniformly by calculating the significant wave height in front of the revetments using the approximated wave height calculation equation⁹³⁾ in a surf zone.

⑨ Effects of Parapet

Parapet on a revetment is effective in reducing wave overtopping. **Reference 127)** can be referred for wave overtopping of sloping dikes with parapet. However, since the upward force acts on the wall body of parapet depending on the condition of waves and parapet structures, this upward force needs to be fully taken into consideration in examination of stability of a wall body.

⑩ Wave Overtopping of Multidirectional Random Waves

In waters where the multidirectionality of waves is well clarified, the wave overtopping rate may be corrected in accordance with S_{\max} , as in **Reference 119)**.

⑪ Permissible Wave Overtopping Rate

The permissible wave overtopping rate depends on factors such as the structural type of the seawall, the situation with regard to land usage behind the seawall, and the capacity of drainage facilities; therefore it needs to be set appropriately depending on the situations. Although it is impossible to give one standard value for the permissible wave overtopping rate, Goda¹²⁸⁾ gave the values for the threshold rate of wave overtopping for inducing damage (**Table 4.4.5**) on the basis of the past cases of disasters. Furthermore, Fukuda et al.¹²⁹⁾ gave the values shown in **Table 4.4.6**, and Allsop et al.¹³⁰⁾ and Kimura et al.¹³¹⁾ gave the values shown in **Table 4.4.7** as values for the permissible wave overtopping rate in view of the land usage behind the seawall. Furthermore, Nagai and Takada¹³²⁾ have considered the degree of importance of the facilities behind the seawall and have come up with the values for the permissible wave overtopping rate (**Table 4.4.8**) by using the results of experiments with regular waves. Suzuki et al.¹³³⁾ proposed $0.01 \text{ m}^3/\text{s}/\text{m}$ as the permissible wave overtopping rate for amenity-oriented revetment. When conducting the performance verification, these must be set appropriately by considering the importance of the facilities and the capacity of drainage facilities.

CADMAS-SURF³¹⁾ or flooding analysis models, such as those that use the MARS method,¹³⁴⁾ can be used when calculating wave overtopping precisely with the inclusion of items, such as the permeability of the soil behind the seawall and the characteristics of wave-dissipating work configurations.

Table 4.4.5 Threshold Rate of Wave Overtopping for Inducing Damage

Type	Armor Layer	Wave Overtopping Rate (m ³ /s/m)
Seawall	Paved behind	0.2
	Not paved behind	0.05
Levee	Covered with concrete on three sides	0.05
	Crown paving/rear slope non constructed	0.02
	Crown not paved	0.005 or less

Table 4.4.6 Permissible Wave Overtopping Rate in View of the Usage Condition of Hinterland (1)

User	Distance from dike	Wave overtopping rate (m ³ /s/m)
Pedestrian	Land right in back (50% degree of safety)	2×10^{-4}
	Land right in back (90% degree of safety)	3×10^{-5}
Automobile	Land right in back (50% degree of safety)	2×10^{-5}
	Land right in back (90% degree of safety)	1×10^{-6}
House	Land right in back (50% degree of safety)	7×10^{-5}
	Land right in back (90% degree of safety)	1×10^{-6}

Table 4.4.7 Permissible Wave Overtopping Rate in View of the Usage Condition of Hinterland (2)

User	Condition	Wave overtopping flow rate (m ³ /s/m)
Pedestrian	• Those who are paying attention to wave overtopping	10^{-4}
	• Those who are paying no attention	3×10^{-5}
Automobile	• Stopping or driving at low speed	0.01 to 0.05
	• Normal driving, damage to vehicles	1.1×10^{-5}
Building	• Structural damage	3×10^{-5}
	• Damage to joinery	10^{-6} to 3×10^{-5}
	• No damage	10^{-6}

Table 4.4.8 Permissible Wave Overtopping Rate in View of the Degree of Importance of Hinterland (m³/s/m)

Districts where significant damage is expected, particularly because of the invasion of wave overtopping and spray due to a dense concentration of residential houses and public facilities in the rear.	Around 0. 01
Other important districts	Around 0. 02
Other districts	0. 02–0. 06

Table 4.4.6 is a table created with the results where people who watch a wave overtopping observation video make a judgment and indicate a wave overtopping rate that at least that percentage of people judged safe. Moreover, **Table 4.4.7** does not indicate the values measured in the field but was estimated in the hydraulic model experiment after the occurrence of damages or by using the wave overtopping rate estimation diagram. Therefore, they were possibly affected by the model scale and care should be taken that much more wave overtopping rate might have been experienced in the field.

⑫ Effect of Winds on the Wave Overtopping Quantity

In general, winds have a relatively large effect on small wave overtopping quantity, although there is a lot of variation. However, the relative effect of winds decreases as the wave overtopping rate increases. **Fig. 4.4.27**¹²⁹⁾ shows the results of an investigation on the wind effect on wave overtopping quantity based on field

observations. The abscissa shows the spatial gradient of the horizontal distribution of the wave overtopping quantity, whereas the ordinate shows the wave overtopping quantity per unit area. As seen from the figure, when the wave overtopping quantity is small, a larger wind velocity corresponds to a smaller spatial gradient of the horizontal distribution of the wave overtopping quantity. When the wave overtopping quantity is large, the spatial gradient of the horizontal distribution of the wave overtopping quantity increases. This shows that when the wave overtopping quantity is small, the distance over which a mass of water splashes is strongly affected by the wind velocity, with a larger distance at a higher wind velocity; however, when the wave overtopping quantity is large, the difference in the splash distance becomes small. Moreover, Yamashiro et al.¹³⁵⁾ rearranged the data at that time, added a wind tunnel water tank experiment, made a regression equation of the wind velocity effect, and reported that it was appropriate that the model wind velocity should be approximately 1/3 of the field wind velocity when reproducing the effect of wind in the wind tunnel water tank.

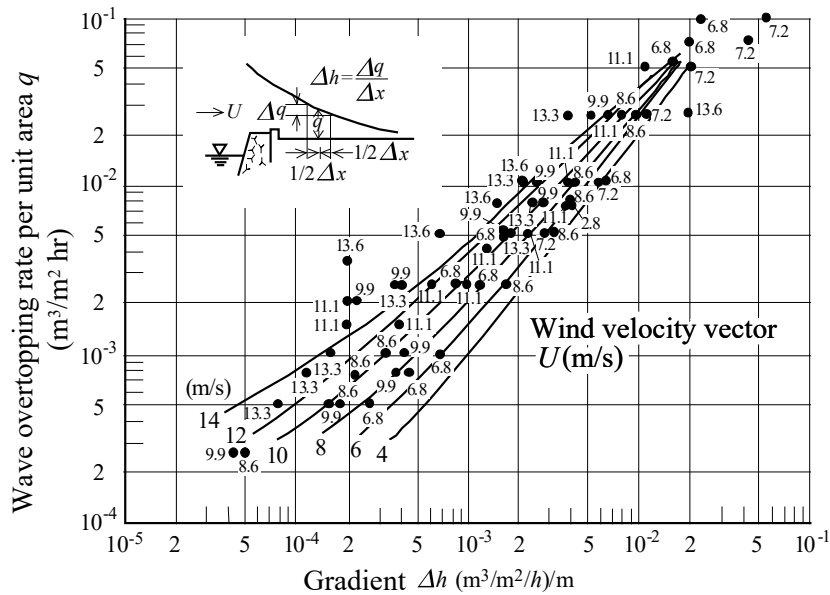


Fig. 4.4.27 Wind Effect on the Spatial Gradient of Horizontal Distribution of Wave Overtopping Quantity¹²⁹⁾

(3) Transmitted Wave Height

- ① The height of waves transmitted behind a breakwater by overtopping and/or permeation via the breakwater or the foundation mound of breakwater are calculated by referring to either the results of hydraulic model tests or the past data.
- ② It is necessary to appropriately estimate the transmitted wave height after waves have overtopped and/or passed through a breakwater because the transmitted waves affect the wave height distribution behind the breakwater. Transmitted waves include waves that have overtopped and/or overflowed, as well as waves that have permeated through a permeable rubble-mound breakwater or a foundation mound of composite breakwater. The latter in particular is sometimes referred to as permeated waves. Recently, several breakwaters have been built with caissons, which are originally not permeable, with through-holes to enhance the exchange of the seawater in a harbor. In this case, it is necessary to examine the wave coefficient of wave transmission (wave permeation) because the coefficient serves as an indicator of the efficiency of the exchange of seawater.
- ③ Coefficient of Wave Transmission to Inside of the Port at Breakwater

(a) **Fig. 4.4.28**¹³⁶⁾ may be used to calculate the height of waves that are transmitted into a harbor when they overtop a composite breakwater or permeate through a foundation mound. Even when the waves are random, the coefficient of wave transmission agrees pretty well with that shown in **Fig. 4.4.28**. It has also been shown that **Fig. 4.4.28** is valid not only for the significant wave height but also for the highest one-tenth wave height and the mean wave height.¹³⁷⁾ The period of the transmitted waves drops to approximately 50% to 80% of the corresponding incident wave period in both the significant wave and mean wave.¹³⁷⁾ On the contrary, when wave overtopping transmitted waves dominate compared with waves permeating through a foundation mound, there is an example where an approximate value of coefficient of transmission was estimated using the wave overtopping rate on the breakwater crown.¹³⁸⁾

Moreover, there is a trial to calculate the overtopping transmitted waves behind the breakwater at the same time in wave transformation calculation for the targeting ports and harbors.¹³⁹⁾ Furthermore, Matsumoto¹⁴⁰⁾ indicated that CADMAS-SURF (the Super Roller Flume for Computer Aided Design of Maritime Structure) can be applied to the calculation of wave overtopping transmitted waves.

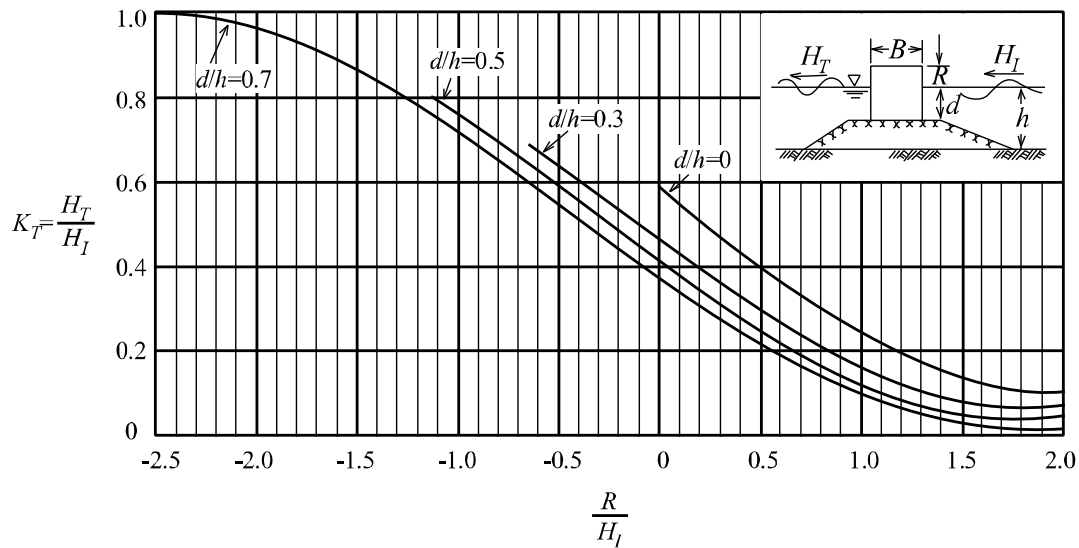


Fig. 4.4.28 Diagram for Calculating Coefficient of Wave Height Transmission¹³⁶⁾

- (b) The transmitted wave height for breakwater covered with wave-dissipating blocks was experimented by Kondo and Sato¹⁴¹⁾ and Tanimoto and Oosato¹⁴²⁾. Moreover, Sakamoto et al.¹⁴³⁾ experimented the wave-dissipating block-type sloping breakwater.
- (c) A submerged breakwater is usually made by piling up crushed rock to form a mound and covers the surface with concrete blocks to prevent underlayers from sucking out. For wave transmission on a submerged breakwater of crushed rock, a diagram¹⁴⁴⁾ showing the relationship between the crown height of the breakwater and the coefficient of wave permeation is available.

④ Coefficient of Wave Permeation at Breakwaters

- (a) For a porous and permeable structure, such as a rubble-mound breakwater or a deformed wave-dissipating concrete block-type breakwater, the theoretical analysis of Kondo and Takeda¹⁴⁵⁾ may be used as a reference. The following empirical equation may be used to obtain the coefficient of wave permeation of a typical structure.

$$\text{Stone breakwater }^{146)} : K_T = 1 / (1 + k_t \sqrt{H/L})^2 \quad (4.4.27)$$

where

$$k_t : \text{in the case of rubble-mound breakwater } k_t = 1.26 \left(\frac{B}{d_t} \right)^{0.67},$$

$$\text{in the case of deformed block-type breakwater } k_t = 1.184 \left(\frac{B}{d_t} \right)^{0.895}$$

B : crown width of the structure

d_t : nominal diameter of rubble or height of deformed block

H : height of incident waves

L : wavelength of incident waves

- (b) For a curtain wall-type breakwater, the theoretical solutions of Morihira et al.¹⁴⁷⁾ may be used.

- (c) For the coefficient of the wave transmission of an upright wave-dissipating breakwater of permeable type that has slits in both the front and rear walls, the experimental results are available.¹⁴⁸⁾
- (d) Types of breakwater aiming to promote the exchange of seawater include multiple-wing-type permeable breakwaters, multiple-vertical-cylinder breakwaters, horizontal-plate-type permeable breakwaters, and pipe-type permeable breakwaters. The coefficient of wave permeations of these types of breakwater is obtained.¹⁴⁸⁾

4.4.8 Rise of Mean Water Level due to Waves and Surf Beats

(1) Wave Setup

- ① When constructing structures within the surf zone, it is preferable to consider the phenomenon of wave setup as necessary, which occurs in the surf zone owing to wave breaking as they approach the coast.

② Rise of the mean water level due to breaking waves

The phenomenon where the mean water level near the shoreline rises due to breaking waves (i.e., "wave set up") was known long ago via observations at the seashore and so on, but theoretical proof about the causes for the occurrence of this phenomenon has been lacking. In 1962, Longuet-Higgins and Stewart¹⁴⁹⁾ indicated that when a series of waves whose wave height varies approach the shore, this becomes the conveyance of a large momentum at the places where the wave height is large, and it becomes smaller at places wherein the wave height is small; therefore, apparent stress ends up being generated, and the mean water level changes. This apparent stress was called the radiation stress. This radiation stress is an amount proportionate to the square of the wave height and is an amount with the same order as the energy of a wave.

③ Radiation Stress

With the introduction of the concept of radiation stress, the change in the mean water level can be explained as follows.

When a wave approaching from offshore reaches shallow waters, the wave height increases owing to shallow water deformation as the water depth becomes shallower. When the wave height becomes larger, the conveyance of momentum becomes larger, and the mean water level begins to decrease (wave set down).

When the wave approaches the place where the water is even shallower, it breaks due to the wave height corresponding to the seabed slope and water depth. The wave height is suddenly diminished, the sudden decline of this wave height causes the conveyance of momentum to decrease suddenly, and the mean water level rises. The rise in the mean water level in the vicinity of the shoreline is viewed as a typical example of a phenomenon caused by such radiation stress.

④ Diagrams for Estimating the Amount of Wave Setup

Fig. 4.4.29 and **Fig. 4.4.30** show the changes in the mean water level by random wave breaking on the seabed slopes of 1/100 and 1/10, as calculated by Goda⁹³⁾. A smaller wave steepness (H_0'/L_0) corresponds to a faster and larger rise in mean water level. Furthermore, a larger seabed slope corresponds to a larger rise in water level. **Fig. 4.4.31** shows the rise of mean water level at the shoreline. A smaller the wave steepness and steeper seabed slope leads to a larger rise of mean water level. When H_0'/L_0 is 0.01–0.05, with the exception of a very steep seabed slope, the rise of mean water level near the shoreline is 0.1–0.15 H_0' , where H_0' is the equivalent deepwater wave height and L_0 is the wavelength of the deepwater wave. **Fig. 4.4.32** is a diagram for estimating the amount of wave setup that has been newly proposed by taking the directional wave spectrum into account. The values are slightly smaller than the values in **Fig. 4.4.31**, where the wave steepness is small.¹⁵⁰⁾

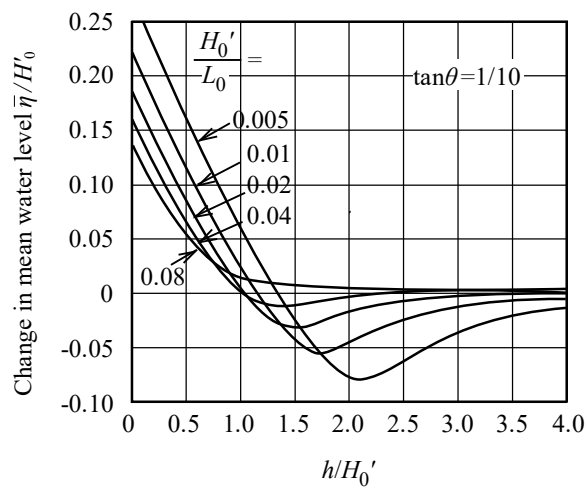


Fig. 4.4.29 Change in Mean Water Level
(Seabed Slope 1/10)

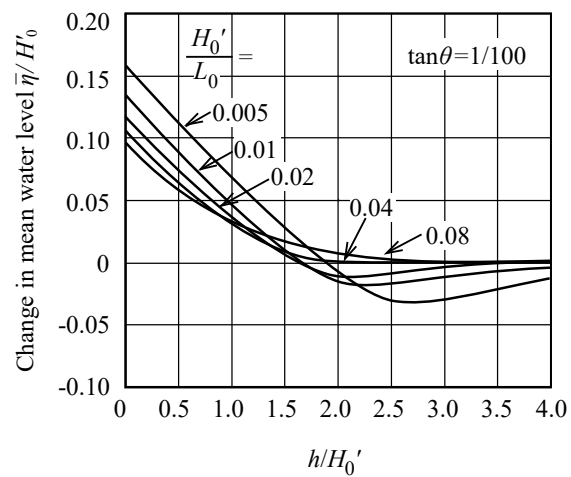


Fig. 4.4.30 Change in Mean Water Level
(Seabed Slope 1/100)

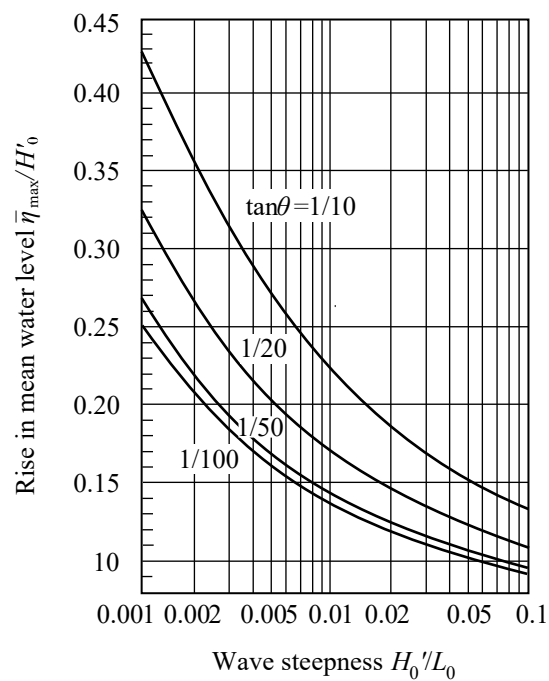


Fig. 4.4.31 Rise in Mean Water Level at Shoreline

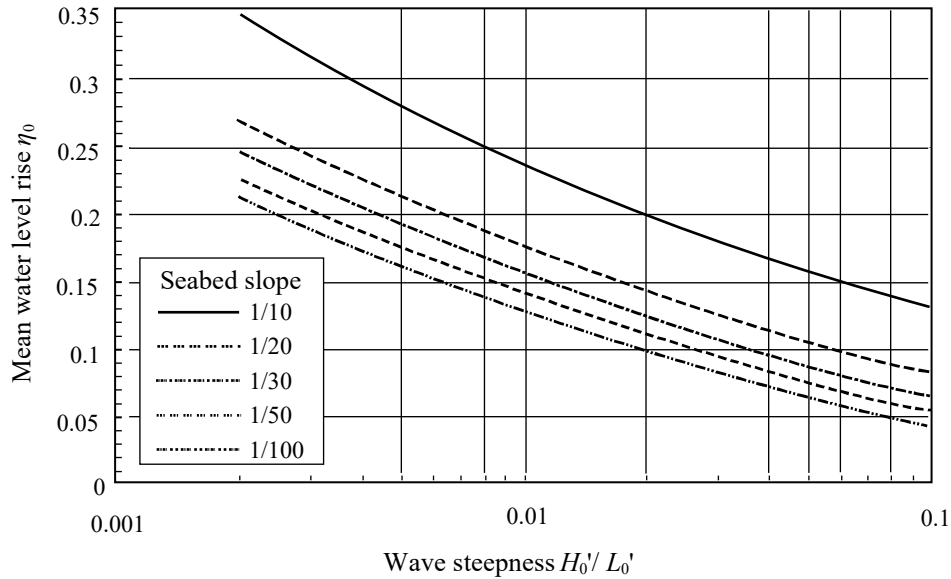


Fig. 4.4.32 Diagram of Water Level Rise at Shoreline considering the Multidirectionality of Waves

⑤ Consideration of the rise in mean water level in the performance verification

Given that the wave breaking point moves and that the breaking wave height becomes larger, owing to the rise of the mean water level, it is important to consider the rise in mean water level in performing an accurate computation of the design wave height in shallow waters.

(2) Surf Beats

- ① Surf beat with a period of one to several minutes, which occurs along with wave transformation in shallow waters, shall be examined as necessary in cases such as when using a numerical calculation model, which does not theoretically consider it, and when phenomenon exceeding what is implied by the calculation diagram based on the results of experiments.
- ② Random water level fluctuations lasting one to several minutes in the vicinity of the shoreline are called surf beat, and this has a major effect on the run-up height of waves, wave overtopping, and stability of beaches at the beach. The size of the surf beat should be estimated using either the approximation formulas of Goda⁹³⁾ or on-site observations.

③ Goda's Formulas for Estimating Surf Beat Amplitude

On the basis of the results of field observations of surf beat, Goda⁹³⁾ has proposed the following relationship:

$$\zeta_{rms} = \frac{0.04(\eta_{rms})_0}{\sqrt{\frac{H_0'}{L_0} \left(1 + \frac{h}{H_0'}\right)}} = \frac{0.01H_0'}{\sqrt{\frac{H_0'}{L_0} \left(1 + \frac{h}{H_0'}\right)}} \quad (4.4.28)$$

where

ζ_{rms} : root mean square amplitude of the surf beat wave profile

$(\eta_{rms})_0$: root mean square amplitude of the deepwater wave profile

H_0' : equivalent deepwater wave height

L_0 : wavelength in deepwater

H : water depth

This equation shows that the amplitude of the surf beat is proportional to the equivalent deepwater wave height, that it falls as the water depth increases, and that it increases as the deepwater wave steepness (H_0'/L_0)

decreases. **Fig. 4.4.33** shows an example of the surf beat observation by Goda. **Fig. 4.4.34** compares **equation (4.4.28)** with the observation values.

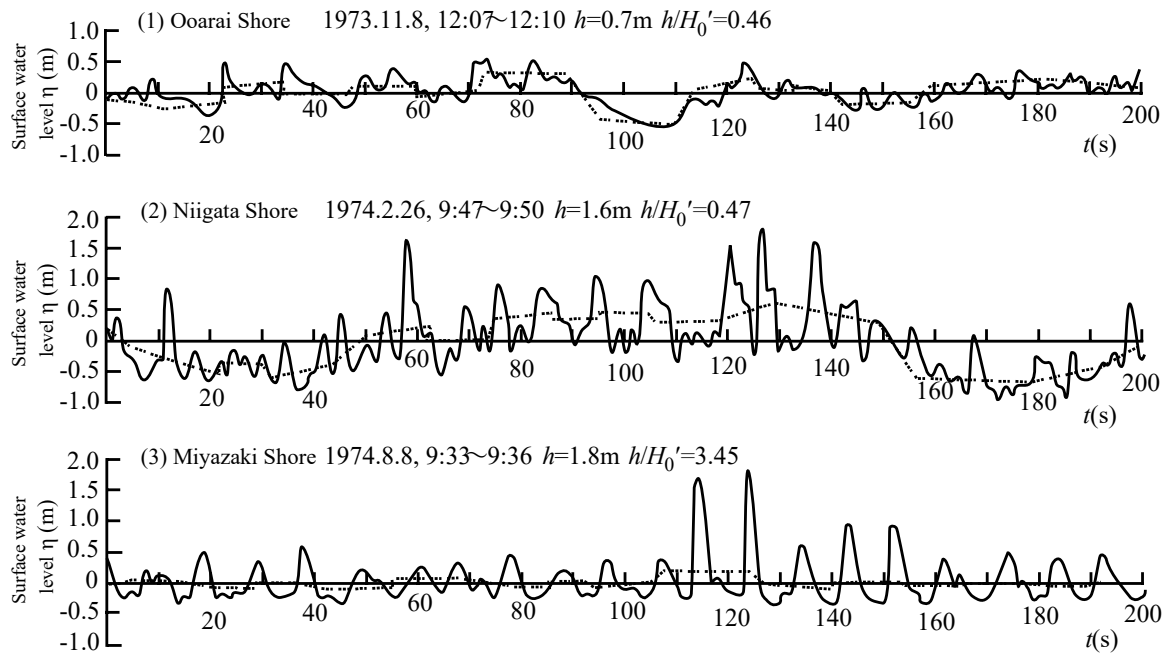


Fig. 4.4.33 Example of Waves and Surf Beats at Shores

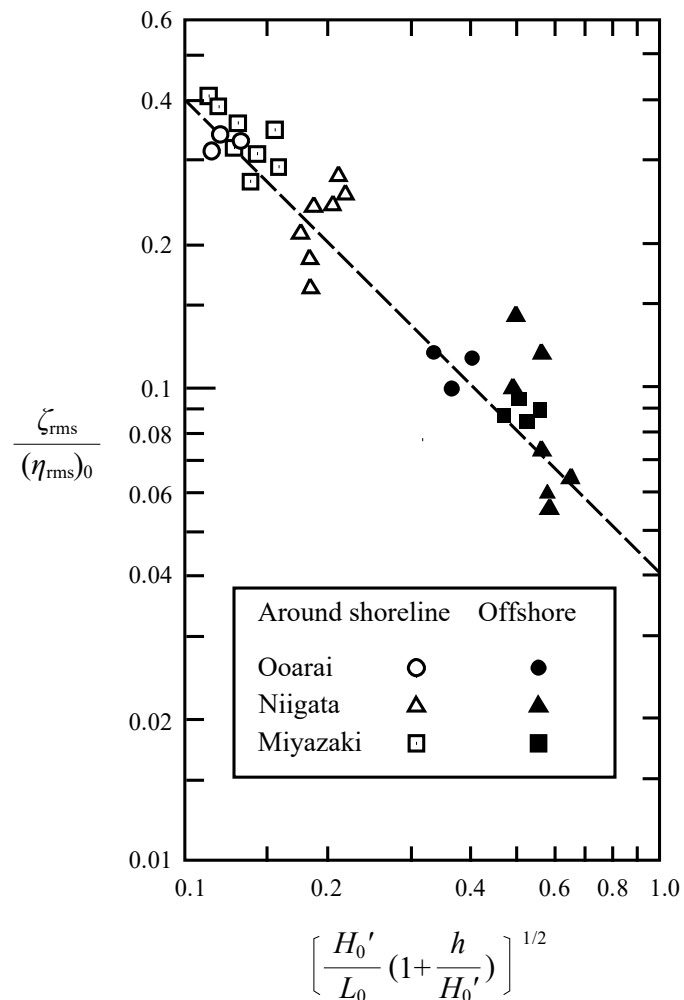


Fig. 4.4.34 Ratio of Surf Beat Amplitude for Deepwater Wave

4.5 Long-period Waves

(1) Setting Method of Long-Period Waves

① Definition of Long-Period Waves

With regard to long-period waves and harbor resonance, field observations should be performed as far as possible, and appropriate measures to control them must be taken on the basis of the results of these observations. Here, long-period waves are defined as waves composed of component waves with periods from 30 seconds to 300 seconds in the frequency spectrum analyzed from an uninterrupted wave record observed for the period more than 20 minutes.

② Distinction between Long-period Waves and Harbor Resonance

Water level fluctuations with the period between 30 seconds and several minutes sometimes appear at observation points in harbors and off the shore. Such fluctuations are generally called long-period waves. If the period of such long-period waves is close to the natural period in the surge motion of a ship moored at a quay wall by ropes, the phenomenon of resonance can give rise to a large surge motion with the amplitude of several meters even if the wave height is small, thus resulting in large effects on the cargo-handling efficiency of the port. The critical wave height for cargo handling affected by long-period waves differs by periods, specifications of ships, mooring conditions, loading conditions, and others. However, if it is clear that long-period waves of significant wave height 10–15 cm or more frequently appear in a harbor like the field observation results¹⁵¹⁾ at Port of Tomakomai, it is advisable to investigate countermeasures from the hardware or software aspect¹⁵²⁾.

When conspicuous water level fluctuations with the period of several minutes or longer occur at an observation point in a harbor, it is highly likely that the phenomenon of harbor resonance is occurring. This phenomenon occurs when small disturbances in water level generated by changes of air pressure in offshore sea and amplifies the natural fluid motion in the harbor or bay by the resonance. If the harbor resonance becomes significantly large, the inundation at the innermost part of the bay or reverse outflow from municipal drainage channels may occur. Furthermore, high-current velocities may occur locally in a harbor, thus resulting in breaking of the mooring ropes of small ships. When drawing up a harbor plan, it is preferable to give consideration to making the shape of the harbor to minimize the harbor resonance motion as much as possible. The resonant period in small ports like marinas may be close to the period of long-period waves and the propagation of long-period waves from the open sea may excite the harbor resonance in the port. The two aspects of the long period wave and the harbor resonance are therefore highly correlated. If harbor resonance excitation by long-period waves becomes apparent from observations or numerical calculations, it is preferable to deliberate countermeasures while giving thought to these aspects.

In an ordinary harbor, the period of harbor resonance is several minutes or more, which is longer than that of long-period waves, and it is possible to distinguish the two from analysis of the oscillation period. However, the period of harbor resonance may become shorter to 2 to 3 minutes in the case of small craft basins and marinas, and this makes the discrimination difficult. In that case, it is preferable to make a judgment as suitable on the basis of the observation results for offshore waters and the circumstances in the surrounding harbor.

③ Occurrence Factor of Long-period Waves

The radiation stress¹⁴⁹⁾ indicated by Longuet Higgins and Stewart distributes unevenly for waves having prominent wave groups, and the long-period fluctuation of water level occurs. As this wave proceeds along with the wave group, it is called the bound wave. This wave theoretically proceeds at the wave group velocity C_G , and its amplitude is proportional to the square of the wave height of wind waves composing the wave group. Moreover, the amplitude increases as the water depth becomes shallower. If the wind waves are diffracted by a breakwater or a cape, the bound wave decreases because the diffracted wave height becomes smaller. However, given that the long period fluctuation induced so far does not disappear drastically, it is seemingly transformed to unbound long-period wave and propagated freely in the port. This wave is called a free progressive long wave, and its propagation velocity is expressed in \sqrt{gh} as the long wave celerity.

Moreover, when waves with a wave group form break, the variation of their heights moves the wave breaking point onshore or offshore, the slope of the radiation stress is changed with time, and free progressive long waves are generated in the surf zone¹⁵³⁾. Long-period waves invaded in a port as free progressive long waves are reflected by the quaywalls or beach, and some energies of the long waves propagate out of the port again. Therefore, long-period waves observed at an observation point outside a port include the component of bound

waves, and the component of free progressive long waves advances onshore and offshore. However, some of the occurrence process of long-period waves are complicated and still unexplained. Here, countermeasures and others are presented by considering that the majority of long-period waves observed in a port is expressed as free progressive long waves advancing toward the shore. However, in reality, not only the component of free progressive long waves but also the component remaining as bound waves and the long-period wave induced by the change in wave height at the port entrance may exert some influence. Therefore, it is necessary to evaluate the effect of countermeasures against the long waves through the numerical analysis, model experiment, or others if any structures are constructed as the countermeasures.

(2) Representation of Long-Period Waves

① Standard Spectrum for Long-Period Waves

When there are insufficient field observation data of long-period waves in offshore sea and the property of the long-period waves are not sufficiently derived, the standard spectrum shown in **Reference 154)** or its approximate expression may be used for the long-period wave performance verifications. Here, the standard spectrum is proposed as the spectral form that superimposes uniform spectral density in the long-period wave side to the short-period wave spectrum represented by the Bretschneider–Mitsuyasu type.

Fig. 4.5.1 shows a comparison between an observed spectrum and an approximate form of the standard spectrum. The term α_l in the figure denotes a parameter that represents the energy level of the long-period waves. The parameter shows the relationship between the spectrum peak frequency f_p of short-period wave components and boundary frequency f_b for calculating the energy of long-period waves components. The parameter α_l is given as $\alpha_l = f_p / f_b$. The past observations show that the value of the parameter exists between 1.6 and 1.7. A smaller value of α_l leads to the larger energy of the long-period waves.

Given that the values of the parameter are determined as the mean values estimated from observation data with the significant wave heights of 3 m or more, the wave heights of the long-period wave components are prone to be overestimated for normal waves. Therefore, for the normal waves, it is needed to use the relations between the proper wave height ratio $R_L (= H_L / H_{1/3}$; where H_L is the significant wave height of the long-period wave component, and $H_{1/3}$ is the significant wave height of the whole frequency band) and α_l corresponding to the spectral form of short-period wave components. **References 155)** and **156)** are helpful because they propose the equation to directly calculate α_l from the height and period of the wind waves observed at the sea shallower than 50 m, in addition to the correlation equation between R_L and α_l for each frequency spectrum of the Bretschneider–Mitsuyasu type (**equation (4.2.12)**), modified Bretschneider–Mitsuyasu type (**equation (4.2.13)**), and JONSWAP type (**equation (4.2.14)**).

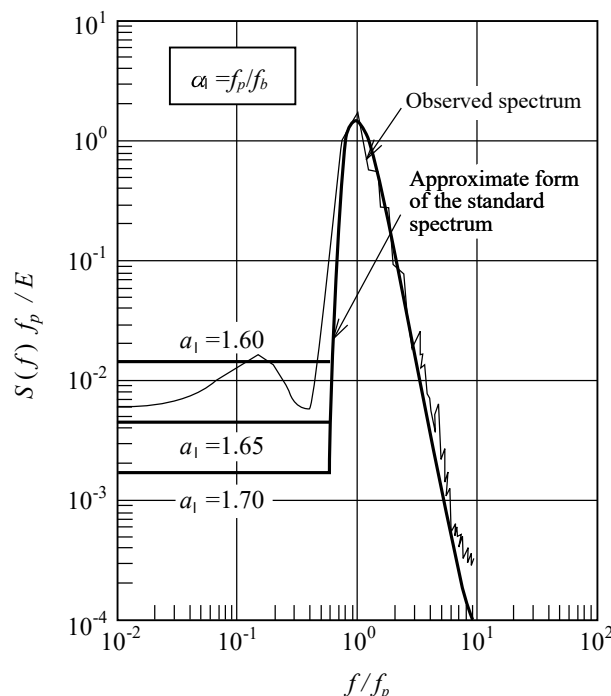


Fig. 4.5.1 Comparison between Standard Spectrum with Long-period Wave Components and Observed Spectrum

② Direction of Long-period Waves

At the propagation of the long-period waves they frequently overlap with the waves reflected from the longshore, and consequently it is difficult to determine their direction. However, if the main energy of the long-period waves advances toward the shore as the free progressive long waves, its wave direction may be conveniently assumed to be same as the principal direction of short-period waves (wind waves).

(3) Handling of Long-Period Waves

① Calculating the Propagation of Long-Period Waves

It is preferable to calculate the propagation of long-period waves into a harbor by setting up incident wave boundary in offshore sea and then by using either the Boussinesq equation or the linear long wave equations.¹⁵⁷⁾ At this time, random waves for the calculation shall be the basic target. However, if there are any special circumstances such as the period restriction of the incident long waves to some specific period band, several calculation results for the regular waves with different periods may be synthesized in energy and used. See **Part II, Chapter 2, 3.3 Harbor Resonance** for the method for calculating harbor resonance.

② Countermeasures against Long-Period Waves and Harbor Resonance

In waters where long-period waves are marked, it is preferable to establish a breakwater layout plan to inhibit the ingress of long-period waves into the harbor. At this time, in the event that the particle diameter of the mound materials is large, almost all of the energy of the long-period waves is transmitted into the harbor; therefore, it is necessary to thoroughly examine the structures of the breakwater and mound.

To control the surge oscillation of ships, it is preferable to shift the resonant period of the ship mooring system from the period of the invading long-period waves. To this end, it is preferable to take such measures as changing the places and the initial tensions of the mooring ropes, as well as improvement of rope material and increase of the number of the mooring ropes by new installation of land winches. The effects of such measures should be examined beforehand, and appropriate measures should be devised on the basis of suitable numerical calculations.

The long-period waves are frequently amplified by the reflection from the facilities in a harbor; in particular, upright wave-dissipating revetments have almost no wave-dissipating functions for long-period waves and swells. Therefore, the review of the reflection coefficient of the facilities is necessary to accurately estimate the long-period wave heights inside harbors. **The Environment Assessment Manual of Long-Period Waves in Harbors**¹⁵⁸⁾ can be used as a reference for the rough order of magnitude and calculation method of the reflection coefficient.

Structures that control the reflection of long-period wave and lower the long-period wave height inside ports and harbors are called the long-period wave countermeasure construction, and many of them are installed behind the breakwater or in front of the revetment in ports and dissipate long-period waves by turbulence generated at the wave penetration through the permeable mound of gravel material and so on.¹⁵⁹⁾ In this case, if the width of the permeable mound is approximately 5% of the long-period wave length in the state of direct incidence, the reflection coefficient of the long-period waves is on the order of 0.8.¹⁶⁰⁾ Furthermore, long-period wave-dissipating revetments which are composed of a two-sided slit caisson and backfilling materials of large gravels have been developed to dampen the long-period waves in a harbor. It is preferable to set the width of the water transmitting layer, place of installation, and installation range through the hydraulic model test and numerical calculations to achieve the maximum effects.^{161) 162)} Studies need to be conducted to examine the wave-dissipation effect by widening the virtual width of permeable mound for oblique incident long-period waves to the permeable mound¹⁶³⁾ and to examine the wave-dissipation performance of water-submerging-type long-period wave-dissipating works by expecting the friction effect on the permeable mound.¹⁶⁴⁾

Considering that the distribution of long-period wave height is not uniform in the harbor, it is preferable to examine the modification of the berthing location at the planning stage in the event that the height of long-period waves in the target berth clearly exceeds the limit values.

4.6 Concept of Harbor Calmness

(1) Factors of Calmness and Disturbance

- ① The factors causing disturbances in the harbor need to be set appropriately for the evaluation of harbor calmness.
- ② The problem of harbor calmness is extremely complex. It involves not only physical factors such as waves, winds, ship motions, and wind- and wave-resistance of working machinery but also the factors requiring human judgment, such as the ease with which ships can enter and leave the harbor, ship refuge during stormy weather, and critical conditions of works at sea. Harbor calmness is further related with economic factors, such as the efficiency of cargo handling works, the operating rate of ships, and the cost of constructing the various facilities required to improve the harbor calmness. The factors that cause the harbor disturbances related to waves, which constitute the basis of the criteria for the evaluation of the harbor calmness, include the following:
 - (a) Invading waves from harbor entrance
 - (b) Transmitted waves into the harbor
 - (c) Reflected waves
 - (d) Long-period waves
 - (e) Harbor resonance

In large harbors, wind waves generated within the harbor may require attention, and the ship wake waves by larger ships may cause troubles for small ships.

(2) Points to remember for calculations of harbor calmness

It is necessary to bear the following points in mind when performing harbor calmness calculations.

- ① Set the wave height and period frequency distribution at the port entrance.
- ② In the event that the water depth in navigation channel differs significantly from the surrounding water depth, shoals exist inside the harbor, or the water depth changes suddenly in the port entrance, consider the water depth change in the calculation of wave height inside the harbor.
- ③ Introduce the effects of the period as concerns the permissible value of the wave height in the harbor.
- ④ Consider the future state of the port utilization to set up the target value for harbor calmness.

(3) Computation of Harbor Calmness for Normal Waves

Harbor calmness is generally set with the occurrence probability of the significant waves that does not exceed the critical wave height for cargo handling works or for ship anchoring. The critical wave height for cargo handling works means the upper limit of the significant wave height at which the ships moored at the quay wall or dolphin can safely perform cargo handling activities. The critical wave height for anchoring means the upper limit of the significant wave height at which ships can safely anchor in the berthing basin and moored at the buoy as well as at the mooring facilities. The occurrence probability of the significant waves that does not exceed the critical wave height for cargo handling works is called the cargo handling operating rate. In general, the harbor calmness is assessed by the cargo handling operating rate. The following methods may be used for computation of harbor calmness ^{165) 166)} (see Fig. 4.6.1).

① Computation of the cargo handling operating rate for normal waves (wind waves and swells)

- (a) Prepare a frequency table of wind waves (wave height, period) by the wind direction outside the harbor.
- (b) Set several representative waves outside the harbor for the computation

Set several representative waves (combination of wave height and period and wave directions) outside the harbor for the computation considering the topography of ports and referring to the frequency table of wind waves and swells by the wave direction at a point outside the harbor. If the waves' nonlinear transformation can be ignored inside and outside the harbor or if the wave direction and height at the harbor entrance are computed by using the linear models of the energy balance equation and others per combination of wave period and direction outside the harbor, the occurrence frequency of wave heights outside the harbor may not necessarily be considered in setting the height of representative waves.

(c) Compute the wave heights at points inside the harbor and prepare their occurrence frequency tables

If the wave transformation inside and outside the harbor can be computed at the same time by using a nonlinear wave model like the Boussinesq model, determine the ratio of the wave height at each point inside the harbor to the incident wave height outside the harbor per representative wave, and then, determine the ratio of the wave heights by interpolation to the class values of period and wave direction in the wind wave and swell frequency table at point outside the harbor or their original values of period and wave direction in the wave dataset observed at point outside the harbor. If the transformation of waves due to the seabed topography inside the harbor can be ignored because of the relatively small change of the water depth inside the harbor, it is possible to employ the ratios obtained by multiplying the wave height ratios inside the harbor, computed with Takayama or other methods for the incident wave at the harbor entrance, with the wave height ratio at the harbor entrance to the outside harbor previously computed with the energy balance equation and others. The wave height occurrence frequency table in front of the target facilities and inside the harbor can be computed by multiplying these ratios of wave heights with each of class values or original values of wave height. When the transmitted and permeated waves into the harbor are considered together as needed, these wave heights and the computed wave heights obtained above are squared individually, and the square root of their sum (mean wave of wave energy) may be considered as the wave height inside the harbor. In a harbor where the influence of the transmitted or the permeated waves is relatively small, the wave period inside the harbor may be represented by the wave period obtained from the above wave transformation computation inside the harbor. It was reported that the wave transmission rate becomes significant when the wave overtopping rate is at least $0.02\text{m}^3/\text{s}/\text{m}$ or more for a composite breakwater where transmitted waves caused by wave overtopping are more prominent than waves permeating through the foundation mound.¹³⁸⁾

(d) Compute the cargo handling operating rate for normal wave (wind waves and swells) components

The cargo handling operating rate can be computed in the following procedures:

- 1) Setting the critical wave height for cargo handling works (if there is or may be a trouble in cargo handling due to swells and others, set by the type and deadweight tonnage of ships used and the wave direction, period, and the like per mooring facility as necessary). **The Environmental Assessment Manual of Long-Period Waves in Harbors**¹⁶⁷⁾ lists standard values of the critical wave height for cargo handling works, which can be used as a reference.
- 2) Accumulating the occurrence frequency of the wave heights which exceed the critical wave height for cargo handling works in front of the target facilities.
- 3) Determining the cargo handling non-operating rate (%) by dividing the cumulative frequency in 2) by the number of whole data and adding up by all periods and wave directions. Obtaining the cargo handling operating rate by subtracting the non-operating rate from 100%.

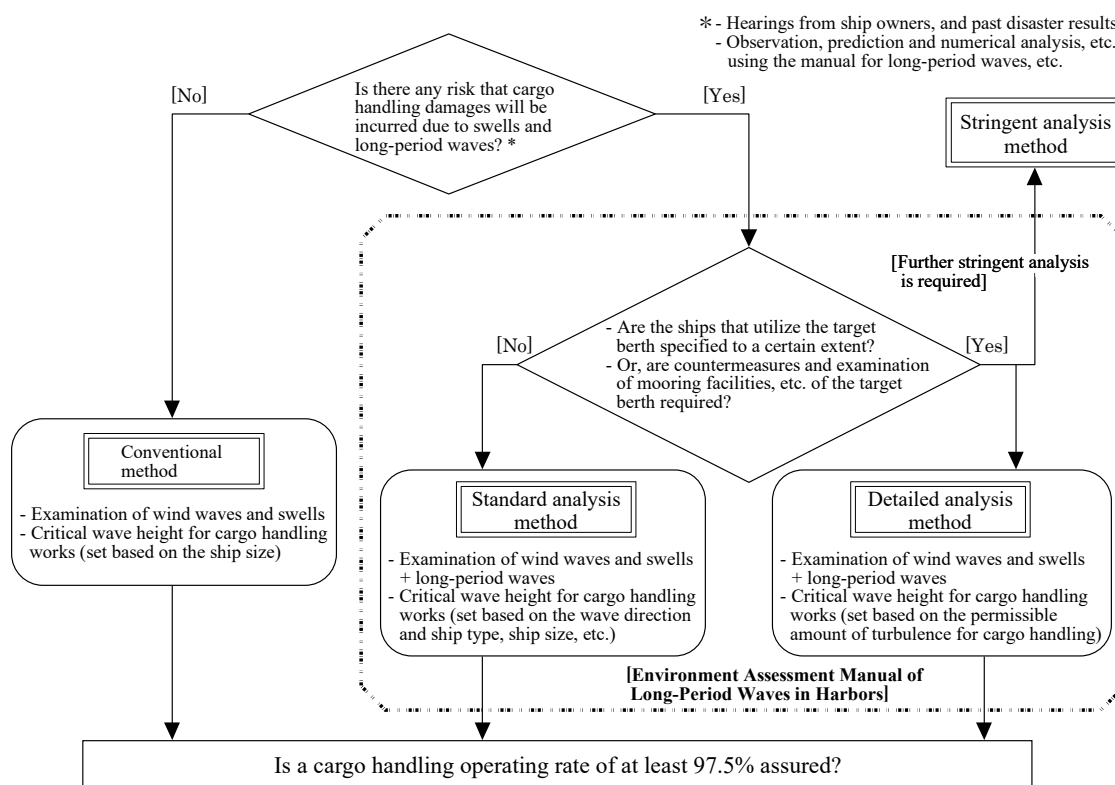


Fig. 4.6.1 Example of Performance Verification Steps Relating to Harbor Calmness

② Calculation of the cargo handling operating rate for long-period waves

Prepare a frequency table of long-period waves by the wave direction outside the harbor

If a frequency table of long-period waves measured in the field by the wave direction cannot be obtained, prepare a frequency table of long-period waves by the wave direction outside the harbor by utilizing the frequency table of the wind waves outside the harbor. In this case, the standard spectrum of the long-period waves may be used (see **Part II, Chapter 2, 4.5 Long-period Waves**).

(b) Set several wave directions and heights of long-period waves outside the harbor to compute

Set several wave directions and heights of long-period waves outside the harbor for the computation considering the topography of ports and referring to the frequency table of long-period waves by the wave direction at a point outside the harbor. In the application range of the linear theory, the heights of representative long-period waves outside the harbor may be set without considering the occurrence frequency. The period band of the component waves may be set from 30 s to 300 s according to the definition.

(c) Compute the wave heights inside the harbor and prepare the occurrence frequency table of long-period wave heights inside the harbor

By using a wave model like the Boussinesq model that can compute the wave transformation occurring inside and outside the harbor at the same time, determine the ratio of the wave height at each point inside the harbor to the incident long wave height outside the harbor per long-period wave direction, and then, determine the ratio of the wave heights by interpolation to the class values of wave direction in the long-period wave frequency table at point outside the harbor or their original values of wave direction in the wave dataset observed at point outside the harbor. It is preferable to consider the transformation of random waves at this time. The occurrence frequency table of wave heights in front of the target facilities and inside the harbor can be computed by multiplying these ratios of the wave heights with each of class values or original values of wave height.

(d) Compute the cargo handling operating rate for long-period wave components

The cargo handling operating rate for long-period wave components can be computed in the following procedures:

- 1) Setting the critical long-period wave height for cargo handling works. For this setting, it is preferable to consider the type of ship and the cargo handling system in question and to determine the wave heights separately based on a survey of the actual state of cargo handling. The critical wave height for cargo handling works for long-period waves is defined in **Table 4.6.1**.¹⁶⁸⁾
- 2) Accumulating the occurrence frequency of the wave heights which exceed the critical wave height for cargo handling works in front of the target facilities.
- 3) Determining the cargo handling non-operating rate (%) by dividing the cumulative frequency in 2) by the number of whole data and adding up for all wave directions. Obtaining the cargo handling operating rate by subtracting the non-operating rate from 100%.

Table 4.6.1 Critical Wave Height for Cargo Handling Works for Long-Period Waves ¹⁶⁸⁾

Level of the significant wave height of long-period waves	Assumed conditions	Critical wave height for cargo handling works (m)
1	Ship classes for which the permissible amount of motions in cargo handling is relatively large for surging, or ships whose resonant period for surging is 1.5 minutes and under (medium sized ships: 1,000 to 5,000 DWT)	0.20
2	Ship classes for which the permissible amount of motions in cargo handling is moderate for surging, and ships whose resonant period for surging is 1.5 minutes and under (general cargo ships: 5,000 to 10,000 DWT)	0.15
3	Ship classes for which the permissible amount of motions in cargo handling is small for surging, or ships whose resonant period for surging is 2–3 minutes (container ships, mineral ore ships: 10,000 to 70,000 DWT)	0.10

(4) Harbor calmness for abnormal waves

The harbor calmness for abnormal waves which is equivalent to a probabilistic wave with a return period of 50 years, for facilities with a design service life of 50 years in the case of waves as variable action can be generally assessed by considering the fact that the waves in an abnormal state have a major effect on the performance of the facilities in harbors. The evaluation of the harbor calmness can be performed by setting the critical value of the abnormal wave height inside the harbor and confirming that the wave heights computed inside the harbor in the abnormal state does not exceed this critical value.

It is preferable to set the critical wave height for ship refuge among the critical waves as 0.7 to 1.5 m for ships in the order of 5,000 to 10,000 GT class or less according to the type of ship and the refuge condition (mooring to a wharf, mooring to a buoy, anchoring). It may be on the order of 0.5 m in a small craft basin for small ships. A crown height of the wharf shall ensure no inundation behind owing to wave overtopping and others, and the critical wave height for that needs to be set properly.

(5) Harbor resonance

The period of the harbor resonance is approximately 5 minutes or more and is not a factor to extremely worsen the cargo handling works. However, a harbor shape that does not generate big harbor resonance is preferable because a large amplitude causes damage, such as troubles in mooring small ships, reverse flow from drains, flooding of quaywalls, etc. (See **Part II, Chapter 2, 3.3. Harbor Resonance**).

4.7 Ship Wake Waves

- (1) It is preferable to consider ship wake waves due to ship navigation in canals and waterways.
- (2) Ship wake waves are caused when ships navigate. A larger and faster ship leads to the greater ship wake waves. As the ship wake waves propagate longer, they attenuate gradually; therefore, they do not cause serious problems in wide water areas. However, they sometimes cause undesirable motions in moored small ships, floating piers, etc., inside harbors or in narrow waterways such as channels and canals. Furthermore, they infrequently affect wave overtopping, the scouring and stability of armored blocks at revetments on both sides of a waterway.

(3) Pattern of Ship Wake Waves

If the ship wake waves are viewed from air, they appear as shown in **Fig. 4.7.1**. It is composed of two groups of waves. One group spread out in a shape like "八" from a point slightly ahead of the bow of the navigation ship. The other group is behind the ship, and the wave crest is perpendicular to the ship's navigation line. The former waves are called "divergent waves," whereas the latter are called "transverse waves." The divergent waves form concave curves; the closer to the navigation line, the shorter the distance between the adjacent wave crests. On the contrary, the transverse waves are approximately arc-shaped, with the constant distance between the adjacent wave crests. In deep water, the area over which the ship wake waves extend is limited within the area bounded by the two cusplines, with the angles $\pm 19^\circ 28'$ from the navigation line and starting from the origin lying somewhat in front of the bow of the ship. The divergent waves cross the transverse waves just inside the cusplines; this is where the wave height is the largest. Wave steepness is smaller for the transverse waves than for the divergent waves, thus implying that the transverse waves often cannot be distinguished from an aerial photograph.

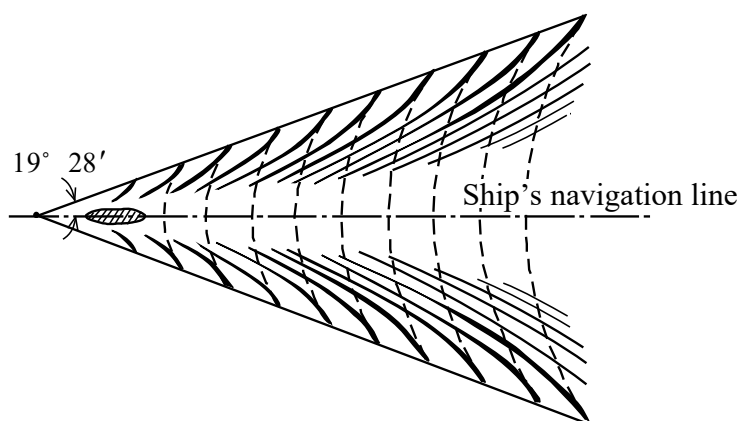


Fig. 4.7.1 Plan View of Ship Wake Waves (Solid lines show the crests of divergent waves, and dotted lines show the crests of transverse waves.)

(4) Wavelength and Period of Ship Wake Waves

The wavelength and period of ship wake waves are different between the divergent waves and the transverse ones, with the latter having both a longer wavelength and a longer period. Amongst the divergent waves, the wavelength and period are both the longest for the first wave and then become progressively shorter.

- ① The wavelength of the transverse waves can be obtained by the numerical solution of **equation (4.7.1)**, which is derived from the condition that the velocity of the transverse waves must be same as the speed of the ship navigation.

$$\frac{gL_t}{2\pi} \tanh \frac{2\pi h}{L_t} = V^2 \quad (\text{when } V < \sqrt{gh}) \quad (4.7.1)$$

where

L_t : wavelength of transverse waves (m)

h : water depth (m)

V : ship navigation speed (m/s)

When the water is sufficiently deep compared with the wavelength of transverse waves, the wavelength of the transverse waves is given by the following equation:

$$L_0 = \frac{2\pi}{g} V^2 = 0.169 V_k^2 \quad (4.7.2)$$

where

L_0 : wavelength of transverse waves at places where the water is sufficiently deep (m)

V_k : ship navigation speed (kt) ($V_k = 1.946 V$)

- ② The period of the transverse waves is equal to the period of progressive waves with the wavelength L_t in water of depth h . It is given by **equations (4.7.3) or (4.7.4)**.

$$T_t = \sqrt{\frac{2\pi}{g} L_t \coth\left(\frac{2\pi h}{L_t}\right)} = T_0 \coth\left(\frac{2\pi h}{L_t}\right) \quad (4.7.3)$$

$$T_0 = \frac{2\pi}{g} V = 0.330 V_k \quad (4.7.4)$$

where

T_t : period of transverse waves in water of depth h (s)

T_0 : period of transverse waves at places where the water is sufficiently deep (s)

- ③ The wavelength and period of the divergent waves are given by **equations (4.7.5) and (4.7.6)**, which are derived from the condition that the component of the ship's speed in the direction of travel of the divergent waves must be equal to the velocity of the divergent waves.

$$L_d = L_t \cos^2 \theta \quad (4.7.5)$$

$$T_d = T_t \cos \theta \quad (4.7.6)$$

where

L_d : wavelength of divergent waves as measured in the direction of travel (m)

T_d : period of divergent waves (s)

θ : angle between the direction of travel of the divergent waves and the navigation line ($^\circ$)

According to Kelvin's theory of wave-generation at places where the water is sufficiently deep, the angle of travel θ of the divergent waves can be obtained, as shown in **Fig. 4.7.2**, as a function of the position of the place of interest relative to the ship. For actual ships, the minimum value of θ is generally approximately 40° , and θ is usually 50° to 55° for the point on a particular divergent wave at which the wave height is the maximum. The illustration in the figure shows that the angle θ directs the location of the source point Q where the divergent wave has been generated and α is the angle between the cuspline and the navigation line.

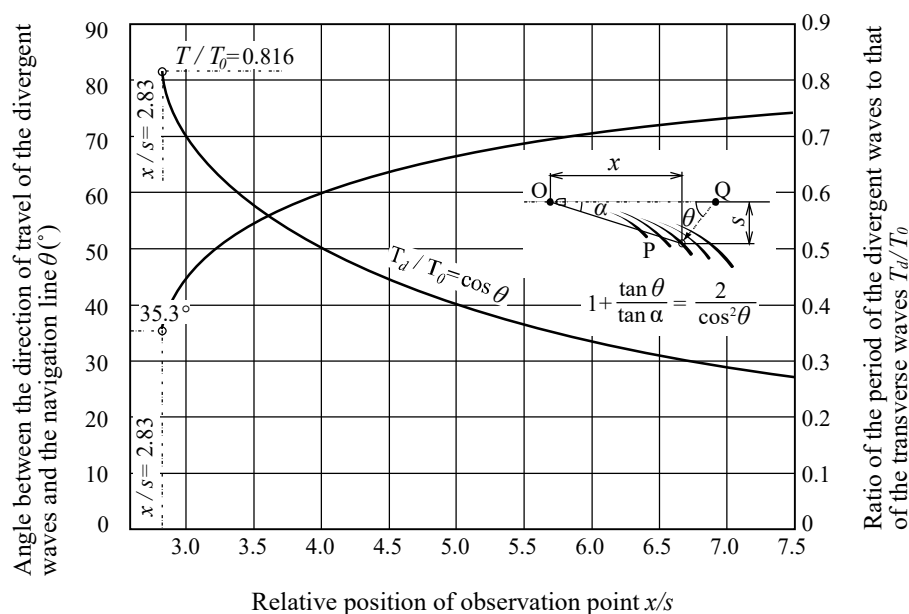


Fig. 4.7.2 Wave Direction and Period of Divergent Waves at Places where the Water is Sufficiently Deep

(5) Shoaling Effect on Ship Wake Waves

As same as normal water waves, ship wake waves are affected by the water depth, and their properties vary when the water depth decreases relative to their wavelength. This shoaling effect on the ship wake waves may be ignored if the condition defined by **equation (4.7.7)** is satisfied¹⁶⁹⁾:

$$V \leq 0.7\sqrt{gh} \quad (4.7.7)$$

The critical water depth above which ship wake waves may be regarded as deepwater waves is calculated by **equation (4.7.7)**, as shown in **Table 4.7.1**. As can be seen from this table, the waves generated by ships in normal conditions can generally be regarded as deepwater waves. Situations in which they must be regarded as shallow water waves include the following cases: a high-speed ferry travels through relatively shallow waters, a motorboat travels through shallow waters, and ship wake waves propagate into shallow waters.

Note that ship wake waves generated in shallow water have a longer wavelength and period than those generated by the ship navigating in deep water at the same speed.

Table 4.7.1 Conditions under which Ship Wake Waves can be regarded as Deepwater Waves

Speed of ship	$V_k(\text{kt})$	5.0	7.5	10.0	12.5	15.0	17.5	20.0	25.0	30.0
Water depth	$h(\text{m}) \geq$	1.4	3.1	5.5	8.6	12.4	16.9	22.0	34.4	49.6
Period of transverse waves	$T_0(\text{s})$	1.7	2.5	3.3	4.1	5.0	5.8	6.6	8.3	9.9

(6) Height of Ship Wake Waves

The ship wake waves research committee of the Japan Association for Preventing Maritime Accidents has proposed the following **equation (4.7.8)** for giving a rough estimate of the height of ship wake waves¹⁶⁹⁾:

$$H_0 = \left(\frac{L_{pp}}{100} \right)^{1/3} \sqrt{\frac{E_{HPW}}{1620 L_{pp} V_K}} \quad (4.7.8)$$

where

H_0 : characteristic wave height of ship wake waves (m), or the maximum wave height observed at a distance of 100 m from the navigation line when a ship is navigating at its full-load cruising speed

- L_{pp} : length between perpendiculars of the ship (m)
 V_K : full-load cruising speed of the ship (kt)
 E_{HPW} : wave-generation horsepower of the ship (W)

The wave-generating horsepower E_{HPW} of a ship is calculated as follows. For the ship dimensions necessary for these equations, reference 170) can be referred to.

$$E_{HPW} = E_{HP} - E_{HPF} \quad (4.7.9)$$

$$E_{HP} = 0.6S_{HPm} \quad (4.7.10)$$

$$E_{HPF} = \frac{1}{2} \rho_0 S V_0^3 C_F \quad (4.7.11)$$

$$S = 2.5 \sqrt{\nabla L_{pp}} \quad (4.7.12)$$

$$C_F = 0.075 \left/ \left(\log \frac{V_0 L_{pp}}{\nu} - 2 \right) \right.^2 \quad (4.7.13)$$

where

- S_{HPm} : continuous maximum shaft horsepower of the ship (W)
 ρ_0 : density of seawater (kg/m³) $\rho_0 = 1030 \text{ (kg/m}^3\text{)}$
 V_0 : full-load cruising speed of the ship (m/s) $V_0 = 0.514 V_K$
 C_F : frictional resistance coefficient
 ν : coefficient of kinematic viscosity of water (m²/s) $\nu \doteq 1.2 \times 10^{-6} \text{ (m}^2\text{/s)}$
 ∇ : full-load displacement of the ship (m³)

Equation (4.7.13) has been obtained by assuming that the ship's energy consumed through wave-generation resistance is equal to the propagation energy of ship wake waves, whereas the values of the coefficients have been determined as averages of the data from ship towing tank tests. The characteristic wave height H_0 of ship wake waves depends on an individual ship, although for medium and large-size ships it is approximately 1.0 to 2.0 m. Tugboats sailing at full speed produce relatively large waves as well. The characteristic wave height H_0 shall be calculated by setting values of ship's length between perpendiculars L_{pp} , full-load displacement ∇ , full-load cruising speed V_K , and continuous maximum shaft horsepower S_{HPm} in **equations (4.7.8) to (4.7.13)** from the documents describing ship specifications, such as reference 170). Here, the horsepower described in reference 170) can be used for the continuous maximum shaft horsepower S_{HPm} .

It can be considered that the wave height of ship wake waves attenuates in proportion to $S^{-1/3}$, where S is the distance of the observation point from the navigation line. It is also considered that the wave height is proportional to the cube of the cruising speed of the ship. Accordingly, the maximum wave height H_{max} of ship wake waves can be calculated by the following equation:

$$H_{max} = H_0 \left(\frac{100}{S} \right)^{1/3} \left(\frac{V_k}{V_K} \right)^3 \quad (4.7.14)$$

where

- H_{max} : maximum wave height of ship wake waves at any chosen observation point (m)
 S : distance from the observation point to the navigation line (m)
 V_k : actual cruising speed of the ship (kt)

Equation (4.7.14) cannot be applied if the distance S is too small. However, **equation (4.7.14)** can be applied to the smaller value of the ship's length between perpendiculars L_{pp} or 100 m.

The upper limit of the height of ship wake waves occurs when the wave steepness of the maximum wave height of the divergent wave reach to the breaking criterion of $H_{\max}/L_t = 0.14$. If the angle between the wave direction and the navigation line is assumed to be $\theta = 50^\circ$ at the point on a divergent wave where the wave height becomes largest, the upper limit of the wave height at any given point can be given by **equation (4.7.15)**. However, the conditions for deepwater waves shall be satisfied.

$$H_{\text{limit}} = 0.010V_k^2 \quad (4.7.15)$$

where

H_{limit} : upper limit of the height of ship wake waves derived from the wave breaking conditions (m)

The ship wake waves are largely affected by the ship's conditions such as size, shape, and cruising speed and topographical conditions such as water depth. Therefore, it is practically preferable to consider these conditions in the estimation of the ship wake waves. The method described here is for quick calculation of the height of the ship wake waves. Other methods such as the numerical calculation method of the ship wake waves are also proposed.¹⁷¹⁾

(7) Propagation of Ship Wake Waves

- ① Among the two groups of ship wake waves, the transverse waves propagate in the direction of ship's navigation, and continue to propagate even if the ship changes course or stops. In this case, the waves have a typical nature of regular waves with the period given by **equation (4.7.3)**, and they propagate at the group velocity, undergoing transformation such as refraction and others. Takeuchi and Nanasawa¹⁷²⁾ gave an example of such transformations. As the waves propagate, the length of wave crest spreads out. Even when the water is of uniform depth, the wave height attenuates in a manner that is inversely proportional to the square root of the distance traveled.
- ② The direction of propagation of a divergent wave varies from point to point on the wave crest. According to Kelvin's theory of wave-generation, the angle between the direction of propagation and the navigation line is $\theta = 35.3^\circ$ at the outer edge of a divergent wave. As one moves inwards along the wave crest, the value of θ approaches 90° . The first wave arriving at any particular point has the angle $\theta = 35.3^\circ$, whereas the value of θ becomes gradually larger for subsequent waves. This spatial change in the direction of propagation of the divergent waves can be estimated by using **Fig. 4.7.2**.
- ③ The propagation velocity of a divergent wave at any point on the wave crest is the group velocity corresponding to the period T_d at that point (see **equation (4.7.6)**). In the illustration in **Fig. 4.7.2**, the time necessary for a component wave to propagate at the group velocity from point Q at wave source to point P is equal to the time taken for the ship to travel at the speed V from point Q to the point O. Considering that each wave profile propagates at the wave velocity (phase velocity), the waves pass beyond the cuspline and appear to vanish one after the other at the outer edge of the divergent waves.

(8) Generation of Solitary Waves

When a ship navigates through shallow waters, there are cases when solitary waves are generated in front of the ship if the cruising speed V_k approaches \sqrt{gh} . Around the river mouths, there is a possibility of small ships being affected by such solitary waves generated by other large ships.¹⁷³⁾

4.8 Actions on Floating Body and its Motions

4.8.1 General

- (1) The performance verification of a floating body shall be conducted under the appropriate consideration of the motions and mooring forces of the floating body due to wind, currents, and waves.
- (2) In general, a floating body refers to a structure that is buoyant in water and makes allowable motions within a certain range.¹⁷⁴⁾ When verifying the performance of a floating body, both its required functions and its stability

shall be examined. It is necessary to pay attention to the matter that the required performance on each case is different in general.

- (3) Mooring equipment includes a variety of types and is generally composed of a combination of mooring lines (ropes or chains), anchors, sinkers, intermediate weights, intermediate buoys, mooring piles, connection joints, and fenders. The mooring equipment has a large influence on the motions of a floating body; therefore, it is important to verify the stability of this equipment appropriately.
- (4) The floating bodies used as port facilities can be classified into floating wharves,¹⁷⁵⁾ offshore floating petroleum stockpiling bases,¹⁷⁶⁾ floating breakwaters,¹⁷⁷⁾ floating bridges,^{178) 179)} and floating disaster-prevention bases.^{180) 181)} Moreover, the investigation and development of very large floating type structures^{182) 183) 184) 185)} have been performed.
- (5) Floating bodies can also be classified by the types of mooring methods. As described below, mooring methods include catenary mooring (slack mooring), dolphin mooring, taut mooring etc.

① **Catenary mooring (Fig. 4.8.1(a))**

This is the most common mooring method. With this method, the chains or other materials used in the mooring are given sufficient lengths to make them slack. This means that the force restraining the motions of the floating body is small, but the mooring system fulfills the function of keeping the floating body in more-or-less the same position. There are various types of catenary mooring depending on factors such as the material of the mooring lines, number of mooring lines, and presence or absence of intermediate buoys and sinkers.

② **Dolphin mooring (Fig. 4.8.1(b))**

With this method, mooring is maintained using either a pile-type dolphin or a gravity-type dolphin. In general, this method is suitable for restraining the motions of a floating body in the horizontal direction, but a large mooring force acts on the dolphin. This method has been used for mooring floating units of offshore petroleum stockpiling bases. Moreover, there is a pile mooring as a mooring method similar to the dolphin mooring. This mooring method is often used for relatively small floating piers and others. It generally uses a guide roller instead of a fender in the contact part with a floating body.

③ **Taut mooring (Fig. 4.8.1(c))**

This is a mooring method that reduces the motions of a floating body greatly; a Tension Leg Platform (TLP) is an example. With this method, the mooring lines are given a large initial tension so that they do not become slack even when the floating body moves. The advantages of this mooring method are as follows: The floating body does not move much, and only a small area is needed for installing the mooring lines. However, it is necessary to take note of the fact that because a large tensile force is generated in the mooring lines, the specifications of the lines become the critical factor on the stability of the floating body. This method is often used for mooring platforms for oil drilling and others in overseas.

④ **Mooring using a universal joint (Fig. 4.8.1(d))**

This is a mooring method with a mechanism that allows operation in every direction so as not to give the large restraining force to a floating body. The mooring equipment shown in the figure is an example of a mooring method that can be used to moor a large offshore floating body. The examples of mooring equipment that uses a universal joint on the sea bottom include a SALM (Single Anchor Leg Mooring) type single point mooring buoy¹⁸⁶⁾ and the mooring of a MAFCO (MARitime Facility of Cylindrical Construction) tower.¹⁸⁷⁾

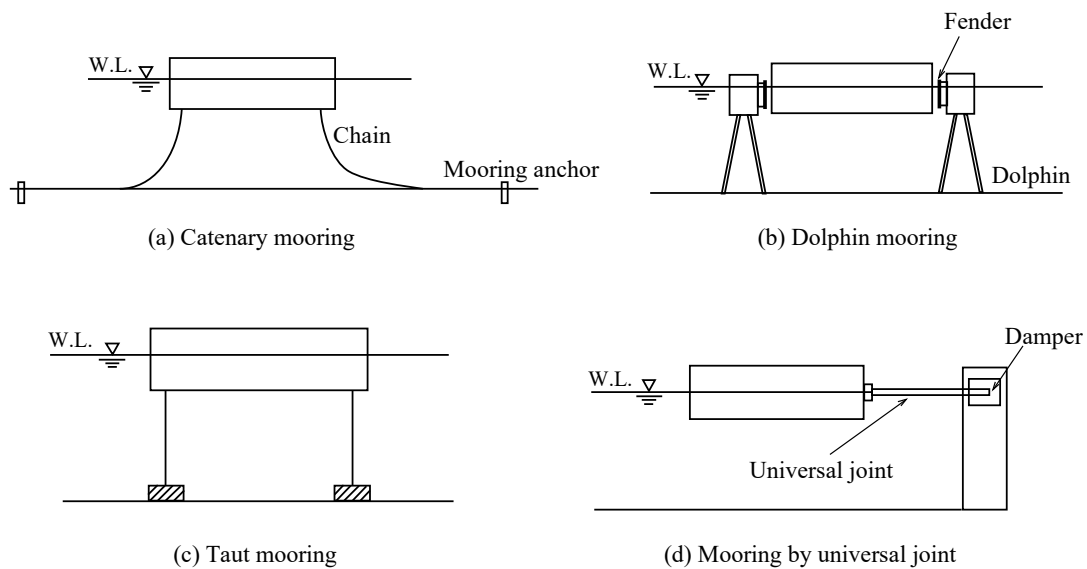


Fig. 4.8.1 Examples of Mooring Methods for Floating Body

4.8.2 Action on Floating Body

(1) Types of Actions and Calculation Methods

When a port facility is made of floating structures, the forces acting on the floating structures and caused by their motions shall be composed of the following forces: wind drag force, drag force by currents, wave-exciting force, wave drift force, wave making resistance force, restoring force, and mooring force. These forces shall be estimated by an appropriate analytical method or hydraulic model tests, in accordance with the mooring method for the floating body and the size of facility.

(2) Wind Drag Force

With a structure for which a part of the floating body is above the sea surface, wind exerts an action on the structure. This action is called the wind drag force or wind pressure and is composed of a pressure drag and a friction drag. If the floating body is relatively small in size, the pressure drag is dominant. The pressure drag is proportional to the square of the wind velocity and is expressed as follows. The subscript k in the following equation refers to the characteristic value:

$$F_{w_k} = \frac{1}{2} \rho_a C_{DW} A_w |U_{w_k}| U_{w_k} \quad (4.8.1)$$

where

F_w : wind drag force (kN)

ρ_a : density of air (t/m³)

A_w : projected area of the part of the floating body above the sea surface as viewed from the direction in which the wind is blowing (m²)

U_w : wind velocity (m/s)

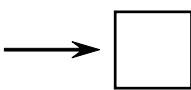
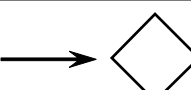
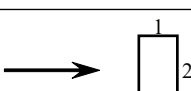

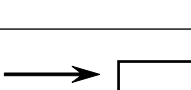

C_{DW} : wind drag force coefficient

The wind drag force coefficient is proportionality constant and is also known as the wind pressure coefficient. It can be determined by wind tunnel tests and others. However, it is also acceptable to use a value that has been obtained in past experiments for a structure with a shape similar to the structure of interest.

Values such as those listed in **Table 4.8.1** have been proposed as the wind drag force coefficients of objects in the uniform flow. As can be seen from this table, the wind drag force coefficient varies with the shape of the floating body, but it is also affected by the wind direction and the Reynolds number. It is considered that the wind pressure

acts in the direction of the wind flow and at the centroid of the projection of the part of the floating body above the water surface. However, it is necessary to pay attention to the fact that this may not necessarily be the case if the floating body is large. Moreover, the velocity of the actual wind is not uniform vertically. Therefore, the value of the wind velocity at the elevation of 10 m above the sea surface is generally employed as the representative wind speed U_W for the wind pressure calculation.

Table 4.8.1 Wind Pressure Coefficients

	Square cross-section	2.0 [1.2] (0.6)
	Square cross-section	1.6 [1.4] (0.7)
	Rectangular cross-section (ratio of side lengths = 1:2)	2.3 [1.6] (0.6)
	Rectangular cross-section (ratio of side lengths = 1:2)	1.5 (0.6)
	Rectangular cross-section (ratio of side lengths = 1:2, when one face is in contact with the ground)	1.2
	Circular cross-section (smooth surface)	1.2 (0.7)

[] is a value when chamfered with a diameter equal to 1/4 of one side
() is a numerical value equal to or more than the critical Reynolds number

(3) Drag Force by Currents

When there is a current, such as tidal currents, these currents exert forces on the submerged part of the floating body. These forces are referred to as the flow pressure or the drag force by currents. Similar to the wind drag force, they are proportional to the square of the flow velocity. Considering that the velocity of the current is generally small, the drag force by current is actually expressed as being proportional to the square of the relative velocity of the current to the motion of the floating body, as shown in the following equation. The subscript k in the following equation refers to the characteristic value:

$$F_{C_k} = \frac{1}{2} \rho_0 C_{DC} A_C |U_{C_k} - U_k| (U_{C_k} - U_k) \quad (4.8.2)$$

where

F_C : drag force by currents (kN)

ρ_0 : density of fluid (t/m³)

A_C : projected area of the submerged part of the floating body as viewed from the direction of the currents (m²)

U_C : velocity of the currents (m/s)

U : velocity of motion of the floating body (m/s)

C_{DC} : drag coefficient with respect to the currents

The drag coefficient with respect to the current C_{DC} is a function of the Reynolds number. However, when the Reynolds number is large, the values for steady flow shown in **Table 7.2.1** may be used.

The drag coefficient for the currents generally varies with the shape of the floating body, the direction of the currents, and the Reynolds number. Similar to the wind pressure, the direction of the force exerted by the currents and the direction of the currents itself are not necessarily the same.¹⁸⁸⁾ In general, the deeper the draft of the floating body relative to the water depth, the larger the drag coefficient for the currents becomes. This is referred to as the shoaling effect, and the drag coefficient increases because a smaller gap between the sea bottom and the base of the floating body increases the difficulty for water to flow through this gap.

(4) Wave-Exciting Force

The wave-exciting force is the force exerted by incident waves on the floating body when the floating body is considered to be fixed in the water. It is composed of a linear force that is proportional to the amplitude of the incident waves and a nonlinear force that is proportional to the square of the amplitude of the incident waves. The linear force is the force that the floating body receives from the incident waves as reaction when the floating body deforms the incident waves. The velocity potential for the deformed wave motion can be obtained by using wave diffraction theory. On the contrary, the nonlinear force is composed of a force that accompanies the finite amplitude nature of waves and a force that is proportional to the square of the flow velocity. The former force due to the finite amplitude effect can be analyzed theoretically; however, it is often ignored in practice. The latter force that is proportional to the square of the flow velocity becomes large, particularly when the diameter of the floating body is small relative to the wavelength; it is preferable to determine this force experimentally.

(5) Wave Drift Force

When waves act on a floating body, the center of the motion of the floating body gradually shifts in the direction of wave propagation. The force that causes this shift is called the wave drift force. If it is assumed that the floating body is 2-dimensional and the wave energy is not dissipated, the wave drift force is given by the following equations.¹⁸⁹⁾ The subscript k in the equation refers to the characteristic value:

$$F_{d_k} = \frac{1}{8} \rho_0 g H_{i_k}^2 R \quad (4.8.3)$$

$$R = K_R^2 \left\{ 1 + \frac{4\pi h / L}{\sinh(4\pi h / L)} \right\} \quad (4.8.4)$$

where

F_d : wave drift force per unit width (kN)

$\rho_0 g$: unit weight of seawater (kN/m³)

H_i : incident wave height (m)

R : wave drift force coefficient

K_R : reflection coefficient

h : water depth (m)

L : wavelength (m)

If the dimensions of the floating body are extremely small relative to the wavelength, the wave drift force may be ignored as being much smaller than the wave-exciting force. However, the wave drift force becomes dominant as the floating body becomes larger.

When random waves act on a floating body moored at a system with only a small restraining force, such as a single-point mooring buoy designed for supertankers, the wave drift force becomes a dominant factor because it may give rise to slow drift oscillations. In this case, the long-period fluctuating wave drift force in the form of the wave drift force has a large effect on the slow drift oscillations of the floating body. For example, if random waves are comprised of waves with two different frequencies, the fluctuating wave drift force is given by the following equation.¹⁹⁰⁾ The subscript k in the equation refers to the characteristic value:

$$F_{d_k} = \frac{1}{4} \rho_0 g H_{i_k}^2 R \left(\frac{\omega_1 + \omega_2}{2} \right) \left\{ 1 + \cos \left(\frac{\omega_1 - \omega_2}{2} \right) t \right\} \quad (4.8.5)$$

where

F_d : wave (fluctuating) drift force per unit width (kN)

$\rho_0 g$: unit weight of seawater (kN/m³)

H_i : incident wave height (m)

$R((\omega_1 + \omega_2)/2)$: wave drift force coefficient by regular wave of $\cos((\omega_1 + \omega_2)/2)$

ω_1 and ω_2 : wave frequency (rad/s)

t : time (s)

(6) Wave Making Resistance Force

When a floating body moves in still water, the floating body exerts a force on the surrounding water, and the floating body receives a corresponding reaction force from the water; this reaction force is called the wave making resistance force. This force can be determined by forcing the floating body to move through the still water and by measuring the force acting on the floating body. However, an analytical method is generally used wherein each mode of the floating body motions is assumed to be realized separately, and the velocity potential, which represents the motion of the fluid around the floating body, is obtained. Only forces that are proportional to the motion of the floating body can be determined analytically; the nonlinear forces that are proportional to the square of the motion cannot be determined analytically. Among the terms of the linear forces, i.e., those that are proportional to the motion of the floating body, the term that is proportional to the acceleration of the floating body is called the added mass term, whereas the term that is proportional to the velocity is called the linear damping term.

(7) Restoring Force

The static restoring forces make a floating body return to its original position when the floating body moves in still water. They are generated in the unbalance state of buoyancy and gravity when the floating body heaves, rolls, or pitches. They are generally treated as proportional to the amplitude of the motion of the floating body, although this proportionality is gradually lost as the amplitude becomes large. However, the static restoring force is often treated as proportional to the amplitude.

(8) Mooring Force

The mooring force is the force (restraining force) that is generated to restrain the motion of the floating body with mooring equipment such as mooring lines. The magnitude of this force depends greatly on the displacement-restoration characteristics of the mooring equipment. Reference 191) can be referred for the materials used in mooring equipment and their characteristic features.

(9) Analytical Method for Wave-Exciting Force and Wave Making Resistance Force by Using Velocity Potential

In the estimation of the wave-exciting force and the wave making resistance force, the velocity potentials which represent the motion of the fluid are derived first and then these two forces are calculated by using the velocity potentials. The derivation methods of the velocity potentials for both forces are fundamentally same except only difference in the boundary conditions. The velocity potentials can be obtained by using any of a number of methods, such as a domain decomposition method, an integral equation method, a strip method, or a finite element method. The outline of the abovementioned numerical calculation methods is introduced in references 192) 193) 194).

When a floating body is fixed in position, the wave force acting on the floating body can be calculated from the velocity potential that satisfies the boundary conditions at the sea bottom and around the floating body. For example, the wave force acting on a floating body with a long rectangular cross-section, such as a floating breakwater, can be determined using the approximate theory of Ito *et al.*¹⁹⁵⁾.

(10) Forces Acting on a Very Large Floating Type Structure

The external forces described in (2) to (9) above for relatively small floating body cannot be directly applied to a very large floating type structure, because its size is very large and its elastic response cannot be neglected. Therefore, it is necessary to perform sufficient examinations on their characteristics.¹⁹⁶⁾

4.8.3 Motions of Floating Body and Mooring Forces

(1) Calculation Methods of Motions of Floating Body and Mooring Forces

The motions of a floating body and the mooring forces shall be calculated by an appropriate analytical method or hydraulic model tests, in accordance with the shape of the floating body and the characteristics of the external forces and mooring equipment.

(2) Motions of Floating Body

The motions of a floating body can be determined by solving the dynamic equilibrium equation, with the external forces due to wind and waves, the restoring force of the floating body itself, and the reaction forces of the mooring equipment. If the floating body is assumed to be a rigid body, then its motions comprise six motion components (**Fig. 4.8.2**): surging, swaying, heaving, pitching, rolling, and yawing. Among these, the horizontal motions of surging, swaying, and yawing, may show slow motions with the period of a few minutes or more in some cases. Such long-period motions have a large influence on the extension range of mooring lines and the performance verification of the mooring equipment. Thus, one may give separate consideration to the long-period motions, by taking only the wave drift force and the long-period fluctuating components of the wind and waves as the external forces when doing analysis. If the floating body is very long, elastic deformation may accompany the motions of the floating body and this should be examined if necessary.

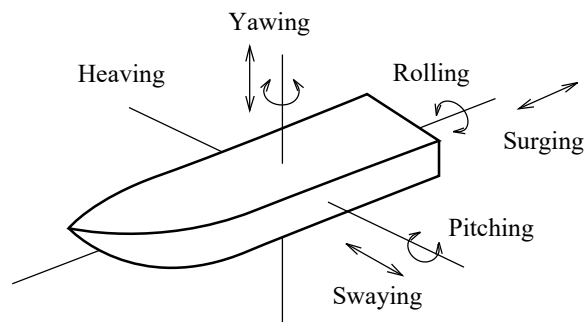


Fig. 4.8.2 Components of Motions of Floating Body

(3) Methods for Solving the Equations of Motion

① Steady state solution method for the nonlinear equations of motion

The equations of motion for a floating body are nonlinear. Therefore, it is not easy to solve the equations. Nevertheless, if the nonlinear terms in the equations of motion are linearized under the assumption that the motion amplitudes are small, the solutions can be obtained relatively easily. For example, the equations for the motions of a 3-dimensional floating body ends up with a system of six simultaneous linear equations for the amplitudes and phases of the six modes of motions. Note that if the floating body is assumed to be a rigid body and its motions are linear, the motions are proportional to the external forces. In particular, if there are no currents or wind, the motions are proportional to the wave height.

② Numerical simulation of nonlinear motions

The wind drag force and the drag force by currents are in general nonlinear, and the mooring force is also often nonlinear. In this case, an effective and general solution method is to use a numerical simulation where the equations of motion are progressively solved for a series of time steps. The equations of motion for the floating body can be divided into the constant coefficient method,¹⁹⁷⁾ in which the coefficient values of the added mass term and linear wave damping term within the equations of motion are fixed at a specific frequency, and the phase lag function method,^{198) 199)} in which these terms are changed over time in a simulation using a phase lag function. The phase lag function method is also called the memory influence function method. In the numerical simulation, the time-series data of the wave-exciting force and the wave induced flow velocity are obtained from the incident wave spectrum, and data of the fluctuating wind speed are obtained from the wind spectrum. The external forces obtained from these time-series data are then placed into the equations of motion for the floating body, and the time-series of the floating body motions and the mooring forces are calculated.

Numerical simulations are applied to the analyses of the motions of various floating bodies. For example, Ueda and Shiraishi¹⁹⁷⁾ performed numerical simulations on the motions of a moored ship, and Suzuki and Moroishi²⁰⁰⁾ analyzed the swinging motion of a ship moored at a buoy. The numerical simulation generally assumes as the preconditions that the fluid is ideal, that the motions of the floating body are small, and that the incident waves are linear and their superposition is allowed. If these assumptions cannot be held, it is preferable to perform hydraulic model tests.

The approximation theory of Ito *et al.*¹⁹⁵⁾, which is relatively easy to handle, can be applied for calculating the motions and mooring forces for a rectangular cross-sectional floating body.

(4) Hydraulic Model Tests

Hydraulic model tests provide a powerful technique for determining the motions of a floating body and the mooring forces. Up to the present time, hydraulic model tests have been performed for various types of floating bodies. For examples, **References 201) 202) 203) and 204)** can be used.

When conducting hydraulic model tests of a floating body, sufficient attention shall be paid to any similarities in the inertia moments of the floating body and the characteristics of mooring equipment. Given that the motion characteristics of the floating body vary significantly by the mooring method, it is particularly important to properly analogize the displacement-restoration characteristics of the mooring equipment. For example, considering that the similarity law for mooring line does not hold just by using the same materials at the site and analogizing the shape, it is necessary to reduce the elastic coefficients of the model materials just by the scale size from those at the site. However, it is practically difficult to look for such a material, and a variety of creative measures needs to be taken.

(5) Statistical Treatment of Motions of Floating Body and Mooring Forces

The motions and mooring forces for a floating body obtained by numerical simulation and hydraulic model tests for random waves vary irregularly with time. Therefore, the peak values of the motion amplitudes and mooring forces for the floating body also vary with time. Even if the wave spectrum is identical, the maximum values for these vary when the duration time or the wave run is different. In other words, given that the motion amplitudes and mooring forces for the floating body are probability variables, statistical treatment should be performed to estimate the expected values. In the usual statistical treatment, a normal distribution or a Rayleigh distribution is applied to the probability density distributions of the peak values of the obtained motion amplitudes and mooring forces, and the expected values are estimated.

(6) Methods for Estimating Expected Values of Motions of Floating Body

The expected values for the motions of a floating body can be estimated by taking into consideration its motion characteristics and by assuming either a normal distribution or a Rayleigh distribution.²⁰¹⁾ The procedure is described below.

① Simulation of oscillation

A simulation of oscillation of a floating body is performed for adequate calculation time, and the values of double amplitudes of the motions are calculated for each wave. The motion double amplitude is defined as a sum of the maximum amplitude and the minimum one for a wave in the time series of the motion of a floating body, similar to the definition of the wave height to the surface wave. The number of waves needed to accurately estimate the expected value of the maximum motions is approximately 100 or more.

② Assumption of the distribution shape of the motion double amplitude

A suitable distribution shape for the double amplitudes of the motions obtained by the simulation of oscillation is assumed. A Rayleigh distribution or a normal distribution shown below may be adopted as the distribution shape.

$$\text{Rayleigh distribution: } P(x)dx = 2a^2 \exp(-a^2 x^2) dx \quad (4.8.6)$$

$$\text{Normal distribution: } P(A) = \frac{1}{\sqrt{2\pi}\sigma^2} \exp\left\{-\frac{1}{2}\left(\frac{A-\bar{A}}{\sigma}\right)^2\right\} \quad (4.8.7)$$

where

$$x=A/A^*$$

A : motion double amplitude

A^* : arbitrary base motion double amplitude

$$a = A^*/(8 m_0)^{1/2}$$

$$(8 m_0)^{1/2} = A_{rms} \text{ (root mean square of the motion double amplitudes)}$$

σ : standard deviation of the motion double amplitudes

\bar{A} : mean value of the motion double amplitudes

However, the value of parameter a is 1.416 when the arbitrary base motion double amplitude A^* is the significant value $A_{1/3}$, and $\sqrt{\pi}/2$ when it is the mean value \bar{A} .

③ Estimation method of the expected value of the maximum values

Assuming that the number of waves is N and that the value at which the exceedance probability becomes $1/N$ is the expected value of the maximum values at that number of waves, the expected value of the ratios of double amplitudes of motions in a Rayleigh distribution is approximated by the following equation when N is sufficiently large.

$$x_N = \frac{1}{a} (\ln N)^{1/2} \quad (4.8.8)$$

On the contrary, in a normal distribution, the expected value of the motion double amplitudes is expressed by the following equation.

$$A_N = \bar{A} + \mu_N \sigma \quad (4.8.9)$$

The expected value of the maximum values varies depending on the number of waves N . **Table 4.8.2** shows the values of x_N and the values of μ_N , which is the parameter of the deviation of a standard normal distribution, relative to the representative values of N .

Table 4.8.2 Values for the Estimation of the Expected Value of the Maximum Values

Number of samples N relative to the expected value of the maximum values	100	200	500	1000	10000
Rayleigh distribution x_N	1.52	1.63	1.76	1.86	2.14
Normal distribution μ_N	2.33	2.58	2.88	3.09	3.96

④ Calculation example of the expected value of the maximum values

For example, assuming a Rayleigh distribution as the distribution shape, consider a case wherein the expected value of the maximum values for the number of waves of 1,000 is calculated. First, the significant value A^* of the double amplitudes of motions is calculated from the simulation results. Thereafter, $a = 1.416$ and $N = 1,000$ are substituted into **equation (4.8.8)**, and the value of x_N is calculated. Finally, the expected value A can be obtained from $x_N = A/A^*$.

4.9 Wave Observations and Investigation

(1) Overview

In shallow water, waves are transformed by processes such as refraction, breaking, and shoaling; therefore, offshore observations are necessary to understand their actual states. Notwithstanding its importance, it has been about 40 years only since the longshore wave observation using measuring instruments began as the routine in Japan. The volume of accumulated wave data is not necessarily enough at present compared with the observed data of tidal level or wind, and wave observation data must be accumulated further for a long time. See **Reference (Part II), 2.4 Observation and Examination of Waves** for details.

The objectives and items of wave observation need to be determined, and the types of observation instruments to use need to be selected depending on observation items. Moreover, with due consideration for the following points the observation point should be selected ³⁾ so that the waves observed at the point can show the representative characteristics of waves in the sea area of interest:

① **A place where the principal wave direction can be observed**

A place that is open to the direction from which the most influential principal waves directly attack the target sea area.

② **Not affected by structures**

No affection of sheltering, reflection, diffraction, or others caused by existing or soon constructed structures such as breakwaters.

③ **Not complicated sea bottom topography**

Not near the steep sloping land or submarine escarpment but relatively flat sea bottom topography. A place where rapid tidal flows should also be avoided.

④ **Not affected by sailing ships and fish catching activities**

There is no frequent traffic of ships or activities of fish boats on the sea where wave observation instruments are installed.

⑤ **Others**

Select an observation point where the observation purpose is fulfilled as far as possible by coordinating with the jurisdictional Maritime Safety Agency, port and coast managing bodies (national government, autonomous bodies, etc.), and concerned parties of users (shipping lines, fishery cooperatives, etc.).

(2) Observation of Tsunamis and Long-period Waves with Offshore Wave Meters

Normally, 20-minute long sea surface observation data are used as a basis for analysis and arrangement of significant wave and so on, but a long-duration sea surface observation data also enable the analysis and arrangement of tsunamis and long-period waves.

① **Recording of offshore tsunami profile**

Previously, the only actual measured data at the sites of tsunamis were run-up traces and tide level recordings. Such data are important for clarifying the actual conditions of tsunamis, but it is not sufficient. In particular, the tidal level variations observed at tide measurement wells inside harbors were records of water level changes through inlet pipes; therefore, in actuality, it was extremely difficult to clearly measure vibration components with short periods less than 10 minutes. For this reason, the offshore tsunami wave profile recordings have a significant meaning.

② **Observation of long period waves**

Information concerning long-period waves from continuous observation data taken using offshore wave gauges is expected to be useful not just when tsunamis occur but also at normal times.

It is often impossible to correctly evaluate harbor calmness on the basis of significant wave height alone, as has been the custom to date. Even when the significant wave height is low and when the waves appear calm in the port, there have been many reports of cases where mooring ropes broke, which made cargo operations impossible, or where maritime construction work was unavoidably interrupted because of the large oscillations of ships and the operation of ships within the port owing to the effects of long-period waves. This is because they can cause resonance with the natural periods of the harbor associated with the port's topography on the order of several minutes to several tens of minutes or with the natural period of mooring systems generated by the mass of the ships and the spring constants of the mooring ropes on the order of several minutes to several tens of minutes.²⁰⁵⁾

(3) Obtaining Wave Observation Documents

Longshore wave observation in Japan is conducted by the Ports and Harbours Bureau of the Ministry of Land, Infrastructure, Transport and Tourism; the Japan Meteorological Agency; electric power companies; local governments; and others. Among them, the **Nationwide Ocean Wave Information Network for Port and HarbourS (NOWPHAS)**, which is administered by Ports and Harbours Bureau of the Ministry of Land, Infrastructure, Transport and Tourism, has the most consummate observation network and data administration and

analysis systems²⁰⁶⁾. Since 1970, NOWPHAS wave observation data have been compiled and published in the Wave Observation Annual Report or Long-Term Statistical Report issued annually.²⁰⁷⁾ NOWPHAS wave observation information is also available on the following site: <http://www.mlit.go.jp/kowan/nowphas/> (Real time wave information)

[References]

- 1) JSCE: Design Handbook for Shore Protection Facilities. JSCE, pp. 301-305, 2000
- 2) Coastal Development Institute of Technology (CDIT): Commentary on analysis and applications of Coastal Waves, Coastal Observation data, p. 181, 2000
- 3) Takayama, T. editorial supervisor, Study Group on Analysis and Utilization of Oceanographic Observation Data Edit: Overview of Waves-Waves, Tsunami, Storm Surge, GPS Ocean Wave Buoy, Coastal Wave Meter-, Coastal Development Institute of Technology (CDIT), 318p, 2013 (in Japanese)
- 4) Borgman, L. E.: Risk criteria, J. Wat. & Harb. Div., Proc. ASCE., Vol. 89, No. WW3, pp. 1-35, 1963
- 5) Hirayama, K., H. Kashima, M. Itsui and T. Naruke: Consideration for Probability of Extreme Swell Occurrences and Characteristics of their Regional Distribution; Journals of JSCE Division B2 (Coastal Engineering), Vol.71 No.2, pp.I_85-I_90, 2015 (in Japanese)
- 6) Matsufuji, E., T. Takayama, M. Miyata, K. Hirayama, H. Kawai, Y. Suzuki, Y. Utsunomiya and Y. Fukunaga: Estimation of Design Wave through Introduction of Swell Effect, Journals of JSCE Division B2 (Coastal Engineering), Vol.73 No.2, pp.I_1153-I_1158, 2017 (in Japanese)
- 7) Hirayama, K., Y. Minami, M. Okuno, K. Minemura, H. Kawai and T. Hiraishi: Case Study on Wave Disaster due to Typhoons in 2004, Technical Note of PHRI, No. 1101, p. 42, 2005
- 8) Takada, E., K. Morohoshi, T. Hiraishi, T. Nagai and S. Takemura: Distribution of wave, storm and tsunami design conditions on Japanese nationwide coastal structures, Technical Note of PARI No. 88, 2003
- 9) Goda, Y.: Revisiting Wilson's formula for simplified wind-wave prediction, J. Waterway, Port, Coastal and Ocean Eng., ASCE, Vol. 129, No. 2, pp. 93-95, 2003
- 10) Hirose, S. and T. Takahashi: Emergence Characteristics of Coastal Waves (Part 2), Proceedings of Coastal Eng. JSCE Vol. 30, JSCE, pp.168-172, 1983
- 11) Gringorten, I.I.: A plotting rule for extreme probability paper, J.Geophysical Res., Vol. 68, No. 3, pp. 813-814, 1963
- 12) Petruaskas, C. and P.M.Aagaard: Extrapolation of historical storm data for estimating design wave heights, Preprints 2nd OTC, No. 1190, 1970
- 13) Goda, Y.: Numerical Investigations on Plotting Formulas and Confidence Intervals of Return Values in Extreme statistics, Rept. of PHRI Vol. 27 No. 1, pp. 31-92, 1988
- 14) Goda, Y.: Wave-resistant Engineering (Wave-resistant design of port and coastal structures), Kashima Publishing, Chapter 13, pp.327-379, 2008
- 15) Goda, Y., O. Kohase and N. Nagai: Demonstrative study on Distribution generating function of extreme wave statistics, Proceedings of Coastal Eng. JSCE Vol. 45, JSCE, pp.211-215, 1998
- 16) Utsunomiya, Y., M. Miyata, T. Takayama, H. Kawai, K. Hirayama, Y. Suzuki, M. Kimizuka and Y. Fukunaga: Estimation and Application of the Largest Class Storm Surge Predicted by Scenario Typhoons, Journals of JSCE Division B2 (Coastal Engineering), Vol.73 No.2, pp.I_1153-I_1158, 2017 (in Japanese)
- 17) NAGAI, T and H. OGAWA: Annual Report on Nationwide Ocean Wave information network for Ports and Harbors (NOWPHAS 2002), Technical Note of PARI, No. 1069, p. 336, 2004
- 18) Nagai, T: Long Term Statistics Report on Nationwide Ocean Wave information network for Ports and Harbors (NOWPHAS 1970-1999), Technical Note of PARI No. 1035, 2002
- 19) Bureau of Port and harbours: Design Manual for prestressed concrete port facilities, 1987
- 20) Coastal Development Institute of Technology (CDIT): Impact Evaluation Manual for long-period waves in ports, Coastal Technology Library No. 21, CDIT, pp.App.B-2-App.B-9, 2004 (in Japanese)
- 21) Goda, Y., "Wave forces on a vertical circular: Experiments and proposed method of wave force computation", Report of the Port and Harbour Research Institute, No. 8, p 24, 1964

- 22) Goda, Y. and K. Nagai: Investigation of the Statistical Properties of Sea Waves with Field and Simulation Data, Report of the Port and Harbour Research Institute, Vol.13, No.1, pp.3-37, 1974 (in Japanese)
- 23) JSCE: Design Handbook for Shore Protection Facilities. JSCE, pp. 31-68, 2000
- 24) Takayama, T., N. Ikeda and T. Hiraishi: Practical Computation Method of Directional Random Wave Transformation, Report of PHRI Vol. 30 No. 1, pp. 21-67, 1991
- 25) Coastal Engineering Committee, JSCE: Coastal waves, JSCE, pp. 46-50, 1994
- 26) Mase, H., T. Takayama, T. Kitano and S. Moriyasu: Study on the Modeling of Diffraction Effect in Phase Averaged Wave Deformation Analysis Model and its Applicability, Journals of JSCE Division B2 (Coastal Engineering), Vol.46, pp.66-70, 1999 (in Japanese)
- 27) HIRAYAMA, K.: Utilization of Numerical Simulation on Nonlinear Irregular Wave for Port and Harbor Design, Technical Note of PARI No. 1036, pp. 162, 2002
- 28) TAKAYAMA, T. and H. FUJI: Probabilistic Estimation of Stability of Slide for Caisson Type Breakwater Author Tomotsuka, Rept. of PHRI Vol. 30 No. 4, pp. 35-64, 1991
- 29) Hiraishi, T.: Generation and Application of Directional Random Waves in a Laboratory, Technical Note PHRI No, 723, p. 176, 1992
- 30) TAKAYAMA, T. and T. HIRAISHI: Amplification Mechanism of Harbor Oscillation Derived From Field Observation And Numerical Simulation, Technical Note of PHRI No. 636, P. 70, 1988
- 31) Coastal Development Institute of Technology (CDIT): Study and Development of Numerical wave channel (CADMAS-SURF), Coastal Development Technology Library No. 12, p 457, 2001
- 32) Hirayama, K and K. Minemura: Simple Estimation for Wave Shoring in an Estuary, Journals of JSCE Division B3 (Ocean Engineering), Vol.21, pp.313-318, 2005 (in Japanese)
- 33) JSCE: Design Handbook for Shore Protection Facilities. JSCE, pp. 9-25, 2000
- 34) Goda, Y.: Wave-resistant Engineering (Wave-resistant design of port and coastal structures), Kashima Publishing, Chapter 13, pp.11-18, 2008 (in Japanese)
- 35) ditto, p.20
- 36) ditto, p.21
- 37) Tanimoto, K., K. Kimura, A. P. dos Santos Pinto: Random Wave Forces and Design Wave Periods of Composite Breakwaters under the Action of Double Peaked Spectral Waves, Rept. Of PHRI, Vol. 25 No. 2, pp. 3-25, 1986
- 38) Goda, Y. and Y. Suzuki: Computation of refraction and diffraction of sea waves with Mitsuyasu's directional spectrum, Technical Note of PHRI, No. 230, p. 45, 1975
- 39) Hashimoto, N.: Study on Estimation Method of Directional Ocean Wave Spectrum, Technical Note of the Port and Harbour Research Institute, No.722, p.118, 1992 (in Japanese)
- 40) GODA, Y.: Numerical Examination of the Measuring Technique of Wave Direction with the 'Covariance Method', Rept. Of PHRI, Vol. 20, No. 3, pp.53-92, 1981
- 41) Sverdrup, H.U. and Munk, W.H.: Wind, sea, and swell; theory of relations for forecasting, U.S. Navy Hydrographic Of.ce, H.O.Pub. 601, pp.1-44, 1947
- 42) Bretschneider, C.L.: Revised wave forecasting relationships, Proc. 2nd Conf. Coastal Engg., ASCE, 1952
- 43) Bretschneider, C.L.: Revisions in wave forecasting, Deep and shallow water, Proc. 6th Conf. Coastal Engg., ASCE, pp. 30-67, 1958
- 44) Wilson, B.W.: Numerical prediction of ocean waves in the Nouth Atlantic for December, 1959, Deut, Hydrogr. Zeit, Jahrgang 18, Heft 3, pp. 114-130, 1965
- 45) JSCE: The Collected Formula of Hydraulics, JSCE, p. 508, 1971
- 46) Mitsuyasu, H.: Development of Wind Wave Spectrum (2)- wind wave spectrum form with finite fetch, Proceedings of Coastal Eng. JSCE Vol. 17, JSCE, pp.1-7, 1970 (in Japanese)
- 47) Wilson, B.W.: Graphical approach to the forecasting of waves in moving fetches, Tech. Memo. No. 73, Beach Erosion Board, U.S. Army Corps of Engrs., 1955

- 48) Ijima, T.: Numerical forecast of waves, JSCE Proceedings of Summer Training on Hydraulic Engineering A, pp. 2-1-2-30, 1968
- 49) Horikawa, K, H. Nishimura, Y. Ozawa and Y. Miyamoto: Wave hindcasting under typhoon in Beppu Bay, Proceedings of the 18th Conference on Coastal Eng. JSCE, pp. 7-12, 1971
- 50) Bretschneider, C.L.: Decay of ocean waves, Fundamentals of ocean engineering-Part 8b, Ocean Industry, pp. 45-50, 1968
- 51) Horikawa, K.: (New Edition) Coastal Engineering, Tokyo University Press, pp. 84-88, 1991
- 52) Isozaki, I. and Uji, T.: Numerical prediction of ocean wind waves, Report of Japan Meteorological Institute Vol. 24, No. 2, pp. 207-231, 1973
- 53) Uji, T.: A coupled discrete wave model MRI-II, J. Oceanogr. Soc. Japan, 40, pp. 303-313, 1984
- 54) Uji, T and Ueno K.: Wave Model MRI-II New, Japan Meteorological Institute Oceanography Division, p. 118, 1987
- 55) Ueno, K. and H. Takano: The third generation wave hindcasting model MRI-3 for on-site operation. Proceeding of Fall Term conference of Oceanographic Society of Japan, P. 153, 1998
- 56) Inoue, T.: On the growth of the spectrum of a wind generated sea according to a modified Miles-Philips mechanism and its application to wave forecasting, Dept. Meteorol. and Oceanogr., New York Univ., TR-67-5, p. 74, 1967
- 57) Yamaguchi, M. and Y. Tsuchiya: Numerical forecast method for waves in finite fetch, Proceedings of the 26th Coastal Engineering, JSCE, pp. 96-100, 1979
- 58) Joseph, P. S. Kawai, S. and Toba, Y.: Ocean wave prediction by a hybrid model-combination of single-parameterized wind waves with spectrally treated swells, Sci. Rept. Tohoku Univ., Ser. 5, Geophs., Vol. 28, No. 1, pp. 27-45, 1981
- 59) The WAMDI Group: The WAM model - A third generation ocean wave prediction model, J. Phys. Oceanogr., 18, pp. 1775-1810, 1988
- 60) Yamaguchi, M, Y. Hatada and Y. Utsunomiya: A shallow water prediction model at a single location and its applicability, Journal of the ASCE Vol. 381/II-7, pp. 151-160, 1987
- 61) Hasselmann, S and K. Hasselmann: Computations and parameterizations of the nonlinear energy transfer in a gravity wave spectrum, Part I, A new method for efficient computations of the exact nonlinear transfer integral, J. Phys. Oceanogr., 15, pp. 1369-1377, 1985
- 62) Janssen, P.A.E.M.: Wave-induced stress and the drag of air flow over sea wave, Journal of Physical Oceanography, vol. 19, pp. 745-754, 1989
- 63) Janssen, P.A.E.M.: Quasi-linear theory of wind wave generation applied to wave forecasting, Journal of Physical Oceanography, vol. 21, pp. 1631-1642, 1991
- 64) Hasselmann, K.: On the non-linear energy transfer in a gravity-wave spectrum, Part 1, General theory, J. Fluid Mech., 12, pp. 481-500, 1962
- 65) Booij, N., Holthuijsen, L. H. and R. C. Ris: The SWAN wave model for shallow water, Proceeding of 25th International Conference on Coastal Engineering, vol. 1, pp. 668-676, 1996.
- 66) Tolman, H. L., and D. V. Chalikov: Source terms in a third-generation wind wave model, J. Phys. Oceanogr., 26, pp. 2497-2518, 1996
- 67) Tolman, H. and the WAVEWATCH III Development Group: User manual and system documentation of WAVEWATCH III version 4. 18, 2014
- 68) Goda, Y: Standard wave spectrum and stochastic characteristics based on numerical simulation, Proceedings of Coastal Eng. JSCE, Vol. 34, pp. 131-135, 1987
- 69) JSCE: Design Handbook for Shore Protection Facilities. JSCE, pp. 33-36, 2000
- 70) Goda, Y.: Wave-resistant Engineering (Wave-resistant design of port and coastal structures), Kashima Publishing, pp.43-45, 2008 (in Japanese)
- 71) Takayama, T.: Wave Diffraction and Wave Height Distribution inside a Harbour, Technical Note of the Port and Harbour Research Institute, No.367, p.140, 1981 (in Japanese)
- 72) Coastal Engineering Committee, JSCE: Coastal waves, JSCE, pp. 27-37, 1994

- 73) Nagai, N., I Tamura and A. Toyoshima: Study on the Diffraction of Irregular Waves due to Breakwaters, Proceedings of the 30th Annual Meeting of JSCE Vol. II-12, pp.22-23, 1975 (in Japanese)
- 74) Goda, Y.: Wave-resistant Engineering (Wave-resistant design of port and coastal structures), Kashima Publishing, pp.49-59, 2008 (in Japanese)
- 75) Sato, S. and Y. Goda: Coast and Harbour, Easy-to-understand Civil Engineering Lecture, Shokokusha Publishing, pp. 72-75, 1971
- 76) Kubo, Y., Y. Kotake, M. Isobe and A. Watanabe: Time-dependent mild slope equation for random waves, Proceedings of Coastal Engineering JSCE No. 38, pp. 46-50, 1991
- 77) Hiraishi, T. I. Uehara and Y. Suzuki: Applicability of Wave Transformation Model in Boussinesq Equation, Technical Note of PHRI No. 814, p. 22, 1995
- 78) Nadaoka, K and Y Nakagawa: Derivation of fully-dispersive wave equations for irregular wave simulation and their fundamental characteristics, Journal of the JSCE, No. 467/II-23, pp. 83-92, 1993
- 79) Coastal Engineering Committee, JSCE: Coastal waves, JSCE, pp. 15-118, 1994
- 80) Hirayama, K.: Wave Transformation Calculation with Boussinesq Model and its Local Applicability, Text of the 43th Summer Workshop on Hydraulic Engineering, B-7, Conferences on Hydraulic Engineering and Coastal Engineering of JSCE, p.20, 2017 (in Japanese)
- 81) Nishimura, K., H. Kato, J. Inoue, I. Nakamura and S. Muratra: Numerical simulation and hydraulic model test on wave height distribution about an island, Proceedings of 27th Coastal Eng. JSCE, pp.65-69, 1980
- 82) Goda, Y.: Wave-resistant Engineering (Wave-resistant design of port and coastal structures), Kashima Publishing, p.83, 2008 (in Japanese)
- 83) Hirayama, K: Numerical Simulation of Nonlinear Partial Standing Waves using the Boussinesq Model with New Reflection Boundary, Rept. of PHRI Vol. 40, No. 4, pp. 3-48, 2001
- 84) Goda, Y., Y. Suzuki, Y. Kishira and O. Kikuchi, Estimation of incident and Reflected Waves in Random Wave Experiments, Technical Note of PHRI No. 248, p. 24, 1976
- 85) Sawaragi, T Edition: New Coastal Engineering for environmental sphere, Fuji Techno System, pp. 251-252, 1999
- 86) ditto, p.253
- 87) Kobune, K and M. Osato: A Study of Wave Height Distribution along a Breakwater with a Corner, Report of PHRI, Vol. 15 No. 2, 1976
- 88) Ito, Y. and K. Tanimoto: Meandering Damages of Composite Breakwaters, Technical Note of PHRI, No. 112, 1971
- 89) Goda, Y. and T. Yoshimura: Wave Force Computation for Structures of Large Diameter, Isolated in the Offshore, Report of PHRI Vol. 10, No. 4, pp. 3-52, 1971
- 90) Shuto, N.: Transformation of long wave- for the case of changing channel width and depth-, Proceedings of 21st Conference on Coastal Engineering JSCE, pp. 57-64, 1974
- 91) Goda, Y: Rearrangement of breaker indices, Journal of Civil Engineering No. 180, JSCE, pp. 39-49, 1970
- 92) Goda, Y.: Reanalysis of Breaking Wave Statistics for Engineering Applications, Proceedings of Coastal Eng. JSCE Vol. 54, JSCE, pp.81-85, 2007 (in Japanese)
- 93) Goda, Y.: Deformation of Irregular Waves due to Depth-controlled Wave Breaking, Report of the Port and Harbour Research Institute, Vol.14 No.3, 1975
- 94) Goda, Y.: Wave-resistant Engineering (Wave-resistant design of port and coastal structures), Kashima Publishing, p.73, 2008 (in Japanese)
- 95) JSCE: Design Handbook for Shore Protection Facilities. JSCE, pp. 90, 2000
- 96) Takayama, T., Y. Kamiyama and O. Kikuchi: Wave Transformation On a Reef, Technical Note of PHRI No. 278, pp. 32, 1977
- 97) Egashira, K, I. Fukuda, Y. Kishira and T. Nishimura: Field observation of transformation of waves on reefs, Proceedings of 32nd conference on Coastal Engineering, JSCE, pp. 90-94, 1985
- 98) Goda, Y.: Revision of 3-D Random Wave Transformation Model with Gradational Breaker Index, Journals of JSCE Division B3 (Ocean Engineering), Vol.19, pp.141-146, 2003 (in Japanese)

- 99) Uno, Y. and K. Hirayama: Characteristics of the Wave Breaking Model on the Production and Dissipation Process of Turbulence, Journals of JSCE Division B2 (Coastal Engineering), Vol.68 No.2, pp.I_026-I_030, 2012 (in Japanese)
- 100) Hirayama, K. and Y. Aida: Characteristics of Surf-beat Distribution on a Reef Estimated by Using Boussinesq Model, Journals of JSCE Division B3 (Ocean Engineering), Vol.72 No.2, pp.I_330-I_335, 2016 (in Japanese)
- 101) Tamada, T., H. Mase and T. Yasuda: Random Wave Runup Formulae for Seawall with Composite Cross Section, Journals of JSCE Division B2 (Coastal Engineering), Vol.B2-65 No.1, pp.936-940, 2009 (in Japanese)
- 102) Mase H.: Random wave runup height on gentle slope, J. Waterway, Port, Coastal and Ocean engineering, ASCE, Vol. 118, No. 5, pp. 649-664, 1989.
- 103) Mase, H., T.S. Hedges M. Share and S. Nagase: Study on wave overtopping rate of sloping coastal dikes considering wave up rush, Journals of JSCE Division B2 (Coastal Engineering), Vol.50, pp.636-640, 2003 (in Japanese)
- 104) Van der meer, J.W. and C.M.Stam: wave runup on smooth and rock slopes of coastal structures, J. Waterway, Port, Coastal and Ocean Engineering, ASCE, Vol. 118, No. 5, pp. 534-550, 1992
- 105) Saville, T. Jr.: Wave run-up on composite slopes, Proc.6th Conf. on Coastal Eng., pp. 691-699, 1958
- 106) Nakamura, A, Y. Sasaski and J. Yamada: Study on wave run-up on the composite slopes, Proceedings of 19th Conference on Coastal Eng., JSCE, pp. 309-312, 1972
- 107) Hosoi, M. and H. Mitsui: Wave up rush on the sea walls placed inner shore inside breaker line, Proceedings of 9th Coastal Eng., JSCE, pp. 143-148, 1962
- 108) Hosoi, M. and N. Shuto: Wave up rush for the case of diagonal incident wave, Proceedings of 9th Coastal Eng., JSCE, pp. 149-152, 1962
- 109) Sakuraba, M., T. Sakakiyama, T. Arikawa, A. Inoue, J. Nakahira and M. Wada: An Investigation for Applicability of Wave Runup by CADMAS-SURF, Journals of JSCE Division B3 (Ocean Engineering), Vol.24, pp.867-872, 2008 (in Japanese)
- 110) Japan Society of Civil Engineers: Numerical Wave Flume- Deepening of Breaking Wave Calculation and Renovation of Wave Resistant Design, pp.43-53, 2012 (in Japanese)
- 111) Sakuraba, M, S. Hirosaki and K. Kashiya: Numerical calculation of wave overtopping and wave run-up by CIVA/Level set method, Proceedings of Coastal Eng. No. 51, JSCE, pp. 36-40, 2004
- 112) Hirayama, K., K. Haruo and I Miyasato: Evaluation of Design Wave Condition for Seawall on Coral Reef Calculated in Boussinesq-type Wave Transformation Model, Report of the Port and Airport Research Institute, Vol.48 No.3, pp.23-74, 2009 (in Japanese)
- 113) Hirayama, K., M. Moriuchi, M. Itsui, T. Kachi and T. Tamada: Evaluation for Distribution of Wave Overtopping Discharge along Coastal Seawall with H2D Boussinesq Model, Journals of JSCE Division B3 (Ocean Engineering), Vol.68 No.4, pp.I_780-I_785, 2012 (in Japanese)
- 114) Honda, T. and K. Ito: Study on Applicability of a Numerical Wave Flume for Overtopping by Irregular Waves, Journals of JSCE Division B2 (Coastal Engineering), Vol.55, pp.816-820, 2008 (in Japanese)
- 115) Goda, Y, Y. Kishira and Y. Kamiyama: Laboratory investigation on the overtopping rate of seawalls by irregular waves, Rept. Of PHRI Vol. 14, No. 4, pp. 3-44, 1975
- 116) GODA Y. and Y. KISHIRA: Experiments on irregular Wave Overtopping Characteristics of Seawalls of Low Crest Types, Technical Note of PHRI No. 242, p. 28, 1976
- 117) TAKAYAMA, T. T. NAGAI and K. NISHIDA: Decrease of Wave Overtopping Amount due to Seawalls of Low Crest Types, Rept. Of PHRI Vol. 21 No. 2, pp. 151-205, 1982
- 118) Takayama, T. T. Nagai, K. Nishida and T. Sekiguchi: Hydraulic Model Test for wave overtopping characteristics of sea walls against diagonal random incident waves, Proceeding of Coastal Eng. JSCE, Vol. 31, pp. 542-546, 1984
- 119) HIRAISHI, T. N. MOCHIZUKI, K. SATO, H. MARUYAMA, T. Kanazawa, 榎本達也: Effect of Wave Directionality on Overtopping at Seawall, Rept of PHRI Vol. 35 No. 1, pp. 39-64, 1996

- 120) Tamada, T., M. Inoue and T. Tezuka: Experimental Study on Wave Overtopping Discharge Calculation Chart of Gentle Slope Revetment and its Overtopping Wave Reduction Effects, Journals of JSCE Division B2 (Coastal Engineering), Vol.49, pp.641-645, 2002 (in Japanese)
- 121) Tamada, T., H. Mase and T. Yasuda: Prediction Formula of Wave Overtopping Discharge Including Wave Runup, Journals of JSCE Division B2 (Coastal Engineering), Vol.66 No.1, pp.926-930, 2010 (in Japanese)
- 122) Mase, H., T. Tamada, T. Yasuda and K. Kawasaki: Integrated Formula of Wave Overtopping and Runup Modeling for Seawalls, Journals of JSCE Division B2 (Coastal Engineering), Vol.72, pp.83-88, 2016 (in Japanese)
- 123) Mase, H., T. Tamada and T. Yasuda: Integrated Formula of Wave Overtopping and Runup Modeling for Vertical Seawalls Based on Clash Datasets, Journals of JSCE Division B2 (Coastal Engineering), Vol.71 No.2, pp.I_847-I_852, 2015 (in Japanese)
- 124) CLASH project: <http://www.clash.ugent.be/>, presented by De Rouck, J., H. Verhaeghe and J. Geeraets, Crest level assessment of coastal structures. General overview, J. Coastal Eng., Vol. 56, Issue 2, pp. 99-107, 2009
- 125) EurOtop: European manual for the assessment of wave overtopping, T. Pullen, N. W. H. Allsop, T. Bruce, A. Kortenhaus, H. Schuttrumpf and J. W. Van der Meer eds., HR Wallingford, Wallingford, U.K., 2007
- 126) Goda, Y.: Proposal of Unified Formulas for Wave Overtopping Rate of Seawalls Based on Clash Database, Journals of JSCE Division B3 (Ocean Engineering), Vol.24, pp.939-944, 2008 (in Japanese)
- 127) Miyajima, S. S. Ogura, Y. Ohashi, T. Morikawa and S. Okuda: Experimental Study on wave overtopping rate of sloping sea wall having parapet, Proceeding of Coastal Eng. JSCE, Vol. 51, pp. 636-640, 2004
- 128) GODA, Y: Estimation of the Rate of Irregular Wave Overtopping of Seawalls, Rept. Of PHRI Vol. 9, No. 4, pp. 3-41, 1970
- 129) Fukuda, N. T. Uno and I. Irie: Field observation of wave overtopping at sea walls (Second Report) Proceeding s of 20th Coastal Eng. JSCE, pp. 113-118, 1973
- 130) Allsop, N. W. H., L. Franco, G. Bellotti, T. Bruce and J. Geeraerts: Hazards to people and property from wave overtopping at coastal structures, Coastlines, Structures and Breakwaters, (Proc. Int. Conf.) Inst. Civil. Engrs., Thomas Telford, pp. 153-165, 2005
- 131) Kimura, K., M. Hamaguchi, M. Okada and T. Shimizu: Characteristics of Wave Overtopping Splash due to Wave Dissipating Seawalls and its Effects on Roads at the Back of Seawalls, Journals of JSCE Division B2 (Coastal Engineering), Vol.50, pp.796-800, 2003 (in Japanese)
- 132) Nagai, S. and A. Takada: Effect of wave absorbing blocks on wave overtopping at coastal dikes, Proceeding of 11th Coastal Eng. JSCE, pp. 279-286, 1964
- 133) Suzuki, Y., T. Hiraishi, N. Mochizuki and T. Morikawa: Hearing Investigation on Wave Overtopping Damage to Seawalls, Journals of JSCE Division B2 (Coastal Engineering), Vol.41, pp.681-685, 1994 (in Japanese)
- 134) YASUDA, T and T. HIRAISHI: Highly Accurate Inundation Simulation by MARS Method on Compound Coastal Urban Area: Rept of PARI Vol. 43, No. 2, pp. 3-34, 2004
- 135) Yamashiro, M., A. Yoshida, H. Hashimoto, N. Kurushima and I. Irie: Conversion of the Wave Velocity in Wave-overtopping Experiment into the Wind Velocity of Real Coast, Journals of JSCE Division B3 (Ocean Engineering), Vol.20, pp.653-658, 2004 (in Japanese)
- 136) Goda, Y.: Wave-resistant Engineering (Wave-resistant design of port and coastal structures), Kashima Publishing, pp.91-96, 2008
- 137) Goda, Y. Y. Suzuki and Y. Kishira: Random wave model test and the characteristics, Proceedings of 21st Coastal Eng. JSCE, pp. 237-242, 1974
- 138) Hirayama, K. and J. Naganuma: Effects of Transmitted Waves through Breakwaters due to Wave Overtopping for Harbor Tranquility, Journals of JSCE Division B2 (Coastal Engineering), Vol.70 No.2, pp.I_761-I_765, 2013 (in Japanese)
- 139) Hirayama, K., H. Kashima, K. Hayashi and Y. Igarashi: Numerical Calculation of Observed Transmitted Waves by Using Boussinesq-type Wave Transformation Model, Journals of JSCE Division B3 (Ocean Engineering), Vol.69 No.2, pp.I_682-I_687, 2013 (in Japanese)
- 140) Matsumoto, A.: Numerical Analysis on Wave Transmission over Breakwaters Using VOF-type Numerical Wave Flume, Journals of JSCE Division B2 (Coastal Engineering), Vol.65 No.1, pp.781-785, 2009 (in Japanese)

- 141) Kondo, T. and I. Sato: A study on the crest height of breakwaters, Journal of Public Works Research Institute (PWRI), Hokkaido Regional Development Bureau (HRDB) No. 117, pp. 1-5, 1964
- 142) Tanimoto, K, M. Osato: An experiment on stability of breakwaters with wave-absorbing blocks against random waves, Proceedings of the 26th Coastal Eng., JSCE, pp. 309-313, 1979
- 143) Sakamoto, Y. Y. Miyaji T. Uenishi and H. Takeda: Experimental study on hydraulic characteristics of sloping sea walls, Journal of Public Works Research Institute, Hokkaido Regional Development Bureau Vol. 82, 1984
- 144) Tanaka, N.: Wave Reduction and Beach Stabilization Effects of Submerged Breakwaters with Wide Crown Widths, Proceedings of Coastal Eng. JSCE Vol. 23, JSCE, pp.152-157, 1976
- 145) Kondo, T. and H. Takeda: wave absorbing facilities, Motikita Publishing, pp. 70-114, 1983
- 146) Numata, A.: Experimental Study on Wave Dissipating Effect of Block Levees, Proceedings of Coastal Eng. JSCE Vol. 22, pp.501-505, 1975
- 147) MORIHIRA, M., S. KAKIZAKI and Y. GODA: EXPERIMENTAL INVESTIGATION OF A CURTAIN-WALL BREAKWATER, Rept. Of PHRI Vol. 3 No. 1, pp. 1-27, 1964
- 148) Sawaragi, T Edition: New Coastal Engineering for environmental sphere, Fuji Techno System, p. 258, 1999
- 149) Longuet-Higgins, M.S. and R.W. Stewart: Radiation stress and mass transport in gravity waves with application to surf beats, Jour. Fluid Mechanics Vol. 13, pp. 481-504, 1962
- 150) Goda, Y. Design diagram of wave set-up and longshore currents under directional random waves, Proceedings of Ocean Development Vol. 21, pp. 301-306, 2005
- 151) HIRAISHI, T, A. TADOKORO and H. FUJISAKU: Characteristics of Long Period Wave Observed in Port, Rept. Of PHRI Vol. 35 No. 3, pp. 3-36, 1996
- 152) Coastal Development Institute of Technology (CDIT): Impact Evaluation Manual for long-period waves in ports, Coastal Technology Library No. 21, CDIT, pp. 1-14, 2004
- 153) KATO, K., S. NAKAMURA and N. IKEDA: Estimation of Infragravity Waves in Consideration of Wave Groups (An Examination on Basis of Field Observation at HORF), Rept of PHRI Vol. 30 No. 1, pp. 137-163, 1991
- 154) Hiraishi, T., S. Kawano S. Tamaki and J. Hasegawa: Standard wave spectrum of long period wave employed in the design of port and harbour facilities, Proceeding of Coastal Eng. JSCE No. 44, pp. 246-250, 1997
- 155) Hirayama, K., H. Kashima, J. Naganuma and Y. Uno: Harbor Tranquility Analysis for Long Period Waves Propagated from Offshore and Generated on Harbor Entrance, Journals of JSCE Division B3 (Ocean Engineering), Vol.70 No.2, pp.I_211-I_216, 2014 (in Japanese)
- 156) Hirayama, K. and H. Kashima: Estimation of Infragravity Wave Spectrum with Variable Parameter Related to Properties of Wind Wave, Journals of JSCE Division B2 (Coastal Engineering), Vol.70 No.2, pp.I_116-I_120, 2014 (in Japanese)
- 157) Coastal Development Institute of Technology (CDIT): Impact Evaluation Manual for long-period waves in ports, Coastal Technology Library No. 21, CDIT, pp. 48-52, 2004
- 158) ditto, p.49
- 159) Hiraishi, T, K. Hirayama, K. Ozawa and Y. Moriya: Wave Absorbing Capacity of Long Period Wave Countermeasures in Harbor, Technical Note of the Port and Airport Research Institute, No.1205, p.16, 2009 (in Japanese)
- 160) Yamada, A., H. Kunisu, T. Tamehiro, K. Kohirata and T. Hiraish: Examination of Wave Dissipating Structures to the Long Period Wave in the Ishinomaki Harbor, Journals of JSCE Division B3 (Ocean Engineering), Vol.21, pp.785-790, 2005 (in Japanese)
- 161) Ozawa, K, Y. Moriya, S. Yamamoto, K. Hirayama and T. Hiraishi: Harbor Tranquility Improvement Effect of Long Period Wave Countermeasure Facility in Akita Harbor, Journals of JSCE Division B3 (Ocean Engineering), Vol.25, pp.653-658, 2009 (in Japanese)
- 162) Matsuno, K., T. Yano, H. Kasai, T. Yamamoto, T. Hiraishi and K. Kimura: Field Observation of Long-period Wave Absorbers in Tomakomai Nishi Port, Journals of JSCE Division B2 (Coastal Engineering), Vol.67 No.2, pp.681-685, 2011 (in Japanese)

- 163) Hirayama, K., K. Kawauchi and I. Miyazato: Experimental Study on Wave Reflection Coefficients of Wave Dissipating Works for Oblique Incident Waves, Journals of JSCE Division B2 (Coastal Engineering), Vol.67 No.2, pp.I_686-I_690, 2011 (in Japanese)
- 164) Tanaka, M., A. Mtsumoto, M and Hanzawa: Experimental Study on Wave Absorbing Properties of Submerged Mound Type Long-period Wave Absorbing Structures, Journals of JSCE Division B3 (Ocean Engineering), Vol.68, pp.I_816-I_816, 2012 (in Japanese)
- 165) UEDA, S., S. SHIRAISHI, H. OSHIMA and K. ASANO: Allowable Wave Height and Wharf Operation Efficiency Based on the Oscillations of Ships Moored to Quay Walls, Technical Note of PHRI No. 779, p. 44, 1994
- 166) Hirayama, K.: Harbor Tranquility Analysis Method for Using Boussinesq-type Nonlinear Wave Transformation Model, Technical Note of the Port and Airport Research Institute, No.1159, p.90, 2007 (in Japanese)
- 167) Coastal Development Institute of Technology (CDIT): Impact Evaluation Manual for long-period waves in ports, Coastal Technology Library No. 21, CDIT, pp.17-18 and App.A-2-App.A-7, 2004
- 168) ditto, p.19
- 169) Japan Association of Marine Safety: Survey and Study on Fundamental Elements of Sea Transport Safety (Report 3) - Effect of Ship Waves on Small Crafts, p.83, 1976. (in Japanese)
- 170) Japan Shipping Exchange, Inc.: Register of Ships (2017), 2017. (in Japanese)
- 171) Shiotani, S.: On comparison of estimation methods of ship waves, Journal of Japan Institute of Navigation, Vol.106, pp.271-277, 2002. (in Japanese)
- 172) Takenouti, Y. and K. Nanasawa: About "GUNKAN-NAMI" (warship wave) which reaches on the Imabari Beach as significant breakers, Journal of the Oceanographical Society of Japan, Vol.17, No.2, pp.80-90, 1961. (in Japanese)
- 173) Ertekin, R. C., W. C. Webster and J. V. Wehausen: Ship-generated solitons, Proc. of the 15th Symposium on Naval Hydrodynamics, pp.347-364, 1985.
- 174) Coastal Development Institute of Technology: Technical Manual for Floating Structure, p.115, 1991. (in Japanese)
- 175) Kanda, K., N. Shiraishi and Y. Takino: About oscillation characteristics of floating type wharves, Proceedings of Civil Engineering in the Ocean, Vol.2, pp.163-168, 1986. (in Japanese)
- 176) Toyoda, S.: Floating oil storage system, The 4th Ocean Engineering Symposium, Society of Naval Architects of Japan, pp.25-50, 1979. (in Japanese)
- 177) Kogure, K., Y. Suzuki, M. Katagiri and T. Yakuwa: Design and construction of floating breakwater, Proceedings of Coastal Engineering, Vol.30, pp.435-439, 1983. (in Japanese)
- 178) Maruyama, T.: Construction of movable floating bridge, The 14th Ocean Engineering Symposium, Society of Naval Architects of Japan, pp.327-334, 1998. (in Japanese)
- 179) Public Works Bureau, Osaka City: Record of Construction of YUMEMAI Bridge, Osaka City, 2002. (in Japanese)
- 180) Miyamoto, T.: Floating disaster prevention basis, Cargo-handling, Vol.44, No.3, Japan Association of Cargo-handling Mechanization, 1999. (in Japanese)
- 181) Kozawa, T., Y. Miyachi, T. Koizumi, K. Wada and Y. Matsushita: Provision of Floating Disaster Prevention Basis, Proceedings of Techno-Ocean 2000 International Symposium, Techno-Ocean Network, pp.623-628, 2000.
- 182) Coastal Development Institute of Technology and Floating Structures Association of Japan: Study Report of Large Scale Floating Structure, p.638, 1995. (in Japanese)
- 183) Technological Research Association of Mega-Float: Fiscal Year 1997 Study Report of Very Large Floating Offshore Structure (Mega-Float), p.350, 1998. (in Japanese)
- 184) Floating Structures Association of Japan: Large Scale Floating Structure, Kajima Institute Publishing, p.172, 2000. (in Japanese)
- 185) Technological Research Association of Mega-Float: Demonstrative Study on Utilization of Mega-Float as Airport (Mega-Float Technology Study Report) -Summary of the Results of Phase II and the Results in Fiscal Year 2000-, p.228, 2001. (in Japanese)

- 186) Takayama, T., T. Hiraishi, M. Furukawa, K. Sao and S. Tachino: Field Observation of Motions of a SALM Buoy and Tensions of Mooring Hawsers, Technical Note of PHRI, No.542, p.38, 1985. (in Japanese)
- 187) Iwatani, F., S. Miyai and K. Mishina: Wave observation at Sakata Port utilizing new structural type, Proceedings of Civil Engineering in the Ocean, Vol.2, pp.97-102, 1986. (in Japanese)
- 188) Tsuji, T., N. Mori and Y. Yamanouchi: On the Force Acting on a Ship in Oblique Flow, Rept. of Ship Research Institute, Vol.6, No.5, pp.15-28, 1969. (in Japanese)
- 189) Nojiri, N. and K. Murayama: Study on drift force acting on 2-dimensional floating body in regular waves, Transactions of the West-Japan Society of Naval Architects, Vol.51, pp.131-152, 1976. (in Japanese)
- 190) Matora, S., T. Koyama, M. Fujino and H. Maeda: (Revised Edition) Dynamics of Ships and Offshore Structures, Seizando-Shoten Publishing, pp.220-224, 1997. (in Japanese)
- 191) Port and Harbour Research Institute and Ports and Harbours Bureau, Ministry of Transport: Study Report on Development of Construction Methods of Floating Structures, p.171, 1985. (in Japanese)
- 192) Coastal Engineering Committee, JSCE: Coastal Waves, JSCE, pp.291-429, 1994. (in Japanese)
- 193) Akishima Laboratories (Mitsui Zosen): Akishima Laboratories 15th Anniversary -Trace of Research and Development-, pp.105-130, 1995. (in Japanese)
- 194) Performance Working Group, Ocean Engineering Committee, Society of Naval Architects of Japan: Practical Guide for Hydrodynamics of Floating Body (First Part) Numerical Calculation Methods for Oscillation Problems, Seizando-Shoten Publishing, p.291, 2003. (in Japanese)
- 195) Itou, Y. and S. Chiba: An Approximate Theory of Floating Breakwaters, Rept. of PHRI, Vol.11, No.2, pp.15-28, 1972. (in Japanese)
- 196) Ocean Engineering Committee, Society of Naval Architects of Japan: Mega-Float Offshore Structure, Seizando-Shoten Publishing, p.351, 1995. (in Japanese)
- 197) Ueda, S. and S. Shiraishi: Method and its Evaluation for Computation of Moored Ship's Motions, Rept. of PHRI, Vol.22, No.4, pp.181-218, 1983. (in Japanese)
- 198) Cummins, W. E.: The impulse response function and ship motions, Schiffstechnik, Bd.9, Heft 47, pp.101-109, 1962.
- 199) Kubo, M. and S. Okamoto: Study on precision improvement of time series analysis of a moored floating body in front of a quaywall using retarded function, Proceedings of Coastal Engineering, Vol.34, pp.611-615, 1987. (in Japanese)
- 200) Suzuki, Y. and K. Moroishi: On the Slow Motions of Ships Moored to Single-Point Mooring Systems, Rept. of PHRI, Vol.21, No.2, pp.107-150, 1982. (in Japanese)
- 201) Ueda, S.: Analysis Method of Ship Motions Moored to Quay Walls and the Applications, Technical Note of PHRI, No.504, p.372, 1984. (in Japanese)
- 202) Suzuki, Y.: Study on the Design of Single Point Buoy Mooring, Technical Note of PHRI, No.829, p.48, 1996. (in Japanese)
- 203) Shiraishi, S., K. Nazato and H. Kawahara: A Study on the Characteristics of Motions of Pleasure Boats and Floating Piers in a Marina, Technical Note of PHRI, No.950, p.63, 1999. (in Japanese)
- 204) Yoneyama, H., K. Ohgaki, M. Tsuda, A. Kurihara, T. Hiraishi and T. Aono: Model Experiments and Numerical Simulation on Tsunami Impact to a Moored Ship, Technical Note of PARI, No.1213, p.27, 2010. (in Japanese)
- 205) Coastal Development Institute of Technology (CDIT): Impact Evaluation Manual for long-period waves in ports, Coastal Technology Library No. 21, CDIT, p. 86, 2004
- 206) Nagai, T: Study on Japanese Coastal Wave Characteristics Obtained from the NOWPHAS Wave Observation Network, Technical Note of PHRI No. 863, p. 113, 1997 (in Japanese)
- 207) Kawaguchi, K., S. Sakuraba and T. Fujiki : Annual Report on Nationwide Ocean Wave Information Network for Ports and Harbours (NOWPHAS2014), Technical Note of PHRI, No.1319, p.126, 2016 and so on (in Japanese)
- 208) JSCE: The Collected Formula of Hydraulics (1971 Edition), JSCE, p. 533, 1971

5 Tsunamis

[Public Notice] (Design Tsunami)

Article 9

Design tsunamis shall be appropriately defined in terms of the tsunami height and others based on historical tsunami records or numerical analyses.

[Interpretation]

7. Setting of Natural Conditions, etc.

(3) **Items related to waves** (Article 6 of the Ministerial Ordinance and the interpretation related to Article 8 and 9 of the Public Notice)

④ Setting of the design tsunami

The design tsunami and the excess design tsunami used to performance verification shall be larger than the frequent tsunami of several ten year- to one hundred and several ten year-return period and be properly set according to the importance of the facilities concerned.

(1) Definition of Terminology Related to Tsunamis

Most of tsunamis are a series of waves that are generated as vertical fluctuation of the sea surface by the uplift and subsidence of sea bottom due to submarine earthquakes and propagate to the coast. Other causes of the tsunamis are large landslides into or in sea, the undersea volcano eruptions, etc.

The sea bottom displacement may extend in a horizontal direction for several tens of kilometers but water depth is several kilometers at most. As the range of a crustal movement is considerably wider than the range to which surface waves propagate during crustal movement, sea surface fluctuation occurs. This sea surface fluctuation becomes the initial tsunami profile. The sea surface fluctuation due to crustal movement can be treated as the sum of vertical amount of sea bottom displacement and the vertical amount of sea bottom displacement due to horizontal movement of undulating topography of the sea bed ¹⁾. As an initial tsunami profile has an extremely long wavelength compared to the water depth, the sea surface fluctuation propagates outward as a long wave.

Terminology of the tsunamis is as shown in **Fig. 5.1.1**.

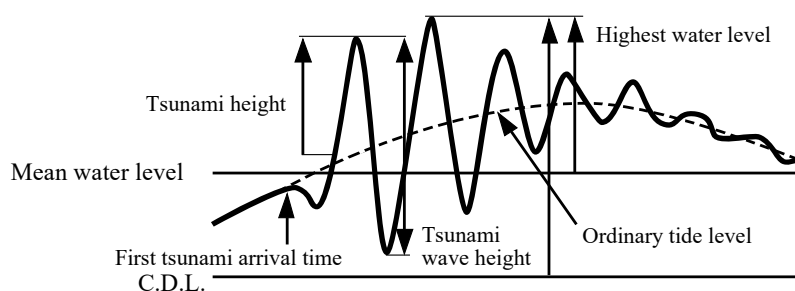


Fig. 5.1.1 Tsunami Terminology

① Ordinary tide level

Ordinary tide level is the level of the sea surface when there is no tsunami. It is expressed in height relative to the mean sea level (M.S.L.) in Tokyo Bay (T.P.) or the lowest astronomical tide (D.L.). It may be deviated from the astronomical tide level calculated from harmonic components of tide due to factors such as atmospheric pressure changes, winds, and changes in ocean currents.

② Tsunami height

The value of the difference between the actual tidal level and the ordinary tidal level is referred to as deviation. The maximum value of the deviation when the actual tidal level is higher than the estimated tidal level is

referred to as the maximum deviation or the tsunami height. It is necessary to recognize that the tsunami height is different from the tsunami wave height as described later.

③ Highest water level

The maximum value of the tidal level that is measured during a tsunami is called the highest water level. It is indicated by the sea-surface height relative to the mean sea level (M.S.L.) in Tokyo Bay (T.P.) or the lowest astronomical tide (D.L.).

④ Tsunami wave height and period

Wave profiles of tsunami are irregular. In the same way as analysis of wind waves, the tsunami can be analyzed by the zero up-crossing method to define the tsunami wave height and period for an individual wave. An individual wave is defined to extend from a point where the observed sea surface water level crosses over the ordinary tide level from the negative side to the positive side, to the next such point. The difference between the highest water level and the lowest water level within the individual wave is defined as the tsunami wave height, while the time duration of the individual wave is defined as the tsunami period. Finally, the highest value within a series of tsunami wave heights is called the highest tsunami wave height.

⑤ Initial movement

Initial movement refers that the detaching of observed tidal level from the ordinary tidal level. When the first observed level is higher than the ordinary tidal level, such initial motion is referred to as the pushing initial motion; when it is lower than the ordinary tidal level, the initial motion is called the drawing initial motion.

⑥ Run-up height and tsunami trace height

Run-up height of tsunami is the maximum water level on land or facilities. It is expressed in the height relative to the mean sea level (M.S.L.) in Tokyo Bay (T.P.) or the lowest astronomical tide (D.L.). The run-up height is often determined by the trace that the tsunami leaves at that location, and the height of that trace is also called the tsunami trace height.

(2) Tsunami Period

The predominant period of a tsunami depends on factors such as the size of the source area of the tsunami and the distance from the epicenter. A tsunami may have components whose periods are the same as the natural periods of the bay or harbor and which are amplified through resonance. Therefore, it is preferable to investigate not only tsunamis caused by expected earthquakes but also tsunamis with the periods that are the same as the natural periods of bays and harbors by numerical simulation etc.

(3) Tsunami wave celerity

Tsunami wave celerity is usually well approximated by the celerity of long wave that is a function only of the water depth, as in the following formula:

$$C = \sqrt{gh} \quad (5.1.1)$$

where

C : wave celerity (m/s)

g : gravitational acceleration (m/s²)

h : water depth (m)

For example, the tsunami wave celerity would be 198 m/s (713 km/h) in the average depth of the Pacific Ocean which is about 4,000 meters. In 1960, the tsunami that formed off the coast of Chile reached Japan about one day later. At the shore, with a depth of 20 m, the wave celerity decreases to 14 m/s (50 km/h).

If the time when a tsunami arrives at various coastal locations is known from the tide observation record or others, the tsunami wave source area can be estimated by reverse propagation calculation toward offshore from observation points.

(4) Tsunami Transformation

① Wave shoaling, refraction, and diffraction

In the deep sea, the common wavelength of a tsunami is several tens of kilometers or more, while the wave height is only about several meters. Therefore, tsunami is not distinguishable at the deep sea. However, in the process of propagation to the coast, the tsunami is transformed by wave shoaling and refraction in the same way as wind waves. This process provides the increase of tsunami wave height and the wave height can exceed 10 m. In addition, the affection of the local topological features along the shore, on a scale of several hundreds of meters, occasionally makes it possible for the tsunami to run up the shore several tens of meters in height. For example, the tsunami by the 1993 Hokkaido-oki earthquake (the 1993 Okushiri Tsunami) ran up 32 m high at the V-shaped cliff of Okushiri Island.^{2) 3)} A 40 m wave run-up height was recorded at a V-shape valley on the Sanriku ria coast also in the 2011 Tohoku District off the Pacific Ocean Earthquake tsunamis⁴⁾. Also, a tsunami can be concentrated at a cape due to refraction induced by bathymetry change off the cape. Further, due to diffraction, a tsunami wave may reach the opposite side of an island or cape to the direction of approach of the tsunami. For example, the 1993 Okushiri tsunami approached Okushiri Island from the west side, but tsunami caused damages even on the east side as well as the west side of the island, and the 2004 Indian Ocean tsunami by the Sumatra-Andaman earthquake reached Sri Lankan Island from the east side but the tsunami of about 5 m high also hit the southwest shore.

② Transformation of tsunamis in a bay

A tsunami increases its wave height and fluid velocity if it propagates into a bay where the water depth becomes shallower and the width of the bay becomes narrower. The wave height can be calculated from Green's law, as shown in **equation (5.1.2)**:

$$\frac{H_2}{H_1} = \left(\frac{b_1}{b_2} \right)^{1/2} \left(\frac{h_1}{h_2} \right)^{1/4} \quad (5.1.2)$$

where

H_1 : the tsunami wave height for a cross-section of width b_1 and water depth h_1

H_2 : the tsunami wave height for a cross-section of width b_2 and water depth h_2

Equation (5.1.2) only holds if one assumes that the ratio of the wave height to the water depth is small, the width and water depth change gradually, there is no energy loss due to sea bottom friction, and there is no reflected wave. It cannot be applied in places such as shallow water area and the inner portion of a bay where there is a strong effect of the reflected wave.

(5) Bore Type Tsunamis⁵⁾

The tsunami by the 1983 Nihonkai-Chubu earthquake (the 1983 Sea of Japan Earthquake) attacked along the northern shore of Akita prefecture where the shore has a mild bottom slope of about 1/200 that extends for 30 km. The tsunami was greatly deformed into a bore, accompanied by short periodic waves of about 5 to 10 seconds. On the other hand, when this same tsunami hit a shore with a relatively steep slope of about 1/50, such as the western shore of Oga peninsula, it became rather similar to standing waves. A bore type tsunami tends to have a greater run-up height than a standing-wave type tsunami, even if the heights of two tsunami are same.

(6) Edge Waves

If a tsunami approaches a coast obliquely, the wave refraction can make the tsunami reflected from a coast propagate along the coast and consequently part of energy of the tsunami can be trapped near the coast. For example, in the 2003 Tokachi-oki earthquake in the sea off Tokachi in Hokkaido, a tsunami that could be considered an edge wave was detected along the coast from Cape Erimo to Kushiro in the southeastern coast of Hokkaido, Japan. The fact that a tsunami can continue for a long time due to formation of edge waves means the increase of possibility that the tsunami can meet a high tide resulting in inundation in coastal areas.⁶⁾

(7) Tsunami Wave Force

Part II, Chapter 2, 6.7 Tsunami Wave Force may be referred to for the tsunami wave force.

(8) Fluid Velocity of Tsunami

For a tsunami different from a wind wave, the movement of the sea water is uniform from the sea surface to the sea bottom. The fluid velocity u may be given by **equation (5.1.3)** and it is faster in the shallower water.

$$u = \frac{C\eta}{h} = \eta \sqrt{\frac{g}{h}} \quad (5.1.3)$$

where

η : sea surface deviation due to the tsunami (m)

C : wave celerity (m/s)

h : water depth (m)

g : gravitational acceleration (m/s²)

(9) Tsunamis in Tide Records

Tide records are extremely useful as records of tsunamis. However, when using such data, it is necessary to keep in mind the following items.²⁾

- ① Tsunami records measured at a tide station in a harbor may indicate different characteristics of tsunami, from those outside the harbor, because they are affected by harbor facilities such as breakwaters.
- ② A tsunami with a relatively short period will be measured to be smaller than the tsunami around tide station because of an energy loss due to the tsunami water flows through the tide station's inlet pipe. **Table 5.1.1** shows the tidal levels of the Middle Japan Sea Earthquake tsunami recorded in each harbor, the flood trace height obtained near tide observatories, or the estimated height from the visual observation. Comparing these levels shows that the tide records are somewhat lower than the flood trace height and others.

(10) Impact of Crustal Movement on Water Level Records of Tsunamis

In addition to the tidal observation records, water level records of tsunamis obtained from the ocean bottom pressure gauge, GPS wave buoy, and other instruments are very efficient as tsunami records.

However, when the vertical displacement of observation benchmarks, due to crustal movement, cannot be ignored, data should be handled carefully. **Part II, Chapter 5, 2 Crustal Movement due to Earthquake** may be referred to for this. The water level data in this case records superimposed changes in the water level, due to the tsunami itself, and in the observation benchmark accompanied by vertical displacement of the crust. To extract the change in the water level due to tsunamis, the impact of crustal movement needs to be deducted. The vertical displacement of the observation benchmark accompanied by crustal movement can be calculated from the difference in the mean value of tide levels before and after the earthquake⁷⁾.

Table 5.1.1 Ratio of Tide Observation Records to the Flood Trace Heights (Based on Level)⁵⁾

	<i>A</i> Level recorded in tide observation records (m)	<i>B</i> Level recorded in trace or visual observation (m)	<i>A/B</i>
Ishikari Bay Shinko	0.56	0.63	0.89
Iwanai Port	1.25	1.3	0.96
Esashi Port	0.75	1.1	0.68
Fukaura Port	0.61	3.2	0.19
Noshiro Port *	1.94	2.8	0.69
Funagawa Port	0.32	0.7	0.46
Sakata Port	0.81	1.3	0.62
Iwafune Port *	0.73	0.7	1.04
Niigata Higashi Port	0.78	1.0	0.78
Niigata Nishi Port	0.50	1.0	0.50
Ryotsu Port	1.17	1.5	0.78

	<i>A</i> Level recorded in tide observation records (m)	<i>B</i> Level recorded in trace or visual observation (m)	<i>A/B</i>
Teradomari Port	0.59	0.6	0.98
Kashiwazaki Port	1.01	1.0	1.01
Naoetsu Port	0.72	0.7	1.03

* The first wave reached the highest water level.

(11) Model Experiments of Tsunamis

In model experiments, a water area including a harbor or the sea bottom topography around a structure is reproduced. And then, around that, by reproducing tsunami waveforms determined by numerical simulations, it is possible to investigate the stability and protective effect of tsunami breakwaters⁸⁾ and the effect of topological alterations such as reclamations on tsunamis. The scouring of a breakwater entrance mound by the 1993 Okushiri tsunami has been investigated in the model experiments.⁹⁾

(12) Numerical Simulations of Tsunamis

- ① Numerical simulations of tsunamis must use appropriate numerical models which are based on fundamental equations that can reproduce the subject tsunamis. The following two types of theories are mainly used for regional tsunamis that occur near the coast:
 - (a) Non-dispersive theories¹⁰⁾: There are the linear long wave theories that apply to waves whose wavelengths are long compared to the water depth, and also the ratio of wave height to water depth is small, and nonlinear long wave theories that apply to long waves when the ratio of wave height to water depth is not small. According to Shuto¹¹⁾, the linear long wave theory may be applied in the water 200 meters or deeper.
 - (b) Dispersive theories: Dispersion of tsunami, such as observed near the coast for the tsunami by the 1983 Nihonkai-Chubu earthquake, can be reproduced with a nonlinear dispersed-wave theory^{12) 13)}. This theory includes factors that take wave dispersion into account (dispersion terms) to a nonlinear long wave theory.

For a distant tsunami (teletsunami) that originates from a faraway source, it is possible to use linear dispersive wave theories, which add dispersion terms to the linear long wave theory. Since a tsunami in general is a series of waves whose components have various periods and a wave component with longer period has slightly faster wave celerity in deep water, wave components with shorter periods delay and the waves disperse while traveling long distance like the Pacific Ocean. Further, accurate calculation of a distant tsunami generally needs to consider the Coriolis force and to use the spherical coordinates.

- ② In numerical simulations of tsunami, a tsunami incident waveform shall be provided at the boundary of the calculation region¹⁴⁾. Otherwise, displacement of the sea bottom shall be calculated by an earthquake fault model¹⁵⁾ and then the sea level displacement at the initial stage of the tsunami is calculated to provide the initial spatial waveform of the tsunami. In calculating the displacement from an earthquake fault model, the elastic theory solution of Mansinha and Smylie¹⁶⁾ and Okada¹⁷⁾ may be used. The sea surface movement due to the crustal movement can be treated as the sum of vertical amount of sea bottom movement and the vertical movement generated by horizontal displacement of uneven bottom.¹⁾ Moreover, there are some cases where spatiotemporally uneven fault slip distribution is given considering the asperity in the fault or a large slip near the trench axis confirmed at the 2011 off the Pacific coast of Tohoku Earthquake¹⁾.
- ③ In order to calculate the tsunami runup on the land, the method of Iwasaki and Mano,¹⁸⁾ or improvements on it¹⁹⁾ can be used. If the tsunami overflows structures such as breakwaters or seawalls, it is possible to use the Honma formula^{20) 21)} to calculate the amount of overflow for a unit width. In order to evaluate tsunami reduction effect of breakwaters and other structures, momentum loss at the opening section should be considered. The momentum loss, which is proportional to the mean flow velocity calculated by the long wave theory models, includes the sea bottom friction that can be evaluated by Manning's roughness coefficients and others, and the momentum loss due to abrupt narrowing and widening of the cross-section as seen in the opening section of breakwater. Comparing model experiments²²⁾ with numerical simulations for the breakwaters at the entrance to Kamaishi Bay provided a value of 0.5 for the coefficient of the momentum loss due to the breakwaters.¹⁰⁾ Recently it has also become possible to calculate the flows near submerged breakwaters in the opening section of tsunami breakwater as well as the tsunami wave force that acts on the submerged breakwaters^{23) 24) 25)} by using non-hydrostatic and three-dimensional numerical models.

(13) "Design Tsunami" and "Excess Design Tsunami"

When constructing tsunami countermeasures, two levels of tsunamis shall be considered; one is the "design tsunami," the other is the "excess design tsunami," used to performance verification. They are set between high-frequency tsunamis and maximum-class tsunamis according to the importance of the facilities concerned^{26) 27)}.

The high-frequency tsunamis shall be set by properly considering the highest past tsunami in the target region, tsunamis of the scale deemed appropriate in terms of disaster prevention among recent tsunamis, of which relatively large amounts data are available, and tsunamis based on the scenario earthquake in the seismic gap. "A setting method of the water level of design tsunami²⁸⁾," can be referred to. In the method, high-frequency tsunami with some specific return period (e.g. once in several ten years to one hundred and some ten years) can be set in consideration of the record of past tsunamis, revealed by flood trace heights, and investigating historical documents, such as historical records and literature, and data based on the simulation conducted as needed.

In order to set the maximum-class tsunamis a scientific comprehensive survey on past tsunamis and earthquakes is required. It shall be composed of the analysis of historical materials, sedimentary records, coastal topography, etc. The result of physical survey shall be summarized from the viewpoint of disaster prevention and the maximum-class tsunami is set in consideration of all possibilities²⁹⁾. The tsunami fault model published by the Central Disaster Prevention Council may be referenced.

These tsunamis shall be properly set in consideration of the regional disaster prevention plan under the careful coordination among persons concerned.

(14) Determination of Tsunami for the Performance Verification of Facilities

Two grade tsunamis, "design tsunami" and "excess design tsunami" is considered in the design of port facilities. "Design tsunamis" is utilized to verify the facilities' stability and "Excess design tsunami" is considered in the design process of contingency-prepared facilities (e.g. breakwaters, seawalls, water gates, locks, revetments, dikes, parapets, and waste disposal sites) in order to maximize the stability and resilience of facilities, to minimize the damage of disaster and to maintain the calmness of the harbor for promotion of early recovery and reconstruction.

It seems that high-frequency tsunamis are generally set to the "design tsunami." When protecting significantly important facilities, like electric power stations and others, or regions where people, property, industry, and others are present in large numbers, it is necessary to set the tsunami magnitude properly even in consideration of maximum-class tsunami, according to the importance of facilities concerned.

A proper magnitude of tsunami needs to be set to the "excess design tsunami" in the range up to the maximum-class tsunami, from the view point of the cost and benefit of additional structural treatment to stabilize the facilities and the importance of facilities concerned²⁷⁾.

Moreover, it is important to consider the effects of settlement, deformation, remaining bearing force and others of facilities due to earthquake ground motion and crustal movement in performance verification by tsunami actions, as the facilities are often influenced by the earthquake before the attack of tsunamis.

[References]

- 1) Nankai trough giant earthquake research committee of the central disaster management council: Seismic intensity distribution and tsunami heights of Nankai trough mega earthquake (first report), p. 44, 2012.3.31
- 2) Takayama, T., Y. Suzuki, H. Tsuruya, S. Takahashi, C. Gotoh, T. Nagai, N. Hashimoto, T. Nagao, T. Hosoyamada, K. Shimosako, K. Endo and T. Asai: Field investigations of the tsunami caused by 1993 HokkaidoNansei-oki Earthquake, Technical Note of PHRI No. 775, p. 225, 1994
- 3) Shuto, N. H. Tomimatsu and M. Ubana: Characteristics of Off-Hokkaido Southwest Earthquake and outstanding issues towards future, Proceedings of Coastal Eng. JSCE Vol. 41, pp. 236-240, 1994
- 4) The 2011 Tohoku Earthquake Tsunami Joint Survey (TTJS) Group: Field survey report, URL: <http://www.coastal.jp/ttjt/>, 2012
- 5) Tanimoto, K., T. Takayama, K. Murakami, S. Murata, H. Tsuruya, S. Takahashi, M. Morikawa, Y. Yoshimoto, S. Nakano and T. Hiraishi: Field and laboratory investigations of the tsunami caused by 1983, Nihonkai Chubu Earthquake, Technical Note of PHRI No. 470, pp. 299, 1983
- 6) Tomita, T., H. Kawai and T. Kakinuma: Tsunami disasters and tsunami characteristics due to the Tokachi-oki Earthquake in 2003, Technical Note of PHRI No. 1082, pp. 30, 2004

- 7) Kawai, H., M. Satoh, K. Kawaguchi, K. Seki: Characteristics of the 2011 off the Pacific Coast of Tohoku Earthquake Tsunami, Report of PARI, Vol. 50, No. 4, pp. 3-63, 2011
- 8) Takayama, T. and T. Hiraishi: Hydraulic model tests on tsunamis at Suzaki-port, Technical Note of PHRI, No. 549, pp. 131, 1986
- 9) Tsuruya, K. and Y. Nakagawa: Model experiment for reproduction of disaster at Okushiri-higashi breakwater by Hokkaido-Nansei-oki Earthquake Tsunami, Technical Note of PHRI, No. 789, pp. 20, 1994
- 10) Goto, C. and K. Sato: Development of tsunami numerical simulation system for Sanriku coast in Japan, Rept of PHRI, Vol. 32, No. 2, pp. 3-44, 1993
- 11) Shuto, N: Tsunami and countermeasures, Jour. of the JSCE, No. 369/II-5, pp. 1-11, 1986
- 12) Iwase, H, T. Mikami and C. Goto: Practical tsunami numerical simulation model by use of non-linear dispersive wave theory, Jour. Of JSCE, Vol. 600/11-44, pp. 119-124, 1998
- 13) Iwase, H. K. Fujima. T. Mikami, H. Shibaki and C. Goto: Calculation of Central Japan Sea Earthquake Tsunami run-up considering wave number dispersion effect., Proceedings of Coastal Eng. JSCE Vol. 49, pp. 266-270, 2002
- 14) Arikawa, T., M. Sato, K. Shimosako, T. Tomita, D. Tatsumi, G. Yeom and K. Takahashi: Investigation of the failure mechanism of Kamaishi breakwaters due to tsunami – initial report focusing on hydraulic characteristics –, Technical Note of PARI, No. 1251, p. 53, 2012
- 15) Sato, R., K. Abe, Y. Okada, K. Shimazaki and Y. Suzuki: Parameter handbook of seismic faults in Japan, Kajima Institute Publishing, pp. 10-27, 1989
- 16) Mansinha, L. and D. E. Smylie: The displacement fields of inclined faults, Bulletin of the Seismological Society of America, Vol. 61, No. 5, pp. 1433-1440, 1971
- 17) Okada Y.: Internal deformation due to shear and tensile faults in a half-space, Bulletin of the Seismological Society of America, Vol. 82, No. 2, pp. 1018-1040, 1992
- 18) Iwasaki, T. and A. Mano: Numerical calculation of 2-dimensional tsunami run-up in Euler coordinates, Proceedings of 26th Conference on Coastal Eng. JSCE, pp. 70-74, 1979
- 19) Kotani, Y., F. Imamura and N. Shuto: Calculation of Tsunami Run-up and damage estimation utilizing GIS, Proceedings of Coastal Eng. JSCE Vol. 45, pp. 356-360, 1998
- 20) Honma, M. and K. Akishiro: Mononobe Hydraulics, Iwanami Publishing, pp. 232-237, 1962
- 21) JSCE: The Collected Formula of Hydraulics (1999 Edition), Maruzen Publishing, p. 713, 1999
- 22) Tanimoto, K., K. Kimura and K. Miyazaki: Study on stability of submerged dike at the opening section of tsunami protection breakwaters, Rept of PHRI, Vol. 27, No. 4, pp. 93-122, 1988
- 23) Masamura, K., K. Fujima, C. Goto, K. Iida and T. Shigemura: Numerical analysis of tsunami by using 2D/3D hybrid model, Jour. of JSCE, No. 670/II-54, pp. 49-61, 2001
- 24) Tomita, T., T. Kakinuma and A. Shimada: Numerical calculation of effect of Tsunami breakwater utilizing 3-dimensional wave model, Proceedings of Coastal Eng. JSCE Vol. 51, pp. 296-300, 2004
- 25) Tomita, T., K. Honda and Y. Chida: Numerical simulation on tsunami inundation and debris damage STOC Model, Report of PARI Vol. 55, No. 2 pp. 3-33, 2016
- 26) Transportation Policy Council Harbor Disaster Prevention Subcommittee: The way of earthquake and tsunami countermeasures in harbors - to maintain the lifeline of island country Japan, p. 20, 2012.6.13
- 27) MLIT Ports and Harbours Bureau: Guideline for Tsunami-Resistant Design of Breakwaters, p. 37, 2015
- 28) MAFF and MLIT: About setting method of water level of design tsunami, 2011.7.8
- 29) Central Disaster Management Council: Report of the committee for technical investigation on countermeasures for earthquakes and tsunamis based on the lessons learned from the “2011 off the Pacific coast of Tohoku Earthquake, 2011.9.28

6 Wave Force

6.1 General

6.1.1 Wave Forces due to Waves and Tsunamis and Wave Forces at Storm Surges

Wave forces are classified roughly as due to waves, tsunamis, or storm surges. As shown in **Figs. 6.1.1, 6.2, 6.3, 6.4,** and **6.5** deal with wave forces due to waves, **6.6** deals with wave forces due to tsunamis, and **6.7** deals with wave forces due to storm surges.

6.1.2 Classification of Wave Forces by Structure Type

Wave forces can be generally classified by the type of structure. Wave forces acting on upright walls are described in **6.2**, wave forces acting on submerged members in **6.3**, wave forces acting on structures near the water surface in **6.4**, and wave forces acting on armor stones or concrete blocks in **6.5**.

The wave forces are different for each type of structure. It is thus necessary to use an appropriate calculation method in accordance with the conditions including structural type. Wave forces and resistance forces acting on armor stones and concrete blocks in **6.5** differ greatly depending on their shapes and positions in addition to conditions of the waves acting on them. Therefore, when verifying performance, the required mass for the armor stones and concrete blocks are usually determined directly from wave conditions rather than calculating the acting wave force.

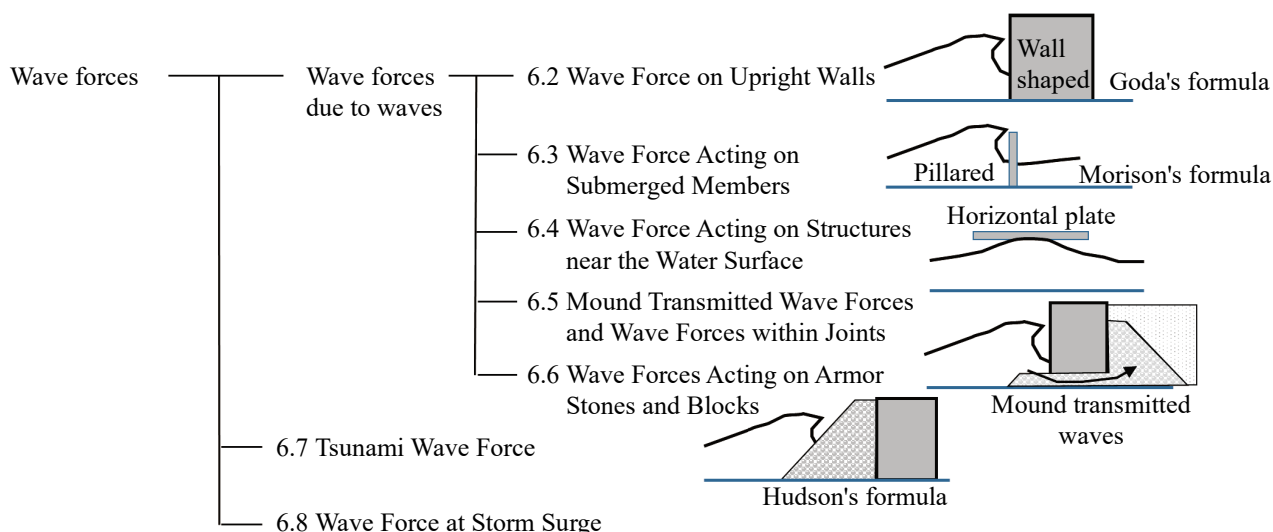


Fig. 6.1.1 Classification of Wave Forces

6.1.3 Examination of Wave Force by Hydraulic Model Tests

In the case of structures in which there is a lack of construction experience, wave actions have not been sufficiently resolved, and therefore it is preferable to carry out studies including hydraulic model tests for such structures. When examining wave force by hydraulic model tests, it is necessary to give sufficient consideration to the failure process of the structure and to use an appropriate measurement method. It is also preferable to give sufficient consideration to the irregularity of waves in the field concerned. In particular, when carrying out experiments using regular waves, an examination against the highest wave should be included in principle.

6.1.4 Examination of Wave Force by Numerical Calculation

A great deal of labor and expense is required for examining the wave force with hydraulic model tests, and usually there are limits to the experimental cases and the measurement items. On the other hand, in recent years it has become possible to employ numerical calculations. If the accuracy of the calculation models is verified by the comparison with on-site observations and hydraulic model tests at the employment of the numerical calculation in actual design, the computation of wave force can save labor and expense more than the hydraulic model test. The CADMAS-SURF¹⁾ is a numerical computation program developed for the purpose of assisting the structurally resistive design against wave

action and with the program it is possible to examine the interactions among waves, ground and structures and the impulsive breaking wave pressure. In addition, numerical models, such as OpenFOAM²⁾ or the particle method,³⁾ can be used. However, it is essential to verify the calculated results in spite of the calculation methods with the hydraulic model experimental data, and others, when applying to complicated phenomena such as impulsive breaking wave pressure.

6.2 Wave Force on Upright Walls

6.2.1 General Characteristics of Wave Force on Upright Walls^{4) 5) 6) 7)}

(1) Parameters affecting wave force on upright walls

The major parameters that affect the wave force acting on an upright wall are wave period, wave height, wave direction, tidal level, water depth, bottom slope, water depth of the crown of the foundation mound, the front berm width of foundation mound, slope of foundation mound, the crown height of upright wall, and water depth at base of the upright wall. In addition, it is also necessary to consider the effect of the wall alignment. The wave force on an upright wall with a concaved alignment may be larger than that on an upright, straight wall of infinite length. Furthermore, if the front of upright wall is covered with wave-dissipating concrete blocks, the characteristics of these blocks and the crown height and width will affect the wave force.

(2) Types of wave force

The wave force acting on an upright wall can be classified according to the type of waves such as a standing wave force, a breaking wave force, or a wave force after breaking. It is considered that the changes of wave forces are continuous. A standing wave force is produced by waves whose height is small compared with the water depth, and the change in the wave pressure over time is gradual. As the wave height increases, the wave force also increases. In general, the largest wave force is generated by the waves breaking just a little off the upright wall. Accordingly, with the exception of very shallow water conditions, the force exerted by waves breaking just in front of an upright wall is larger than the wave force by higher waves that have already broken offshore. It is necessary to note that especially when breaking waves act on an upright wall on a steep seabed, or on an upright wall set on a high mound even on a mild slope, a very strong impulsive breaking wave force may appear.

(3) Wave Irregularity and Wave Force

Sea waves are irregular with the wave height and period. Depending on the water depth where facilities are to be installed and the topography of the sea bottom, wave forces such as non-breaking, breaking or after breaking act on the structure. When calculating the wave force, it is important to include the waves that cause the severest effect on the structure. It is necessary to give sufficient consideration to wave irregularity and to the characteristics of the wave force in accordance with the type of structure.

In general, it may be assumed that the larger the wave height, the greater the wave force becomes. It is thus acceptable to focus on the wave force of the highest wave among a train of random waves attacking the structure. However, with regard to the stabilities of concrete blocks or armor stones on the slope and wave force acting on the floating structures and cylindrical structures with small rigidity, it is preferable to consider the effect of the successive action of the random waves.

6.2.2 Wave Forces of Standing Waves or Breaking Waves when the Peak of Waves is on the Wall Surface

(1) Goda's formula (General)

The maximum horizontal wave force acting on an upright wall and the simultaneous uplift is generally calculated using Goda's formula as shown below. Goda's formula⁸⁾ takes into consideration results of wave pressure experiments and application of the formula to the existing breakwaters and has been modified to include the effects of wave direction⁹⁾. Its single-equation formula enables one to calculate the wave force from the standing to breaking wave conditions without making any abrupt transition. However, where the upright wall is located on a steep seabed, or built on a high mound, and is subjected to a strong impulsive wave pressure due to breaking waves, the formula may underestimate the wave force. It should therefore be applied preferably with consideration of the possibility of occurrence of impulsive wave pressure due to breaking waves (see **Part II, Chapter 2, 6.2.4 Impulsive Breaking Wave Force**). The wave pressure given by Goda's formulas takes the hydrostatic pressure at the still water condition as the reference value. Any hydrostatic pressure before wave action should be considered separately. Further, the formula aims to examine the stability of the whole body of an upright wall. When breaking

wave actions exist, the formula does not necessarily express the local maximum wave pressure at the respective positions; thus, such should be considered during examination of the stress of structural members.

(2) Wave pressure on the front face according to the Goda's formulas

The wave pressure on the front face of an upright wall in the Goda's formula is a linear distribution. Wave pressure is 0 at the height expressed as η^* in **equation (6.2.1)**, maximum value expressed as p_1 in **equation (6.2.2)** at still water level, and expressed as p_2 in **equation (6.2.3)** at the sea bottom. The formula considers wave pressure from the bottom to the crown of the upright wall (see **Figs. 6.2.1** and **6.2.2**).

$$\eta^* = 0.75(1 + \cos \beta) \lambda_1 H_D \quad (6.2.1)$$

$$p_1 = 0.5(1 + \cos \beta) \left(\alpha_1 \lambda_1 + \alpha_2 \lambda_2 \cos^2 \beta \right) \rho_0 g H_D \quad (6.2.2)$$

$$p_2 = \frac{P_1}{\cosh(2\pi h/L)} \quad (6.2.3)$$

$$p_3 = \alpha_3 p_1 \quad (6.2.4)$$

In this equation, η^* , p_1 , p_2 , p_3 , $\rho_0 g$, β , λ_1 , λ_2 , h , L , H_D , α_1 , α_2 , and α_3 respectively represent the following values:

- η^* : height above still water level at which intensity of wave pressure is 0 (m)
- p_1 : intensity of wave pressure at still water level (kN/m²)
- p_2 : intensity of wave pressure at sea bottom (kN/m²)
- p_3 : intensity of wave pressure at toe of the upright wall (kN/m²)
- $\rho_0 g$: unit weight of water (kN/m³)
- β : angle between the most dangerous direction within the range of $\pm 15^\circ$ from the main wave direction and the line perpendicular to the faceline of the upright wall ($^\circ$)
- λ_1, λ_2 : wave pressure correction coefficient (1.0 is the standard value)
- h : water depth in front of the upright wall (m)
- L : wavelength at water depth h used in calculation as specified in the item (4) below (m)
- H_D : wave height used in calculation as specified in the item (4) below (m)
- α_1 : value expressed by the following equation

$$\alpha_1 = 0.6 + \frac{1}{2} \left\{ \frac{4\pi h/L}{\sinh(4\pi h/L)} \right\}^2 \quad (6.2.5)$$

- α_2 : value expressed by the following equation

$$\alpha_2 = \min \left\{ \frac{h_b - d}{3h_b} \left(\frac{H_D}{d} \right)^2, \frac{2d}{H_D} \right\} \quad (6.2.6)$$

- α_3 : value expressed by the following equation

$$\alpha_3 = 1 - \frac{h'}{h} \left\{ 1 - \frac{1}{\cosh(2\pi h/L)} \right\} \quad (6.2.7)$$

In this equation, h_b , d , and h' respectively represent the following values:

- h_b : water depth at an offshore distance of 5 times the significant wave height from the front face the upright wall (m)
- d : water depth at the crest of either the foot protection works or the mound armoring units of whichever is higher (m)
- h' : water depth at toe of the upright wall (m)

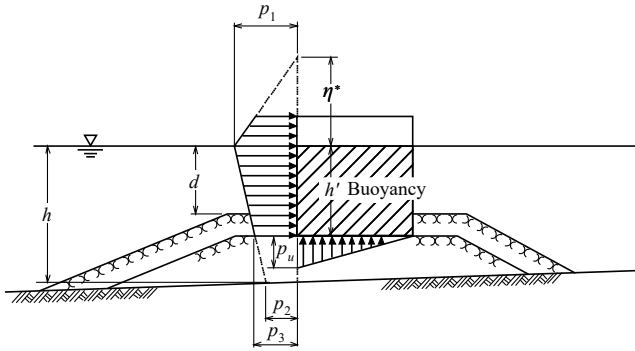
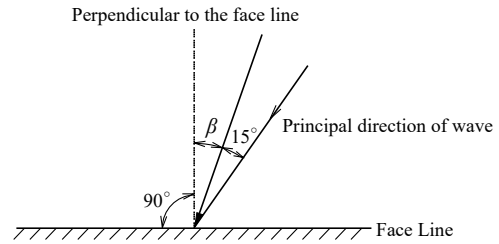


Fig. 6.2.1 Wave Pressure Distribution Used in Design Calculation


 Fig. 6.2.2 Way of Obtaining Incident Wave Angle β

(3) Uplift on the bottom of upright wall

In Goda's formulas, the uplift acting on the bottom of an upright wall is described by a triangular distribution, with the pressure intensity at the front toe p_u given by the following equation and 0 at the rear toe.

$$p_u = 0.5(1 + \cos \beta) \alpha_1 \alpha_3 \lambda_3 \rho_0 g H_D \quad (6.2.8)$$

In this equation, p_u and λ_3 respectively represent the following values:

p_u : uplift pressure acting on the bottom of the upright wall (kN/m²)

λ_3 : uplift pressure correction coefficient (1.0 is the standard value)

(4) Wave height and wavelength used in the wave pressure calculation

In Goda's formulas, the wave height H_D and the wavelength L are the height and wavelength of the highest wave. The wavelength of the highest wave is that corresponding to the significant wave period, while the height of the highest wave is as follows:

① When the highest wave does not have effect of wave breaking:

$$H_D = H_{\max} = 1.8 H_{1/3} \quad (6.2.9)$$

In this equation, H_{\max} and $H_{1/3}$ respectively represent the following values:

H_{\max} : highest wave height of incident waves as a progressive wave at the water depth of the upright wall (m)

$H_{1/3}$: significant wave height of incident waves as a progressive wave at the water depth of the upright wall (m)

② When the highest wave has effect of wave breaking:

H_D : maximum wave height considering transformation due to the breaking of random waves (m)

(5) Highest wave

Since Goda's formulas represents the wave force on an individual wave, in the breakwater performance verifications in general, it is necessary to use the wave parameters of the severest wave force from a wave group. The highest wave shall be subject to consideration. The occurrence of the highest wave in a random wave group is probabilistic, and so it is not possible to determine the parameters of the wave explicitly. Nevertheless, after examination of the results of applying the current method to breakwaters in the field, it is standard to use 1.8 times the significant wave height as the height of the highest wave where no transformation of breaking wave is observed. It has also become standard to use the wavelength corresponding to the significant wave period as the wavelength of the highest wave.

In order to determine whether or not the highest wave is subject to wave breaking, the diagrams for determining the highest wave height (Figs. 4.4.15 (a)–(e) in Part II, Chapter 2, 4.4.6 Wave Breaking) should be used by referring to the location of the peak wave height in the zone in the onshore side of the 2% attenuation line. It is acceptable to consider that the highest wave is not subject to wave breaking when the water is deeper than that at the peak height,

but that it is subject to wave breaking when the water is shallower than this. If the highest wave height is to be obtained using the approximate **equation (4.4.11)** in **Part II, Chapter 2, 4.4.6 Wave Breaking** h_b should be substituted as h in the first term in the braces { } on the right-hand side of the equation.

If using a value other than 1.8 as the coefficient on the right-hand side of **equation (6.2.9)**, it is necessary to conduct sufficient examinations into the occurrence of the highest wave and then choose an appropriate value (see **Part II, Chapter 2, 4.2 Handling of Waves Used for Design**).

(6) Wave pressure correction coefficient $\lambda_1, \lambda_2, \lambda_3$

Equations (6.2.1) to (6.2.8) are the generalized version of Goda's formulas. They contain three correction coefficients so that they can be applied to walls of different conditions. For an upright wall, the correction coefficients are of course 1.0. The wave pressure acting on other types of wall such as a caisson covered with wave-dissipating concrete blocks or an upright wave-dissipating caisson may be expressed using the generalized Goda's formulas with appropriate correction coefficients (see **Part II, Chapter 2, 6.2.5 Wave Force Acting on Upright Wall covered with Wave-dissipating Concrete Blocks** and **Part II, Chapter 2, 6.2.7 Wave Force Acting on Upright Wave-absorbing Caisson**).

(7) Features and application limits of the Goda's formulas

The first feature of Goda's formulas is that the wave force from standing waves to breaking waves can be calculated continuously, including the effect of surrounding conditions. The parameter α_1 given by **equation (6.2.5)** expresses the effect of the period (strictly speaking h/L); it takes the limiting values of 1.1 for shallow water waves and 0.6 for deepwater waves. The effect of period also appears when determining the maximum wave height to be used in the calculation; for a constant deepwater wave height, the longer the period, the larger the maximum wave height in a shallow sea. Goda's formulas incorporate the effect of period on the wave pressure as well as on the maximum wave height.

Another feature of Goda's formulas is that the change in the wave force with the foundation mound height and the bottom slope is considered by means of the parameter α_2 . As can be seen from **equation (6.2.6)**, as the foundation mound height is gradually increased from zero (i.e., $d = h$) with constant H_D , α_2 gradually increases from zero to its maximum value. After reaching its limit value, α_2 then decreases until it reaches zero again when $d = 0$. The limit value of α_2 is 1.1; combining this with the limit value of α_1 of 1.1, the intensity of the wave pressure p_1 at the still water level is given $2.2\rho_0gH_D$.

With regard to the effect of the bottom slope, h_b within the equation for α_2 is taken as the water depth at the distance of 5 times the design significant wave height from the upright wall. Because of this artifice, a steep bottom slope results in the same effect as having a high foundation mound. The highest wave height at $5H_{1/3}$ apart was used to calculate regions affected by wave breaking because it was considered that the waves that break slightly offshore, as progressive waves exert the largest wave force on upright walls. The effect of the bottom slope also appears when determining the maximum wave height to be used in the calculation. In the wave breaking zone, the steeper the bottom slope, the larger the wave height, because the wave height used in the calculation is the maximum wave height at a distance $5H_{1/3}$ offshore from the upright wall. The bottom slope thus has a strong influence on the wave force.

As explained above, Goda's formulas consider the effects of the foundation mound height and the bottom slope on the wave pressure. Nevertheless, for an upright wall on a high mound or a steep seabed, a large impulsive breaking wave force may act, and under such conditions Goda's formulas may underestimate the wave force. When applying the Goda's formulas, it is thus preferable to pay attention to the risk of an impulsive breaking wave force arising. In particular, with a high mound, it is necessary to consider not only α_2 in **equation (6.2.6)** but also the impulsive breaking wave force coefficient α_1 by Takahashi et al.¹⁰⁾ (see **Part II, Chapter 2, 6.2.4 (6) Impulsive breaking wave forces acting on composite breakwater**), and to use α_1 in place of α_2 when α_1 is the larger of the two.

One more problem with Goda's formulas concerns its applicability to extremely shallow waters, for example near to the shoreline. The applicable range of Goda's formula is rigidly where the waves that break slightly offshore on the side of the upright walls exert the maximum wave force. It is difficult, however, to clearly define where the limit of applicability lies. For cases such as the wave force acting on an upright wall near the shoreline, it is advisable to use other calculation equations together with the Goda formula. (See **Part II, Chapter 2, 6.2.11 Wave Force Acting on Upright Wall Located Considerably Toward the Landside from the Breaker Line**.)

(8) Effect of wave direction in Goda's formula

Although a number of experiments have been carried out for the effect of wave direction on the wave force, there are still many points unclear. Traditionally, for standing waves, no correction has been made for wave direction to

the wave force. The effects of wave direction have been considered only for breaking waves, by multiplying the wave force by $\cos^2\beta$. However, it is irrational that the breaking wave force is assumed to decrease as the wave angle increases, reaching zero at the limiting value $\beta = 90^\circ$, and on the other hand the standing waves are assumed to remain at the perfect standing wave condition. In other words, when the incident wave angle is large (i.e., oblique wave incidence), it takes a considerably large distance from the tip of breakwater until the wave height becomes twice the incident height. At the limiting value of $\beta = 90^\circ$, it becomes an infinite distance. In this case, because actual breakwaters are finite in extension, it is appropriate to consider that the wave pressure of progressive waves acts on the upright wall. Furthermore, even in cases where the breakwater can be taken to extend infinitely, when using second-order approximation finite amplitude wave theory, the wave pressure from oblique incident waves decreases slightly in comparison to incidence at right angles and its degree becomes proportionate to the wave steepness. Considering these points and application to the breakwaters in the field, **equation (6.2.2)** for wave direction has been corrected by multiplying α_2 which represents mound effects with $\cos^2\beta$, and then multiplying the whole term by $0.5(1 + \cos\beta)$.

(9) Application of other theory and formulas

Goda's formula enables continuous determination of wave forces with considerable precision from standing waves to breaking waves without categorizing them by their application limits. But when the ratio of the wave height to the water depth is small and a standing wave force is obviously exerted on an upright wall, a high-accuracy standing wave theory may be applied. In this case, however, it is necessary to give sufficient consideration to the irregularity of waves in the field, and preferable to examine the force for the highest wave. Moreover, the Sainflou formula ¹¹⁾ and Hiroi's formula ¹²⁾ may also be used for wave force calculations¹³⁾. When applying these methods, adequate care is needed in determining applicability.

(10) Wave force and significant wave period for waves composed of two wave groups with different periods

An example of two wave groups with different periods being superimposed is the superimposition of waves entering a bay from the outer sea and another group of waves generated within the bay. Another case is the superposition of waves diffracted at the entrance of a harbor and waves transmitted by wave overtopping. In such cases, the spectrum is bimodal (i.e., having two peaks) ¹⁴⁾. Tanimoto, Kimura et al. ¹⁵⁾ carried out experiments on the wave force acting on the upright section of a composite breakwater by using waves with a bimodal spectrum, and verified that Goda's formulas can be applied even in such a case. They also proposed a method for calculating the significant wave period to be used in the wave force calculation (see **Part II, Chapter 2, 4 Waves**). If each frequency spectrum of the two wave groups before superimposition can be considered to be a Bretschneider-Mitsuyasu type, the significant wave period after superimposition may be obtained by the method proposed by Tanimoto et al. Then this significant wave period may be used in wave force calculation.

(11) Wave force for low crested upright wall

If the crown height of the upright wall is low, the reduction in resistance force due to the weight fall owing to the crest lowering becomes greater than the reduction in wave force resulting from the decrease in the range of wave pressure acting on the wall. Therefore, in general, the wall needs to be widened. However, there are cases that the stability of an upright wall increases as the crown height is reduced. Nakata, Terauchi et al. ¹⁶⁾ have proposed a method for calculating the wave force for a breakwater with a low crown height. In the method, the terms of the front wave pressure and the uplift in the Goda's formulas are multiplied by a reduction coefficient λ_h , thus reducing the wave force.

(12) Wave force for high crested upright wall

When the crown of the upright wall is considerably higher than that for a normal breakwater, there will be no wave overtopping, meaning that the wave force may be larger than that given by Goda's formulas. Mizuno, Sugimoto et al. ¹⁷⁾ carried out experiments on the wave force acting on a breakwater with a high crown.

(13) Wave force on inclined walls

When the wall is slightly inclined, such as a trapezoidal caisson, the horizontal wave force is more-or-less the same as that for an upright wall. However, it is necessary to consider the vertical component of the wave force acting on the inclined surface, along with the reduction in uplift. Tanimoto and Kimura ¹⁸⁾ have carried out experiments on the wave force for slightly inclined walls, and have proposed a method for calculating the wave force.

(14) Uplift on caisson with footing

When a caisson has a footing, a wave force acts downwards on the upper surface of the footing on the seaside, and an uplift of p_u' acts at the front toe, while the uplift at the rear toe is zero. Nevertheless, in general the resultant force

is not significantly different to the uplift without the footing. It is thus acceptable to ignore the footing, and to assume that the uplift has a triangular distribution as shown in **Fig. 6.2.3**, with the uplift p_u at the front toe being given by **equation (6.2.8)**, and the uplift at the rear toe being zero. If the footing is extremely long, however, it is necessary to calculate the uplift appropriately, considering the change in the uplift p_u at the front toe of the footing. Esaki et al.^{19), 20)} have proposed a calculation equation of uplift and others acting on large footing based on the hydraulic model.

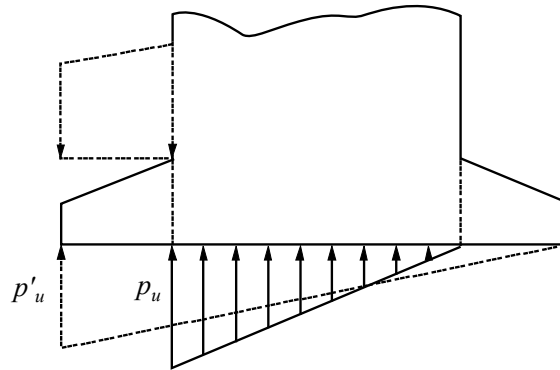


Fig. 6.2.3 Uplift when there is a Footing

(15) In case of wide mound berm in front of upright wall

The wave force acting on the upright wall of a composite breakwater varies not only with the mound height but also with the berm width and the front slope of foundation mound (see **Part II, Chapter 2, 6.2.4 Impulsive Breaking Wave Force**). As explained, of these three coefficients, Goda's formulas incorporates only the effect of the mound height. Consequently, if the width and/or slope of the foundation mound are considerably different from normal, it is preferable to carry out examination using hydraulic model tests. Note however that if the berm is sufficiently wide, it may be considered as a part of the topography of the sea bottom. Even with the standard formula, if the width is more than one half of the wavelength, it is possible to use the water depth on the mound for calculation of both the wave height and the wavelength.

(16) Wave force acting on an upright wall comprised of vertical cylinders

Nagai, Kubo et al.²¹⁾ as well as Hayashi, Karino et al.²²⁾ have carried out studies on the wave force acting on an upright wall comprised of cylinders such as a pile breakwater. Through their researches, it has been verified that the wave force is not greatly different from that acting on an upright wall with a flat face. It is thus acceptable to treat an upright wall comprised of cylinders as having a flat face and calculate the wave force using Goda's formulas.

6.2.3 Negative Wave Force of Wave Troughs on Wall Surfaces

(1) General

When the trough of a wave is at a wall, a negative wave force acts corresponding to the trough depth of the water surface from the still water level. A negative wave force is a wave force that is obtained through suitable hydraulic model tests or through appropriate calculations. It is a force directed seaward and may be comparable in magnitude to a positive wave force when the water is deep and the wavelength is short.

(2) Negative wave pressure distribution

The negative wave pressure acting on the front side of an upright wall at the wave trough can be approximately estimated as shown in **Fig. 6.2.4**. Specifically, it can be assumed that a wave pressure acts toward the sea, with the magnitude of this wave pressure being zero at the still water level and having a constant value of p_n from a depth $0.5H_D$ below the still water level right down to the toe of the wall. Here p_n is given as follows:

$$p_n = 0.5\rho_0 g H_D \quad (6.2.10)$$

where

p_n : intensity of wave pressure in constant region (kN/m²)

$\rho_0 g$: unit weight of seawater (kN/m³)

H_D : wave height used in performance verification (m)

In addition, the negative uplift acting on the bottom of the upright wall can be assumed to act as shown in **Fig. 6.2.4**. Specifically, it can be assumed that an uplift acts downwards with its intensity being p_n as given by **equation (6.2.10)** at the front toe, zero at the rear toe, and having a triangular distribution in-between. Incidentally, it is necessary to use the highest wave height as the wave height H_D used in the performance verification.

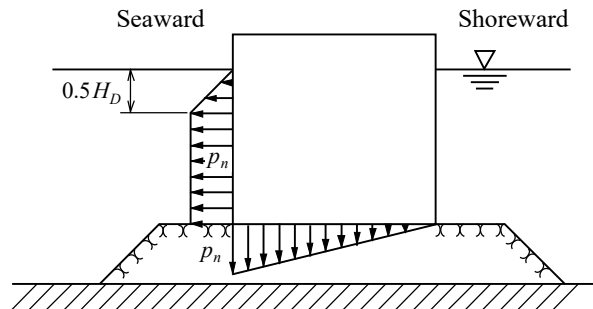


Fig. 6.2.4 Negative Wave Pressure Distribution

(3) Negative wave force by finite amplitude wave theory

Goda and Kakizaki²³⁾ have carried out a wave force calculation based on the fourth order approximate solutions of a finite amplitude standing wave theory, and presented calculation diagrams for negative wave pressure. It has been verified that their calculation results agree well with experimental results. When the water is deep and standing waves are clearly formed, it is acceptable to use the results of this finite amplitude standing wave theory of higher order approximation. It should be noted that, for a deepwater breakwater, the negative wave force at the wave trough may become larger than the positive wave force at the wave crest, and that the upright wall may slide toward offshore.

6.2.4 Impulsive Breaking Wave Force

(1) General

An impulsive breaking wave force is generated when the steep front of a breaking wave strikes a wall surface. Hydraulic model tests have shown that under certain conditions the maximum wave pressure may rise as much as several tens of times the hydrostatic pressure corresponding to the wave height ($1.0\rho_0 g H_D$). However, such a wave pressure acts only locally and for a very short time, and even slight changes in conditions lead to marked variation in the wave pressure. Because of the impulsive nature of the wave force, the effects on stability and the stress in structural elements vary according to the dynamic properties of the structure. Accordingly, when there is a risk of a large impulsive force due to breaking waves being generated, it is necessary to take appropriate countermeasures by understanding the conditions of the impulsive breaking wave force generation and the wave force characteristics by means of hydraulic model tests. It is preferable to avoid the use of cross-sectional shapes and structures that may give rise to a strong impulsive breaking wave force. Where generation of strong impulsive breaking wave force is unavoidable due to steep sea bottom or other reasons, it would be preferable to arrange ways of mitigating wave forces such as by installing appropriate wave-dissipating works.

(2) Conditions of Generation of Impulsive Breaking Wave Forces

A whole variety of coefficients contribute to generation of an impulsive breaking wave force, and so it is difficult to describe the conditions in general. Nevertheless, based on the results of a variety of experiments, it can be said that an impulsive breaking wave force is liable to occur in the following cases when the wave incident angle β (see **Fig. 6.2.2**) is less than 20° .

① **In the case of steep bottom**

When the three conditions, such that the bottom slope is steeper than about 1/30; there are waves that break slightly off the upright wall; and their equivalent deepwater wave steepness is less than 0.03, are satisfied simultaneously, then an impulsive breaking wave force is liable to be generated.

② **In the case of high foundation mound**

Even if the bottom slope is mild, the shape of the rubble mound may cause an impulsive breaking wave force to be generated. In this case, in addition to the wave conditions, the crown height, the berm width, and the slope gradient of the mound all play a part, and so it is hard to determine the conditions under which such an impulsive breaking wave force will be generated. In general, an impulsive breaking wave force will be generated when the mound is relatively high, the berm width is relatively wide or the slope gradient is gentle, and breaking waves form a vertical wall of water at the slope or at the top of the mound.²⁴⁾

When the seabed slope is gentler than about 1/50 and the ratio of the water depth above the top of the mound including armor units to the water depth above the seabed is greater than 0.6, it may be assumed that a large impulsive breaking wave force will not be generated.

(3) Countermeasures

If a large impulsive wave force due to breaking waves acts on an upright wall, the wave force can be greatly reduced by sufficiently armoring the front with wave-dissipating concrete blocks. In particular, with a high mound, a sufficient covering with wave-dissipating concrete blocks can prevent the generation of the impulsive breaking wave force itself. In some cases, the action of an impulsive wave force can also be avoided by using special caissons such as perforated-wall caissons or sloping-top caissons.²⁴⁾ The wave direction also has a large effect on the generation of an impulsive breaking wave force, and therefore, one possible countermeasure is to ensure that the wave direction is not perpendicular to the breakwater alignment.

(4) Examining wave force using hydraulic model tests

When examining the wave force using hydraulic model tests for the case that an impulsive force due to breaking wave acts, it is necessary to give consideration to the response characteristics of the structure. For example, the examination of the stability of upright wall as a whole is preferably conducted by sliding experiment and the strength of members such as parapets by stress measurement experiment.

(5) Impulsive breaking wave force due to breaking waves acting on an upright wall on a steep seabed

① **Water depth of upright wall inducing maximum wave pressure and the mean intensity of wave pressure**

Mitsuyasu²⁵⁾, Hom-ma, Horikawa et al.²⁶⁾, Morihira, Kakisaki et al.²⁷⁾, Goda and Haranaka²⁸⁾, Horikawa and Noguchi²⁹⁾, and Fujisaki, Sasada et al.³⁰⁾ have all carried out studies on the impulsive breaking wave force due to breaking waves acting on an upright wall on a steeply sloping sea bottom. In particular, Mitsuyasu carried out a wide range of experiments using regular waves whereby he studied the breaking wave force acting on an upright wall on uniform slopes of gradient 1/50, 1/25, and 1/15 for a variety of water depths. He investigated the change in the total wave force with the water depth at the location of the upright wall, and obtained an equation for calculating the water depth h_M at the upright wall for which the impulsive wave force is largest. When the Mitsuyasu equation is rewritten in terms of the deepwater wavelength, it becomes as **equation (6.2.11)**:

$$\frac{h_M}{H_0} = C_M \left(\frac{H_0}{L_0} \right)^{-1/4} \quad (6.2.11)$$

where

$$C_M = 0.59 - 3.2 \tan \theta \quad (6.2.12)$$

H_0 : deepwater wave height (m)

L_0 : deepwater wavelength (m)

$\tan \theta$: gradient of uniform slope

Hom-ma and Horikawa et al.²⁸⁾ have proposed a slightly different value for C_M based on the results of experiments with a gradient of 1/15 and other data. In any case, the impulsive breaking wave pressure is largest when the structure is located slightly shoreward of the wave breaking point for progressive waves.

Fig. 6.2.5 shows the total wave force when the impulsive breaking wave force is largest for a number of slope gradients, as based on the results of Mitsuyasu's²⁵⁾ experiments. In this figure, the mean intensity of the wave pressure \bar{p} , determined by assuming that wave pressure acts from the sea bottom to the height of 0.75 times limiting breaker height H_b above the still water surface, has been obtained and then divided by $\rho_0 g H_b$ to make it dimensionless; it has then been plotted against the deepwater wave steepness. Specifically, it can be seen that the smaller the wave steepness i , the larger the impulsive breaking wave force is generated. Also, as the slope gradient becomes smaller, the intensity of the maximum impulsive breaking wave force decreases.

② Conditions for generation of impulsive breaking wave force

The conditions for the occurrence of an impulsive breaking wave force on a steep seabed, as described in **Part II, Chapter 2, 6.2.4 (2) ① In the case of steep sea bottom**, have been set by primarily employing **Fig. 6.2.5** as a gross guideline. For random waves in the sea, the equivalent deep water wave steepness can be calculated as the ratio of the equivalent deepwater wave height corresponding to the highest wave height H_{\max} to the deepwater wavelength corresponding to the significant wave period: where the wave height H_{\max} is to be calculated at the distance $5H_{1/3}$ from the upright wall taking into account of wave transformation due to random wave breaking. One may refer to **Fig. 6.2.5** in order to obtain an approximate estimate of the mean intensity of the wave force for this equivalent deepwater wave steepness. In this case, H_b should be taken to be the aforementioned H_{\max} . One can also envisage an installation of a breakwater at a place where the risk of impulsive breaking wave force generation is not large for the design waves. However, when placing an upright wall closer to the shore where waves already broken act upon, it becomes important to carry out examination for waves with a height lesser than that of the design waves because it is possible that the waves breaking in front of the upright wall exert more wave force than the design waves that lower the wave height, due to wave breaking, among waves of lower height than design waves.

③ Impulsive breaking wave force acting on an upright wall on a horizontal floor adjoining a steep slope

Takahashi and Tanimoto et al.³¹⁾ have carried out studies on the impulsive breaking wave force acting on an upright wall on a horizontal floor joining to a steep slope. They employed a horizontal berm connected to a slope of uniform gradient 1/10 or 3/100 in a water tank, and then measured the wave pressure that acts on an upright wall at a variety of positions on the horizontal berm with regular waves. They have proposed an equation valid for certain wave conditions for calculating the upright wall position at which the wave force is largest and the maximum wave force in that condition.

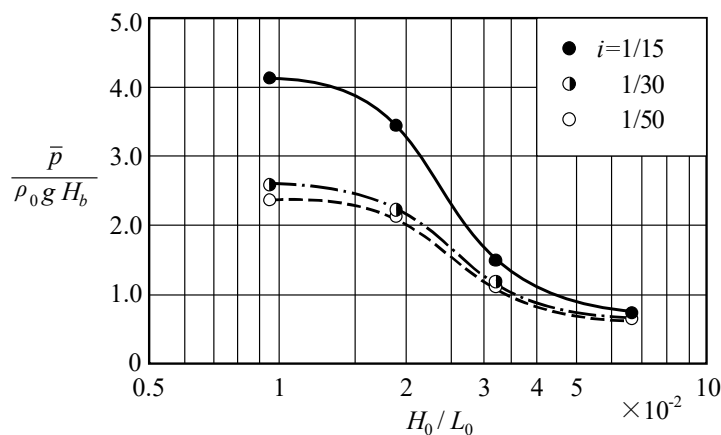


Fig. 6.2.5 Mean Intensity of Wave Force for the Severest Wave Breaking (Upright Wall on a Steep Slope)

(6) Impulsive breaking wave force acting on composite breakwater

① Effect of the mound shape (impulsive breaking wave pressure coefficient)

Takahashi et al.¹⁰⁾ have proposed, based on the results of sliding experiments²⁴⁾, the impulsive breaking wave force coefficient α_1 . This is a coefficient that represents the extent of the impulsive force due to breaking waves when the foundation mound is high. It is expressed as the function of the ratio of the wave height to the depth of water above the mound in front of the caisson H_D/d , the ratio of the depth of water above the mound to the original water depth at the upright wall d/h , and the ratio of the front berm width of the mound to the wavelength at this place B_M/L . Note that the wave height H_D is the design wave height, namely highest wave height. The impulsive breaking wave force coefficient α_1 is expressed as the product of α_{10} and α_{11} as in the following equations:

$$\alpha_1 = \alpha_{10}\alpha_{11} \quad (6.2.13)$$

$$\alpha_{10} = \begin{cases} H_D/d & (H_D/d \leq 2) \\ 2 & (H_D/d > 2) \end{cases} \quad (6.2.14)$$

Fig. 6.2.6 shows the distribution of α_{11} . It attains the maximum value of 1 when d/h is 0.4 and B_M/L is 0.12. The impulsive breaking wave force coefficient α_1 takes values between 0 and 2; the larger the value of α_1 , the larger the impulsive breaking wave force is. When calculating the wave force using conventional Goda's formulas, among α_1 and α_2 , whichever larger shall be used. The equation for α_1 has been formulated based mainly on the results of sliding experiments when H_D/h is relatively large and may be used when examining the sliding of an upright wall on the condition of $H_D/h \geq 0.5$. When $H_D/h < 0.5$, $h = 2H_D$ may be used, for the sake of convenience, in the calculation of α_{11} .³²⁾

② Effect of the crown height of the upright wall

The higher the crown height, the greater the risk of an impulsive breaking wave force being generated. This is because the steep front of a breaking wave often takes a nearly vertical cliff of water above the still water level, and if there is an upright wall at this place, the impact of the wave front results in the generation of an impact load. For example, Mizuno, Sugimoto et al.¹⁷⁾ have pointed out the tendency that, when the crown is high, an impulsive breaking wave force is generated even when the mound is relatively low.

③ Effect of the wave direction

According to the results of the sliding experiments of Tanimoto et al.²⁴⁾, even if conditions are such that a large impulsive breaking wave force is generated when the wave angle β is 0° , there is a rapid drop in the magnitude of the wave force as β increases to 30° or 45° . When the alignment of breakwater is oblique at the direction of incident waves, the impulsive breaking wave force will not generate or actually be neglected because of the weak effect of it against sliding, even if generated. By considering the fluctuation in the wave direction, it is reasonable to assume that the condition for the generation of an impulsive wave force is that β is less than 20° .

④ Dynamic response of the upright section to an impulsive breaking wave force and the sliding of upright section

When an impulsive breaking wave force due to breaking waves acts on an upright section, the instantaneous local pressure can rise up to several tens of times the hydrostatic pressure corresponding to the wave height, although the fluctuation of the impulse is not large and the duration time of the strong impulsive breaking wave force is very short. It is necessary to evaluate the contribution of the impulsive breaking wave force to sliding of the upright section in terms of the dynamic response, considering deformation of the mound and the subsoil. Goda³³⁾ as well as Takahashi and Shimosako³³⁾ have carried out calculations of the shear force at the bottom of an upright section using dynamic models. Judging from the results of these calculations and the results of various sliding experiments, it would seem reasonable to take the mean intensity of the wave pressure of the extreme impulsive breaking wave force statically equivalent to the sliding of the upright wall on the mound to be $(2.5-3.0) \rho_0 g H$. The impulsive breaking wave force coefficient has been introduced based on the results of sliding experiments with consideration of such dynamic response effects to a certain extent.

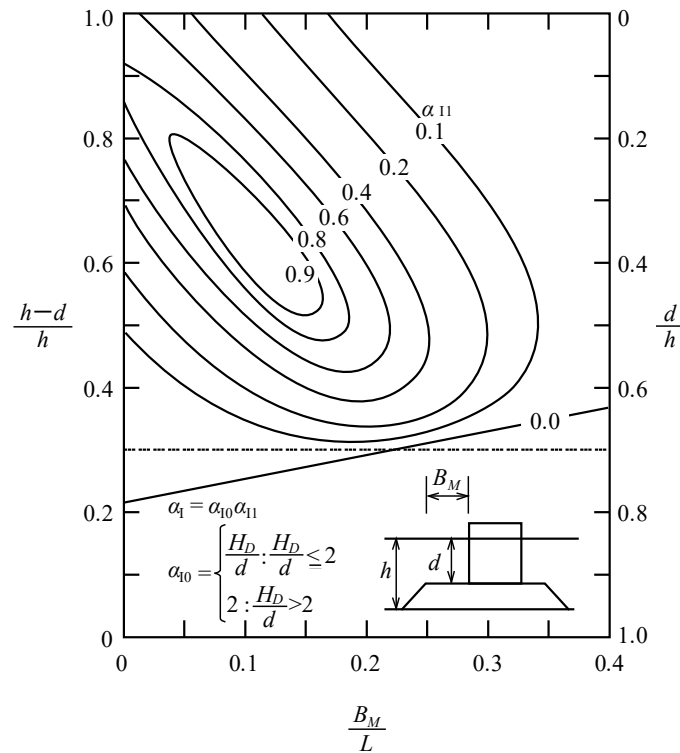


Fig. 6.2.6 Impulsive breaking wave force coefficient

6.2.5 Wave Force Acting on Upright Wall Covered with Wave-dissipating Concrete Blocks

(1) General

If the front of an upright wall is covered with wave-dissipating deformed concrete blocks, the features of wave force acting on the wall varies. The extent of this variation depends on the characteristics of incident waves, along with the crown height and width of the wave-dissipating work, the size and the type of wave-dissipating concrete blocks used, and the composition of the wave-dissipating work including the presence or non-presence of core materials such as rubble. In general, when standing waves act on an upright wall, the wave force does not change drastically by introducing wave-dissipating works. However, when a large impulsive breaking wave force acts, the wave force can be reduced significantly by covering the upright wall with wave-dissipating blocks. Nevertheless, such a reduction in the wave force is only achieved when the wave-dissipating work has a sufficient width and crown height; in particular, it should be noted that if the crown of the wave-dissipating work is below the design tide level, the wave-dissipating work often causes an increase in the wave force.

(2) Wave force calculation formula for upright wall sufficiently covered with wave-dissipating concrete blocks

The wave force acting on an upright wall covered with wave-dissipating concrete blocks varies depending on the composition of the wave-dissipating work, and therefore it should be evaluated using the results of hydraulic model tests. However, if the crown elevation of the wave-dissipating work is as high as the crown of the upright wall and the wave-dissipating concrete blocks are sufficiently stable against the wave actions, the wave force acting on the upright wall may be calculated by applying the extended Goda's formulas. In this method with the standard formula given in **Part II, Chapter 2, 6.2.2 Wave Forces of Standing Waves or Breaking Waves when the Peak of Waves is on the Wall Surface**, the values of η^* , p_1 , and p_u given by equations (6.2.1), (6.2.2), and (6.2.8) are used respectively, but it is necessary to assign appropriate values to the wave pressure correction coefficients λ_1 , λ_2 , λ_3 in accordance with the design conditions.

When in the surf zone where the significant wave height lowers by the effect of wave breaking and fully covered with wave-dissipating blocks, the method proposed by Morihira et al. ²⁷⁾ may be referred to.

(3) Wave pressure correction coefficients to the extended Goda's formulas

The method using the extended Goda's formulas can be applied for not only breaking waves but also non-breaking waves by assigning appropriate wave pressure correction coefficients λ_1 , λ_2 , and λ_3 . Studies about the wave pressure

correction coefficients for the wave-dissipating blocks have been carried out by Tanimoto et al.^{35) 36)}, Takahashi et al.³⁷⁾, Sekino, Kakuno et al.³⁸⁾, and Tanaka, Abe et al.³⁹⁾ They have revealed the following:

- ① Wave-dissipating concrete blocks result in a considerable reduction in the breaking wave pressure, and so it is generally acceptable to set the breaking wave pressure correction coefficient λ_2 to zero.
- ② The larger the wave height, the smaller the correction coefficient λ_1 for standing wave pressure and the correction coefficient λ_3 for uplift become.
- ③ The larger the ratio of the width of covering block section to the wavelength, the smaller the correction coefficients λ_1 and λ_3 become.
- ④ If even a small portion of the upper part of the upright section is left uncovered, there is a risk of the wave force of the uncovered portion becoming an impulsive breaking wave force.

Based on these, Takahashi et al.³⁷⁾ have proposed that in general, when the upright wall is sufficiently covered with wave-dissipating concrete blocks, the wave pressure reduction coefficient λ_2 may be taken to be zero, while the values of λ_1 and λ_3 depend primarily on the wave height H (the highest wave height). They have thus proposed the following equations:

$$\lambda_1 = \begin{cases} 1.0 & (H/h \leq 0.3) \\ 1.2 - 2(H/h)/3 & (0.3 < H/h \leq 0.6) \\ 0.8 & (H/h > 0.6) \end{cases} \quad (6.2.15)$$

$$\lambda_3 = \lambda_1$$

$$\lambda_2 = 0$$

In the surf zone, where breakwaters covered with wave-dissipating concrete blocks are generally used, the above equations give $\lambda_1 = \lambda_3 = 0.8$.

(4) Wave force acting on the superstructure of a sloping breakwater covered sufficiently by wave-dissipating blocks

Tanimoto and Kojima⁴⁰⁾ have proposed a calculation equation for the wave pressure correction coefficient λ for cases where the foundation ground exists near the still-water surface, and where it is covered sufficiently with wave-dissipating blocks similar to the superstructure of a sloping breakwater.

(5) Block load due to wave action

Wave force as the direct action of waves and the action due to the leaning of the blocks act on an upright wall that is covered with wave-dissipating blocks. The latter is called the block load. Research on the block load has been carried out by Hiromoto, Nishijima, et al.⁴¹⁾, Tanaka, Abe, et al.³⁹⁾, and Takahashi, Tanimoto, et al.³⁷⁾, and the results have been summarized as follows.

- ① The block load in still water when waves are not acting is small immediately after installation, but increases along with the action of waves, and approaches the constant value. It is possible to consider the same distribution as the earth pressure for that load, but the value differs depending on the wave forces that act on.
- ② The block load during wave action can be ignored in ordinary cases. This is because the upright wall is displaced, albeit slightly, by the action of the waves, and the block load decreases, and becomes almost 0 when the wave height becomes larger. However, in the event that the wave height is small, or when the water depth is large and the block load in still water is large, it can no longer be ignored.

(6) Impact force of wave-dissipating blocks

Immediately after installation of the blocks or in the event that settlement of the blocks has occurred, when they are subjected to the action of waves in a state where the interlocking between blocks is loose, there are cases where the blocks move due to the waves, and strike the upright wall. In particular, when a wave-dissipating block is large, a powerful impact force acts. This collision of blocks may result in local failure on the caisson's side wall, which makes a bore. Kawabata et al.⁴⁰⁾ indicated a design and verification method of local failure on the caisson's side wall.

(7) Wave force on the discontinuous part of wave-dissipating block covering

In those cases where wave-dissipating blocks are placed partially at corners of breakwater alignment, a discontinuous part of a wave-dissipating block covering appears at the end of wave-dissipating works. In cases

where the crest height of a wave-dissipating work is lower than the design tide level, care is required since the wave force may increase greatly from when it is not armored, and a similar large increase in the wave force may occur also at the discontinuous part of the wave-dissipating block covering.⁴³⁾

Shiomi, Yamamoto, et al.⁴⁴⁾ have conducted a 3-D experiment for the wave force at the discontinuous part of the wave-dissipating block armoring and examined the calculation method shown in **Fig. 6.2.7**. The target range for wave force calculation of the discontinuous part is set as from the slope toe end of the wave-dissipating work to the point where H.W.L. crosses the slope. The target range is divided into unit lengths l . For each divided section, water depth of the wave-dissipating work is assumed to be the water depth d on the mound armored work crest, and the wave-dissipating work crest width is assumed to be the mound crest width B_M . The wave pressure and uplift intensity is calculated by Goda's formulas (employing the impulsive breaking wave force coefficient α_i) in **Part II, Chapter 2, 6.2.2 Wave Forces of Standing Waves or Breaking Waves when the Peak of Waves is on the Wall Surface**, and the wave pressure of each divided section is determined. The wave force is calculated such that the mean wave pressure intensity (p_1, p_3, p_4) and the uplift pressure intensity (p_u) of the one caisson act on the entire caisson located in the discontinuous portion. The division length l is determined such that the full wave force over the length of one caisson becomes maximum, but in general it is set at 1/4 to 1/1 of the partition wall interval of the caisson.

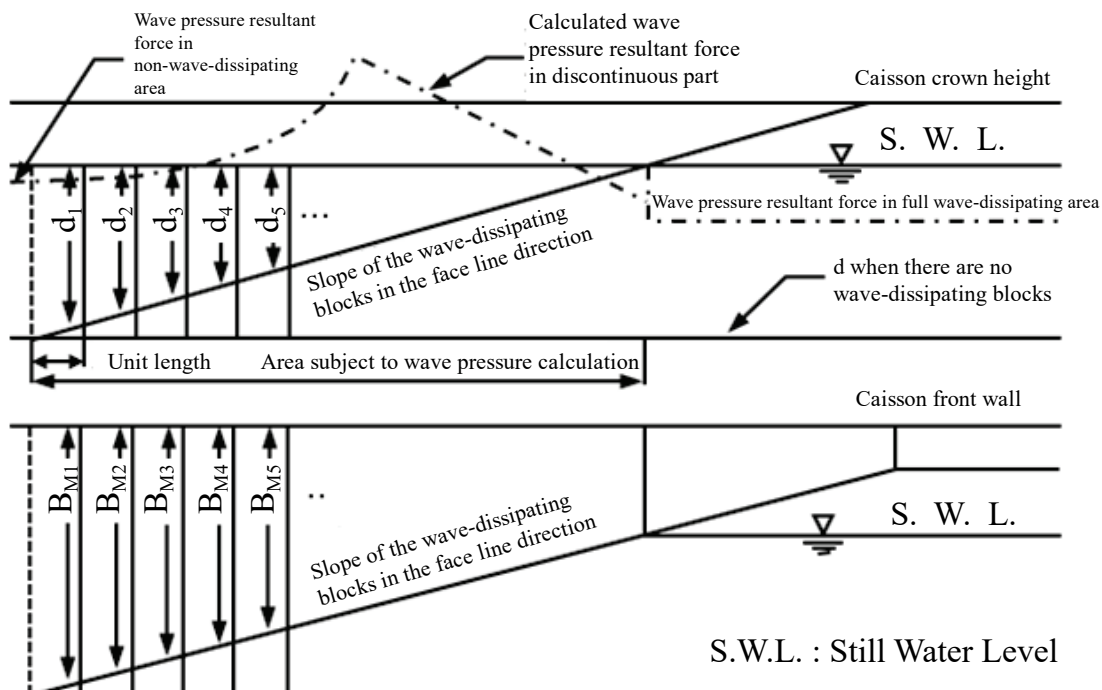


Fig. 6.2.7 Calculation Method of Wave Force at Discontinuously Covered Part of the Wave-Dissipating Blocks (Shiomi et al.⁴⁴⁾)

(8) Wave force on the cross section incompletely covered with wave-dissipating blocks

Even if the crown height of wave-dissipating blocks is higher than the still water level, the wave force may become larger than when there are no wave-dissipating works, provided that the wave-dissipating works provide insufficient cover and the upper part of the upright walls in the front side is not covered with wave-dissipating works. When wave-dissipating works do not completely cover the front side of the upright walls of the breakwater, revetment, and seawall that are covered with the wave-dissipating blocks, the simultaneous action of the storm surge and high waves may exert a strong wave force on upright walls or parapets.

Takahashi et al.⁴⁵⁾ conducted an experiment on an incompletely covered cross section of these wave-dissipating works to obtain a calculation method of wave pressures. This calculation method divides the wave pressure correction coefficient expressed in **equation (6.2.15)** into three regions, as shown in **Table 6.2.1** and **Fig. 6.2.8**. Region 1 is the area not covered with the wave-dissipating works, region 2 is the area covered with wave-dissipating works, on which the impulsive breaking wave exerts a force, and region 3 is the area covered with the wave-dissipating works and on which the impulsive breaking wave does not exert a force. Region 2 extends

down by d_p below from the crown height of the wave-dissipating works. The value of d_p can be calculated by the following equation.

$$d_p = \min[H_{1/3}/3, (h_c - h_B)] \quad (6.2.16)$$

where

h_c is the crown height of the superstructure above the still water level, and h_B is the crown height of the wave-dissipating works above the still water level.

Table 6.2.1 Wave Pressure Correction Coefficient on Incompletely Covered Cross Section, λ_1 , λ_2

	λ_1	λ_2
Region 1	1.0	$1.0 \quad (h_B/H < 0.0)$ $1.0 - 10/7(h_B/H) \quad (0.0 \leq h_B/H \leq 0.7)$ $1.0 - 10h_B/7H \quad (0.7 < h_B/H)$ 0.0
Region 2	$\lambda_{10} \lambda_{11}$	$1.0 \quad (h_B/H < 0.0)$ $1.0 - 10/7(h_B/H) \quad (0.0 \leq h_B/H \leq 0.7)$ $0.0 \quad (0.7 < h_B/H)$
Region 3	$\lambda_{10} \lambda_{11}$	0.0

where, λ_{10} is the reduction coefficient of the standing wave pressure component on the cross section fully covered with wave dissipating blocks and λ_{11} is expressed by the following equation.

$$\lambda_{10} = 0.8 \sim 1.0 \quad (6.2.17)$$

$$\lambda_{11} = \begin{cases} 1.0/\lambda_{10} & (h_B/H < 0.0) \\ \left\{ 1.0 - \frac{1.0 - \lambda_{10}}{0.35} \left(\frac{h_B}{H} \right) \right\} / \lambda_{10} & (0.0 \leq h_B/H \leq 0.35) \\ 1.0 & (0.35 < h_B/H) \end{cases} \quad (6.2.18)$$

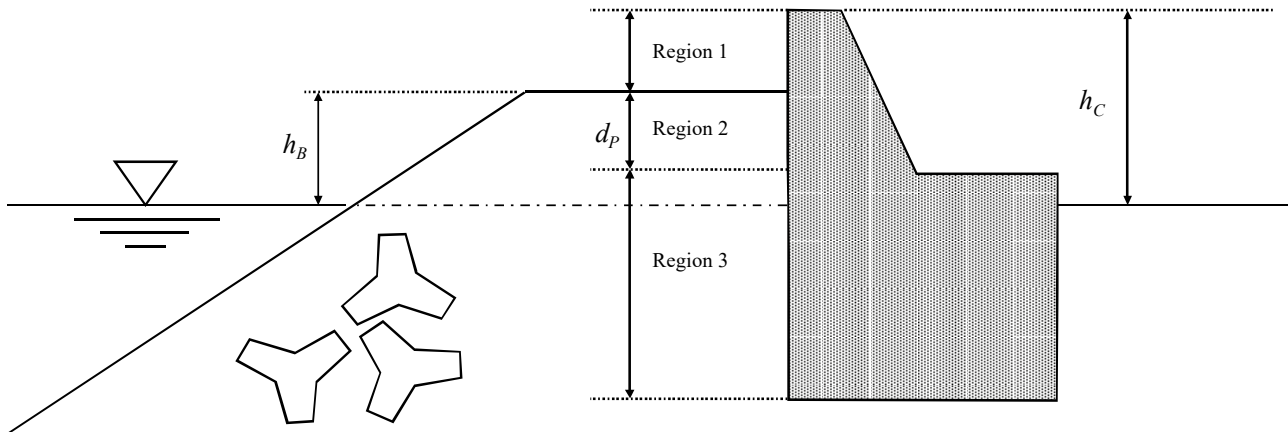


Fig. 6.2.8 Three Regions Distinguishing the Wave Pressure Correction Coefficients on Incompletely Covered Cross Section, λ_1 , λ_2

6.2.6 Wave Force on Sloping-top Caisson Breakwaters

(1) Wave force calculation equation of the sloping-top caisson breakwaters not covered with wave-dissipating blocks

The wave force on sloping-top caisson breakwaters should be calculated based on the hydraulic model test results that are suited to the conditions. However, it is possible to use the following calculation equations, if the conduct of the model test is difficult.⁴⁶⁾ (See Fig. 6.2.9)

$$F_X = F_{SH} + F_V = \lambda'_{SL} F_1 \sin^2 \alpha + \lambda_V F_2 \quad (6.2.19)$$

$$F_Z = -F_{SV} + F_U = -\lambda'_{SL} F_1 \sin \alpha \cos \alpha + 0.5 p_u B \quad (6.2.20)$$

$$\lambda'_{SL} = \min \left[\max \left\{ 1.0, -23(H/L) \tan^{-2} \alpha + 0.46 \tan^{-2} \alpha + \sin^{-2} \alpha \right\}, \sin^{-2} \alpha \right] \quad (6.2.21)$$

$$\lambda_V = \min [1.0, \max \{1.1, 1.1 + 11 d_c / L\} - 5.0(H/L)] \quad (6.2.22)$$

Here,

F_X : total horizontal wave force acting on the sloping-top breakwater (kN/m)

F_Z : total vertical wave force acting on the sloping-top breakwater (kN/m)

F_{SH} : horizontal component of the wave force acting on the sloping part (kN/m)

F_{SV} : vertical component of the wave force acting on the sloping part (with the upwards direction being positive) (kN/m)

F_V : wave force acting on the upright part (kN/m)

F_U : uplift acting on the bottom surface (kN/m)

F_1 : component corresponding to the sloping part out of the horizontal wave force acting on the upright wall calculated by Goda's formulas (kN/m)

F_2 : component corresponding to the upright part out of the horizontal wave force acting on the upright wall calculated by Goda's formulas (kN/m)

λ'_{SL} : correction coefficient for the wave force acting on the sloping part

λ_V : correction coefficient for the wave force acting on the upright part

α : angle of the sloping part (°)

p_U : uplift pressure at the front toe of an ordinary caisson calculated by Goda's formulas (kN/m²)

B : caisson width of a sloping-top breakwater (m)

H : wave height (m)

L : wavelength (m)

d_c : height from the still-water surface to the lower end of the slope (with a case where it is located above the still-water surface taken to be positive) (m)

λ'_{SL} is defined by the following three areas.

① Where H/L is relatively small

$\lambda'_{SL} = \sin^{-2} \alpha$, that is, $F_{SH} = F_1$, $F_{SV} = F_1 \cdot \tan^{-1} \alpha$

② Where H/L is large

$\lambda'_{SL} = 1.0$, that is, $F_{SH} = F_1 \cdot \sin^2 \alpha$, $F_{SV} = F_{SV} \cdot \sin \alpha \cdot \cos \alpha$

③ Where H/L is between ① and ②

λ'_{SL} decreases as H/L becomes larger

In addition, with respect to λ_V , $\lambda_V=1.0$ when H/L is relatively small, and λ_V decreases as H/L becomes larger. However, this wave force calculation equation is applied in the cases where the water depth is relatively deep and the period of the design wave is long, and the value of λ_V should be set at a lower limit of around 0.75.³²⁾ Before this calculation equation was proposed, it had been calculated as $\lambda_{SL}' = \lambda_V = 1.0$ as a convenient and simple method.⁴⁷⁾ In this case, the calculated results are somewhat on the safe side in those cases other than when H/L is relatively small.

(2) Wave force acting on sloping-top caisson breakwaters covered with wave-dissipating concrete blocks

The research of Sato, et al.⁴⁸⁾ can be referenced as concerns the wave force acting on sloping-top caisson breakwaters covered with wave-dissipating blocks. In addition, Katayama, et al.⁴⁹⁾ have proposed a wave force calculation equation for the semi-submerged type, as when the lower end of the sloping part is under the water surface.

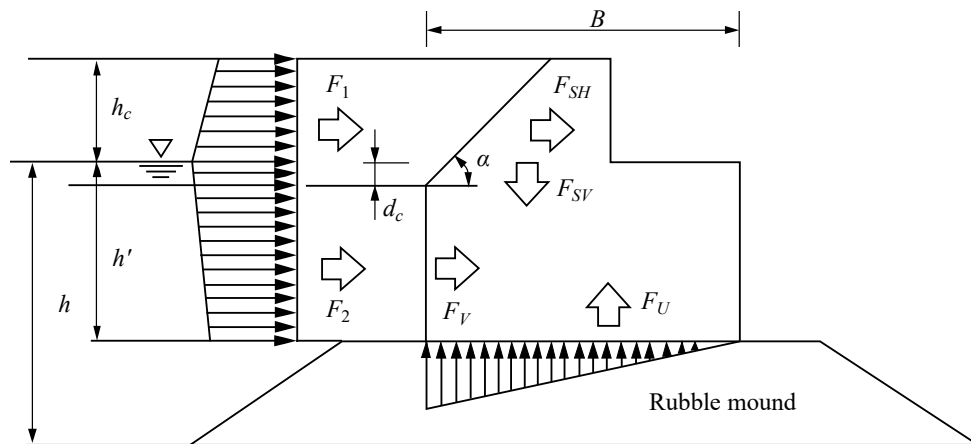


Fig. 6.2.9 Wave Force Acting on Sloping-top Caisson Breakwater

6.2.7 Wave Force Acting on Upright Wave-absorbing Caisson

(1) General

The wave force acting on an upright wave-absorbing caisson varies in a complex way. Specifically, it varies with the wave characteristics, the water level, the water depth, the topography of sea bottom and the shape of the foundation mound as with the case of an ordinary upright wall, but it also varies with the structure of the wave-dissipating structure. It is thus difficult to designate a general calculation method that can be used in all cases. Consequently, if the calculation method that is sufficiently reliable for the structure in question is not proposed, it is necessary to carry out the hydraulic model tests matched to the individual conditions. It is preferable to sufficiently examine not only the wave force to be used in the stability examination but also the wave force acting on structural members. Moreover, it should be noted that the wave force varies significantly according to whether or not the top of wave chamber is covered with a ceiling slab.

(2) Wave force without a ceiling slab in the wave chamber

For the ordinary case where there is no ceiling slab in the wave chamber, one can apply the extended Goda's formulas to calculate the wave force. Takahashi, Shimosako, et al.⁵⁰⁾ have carried out experiments on a vertical-slit wall caisson, and have presented a method for calculating the wave pressure acting on the slit and rear walls for four representative phases, where the wave pressure given by the Goda's formulas is multiplied by a correction coefficient λ . They give specific values for the correction coefficient for the slit and rear walls for each phase. This method can be used to give not only the wave force that is severest in terms of the sliding or overturning of the caisson, but also the wave force that is severest in terms of the performance verification of the structural members for each wall. Note, however, that the experiments which form the basis for this calculation method were conducted under limited structural conditions. Discretion should therefore be exercised in the scope of application for this method.³²⁾

(3) Simplified method to examine the stability of a wave chamber without a ceiling slab

A simpler form of the Goda's formulas can similarly be applied when examining the stability of a caisson. In this method, it is assumed that the wave pressure acts on the main body of the caisson disregarding the wave-dissipating structure (see Fig. 6.2.10), and then the wave force is calculated using η^* obtained using equation (6.2.1), p_1 from equation (6.2.2) and p_u from equation (6.2.8), as described in the Goda's formulas in Part II, Chapter 2, 6.2.2 **Wave Force of Standing Waves or Breaking Waves when the Peak of Waves is on the Wall Surface**. In this case, with respect to the wave-dissipating structure, buoyancy of the entire section should be taken into account. With regards the main body of the caisson, on the other hand, buoyancy under the still water should be considered. However, the wave pressure correction coefficient λ_1 , λ_2 and λ_3 should be assigned appropriately according to structural conditions. There are examples of examinations²⁴⁾ on the correction coefficients λ_1 and λ_2 on curved-slit caissons,⁵¹⁾ perforated-wall caissons and vertical-slit wall caissons.

(4) Wave force used for the examination of the stability with a ceiling slab in the wave chamber

When the top of the wave chamber is closed off with provision of a ceiling slab, an impulsive breaking wave force is generated at the instant when the air layer in the upper part of the wave chamber is trapped in by the rise of water surface. It is thus necessary to give consideration to this impulsive breaking wave force in particular with regard to the wave pressure used in the performance verification of structural elements. This impulsive breaking wave force can be reduced by providing suitable air holes. However, it should be noted that if these air holes are too large, the rising water surface will directly strike the ceiling slab without air cushion, meaning that the wave force may actually increase.^{52) 53)}

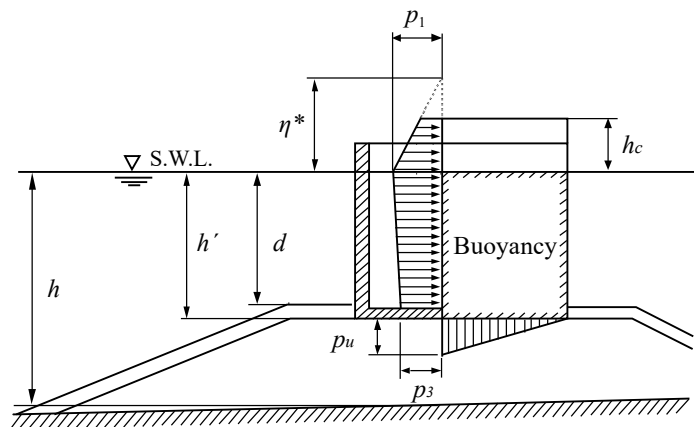


Fig. 6.2.10 Wave Pressure Distribution Employed for Examining Stability
(In case no ceiling slab is installed for wave chamber)

6.2.8 Calculation of Wave Force considering Effect of Alignment of Breakwater**(1) General**

When the alignment of breakwater is discontinuous, the distribution of the wave height along the alignment of breakwater becomes non-uniform due to the effects of wave reflection and diffraction. Ito and Tanimoto⁵⁴⁾ have pointed out that most breakwaters having been damaged by storm waves show a pattern of meandering distribution of sliding distance. They have termed this "meandering damage," and pointed out that one of the causes of this type of damage is the differences in the local wave forces induced by the non-uniform wave height distribution. The variation of wave heights along the breakwater is particularly prominent when the breakwater alignment contains a concave corner with respect to the direction of wave incidence (see Part II, Chapter 2, 4.4.4 **(3) Transformation of Waves at Concave Corners, near the Heads of Breakwaters, and around Detached Breakwaters**). This should be considered in the calculation of the wave forces.^{55) 56)} Variations in wave heights along the breakwater alignment may also occur near the head of the breakwater. In particular, for a detached breakwater that extends over a short length only, diffracted waves from the two ends may cause large variations in wave heights.⁵⁶⁾ These aspects should be considered in the calculation of the wave forces, as necessary.

(2) Wave force calculation method taking increase in wave height into consideration

Wave force calculation methods that consider the effects of the shape of the breakwater alignment have not reached to the level of reasonable reliability yet. It is thus preferable to carry out an examination using hydraulic model tests suited to the conditions. Nevertheless, there is a good correlation between the increase in the wave height owing to the shape of the breakwater alignment and the increase in the wave force. It is thus acceptable to increase the wave height for the performance verifications in accordance with the effect of the shape of the breakwater alignment as in **equation (6.2.23)**, and then calculate the wave force based on the standard calculation equation.

$$H_D' = \min\{K_c H_D, K_{cb} H_b\} \quad (6.2.23)$$

where

H_D' : wave height to be used in the wave force calculation in consideration of the effect of the shape of breakwater alignment (m)

K_c : coefficient for the increase in wave height due to the effect of the shape of breakwater alignment; $K_c \geq 1.0$

K_{cb} : limit value of increase coefficient for limiting breaking wave height; $K_{cb} \doteq 1.4$

H_D : wave height used in the wave force calculation when the effects of the shape of breakwater alignment are not considered (m)

H_b : limiting breaking wave height at the offshore location with the distance of 5 times the significant wave height of progressive waves from the breakwater (m)

The wave height increase coefficient K_c in **equation (6.2.23)** is generally expressed as in **equation (6.2.24)**. It can be appropriately determined based on the distribution of the standing wave height (see **Part II, Chapter 2, 4.4.4 (3) Transformation of Waves at Concave Corners, near the Heads of Breakwaters, and around Detached Breakwaters**) along the alignment of breakwater as determined under the condition that the waves do not break.

$$K_c = H_s / \{H_I(1 + K_R)\} \quad (6.2.24)$$

where

H_s : standing wave height along the wall of breakwater (m)

H_I : incident wave height (m)

K_R : reflection coefficient for the breakwater in question

If the waves are treated as regular waves, then the coefficient for wave height increase varies considerably along the breakwater. Moreover, the height increase coefficient is very sensitive to the period of the incident waves and the direction of waves. It is thus reasonable to consider the irregularity of the period and the direction of waves. It should be noted that the value of K_c obtained in this way varies along the breakwater and that there may be regions where $K_c < 1.0$. In that case, $K_c = 1.0$ shall be applied.

The second term in the braces $\{ \}$ on the right-hand side of **equation (6.2.23)** was introduced in view of the fact that the increase in wave height from the effects of the shape of the breakwater alignment is limited by the water depth. The height of limiting breaking wave H_b can be taken to be the highest wave height H_{\max} in **Part II, Chapter 2, 4.4.6 Wave Breaking** when there is an upright wall in a region where the highest wave would be affected by breaking waves. If it is further offshore, values of limiting breaking wave height of regular waves provided in the breaker index diagram (see **Fig. 4.4.13**) in **Part II, Chapter 2, 4.4.6 Wave Breaking** can be applied. The limit value K_{cb} of increase coefficient for limiting breaking wave height has not been clarified in detail. Nevertheless, it may be considered to be about 1.4 based on experimental results up to the present time.

6.2.9 Wave Force acting on Upright Wall in Abrupt Depth Change

For an upright wall located in a place where the water depth changes abruptly owing to the presence of reefs and others, waves transform significantly and strong impulsive breaking wave force or wave force after breaking act on the upright wall in accordance with the conditions such as the location of the breakwater. Therefore, it is preferable to calculate the wave force acting on the upright wall based on hydraulic model tests, by taking the rapid transformation of waves into consideration.

Ito et al.⁵⁸⁾ have carried out experiments on the wave force acting on an upright wall located on or behind a reef with the uniform water depth and with the offshore slope of about 1/10.

6.2.10 Wave Force acting on Upright Wall Located Toward the Landside from the Breaker Line and Near the Shoreline

(1) Wave force acting on an upright wall located at the seaside of the shoreline near the shoreline

① General

When the changes in wave force due to the installation depth of an upright wall on a uniform slope are examined under conditions of the specified waves, in general the wave force reaches a maximum when the upright wall is located somewhat to the shore side from the breaker point as the progressive wave, and the wave forces decrease as the installation depth becomes shallower than that. Given such a tendency, it is considered that the wave force due to the smaller waves that break somewhat at the offing of the upright wall is greater than wave force after the breaking of a large wave that breaks considerably toward the offing from the upright wall, when it has a certain degree of water depth.

Goda's formula, which are stipulated in **Part II, Chapter 2, 6.2.2 Wave Force of Standing Waves or Breaking Waves when the Peak of Waves is on the Wall Surface**, provide a wave force based on the waves breaking somewhat in the offing of such an upright wall. However, in those places where the water depth in the vicinity of the shoreline is shallow, not only does the breaking wave height vary greatly depending on the changes in water level due to surf beat and so on, but also the breaking wave force varies greatly due to the sea bottom gradient, the wave steepness of offshore waves and the irregularity of the waves, so it is not appropriate to employ Goda's formulas, and it should be calculated with an equation suited to the conditions or the results of a hydraulic model test. In addition, the fact that the water depth itself changes due to the littoral drift, or that the effects of storm surge are great, should also be taken into consideration.

② Calculation method of wave force acting on an upright wall at the seaward side of shoreline near the shoreline

A number of different wave force formulas have been proposed for upright walls near the shoreline. It should be necessary to carry out an appropriate wave force calculation in line with the design conditions. Very roughly speaking, the standard formula in **Part II, Chapter 2, 6.2.2 Wave Forces of Standing Waves and Breaking Waves when the Peak of Waves is on the Wall Surface** are applicable in the regions where the seabed slope is mild and the water is relatively deep. The formula of Tominaga and Kutsumi⁵⁹⁾ is applicable in the regions near the shoreline. The formula of Hom-ma, Horikawa and Hase²⁶⁾ is applicable in the regions where the seabed slope is steep and the water is of intermediate depth. When applying Goda's formula to the places where the water depth is less than one half the equivalent deepwater wave height, it may be preferable to use the values for the wavelength and wave height at the water depth equal to one half the equivalent deepwater wave height in the calculation.

(2) Wave force acting on an upright wall located at the land side of the shoreline

① General

Since the wave force acting on an upright wall located at the land side of the shoreline varies greatly depending on the rise in the water level due to surf beat or the runup of the waves, it should be calculated with an equation suited to the conditions or the results of a hydraulic model test. In addition, the fact that the topology in the vicinity of the shoreline changes due to the littoral drift, or that the effects of storm surge are great, should also be taken into consideration.

② Calculation method of wave force acting on an upright wall at the landward side of shoreline near the shoreline

For an upright wall located on the landward side of the shoreline, the formula by the US Army Coastal Engineering Research Center (CERC)⁶⁰⁾ is available. Moreover, one may refer to the research that has been carried out by Tominaga and Kutsumi⁵⁹⁾ on the wave force acting on an upright wall located on the landward side of the shoreline.

6.3 Wave Force Acting on Submerged Members and Large Isolated Structures

6.3.1 Wave Force Acting on Submersed Members ⁶¹⁾

(1) Morison's Formula

① General

Structural members such as piles that have a small diameter relative to the wavelength hardly disturb the propagation of waves. The wave force acting on such members can be obtained using the Morison's formula as shown in **equation (6.3.1)**, in which the wave force is expressed as the sum of a drag force that is proportional to the square of the velocity of the water particles and an inertia force that is proportional to the acceleration.

$$\vec{f}_n = \frac{1}{2} C_D \rho_0 |\vec{u}_n| \vec{u}_n D \Delta S + C_M \rho_0 \vec{a}_n A \Delta S \quad (6.3.1)$$

where

\vec{f}_n : force that acts on a small length ΔS (m) in the axial direction of the member, where the direction of this force lies in the plane containing the member axis and the direction of motion of the water particles and is perpendicular to the member axis (kN)

\vec{u}_n, \vec{a}_n : components of the water particle velocity (m/s) and acceleration (m/s²), respectively, in the direction perpendicular to the member axis that lies within the plane containing the member axis and the direction of motion of the water particles (i.e., the same direction as \vec{f}_n) (these components are for incident waves that are not disturbed by the presence of member)

$|\vec{u}_n|$: absolute value of \vec{u}_n (m/s)

C_D : drag coefficient

C_M : inertia coefficient

D : width of the member in the direction perpendicular to the member axis as viewed from the direction of \vec{f}_n (m)

A : cross-sectional area of the member along a plane perpendicular to member axis (m²)

ρ_0 : density of seawater (normally 1.03 t/m³)

Equation (6.3.1) is a generalized form of the equation presented for mooring posts by Morison et al. ⁶²⁾, to give the wave force acting on a section of a very small length ΔS of a member orientated in any given direction. The arrows on top of symbols indicate that the force, velocity and acceleration are the components in the direction perpendicular to the member. The first term on the right-hand side represents the drag force, while the second term represents the inertia force. The water particle velocity and acceleration components in the equation both vary in time and space. It is preferable to pay sufficient attention to these variations, and to examine the distribution of the wave force that is severest to the member or structure in question. Because of the phase deviation between velocity and acceleration, the inertia force does not become highest when the drag force is highest. When a member's diameter is quite small compared to the wavelength, the drag force is dominant and the inertia force can be ignored, but it cannot be ignored as the member's diameter becomes larger. It should be also necessary to appropriately evaluate the drag coefficient and the inertia coefficient by hydraulic model tests or field measurement results.

② Water particle velocity and acceleration components

The components of water particle velocity and acceleration (\vec{u}_n, \vec{a}_n) in **equation (6.3.1)** represent the component of the water particle motion at the center axis of the member. These components are in the direction perpendicular to the member axis, and are evaluated under the assumption that waves are not disturbed by the presence of the structure in question. When calculating the wave force, it is necessary to estimate these components as accurate as possible, based on either experimental data or theoretical prediction. In particular, the water particle velocity component contributes to the wave force with its square, meaning that when the wave height is large, an approximation using small amplitude wave theory becomes insufficient to yield reliable estimate. Moreover, when the member extends above the water level, it is necessary to give sufficient

consideration to the range over which the wave force acts, i.e., the elevation of wave crest. When calculating these terms using theoretical values, it is preferable to use the finite amplitude wave theory that agrees with the characteristics of the design waves, based on **Part II, Chapter 2, 4.2.1 Setting Procedure of Waves**. Note also that it is necessary to take full account of wave irregularity with regard to the wave height and period used in the wave force calculation, and to study the wave characteristics that are severest to the safety of member or structure in question. In general, the highest wave height and the significant wave period may be used in the analysis for rigid structures.

③ Drag coefficient C_D

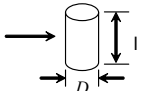
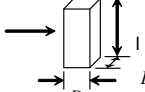
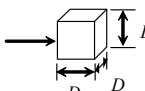
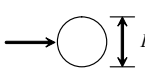
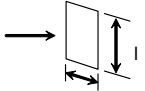
In general, the drag coefficient C_D for steady flow can be used as the drag coefficient C_D for wave force. Note, however, that the drag coefficient varies with the shape of the member, the surface roughness, the Reynolds number Re , and the separation distance between neighboring members. It also varies with the Keulegan-Carpenter number (KC number). It is necessary to consider these conditions when setting the value of drag coefficient. For a circular cylindrical member, it is standard to set $C_D = 1.0$ if the finite amplitude properties of the waves are fully considered. A lower value may be used according to the importance of the facilities if its value is based on the results of hydraulic model tests. Even in this case, however, C_D should not be set below 0.7. Note also that when estimating the water particle velocity by an approximate equation, it is preferable to use a value for the drag coefficient that has been adjusted for the estimation error in the water particle velocity. If the velocity of the water particle motion can be calculated accurately, drag coefficient values for steady flow in **Table 7.2.1** in **Part II, Chapter 2, 7.2 Fluid Force due to Current** may be used with necessary modifications.

④ Inertia coefficient C_M

The value by the small amplitude wave theory may be used for the inertia coefficient C_M . Note, however, that the inertia coefficient varies with the shape of the member and other coefficients such as the Reynolds number, the KC number, the surface roughness, and the separation distance between neighboring members. The value of the inertia coefficient should be set appropriately in line with the given conditions.

When the diameter of the object in question is no more than 1/10 of the wavelength, it is standard to use the value listed in **Table 6.3.1** for the inertia coefficient C_M . However, when estimating the water particle acceleration by an approximate equation, it is necessary to adjust the value of C_M for the error in the estimate of water particle acceleration. The values of inertia coefficient shown here are mostly from the study by Stelson and Mavis.⁶³⁾ According to the experiments of Hamada, Mitsuyasu et al.⁶⁴⁾, the inertia coefficient C_M for a cube is in the range of 1.4 to 2.3.

Table 6.3.1 Inertia Coefficient

Shape of the object	Basic volume	Inertia coefficient
Cylinder 	$\frac{\pi}{4} D^2 l$	2.0 ($l > D$)
Regular prism 	$D^2 l$	2.19 ($l > D$)
Cube 	D^3	1.67
Sphere 	$\frac{\pi D^3}{6}$	1.5
Flat plate 	$\frac{\pi}{4} D^2 l$	When $D/l = 1$, 0.61 When $D/l = 2$, 0.85 When $D/l = \infty$, 1.00

⑤ Experimental values for drag coefficient and inertia coefficient of cylinder

There are many experimental values for the drag coefficient and inertia coefficient of a vertical cylinder; for example, those of Keulegan and Carpenter, ⁶⁵⁾ Sarpkaya, ^{66) 67) 68)} Goda, ⁶⁹⁾ Yamaguchi, ⁷⁰⁾ Nakamura, ⁷¹⁾ Chakrabarti, ^{72) 73)} and Koderayama and Tashiro. ⁷⁴⁾ There are many variations between these values. However, there is not sufficient data in the region of high Reynolds number, which is subject to the actual performance verification. Oda ⁷⁵⁾ has produced a summary of these researches which may be referred to.

⑥ On-site measurement values for drag coefficient and inertia coefficient of cylinder

The drag coefficient and inertia coefficient of a cylinder is also obtained by measuring the wave force at on-site facilities. For example, Mizuno et al. ⁷⁶⁾ obtained $C_D = 0.60 \pm 0.17$, $C_M = 1.23 \pm 0.34$ for a steel pipe structure. Many other on-site measurement results, such as Kim's, ⁷⁷⁾ have been reported, but they are not coincident, partly because of restrictions on accuracy in the on-site experiments, etc.

⑦ Effects of neighboring members

When structural members neighbor one another, the values of the drag coefficient and inertia coefficient vary due to the effects of the other structural members. According to experiments on cylindrical columns, the drag coefficient increases in the event that two columns are arranged in a row perpendicular to the direction of the flow, but it has been known that if the net space between the columns (s) is at least 2.5 times its diameter (D), its effects are small. In addition, in the event that they are arranged in a row in the direction of the flow, the drag coefficient for the column in back exhibits a tendency to decrease over a considerable range ($s/D =$ about 9). However, it cannot be recognized that its effects have been phenomenaadequately solved already, and in general it is better not to consider this as a decrease in the drag coefficient due to the neighboring effect.

In addition, the value of the inertia coefficient considering the effects of neighboring columns has been calculated by diffraction theory, and an increase or decrease has been known compared with the case of a single column depending on the values of s/D and D/L , ⁷⁸⁾ but when D/L is small, its effects are small. Nakamura and Abe ⁷⁹⁾ have investigated experimentally the increase in the inertia coefficient in a range of $D/L < 0.1$, and have pointed out that although the results are scattered, the upper limit of the coefficient value is extremely large in the vicinity of $s/D = 2$ to 3, and it is better to avoid a situation where the interval between the two columns matches such conditions.

⑧ Facilities composed of many structural members

The wave force that acts on an entire facility composed of upright columns, slanted members and/or horizontal members is calculated by **equation (6.3.1)** considering the phase difference of the wave force acting on each structural member, and by compounding the vector sums of these. In the case of facilities composed of many of structural members, there is a risk that the whole might collapse due to the failure of one point in the structural member, so the distribution of the wave force that is most severe for the individual structural members and the entire facility should be considered in particular.

⑨ Resonance with waves and random wave force

In the event that the rigidity of the facilities is low, and the natural frequency period is long, it is preferable to consider the effects of the dynamic response on the wave force that acts periodically. The wave force in this case may be calculated for the temporal changes of \vec{u}_n , \vec{a}_n based on **equation (6.3.1)**. However, since only the specific dynamic effects are reflected in the examination for waves with a constant period, it is reasonable to view this as the continuous action of random waves. When calculating the wave force for random waves, suitable measures may be devised for the way to provide the height of the wave crest and the drag coefficient, and the water particle movement component may be calculated based on small amplitude wave theory.

(2) Wave force when breaking waves act

When breaking waves act on facilities on a steep sea bottom surface, there are cases when an impulsive wave force similar to the impulsive breaking wave pressure that acts on upright walls acts in addition to the drag and inertia forces given by **equation (6.3.1)**. Since the response characteristics of the facilities become the dominant effective factor for such an impulsive action, not only a calculation of the wave force but also an examination that includes the behavior of the entire facility as well as the structural members should be carried out. ^{80) 81)}

(3) Uplift

In addition to the drag and inertia forces of **equation (6.3.1)**, wave force acting on submerged members is the uplift acting in the direction perpendicular to the plane containing the member axis and the direction of the water particle

motion. In general, it is acceptable to ignore this uplift, but it is necessary to pay attention to the fact that the uplift may become a problem for horizontal members that are placed near to the seabed.^{82) 83) 84) 85) 86) 87)} Moreover, for long and thin members, it is necessary to pay attention to the fact that the uplift may induce vibrations.

(4) Wave force due to random waves

Of the wave force components acting on structural members in the sea, the inertia force is linear, so the spectrum of the wave force can be calculated easily from the spectrum of the waves, but when the drag force is included this becomes difficult owing to its nonlinearity. Borgman⁸⁸⁾ has introduced a theoretical equation for the wave force spectrum that includes drag force based on probability theory. The first approximation of this drag force corresponds to something where the nonlinear drag force is made linear in a form in which the root-mean-square value of the water particle speed is incorporated in the coefficient, and this is employed occasionally in spectrum analysis of on-site observational data and other cases. In addition, Hino⁸⁹⁾ has introduced a theory of a case where waves and a uniform flow co-exist by using the characteristic function method. A simulation method where the random wave forms and water particle movement are simulated based on a prescribed wave spectrum, and its time series is inputted and the wave force is calculated, is also being employed commonly as a method for studying the statistical nature of random waves including the nonlinear drag and the dynamic response of the facilities. Borgman⁹⁰⁾ has explained this method, and there is the calculation example of Ito et al.⁹¹⁾. These are simulations based on linear theory, but recently nonlinear simulation calculations that consider everything up to the second-order interference terms between component waves have also been carried out,⁹²⁾ and in addition, nonlinear simulation calculations of multi-directional random waves have also been tried.⁹³⁾ As for the probability distribution of the wave force, the wave height exhibits a Rayleigh distribution, whereas the distribution of its local maximum value may become considerably different from the Rayleigh distribution owing to the nonlinearity of the drag force etc. and the incidence rate of large maximum values may become considerably high. Tickell-Elwany⁹⁴⁾ has calculated the theoretical value of the wave force distribution based on three-dimensional random waves. In addition, Kimura et al.⁹⁵⁾ has calculated the probability distribution of the wave force acting on a single cylindrical column based on the joint distribution of the wave height and period of random waves, and shown a method for calculating the anticipated values for the maximum wave force.

(5) Equation for calculating the breaking wave force acting on slanted columns

Tanimoto, Takahashi, et al.⁸¹⁾ have developed the research of Goda et al.⁸⁰⁾, and have proposed a method for calculating the breaking wave force acting on cylindrical columns based on experimental results. The calculation of the impulsive breaking wave force acting on upright cylindrical columns or slanted cylindrical columns installed on a sea bottom with a uniform slope may be carried out based on this method. In the experiments both regular and random waves were employed, and the experiments were carried out with a cylindrical column with a $D/h = 1/5$, for gradients $i = 1/100$ and $1/30$, and $\theta = -30^\circ, -15^\circ, 0^\circ, +15^\circ$ and $+30^\circ$. The position of the impulsive wave force that acts and the changes over time can be calculated by the proposed calculation method, and the response of the cylindrical column member to the impulsive wave force can also be calculated by applying appropriate methods.

(6) Breaking wave force acting on small diameter cylindrical columns on a reef

Goda et al.⁹⁶⁾ have proposed a method for calculating the breaking wave force that acts on upright cylindrical columns on reefs, where the water depth changes suddenly, and it is possible to carry out calculations of the wave force based on this method for waves like those that break on the slope of reefs.

(7) Effects of multi-directionality of waves

As the multi-directionality of waves becomes stronger, the components of the wave force other than the principal direction of the waves becomes larger. Therefore, the multi-directional dispersion of the waves should be considered in facilities constructed in deep waters where the multi-directionality is strong.⁹⁷⁾

6.3.2 Wave Force Acting on Large Isolated Structures

(1) General

The wave force acting on a large isolated structure whose dimensions are comparable to the wavelength can be calculated using the velocity potential, because it is generally possible to ignore the drag force. In particular, for structures of a simple shape, analytical solutions obtained by diffraction theory are available. However, it is necessary to calculate the breaking wave force by hydraulic model tests if there is a possibility of breaking wave force exerted on structure.

(2) Diffraction theory

MacCamy-Fuchs⁹⁸⁾ have determined the velocity potential of waves around an upright cylindrical column of large diameter using diffraction theory, and calculated the wave force from the water pressure distribution at the surface of cylinder. Goda and Yoshimura⁹⁹⁾ have applied diffraction theory to an upright elliptic cylinder, and presented their results in terms of the inertia coefficient C_M . Yamaguchi¹⁰⁰⁾ has examined the effect of the wave nonlinearity on the wave force acting on an upright cylindrical column of large diameter by nonlinear diffraction theory, and pointed out that it is necessary to consider these effects when the water is shallow.

(3) Isolated structure of arbitrary shape

For a structure that is complex in shape, it is difficult to obtain the wave force analytically, and so it is necessary to carry out a numerical calculation. Various methods are available, such as integral equation methods (see **Part II, Chapter 2, 4.8 Action on Floating Body and its Motions**).

6.4 Wave Force Acting on Structures near the Water Surface

6.4.1 Uplift Acting on Horizontal Plates near the Water Surface

(1) General

In the case of facilities near still water surface, such as the superstructure of piled piers or pile-type dolphins, and in particular those facilities that are roughly parallel to the water surface, there is a risk that a rising wave surface will strike on the bottom surface of the facilities and an impulsive wave force (uplift) will act on. In particular, it becomes a large impact load when the wave height is large and the clearance with the still water surface is small. In addition, in a case where there is a reflecting wall at the rear as in the case of open type wharf, and the waves become standing waves and act on this, the wave surface rise rate increases and so does the impact load. If there is a risk of an impact load, the impulsive uplift should be calculated by a suitable method such as a hydraulic model test. Due attention should also be paid to the fact that ordinary uplift that is not an impact load also acts on the bottom surface of such structures, in addition to the impulsive uplift.

(2) Characteristics of impulsive uplift

If the bottom surface of the plate is flat, the impulsive uplift acting on a horizontal plate near the still water surface level varies with the impact velocity of the wave surface and the angle between the wave surface and the plate. As shown in **Fig. 6.4.1 (a)**, when there is an angle between the wave surface and the plate, the wave surface runs along the bottom surface of the plate and the wave pressure distribution becomes as shown there. The distinct feature of the wave pressure in this case is its rapid rise in time. On the other hand, when the angle between the wave front and the plate is close to 0, as shown in **Fig. 6.4.1 (b)**, a layer of air is trapped between the wave surface and the plate, and compression of this layer of air results in the almost uniform wave pressure distribution. The distinct feature of the wave pressure in this case is its oscillation in time with having a short-period damping vibration.

In case of a piled pier with a deck plate supported by horizontal beams, the wave surface is disturbed by the beams, and the uplift becomes of complex nature. With beams, a layer of trapped air is often formed and this layer of air is compressed by the uprising wave surface. It is thus necessary to give consideration to the change in the uplift with respect to the shape of the bottom face of the horizontal plate. The shape of the impacting wave surface varies greatly according to the condition whether the wave is progressive or standing in nature. With standing waves, the shape of the impacting wave front varies with the distance between the position of wave reflection and the horizontal plate. It is thus necessary to consider such differences.

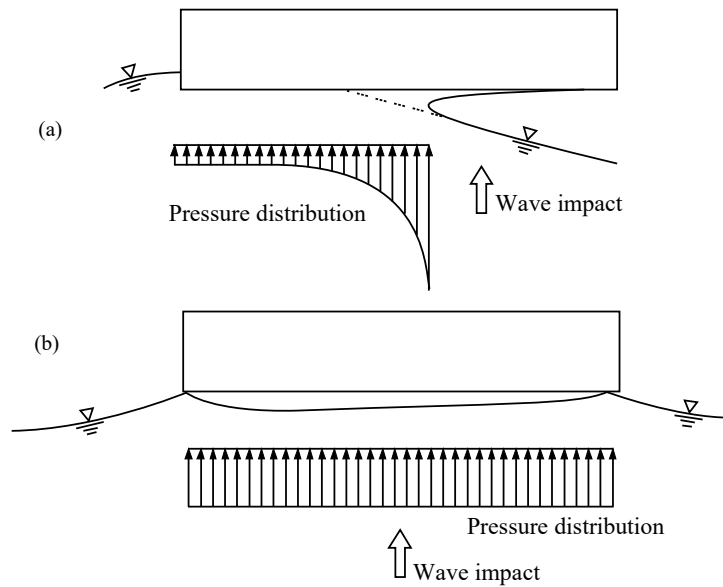


Fig 6.4.1 Impact between Wave Front and Horizontal Plate

(3) Calculation of uplift from standing waves

① Uplift acting on horizontal plate with flat bottom surface

Goda ⁶⁾ considered the uplift acting on a horizontal plate as being the force resulted from the sudden change in the momentum of wave by its impact on the plate. Using von Karman's theory, he obtained the following formulas for calculating the uplift of standing waves acting on a horizontal plate.

$$P = \zeta \frac{\rho_0 g}{4} HLB \tanh \frac{2\pi h}{L} \left(\frac{H}{s'} - \frac{s'}{H} \right) \quad (6.4.1)$$

$$s' = s - \pi \frac{H^2}{L} \coth \frac{2\pi h}{L} \quad (6.4.2)$$

where

P : total uplift (kN)

ζ : correction coefficient

$\rho_0 g$: unit weight of seawater (kN/m³)

H : wave height of progressive waves, generally the highest wave height H_{\max} (m)

L : wavelength of progressive waves (m)

B : width of plate (m)

h : water depth (m)

s : clearance of the plate above the still water surface (m)

s' : clearance of the plate above the level corresponding to the middle of the wave crest and trough (m)

It is necessary to pay attention to the fact that the uplift in the above equations does not depend on the length of the horizontal plate l .

The impact force has the magnitude given by the above equations and takes the form of a pulse that lasts for a time τ from the moment of the impact, that is given as follows:

$$\tau = \frac{\pi T^2}{L^2} \frac{s'}{\sqrt{H^2 - s'^2}} \quad (6.4.3)$$

Where T is the wave period and l is the length of the horizontal plate. Provided the length of the horizontal plate is sufficiently short compared with the wavelength L and the bottom surface of the horizontal plate is flat, **equation (6.4.1)** well represents the features of the uplift well with simple equation. Comparing calculated values with $\zeta = 1.0$ to experimental values, agreement is relatively good provided H/s' is no more than 2.

Tanimoto, Takahashi et al.¹⁰¹⁾ have proposed another method for calculating the uplift acting on horizontal plate based on Wagner's theory. With this calculation method, the angle of contact β between the wave surface and the horizontal plate as well as the impact velocity V_n are given by Stokes' third order wave theory, making it possible to obtain the spatial distribution of the impact pressure and its change over time. Note, however, that the use of Stokes' third order wave theory makes the calculation rather complex. This calculation method is intended for use when the bottom face of the horizontal plate is flat. It cannot be applied directly to structures of complicated shape such as an ordinary piled pier that have beams under the floor slab; the impact between the wave surface and the floor slab is disturbed by the beams. In general, the presence of beams causes air to become trapped in and the wave surface to be disturbed, the result being that the impact force is less than for a horizontal plate with a flat surface. Accordingly, the value obtained from this calculation method may be considered as being the upper limit of the uplift for an ordinary piled pier.

② Uplift Acting on Piled Pier

Ito and Takeda¹⁰²⁾ have conducted scale model tests of piled pier to obtain the uplift acting on an access bridge, and its vibration threshold weight and falling threshold weight. The peak value of the uplift obtained by the experiment varied considerably from wave to wave even under the same conditions. Nevertheless, the mean of these peak values is given approximately by the following **equation (6.4.4)**:

$$p = \rho_0 g (8H - 4.5S) \quad (6.4.4)$$

where

p : mean peak value of uplift (kN/m²)

$\rho_0 g$: unit weight of seawater (kN/m³)

H : incident wave height (m), (highest wave height)

S : distance from the water level to the underside of access bridge (m)

Note however that the peak value of the intensity of the uplift given by **equation (6.4.4)** acts only for an extremely short time, and that the phase of this uplift varies from place to place. This means that even if the uplift p exceeds the self weight of the access bridge, the bridge will not necessarily move or fall down immediately. Based on this perspective, Ito and Takeda have obtained the threshold weight at which the access bridge vibrates and that at which the deck slab falls down. The relationship between the vibration threshold weight and the wave height is given below:

$$q = \rho_0 g (1.6H - 0.9S) \quad (6.4.5)$$

The vibration threshold weight given by **equation (6.4.5)** is one fifth of the intensity of the uplift as given by **equation (6.4.4)**. The falling threshold weight was found to be 1/2 to 1/3 of the vibration threshold weight.

In these access bridge experiments, Ito and Takeda also tested the access bridge with holes or slits of various sizes, and investigated how the threshold weights changed when the void ratio was changed. In general, the change in the vibration threshold weight by the void ratio is only slight compared to access bridges without holes, when the void ratio is small i.e., around 1%, air escapes easily and the water surface strikes the access bridge impulsively. The falling threshold weight, on the other hand, drops noticeably when the void ratio exceeds 20%. Note that the bridge weight referred to here is the weight per unit area of the substantial part i.e., the weight per unit area excluding the voids. In this way, since there is little change to the vibrating threshold weight, namely the stable weight per unit area of the substantial part of the access bridge, the weight of an entire surface area can be reduced by boring holes. What is more, the falling threshold weight decreases with the increase in the void rate. From these two reasons, it can be concluded that it is best to raise the void rate.

Furthermore, Ito and Takeda¹⁰²⁾ have attached a strain gage to the deck slab in the superstructure of the model of piled pier and measured the stress. Based on their results, they proposed the following equation for the equivalent static load (kN/m²) assumed to act with uniform distribution on the deck slab.

$$p = 4\rho_0 gH \quad (6.4.6)$$

Note, however, that the value given by this equation corresponds to the upper limit of the experimental values and should, thus, be considered corresponding to the case that the distance s from the water level to the underside of the superstructure is almost 0. The equivalent static load, given by **equation (6.4.6)**, is generally lower than the uplift acting on a horizontal plate with a flat bottom face. It is considered that this is partly because the beams disturb the impacting wave front, trapping air. Experimental research into the uplift acting on a piled pier has also been carried out by Murota and Furudoi,¹⁰³⁾ Nagai and Kubo et al.¹⁰⁴⁾, Horikawa and Nakao et al.¹⁰⁵⁾, and Sawaragi and Nochino.¹⁰⁶⁾

(4) Calculation of uplift from progressive waves

① Uplift acting on horizontal plate with flat bottom surface

An impulsive uplift also acts when progressive waves act on a horizontal plate that is fixed near to the still water level. Tanimoto and Takahashi et al.¹⁰⁷⁾ have proposed a method for calculating this impulsive uplift, based on the same theory that was used for impulsive uplift by standing waves.

② Uplift acting on superstructure of detached pier

- (a) Ito and Takeda¹⁰²⁾ have also carried out studies on the uplift of progressive waves acting on a detached pier. Specifically, they measured the stress occurring in the deck slabs of a detached pier model. Based on the upper limits of their experimental results, they proposed the following equation for the uniformly distributed equivalent static load.

$$p = 2\rho_0 gH \quad (6.4.7)$$

- (b) Allsop and Cuomo, et al.^{108) 109) 110) 111)} have undertaken a systematic examination of the uplift due to progressive waves that act on detached pier by hydraulic model tests based on random waves and theoretical analysis. They have proposed calculation equations concerning the ordinary uplift that is not an impact load.¹⁰⁹⁾

6.4.2 Horizontal Wave Force Acting on the Vertical Plate near the Water Surface

A horizontal wave force acts on thin, vertical plates, such as curtain walls installed near the water surface, or the vertical surface of the horizontal plates, such as the dolphin superstructure of the stationary offshore berth. The water surface location and the wave making resistance force, due to the existence of the free surface, should be considered when calculating this horizontal wave force.

Tanimoto, Takahashi et al.¹⁰⁷⁾ proposed a calculation equation for the horizontal wave force acting on the stationary structure near the water surface, primarily targeting the dolphin superstructure, and also proposed to use this horizontal wave force calculation equation for the horizontal wave force acting on the curtain walls fixed near the water surface. Moreover, Kubou, Takezawa et al.¹¹²⁾ also proposed a calculation equation for curtain walls with a shallow submersion depth.

Morihira, Kakizaki et al.¹¹³⁾ experimentally obtained the horizontal wave force acting on curtain walls used as breakwater. Also, Sekimoto et al.¹¹⁴⁾ indicated a calculation method for the wave force acting on curtain walls, considering the incidence angle.

6.5 Mound Transmitted Wave Pressure of Caisson Type Seawall and Wave Pressure within Joints of Caissons

6.5.1 General

In the caisson-type seawalls, waves may transmit rubble mounds and back fill stones, as in **Fig. 6.5.1**, and act on the reclaimed sand. As the rubble and reclaimed sand significantly differ in grain size, sand leakage prevention sheets and joint plates between caissons are installed to prevent the leakage of reclaimed sand. However, these sand leakage prevention sheets and joint plates are frequently damaged by the mound transmitted waves during and after construction to result in the leakage of the reclaimed sand.

Here, the mound transmitted waves and the wave pressure generated in the joint of caissons are explained.

6.5.2 Mound Transmitted Wave Pressure

After installation of impermeable sand leakage prevention sheets or reclaimed soil behind the backfill stones as in **Fig. 6.5.1**, the inside of the rubble mound or backfill stones becomes sealed. In this condition, the pressure exerted to the front toe of the caisson acts on the sand leakage prevention sheets or the reclamation gravel without attenuation¹¹⁵⁾. The wave pressure p_w acting on the front toe can be calculated by Goda's formula (**equation (6.2.4)**)¹¹⁶⁾, and the pressure almost equal to the wave pressure is generated inside the backfill stones

The uplift of the sand leakage prevention sheets due to this wave force, needs to be prevented because it causes damage of the sheets during construction.

Moreover, even after construction period, mound transmitted strong waves may blow off the reclaimed soil if it is thin at the back. Depressurizing works may be installed in the upper part of the mound to reduce such strong mound transmitted waves. See "Design, construction and control manual for the controlled type waste disposal site (Revised)"¹¹⁶⁾ for the pressure calculation method inside the mound with depressurizing works.

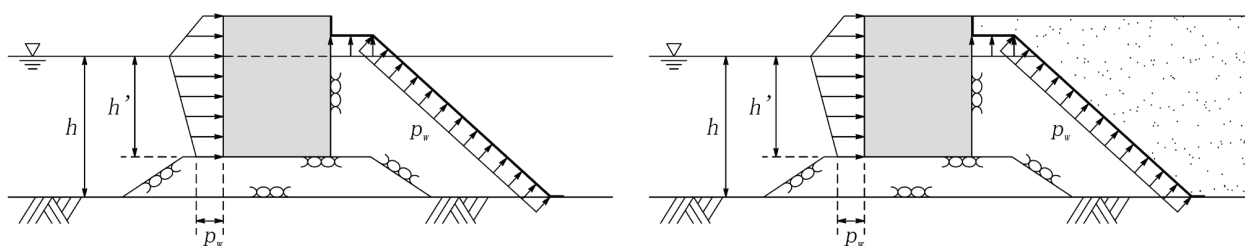


Fig. 6.5.1 Mound Transmitted Wave Pressure Applied behind the Caisson Type Seawall
(left: during construction, right: after completion)

6.5.3 Wave Pressure within Joints

The joint plates are installed behind the joints, between the caissons, to prevent the leakage of backfill stones or reclaimed soil. The impulsive wave pressure may be generated inside the joints, as shown in **Fig. 6.5.2**, when the wave surface acts on the joint plates. This wave pressure is often larger than the one acting on the front side of caisson and is expressed by **equation (6.5.1)**¹¹⁵⁾.

The stability and tensile strength of the sand leakage prevention plate can be obtained by using Takebe et al's method.¹¹⁷⁾

Moreover, as the joint plate deforms even slightly by such wave force after construction of the seawall, sediment with small grain sizes, like sand, may leak out. Therefore, it is necessary to avoid putting reclaimed sand just behind the joint plate, but to install the back fill stones just behind the joint plate or in other ways.

$$p = 2\rho_0 g H \quad (6.5.1)$$

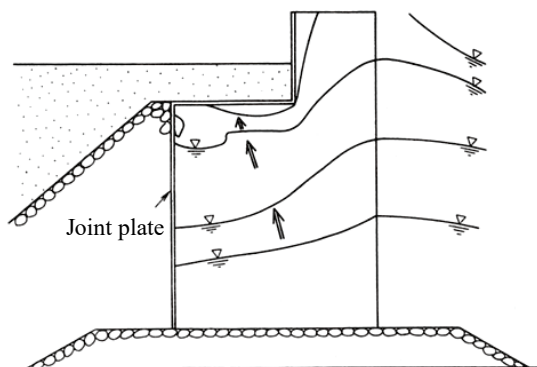


Fig. 6.5.2 Behavior of Wave Surface inside the Joint

6.6 Stability of Armor Stones and Blocks against Waves

6.6.1 Required Mass of Armor Stones and Blocks on Slope^{118) 119)}

(1) General

The armor units for the slopes such as sloping breakwaters are placed to protect the rubble stones inside; it is necessary to ensure that an armor unit has a mass sufficient to be stable so that it is not scattered itself. This stable mass (the required mass) can generally be obtained by hydraulic model tests or calculations using appropriate equations.

(2) Basic Equation for Calculation of Required Mass

When calculating the required mass of rubble stones and concrete blocks covering the slope of a sloping structure which is affected by wave forces, Hudson's formula with the stability number N_s , which is shown in the following equation, may be used.¹²⁰⁾

$$M = \frac{\rho_r H^3}{N_s^3 (S_r - 1)^3} \quad (6.6.1)$$

where

M : required mass of rubble stones or concrete blocks (t)

ρ_r : density of rubble stones or concrete blocks (t/m³)

H : wave height used in stability calculation (m)

N_s : stability number determined primarily by the shape, slope, damage rate of the armor, etc. of the armor units

S_r : specific gravity of rubble stones or concrete blocks relative to water

(3) Stability Number and Nominal Diameter

The stability number directly corresponds to the size (nominal diameter) of the armor required for a certain wave height H . Assume the nominal diameter $D_n = (M/\rho_r)^{1/3}$ and $\Delta = S_r - 1$ and substitute into **equation (6.6.1)**, a simple equation

$$H / (\Delta D_n) = N_s \quad (6.6.2)$$

is obtained to show that the wave height and the nominal diameter are proportional with ΔN_s as its proportional constant.

(4) Design Wave Height H Used in the Performance Verification

Hudson's formula was proposed based on the results of experiments in regular waves. When applying it to the action of actual waves which are random, there is thus a problem of which definition of wave heights shall be used. However, with structures that are made of rubble stones or concrete blocks, there is a tendency for damage to occur not when one single wave having the maximum height H among a random wave train attacks the armor units, but rather for damage to progress gradually under the continuous action of waves of various heights. Considering this fact and past experiences, it has been decided to make it standard to use the significant wave height of progressive waves at the place where the slope is located as the wave height H in **equation (6.6.1)**, because the significant wave height is representative of the overall scale of a random wave train. Note however that for places where the water depth is less than one half of the equivalent deepwater wave height, the significant wave height at the water depth equal to one half of the equivalent deepwater wave height should be used.

(5) Parameters Affecting the Stability Number N_s

As shown in **equation (6.6.1)**, the required mass of armor stones or concrete blocks varies with the wave height and the density of the armor units, and also the stability number N_s . The N_s value is a coefficient that represents the effects of the characteristics of structure, those of armor units, wave characteristics and other factors on the stability. The main coefficients that influence the N_s value are as follows.

① Characteristics of the structure

- (a) Type of structure; sloping breakwater, breakwater covered with wave-dissipating concrete blocks, and composite breakwater, etc.

- (b) Gradient of the armored slope
- (c) Position of armor units; breakwater head, breakwater trunk, position relative to still water level, front face and top of slope, back face, and berm, etc.
- (d) Crown height and width, and shape of superstructure
- (e) Inner layer; permeability coefficient, thickness, and degree of surface roughness

② **Characteristics of the armor units**

- (a) Shape of armor units (shape of armor stones or concrete blocks; for armor stones, their diameter distribution)
- (b) Placement of armor units; number of layers, and regular laying or random placement, etc.
- (c) Strength of armor material

③ **Wave characteristics**

- (a) Number of waves acting on armor layers
- (b) Wave steepness
- (c) Form of seabed (seabed slope, where about of reef, etc.)
- (d) Ratio of wave height to water depth as indices of non-breaking or breaking wave condition, breaker type, etc.
- (e) Wave direction, wave spectrum, and wave group characteristics

④ **Extent of damage (damage ratio, deformation level, relative damage level)**

Consequently, the N_S value used in the performance verification must be determined appropriately based on hydraulic model experiments in line with the respective design conditions. By comparing the results of regular waves experiments with those of random wave experiments, ¹²¹⁾ it was found that the ratio of the height of regular waves to the significant height of random waves that gave the same damage ratio, within the error of 10%, varied in the range of 1.0 to 2.0, depending on the conditions. In other words, there was a tendency for the random wave action to be more destructive than the action of regular waves. It is thus better to employ random waves in experiments.

(6) Stability Number N_S and K_D Value

In 1959, Hudson published the so-called Hudson's formula, ¹²⁰⁾ replacing the previous Iribarren-Hudson's formula. Hudson developed **equation (6.6.1)** by himself using $K_D \cot \alpha$ instead of stability number N_S .

$$N_S^3 = K_D \cot \alpha \quad (6.6.3)$$

where

α : angle of the slope from the horizontal line (°)

K_D : constant determined primarily by the shape of the armor units and the damage ratio

The Hudson's formula was based on the results of a wide range of model experiments and has proved itself well in usage in-site. This formula using the K_D value has thus been used in the calculation of the required mass of armor units on a slope.

However, the Hudson's formula that uses the stability number in **equation (6.5.1)** has been used for quite a while for calculating the required mass of armor units on the foundation mound of a composite breakwater as discussed in **Part II, Chapter 2, 6.5.2 Required Mass of Armor Stones and Blocks in Composite Breakwater Foundation Mound against Waves**, and is also used for the armor units of other structures such as submerged breakwaters. It is thus now more commonly used than the old formula with the K_D value.

The stability number N_S can be derived from the K_D value and the angle α of the slope from the horizontal line by using **equation (6.5.3)**. There is no problem with this process if the K_D value is an established one and the slope angle is within a range of normal design. However, most of the K_D values obtained up to the present time have not sufficiently incorporated various coefficients like the characteristics of the structure and the waves. Thus, this method of determining the stability number N_S from the K_D value cannot be guaranteed to obtain economical design

always. In order to calculate more reasonable values for the required mass, it is thus preferable to use the results of experiments matched to the conditions in question, or else to use calculation formulas, calculation diagrams, that include the various relevant coefficients as described below.

(7) Van der Meer's Formula for Armor Stones

In 1987, van der Meer carried out systematic experiments concerning the armor stones on the slope of a sloping breakwater with a high crown. He proposed the following calculation formula for the stability number, which can consider not only the slope gradient, but also the wave steepness, the number of waves, and the damage level.¹²²⁾ Note however that the following equations have been slightly altered in comparison with van der Meer's original one in order to make calculations easier. For example, the wave height $H_{2\%}$ for which the probability of exceedance is 2% has been replaced by $H_{1/20}$.

$$N_S = \max(N_{spl}, N_{ssr}) \quad (6.6.4)$$

$$N_{spl} = 6.2 C_H P^{0.18} (S^{0.2} / N^{0.1}) I_r^{-0.5} \quad (6.6.5)$$

$$N_{ssr} = C_H P^{-0.13} (S^{0.2} / N^{0.1}) (\cot \alpha)^{0.5} I_r^P \quad (6.6.6)$$

where

N_{spl} : stability number for plunging breakers

N_{ssr} : stability number for surging breaker

I_r : iribarren number ($\tan \alpha / S_{om}^{0.5}$), also called the surf similarity parameter

S_{om} : wave steepness ($H_{1/3} / L_0$)

L_0 : deepwater wavelength ($L_0 = g T_{1/3}^2 / 2\pi$, $g = 9.81 \text{ m/s}^2$)

$T_{1/3}$: significant wave period

C_H : breaking effect coefficient $\{= 1.4 / (H_{1/20} / H_{1/3})\}$, ($= 1.0$ in non-breaking zone)

$H_{1/3}$: significant wave height

$H_{1/20}$: highest one-twentieth wave height, see **Fig. 6.6.1**

α : angle of slope from the horizontal surface ($^\circ$)

D_{n50} : nominal diameter of armor stone ($= (M_{50} / \rho_r)^{1/3}$)

M_{50} : 50% value of the mass distribution curve of an armor stone namely required mass of an armor stone

P : permeability index of the inner layer, see **Fig. 6.6.2**

S : deformation level ($S = A / D_{n50}^2$), see **Table 6.6.1**

A : erosion area of cross section, see **Fig. 6.6.3**

N : number of acting waves

The wave height $H_{1/20}$ in **Fig. 6.6.1** is for a point at a distance $5H_{1/3}$ from the breakwater, and H_0' is the equivalent deepwater wave height. The deformation level S is an index that represents the amount of deformation of the armor stones, and it is a kind of damage ratio. It is defined as the result of the area A eroded by waves, see **Fig. 6.6.3**, being divided by the square of the nominal diameter D_{n50} of the armor stones. As shown in **Table 6.6.1**, three stages are defined with regard to the deformation level of the armor stones: initial damage, intermediate damage, and failure. With the standard performance verification, it is common to use the deformation level for initial damage for $N = 1000$ waves. However, in case where a certain amount of deformation is permitted, usage of the value for intermediate damage may also be envisaged.

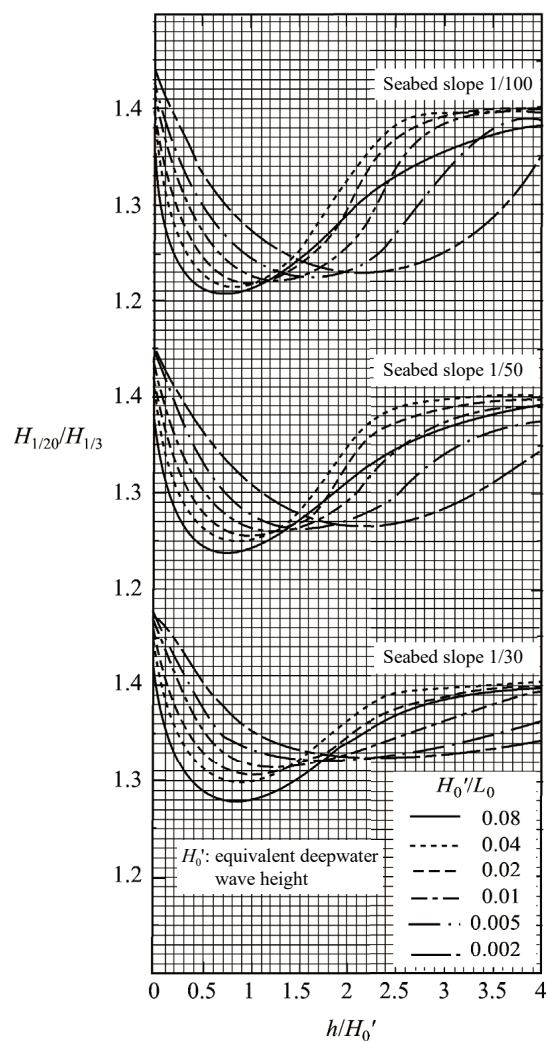


Fig. 6.6.1 Ratio of $H_{1/20}$ to $H_{1/3}$ ($H_{1/20}$ Values are at a Distance $5H_{1/3}$ from the Breakwater)

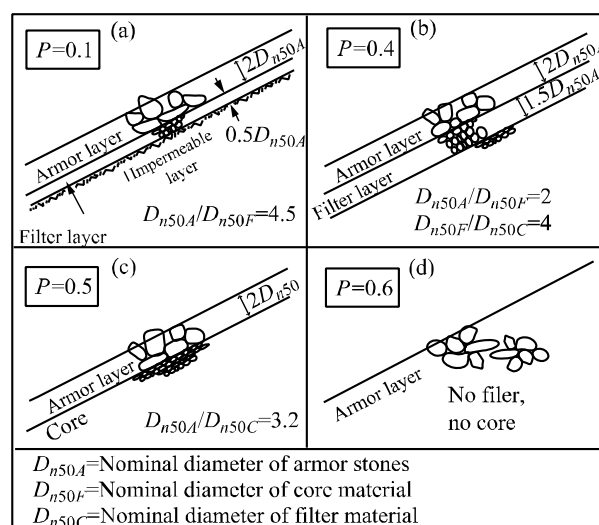


Fig. 6.6.2 Permeability Index P

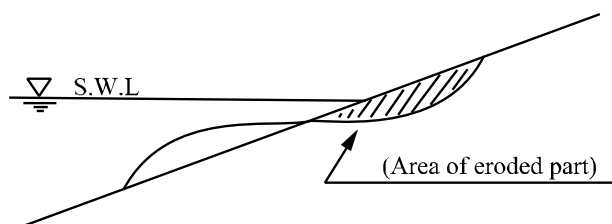


Fig. 6.6.3 Erosion Area A

Table 6.6.1 Deformation Level S for Each Failure Stage for a Two-layered Armor

Slope	Initial damage	Intermediate damage	Failure
1:1.5	2	3-5	8
1:2	2	4-6	8
1:3	2	6-9	12
1:4	3	8-12	17
1:6	3	8-12	17

(8) Formulation for Calculating Stability Number for Armor Blocks including Wave Characteristics

Van der Meer has carried out hydraulic model experiments on several kinds of precast concrete blocks, and proposed the formulas for calculating the stability number N_S .¹²³⁾ In addition, other people have also conducted research into establishing calculation formulas for precast concrete blocks. For example, Burcharth and Liu¹²⁴⁾ have proposed a calculation formula. However, it should be noted that these are based on the results of experiments for a sloping breakwater with a high crown.

Takahashi et al.¹²⁹⁾ showed a performance verification method of the stability against wave action for armor stones of a sloping breakwater using Van der Meer's formula as the verification formula, and proposed the performance matrix used for performance verification.

(9) Formulas for Calculating Stability Number for Concrete Blocks of Breakwater Covered with Wave-dissipating Blocks

The wave-dissipating concrete block parts of a breakwater covered with wave-dissipating blocks may have various cross sections. In particular, when almost all the front face of an upright wall is covered by wave-dissipating concrete blocks, the stability is higher than that of armor concrete blocks of an ordinary sloping breakwater because the permeability is high. In Japan, much research has been carried out on the stability of breakwaters covered with wave-dissipating concrete blocks. For example, Tanimoto et al.¹²⁶⁾, Kajima et al.¹²⁷⁾, and Hanzawa et al.¹²⁸⁾ have carried out systematic research on the stability of wave-dissipating concrete blocks. In addition, Takahashi et al.¹²⁹⁾ have proposed the following equation for wave-dissipating concrete blocks that are randomly placed in all the front face of an upright wall.

$$N_S = C_H \left\{ a \left(N_0 / N^{0.5} \right)^{0.2} + b \right\} \quad (6.6.7)$$

where

- N_0 : degree of damage, a kind of damage rate that represents the extent of damage: it is defined as the number of concrete blocks that have moved within a width D_n in the direction of the breakwater alignment
- D_n : nominal diameter of the concrete blocks: $D_n = (M/\rho_r)^{1/3}$, where M is the mass of a concrete block
- C_H : breaking effect coefficient; $C_H = 1.4/(H_{1/20}/H_{1/3})$, in non-breaking zone $C_H = 1.0$
- a, b : coefficients that depend on the shape of the concrete blocks and the slope angle. With deformed shape blocks having a K_D value of 8.3, it may be assumed that $a = 2.32$ and $b = 1.33$, if $\cot\alpha=4/3$, and $a = 2.32$ and $b = 1.42$, if $\cot\alpha=1.5$

Takahashi et al.¹²⁵⁾ have further presented a method for calculating the cumulative degree of damage, the expected degree of damage, over the service lifetime. In the future, reliability design methods that consider the expected degree of damage is important as the more advanced design method. In the region where wave breaking does not occur, if the number of waves N is 1000 and the degree of damage N_0 is 0.3, the design mass as calculated using the method of Takahashi et al. is more-or-less the same as that calculated using the existing K_D value. The value of $N_0 = 0.3$ corresponds to the conventionally used damage rate of 1%.

(10) Increase of Mass in Breakwater Head

Waves attack the head of a breakwater from various directions, and there is a greater risk of the armor units on the top of the slope falling to the rear rather than the front. Therefore, rubble stones or concrete blocks which are to be used at the head of a breakwater should have a mass greater than the value given by **equation (6.6.1)**.

Hudson proposed increasing mass by about 10% in the case of rubble stones and about 30% in the case of concrete blocks. However, because this is thought to be insufficient, it is preferable to use rubble stones or concrete blocks with a mass at least 1.5 times the value given by **equation (6.6.1)**. Kimura et al.¹³⁰⁾ have shown that, in a case where perpendicular incident waves act on the breakwater head, the stable mass can be obtained by increasing the required mass of the breakwater trunk by 1.5 times. In case of oblique incidence at 45° , in the breakwater head on the upper side relative to the direction of incidence of the waves, the necessary minimum mass is the same as for 0° incidence, whereas, on the lower side of the breakwater head, stability is secured with the same mass as the in the breakwater trunk.

As there is a risk of an impulsive breaking wave force at the end of wave-absorbing works, it is preferable to round the breakwater head, circumvoluting inside the port. The range is commonly set to on the order of one caisson.

(11) Mass of Submerged Armor Units

Since the action of waves on a sloping breakwater below the water surface is weaker than above the water surface, the mass of stones or concrete blocks may be reduced at depths greater than $1.5H_{1/3}$ below the still water level.

(12) Correction for Wave Direction

In cases where waves act obliquely to the breakwater alignment, the extent to which the incident wave angle affects the stability of the armor stones has not been investigated sufficiently. However, according to the results of experiments carried out by Van de Kreeke,¹³¹⁾ for the wave angles of 0° , i.e., direction of incidence is perpendicular to the breakwater alignment, 30° , 45° , 60° and 90° , i.e., direction of incidence is parallel to the normal line were adopted, the damage rate for a wave direction of 45° or smaller is more-or-less the same as that for a wave direction of 0° , and when the wave direction exceeds 60° , the damage rate decreases. Considering these results, when the incident wave angle is 45° or less, the required mass should not be corrected for wave direction. Moreover, Christensen et al.¹³²⁾ have shown that stability increases when the directional spreading of waves is large.

(13) Strength of Concrete Blocks

In case of deformed shape concrete block, it is necessary not only to ensure that the block has a mass sufficient to be stable for the variable situation in respect of waves, but also to confirm that the block itself has sufficient structural strength.

(14) Stability of Wave-dissipating Blocks in Reef Area

In general, a reef rises up at a steep slope from the relatively deep sea, and forms a relatively flat and shallow sea bottom. Consequently, when a large wave enters at such a reef, it breaks around the slope, and then the regenerated waves afterward propagate over the reef in the form of surge. The characteristics of waves over a reef are strongly dependent on not only the incident wave conditions but also the water depth over the reef and the distance from the shoulder of the reef. The stability of wave-dissipating concrete blocks situated on a reef also varies greatly due to the same reasons. Therefore, the characteristics over a reef are more complicated than those in general cases. The stability of wave-dissipating concrete blocks situated on a reef must thus be examined based either on hydraulic model experiments matching the conditions in question or on field experiences for sites having similar conditions.

(15) Stability of Wave-dissipating Blocks on Low Crest Sloping Breakwater

For a low crown sloping breakwater covered by wave-dissipating blocks without a supporting wall, it is necessary to note that the wave-dissipating blocks around its crown in particular at the rear are easily damaged by waves.¹³³⁾ For example, for detached breakwater composed of wave-dissipating blocks, unlike a caisson breakwater covered with wave-dissipating blocks, there is no supporting wall at the back and the crown is not high. This means that the concrete blocks near the crown in particular at the rear are easily damaged, and indeed such cases of block damage have been reported. In the case of a detached breakwater, it is pointed out that some kind of concrete blocks at the rear of the crown should have a larger size compared to those at the front of the crown.

(16) Stability of Blocks on Steep Slope Seabed

In cases where the bottom slope is steep and waves break in a plunging wave form, a large wave force may act on the blocks, depending on their shapes. Therefore, appropriate examination should be carried out, considering this fact.^{134), 135), 136)}

(17) High-density Blocks

The required mass of blocks that are made of high-density aggregate may also be determined using the Hudson's formula with the stability number shown in **equation (6.5.1)**. As shown in the equation, high-density blocks have a high stability, so a stable armor layer can be made using relatively small blocks.¹³⁷⁾

(18) Effect of Structural Conditions

The stability of wave-dissipating blocks varies depending on structural conditions and on the method of placement, such as regular or random placement etc. According to the results of experiments under conditions of random placement over the entire cross section and regular two-layer placement on a stone core, the regular placement with good interlocking had remarkably higher stability in almost all cases.¹²⁶⁾ Provided, however, that if the layer of blocks is thinner and the permeability of fill material is lower, the stability of blocks actually decreases in some cases.¹³⁸⁾

The stability of wave-dissipating blocks is also affected by the crown width and crown height of the blocks. For example, according to the results of a number of experiments, there is a tendency of having greater stability when the crown width and the crown height are greater.

(19) Standard Method of Hydraulic Model Tests

The stability of concrete blocks is influenced by a very large number of coefficients, and so it has still not been sufficiently elucidated. This means that when actually verifying the performance, it is necessary to carry out studies using hydraulic model experiments, and it is needed to progressively accumulate the results of such tests. The following points should be noted when carrying out model hydraulic experiments.

- ① It is standard to carry out experiments using random waves.
- ② For each particular set of conditions, the experiment should be repeated at least three times i.e., with three different wave trains. However, when tests are carried out by systematically varying the mass and other coefficients and a large amount of data can be acquired, one run for each test condition will be sufficient.
- ③ It is standard to study the action of 1000 waves in a run for each wave height level. Even for the systematic experiments, it is desirable to apply more than 500 waves or so in a run.
- ④ For the description of the extent of damage, in addition to the damage ratio which has been commonly used in the past, the deformation level or the relative damage level may also be used. The deformation level is suitable when it is difficult to count the number of armor stones or concrete blocks that have moved, while the degree of damage is suitable when one wishes to represent the damage to wave-dissipating blocks. The damage rate is the ratio of the number of damaged armor units in an inspection area to the total number of armor units in the same inspection area. The inspection area is taken to whichever is shallower, the depth of $1.5H$ below the still water level or to the bottom elevation of the armor layer, where the wave height H is inversely calculated from the Hudson's formula by inputting the mass of armor units. However, for the deformation level and the degree of damage, there is no need to define the inspection area. For evaluating the damage rate, an armor block is judged to be damaged if it has moved over a distance of more than about $1/2$ to 1.0 times its height.

(20) K_D Value Proposed by C.E.R.C.

Table 6.5.2 shows the K_D value of armor stones proposed by the Coastal Engineering Research Center, C.E.R.C., of the United States Army Corp of Engineers. This value is proposed for the breakwater trunk, parts other than the breakwater head, in the 1984 Edition of the C.E.R.C.'s **Shore Protection Manual**.¹³⁹⁾ In the table, the values not in parenthesis are based on experiment results by regular waves, and it is considered that those corresponds to 5% or less of the damage rate due to action of random waves. The values in parentheses are estimated values. For example, the value (1.2) for rounded rubble stones which are randomly placed in two-layer under the breaking wave conditions is estimated as the value which is half of 2.4, because the K_D value of two-layer angular rubble stones under the breaking waves condition is $1/2$ of the value under the non-breaking wave conditions.

However, in cases where the wave height of regular waves corresponds to the significant wave height, the wave which is close to the maximum wave height of random waves acts continuously under the breaking wave condition in the regular wave experiments. Therefore, the regular wave experiment under the breaking wave condition falls into an extremely severe state in comparison with that under the non-breaking wave conditions. In random waves experiments, as described previously, it is considered that so long as the significant wave height is a standard, K_D has a tendency to increase, conversely, as the breaking wave conditions gets severe. Thus, at least it is not necessary to reduce the value of K_D under the breaking wave conditions.

Table 6.5.2 K_D Value of Rubble Stones Proposed by C.E.R.C. (Breakwater Trunk)

Type of armor	Number of layers	Placement method	K_D		$\cot \alpha$
			Breaking waves	Non-breaking waves	
Rubble stones (rounded)	2 3 or more	Random placement "	(1.2) (1.6)	2.4 (3.2)	1.5–5.0 "
Rubble stones (angular)	2 3 or more	" "	2.0 (2.2)	4.0 (4.5)	" "

() shows estimated values.

6.6.2 Required Mass of Armor Stones and Blocks in Composite Breakwater Foundation Mound against Waves

(1) General

The required mass of armor stones and blocks covering the foundation mound of a composite breakwater varies depending on the wave characteristics, the water depth where the facility is placed, the shape of the foundation mound such as thickness, front berm width and slope angle etc., and the type of armor unit, the placement method, and the position (breakwater head or breakwater trunk), etc. In particular, the effects of the wave characteristics and the foundation mound shape are more pronounced than those of the armor stones and blocks on a sloping breakwater. Adequate consideration should also be given to the effects of wave irregularity. Accordingly, the required mass of armor stones and blocks on the foundation mound of composite breakwater shall be determined by performing hydraulic model experiments or proper calculations using an appropriate equation in reference with the results of past research and actual experiences in the field. However, the stability of the armor units covering the foundation mound of a composite breakwater is not necessarily determined purely by their mass. Depending on the structure and the arrangement of the armor units it may be possible to achieve stability even when the armor units are relatively small in mass.

(2) Basic Equation for Calculation of Required Mass

As the equation for calculation of the required mass of armor stones and blocks in the foundation mound of a composite breakwater, Hudson's formula with the stability number N_s , as shown in the following equation, can be used in the same manner as with armor stones and blocks on sloping breakwater. This partial safety coefficient is the value in cases where the limit value of the damage rate is 1% or the limit value of the degree of damage is 0.3.

$$M = \frac{\rho_r H^3}{N_s^3 (S_r - 1)^3} \quad (6.6.1) \text{ reshown}$$

This equation was widely used as the basic equation for calculating the required mass of the foundation mounds of upright walls by Brebner and Donnelly.¹⁴⁰⁾ In Japan, it is also called Brebner-Donnelly's formula. Because it has a certain degree of validity, even from a theoretical standpoint, it can also be used as the basic equation for calculating the required mass of armor unit on the foundation mound of a composite breakwater.¹⁴¹⁾ However, the stability number N_s varies not only with the water depth, the wave characteristics, the shape of the foundation mound, and the characteristics of the armor units, but also with the position of placement, breakwater trunk, breakwater head etc. Therefore, it is necessary to assign the stability number N_s appropriately based on hydraulic model experiments corresponding to the conditions. Moreover, the wave height used in the performance verification is normally the significant wave height, and the waves used in the hydraulic model experiments should be random waves.

(3) Stability Number for Armor Stones

The stability number N_s may be obtained using the method proposed by Inagaki and Katayama,¹⁴²⁾ which is based on the work of Brebner and Donnelly and past damage case of armor stones. However, the following formulas proposed by Tanimoto et al.¹⁴¹⁾ are based on the current velocity in the vicinity of the foundation mound and allow the incorporation of a variety of conditions. These formulas have been extended by Takahashi et al.¹⁴³⁾ so as to include the effects of wave direction.

(a) Extended Tanimoto's formulas

$$N_s = \max \left\{ 1.8, 1.3 \frac{1-\kappa}{\kappa^{1/3}} \frac{h'}{H_{1/3}} + 1.8 \exp \left[-1.5 \frac{(1-\kappa)^2}{\kappa^{1/3}} \frac{h'}{H_{1/3}} \right] \right\} : B_M / L' < 0.25 \quad (6.6.8)$$

$$\kappa = \kappa_1 (\kappa_2)_B \quad (6.6.9)$$

$$\kappa_1 = \frac{4\pi h' / L'}{\sinh(4\pi h' / L')} \quad (6.6.10)$$

$$(\kappa_2)_B = \max \left\{ \alpha_s \sin^2 \beta \cos^2 (2\pi l \cos \beta / L'), \cos^2 \beta \sin^2 (2\pi l \cos \beta / L') \right\} \quad (6.6.11)$$

where

h' : water depth at the crown of rubble mound foundation excluding the armor layer (m) (see Fig. 6.6.4)

λ : in the case of normal wave incidence, the front berm width of foundation mound B_M (m)

in the case of oblique wave incidence, either B_M or B'_M , whichever gives the larger value of $(\kappa_2)_B$ (see Fig. 6.6.4)

- L' : wavelength corresponding to the design significant wave period at the water depth h' (m)
 α_s : correction coefficient for when the armor layer is horizontal ($=0.45$)
 β : incident wave angle, angle between the line perpendicular to the breakwater face line and the wave direction, no angle correction of 15° is applied (see Fig. 6.6.5)
 $H_{1/3}$: design significant wave height (m)

The validity of the above formulas has been verified for the breakwater trunk for oblique wave incidence with an angle of incidence of up to 60° .

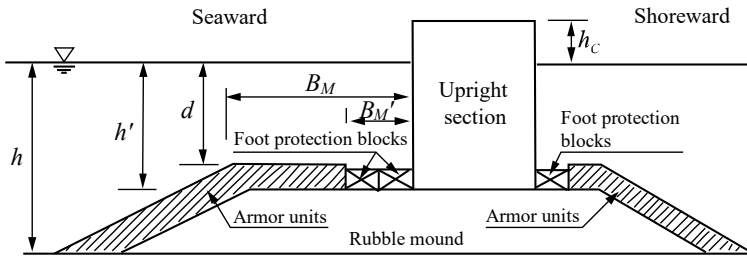


Fig. 6.6.4 Standard Cross Section of a Composite Breakwater and Notations

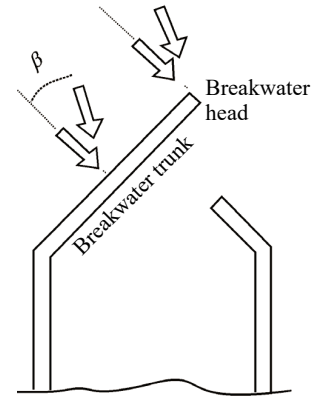


Fig. 6.6.5 Effects of Shape of Breakwater Alignment and Effects of Wave Direction

(b) Stability Number When a Certain Amount of Damage is Permitted

Sudo et al.¹⁴⁴⁾ have carried out stability experiments for the special case such that the mound is low and no wave breaking occurs. They proposed the following equation that gives the stability number N_S^* for any given number of waves N and any given damage rate D_N (%).

$$N_S^* = N_S [D_N / \exp\{0.3(1 - 500/N)\}]^{0.25} \quad (6.6.12)$$

where N_S is the stability number given by the conventional Tanimoto's formula when $N = 500$ and the damage rate is 1%. In the performance verification, it is necessary to take $N = 1000$ considering the progress of damage, while the damage rate 3% to 5% can be allowed for a 2-layer armoring. If $N = 1000$ and $D_N = 5\%$, then $N_S^* = 1.44 N_S$. This means that the required mass decreases to about 1/3 of that required for $N = 500$ and $D_N = 1\%$, which leads to $N_S^* = N_S$.

(4) Stability Number for Concrete Units

The stability number N_S for concrete blocks varies according to the shape of the block and the method of placement. It is thus desirable to evaluate the stability number by means of hydraulic model experiments.^{145) 146)}

Based on the calculation method proposed by Tanimoto et al.,¹⁴¹⁾ Fujiike et al.¹⁴⁷⁾ newly introduced reference stability number, which is a specific value for blocks, and separating the terms which is determined by the structural conditions of the composite breakwater etc., and then, presented the following equation regarding the stability number for armor blocks in cases where wave incidence is perpendicular.

$$N_S = N_{S0} \max \left\{ 1.0, A \frac{1-\kappa}{\kappa^{1/2}} \frac{h'}{H_{1/3}} + \exp[-0.9 \frac{(1-\kappa)^2}{\kappa^{1/2}} \frac{h'}{H_{1/3}}] \right\} \quad (6.6.13)$$

$$\kappa = \kappa_1 (\kappa_2)_B$$

refer to (6.6.9)

$$\kappa_1 = \frac{4\pi h' / L'}{\sinh(4\pi h' / L')} \quad \text{refer to (6.6.10)}$$

$$(\kappa_2)_B = \begin{cases} \sin^2 \frac{2\pi B_M}{L'} & \left(\frac{B_M}{L'} \leq 0.15 \right) \\ 1.309 - \sin^2 \frac{2\pi B_M}{L'} & \left(0.15 < \frac{B_M}{L'} \leq 0.25 \right) \\ 0.309 & \left(0.25 < \frac{B_M}{L'} \right) \end{cases} \quad (6.6.14)$$

where

N_{S0} : reference stability number

A : constant determined based on wave force experiments (= 0.525)

(5) Conditions for Application of Stability Number to Foundation Mound Armor Units

In cases where the water depth above the armor units on the mound is shallow, wave breaking often causes the armor units to become unstable. Therefore, the stability number for foundation mound armor units shall be applied only when $h'/H_{1/3} > 1$, and it is appropriate to use the stability number for armor units on a slope of a slope structure when $h'/H_{1/3} \leq 1$. The stability number for armor stones in the Tanimoto's formulas have not been verified experimentally in cases where $h'/H_{1/3}$ is small. Accordingly, when $h'/H_{1/3}$ is approximately 1, it is preferable to confirm the stability of the armor units by hydraulic model experiments.

On the other hand, Matsuda et al.¹⁴⁸⁾ carried out model experiments in connection with armor blocks, including the case in which $h'/H_{1/3}$ is small and impulsive waves act on the blocks, and proposed a method that provides a lower limit of the value of κ corresponding to the value of the impulsive breaking wave force coefficient α_1 of **equation (6.2.13)** in the case where α_1 is large.

(6) Armor Units Thickness

Two-layers are generally used for armor stones. It may be acceptable to use only one layer provided that consideration is given to examples of armor units construction and experiences of damaged armor units. It also may be possible to use one layer by setting the severe damage rate of 1% for $N=1000$ acting waves in **equation (6.5.12)**. One layer is generally used for armor blocks. However, two layers may also be used according to the shape of the blocks or sea conditions.

(7) Armor Units for Breakwater Head

At the head of a breakwater, strong currents occur locally near the corners at the edge of the upright section, meaning that the armor units become liable to move. It is thus necessary to verify the extent to which the mass of armor units should be increased at the breakwater head by carrying out hydraulic model experiments. If hydraulic model experiments are not carried out, the mass should be increased to at least 1.5 times that at the breakwater trunk. As the extent of the breakwater head in the case of caisson type breakwater, the length of one caisson may be usually adopted. The mass of the armor stones at the breakwater head may also be calculated using the extended Tanimoto's formula. Specifically, the dimensionless velocity parameter κ in **equation (6.6.9)** should be rewritten as follows:

$$\kappa = \kappa_1 (\kappa_2)_T \quad (6.6.15)$$

$$(\kappa_2)_T = 0.22 \quad (6.6.16)$$

Note however that if the calculated mass turns out to be less than 1.5 times that for the breakwater trunk, it is preferable to set the mass to 1.5 times that for the breakwater trunk.

(8) Armor Units at Harbor Side

It is preferable to decide the necessity and required mass of armor units at the harbor side, not only referring to past examples, but also performing hydraulic model experiments if necessary, under the consideration of the waves at the harbor side, the wave conditions during construction work and wave overtopping etc.

(9) Reduction of Mass of Armor

The equations for calculation of the required mass of armor units are normally applicable to the horizontal parts and the top of slope. In cases where the mound thickness is minimal, armor units of the entire slope have the same mass in many cases. However, in cases where the mound is thick, the mass of armor units placed on the slope in deep water may be reduced.

(10) Foundation Mound Armor Units in Breakwaters Covered with Wave-dissipating Blocks

In the case of breakwaters covered with wave-dissipating blocks, the uplift pressure acting on the armor and the current velocities in the vicinity of the mound are smaller than those of conventional composite breakwaters. Fujiike et al. ¹⁴⁷⁾ carried out hydraulic model experiments in connection with the stabilities of both the armor units of the conventional composite breakwaters and the breakwaters covered with wave-dissipating blocks, and proposed a method of multiplying **equation (6.6.9)** by the compensation rate for breakwater shape influence. Namely,

$$\kappa = C_R \kappa_1 (\kappa_2)_B \quad (6.6.17)$$

where

C_R : breakwater shape influence coefficient, 1.0 may be used for conventional composite breakwaters and approximately 0.4 for breakwaters covered with wave-dissipating blocks.

(11) Flexible Armor Units

Using bag-type foot protection units, consisting of synthetic fiber net filled with stones, as the flexible armor units on the rubble mound has various advantages: large stones are not required, and mound leveling is almost unneeded because they have high flexibility and can adhere to the irregular sea bed. Shimosako et al. ¹⁴⁹⁾ proposed a method for calculating the required mass of such armor units on the rubble mound, and also examined their durability. Moreover, a durable stone net filled with fillings in steel wires, covered with resin, may be used as armor units on the rubble mound ¹⁵⁰⁾. It is preferable to use these considering the strength of synthetic fibers or steel wires against wave actions.

6.6.3 Required Mass of Armor Stones and Blocks against Currents

(1) General

The required mass of rubble stones and other armor materials for foundation mounds to be stable against water currents may generally be determined by appropriate hydraulic model experiments or calculated using the following equation.

$$M = \frac{\pi \rho_r U^6}{48 g^3 (y)^6 (S_r - 1)^3 (\cos \theta - \sin \theta)^3} \quad (6.6.18)$$

where

M : stable mass of rubble stones or other armor material (t)

ρ_r : density of rubble stones or other armor material (t/m³)

U : current velocity of water above rubble stones or other armor material (m/s)

g : gravitational acceleration (m/s²)

y : Isbash's constant, for embedded stones, 1.20; for exposed stones, 0.86

S_r : specific gravity of rubble stones or other armor material relative to water

θ : slope angle in axial direction of water channel bed (°)

This equation was proposed by the C.E.R.C. for calculation of the mass of rubble stones required to prevent scouring by tidal currents and is called Isbash's formula.¹³⁹⁾ As also shown in the equation, attention should be given to the fact that the required mass of armor units against currents increases rapidly as the current velocity increases. The required mass also varies depending on the shape and density of the armor units, etc.

(2) Isbash's Constant

Equation (6.6.18) was derived considering the balance of the drag force of the flow acting on a spherical object on a slope and the friction resistance force. The constant y is Isbash's constant. The values of 1.20 and 0.86 for embedded stones and exposed stones, respectively, are given by Isbash, and are also cited by Kudo¹⁵¹⁾. It should be noted that, because **equation (6.6.18)** was obtained considering the balance of forces in a steady flow, it is necessary to use rubble stones with a larger mass in the place where strong vortices will be generated.

(3) Armor Units on Foundation Mound at Openings of Tsunami Protection Breakwaters

Iwasaki et al.¹⁵²⁾ conducted experiments on 2-dimensional steady flows for the case in which deformed concrete blocks are used as the armor units on a foundation mound in the opening of the submerged breakwaters of tsunami protection breakwaters, and obtained a value of 1.08 for Isbash's constant in **equation (6.6.18)**. Tanimoto et al.¹⁵³⁾ carried out a 3-dimensional plane experiment for the opening of breakwaters, clarifying the 3-dimensional flow structure near the opening, and also revealed the relationship between Isbash's constant and the damage rate for the cases where stone materials and deformed concrete blocks are used as the armor units.

6.7 Tsunami Wave Force

6.7.1 Tsunami Wave Force Acting on Composite Type Breakwater

(1) General

Tsunami wave force acting on composite type breakwater can be calculated according to the calculation procedure shown in **Fig. 6.7.1**, considering whether tsunami bores or overflowing exist¹⁵⁴⁾.

Tsunamis can, firstly, be classified into bore condition or not. Tsunami bores, which become bore shaped by breaking of the front end of tsunamis with long wave lengths, into several short-period waves (soliton fission) may have quite large impulsive bore wave forces. Therefore, Tanimoto's formula is used in the case of no tsunami bores. As the tsunami bores strengthen the tsunami wave force, modified Tanimoto's formula is used, corresponding to this case.

Tsunami bores occur when the seabed slope is quite gentle, while a small ratio of tsunami wave height to water depth (tsunami height / water depth) or relatively steep seabed slope does not generate bores. The soliton fission is considered generated when the incident tsunami height is 30% or more of the water depth (the height of tsunami standing waves generated by simulation or others is 60% or more of the water depth) and in a shoal with the seabed slope around 1/100 or less.

If no tsunami bores occur, but overflowing does, calculation equations, corrected by the coefficients of the hydrostatic pressures acting on the front side and rear side of a caisson, are applied. The overflowing case indicates the state that the tsunami height, calculated with the numerical simulation, exceeds the crown height of the breakwater. When a calculation equation correcting the hydrostatic pressure is applied to a slightly overflowing condition, compare the equation and Tanimoto's formula and adopt the result of larger tsunami force. Applying Tanimoto's formula to the condition just before overflowing, which is shallower in water level, may show a larger wave force.

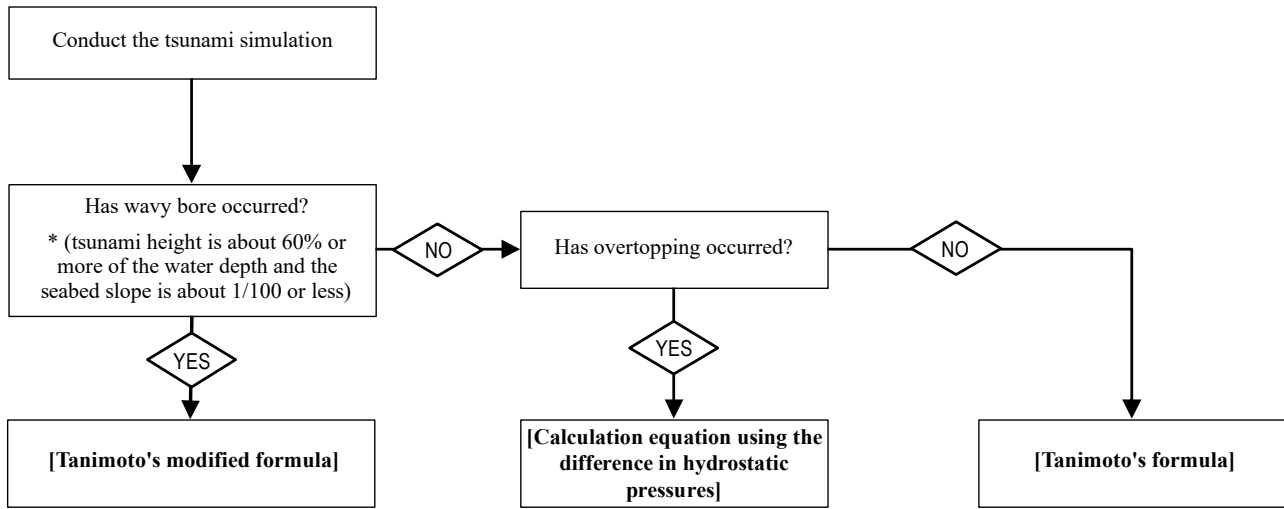


Fig. 6.7.1 Calculation Procedure of Tsunami Wave Force

The tsunami height for calculating the tsunami wave force acting on the breakwater is basically calculated using the numerical simulation result under the condition where the breakwater has been installed. The height of an incident tsunami above the still water a_I for Tanimoto's formula and modified Tanimoto's formula is used to calculate the wave force by defining the incident tsunami height as 1/2 of the tsunami height (above the still water level) numerically simulated. Here, the still water level is the standard water level for the calculation of the tsunami height on the surface on which the tsunami acts. The tsunami height is generally the water level (including the effect of reflected waves) to consider the effect of inundation, etc. Therefore, half of the tsunami height is also defined, in principle, as the incident tsunami height a_I . Since the tsunami height is generally, and often expressed in, the water level above T.P., it must be halved after converting to the height above the design tide level (normally H.W.L.).

(2) Tanimoto Method and Modified Tanimoto Method

Tsunami wave force on an upright wall may be determined as in Fig. 6.7.2 (a), in which the wave pressure distribution can be assumed as a linear distribution with a value of $p=0$ at a height of $\eta^* = 3.0 a_I$ above the still water level and a value of $p=2.2\rho_0 g a_I$ (Tanimoto method) or $p=3.0\rho_0 g a_I$ (modified Tanimoto method) at the still water level, and a constant value in the depth direction for the wave pressure below the still water level.

When the water level behind the breakwater becomes lower than the still water level, negative wave force is generated behind the breakwater, as shown in Fig. 6.7.2 (b), and the distribution of the uplift pressure is a distribution obtained by linearly connecting the pressures on the front side and the rear side. The breakwater buoyancy is calculated as the volume (hatched line part), assuming that the foreside still water level extends to the rear side.

Maruyama et al.¹⁵⁵⁾ indicated that the impact force by the wave breaking of soliton fission is mitigated when the upright walls are covered with the wave-dissipating blocks.

$$\eta^* = 3.0 a_I \quad (6.7.1)$$

$$p_1 = \begin{cases} 2.2\rho_0 g a_I & : \text{Tanimoto's formula} \\ 3.0\rho_0 g a_I & : \text{Tanimoto's modified formula} \end{cases} \quad (6.7.2)$$

$$p_2 = \rho_0 g \eta_B \quad (6.7.3)$$

$$p_u = p_1 \quad (6.7.4)$$

$$p_L = p_2 \quad (6.7.5)$$

where

η^* : wave pressure acting height above the still water level (m)

η_B : water level behind the caisson (m)

a_I : incident tsunami height (amplitude) (m)

- $\rho_0 g$: unit weight of the seawater (kN/m³)
 p_1 : wave pressure at the still water level (kN/m²)
 p_u : uplift pressure at the lower edge of the front wall of the caisson (kN/m²)
 p_2 : negative pressure on the rear side of the caisson (kN/m²)
 p_L : uplift pressure at the lower edge of the rear surface of upright walls (kN/m²)

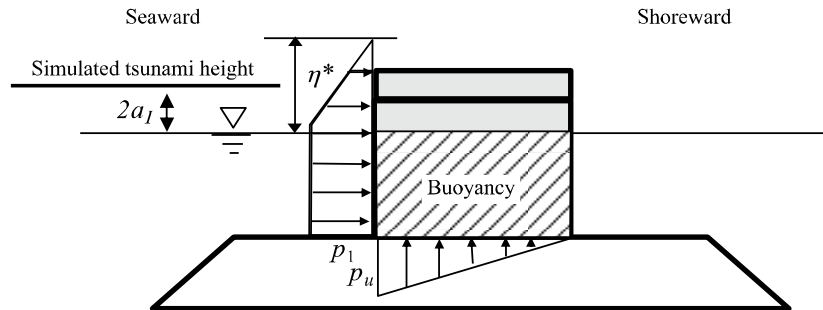


Fig. 6.7.2 (a) Tanimoto's Formula and Tanimoto's Modified Formula
(When the rear water level is not lower than the still water level)

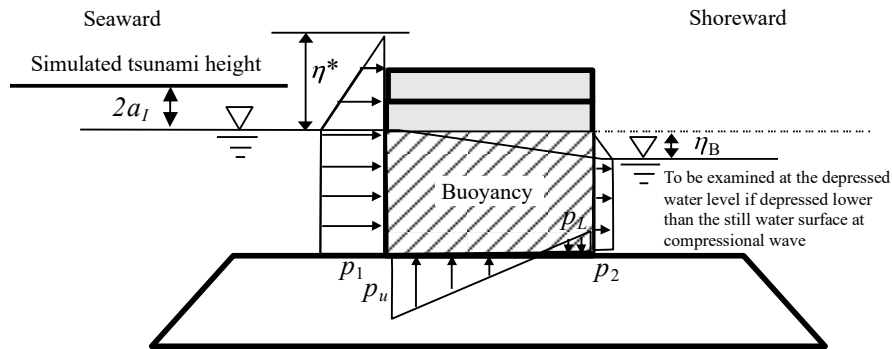


Fig. 6.7.2 (b) Tanimoto's Formula and Tanimoto's Modified Formula
(When the rear water level is lower than the still water level)

(3) Calculation Equation Using the Difference in Hydrostatic Pressure (When tsunami overflows breakwater)

When tsunamis overflow the breakwater, calculate the difference in the highest water levels between the front wall and the rear one, and confirm the breakwater's stability using the difference in hydrostatic pressure between the breakwater's front and rear water level, as shown in Fig. 6.7.3.

The hydrostatic pressure on the front wall shall be multiplied by $\alpha_f (= 1.05)$ and on the rear wall by $\alpha_r (= 0.9)$. The rear wall hydrostatic pressure correction coefficient α_r significantly decreases as the difference between the front water level and the rear one at upright walls increases¹⁵⁶⁾. Tsuruta et al.¹⁵⁷⁾ proposed a calculation equation for the hydrostatic pressure correction coefficient, which may be referenced.

$$p_1 = \alpha_f \rho_0 g (\eta_f + h') \quad (6.7.6)$$

$$p_2 = \frac{\eta_f - h_c}{\eta_f + h'} p_1 \quad (6.7.7)$$

$$p_3 = \alpha_r \rho_0 g (\eta_r + h') \quad (6.7.8)$$

where

- p_1 : wave pressure at the front bottom of caissons (kN/m²)
 p_2 : wave pressure at the front crown of caissons (kN/m²)

- p_3 : wave pressure at the rear bottom of caissons (kN/m²)
 $\rho_0 g$: unit volume weight of the seawater (kN/m³)
 h' : water depth at the bottom of caissons (m)
 h_c : height between the still water level and the crown height of upright walls (m)
 η_f : tsunami height from the still water level at the front side of upright walls (m)
 η_r : tsunami height from the still water level at the rear side of upright walls (m)
 α_f : hydrostatic pressure correction coefficient at the front side of upright walls
 α_r : hydrostatic pressure correction coefficient at the rear side of upright walls

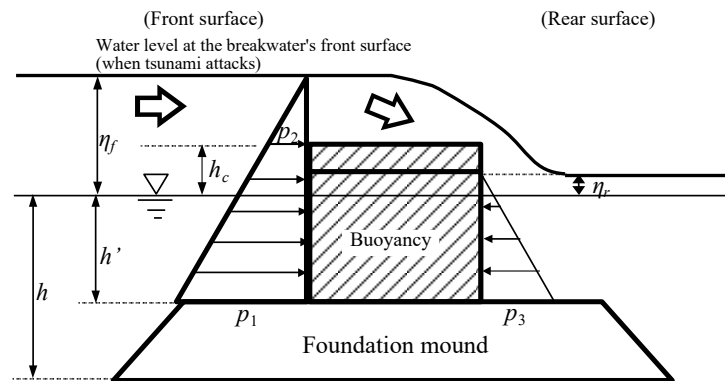


Fig. 6.7.3 Hydrostatic Pressure Difference Equation (Wave Force Equation When Tsunami Overflows Breakwater)

- (a) The buoyancy shall be calculated as the submerged whole wall body (hatched line part), excluding the uplift. However, when the parapet is large, the uplift becomes large. When the overflowing velocity is large, the centrifugal force applied to the water mass at the front crown part of the upright wall decreases the pressure. In these cases, the vertical upward force may become larger than the buoyancy¹⁵⁸⁾.
- (b) When applying a calculation equation of the hydrostatic pressure difference to the slightly overflowing condition, compare to the case where Tanimoto's formula is applied to the condition just before overflowing and adopt a more disadvantageous case to the caisson's stability.

6.7.2 Tsunami Wave Force Acting on Onshore Upright Walls

(1) General

The tsunami wave force acting on onshore upright walls, such as the parapet, shall be calculated according to the procedure shown in **Fig. 6.7.4**, referring to the wave force calculation equation, considering the existence of tsunami overflowing in **Concept of Parapet Design Considering Tsunami (Preliminary Version)**¹⁵⁹⁾.

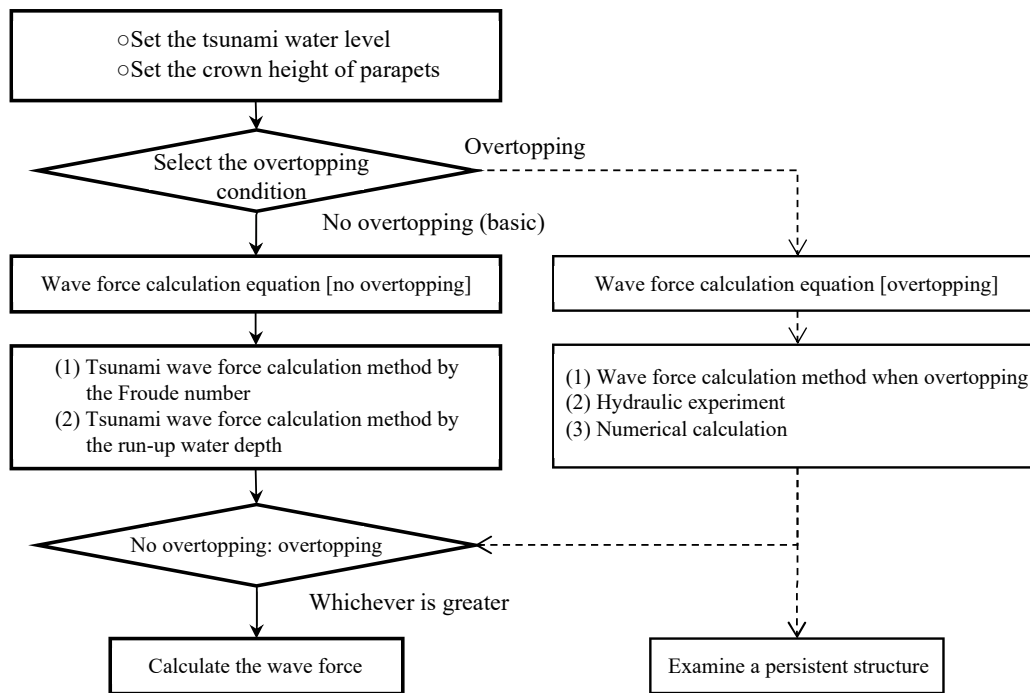


Fig. 6.7.4 Procedure for Calculating Tsunami Wave Force Acting on Parapets

(2) Tsunami wave force without overflowing

The tsunami wave force without overflowing can be calculated by using the run-up water depth or the Froude number.

① Tsunami wave force estimating from inundation depth of tsunami standing wave

The inundation depth η of running-up tsunami in front of upright walls shall be calculated by the tsunami run-up simulation. Then, the wave force shall be calculated from this inundation depth η , as shown in Fig. 6.7.5. The wave pressure acting height shall be the inundation depth η , and the acting water pressure is expressed by equation (6.7.9).

$$p_1 = \alpha \rho_0 g \eta \quad (6.7.9)$$

where

- p_1 : wave pressure at the lower edge of upright walls (kN/m²)
- η : inundation depth of tsunami standing wave in front of upright walls (m)
- $\rho_0 g$: unit volume weight of the seawater (kN/m³)
- α : wave pressure coefficient of hydrostatic pressure (= 1.1)

However, the maximum wave pressure, significantly exceeding the hydrostatic pressure, may be generated at the bottom of the upright wall. Moreover, note that the wave pressure may exceed 1.1 times of the hydrostatic pressure when breaking tsunami acts on the upright wall.

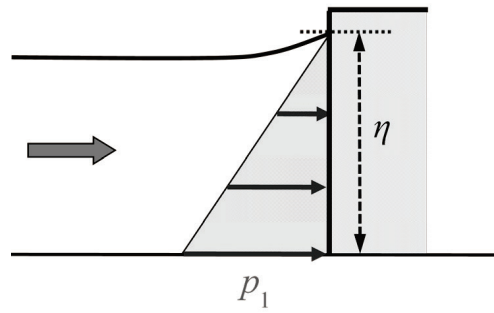


Fig. 6.7.5 Wave Pressure Distribution of Wave Force Calculation Equation without Overtopping
(Tsunami Wave Force Calculation by Wall Erection Calculation)

② Wave force estimation as progressive tsunami with Froude number

The inundation depth of progressive tsunami shall be calculated by the tsunami inundation simulation without upright walls.

When the Froude number F_r of progressive tsunami is less than 1.5, the wave pressure is expressed by **equation (6.7.10)**. The wave pressure acting height shall be α' times the inundation depth of progressive tsunami.

$$\frac{P_{\max}}{\rho_0 g \eta_{\max}} = \alpha \left(1 - \frac{z}{\alpha' \eta_{\max}} \right) \quad (6.7.10)$$

$$\alpha' = \max \{ 3, \alpha \} \quad \begin{array}{l} \text{Coefficient of the dimensionless} \\ \text{wave pressure acting height} \end{array} \quad (6.7.11)$$

where

- p_{\max} : maximum tsunami wave pressure (kN/m²)
- η_{\max} : maximum inundation height of progressive waves (m)
- $\rho_0 g$: unit volume weight of the seawater (kN/m³)
- z : height of the wave pressure acting location from the ground (m)

The dimensionless wave pressure coefficient α is given as the following equation.

$$\alpha = 1.0 + 1.35 F_r^2 \quad \begin{array}{l} \text{Coefficient of the dimensionless wave pressure acting height} \end{array} \quad (6.7.12)$$

When the Froude number F_r exceeds 1.5, examine the dimensionless wave pressure coefficient α (wave pressure acting height coefficient α' shall be 3) using the existing research results, hydraulic experiments, numerical calculations, etc.

If the Froude number F_r is unknown, employ the maximum water depth $\eta_{0\max}$ at the shore line as the water depth η_{\max} , and apply Tanimoto's formula ($\alpha' = 3.0$, $\alpha' = 2.2$) in **Part II, Chapter 2, 6.7.1 (1)**.

The dimensionless wave pressure coefficient α can be calculated with the method of Ishida et al,¹⁶⁰⁾ which uses the inundation depth and flow rate at the highest specific energy. As η_{\max} and the Froude number vary according to the topography behind the parapet or existence of structures, it is preferable to consider the effects of them.¹⁶¹⁾

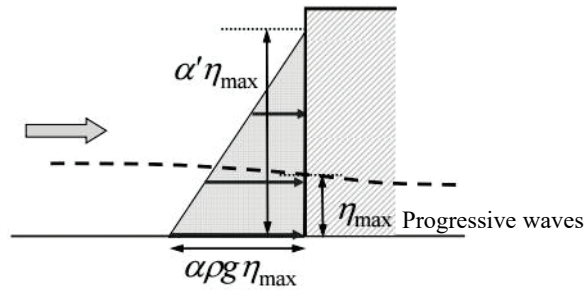


Fig. 6.7.6 Wave Force Distribution without Overtopping (Method Using the Froude Number)

③ Uplift applied to the upright wall

The upright wall is subjected to the uplift when there is rubble mound beneath it.

(3) Tsunami wave force during overflowing

The tsunami wave force during overflowing shall be calculated as shown in **Fig. 6.7.7** by using the water levels at the front and rear sides of the upright wall. The water levels are calculated by tsunami inundation simulation.

① Wave pressure on front side

$$p_1 = \alpha_1 \rho_0 g \eta \quad (6.7.13)$$

$$p_2 = p_1 (\eta - h_c) / \eta \quad (6.7.14)$$

The value of α_1 shall be calculated by the following equation when using the water depth η at the foot of a front slope of the wall.

$$\alpha_1 = -0.17h_c / \eta + 1.27 \quad 0.4 \leq h_c / \eta < 1.0 \quad (6.7.15)$$

The value of α_1 shall be given by the following equation when using the offshore water level η_0 (where the water level varies little).

$$\alpha_1 = 1.1 \quad (6.7.16)$$

② Wave pressure on rear side

$$p_3 = \alpha_{1B} \rho_0 g \eta^* \quad (6.7.17)$$

$$p_4 = p_3 (\eta^* - h_{CB}^*) / \eta^* \quad (6.7.18)$$

$$h_{CB}^* = \min\{\eta^*, h_c\} \quad (6.7.19)$$

Here, the water level at the rear η_B shall be used as water depth η^* . Note that the wave pressure at the rear differs by the effect of topography behind, etc.

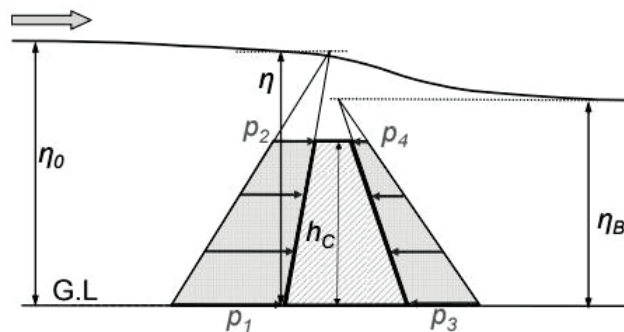


Fig. 6.7.7 Wave Pressure Distribution during Tsunami Overflowing

③ Vertical force

Although the water pressure is applied to the upper part of the upright wall during tsunami overflowing, it is reduced by the effect of centrifugal force when the overflowing velocity is fast. Also, the uplift force acts on the bottom face of the upright wall when there is rubble mound under the upright walls.

④ Wave force applied to the ground behind

Naito et al.¹⁶²⁾ may be referred to for the tsunami overflowing force applied to the ground behind the wall.

6.7.3 Required mass for an armor unit against the tsunami overflowing

(1) General

Rubble mound and armor works behind the upright wall may be scoured by tsunami overflowing. As the overflowing phenomenon changes intricately in accordance with the shape of the upright wall, the required mass of armor units shall basically be obtained by the hydraulic model experiments. However, if the upright wall shape is relatively simple, the following method may be used to verify the required mass.

(2) Calculation using the Isbash formula

The required mass can be verified by obtaining the overflow velocity acting on the armor works through hydraulic model experiments or numerical simulations and by using the Isbash formula explained in **Part II, Chapter 2, 6.5.3, Required Mass of Armor Stones and Blocks against Currents**^{163) 164)}.

(3) Stability number against overflowing

The required mass may also be verified using the stability number N_s against the overflowing shown below¹⁶⁵⁾. In this case, the required mass of the armor works against overflowing shall be calculated with the following equations.

$$M = \rho_r D_n^3 \quad (6.7.20)$$

$$D_n = \frac{h_1}{(\rho_r / \rho_w - 1) N_s} \quad (6.7.21)$$

Here, ρ_w and ρ_r are the density of seawater and concrete, respectively. D_n is the nominal diameter of armor works and is the cube root of the armor unit volume. h_1 is the overflowing depth shown in **Fig. 6.7.8**.

The stability number N_s is the function of ratio B/L , where B is the mound crown width, L is the driving position of overtopping shown in **Fig. 6.7.8**, and the ratio d_2/d_1 where d_2 is the height between the mound crown height and the still water level, d_1 is the height between the caisson crown height and the still water level, and is calculated using the calculation diagram obtained from experiments per various armor units. The manual for required mass calculation of armor works on the additional rubble mound behind the breakwater against tsunami overflowing describes calculation diagrams for various armor units¹⁶⁶⁾.

The driving position of overflowing L can be calculated by the following equations.

$$u_2 = q/h_2 = 0.35 \frac{h_1}{h_2} \sqrt{2gh_1} \quad (6.7.22)$$

$$h_2 = rh_1 \quad (6.7.23)$$

$$x_3 = u_2 \sqrt{2(d_1 + h_2/2)/g} \quad (6.7.24)$$

$$u_{3x} = u_2 \quad (6.7.25)$$

$$u_{3z} = \sqrt{2g(d_1 + h_2/2)} \quad (6.7.26)$$

$$L = x_3 + (u_{3x}/u_{3z})d_2 \quad (6.7.27)$$

Here, q is the overflowing rate, r is the ration of overflowing depth expressed as $r = h_2/h_1$. The above equations can be applied when $h_1/B < 0.5$. $r = 0.42$ to 0.45 , or the following calculation equation can be used for the ratio of overflowing depth r ¹⁵⁶⁾.

$$r = 0.43 + 0.324 \times (h_1 / B) - 0.5 \quad (6.7.28)$$

However, as the ratio of overflowing depth r needs caution against versatility and applicability to various structures, the driving position of overtopping L shall be estimated preferably with the aid of numerical simulation, such as CADMAS-SURF¹⁾.

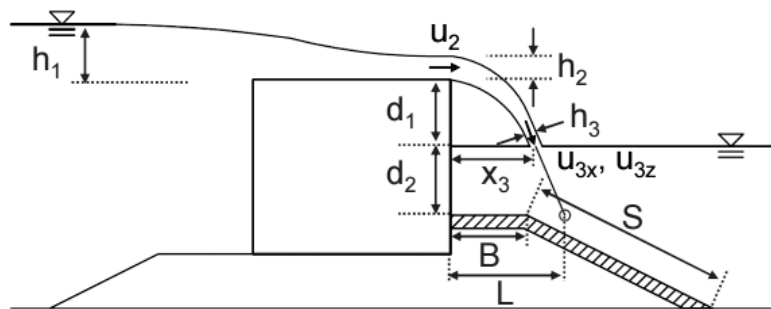


Fig. 6.7.8 Definition of Variables for Calculation Equation of the Mass Required for Armor Blocks

(4) Stability of armor works where overflowing concentrates

The concentrated overflowing may increase the flow rate acting on the armor works at the corner of breakwater or where the breakwater width becomes discontinuous¹⁶⁷⁾. When verifying the blocks' stability, it is preferable to estimate the flow velocity with the numerical simulation and verify the stability using the Isbash formula, or estimate the stability with the hydraulic model experiments.

6.8 Wave Force during Storm Surge

6.8.1 When the Tide Level during Storm Surge is Lower than the Crown Height of Structures

(1) Simultaneous action of storm surges and high waves

During storm surges, the storm surges and high waves generally act on structures at the same time. Therefore, the water pressures increased by the storm surge, and the wave one due to high waves, simultaneously act on the protective facilities for the harbor, such as breakwaters, seawalls, dikes, and parapets. When verifying this stability, calculate the increased hydrostatic pressure due to storm surges, and the wave pressure due to high waves, as shown in Fig. 6.8.1.

However, because of the effect of seabed topography or the rubble mound in front of structures, the wave force most disadvantageous to structures does not necessarily occur when the tidal level is highest, but the broken wave may generate stronger impulsive wave force at the lower tidal level (**Part II, Chapter 2, 6.2.4, Impulsive Breaking Wave Force**). Therefore, it is necessary to calculate the wave force by varying the tidal levels from low tide to the highest water level during storm surge.

Moreover, when the wave-dissipating blocks do not shield the front surface wall up to its crown height, the increased tide level makes the wall surface an incompletely shielded cross section and generates the impulsive wave force (**Part II, Chapter 2, 6.2.5 Wave Force Acting on Upright Wall Covered with Wave-dissipating Concrete Blocks**) and may break the parapet. The front surfaces of shore seawalls or revetments, in particular, are often shielded incompletely and may apply strong impulsive wave forces to the parapet. Therefore, it is preferable to verify the stability of the whole parapet or the strength of internal arrangement of reinforcement bars¹⁶⁸⁾.

The seawalls, dikes, and parapets have intricate cross sections due to topography at the front surface of structures, hinterland utilization, or others, which often make it difficult to calculate the wave force. Therefore, it is preferable, in principle, to conduct a hydraulic model experiment to calculate the wave force.

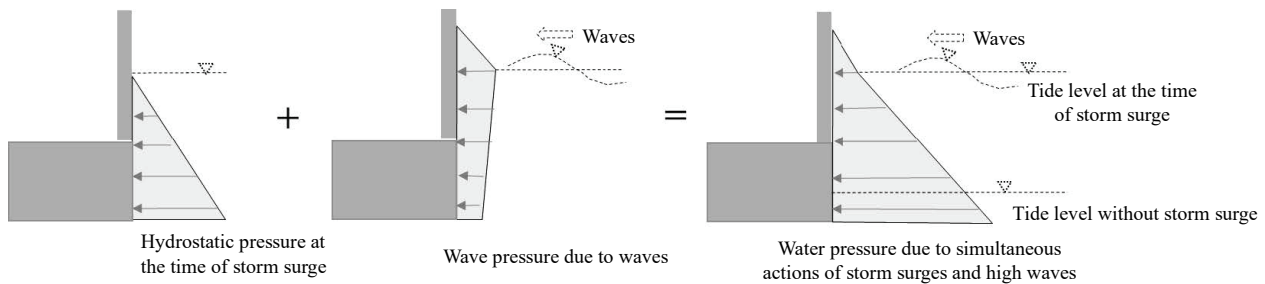


Fig. 6.8.1 Wave Pressure Distribution during Storm Surge

(2) Uplift and mound transmitted waves applied to gravity-type structures at storm surges

The increased hydrostatic pressure (or buoyancy), due to storm surges, and the uplift, due to high waves, simultaneously act on the bottom part of wall body of the caisson type or block type breakwater. Therefore, these vertical upward pressures shall be considered when verifying breakwater stability. On the other hand, the increased hydrostatic pressure, due to storm surges, and the mound transmitted wave pressure, due to high waves (**Part II, Chapter 2, 6.5 Mound Transmitted Wave Pressure and Wave Pressure within Joints Acting on behind the Revetments**), occur simultaneously inside the rubble mound or backfill stones behind the caisson type or block type seawall. Therefore, the hinterland ground stability shall be verified as the reclamation ground in the upper part of the backfill stones may be uplifted by this pressure and broken¹⁶⁹⁾. The seawater may invade the hinterland through the mound when the ground height behind the seawall is lower than the tide level during storm surges.

(3) Wave overtopping

If the storm surge raises the tidal level higher than the design high water level, the amount of wave overtopping increases and may break pavement behind the structures. To prevent these phenomena, the crown height of seawall shall be verified so the permissible amount of wave overtopping is not exceeded.

6.8.2 When the Tide Level during Storm Surge is Higher than the Crown Height of Structures

If the tidal level during storm surge is higher than the crown height of structures, the overflowing and wave overtopping occur at the same time, and the massive seawater flows in behind the coastal defenses to cause huge flood damage¹⁶⁹⁾. Furthermore, increased hydrostatic pressure due to storm surge, and the wave force due to high waves, simultaneously act on the lower part of and behind the structures, and the seawater may permeate the mound and inundate the hinterland. As these phenomena intricately vary according to the shape of structures and usage condition of hinterland, it is preferable to conduct a hydraulic model experiment for calculating the wave force or the amount of overtopping. Moreover, as the storm surge continues for a long time, it is preferable to verify to avoid scouring, or leakage of reclaimed soil, from the sandy ground behind the seawall.

It is necessary to append toughness to structures to cope with such storm surges exceeding the design tide level. One simple and indirect rule of thumb for "toughness" can be the degree of margin for the simultaneous action of the hydrostatic pressure at the time of storm surge, and the force of high waves in the verification equation of sliding and overturning of wall body, the strength of reinforcing bars inside the parapet and others, i.e., the level of safety coefficient exceeding 1.0.

Moreover, a construction method to avoid failures of coastal defenses in the elongation direction by installing an intervening wall in the elongation direction of revetments or seawalls as a tough structure¹⁷⁰⁾ may be an option.

[References]

- 1) Study Group on application of numerical wave tank to structural design against waves: Study and development of numerical wave channel, Coastal Development Technology Library, CDIT, pp. 156-163, 2001

- 2) Koji Kawasaki, Sho Matsuura and Taiki Sakatani: Validation of Free Surface Analysis Method in Three-Dimensional Computational Fluid Dynamics Tool “OpenFOAM”, JJSCE, Ser.B3, Ocean Engineering, I_748-I_753
- 3) Hitoshi Gotoh • Kojiro Suzuki • Hiroyuki Ikari • Taro Arikawa • Abbas Khayyer • Naoki Tsuruta: Development of Particle-Based Numerical Wave Flume for Multiphase Flow Simulation, JJSCE, Ser.B2, Coastal Engineering, I_25-I_30.
- 4) Mitsuyasu, H. : Theory of wave pressure, Summer Training on Hydraulic Engineering B Coast and Harbour 1965, Hydraulic Committee, JSCE pp. B-16-1-B-16-25, 1965
- 5) ITO, Y. M. FUJISHIMA and T. KITATANI: ON THE STABILITY OF BREAKWATERS, Rept. Of PHRI Vol. 5 No. 4, p. 134, 1966
- 6) Goda, Y.: Wave forces on port facilities, Lecture Note of Summer Training on Hydraulic Engineering B Coast and Harbour 1967, Hydraulic Committee, JSCE pp. B-10-1-B-10-34, 1967
- 7) Tanimoto, K: Wave forces on composite breakwaters, Proceeding of Lecture Meeting of PHRI 1976, pp. 1-26, 1976
- 8) Goda, Y.: Motion of Composite Breakwater on Elastic Foundation under the Action of Impulsive Breaking Wave Pressure, Rept. Of PHRI Vol. 12 No. 3, pp. 31-69, 1973
- 9) Tanimoto, K, K. Moto, S. Ishizuka and Y. Goda: Discussions on formula of design wave forces on breakwaters, Proceedings of 23rd Coastal Eng. JSCE pp. 11-16, 1976
- 10) Takahashi, S., K. Tanimoto, K. Shimosako and T. Hosoyamada: Proposal of Pressure coefficient of impact-breaking waves on composite type breakwater considering foundation mound profile, Proceedings of Coastal Eng. JSCE Vol. 39, pp. 676-680, 1992
- 11) G. Sainflou: Essai sur les diques maritimes verticales, Annales des Ponts et Chaussees, Vol. 98, No. 1, pp.5-48, 1928
- 12) I. Hiroi: On a method of estimating the force of waves, Journal of School of Engineering, Tokyo Imperial University, Vol. X, No. 1, p. 19, 1919
- 13) Kuroda, S. and T. Ishiwata: Disaster Prevention Engineering, Sankaido Publishing Co., 1960, 276p
- 14) Nagai, K, T. Ozawa, Y. Hishira and T. Nishimura: Characteristics of field waves having a bi-modal wave spectrum generated by typhoon, Proceeding s of 33rd Coastal Eng. JSCE, pp. 144-148, 1986
- 15) Tanimoto, K, K. KIMURA, A. P. dos Santos Pinto: Random Wave Forces and Design Wave Periods of Composite Breakwaters under the Action of Double Peaked Spectral Waves, Rept of PHRI Vol. 25 No. 2, pp. 3-25, 1986
- 16) Nakata, K, K. Terauchi, H. Nishida and I. Umeki: Characteristics of low crest breakwaters, Proceedings of 31st Coastal Eng. JSCE, pp. 532-536, 1984
- 17) Mizuno, Y. Y. Sugimoto, K. Kimura, K. Yamanaka and S. Kikuchi: Study of Characteristics of wave force on high crest breakwaters, Proceedings of Coastal Eng. JSCE Vol. 40, pp. 721-725, 1993
- 18) TANIMOTO, K., K. KIMURA: A Hydraulic Experimental Study on Trapezoidal Caisson Breakwaters, Technical Note of PHRI No. 528, p. 28, 1985
- 19) Keiji Esaki • Tomotsuka Takayama • Tae-Min Kim • Masaki Arai: Experimental Investigation of Uplift and Compressive Pressures on a Footing of a Hybrid Caisson, Proceedings of Civil Engineering in the Ocean, Vo.20, p.73-78, 2004.
- 20) Keiji Esaki • Tomotsuka Takayama • Tomohiro Yasuda : Verification of Wave Pressure Acting on a Breakwater with Footing, Proceedings of Civil Engineering in the Ocean, Vo.22, p.319-324, 2006.
- 21) Nagai, S, T. Kubo and K. Tokikawa: Study on Steel pile breakwater (First Report) Proceeding of Coastal Eng, JSCE, pp. 209-218, 1965
- 22) Hayashi, T, T. Kano, M. Shirai and S. Hattori: Hydraulic characteristics of cylindrical permeable breakwaters, Proceeding of 12th Coastal Eng. JSCE, pp. 193-197, 1965
- 23) Goda, Y. and S. Kakizaki: STUDY ON FINITE AMPLITUDE STANDING WAVES AND THEIR PRESSURES UPON A VERTICAL WALL, Repot of PHRI Vol. 5 No. 10, pp. 1-57, 1966
- 24) TANIMOTO, K., S. TAKAHASHI and T. KITATANI: Experimental Study of Impact Breaking Wave Forces on a Vertical wall Caisson of Composite Breakwater, Rept of PHRI Vol. 20 No. 2, pp. 3-39, 1981

- 25) H. Mitsuyasu: Experimental study on wave force against a wall, Report of Trans. Tech. Res. Inst. No. 47, pp.1-39, 1962
- 26) Honma, M., K. Horikawa and N. Hase: Wave forces on sea dikes, Proceeding of 9th Coastal Eng. JSCE, pp. 133-137, 1962
- 27) MORIHIRA, M. S. KAKIZAKI and T. KIKUYA: EXPERIMENTAL STUDY ON WAVE FORCE DAMPING EFFECTS DUE TO DEFORMED ARTIFICIAL BLOCKS, Rept. PHRI Vol. 6 No. 4, pp. 3-31, 1967
- 28) GODA, Y. and S. HARANAKA: Title AN EXPERIMENT ON THE SHOCK PRESSURE OF BREAKING WAVES, Technical Note of PHRI No. 32, pp. 1-18, 1967
- 29) Horikawa, K. and Y. Noguchi: Relationship between breaker pressure and wave profile acting on a vertical wall, Proceeding of 17th Coastal Eng. JSCE, pp. 177-184, 1970
- 30) Fujisaki, H, A. Sasada and Y. Takahashi: Discussion on the construction techniques of breakwaters on steep slope sea bed, Proceeding of Chubu Branch of JSCE, pp. 181-183, 1996
- 31) TAKAHASHI, S., K. TANIMOTO and S. SUZUMURA: Generation Mechanism of Impulsive Pressure by Breaking Wave on a Vertical Wall, Rept of PHRI, Vol. 22 No. 4, pp. 3-31, 1983
- 32) Shimosako, K and N. Osaki: Study on the Application of the Calculation Methods of Wave Forces acting on the Various Type of Composite Breakwaters, Technical Note of PHRI, No. 1107, pp. 1-14, 2005
- 33) Goda, Y: Motion of Composite Breakwater on Elastic Foundation under the Action of Impulsive Breaking Wave Pressure, Rept. Of PHRI, Vol. 12 No. 3, pp. 3-29, 1973
- 34) Takahashi, S., K. Shimosako, T. Uwabe and K. Tanimoto: Dynamic response of composite type breakwaters to impact breaking waves, Proceedings of Coastal Engineering JSCE, Vol. 40, pp. 766-770, 1993
- 35) Tanimoto, K, M. Osato, S. Takaoka, T. Uchida and T. Ikada: An experiment on stability of breakwaters with wave-absorbing blocks against random waves, Proceedings of the 26th Coastal Eng., JSCE, pp. 343-347, 1979
- 36) TANIMOTO, K. S. TAKAHASHI and, K. MIYOSE: Title Experimental Study of Random Wave Forces on Upright Sections of Breakwaters, Rept of PHRI Vol. 23 No. 3, pp. 47-100, 1984
- 37) TAKAHASHI, S. K. TANIMOTO and K. SHIMOSAKO: Title Wave and Block Forces on a Caisson Covered with Wave Dissipating Blocks, Rept. Of PHRI Vol. 29 No. 1, pp. 54-75, 1990
- 38) Sekino, T., T. Kadono and T. Imoto: Study on design methods for wave-absorbing block armored breakwaters having unarmored parapet, Journal of Public Works Research Institute, Hokkaido Regional Development Bureau No. 397, pp. 14-20, 1986
- 39) Tanaka, H., N. Abe and M. Kato: Evaluation of horizontal wave force on wave-absorbing block armored caisson breakwater. Proceedings of the 32nd Conference on Coastal Eng. JSCE, pp. 490-494, 1985
- 40) TANIMOTO, K. and R. OJIMA: Title Experimental Study of Wave Forces Acting on a Superstructure of Sloping Breakwaters and on Block Type Composite Breakwaters, Technical Note of PHRI No. 450, p. 32, 1983
- 41) Hiromoto, F., H. Nishijima, S. Konno and I. Kimura: Load of blocks of wave-observing block armored breakwaters under wave actions, Proceedings of the 40th Conference on Coastal Eng. JSCE, pp. 347-351, 1983
- 42) Yuichiro Kawabata • Ema Kato • Mitsuyasu Iwanami : A Study on the Design Method of RC Caissons for Breakwaters against Impact Loads Considering Maintenance Strategy, Technical Note of PARI, No.1279, 56p., 2013.
- 43) Kougamu, Y. and K. Tokikawa: Experimental study on the wave-pressure decreasing effect of wave absorbing blocks during the construction, Report of the Public Works Research Institute (PWRI), Hokkaido Regional Development Bureau (HRDB) No. 53, pp. 81-95, 1970
- 44) Shiomi, M., H. Yamamoto, A. Tsugawa, T. Kurosawa and K. Matsumoto: Damages and countermeasures of breakwaters due to the wave force increase at discontinuous points of wave-absorbing blocks, Proceedings of the 41st conference on Coastal Eng. JSCE, pp. 791-795, 1994
- 45) Shigeo Takahashi • Yasunori Ohki • Ken-ichiro Shimosako • Sadao Isayama • Kunirou Ishinuki : Seawall Failures by Typhoon 9918 and Their Reproduction in Wave Flume Experiments, Technical Note of PARI, No.973, 50p., 2000.
- 46) T. Hosoyamada, S. Takahashi and K. Tanimoto: Application of sloping top caisson breakwater at isolated islands, proceedings of Conference on Coastal Eng. JSCE, Vol. 41, pp. 325-329, 1994

- 47) Morihira, M. and O. Kunita: A model experiments on hydraulic characteristics of sloping breakwater, Proceedings of the 26th Conference on Coastal Eng. JSCE, pp. 295-298, 1979
- 48) Sato, T. N. Yamagata, M. Furukawa, S. Takahashi and T. Hosoyamada: Hydraulic characteristics of sloping-top breakwaters armored with wave-absorbing blocks- Development of a new structural type of breakwaters in deep water area in Naha Port, Proceedings of Coastal Eng. JSCE Vol. 39, pp. 556-560, 1992
- 49) Katayama, H., T. Sekimoto, Y. Kawamata and K. Ueki: On wave force characteristics acting on submerged sloping-top caisson breakwaters, Proceedings of Coastal Eng. JSCE Vol. 45, pp. 776-780, 1998
- 50) TAKAHASHI, S., K. SHIMOSAKO and H. SASAKI: Title Experimental Study on Wave Forces Acting on Perforated Wall Caisson Breakwaters Rept of PHRI Vol. 30 No. 4, pp.3-34, 1991
- 51) TANIMOTO, K., S. HARANAKA, E. TOMIDA, Y. IZUMIDA and S. SUZUMURA : Title A Hydraulic Experimental Study on Curved Slit Caisson Rept of PHRI Vol. 19 No. 4, pp. 3-53, 1980
- 52) TANIMOTO, K., S. TAKAHASHI and T. MURANAGA : Title Uplift Forces on a Ceiling Slab of Wave Dissipating Caisson with a Permeable Front Wall- Analytical Model for Compression of an Enclosed Air Layer-, Rept of PHRI Vol. 19 No. 1, pp. 3-31, 1980
- 53) TAKAHASHI, S. and K. TANIMOTO: Title Uplift Forces on a Ceiling Slab of Wave Dissipating Caisson with a Permeable Front Wall (2nd Report)-Field Data Analysis- Rept of PHRI Vol. 23 No. 2, pp. 3-25, 1984
- 54) ITO, FY. And K. TANIMOTO: Title Meandering Damages of Composite Type Breakwaters. Technical Note of PHRI No. 112, pp. 13, 1971
- 55) Kougami, Y., N. Fujiki and Y. Uehara: An experiment on wave height and pressure at a corner of breakwater, Journal of Public Works Research Institute (PWRI), Hokkaido Regional Development Bureau (HRDB) No. 218, pp. 1-11, 1971
- 56) Y. Kougami, N. Fujiki and T. Tsutsumi: An experiment on wave height and pressure at a corner of breakwater (Second Rep.), Journal of Public Works Research Institute (PWRI), Hokkaido Regional Development Bureau (HRDB) No. 230, pp. 1-13, 1972
- 57) Goda, Y, T. YOSHIMURA and M. ITO: Reflection and Diffraction of Water Waves by an Insular Breakwater, Rept of PHRI Vol. 10 No. 2, pp.3-52, 1971
- 58) ITO, Y., K. TANIMOTO, K. KOBUNE, T. KITATANI and M. TODOROKI: Title An Experimental Investigation of Upright Breakwaters on Reefs, Technical Note of OHRI No. 189, p. 18, 1974
- 59) Tominaga, M. and I. Kuzumi: braking wave pressure on coastal dikes, Proceedings of the 18th Conference on Coastal Eng. JSCE, pp. 215-221, 1971
- 60) Coastal Engineering Research Center, Shore Protection Manual Vol. II, Department of Army Corps of Engineers, 1984
- 61) JSCE Edition: Guideline and commentary for design of Offshore Structures (Draft), JSCE, pp. 28-53, 1973
- 62) J. R. Morison, M. P. O. Brien, J. W. Johnson, S. A. Schaaf: The force exerted by surface waves on piles, Petroleum Trans., 189, TP 2846, pp. 149-154, 1950
- 63) T. E. Stelson and F. T. Mavis: Virtual mass and acceleration in fluids, Proc, ASCE., Vol. 81, Separate No. 670, pp. 670-1-670-9, 1955
- 64) Hamada, H., Mitsuyasu, H. and N. Hasegawa: Wave forces on structures, Proceedings of the 3rd Conference on Coastal Eng. JSCE, pp. 67-83, 1956
- 65) Keulegan, G. H. and L. H. Carpenter: Forces on cylinders and plates in an oscillating fluid, Journal of the National Bureau of Standards, Vol. 60, No. 5, pp. 423-440, 1958.
- 66) Sarpkaya, T.: Forces on cylinders and spheres in a sinusoidally oscillating fluid, Journal of Applied Mechanics, Trans. of ASME, Vol. 42, No. 1, pp. 32-37, 1975
- 67) Sarpkaya, T.: In-line and transverse forces on cylinders in oscillatory flow at high Reynolds number, Proc. of the Offshore Technology Conference, Vol. II, pp. 95-108, 1976
- 68) Sarpkaya, T., N. J. Collins and S.R. Evans: Wave forces on rough-walled cylinders at high Reynolds numbers, Proc. Of OTC, Vol. III, #2901, pp. 167-184, 1977

- 69) Y. Goda: Wave-forces on a vertical circular cylinder; Experiments and proposed method of waveforce computation, Report of P.H.T.R.I., No. 8, p. 74, 1964
- 70) Yamaguchi, M.: Fundamental study on wave forces on sphere and standing waves, Kyoto Univ. Dissertation, p. 147, 1974
- 71) Nakamura, M.: Study on wave forces on coastal structures and their dynamic response, Osaka Univ. Dissertation, p. 297, 1977
- 72) Chakrabarti, S.K., A.L. Wollbert, and A.T. William: Wave forces on vertical circular cylinder, Journal of Waterways, Harbors and Coastal Engineering Division, ASCE, Vol. 102, No. WW2, pp. 203-221, 1976
- 73) Chakrabarti, S.K.: Inline forces on fixed vertical cylinder in waves, Journal of the Waterway, Port, Cow and Ocean Division, ASCE, Vol. 106, WW2, pp. 145-155, 1980
- 74) Koterayama, W. and M. Tashiro: Wave forces on semi-submerged horizontal cylinder in diagonal incident wave and vertical cylinder in deep water waves, Report of Research Institute for Applied Mechanics Kyushu Univ. Vol. 50, pp. 35-61, 1979
- 75) Oda, K.: Wave forces on structures- Cylindrical structures-, Lecture note of Summer training for Hydraulic Engineering 1982, (18th) Course B, Hierodulic Committee of JSCE, pp. B-4-1-B-5-27, 1982
- 76) Mizuno, Y. T. Kadono, Y. Nagai, O. Momose and T. Sekino: Field experiment on offshore structure in a rough sea zone, Rept. of the Public Works Research Institute (PWRI), Hokkaido Regional Development Bureau (HRDB) No. 87, p. 77, 1988
- 77) Kim, Y. Y. and H. C. Hibbard: Analysis of simultaneous wave force and water particle velocity Measurements, Proc. of OTC, Vol. 1, No. 2192, pp. 461-469, 1975
- 78) Ogusu, A.: Wave forces on multiple row cylinders, Proceedings of the Society of Naval Architects of Japan No. 131, 1972
- 79) Nakamura, H. and N. Abe: Hydraulics of intake tower of power plant, Proceedings of the 19th Conference on Coastal Eng. JSCE, pp. 391-394, 1972
- 80) GODA, Y. S. HARANAKA and M. KITAHATA: Title STUDY OF IMPULSIVE BREAKING WAVE FORCES ON PILES, Rept of PHRI Vol. 5 No. 6, pp. 1-30, 1966
- 81) TANIMOTO, K. S. TAKAHASHI, T. KANEKO, K. SHIOTA and K. OGURA: Title Experimental Study on Impulsive Forces by Breaking Waves on Circular Cylinder Rept of PHRI Vol. 2 No.2, pp. 33-87, 1986
- 82) Goda, Y.: Design of marine structures- wave forces-, Jour. of JSCE Vo55 No. 9, pp. 2-7, 1970
- 83) Nagasaki, S. and K. Ogata: Wave forces on underwater pipelines (First Rept.), Proceedings of the 18th Conference on Coastal Eng. JSCE, pp. 223-227, 1971
- 84) T. Sarpkaya, M. Isaacson: Mechanics of Wave Forces on Offshore Structure, Van Nostrand Reinhold Company, p. 651, 1981
- 85) T. Yamamoto, J.H. Nath: Forces on many cylinders near a plane boundary, ASCE, National Water Resources and Ocean Engineering Convention, Preprint No. 2633, 1976
- 86) T. Sarpkaya: In-line and transverse forces on cylinders near a wall in oscillatory flow at high Reynolds numbers, OTC paper No. 2898, pp. 161-166, 1977
- 87) T. Sarpkaya, F. Rajabi.: Hydrodynamic drag on bottom-mounted smooth and rough cylinders in periodic flow, OTC Paper No. 3761, pp. 219-226, 1980
- 88) Borgman, L. E.: Spectral analysis of ocean wave forces on pilling, Proc. ASCE, Vol. 93, No. WW2, pp. 129-156, 1967
- 89) Hino, M.: Spectral theory of wave forces on piles, Proceedings of the 15th Conference on Coastal Eng. JSCE, pp. 103-108, 1968
- 90) Borgman, L. E.: Ocean wave simulation for engineering design, Proc. ASCE, Vol. 95, No. WW4, pp. 557-583, 1969
- 91) ITO, Y. K. TANIMOTO and K. KOBUNE: Title Dynamic Response of an Offshore Platform to Random Waves Rept of PHRI Vol. 11 No. 3, pp. 59-86, 1972
- 92) Hudspeth, R.T.: Wave force prediction from non-linear random sea simulation, 7th OTC, # 2193, pp. 471-486, 1975

- 93) Sharma, J. and Dean, R.G.: Second-order directional seas and associated wave forces, 11th OTC, #3645, pp. 2505-2514, 1979
- 94) Tickell, R.G. and Elwany, M.H.S.: A probabilistic description of forces on a member in a short-crested random sea, *Mechanics of Wave-Induced Forces on Cylinders*, Pitman Pub. Ltd., London, pp. 561-576, 1979
- 95) Kimura, A. A., Seyama and A. Ueno: Stochastic characteristics of random wave forces acting on cylinder, *Proceedings of 27th Conference on Coastal Eng. JSCE*, pp. 373-377, 1980
- 96) GODA, Y. T. IKEDA, T. SASADA and Y. KISHIDA: Title Study on Design Wave Forces on Circular Cylinders Erected upon Reefs Rept of PHRI Vol. 11 No. 4, pp. 45-81, 1972.12
- 97) Hiraishi, T. Y. Tomita and Y. Suzuki: Effect of wave directionality on wave forces on Cylinder, *Proceedings of 27th Conference on Coastal Eng. JSCE Vol. 41*, pp. 836-840, 1994
- 98) MacCamy, R.C. and R.A. Fuchs: Wave Forces on Piles, a Diffraction Theory, U.S. Army, Corps of Engineers, Beach Erosion Board, Tech. Memo. No. 69, p. 17, 1954
- 99) GODA, Y. and T. YOSHIMURA: Title Wave Force Computation for Structures of Large Diameter, Isolated in the Offshore, Rept of PHRI Vol. 10 No. 4, pp. 3-52, 1971
- 100) Yamaguchi, M: Wave forces on pile structures, Lecture note of Summer training for Hydraulic Engineering 1975, (11th) Course B, Hierodulic Committee of JSCE, pp. B-6-1-B-6-26, 1975
- 101) TANIMOTO, K., S. TAKAHASHI and Y. IZUMIDA: A Calculation Method of Uplift Forces on a Horizontal Platform, Rept. of PHRI Vol. 17 No. 2, pp. 3-47, 1978
- 102) ITO, Y. and H. TAKEDA: Uplift on Pier Deck due to Wave Motion, Rept. of PHRI Vol. 6 No. 4, pp. 37-68, 1967
- 103) Murota, A. and M. Furudoi: Experimental study on uplift force on deck of pier, *Proceedings of the 13th Conference on Coastal Eng. JSCE*, pp. 120-125, 1966
- 104) Nagai, S. T. Kobo and K. Tokikawa: Study on uplift on piers (First Rep.), *Proceedings of the 13th Conference on Coastal Eng. JSCE*, pp. 112-119, 1966
- 105) Horikawa, K., T. Nakao and A. Yajima: Experimental study on uplift on piers, *Proceedings of the 14th Conference on Coastal Eng. JSCE*, pp. 148-153, 1967
- 106) Sawaragi, T. and M. Nochino: Discussion on Similarity law for hydraulic model tests on uplift acting on decks of piers, *Proceedings of Coastal Eng. JSCE Vol. 35*, pp. 677-681, 1988
- 107) TANIMOTO, K., Shigeo TAKAHASHI, Masahiko TODOROKI and Yoshikazu IZUMIDA: Horizontal Wave Forces on a Rigid Platform, Rept. of PHRI Vol. 16 No. 3, pp. 39-68, 1977
- 108) Tirindelli, M., Cuomo, G., Allsop, W., and McConnell, K.: Exposed jetties: Inconsistencies and gaps in design methods for wave-induced forces, *Proc. Of the 28th International Conference on Coastal Engineering*, Cardiff, pp. 1684-1696, 2002
- 109) Tirindelli, M., Cuomo, G., Allsop, W., and McConnell, K.: Physical model studies of wave-induced loading on exposed jetties: Towards new prediction formulae, *Proc. Of the International Conference Coastal Structures 2003*, Portland, pp. 382-393, 2003
- 110) Cuomo, G., Allsop, W., and McConnell, K.: Dynamic Wave Loads on Coastal Structures: Analysis of impulsive and pulsating wave loads, *Proc. Of the International Conference Coastal Structures 2003*, Portland, pp. 356-368, 2003
- 111) Bentiba, R., Cuomo, G., Allsop, W., and Bunn, N.: Probability of occurrence of wave loading on fatty deck elements, *Proc. Of the 29th International Conference on Coastal Engineering*, Lisbon, pp. 4113-4125, 2004
- 112) Kubou, M. M. Takezawa and T. Ueki: Experimental study on wave pressure at the vicinity of wave crest, *Proceedings of the 20th Conference on Coastal Eng. JSCE*, pp. 279-284, 1973
- 113) Michio Morihira, Shusaku Kakizaki and Yoshimi Goda :EXPERIMENTAL INVESTIGATION OF A CURTAIN-WALL BREAKWATER ,REPORT OF PORT AND HARBOUR TECHNICAL RESEARCH INSTITUTE MINISTRY OF TRANSPORTATION Vol. 3, No. 1, p. 16, 1964
- 114) Sekimoto, T., H. Kondo, T. Oshita, S. Imai and M. Nakamura: Design wave force of curtain-wall type breakwater considering incident wave angle, *Proceedings of Coastal Eng. JSCE Vol. 35*, pp. 657-661, 1988

- 115) Shigeo Takahashi, Kojiro Suzuki, Katsumasa Tokubuchi, Ken-ichiro Shimosako: Experimental Analysis of the Settlement Failure Mechanism Shown by Casson-Type Seawalls, 25th, I.C.C.E., pp. 1902-1915, 1996
- 116) Waterfront Vitalization and Environment Research Center: Design • Construction • Management Manual of Controlled Type Waste Disposal Revetment (Revised Edition), 134p., 2008.
- 117) Yuichiro Takebe, Kojiro Suzuki, Yoshio Nishino, Yasushi Nishimoto : The Verification of Deformation Model and Design Method of Joint Plate, JJSCE, Ser.B2, Coastal Engineering, Vol.71, No.2, I_1177-I_1182, 2015.
- 118) JSCE Edition: Handbook of design of coastal protection facilities (Revised Edition), pp. 174-176, 1969
- 119) Literature survey Committee: Deformed wave absorbing blocks, Journal of JSCE, Vol. 49, No. 4, pp. 77-83, 1964
- 120) R.Y. Hudson: Laboratory investigation of rubble-mound breakwater, Proc. ASCE., Vol. 85, W.W.3., pp. 93-121, 1959
- 121) Kashima, R., T. Sakakiyama, T. Shimizu, T. Sekimoto, H. Kunisu and O. Kyoutani: Evaluation equation of deformation of wave absorbing works due to random waves, Proceedings of Coastal Eng. JSCE Vol. 40, pp. 795-799, 1995
- 122) J.W. van der Meer: Rock slopes and gravel beaches under wave attack, Doctoral thesis, Delft Univ. of Tech., p. 152, 1988 or J.W. Van Der Meer: Stability of breakwater armor layer -Design formulae, Coastal Engineering, 11, pp. 219-239, 1987
- 123) J. W. van der Meer: Stability of cubes, Tetrapods and Accropode, Proc. of Breakwater. 88, Eastbourne, UK, pp. 71-80, 1988
- 124) H. F. Burcharth and Z. Liu: Design of Dolos armour units, Proc. of the 23rd International Conference on Coastal Engineering, Venice, pp. 1053-1066, 1992
- 125) Takahashi S., M. Hanzawa and K. Shimosako: Performance verification of stability of armour stones of rubble-mound breakwaters against waves, Proceedings of Coastal Eng. JSCE Vol. 50, pp. 761-765, 2003
- 126) Tanimoto, K., Y. Haranaka K. Yamazaki: Experimental Study on the Stability of Wave Dissipating Concrete Blocks against Irregular Waves, Rept. of PHRI Vol. 24, No. 2, pp. 85-121, 1985
- 127) Kashima, r., T. Sakakiyama, T. Shimizu, T. Sekimoto, H. Kunisu and O. Kyoutani: Evaluation equation of deformation of wave absorbing works due to random waves, Proceedings of Coastal Eng. JSCE Vol. 42, pp. 795-799, 1995
- 128) Hanzawa, M., H. Sato, T. Takayama, S. Takahashi and K. Tanimoto: Study on evaluation equation for the stability of wave absorbing blocks, Proceedings of Coastal Eng. JSCE Vol. 42, pp. 886-890, 1995
- 129) Takahashi, S., M. Hanzawa, H. Sato, M. Gomyou, K. Shimosako, K. Terauchi, T. Takayama and K. Tanimoto: Lifetime Damage Estimation with a New Stability Formula for Concrete Blocks, Report of PHRI, Vol.37, No.1, pp.3-28, 1998.
- 130) Kimura, K., K. Kamikubo, Y. Sakamoto, Y. Mizuno, H. Takeda and M. Hayashi: Stability of blocks at the end of breakwaters armored with wave absorbing blocks, Proceedings of Coastal Eng. JSCE Vol. 44, pp. 956-960, 1997
- 131) Van de Kreeke, J.: Damage function of rubble mound breakwaters, ASCE., Journal of the Waterway and Harbors Division, Vol. 95, WW3, pp. 345-354, 1969
- 132) F. T. Christensen, P. C. Broberg, S. E. Sand, and P. Tryde: Behavior of rubble-mound breakwater in directional and uni-directional waves, Coastal Eng., Vol. 8, pp. 265-278, 1984
- 133) Sokabe, T. and T. Yajima: Outstanding technical issues in designing of detached breakwaters, Lecture note of Summer training for Hydraulic Engineering 1982, (18th) Course B, Uralic Committee of JSCE, pp. B-5-1-B-5-24, 1982
- 134) Takeda, H., Y. Yamamoto, K. Kimura and T. Sasazima: Impact wave forces and stability of wave absorbing blocks on breakwaters placed on steep slope, Proceedings Offshore Development Vol. 11, pp. 287-290
- 135) Kamikubo Katsumi, Yasuji Yamamoto, Katsutoshi Kimura, Toshiaki Shimizu, Masafumi Yoshino : Armor Stability of Block Mound Seawall for Steep Foreshore Conditions, Proceedings of Civil Engineering in the Ocean, Vol.26, p.489-494, 2010.
- 136) Kenji Motoyama, Katsumi Kamikubo and Yasuji Yamamoto : Stability of Wave-Dissipating Blocks of Caisson Breakwater for Steep and Shallow Foreshore Conditions, JJSCE, Ser.B3, Ocean Engineering, Vol.70, I_265-I_270, 2014.

- 137) Coastal Development Institute of Technology (CDIT): Technical Manual for wave absorbing blocks of large specific gravity, p. 45, 1995
- 138) Kubota, S., S. Kobayashi, A. Matumoto, M. Hanzawa and M. Matuoka: On the effect of the layer thickness and filling materials of wave absorbing blocks on their stability against waves, Proceedings of Coastal Eng. JSCE Vol. 49, pp. 756-760, 2002
- 139) Coastal Engineering Research Center: Shore Protection Manual, Vol. II, Department of Army Corps of Engineering, 1977
- 140) A. Brebner, D. Donnelly: Laboratory study of rubble foundations for vertical breakwaters, Proc. 8th Conf. of Coastal Engg., New Mexico City, pp. 408-429, 1962
- 141) Tanimoto, K., T. Yanagisawa, T. Muranaga, K. Shibata and Y. Goda: Stability of Armor Units for Foundation Mounds of Composite Breakwaters Determined by Irregular Wave Tests, Rept. of PHRI Vol. 21, No. 3, pp. 3-42, 1982
- 142) Inagaki, K. and T. Katayama: Analysis of damage to armor stones of mounds in composite breakwaters, Technical Note of PHRI No. 127, pp. 1-22, 1971
- 143) Takahashi S., K. Kimura and K. Tanimoto: Stability of Armour Units of Composite Breakwater Mound against Oblique Waves, Rept. of PHRI Vol. 29 No. 2, pp.3-36, 1990
- 144) Sudo, K., K. Kimura, T. Sasajima, Y. Mizuno and H. Takeda: Estimation equation of required weight of armour units of rubble-mound of composite breakwaters considering the allowable deformation, Proceedings of Coastal Eng. JSCE Vol. 42, pp. 896-900, 1995
- 145) Kougami, Y. and T. Narita: On the stability of armour layer, made with wave-absorbing blocks, of rubble foundation of composite breakwaters, Journal of Public Works Research Institute (PWRI), Hokkaido Regional Development Bureau (HRDB) No. 232, pp.1-13, 1972
- 146) Kashima, R., S. Saitou and H. Hasegawa: Required weight of armour concrete cube for rubble mound foundation of composite breakwaters, Report of the Second Technical Research Institute of the Central Research Institute of Electric Power Industry 70022, p. 18, 1971
- 147) Fujiike, T., K. Kimura, T. Hayashi and y. Doi: Stability against waves of armor units placed at front face of rubble-mound of wave-absorbing-block-armored breakwaters, Proceedings of Coastal Eng. JSCE Vol. 46, pp. 881-885, 1999
- 148) Matuda, S., W. Nishikiori, A. Matumoto and M. Saitou: Estimation method of stable weight of armour blocks of rubblemound of composite breakwaters considering impact wave force actions, Proceedings of Coastal Eng. JSCE Vol. 47, pp. 896-900, 2000
- 149) Shimosako, K., S. Kubota, A. Matumoto, M. Hanzawa, Y. Shinomura, N. Oike, T. Ikeya and S. Akiyama: Stability and Durability of Filter Unit Covering Rubble Mound of Composite Breakwater, Report of PARI, Vol.43, No.1, pp.49-83, 2004.
- 150) Association of Nationwide Disaster Prevention: Kujukuri and Minamikujukuri No.1 Coasts Disaster Restoration projects- Composite Measure of Large Gabion Seawall and Foot Protection, Examples of Disaster Restoration Projects in 2013, pp.82-85, 2013 (in Japanese)
- 151) Kudou, T.: Temporary river closing dikes and its overflow, Journal of JSCE, Vol. 58 No. 11, pp. 63-69, 1973
- 152) Iwasaki, T., A. Mano, T. Nakamura and N. Horikoshi : Experimental study on fluid dynamic force in steady flow acting on mound materials of submerged breakwaters and prepacked breakwaters, Proceedings of the 31st Conference on Coastal Eng. JSCE, pp. 527-531, 1984
- 153) Tanimoto, K., K. Kimura and K. Miyazaki: Study on Stability of Submerged Dike at the Opening Section of Tsunami Protection Breakwaters, Rept. of PHRI Vol. 27 No. 4, pp. 93-121, 1988
- 154) Ministry of Land, Infrastructure, Transport and Tourism Port and Harbours Bureau: Guideline for Tsunami-Resistant Design of Breakwaters, p.37, 2015 (in Japanese)
- 155) Sohei Maruyama, Tomotsuka Takayama, Kenichiro Shimosako, Akiihikoo Yahiro, Kojiro Suzuki, Toru Aota, Masashi Tanaka, Akira Matsumoto and Minoru Hanzawa : Estimation of Tsunami Force Acting on the Block Armored Breakwater in the State of Soliton Fission, J.JSCE, Ser.B2, Coastal Engineering, Vol.71, No.2, pp.I_265-I_270, 2015.

- 156) Masafumi Miyata, Yasuo Kotake, Masahiro Takenobu, Tomoaki Nakamura, Norimi Mizutani and Shigeki Asai : Experimental Study on Hydraulic Characteristics of Tsunami Overtopping Flow over a Caisson-Type Breakwater, J.JSCE, Ser.B3, Ocean Engineering, VOL.70, NO.2, PP.I_504-I_509, 2014.
- 157) Naoki Tsuruta, Kojiro Suzuki, Tsukasa Kita, Masafumi Miyata, Masahiro Takenobu, Enhancement of accuracy of prediction of tsunami force in overflow for design of tenacious breakwater, Report of PARI, Vol.56, No.1, pp.26-51., 2016.
- 158) Kojiro Suzuki and Tsukasa Kita: Uplift and overburden pressure acting on breakwater caisson under tsunami overflow, Asian and Pacific Coasts, pp. 817-824, 2017
- 159) Fisheries Agency Fishing Port Fisheries Development Department Disaster Prevention Fishing Village Division • Ministry of Land, Infrastructure, Transport and Tourism Port and Harbours Bureau Coastal and Disaster Management Office: Guideline for design of tidal embankment against tsunami, pp.22., 2015.
- 160) Nobuhiro Ishida, Hiroshi Moritani, Kisaburo Azuma, Takuya Toriyama and Hidetaka Nakamura : Water Depth Coefficients for Evaluating Tsunami Pressure on Seawall, NRA Technical Report, NTEC-2016 -4001, 113p., 2016.
- 161) Kei Ando, Kojiro Suzuki and Naoki Tsuruta : A Study on Inundation Depth in Evaluating Tsunami Wave Pressure Acting on Land Vertical Walls, J.JSCE, Ser.B2, Coastal Engineering, Vol.73, No.2, I_895-I_900, 2017.
- 162) Ryoji Naito, Kentaro Kumagai, Tadashi Asai, Takeshi Suzuki : Measurement of Height, Velocity and Pressure of the Water Overflow over a Seawall, Technical Note of NILIM, No.917, 24p., 2016.
- 163) Jun Mitsui, Akira Matsumoto and Minoru Hanzawa : Derivation Process of the Isbash Formula and Its Applicability to Tsunami Overtopping Breakwater, J.JSCE, Ser.B2, Coastal Engineering, Vol.71, No.2, I_1063-I_1068, 2015.
- 164) Jun Mitsui, Shin-ichi Kubota, Akira Matsumoto and Minoru Hanzawa : Influence of Superstructures on Stability of Armor Units Covering Breakwater Rubble Mounds against Tsunami, J.JSCE, Ser.B2, Coastal Engineering, Vol. 72, No. 2, p. I_1111-I_1116, 2016.
- 165) Jun Mitsui, Akira Matsumoto, Minoru Hanzawa and Kazuo Nadaoka : Stability Verification Method for Armor Units Covering Breakwater Rubble Mounds against Tsunami Overflow, J.JSCE, Ser.B2, Coastal Engineering, Vol.72, No.2, I_1111-I_1116, 2016.
- 166) Association for Innovative Technology on Fishing Ports and Grounds: Manual for calculating required mass of mound covering block with breakwater belly against tsunami overflow, pp.45, 2014 .
- 167) Sogo Jikuhara, Kojiro Suzuki, Kazunori Tatewaki and Yoshihiro Hosokawa : Effect of the Oblique Incident Tsunami on the Mound Cover Layer behind the Vertical Type Breakwater Having Abrupt Change of the Breakwater Width, J.JSCE, Ser.B2, Coastal Engineering, Vol.72, No.2, pp.I_991-I_996, 2016.
- 168) Yoshimi Goda : Coastal Engineering – Its Birth and Development, Gihodo, pp.38, 2012.
- 169) Tsukasa Kita and Kojiro Suzuki: Study on the Stability of Pavement behind Seawall against Overflow with High Waves, J.JSCE, Ser.B2, Coastal Engineering, Vol.73, No.2, I_991-I_996, 2017.
- 170) Senri Tsuruta and Yoshimi Goda: Failure of Coastal Structures by Typhoon Vera and the Characteristics, Proceedings of Coastal Engineering Conference in Japan, Vol.7., pp.195-199., 1960.

7 Water Currents

7.1 The Flow of Sea Water in Coastal Zones

[Public Notice] (Flow of Sea Water)

Article 10

Flow of sea water shall be appropriately defined in terms of current velocity and current direction on the basis of measured values or estimated values.

[Interpretation]

7. Setting of Natural Conditions

(4) **Items related to the flow of water** (Article 6 of the Ministerial Ordinance and the interpretation related to Article 10 to 12 of the Public Notice)

① Setting Methods for the Flow of Sea Water

In the performance verification of facilities subject to the technical standards, when combining the flow of sea water with other actions, out of all the possible flows of sea water that have a high probability of occurring simultaneously with other actions, specify the current velocities and current directions that would be appropriate from the viewpoint of the stability of the target facilities, consideration to the environment, etc.

7.1.1 General

The movements of sea water are the superpositions of currents that have various periods and are caused by different natural actions, and their current velocities and directions are greatly affected by topography and structures and change in complicated ways both in space and time. The movements of sea water cause sediment on the sea bottom to move, thus leading to problems such as siltation in navigation channels and basins and the scouring of the area around facilities. Furthermore, changes in the flow of sea water due to coastal development can cause wide-scale changes in the natural environment, such as water quality, sedimentation changes, and biological and ecosystem¹⁾ changes. With regard to their origins and their scales over time and space, the flows of sea water are classified as ocean currents, tide currents, tidal residual flow, wind-driven currents, density currents, and nearshore currents.

7.1.2 Ocean Current

Ocean current flows in the spatial scale of the ocean with an almost balanced Coriolis force and pressure gradient (geostrophic balance). The effect of the ocean current on the facilities under the technical standards appears as the inflow of oceanic water into the coast, the change in mean water level, etc.

7.1.3 Tidal Current

Tidal current is the horizontal flow of sea water accompanying the wave motion on the sea surface (tidal wave) caused by the tide-producing force generated by the movement of heavenly bodies (mainly the moon and the sun). Considering that the tidal wave is affected by the seabed topography during the propagation process in the ocean, the tide condition differs by location. The tidal current periodically changes according to the four principal tidal constituents (**Part II, Chapter 2, 3.1 Astronomical Tide**). The harmonic constant (i.e., the flow rate amplitude and the lag of each northern and eastern component) obtained by the harmonic analysis of the tidal current observation data differs by sea area and location. The forced oscillation of the bay water caused by the tide in the ocean is significant in Japan's inner bays, where the tidal current amplitude increases from the entrance to the inner part of the bay almost simultaneously, thus repeating the tide. The tidal current becomes faster when the difference in tidal level is larger or when the width of a waterway is narrower such as in a channel. Given that the tidal current is strongly affected by the topography, shape of structures, and other factors, the nearby flow condition varies by the change in topography, shape of structures, and other factors.

7.1.4 Tidal Residual Flow

Tidal residual flow is the flow generated by the nonlinearity of tidal current and the effect of topography when a mean of one tide period is taken. It is important to understand the long-term movement of seawater, such as the mixture and exchange of water in the bay. The tidal residual flow is one of the origins of the permanent current component obtained by the harmonic analysis of flow condition observation data. Other permanent current components include the wind-drive current and the density current.

7.1.5 Wind-Drive Current

Wind-drive current is the flow generated by wind and is an important flow component on the coast and in the inner bay. The wind exerts shear force by friction on the sea surface, and the seawater is dragged to the wind direction. If the sea area is narrow and surrounded by shores, structures, etc., the sea surface in the leeward side rises, and the sea surface in the windward side decreases and causes a slope on the sea surface. This slope on the sea surface acts to press the seawater to the lower sea surface side, thus leading to the generation of vertical return flow to the wind direction on the surface layer and to the opposite direction of the wind in the bottom layer.

If the sea area is broad and the wind-drive time is long, the effect of earth rotation (the Coriolis force) against the generated flow becomes hard to ignore. The force to deflect the flow to its right direction acts in the northern hemisphere and the seawater flows deflecting to the right direction of wind (Ekman wind-drive current). When wind blows constantly for a long time on the borderless ocean of uniform density, the flow is displaced to the right as the depth from the sea surface increases, the velocity is rapidly reduced, and the Ekman spiral flow is generated.

7.1.6 Density Current

Density current is the flow generated by the pressure gradient owing to the uneven distribution of seawater density. The density of seawater is determined by the salt content and the water temperature. On the coast, the uneven distribution of salt content due to the inflow of fresh water from rivers and other factors, the inflow of oceanic water from beyond the bay, and the pressure gradient due to the uneven distribution of water temperature in the shallow sea area by insolation, heat dissipation, etc., drive the density current.

In the inner bay, the low-density river water flows in from the land side, and the high-density seawater flows in from the ocean. This type of inflow causes an unbalanced pressure field, and a flow to coordinate the density field is generated to cancel the imbalance. Light water flows out of the bay on the surface layer, and heavy water flows toward the bay in the bottom layer. This is called estuarine circulation.

7.1.7 Nearshore Current

Nearshore current is the flow generated by the coastal topography and the wave transformation. The water particles of the progressive waves move almost elliptically, but their orbit does not close in one wave period but shifts little by little to the direction of movement of the waves. The movement of water mass from the sea surface to the seabed during this one wave period is called the mass transport by waves and increases with wave shoaling. The seawater pushed to the shore direction by the mass transport of the waves progressing toward the shore increases the mean water level near the shore line (wave setup). The spatial uneven distribution of the increase in mean water level forms the nearshore current system, such as longshore currents, along the shore line and the rip current of converged longshore currents flowing out offshore.

7.2 Fluid Force Due to Currents

(1) General

The fluid force due to currents acting on members and facilities in the water or near the water surface, such as a pile-supported structure (e.g., a piled pier, a pipeline, or armor material of a mound), is proportional to the square of the flow velocity. It may be divided into the drag force acting in the direction of the current and the lift force acting in the direction perpendicular to the current. Also note that a thin, tube-like object in the water may be subject to vibrations excited by induced vortices.

① Drag force

Drag force is generally calculated using the following equation:

$$F_D = \frac{1}{2} C_D \rho_0 A U^2 \quad (7.2.1)$$

where

F_D : drag force acting on the object in the direction of the current (N)

C_D : drag coefficient

ρ_0 : density of water (kg/m³)

A : projected area of the object in the direction of the current (m²)

U : flow velocity (m/s)

② Lift force

Lift force is generally calculated using the following equation:

$$F_L = \frac{1}{2} C_L \rho_0 A_L U^2 \quad (7.2.2)$$

where

F_L : lift force acting on the object in the direction perpendicular to the current (N)

C_L : lift coefficient

A_L : projected area of the object in the direction perpendicular to the current (m²)

(2) Drag Coefficient

The drag force due to currents is expressed as the sum of the surface resistance due to viscosity, and the shape resistance due to pressure is expressed generally in **equation (7.2.1)**. The drag coefficient varies according to the shape and roughness of the object, the direction, and the Reynolds number of the current. Therefore, the value that is appropriate to the conditions in question must be used.

When the Reynolds number is greater than 10³, the values listed in **Table 7.2.1** may be used as standard values for the drag coefficient. Note that for a circular cylinder or sphere with a smooth surface, the value of the drag coefficient decreases suddenly when the Reynolds number is approximately 10⁵. However, for a circular cylinder with a rough surface, this decrease in drag coefficient is not particularly large, and the drag coefficient settles down to a constant value that corresponds to the relative roughness. The data for the cube have been obtained from wave force experiments performed by Hamada, Mitsuyasu, and Hase²⁾. The values for rectangular cylinders and L-shaped members placed diagonally to the current can be found in Ref. ³⁾.

(3) Lift Coefficient

Similar to the drag coefficient, the lift coefficient varies with the shape of the object, the direction of the current, and the Reynolds number, but these values are not well known.

(4) Current Force Acting on the Coping of Submerged Dike at the Opening of Tsunami Protection Breakwater

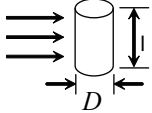
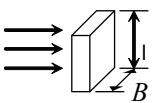
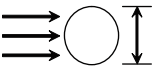
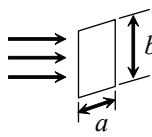
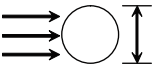
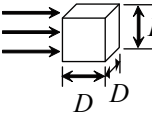
For the current force acting on the coping of the submerged dike at the opening of tsunami protection breakwater, Iwasaki et al.⁴⁾ measured the pressure and obtained a value of 0.84 for the drag coefficient and a value of 0.48 for the lift force coefficient. Tanimoto et al.⁵⁾ performed similar measurements and obtained values of 1.0 to 1.5 for the drag coefficient and 0.5 to 0.8 for the lift coefficient. They have also indicated that when the flow velocity in the breakwater opening is large, the effect of the water surface gradient causes the coefficient values to increase. Sakunaka and Arikawa⁶⁾ conducted a plane experiment of the opening of breakwater and a reproduction calculation by using the numerical wave flume Cadmas-Surf/3D and indicated that Cadmas-Surf/3D can enable the calculation of the experimental values of horizontal pressure and uplift with a 10% to 30% error range. Furthermore, the Isbash formula can be used to determine the initial movement of armor blocks.

(5) Vibration Due to Vortex

Care should be taken because vibration perpendicular to the flow may be generated by the vortex behind a thin member and others by the action of flow. This is because the lift force by vortex varies periodically and because a resonant state is induced when the period come close to the natural period of the member. The period of vortex

generation can be calculated from the diameter of the member, the flow rate, and the Strouhal number. A long natural vibration period necessitates a vibration-proof countermeasure.

Table 7.2.1 Drag Coefficients

Object shape	Standard area	Drag coefficient
Circular cylinder (rough surface) 	Dl	1.0 ($l > D$)
Rectangular cylinder 	Bl	2.0 ($l > B$)
Circular disk 	$\frac{\pi}{4} D^2$	1.2
Rectangular plate 	ab	<i>When</i> $a/b=1$ 1.12 " " 2 1.15 " " 4 1.19 " " 10 1.29 " " 18 1.40 " " ∞ 2.01
Sphere 	$\frac{\pi}{4} D^2$	0.5–0.2
Cube 	D^2	1.3–1.6

7.3 Estuarine Hydraulics

[Public Notice] (Estuarine Hydraulics)

Article 11

The influence of estuarine hydraulics shall be assessed with appropriate methods by taking into account the river flow on the basis of measured values or estimated values.

[Interpretation]

7. Setting of Natural Conditions

(4) Items related to the flow of water (Article 6 of the Ministerial Ordinance and the interpretation related to Article 10 to 12 of the Public Notice)

② Effect of Estuarine Hydraulics

The effects of estuarine hydraulics include tides in rivers, river runoff, density currents at the river mouth, waves entering into the river mouth, and siltation. Their evaluation shall be performed appropriately by considering the action from the seaside on estuaries and also the freshwater and sediment discharge variations from rivers due to flood and drought.

7.3.1 General

The range of estuarine hydraulics to be defined is not necessarily clear. If it is broadly taken as the area over which fresh water and sea water are mixed, this area is a large area that extends from the limit of tidal influence in the upstream river to the mouth of the bay. However, from the viewpoint of actions and effects related to port facilities, the estuarine area is generally defined as extending from the upstream point where salt water reaches by mean tidal motion to the front portion of the estuarine terrace that is composed mainly of sand deposited during floods (hereafter, this will simply be called the estuarine areas). In the estuarine area, in addition to actions such as tidal currents, tide motion, waves, and wave induced nearshore currents, river current fluctuations, such as the outflow of river flood or drought, also occur. There are complex hydraulic and sediment transport phenomena such as density currents represented by vertical circulations and such as chemical flocculation and settlement. In an estuarine area, organisms live in an environment that is affected by physical and chemical actions, and the natural environment and biological environment in the estuarine area can easily be influenced by human activities. Therefore, the development of facilities requires sufficient analysis of the impacts and the continuous monitoring of such influences on the area.

7.3.2 Flow in an Estuary

(1) Tidal Motion, Waves, and Water Currents in an Estuary

In an estuary, complex hydraulic phenomena exist because of the mixture of actions from the sea area, such as tidal level fluctuation and tide currents due to tide motion, water level rise due to waves, fluctuation of nearshore currents, and action from the river. There are still many issues to be resolved to take all of these factors into account in calculating the current field. However, with regard to the intrusion of tidal currents into river channels due to factors such as river bed slope and fresh water discharge, the duration of flood tide is shorter and that of ebb tide is longer, generally; therefore, the maximum and minimum values of the current velocity and discharge occur later than the times of the highest and the lowest water. These various phenomena vary in time and space in accordance with the location of the river mouth, its shape, and the hydraulic parameters of the river and outer sea. In general, the current at the river mouth can be characterized as follows:

- ① The downward current is dominant under higher fresh water discharge through the river and the current is assumed as a uniform flow when it behaves as the gradient current.
- ② When the fresh water discharge is normal condition, the water flow becomes complicated because tidal currents and density currents are superposed onto the gradient current.
- ③ During times of drought, the tidal current characteristics becomes dominant. However, in estuaries where the tidal range is small (e.g., the coast of the Sea of Japan), the tidal current is not strong even during periods of drought and the density current characteristic is intensified.

- ④ In estuaries where the tidal range is large (e.g. the coast of the Pacific Ocean), the tidal current is dominant.

(2) Density Currents at the River Mouth

In an estuary, where river water meets sea water, the sea water penetrates the lower layer of the river water owing to the difference in their densities, and they flow and mix to achieve dynamic equilibrium. These flows are called "density currents at the river mouth" or estuarine circulation. They are divided into three main types, namely, weakly mixing, moderate mixing, and fully mixing, depending on how the density layers form in the river water and sea water. However, even in the same river estuary, the flow field changes according to the change in seasonal or temporal hydraulic conditions, such as river flow rate and tidal phase, and topographical conditions.

① Weakly mixing type

This is a type wherein river water flows down in the upper layer and the wedge-shaped sea water invades the upstream in the lower layer, the river water and the sea water hardly mix, and there is a clear boundary plane where the abrupt density change exists. This type of estuary is generally observed in the river mouth on the coast of the Sea of Japan where the tidal range is small compared to the river flow rate.

② Moderate mixing type

This type appears when the tidal flow slightly increases compared with the river flow. The river water and sea water mix relatively well in this type, and the density gradient appears in the directions of flow down and water depth. This type is generally seen in inner bays on the coast of the Pacific Ocean.

③ Fully mixing type

This type occurs when the tidal flow is quite strong compared with the river flow, and they are mixed by the strong turbulence caused by tide movement. The density will be uniform in the vertical direction, and the distribution of salinity concentration becomes a function of location from the river mouth only. This type is seen in the Chikugo River in the Ariake Sea, at the mouth of the Rokkaku River, and so on.

(3) Waves Entering into a River Mouth

When waves enter an estuary, the waves are transformed by the effects of the topography and the river currents. The wave height increases owing to the refraction and concentration caused by the topography of the estuarine terrace and owing to wave shoaling. Wave propagation is disturbed by river currents that flow in the opposite direction to wave propagation increasing wave height. Given that incident waves with heights that have been increased run up in the river channel, they are attenuated by the effects of wave breakings, bottom friction, and turbulent flow. Furthermore, when the river current is extremely fast, the waves are unable to run up against the current.

7.3.3 Siltation

The sediment within the estuary of a bay is mostly mixture of sand and mud that contains small particles of clay and silt. The sediment moves under the action of wave and current and forms characteristic tidal flats, sand spits, river mouth terraces, and bars in the estuary. When the bottom sediment mainly consists of sand particles, the movement phenomenon of the bottom sediment based on wave and current actions is called littoral drift. Furthermore, fine particles such as clay and silt are widely dispersed because they are suspended by the currents and accumulate in calm areas, such as waterways and basins, or in places with slower currents in the harbor. This causes problems for facility maintenance and environmental management in waterways and basins.

The movement and accumulation phenomenon of mud, which include resuspension of fine particles from the seabed and the supply of high density mud from rivers and their transport by waves and currents, are specifically called "siltation". The main difference between "siltation" and "littoral drift" is that mud flocculates by mixing with sea water in the estuary, thus its settling characteristics are significantly variable. Moreover, it should also be noted that when considering the deposition due to siltation, a transport form called fluid mud, which moves as a gravitational flow along the inclined sea bottom, may occur under a condition with densely concentrated mud before being consolidated. Therefore, it is necessary to examine a numerical simulation⁷⁾ for siltation predictions by using a model that considers the characteristics of such siltation transport form for the siltation phenomenon of navigation channels and basins where a bottom sediment mainly consists of clay and silt.

Furthermore, the mud that is deposited at the bottom of the sea is capable of changing into harder sediment via consolidation over a long period. Their ability to be resuspended by the action of waves and currents is affected by factors such as mud characteristics, salinity of the sea water, particle size, water content, and organic material content, all of which change with time after deposition (degree of consolidation). These characteristics of mud make it difficult

to solve the problems caused by siltation. Moreover, if the strength of mud increases in the vertical direction from a high water content condition near the surface to consolidated mud in deeper layer owing to the characteristics of the time history of deposited mud, it is necessary to note that there is a difference between the result of sounding with an echo sounding equipment and the result with a lead sounding ⁸⁾.

7.4 Littoral Drift^{9) 10) 11) 12) 13) 14) 15)}

[Public Notice] (Littoral Drift)

Article 12

The influence of littoral drift shall be assessed by appropriate methods based on measured values or estimated values.

[Interpretation]

7. Setting of Natural Conditions

(4) Items related to the flow of water (Article 6 of the Ministerial Ordinance and the interpretation related to Article 10 to 12 of the Public Notice)

③ Effect of Littoral Drift

The evaluation of the effect of littoral drift appropriately takes into account seasonal and annual changes in topography due to such factors as sediment grain size, threshold depth of sediment movement, longshore sediment transport rate, predominant direction of longshore sediment transport and cross-shore littoral drift.

7.4.1 General

Littoral drift refers to either the phenomenon wherein the sediment composed mainly of sand on a sea coast and a lakeshore is moved by the actions of some forces such as waves and currents, or the material itself is moved by the above processes. Although the movement of sand by wind and the sand itself that is thus moved is referred to as windblown sand, in the broad definition littoral drift is also considered to include windblown sand at beaches. When port facilities are affected by the littoral drift phenomena, the characteristic values of littoral drift shall be established appropriately for sediment grain size, threshold depth of sediment movement, longshore sediment transport rate, and predominant direction of longshore sediment transport.

Sediment that forms a beach is supplied from nearby rivers, coastal cliffs, and adjacent coastline. The sediment is exposed to the actions of waves and currents during the supply process or after it has accreted on the beach, hence the sediment property reflects the characteristics of external forces such as waves and currents (Refer to **Part II, Chapter 2, 7.4.3 Characteristics and Distribution of Bottom Sediment**). This is referred to as the sediment sorting action by external forces.

When waves approach a coast from offshore, the movement of water particles near the sea floor does not have the force to move the sediment in places with sufficient water depth. However, at a certain water depth, the sediment begins to move. The water depth at the boundary where the sediment begins to move is called the threshold depth of sediment movement (see **Part II, Chapter 2, 7.4.4 Form of Littoral Drift Movement**). Sato¹⁶⁾ studied the movement of sediment by placing radioactive glass sand on the sea floor and by investigating the distribution of their movement. He defined two conditions: the surface layer sediment movement threshold and the total sediment movement threshold. He applied the former term to the situation in which sand in the surface layer on the sea floor is moved collectively in the direction of wave movement. He applied the latter term to the situation wherein sand shows striking movement with a distinctly visible change in water depth.

Given that a natural beach is repeatedly subjected to the process of erosion when storm waves attack and the process of accretion during periods when waves are moderate, a natural beach achieves a relatively balanced topography over a long period. This balance may be lost after a reduction in the supply of sand due to river improvements, changes in sand supply conditions following the construction of coastal structures, and changes in external forces such as waves and currents. Beach deformation will then occur as the beach moves toward new equilibrium conditions. When building structures such as breakwaters, groins, detached breakwaters, and training jetties, careful attention should be paid to the changes that will be caused by construction works in the balance of the beach. Topographical changes that might be induced by a construction project should be sufficiently investigated in advance. Furthermore, careful attention should be paid to the deformation conditions of the beach both during construction and after the completion of any structure, and appropriate coastal protection countermeasures are recommended to be taken when there are concerns about the possibility of a disaster triggered by coastal erosion.

Littoral drift parallel to the coastal line is called longshore sediment transport. Longshore sediment moves in either the right or left direction along a coast, corresponding to the direction of incoming waves. The direction with the larger

volume of movement during a year is called the predominant direction. In the long term, the topographical changes due to longshore sediment transport are often irreversible. For example, considering topographical changes near a groin, if waves come in from the right side (looking out toward the sea from the coast), there will be accumulation and erosion on the right and left sides of the groin, respectively. If the waves originate from the left side, the opposite topographical change occurs. By taking the direction perpendicular to the coastline as a standard, the energy of the waves originating from the right for most coasts is not equal to the energy of the waves coming in from the left, but one of them usually predominates. For example, if the average energy of the waves originating from the right is larger than that of the waves originating from the left, even though the right side of the groin sees repeated accumulation and erosion the amount of accumulation will grow eventually, and erosion will increase on the left side of the groin. Therefore, topographical changes due to longshore sediment transport are considered irreversible. It is desirable to first understand the predominant direction of the longshore sediment transport for that coast, as well as the longshore sediment transport rate, to estimate the degree of coastal deformation in that area if facilities are built.

7.4.2 Coastal Topography

① Terminology for various sections of a beach profile

The typical sections of a sandy beach are defined with the terminology shown in **Fig. 7.4.1**. The "offshore" is the area on the most offshore side where normal waves do not break, and the bottom slope is comparatively gentle in many cases. The "inshore" refers to the area between the landward boundary of the offshore and the ebb tide shoreline, where waves break and cross shore topography as longshore bars or steps are formed. The "foreshore" is the zone from the ebb tide shoreline to the location where waves will reach normally, and the "backshore" is the zone from the landward boundary of the foreshore to the coastline, where waves will reach during stormy weather with the rise in water level.

The names shown along the top row of **Fig. 7.4.1** classify regions based on the types of wave and sediment movement. In the surf zone, the sediment is suspended due to the action of large eddies generated by breaking waves and is carried in high concentration suspended sand. For the littoral drift in the swash zone, when the wave is uprush, the sand is lifted up and carried by the agitation at the front edge of the running-up waves. However, when the wave is in downwash, the agitation on the sea bottom predominates and the sediment is carried as bedload.

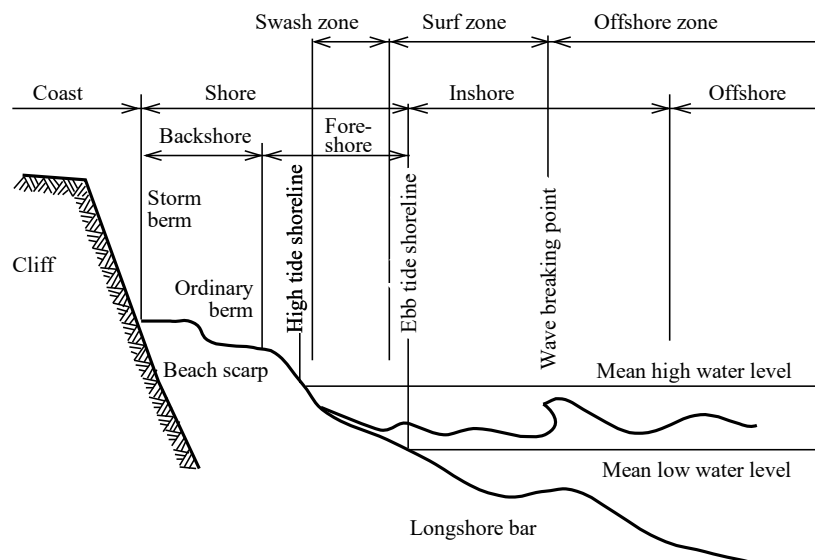


Fig. 7.4.1 Terminology of the Beach Profile¹⁵⁾

② Horizontal Forms of Sandy Beaches

A longshore bar is one of the most distinctive topographical features of a sandy beach. When viewing the shape of a longshore bar horizontally, it is roughly classified into either ①long and linear (roughly parallel to the shoreline, as in **Fig. 7.4.2 (a)**) or ②a repeating arch (**Fig. 7.4.2 (b)**). In particular, the latter type of longshore bar is called a crescentic bar. Furthermore, the longshore bar often forms multiple stages in a sequence leading out to sea; in this

case, it exists on a large scale as an offshore longshore bar. According to **Fig. 7.4.3**, which shows the relation between the water depths at the crest and the trough of longshore bars, their ratio is 1.3 to 1.5.

When an arc-shaped longshore bar is formed, the shoreline often shows periodic longshore undulation in the same phase as that of the longshore bar (**Fig. 7.4.2 (b)**). This undulation of the shoreline does not have any official name but is referred to as cusp or shoreline rhythm^{11) 17)}. The mean distance perpendicular to the shoreline between the most onshore side and most offshore side on one arc of the rhythmic topography is 15 m and the maximum distance is at most around 50 m.

In addition to the periodic longshore undulation described above, there is rhythmic topography with a wave length of several meters to several tens of meters called cusp near the shoreline. **Fig. 7.4.4** shows that the cusp is the topography formed by the repeated wave actions of swash and backwash on the shore. This cusp is the wavelike topography formed along the edge of the rhythmic topography of the shoreline corresponding to the abovementioned longshore bar and is often observed near shorelines.

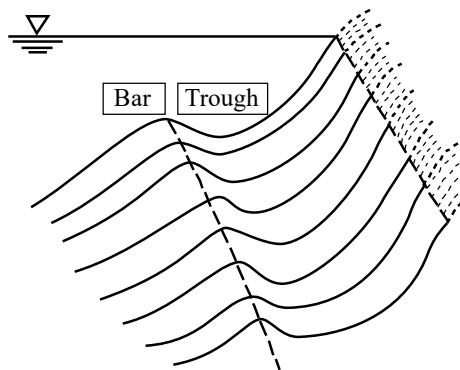


Fig. 7.4.2 (a) Longshore Bar Parallel to the Shoreline

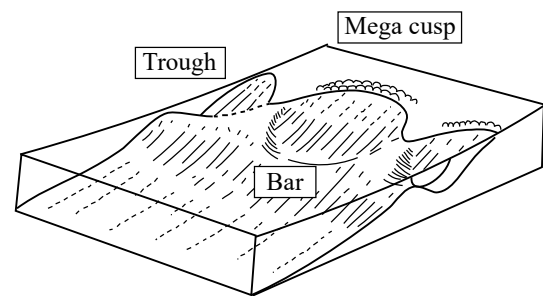


Fig. 7.4.2 (b) Crescentic Bar¹¹⁾

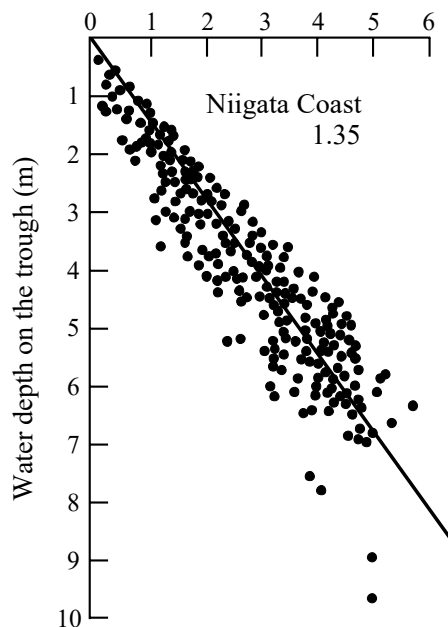


Fig. 7.4.3 Relation between the Water Depth at the Tip of Longshore Bars and the Water Depth on the Trough¹¹⁾

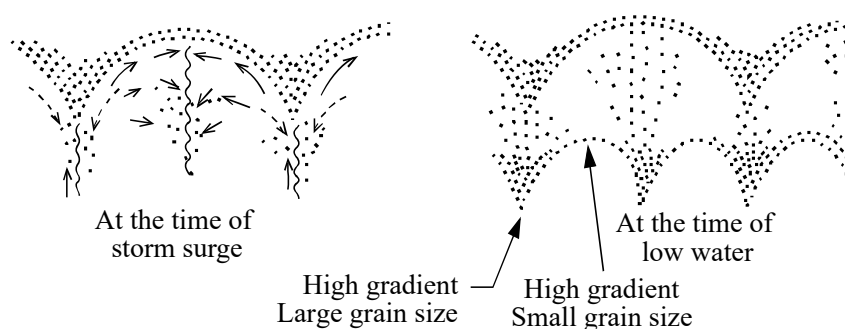


Fig. 7.4.4 Shape of the Cusp¹¹⁾

③ Foreshore topography

As shown in Fig. 7.4.5, when there is continued calmness, a nearly horizontal area or sometimes slanting one toward the land forms in the foreshore, somewhat higher than the high tide level. This topography is called a berm. When conditions are rough, the berm is eroded, thus forming a sandbar called an inner bar near the position of the last breakers. Inner bars dissipate the wave energy when waves break upon them and are thought to prevent the further erosion of the foreshore. The sediments of the inner bars that form during rough conditions gradually return to the foreshore when it is calm, and the foreshore eventually returns to its condition prior to the rough period. The change in the shoreline at this time is described in Part II, Chapter 2, 7.4.8 Topographical or Shoreline Deformation in the Swash Zone.

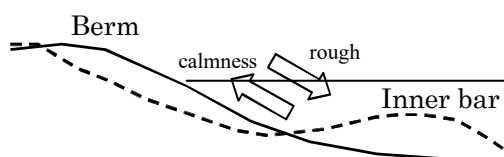


Fig. 7.4.5 Foreshore Topography

④ Other special topography on natural beaches

(a) Tombolo

A relatively calm water area is formed behind offshore islands, ledges, detached breakwaters, etc. A current from an exposed area to a sheltered one is generated, and the sand carried by the current deposits in the sheltered area to form a tongue-shaped topography moving shoreline offshore (Fig. 7.4.6). This tongue-shaped topography connected to an island or others is called Tombolo.

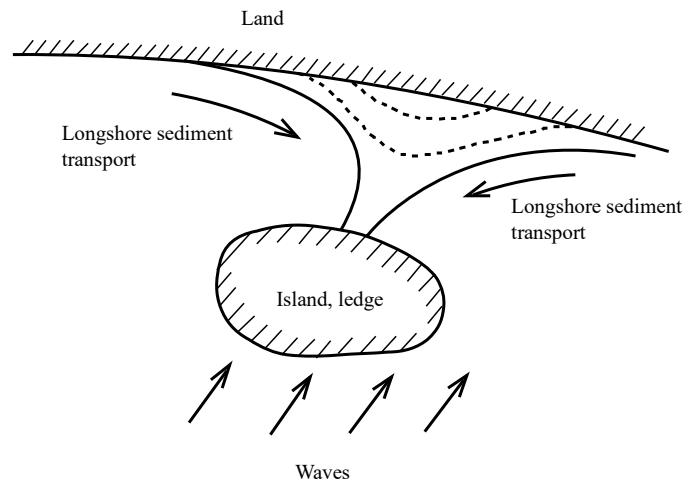


Fig. 7.4.6 Formation of a Tombolo

(b) Sand spit

The sand spit is a sandbar that is grown perpendicular to the shore formulated by the accumulation of sand drifted with longshore currents. A sand spit tends to grow at such a location as near a cape where the shore direction changes significantly (**Fig. 7.4.7**). Its tip slightly curves toward the inner bay in general, and its foreshore slope is larger on the ocean side. Typical examples in Japan include Miho-no-Matsubara, the Notsuke Peninsula in Hokkaido and Ama-no-Hashidate.

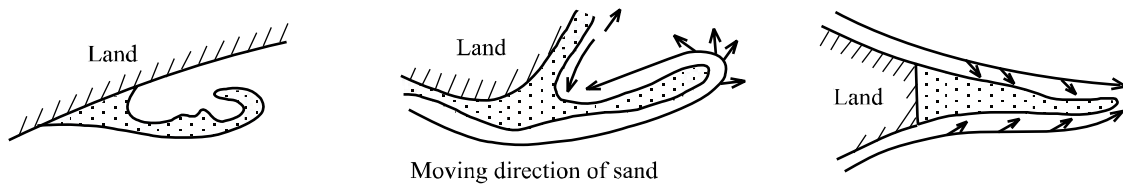


Fig. 7.4.7 Formation of Sand Spit

(c) River mouth bar

The river mouth bar is a bar formed (**Fig. 7.4.8**) by accumulation of sediment near the river mouth discharged through the river or by littoral drift pushed into the river mouth by waves. The intrusion of seawater and the flood of river water make the hydraulic condition at the river mouth complicated and the topography unstable.

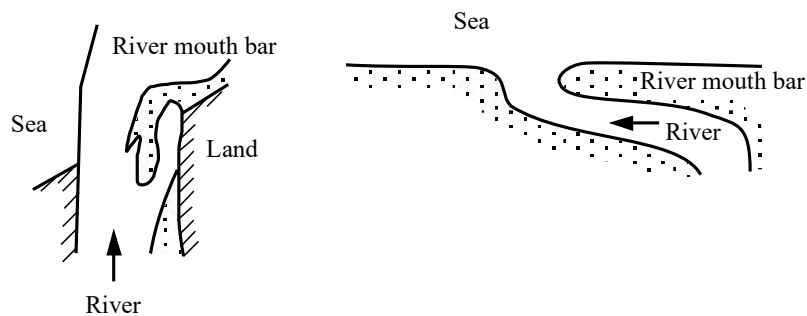


Fig. 7.4.8 Development of a River Mouth Bar

(d) Sand wave

Sand wave is the generic name of the wavelike topography that develops on the surface of sand bed in a broad sense and includes sand ripples of approximately several centimeters to several tens of centimeters in wave length and several centimeters in wave height. In a narrow sense, it indicates that a large-scale wavelike topography of approximately several meters to several hundred meters in wave length and 1 m to 30 m in wave height formed on the seabed or at the river mouth. **Fig. 7.4.9** shows an echo sounding record of a sand wave existing on the seabed of the Bisanseto in the Seto Inland Sea¹⁸⁾.

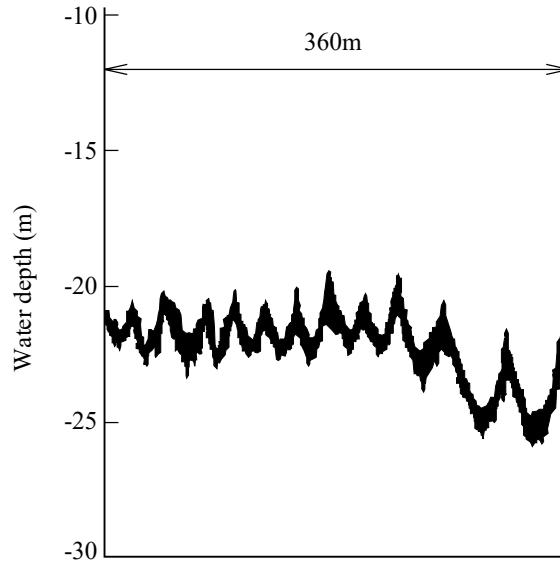


Fig. 7.4.9 Echo Sounding Record of a Sand Wave¹⁸⁾ (Bisan Seto)

(e) Sea cliff^{19) 20)}

A cliff coast made of soft rocks is easily eroded by waves and the accompanying movement of pebbles. This type of erodible cliff is called a coastal cliff, and the collapsed sediment supplies littoral drift. Typical examples in Japan include Byobugaura in Chiba Prefecture²¹⁾, Enshu-Atsumi Coast in Aichi Prefecture, Joban Coast in Fukushima Prefecture, and Tokachi and Nozuka Coasts in Hokkaido.

7.4.3 Characteristics and Distribution of Bottom Sediment

① The grain size characteristics of the bottom sediment are generally shown with the following indices:

- (a) Median diameter (d_{50}): the grain size corresponding to 50 % of the cumulative mass ($p = 50\%$) of the cumulative grain size distribution curve

$$(b) \text{ Mean grain size } (d_m): \quad d_m = \frac{\sum_{p=0}^{100} d_p \Delta p}{\sum_{p=0}^{100} \Delta p} \quad (7.4.1)$$

$$(c) \text{ Sorting coefficient } (S_0): \quad S_0 = d_{75} / d_{25} \quad (7.4.2)$$

$$(d) \text{ Deflection distortion } (S_k): \quad S_k = d_{75} \times d_{25} / (d_{50})^2 \quad (7.4.3)$$

where

p : cumulative percentage (%)

Δp : increment of the cumulative percentage

d_{25} : grain size corresponding to the cumulative percentage (25%)

d_{75} : grain size corresponding to the cumulative percentage (75%)

② Grain Size Distribution of the Bottom Sediment in the Cross Section Perpendicular to the Shoreline

Fig. 7.4.10 shows the survey result of the grain size distribution in the bottom sediment of the cross section perpendicular to the shoreline of the US Pacific coast²²⁾ and shows the sorting situation of the bottom sediment in the cross section. This figure shows the distribution of grain sizes by setting the mean grain size as 100% at a selected foreshore point as standard point, which is easily subjected to wave actions at a mean tide level. In general, this distribution has two peaks: the offshore side and the onshore side across the standard point. One peak is located at the shallowest wave breaking point, and the other peak is located at around the center of the ordinary berm, which is between the foreshore and backshore (Fig. 7.4.1).

The grain size of the bottom sediment near the shoreline greatly affects the foreshore gradient. A coarser bottom sediment corresponds to a steeper gradient of the foreshore.

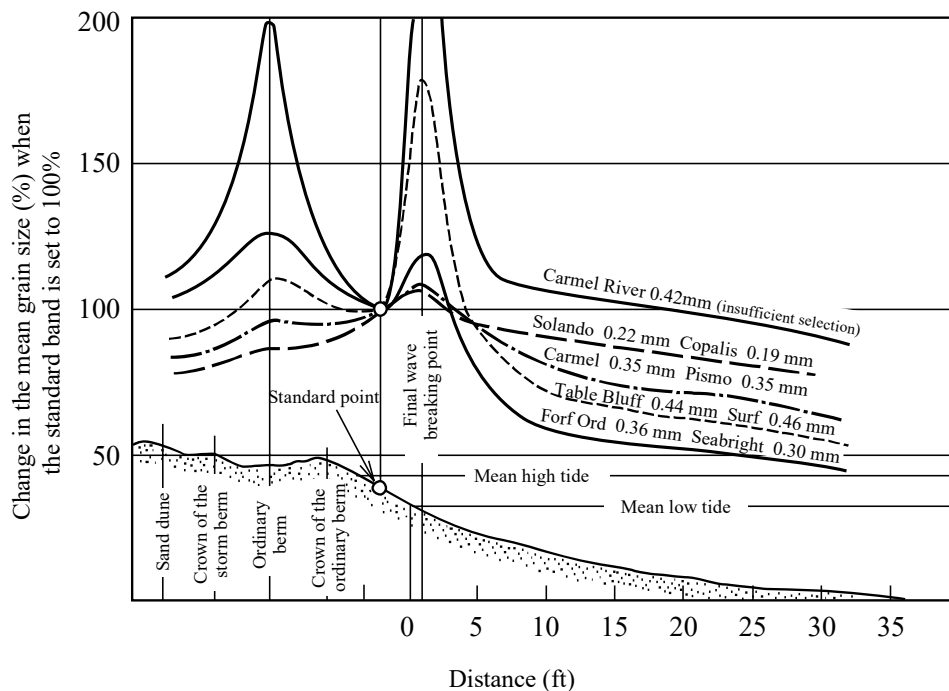


Fig. 7.4.10 Change in the Mean Grain Size on the Cross Section Perpendicular to the Shoreline²²⁾

③ Grain Size Distribution of the Bottom Sediment in the Longshore Direction

The grain size characteristics of the bottom sediment also change in the longshore direction. Among the sediment components supplied from rivers or coastal cliffs, the coarser gravel remains near the point of sediment source and the finer fractions are carried farther. Fig. 7.4.11 shows the spatial distribution of the median diameter on the seabed in front of the mouth of the Yoshino River with the contour of sediment diameter²³⁾. The largest grain size appears near the left bank at the mouth (a sounding-map comparison indicates that this portion is the deepest part of the channel). From the area, the median diameter decreases toward every direction of the sea area. The isoline ($d_{50} = 0.15$ mm) surrounding the river mouth shows onshore retreat most at the slightly right bank at the river mouth and extends to the right and left shores. These features almost correspond to the direction of movement of the littoral drift that was comprehensively estimated from the seabed topography, predominant wave direction, change in river mouth bar, movable bed model experiment, and others.

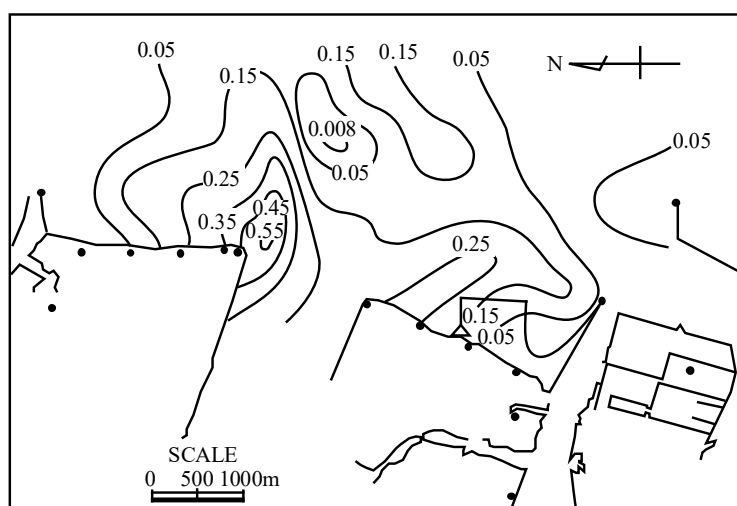


Fig. 7.4.11 Planar Distribution of the Grain Size of the Bottom Sediment in Front of the Mouth of the Yoshino River (Unit in the Figure: mm)²³⁾

④ Mineral composition and heavy mineral analysis of the bottom sediment

The sand on the beach mainly comprises feldspar (specific gravity: 2.5 to 2.9) and quartz (specific gravity: 2.65 to 2.69) but contains some other heavy minerals with a specific gravity of three or more. There are several types of these heavy minerals, and the most commonly seen are five kinds of iron ore, hypersthene, augite, brown amphibole, and green amphibole. When several rivers flow into a shore, if the kinds of heavy minerals in the bottom sediment discharged from the rivers are different, the analysis of heavy minerals of the bottom sediment around the beach and river can provide the direction of the littoral drift.

7.4.4 Form of Littoral Drift Movement

Littoral drift is classified into three categories, namely, bedload, suspended load, and sheet flow, according to the modes of sediment movement.

- ① Bedload: littoral drift that moves by tumbling, sliding, or bouncing along the surface of the sea floor via the direct action of waves and currents
- ② Suspended load: littoral drift that is suspended in seawater by turbulence of breakers and others
- ③ Sheet flow: littoral drift that moves as a layer of high-density flow near the bed surface

Shallow water zones can be classified into three regions (**Fig. 7.4.12**) depending on the physical properties of waves that provide the external forces for the littoral drift phenomenon. The dominant mode of littoral drift movement in each region is as follows:

[Offshore zone] In order for sand to be moved by the action of fluid motion and oscillatory movement, the current velocity of the fluid must exceed a certain value. This condition is generally called the "threshold of movement." For littoral drift, the threshold of movement is defined with the water depth called the threshold depth of sediment movement. When the water depth is shallower than the threshold depth of sediment movement, regular and small undulating topographic contours called sand ripples will form on the sea bottom surface. When sand ripples form, vortices are generated by the fluid motion in the vicinity of the sand ripples, and the movement of suspended sediment trapped in the vortices occurs. As the water depth becomes shallower, sand ripples are extinguished, and a sheet flow condition occurs in which sediment moves in stratified layers extending several layers below the sea bed surface.

[Surf zone] Inside the surf zone, the high-density suspension of sediment is formed by the severe agitation and action of large-scale vortices generated by breakers. The volume of sand that moves near the seabed surface in a bedload state also increases. For convenience, the sand movement inside the surf zone is divided into two components; one is called the longshore sediment transport, which moves parallel to the shoreline, and the other is called the cross-shore sediment transport, which is perpendicular to the shoreline. Although the time frame for the beach deformation caused by longshore sediment transport is long, the time frame for cross-shore sediment transport is relatively short (i.e., from a few days to approximately one week), similar that for periods of storms passing.

[Swash zone] The sand movement in a swash zone differs for the times of wave runup and downflow. During the time of wave runup, sand is placed in suspension by the agitation at the front of a wave and is transported by running-up water. During the downflow, sand is carried in bedload mode.

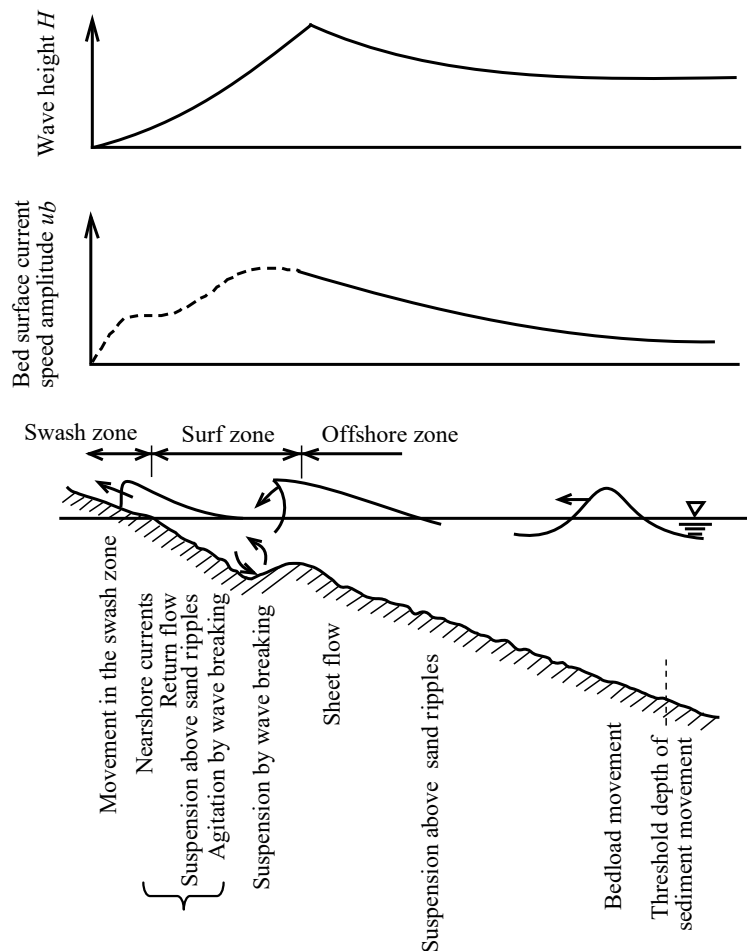


Fig. 7.4.12 Changes in Sediment Movement Modes in Cross-Shore Direction¹⁵⁾

7.4.5 Physical Meaning and Estimation Formulas for the Threshold Depth of Sediment Movement

With respect to the threshold depth of sediment movement, which is required to determine the extension of breakwater or the water depth at the head and offshore boundary of beach deformation, Sato and Tanaka^{16) 24)} conducted a number of field surveys by using radioactive glass sand as a tracer. On the basis of their observed results, they defined the littoral drift movement conditions as follows.

Surface layer sediment movement: As shown in **Fig. 7.4.13 (a)**, the elongation of the isometric lines that show the distribution of radioactive glass sand after waves acted upon it on the sea floor demonstrates that all sand has moved in the direction of the waves. However, the location of the highest count remained at the injection point of glass sand, thus indicating no movement. This corresponds to a situation in which the surface layer sand is moved collectively by traction parallel to the wave direction.

Total sediment movement: As shown in **Fig. 7.4.13 (b)**, this refers to a situation in which both the isometric lines and the portion of the highest count move in the wave direction. This corresponds to a situation of distinct sand movement with the result of apparent change in water depth. The threshold depth of total sediment movement is often used as the threshold depth of sediment movement for engineering purposes.

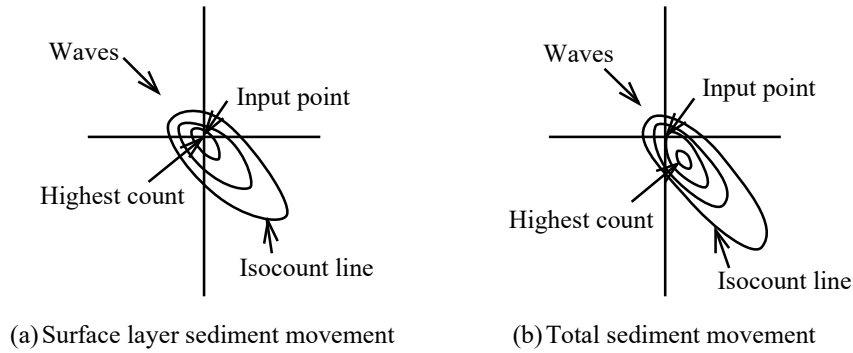


Fig. 7.4.13 Spread of Radioactive Glass Sand in Surface Layer Sediment Movement and Total Sediment Movement

On the basis of the field data, two equations were proposed by Sato and Tanaka for estimating the threshold depth of surface layer sediment movement and the threshold depth of total sediment movement.

① **Threshold depth of surface layer sediment movement**

$$\frac{H_0}{L_0} = 1.35 \left(\frac{d}{L_0} \right)^{1/3} \sinh \frac{2\pi h_i}{L} \frac{H_0}{H} \quad (7.4.4)$$

② **Threshold depth of total sediment movement**

$$\frac{H_0}{L_0} = 2.40 \left(\frac{d}{L_0} \right)^{1/3} \sinh \frac{2\pi h_i}{L} \frac{H_0}{H} \quad (7.4.5)$$

where

L_0 : deepwater wavelength (m)

H_0 : equivalent deepwater wave height (m)

L : wavelength at water depth h_i (m)

H : wave height at water depth h_i (m)

d : sediment grain size, average grain size or median diameter (m)

h_i : threshold depth of sediment movement (m)

Repeated calculations are required to estimate the threshold water depths by using **equations (7.4.4) and (7.4.5)**. Therefore, calculation diagrams such as those in **Fig. 7.4.14 (a) and (b)** have been prepared so that the depths can be easily estimated. By specifying d/L_0 and H_0/L_0 , it is possible to determine h_i/L_0 . Specific calculation examples are shown in Ref. 9).

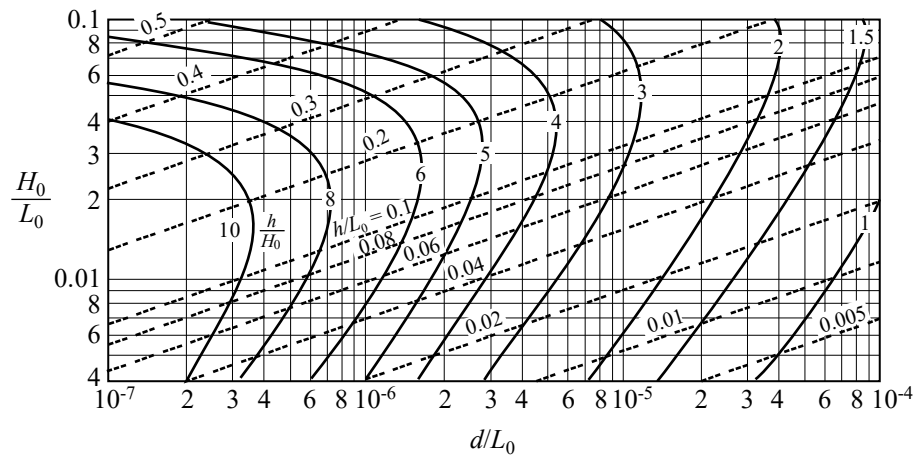


Fig. 7.4.14 (a) Calculation Diagram for Threshold Depth of Surface Layer Sediment Movement⁽⁹⁾

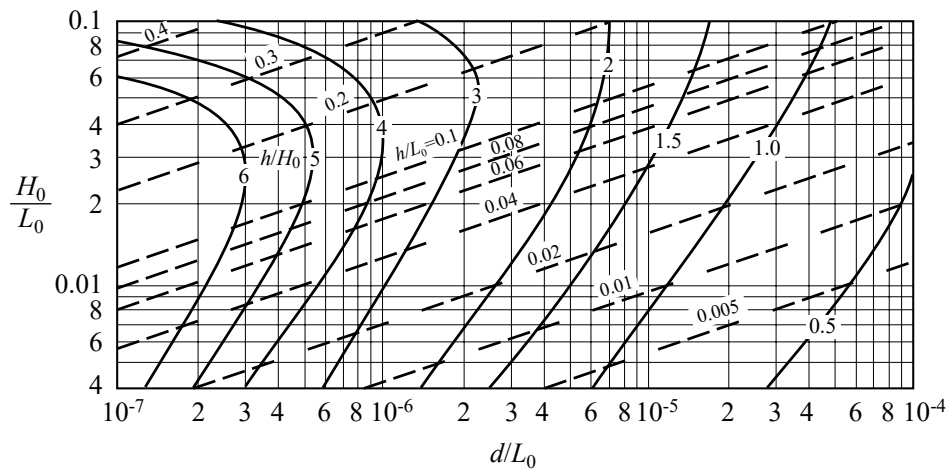


Fig. 7.4.14 (b) Calculation Diagram for Threshold Depth of Total Sediment Movement⁽⁹⁾

7.4.6 Longshore Sediment Transport

① The predominant direction of longshore sediment transport is determined using the following information:

- (a) Topographies of the natural coast and around coastal structures (see **Fig. 7.4.15**)
- (b) Alongshore distribution of the sediment characteristics such as median diameter and mineral composition
- (c) Direction of movement of fluorescent sand tracers
- (d) Direction of incident wave energy flux

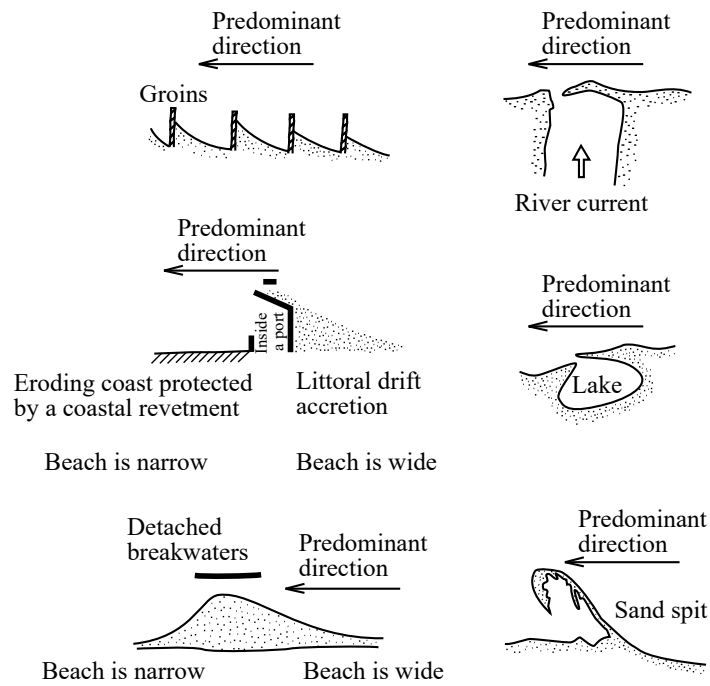


Fig. 7.4.15 Typical Coastal Topography Showing the Predominant Direction of Longshore Sediment Transport

- ② To estimate the longshore sediment transport rate, the following data must be prepared and sufficiently investigated:
- (a) Continuous observation data of the change in sediment volume around a coastal structure
 - (b) Data on the alongshore component of wave energy flux
 - (c) Data concerning the littoral drift rate at the surrounding coast
 - (d) Data on past dredging volume
 - (e) Continuous observation data on deposition volume at the experimental dredging site
 - (f) Data on the volume of movement of tracers, such as fluorescent sand, placed within the surf zone
- ③ Various formulas can be used to estimate an approximate value of longshore sediment transport rate^{9) 25) 26) 27)}. The formulas are normally given in the expression shown in **equation (7.4.6)**, and the coefficient for various formulas is given in **Table 7.4.1**.

$$Q_x = aE_x$$

$$E_x = \sum K_r^2 \left(\frac{n_A w_0 H_A^2 L_A}{8T} \right) \sin \alpha_b \cos \alpha_b \quad (7.4.6)$$

where

- Q_x : longshore sediment transport rate (m³/s)
- E_x : alongshore component of wave energy flux (kN·m/m/s)
- K_r : refraction coefficient between the wave observation point and the wave breaking point
- n_A : ratio of group velocity to wave celerity at the wave observation point
- w_0 : unit weight of sea water (kN/m³)
- H_A : wave height at the wave observation point (m)
- L_A : wavelength at the wave observation point (m)
- T : wave period (s)
- α_b : angle of wave incidence at the wave breaking point (°)

Table 7.4.1 Coefficient a for Longshore Sediment Transport Rate Formula

Savage ²⁶⁾	Sato and Tanaka ²⁵⁾	U.S. Army Corps of Engineers ²⁷⁾
0.022	0.03	0.04

7.4.7 Littoral Drift Phenomena in the Surf Zone

Inside the surf zone, large quantities of sand move by the turbulence caused by breakers, by the increase of the wave orbital velocity near the bottom due to shallower water depth, and by the existence of nearshore currents.

On the basis of the longshore sediment transport rates obtained from studies of fluorescent sand, Komar²⁸⁾ reported that bedload dominates in the surf zone. Sternberg et al.²⁹⁾ reported that most of the longshore sediment transport rate can be explained by suspended load. As a counterpoint to these two conflicting results, Kato et al.³⁰⁾ used fluorescent sand to measure the local sediment transport rates within the surf zone and found that bedload dominates when the velocity of water particle due to waves is small, whereas suspended load dominates when the velocity becomes larger.

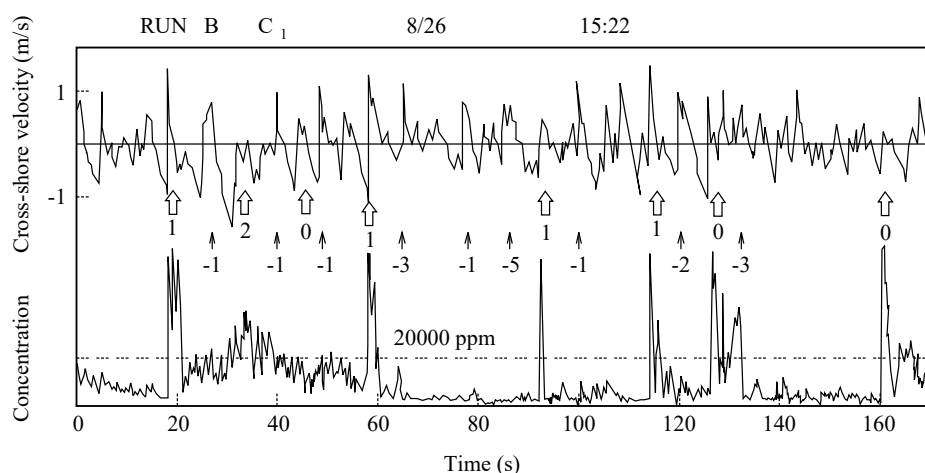
The sediment movement when suspended sediment is predominant can be examined by dividing the movement into two processes.

- ① Sediment suspension process caused by organized vortices formed by wave breaking
- ② Settling process during which sediment is buffeted by random external forces following the breakup of organized vortices

Fig. 7.4.16 shows the temporal variations of suspended sediment concentration and horizontal current velocity measured by Katoh et al.³¹⁾ inside the surf zone in the field. The white arrows in the figure indicate the waves that broke on the seaward side of the observation point, and the black arrows indicate the waves that passed the observation point and broke on the shoreward side. The suspended sediment concentration increased rapidly when waves broke on the seaward side. This result indicates that sediment suspension is related to the organized vortices, particularly obliquely descending vortices³²⁾ that occur after waves break.

The suspended sediment concentration by wave breaking is also related to the type of wave breaking. Kana³³⁾ measured the suspended sediment concentration at the on-site beach and reported that the suspended sediment concentration by plunging wave breaking is approximately 10 times of the suspended sediment concentration by spilling wave breaking.

The bottom sediment suspended by wave breaking is carried to the same direction as the flow by the subsequent flow, i.e., it is carried to the onshore direction by the flow toward the shore just after wave breaking and then to the offshore direction by the flow toward the sea when the next wave trough passes. Therefore, it is carried to the onshore direction if suspended for a short period of time but is carried to the offshore direction if suspended for a long period. Given this situation, Dean³⁴⁾ indicated that the direction of movement of littoral drift at the wave breaking point can be sorted by the ratio of the settling velocity of sand particles to the wave period.

**Fig. 7.4.16** Example of Field Observation of Concentration of Suspended Sediment³¹⁾

7.4.8 Topographical or Shoreline Deformation in the Swash Zone

Horikawa et al.³⁵⁾ investigated the criteria for shoreline advance and retreat due to sand movement in the swash zone on the basis of laboratory experiments and proposed **equation (7.4.7)**, which is also applicable for the field condition.

$$\frac{H_0}{L_0} = C_s (\tan \beta)^{-0.27} \left(\frac{d}{L_0} \right)^{0.67} \quad (7.4.7)$$

where

H_0 : deepwater wave height (m)

L_0 : deepwater wavelength (m)

$\tan \beta$: average bottom slope from the shoreline to a water depth of 20 m

d : sediment grain size (m)

C_s : coefficient

According to **equation (7.4.7)**, a shoreline will retreat when $C_s \geq 18$ (see **Fig. 7.4.17**).

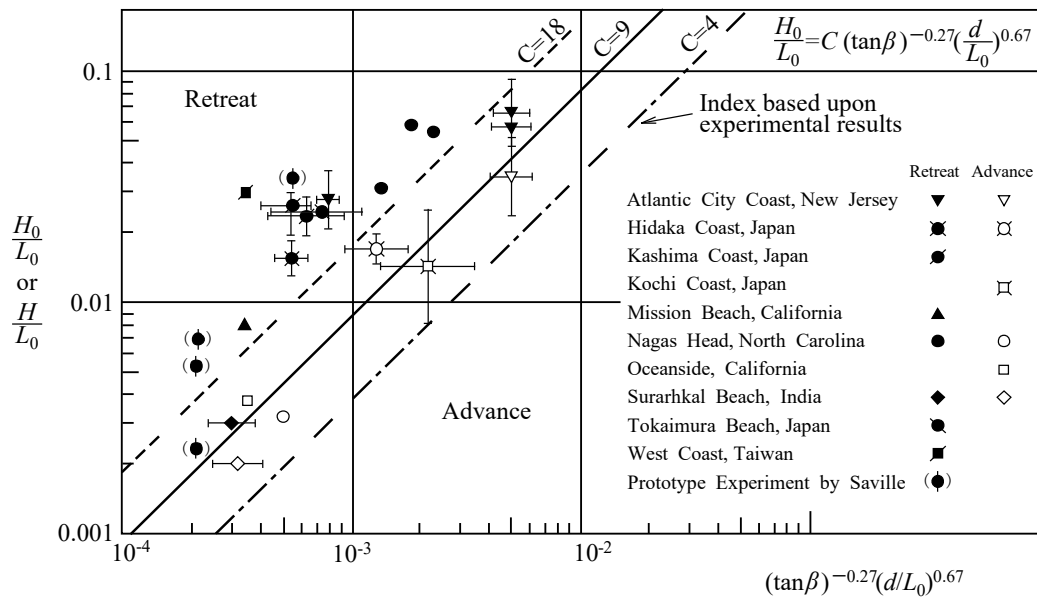


Fig. 7.4.17 Advance and Retreat of Shorelines in the Field³⁵⁾

Katoh et al.³⁶⁾ revised **equation (7.4.7)** by using deepwater wave energy flux and presented a model to predict the daily shoreline change. **Fig. 7.4.18** is a comparison of the predicted and measured results of shoreline location.

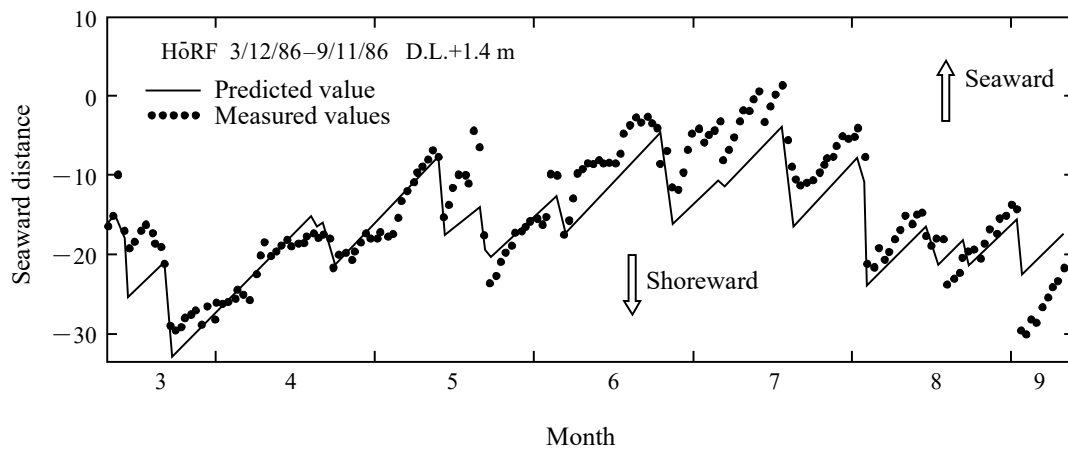


Fig. 7.4.18 Comparison of Prediction and Measurement of Shoreline Location³⁶⁾

7.4.9 Relationship between Foreshore Topographical Changes and Groundwater Level

The topographical changes that accompany the tidal level changes in the foreshore can be explained as follows by using Fig. 7.4.19³⁷⁾. When the tidal level changes, the beach groundwater level also changes as a response. However, because the response of the groundwater level is behind the change of the tidal level, the groundwater level at the flood tide differs from that at the ebb tide even though the tide level is the same. This means that **(a)** during the flood tide, the groundwater level is low, and it is easy for the seawater running up on the beach to permeate underground. Therefore, the sediment carried by the seawater when it runs up on the beach will accrete in this location. **(b)** On the contrary, during the ebb tide the groundwater level is high, and it is difficult for seawater to run up on the beach and to permeate underground. At certain conditions, the groundwater may flow out of the beach surface during the ebb tide. As shown in Fig. 7.4.19, the result is that the sediment that accreted during the flood tide will be eroded and will return to its original location.

When waves run up to a high level on a beach during storms, a high groundwater level condition continues throughout the stormy weather period because the runup seawater permeates into the beach, and the condition becomes that as shown in Fig. 7.4.19 (b). The occurrence of rapid foreshore erosion during such a condition has been confirmed by field data³⁸⁾.

Some shore protection methods make use of this relationship between the foreshore groundwater level and sand movement, i.e., lowering the groundwater level by forced means or gravity to prevent erosion. In the method making use of gravity, a highly water-permeable layer is installed in the foreshore sand to cause the groundwater flow down offshore of the foreshore and to lower the groundwater level. With this method it is possible to preserve beach conditions that are very close to those of a natural beach in appearance because no structures are laid above the beach floor³⁹⁾.

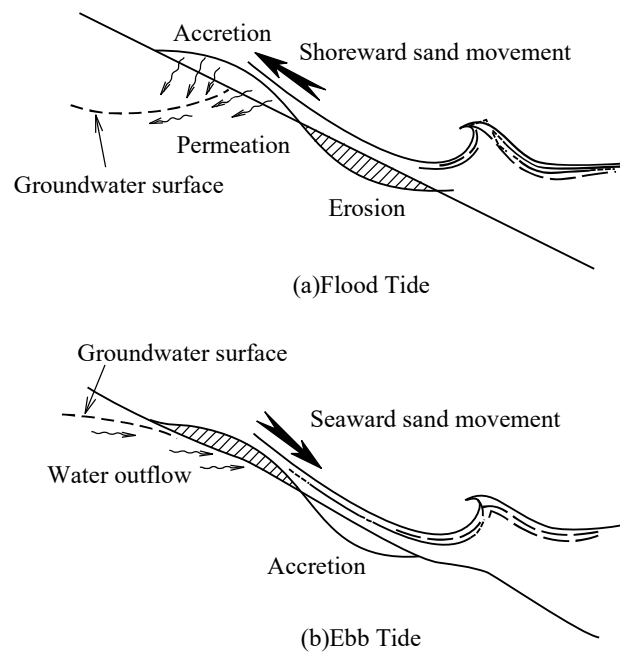


Fig. 7.4.19 Relationship between Foreshore Topographical Changes and Groundwater Level³⁷⁾

7.4.10 Movement of Longshore Bars

Longshore bars form periodically and move offshore⁴⁰⁾. Although longshore bars move offshore, cross-shore sediment transport may occur offshore or onshore in various places; therefore, offshore sediment transport occurs near the bar crests, whereas onshore sediment transport occurs in trough areas⁴⁰⁾. The period of cyclic offshore bar movement depends on the sea coast and can range from 1 year to 20 years.

7.4.11 Windblown Sand¹⁵⁾

The windblown sand causes harbor shoaling or river mouth closure, deteriorates human living environment, and causes problems when utilizing a beach for agriculture or cars passing roads near the beach. The most dominant factor related to the windblown sand is wind, but other factors such as grain size, specific gravity, wet-dry state of ground sand, ground armoring conditions, armor units, topography, and effect of facilities related to the phenomenon. It is said that windblown sand moves in three types of transport states: ① bedload state, ② suspended state, and ③ saltation state. Among them, very few moves in the suspended state. Most sands move in the saltation state while the wind velocity is small. As the wind velocity increases, 20% of the whole windblown sand moves in the bedload state, and the remaining 80% moves in the saltation state⁴¹⁾. Although the vegetation on the shore is just approximately 10 cm in height, but it is shown that it is useful in reducing the amount of windblown sand on the basis of on-site data^{42) 43)}.

7.4.12 Relationship between Climate Change and Topographic Change

It is predicted that the future rise in sea level and the change in wave characteristics probably due to climate change^{44) 45)} cause a long time change in the topography of coastal zones⁴⁶⁾.

The sea level rise causes the erosion of the foreshore and the retreat of shorelines. A change in water depth due to the sea level rise also changes the magnitude of the wave energy acting on the field; therefore, the sandy beach is transformed to the corresponding new equilibrium state. Considering that the coastal topography changes to balance the total amount of erosion and accretion, the shallow sea area, including the foreshore, is eroded (**Fig. 7.4.20**), and the sediment accumulates farther offshore. If the change is small, the amount of change in the shoreline is approximated by **equation (7.4.8)**⁴⁷⁾. **Equation (7.4.8)** is usually called Bruun's law.

$$s = la / h \quad (7.4.8)$$

where

s : amount of retreat of the shoreline (m)

- l : onshore-offshore distance between the threshold depth of the sediment movement of littoral drift and the crown of the berm (m)
 a : amount of sea level rise (m)
 h : vertical height between the threshold depth of the sediment movement of littoral drift and the crown of the berm (m)

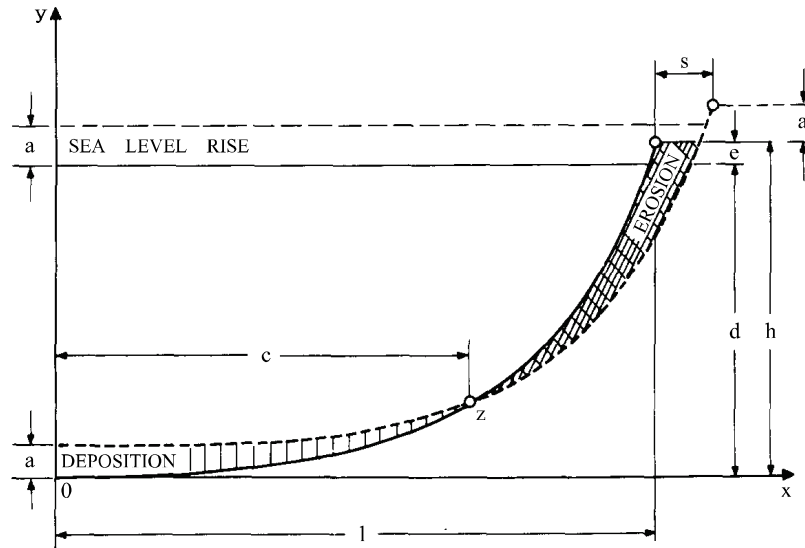


Fig. 7.4.20 Retreat of the Shoreline Caused by the Change in Equilibrium Topographic Cross Section Due to Sea Level Rise⁴⁸⁾

On the contrary, the change in wave characteristics in the future also affects the topographical change. Among the wave statistic, the mean wave affects the beach profile in normal times, and the peak wave is also related to the amount of the maximum erosion or occurrence of coastal disasters due to wave runups. Given that the change in coastal topography due to waves occurs in addition to the erosion of foreshore due to the abovementioned rise in sea level, massive erosion may occur because of the constant erosion due to the sea level rise and the temporary erosion due to the increase of peak waves. Furthermore, if the wave direction changes in the future, the predominant direction of the longshore sediment transport or the longshore sediment transport rate changes, and a littoral drift problem may occur even where no particular problems have occurred thus far⁴⁹⁾.

7.5 Scouring and Sucking

7.5.1 General

If there is a risk of impairing the stability of facilities brought about by scouring of the foundation of the facilities concerned, the ground, and others and by leakage of reclaimed soil in hinterland ground of the structures, it is necessary to take proper countermeasures to prevent scouring and leakage of reclaimed soil, considering the structural types of the facilities concerned.

7.5.2 Scouring

- (1) Scouring shall be taken into consideration, as necessary, if scouring around facilities, such as breakwaters, groins, and training jetties, is proven to affect the safety of the facilities.
- (2) Wave characteristics that act on natural beaches can be considered as nearly constant over a long period of time. Topographies that form in response to these characteristics are nearly stable as well. Scouring will occur when facilities are constructed and the equilibrium between the external forces and topography will be disturbed locally or over a broad area. The mechanism and amount of scouring will change according to the location of a structure because the wave action on the structure changes, and hence, when choosing methods for scouring prevention, the ranges, strength, and the like of such works must be considered carefully.

(3) Scouring in front of coastal revetment

It is well known that scouring in front of coastal revetment is closely correlated with wave reflection coefficient. For example, **Fig. 7.5.1** has been proposed for determining scouring or accretion by means of the reflection coefficient K and the parameter $(H_0/L_0)(l/d_{50}) \sin \alpha$ which is defined with the wave steepness H_0/L_0 , mean diameter of sediment d_{50} , slope gradient of coastal revetment α (for a vertical breakwater, $\alpha = 90^\circ$), and the distance l from the wave run-up point on an equilibrium profile to the location of the coastal revetment⁵⁰⁾. The diagram indicates that all other conditions being equal, it is advantageous against scouring in front of coastal revetment to make the front surface of revetment inclined.

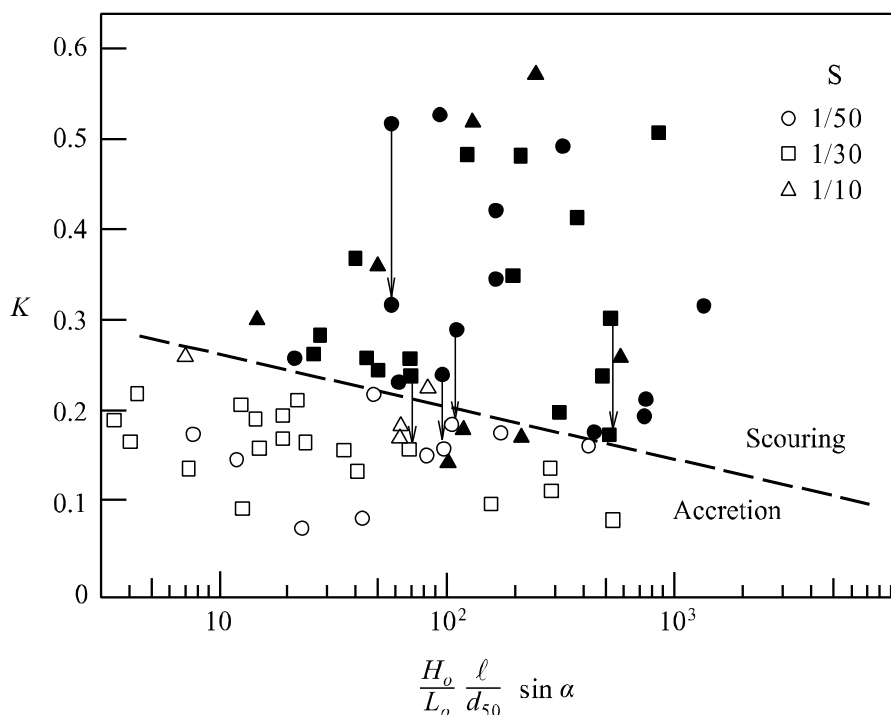


Fig. 7.5.1 Threshold Conditions Between Scouring and Accretion in Front of Coastal Revetment⁵⁰⁾

(4) Local scouring around breakwaters

① Scouring mainly in the surf zone

(a) Local scouring at the breakwater head

Figure 7.5.2 shows the local scouring conditions around a breakwater head, as analyzed by Tanaka.⁵¹⁾ The maximum scouring depth is found to be nearly equal to the maximum significant wave height $(H_{1/3})_{\max}$ during the period up to 15 days prior to the time of scouring measurements. In addition, Fig. 7.5.3 shows the relationship between the water depth around a breakwater head and scouring depth. The scouring depth is at its maximum value when the water depth at the breakwater head is about 3 to 5 m (namely, in the surf zone).

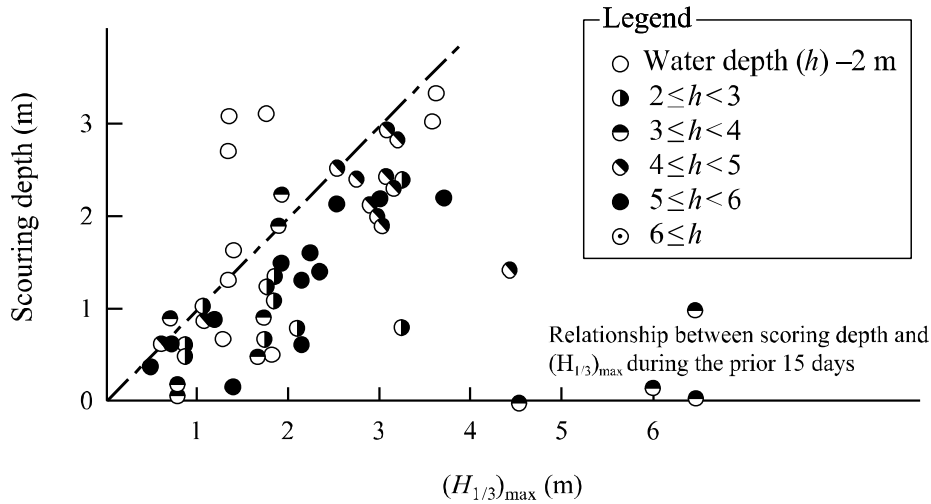


Fig. 7.5.2 Relationship Between Scouring Depth at the Breakwater Head and Maximum Significant Wave Height During the Prior 15 Days⁵¹⁾

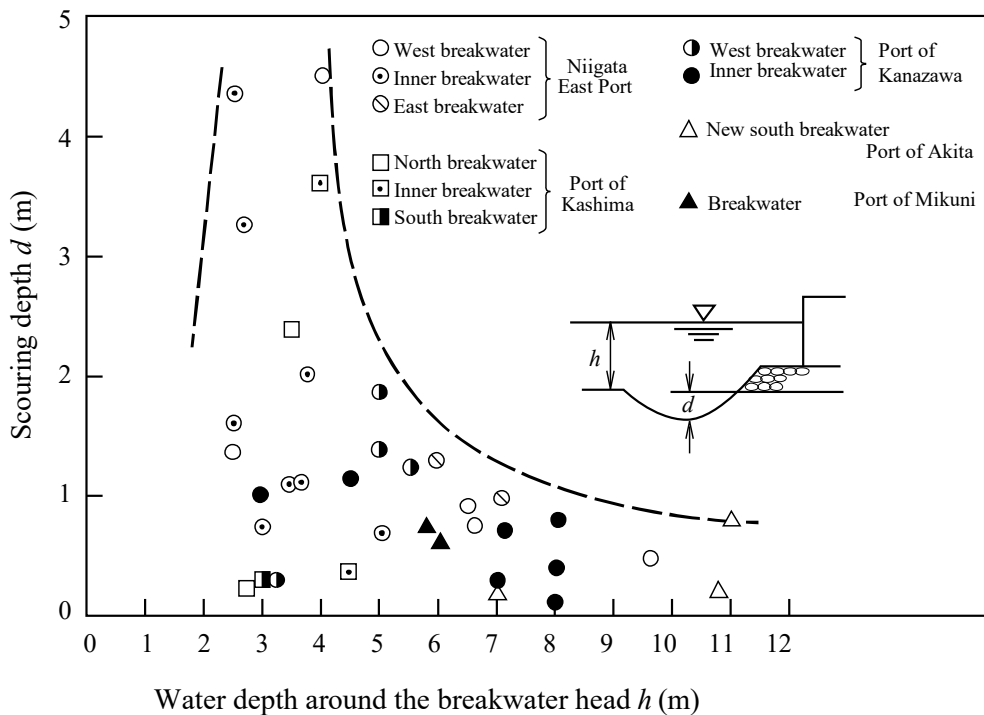


Fig. 7.5.3 Relationship Between Scouring Depth and Water Depth Around the Breakwater Head⁵¹⁾

(b) Scouring in front of breakwaters

Figure 7.5.4 shows the relationship between the scouring depth in front of a breakwater and water depth. ⁵¹⁾ The black circles in the figure indicate the condition of scouring around the oblique part of the breakwater. The scouring depth is at its maximum value at the bend of the breakwater, where the water depth is about 7 m, and gradually decreases seaward. On the other hand, the scouring depth in front of the straight part of the breakwater, which is indicated by the white circles, has its maximum value at around a water depth of 2 m. The location of the maximum scouring depth corresponds to the location of a longshore bar.

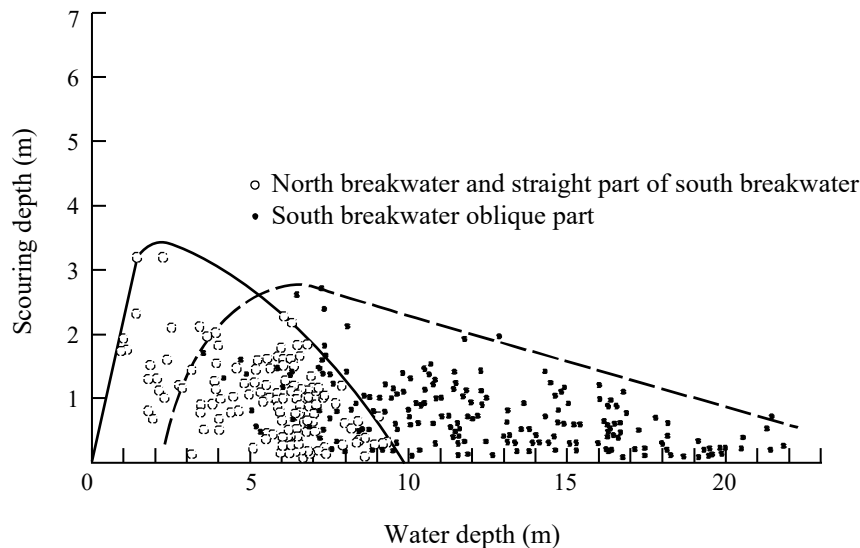


Fig. 7.5.4 Relationship Between Scouring Depth in Front of a Breakwater and Water Depth ⁵¹⁾

(c) Local scouring outside breakwaters

Figure 7.5.5 shows examples of places where typical local scouring occurs as a result of breakwater extension:

- (i) Breakwater head (especially pronounced when the breakwater head is in the surf zone).
- (ii) Around the straight portion of the breakwater (especially pronounced near the point where the breakwater crosses the longshore bar).
- (iii) Around a front mound or a submerged breakwater (especially pronounced inside the harbor).
- (iv) Places where the breakwater bends.

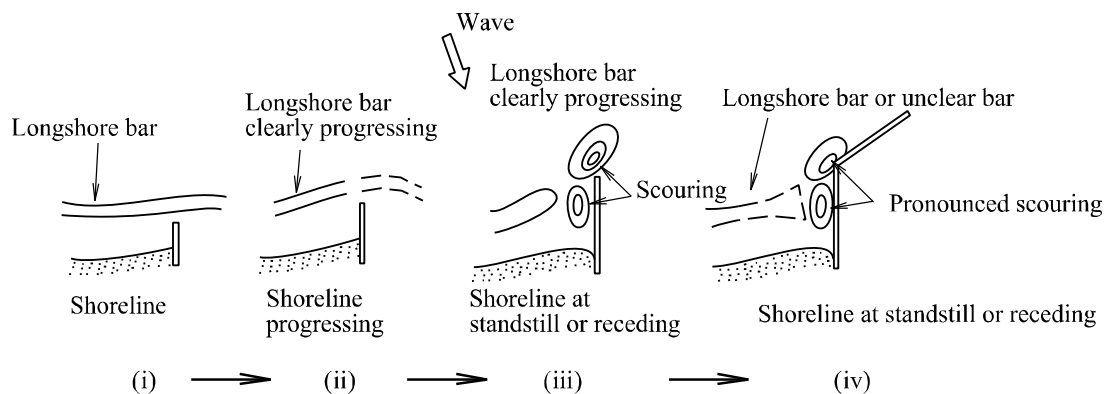


Fig. 7.5.5 Local Scouring Outside the Breakwater ⁵²⁾

② Scouring in standing wave domain

Scouring depth in front of a vertical wall tends to decrease as the initial water depth in front of the wall increases, and the wave condition is shifted into the standing wave domain. In the case of composite-type breakwaters, where the toe of the rubble mound is somewhat away from the wave reflection face of the upright section, scouring at the toe of the rubble mound by standing waves sometimes becomes a problem. Irie et al.⁵³⁾ conducted experiments concerning this type of scouring and highlighted the following issues:

- (a) The basic parameter is U_b/ω , the ratio of the maximum horizontal velocity of water particles at the bottom by incident waves U_b to the settling velocity of sediment ω . When $U_b/\omega > 10$, sediment will move from the location of the node of standing waves to the location of the antinode, with scouring occurring at the node and accretion taking place at the antinode. It is called L-type scouring. When $U_b/\omega < 10$, the opposite phenomenon will occur. It is called N-type scouring (refer to **Fig. 7.5.6**). The L-type scouring refers to the phenomenon where accretion occurs at the antinode of standing waves and scouring occurs at the node, whereas the N-type scouring refers to the opposite phenomenon where scouring occurs at the antinode and accretion occurs at the node.
- (b) As the flow velocity at the sea bottom in the field is higher than that in the experiment, the value of U_b/ω tends to be larger than 10 in the field, and generally, scouring at the node of standing waves is predominant. Normally, because a toe of the rubble mound is located at the distance of about 1/4 wavelength or so from the upright wall, scouring and subsidence of the rubble mound of breakwater will occur at its toe as the sediment there moves toward the location of the antinode at one-half wavelength from the upright wall.

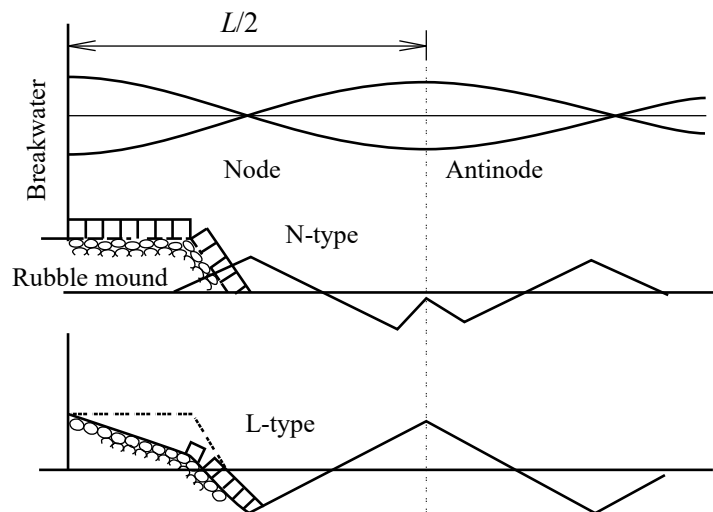


Fig. 7.5.6 Sketch of Scouring by Standing Waves⁵³⁾

③ Scour of sandy seabed under wave-dissipating blocks

One of the causes of settlement failure of wave dissipating blocks is scour of sandy seabed under the blocks. Even if the mass of wave-dissipating blocks satisfies the required mass estimated by Hudson's or other formulas, the scour of sandy seabed gradually settles the blocks. This settlement decreases the interlocking of the blocks resulting in scatter and breakage of the blocks.

Oscillatory flows by waves occur inside the rubble mounds or wave-dissipating blocks, and the flows scour the sandy seabed below the rubble mound or the wave-dissipating blocks. Thus, the wave-dissipating blocks settle down⁵⁴⁾. The sand below the wave-dissipating blocks is often scoured by the wave breaking on the slope of wave-dissipating blocks (**Fig. 7.5.7**). The scoured sand suspends on the sea surface near the wave-dissipating blocks and deposits behind the caisson by wave overtopping.

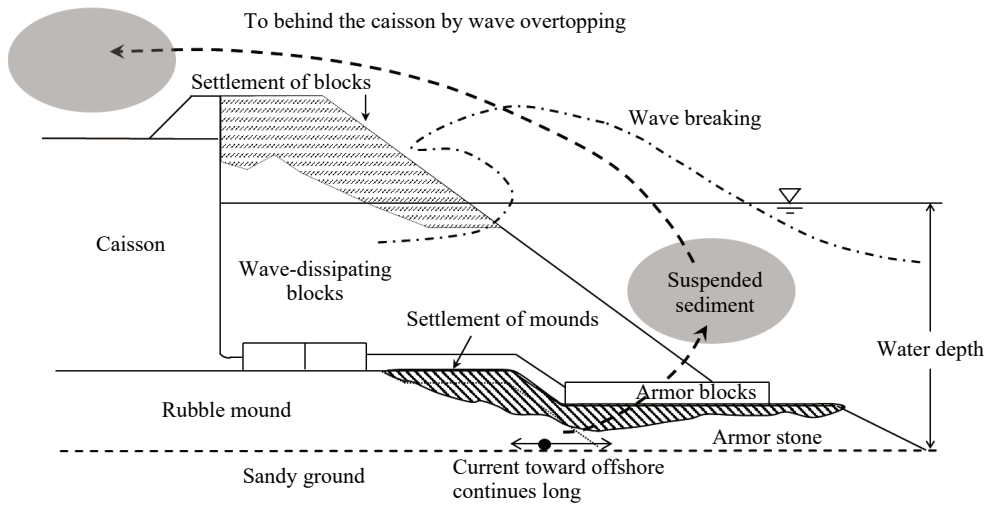


Fig. 7.5.7 Settlement of Mounds and Wave-Dissipating Blocks

The amount of scoured sandy seabed below the wave-dissipating blocks can be estimated by the following equation⁵⁵⁾. The definition of the amount of scour is shown in Fig. 7.5.8.

$$\frac{A_e}{A_T} = F_C \left(\frac{D_m}{B_{mb}} - \frac{800d_{50}}{h^{0.2}} \right) \quad (7.5.1)$$

$$D_m = \frac{H}{\sinh(2\pi h / L)} \quad (7.5.2)$$

where

A_e : amount of scour (m^2) (no scour occurs when negative)

A_T : cross-sectional area of a wave-dissipating block (m^2)

D_m : orbital diameter of a water particle below the wave-dissipating blocks (or in the mound if there is a mound below the wave-dissipating blocks) (m)

H : significant wave height (m)

L : wave length (m)

B_{mb} : length from the caisson wall to the slope of a wave-dissipating block (m)

d_{50} : median grain size of sand in the surface layer of sandy seabed (m)

h : water depth where the breakwater is installed (m)

F_C : coefficient related to the cross-sectional shape below the wave-dissipating blocks (0.84 if $h_F = 0$ and the wave-dissipating blocks are put directly on sandy seabed, 0.64 if the thickness of rubble mound is thin ($h_F < 4d_R$), and 0.32 if the thickness of rubble mound is thick ($h_F \geq 4d_R$). Armor block is not included in this rubble mound.)

h_F : thickness of rubble mound installed at the foot of wave dissipating blocks (m)

$d_R = (M_R/\rho_R)^{1/3}$: nominal diameter of the rubble mound stone(m)

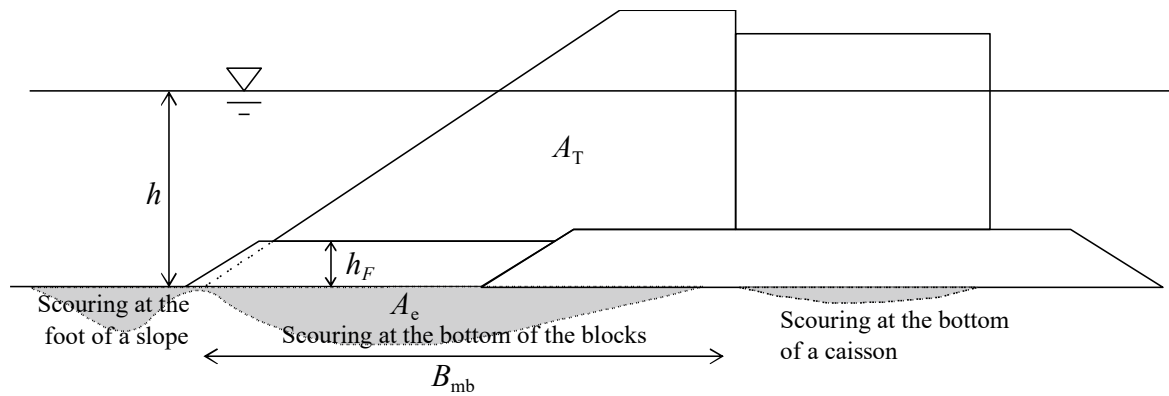


Fig. 7.5.8 Definition of the Amount of Scour (Equation (7.5.1) only Covers Scour below the Wave-Dissipating Blocks)

Scour tends to stabilize at its maximum value with actions by several thousands of waves. The amount of scouring estimated by **equation (7.5.1)** indicates its maximum value. Moreover, scouring is significant in long-period swelling waves, and it may be noticeable in long-period waves even if the wave height is small.

When scour under wave-dissipating blocks is predicted, it is necessary to examine the preliminary countermeasure work considering the type and scale of the target facilities, degree of difficulty, construction period, construction cost, and past scour prevention works and to select proper measures including corrective measures after the settlement of wave dissipating blocks.

The scour prevention work is basically laid under the rubble mound from the front edge to the rear one as shown in **Fig. 7.5.9**. Moreover, stronger scour prevention work such as mats is needed to be installed at the foot of a slope.

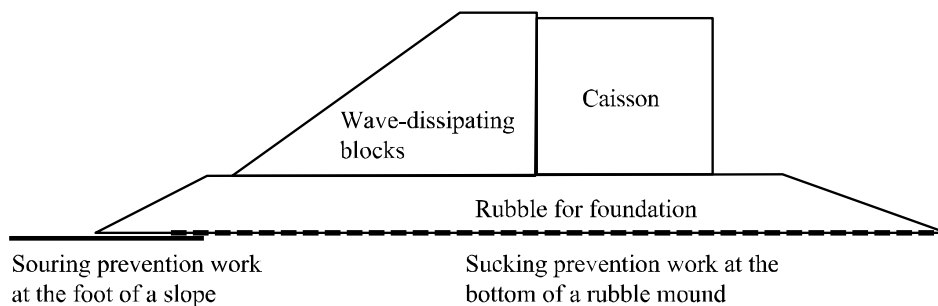


Fig. 7.5.9 Scouring Prevention Work

7.5.3 Leakage of reclaimed soil behind seawalls

- (1) If facilities are predicted to become unstable due to leakage of reclaimed soil behind seawalls, it is necessary to take proper prevention countermeasures considering the structural type of the facilities. The leakage of reclaimed soil is caused by mound-transmitted waves, waves acting through the joint between caissons, or wave overtopping. As the reclaimed soil leaks gradually, a hollow space may be created inside the reclamation soil. Attention should be paid to these hollow spaces as they may result in a significant depression of land. Moreover, if the mound-transmitted waves are large, their uplift may cause extensive damage by boiling of the reclamation sand^{56) 57)}.

(2) Leakage prevention works

Backfills (stones) may be installed behind the caisson to reduce the earth pressure. Geotextile sheets or mats which prevent sand leakage are laid on the slope of the backfills, and the reclamation sand is installed on it. However, if there is a problem in durability of the sand leakage prevention sheets or mats, there may occur a hollow space inside the reclamation sand due to their damages by the mound transmitted waves or tides and subsequent natural dropping or leakage of the reclamation sand into the backfills. Therefore, sufficient attention should be paid to the installation of the sheets or mats that enable the prevention of sand leakage.

The grain size of the stones to be installed may gradually be reduced from the backfilling stone to the reclamation sand according to the filter rule (**Part III, Chapter 4, 3.3 Gravity-type Breakwater (Sloping Breakwaters)**). Moreover, stones of small grain size and sheets or mats may be combined.

A joint plate to prevent sand leakage is installed in the joint between caissons. However, since the wave pressure acting on the joint plate is almost as same as that in the front wall of a caisson, the joint plate that is not durable can easily be broken. Moreover, direct installation of the reclamation sand behind the caisson is not preferable because sand leaks more easily from the joint.

7.6 Prediction of Beach Deformation

All the related factors shall be thoroughly investigated when predicting beach deformation, taking into consideration the predicted results by an appropriate method and the data of past beach deformation at the site in question. Various methods for predicting beach deformation exist, including (1) empirical prediction techniques; (2) estimation based on hydraulic model experiments, especially with movable bed model experiments; and (3) numerical simulations. Because beach deformation is strongly governed by the characteristics of the region in question, it is inappropriate to rely on any single method. It is necessary to predict beach deformation by investigating the local data and information as comprehensively as possible. Moreover, combining two or more prediction methods is desirable.

7.6.1 Empirical Prediction Techniques

The empirical method is a procedure in which, on the basis of analysis of the past examples of beach deformation on the coasts other than the coast in question, the layout and characteristics of the structures to be built on the coast in question are compared with the past examples of similar environment. Based on the similarities, beach deformation caused by the construction of new structures is predicted. Tanaka⁵⁸⁾ has conducted research on modeling of the complicated topographical changes that occur after the construction of structures. He classified characteristics of typical topographical changes in numerous examples of beach deformation. As a result of this research, it is possible to understand the topographical changes in the vicinity of Japanese ports in several representative patterns (see **Fig. 7.6.1**). Exceptions to these patterns are relatively rare. By judging which pattern in **Fig. 7.6.1** is applicable to the coast under investigation, a qualitative prediction of beach deformation becomes possible.

As the empirical prediction method is based on the site-scaled actual performance, it is a powerful method for predicting an outline. However, no quantitative discussion is possible because it has an aspect to pattern the beach deformation.

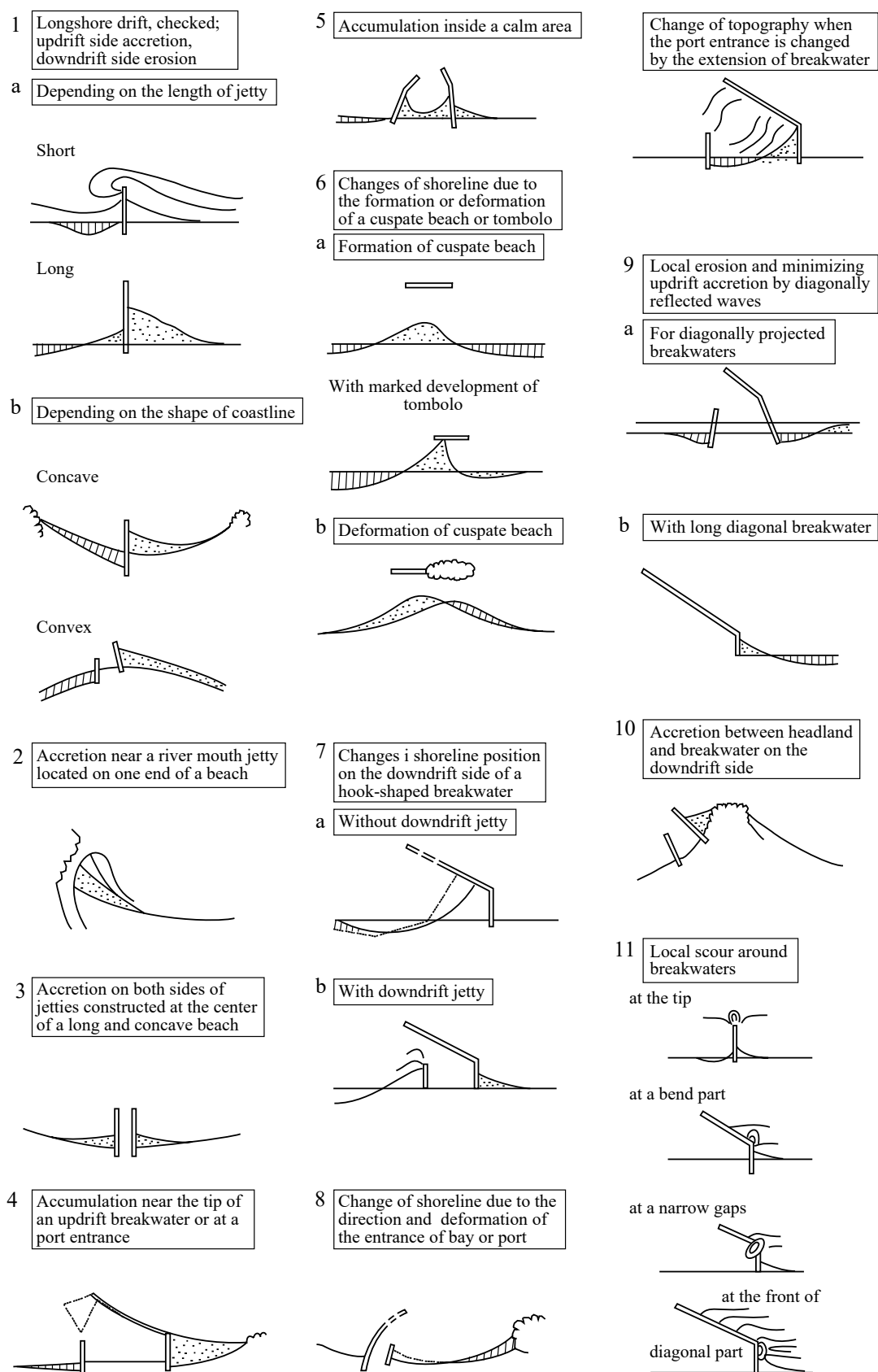


Fig. 7.6.1 Classification of Patterns of Topographical Changes After Construction of Structures

7.6.2 Hydraulic Model Experiments, Particularly Movable Bed Model Experiments

The accuracy of predicting beach deformation based on hydraulic model experiments, particularly movable bed model experiments, is limited because the problem of similarity remains unsolved. But the advantage of model experiments is such that specific topographical changes can be reproduced in a laboratory basin and the phenomenon to be forecasted can be understood visually.

In the experiment, fabricate a model by considering the result of preliminary calculation using an empirical equation concerning the past similarity and setting the model scale and the region to be reproduced. Before predicting future beach deformation, it is necessary to verify the model for reproducibility of the topographical changes that occurred in the past in the study area and to confirm the model's kinematic similarity. The degree of kinematic similarity will be judged by the reproductive accuracy of the experiment, which, therefore, cannot exceed the accuracy of the data collected on beach deformations in the past.

One can assume that adequately effective engineering predictions are possible if sufficient care is taken in the preliminary experiments to study the reproducibility of actual beach deformations, and in particular, the following problems can be addressed:

- ① The area of qualitative topographical changes caused by the construction of coastal facilities.
- ② Comparisons among alternative plans for measures to prevent coastal erosion, such as jetty or detached breakwaters.
- ③ Qualitative evaluation of shoreline changes due to large-scale offshore facilities.

However, predictions of beach deformation are difficult in the following types of cases:

- (a) Stable cross-sectional shapes of large-scale artificial beaches that face rough seas.
- (b) Deformation problems caused by large-scale offshore facilities on beaches that face rough seas.
- (c) Prediction of deposition rates in navigation channels and harbors and effects of their countermeasures.
- (d) Countermeasures against deposition in small-scale ports, such as marinas.
- (e) Experiments concerning effects of permeable detached breakwaters and submerged breakwaters on beach stability.

For details concerning movable bed model experiments, see Reference 58).

7.6.3 Predictions by Numerical Simulations

In the case of numerical simulation, it is preferable to model phenomena that are not yet fully figured out, such as the nearshore current by wave breaking, subsequent shore erosion, and siltation inside the harbor, by focusing on dominating phenomena and introducing various presumptions. Therefore, as in the hydraulic experiments, the validity of the numerical model should be verified by the numerical reproducibility of the past changes in topography of the target shore before the prediction of the future.

At the present time, numerical simulations are divided into two models: those that predict changes in the shoreline location and those that predict three-dimensional changes in water depth, i.e., beach topographical changes. However, many unresolved portions still exist as of today, and such calculations are performed under various assumptions. Therefore, it should be noted that the numerical result may be incorrectly used unless the various assumptions in the simulations are understood until the result can be obtained. Many types of models have been proposed until now to predict various changes in topography (changes in cross sections, changes in shorelines, and three-dimensional changes). The result of estimation and comparison of typical models⁵⁹⁾ shows that it is necessary to use models properly according to the mechanism of changes in the beach of interest and their time and space scales when applying each model to sites.

On the other hand, prediction of changes in beach topography for a long period of some 10 years or longer is required for the topographic changes in coast caused by the sea level rise and changes in the wave field due to future climate changes. The numerical models to predict changes in the shoreline due to these climate changes are currently being developed.

(1) Shoreline Change Model (One-Line Theory)^{15) 60) 61)}

This model predicts the long-time change in the shoreline considering only the longshore sediment transport rate by ignoring the cross shore littoral drift. They are called a shoreline change model, a coastline change model, or a

one-line theory as they predict the change in one shoreline, but they are all essentially the same model. In this model, the shoreline moves by the balance of the longshore sediment transport rate driven by the longshore directional component of the energy flux of the incident wave and finally stabilizes after the shoreline direction changes so that the waves enter perpendicularly to the shoreline. This model is relatively frequently applied, and the results of the predictions are fully put to practical use. However, in order to improve the precision of the prediction, accumulation of enough data concerning a long-time shoreline change should be required and the reproducibility should be verified based on it.

Beach sediment is transported by waves and currents both in the perpendicular direction to the shoreline and in the alongshore direction. Because littoral drift is caused mainly by the direct action of waves, the littoral drift during storm periods will be predominantly towards the offshore, and the coast will be eroded with a retreat of shoreline. When the sea becomes calm, however, the sediment will be carried towards the shore, and the shoreline will advance. Along with these movements, changes of the beach profile will occur. This topographical change in the shoreline location and beach profiles caused by the onshore–offshore transport is normally seasonal. When viewed on the average profile over a long period of time, the changes caused by onshore–offshore transport are less significant compared with those caused by longshore transport. Thus, when focusing on beach erosion or accretion over a period of several years, one can assume that there is no change in the shape of the beach profile and that beach erosion and accretion will correspond to the retreat and advance of the shoreline. Then, the changes in the shoreline location can be predicted primarily from the longshore transport as the basis on the balance of the deposition and removal of the longshore sediment volume.

Figure 7.6.2 illustrates the calculation principles of a shoreline change prediction model. As shown in the figure, the shoreline should be divided into sections of the width Δy along the alongshore direction of the shoreline, and the inflow and outflow of sediment volume between those widths are considered. That is, when the inflow $Q\Delta t$ and

outflow $\left(Q + \frac{\partial Q}{\partial y} \Delta y \right) \Delta t$ of sediment volume during the time period Δt are compared, accretion will occur if the former is larger, and erosion will take place if the latter is larger.

By introducing the assumption that the beach profile remains unchanged over time and any imbalance between the inflow and outflow sediment volumes simply shifts the beach profile parallel to offshore or onshore directions, it is possible to express the advance and retreat of the shoreline as a result of the imbalance. When this is expressed in the continuity of sediment flux, the result is presented by **equation. (7.6.1)**.

$$\frac{\partial x_s}{\partial t} + \frac{1}{D_s} \left(\frac{\partial Q}{\partial y} - q \right) = 0 \quad (7.6.1)$$

where

x_s : shoreline location (m)

t : time (s)

y : coordinate in alongshore direction (m)

D_s : vertical distance of the littoral drift movement zone (m)

Q : longshore sediment transport rate (m^3/s)

q : cross-shore inflow ($q > 0$) or outflow ($q < 0$) of the sediment transport rate across the onshore–offshore boundary per unit width in the alongshore direction ($\text{m}^3/\text{m/s}$)

Therefore, if D_s , Q , and q are given, the time change of the shoreline location can be calculated using **equation (7.6.1)**.

As the evaluation of the cross shore littoral drift rate q is quite difficult, the onshore–offshore boundary should normally be set where the cross shore littoral drift rate can be ignored. In other words, the onshore boundary shall be set to the maximum run-up location of incident waves on the beach, and the movement of the bottom sediment due to wave action is neglected. On the other hand, the offshore boundary should be set to the location of little sand movement, outside of the surf zone at which the littoral drift phenomenon is active. However, when the sediment supplied by rivers is not negligible, when there is sand mining or dumping from the onshore side, or when sand flows out to the offshore direction and never comes back to the beach, their impacts can be incorporated into the model by considering the quantities in the variable of q .

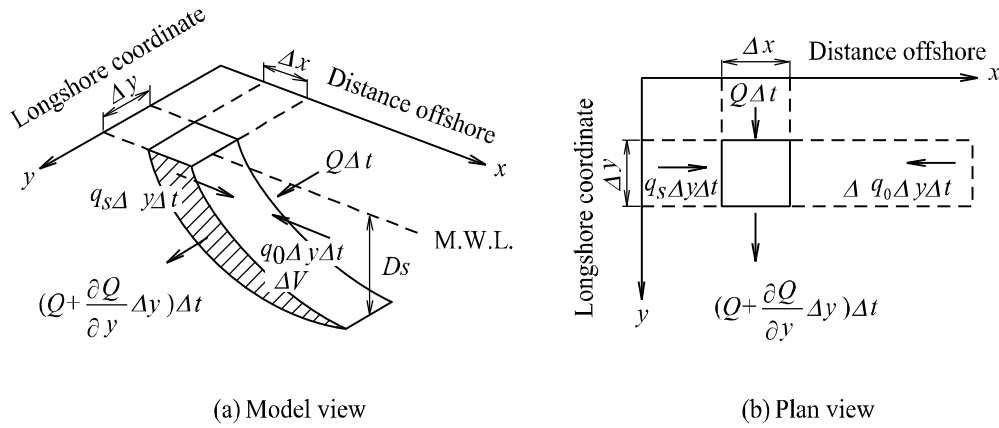


Fig. 7.6.2 Relationship Between Shoreline Change and Sand Movement

The longshore sediment transport rate Q is often estimated using an equation, including the alongshore component of the incident wave energy flux at the wave breaking point. In such equations, the longshore sediment transport rate is determined only from the wave height and direction at the wave breaking point as wave conditions. In the coastal zone where beach deformation is predicted, however, there will normally exist some structures that create an area sheltered from incident waves. Because of this sheltered area, the wave height varies alongshore; thus, currents are induced. Hence, the following equation in which Ozasa and Brampton⁶²⁾ incorporated the abovementioned effect is often used.

$$Q = \frac{H_B^2 C_{gB}}{16s(1-\lambda)} \left(K_1 \sin 2\theta_B - \frac{2K_2}{\tan \beta} \cos \theta_B \frac{\partial H_B}{\partial y} \right) \quad (7.6.2)$$

where

H_B : breaking wave height (m)

C_{gB} : group velocity at the wave breaking point (m/s)

θ_B : angle formed by the wave crest line and the shoreline at the breaker point (°)

$\tan \beta$: equilibrium beach slope

s : $s = (\rho_s - \rho_0) / \rho_0$

ρ_s : density of sediment (g/cm³)

ρ_0 : density of seawater (g/cm³)

λ : void ratio of sediment

K_1, K_2 : coefficients

The width of sediment movement zone D_s is the distance perpendicular to the shoreline from the wave run-up point on the beach to the offshore boundary where longshore sediment transport activity becomes significant. The distance D_s is determined basically by investigating the volume of beach profile area change from the bathymetric data of the coast in question. When the available data are inadequate, an energy-averaged representative wave is estimated, and its dimensions are substituted into the equations for the wave run-up height and the threshold depth of sediment movement as a method to conveniently find the distance D_s .

Because **equation (7.6.2)** cannot be solved analytically, except in extremely simple cases, a computer is required to perform the numerical computation. In the numerical computation, Q must be evaluated at each measuring line. For this purpose, the breaking wave height and angle, the incidence wave angle to the shore line, and the water depth at the wave breaking point at each measuring line must be calculated separately by using the wave transformation calculation (for details concerning numerical computation, see Reference 15).

(2) Three-Dimensional Deformation Models or Prediction Model for Bathymetric Change

While the shoreline change model treats the surf zone phenomena as a black box, the water depth model (three-dimensional model) needs to integrate the phenomena in the surf zone, especially the following phenomena, by properly formulating them.

- ① As wave transformation in shallow sea, refraction, diffraction, wave breaking and wave transformation after wave breaking.
- ② Wave energy attenuation due to wave breaking and roughness coefficient of the sea bottom
- ③ Planar and vertical distributions of the nearshore current
- ④ Mechanisms of bedload, suspended sediment, etc.

Prediction models for bathymetric change predict the change in the water depth at each grid point in a calculation domain, and consider not only longshore sediment transport but also cross-shore sediment transport. Several models have been presented as the prediction model for bathymetric change, but in every model, the method is to first calculate the fields of waves and nearshore currents and then determine the bathymetric changes. As the nearshore currents, depth averaged currents or vertically distributed ones may be employed in the numerical model. (They are called the water depth model, three-dimensional model, coastal topography change prediction model, and so on, but they are all the same.)

Prediction models for bathymetric change are divided into two main types depending on the method of predicting the bathymetric changes. One type of model is based on local sediment transport rates calculated from hydraulic factors and sediment particle diameters at the location in question, and the other type of model considers sediment advection and diffusion. The models based on local sediment transport rates determine bathymetric changes based on the difference between the incoming and outgoing amounts of the local sediment transport, and one of these models is that of Watanabe et al.⁶³⁾, which uses the sediment transport rate formulas of Watanabe et al. Other local sediment transport rate formulas are those of Bijker⁶⁴⁾ and Bailard⁶⁵⁾, which separately calculate the bedload and the suspended load. The model of Watanabe et al.⁶³⁾ has been improved several times and has developed into a model that considers the grain size distribution.⁶⁶⁾

Models that consider the advection and diffusion of sediment, either in three dimensions or just in horizontal two dimensions, have been proposed, for example, by Sawaragi et al.⁶⁷⁾ (hereafter, the Sawaragi model) and by Lesser et al.⁶⁸⁾ (hereafter, the Delft 3D-flow model). In these models, the bathymetric changes are dominated by the difference between the amount of uplifting of suspended sand and its settling rate and by the difference between the incoming amount of bedload and its outgoing amount. The concentration of suspended load at reference points near the sea bottom, which is used in the calculation of uplifted amounts of suspended sand, may be found in the formula of Deguchi and Sawaragi⁶⁹⁾ used in the Sawaragi model or in the formula of van Rijn⁷⁰⁾ used in the Delft 3D-flow model. An example of a formula for bedload is that of van Rijn⁷¹⁾ (used in the Delft 3D-flow model).

The prediction model for bathymetric change have been mainly applied to the areas where offshore topographical changes are significant, such as the problem of siltation in ship channels and basins and bathymetric changes due to large-scale submerged breakwaters.

(3) Prediction Simulation of the Shoreline Change due to Climate Change

In the numerical model where the physical processes are realistically resolved like prediction models for bathymetric change, a vast amount of time is required to calculate the prediction of the shoreline change for a long time of several-year to several-10-year scale. Furthermore, the calculation accuracy is not necessarily improved more than the calculation result using simpler models called process based or empirical model⁷²⁾. Therefore, the latter model is currently often applied for the prediction of long-period phenomenon for several-10-year-scale, such as topographical change due to climate change. They are classified into the following three types:

① Prediction by a shoreline change model

The shoreline change model (one-line theory) explained in 7.6.3 (1) evaluates the topographical change based on the change in future wave height or wave direction. This model is capable of reproducing the shoreline change in a relatively long period.

② Prediction using Bruun's law

Bruun's law calculates the shoreline change caused by the movement of sediment in the onshore–offshore direction (see Part II, Chapter 2, 7.4.12 Relations Between the Climate Change and the Topographical

Change), considering the change in the equilibrium cross section of beach corresponding to the change in sea level. Although this model calculates only the change in equilibrium condition and does not reproduce the change in beach topography according to the temporal variation of wave condition, it has an advantage of allowing relatively easy estimation of future amount of shoreline retreat.

③ Prediction using the equilibrium shoreline change model

This model assumes that the shoreline advances or retreats asymptotically to the equilibrium shoreline location corresponding to the time dependent change in wave condition. This is capable of reproducing not only the short-term shoreline changes caused by waves but also long-term shoreline changes. Although the equilibrium shoreline location or the external force term may be treated differently, it is basically expressed by **equation (7.6.3)**. One-half power of the wave energy is often used as the external force term, and the equilibrium shoreline location is usually dominated by the wave energy^{73) 74)}.

$$\frac{dy}{dt} = CE^{\frac{1}{2}}(y - y_{eq}) \quad (7.6.3)$$

where

dy/dt : shoreline change rate per unit time (m/day)

C : coefficient ($1/N^{0.5}\text{day}^{0.5}$)

E : wave energy (N/day)

y : present shoreline location (m)

y_{eq} : equilibrium shoreline location corresponding to the current waves (m)

Since the above three process-based models basically treat mutually independent events, prediction of the shoreline change, for example, the change due to the changes in sea level and the wave condition, becomes possible by combining each model. Specifically, the Banno-Kuriyama model incorporates the concept of Bruun's law into the equilibrium shoreline change model⁷⁴⁾ or the CoSMoS-COATS model⁷⁵⁾, adding together the results of the three process-based models.

[References]

- 1) Ports and Harbour Bureau of MLIT and Nature Conservation Bureau of MOE: For the Regeneration of Tidal Network, Report of the workshop for the regeneration of ecosystems including tidal flats in Tokyo Bay, National Printing Bureau, p.118, 2004 (in Japanese)
- 2) Hamada, T., H. Mitsuyasu and N. Hase: Wave force on structures, Proceedings of the 3rd Conference on Coastal Eng. JSCE Vol. pp. 67-83, 1956
- 3) Japan Society of Mechanical Engineers: Handbook of Mechanical Engineering, pp. A5-97-106, 1989
- 4) Iwasaki T., A. Mano T. Nakamura and N. Horikoshi: Experimental study on stationary fluid dynamic force acting on mound material of submerged breakwater and pre-packed breakwaters, Proceedings of 31st Conference on Coastal Eng. JSCE, pp. 527-531, 1984
- 5) TANIMOTO, K., K. KIMURA and K. MIYAZAKI: Study on Stability of Submerged Dike at the Opening Section of Tsunami Protection Breakwaters, Rept. of PHRI Vol. 27 No. 4, pp. 93-102, 1988
- 6) Sakunaka, J. and T. Arikawa: Research on Stability of Opening Section at Baymouth Breakwater, Technical Note of the Port and Airport Research Institute, No.1274, p.26, 2013 (in Japanese)
- 7) Tsuruya, H., K. Murakami and I. Irie: Mathematical Modeling Mud Transport in Ports with a Multi-layered Model, Report of the Port and Harbour Research Institute, Vol.29 No.1, pp.3-51, 1990 (in Japanese)
- 8) Nakagawa, Y., K. Watanabe, H. Tanigawa and Y. Kuroda: Measurement of Vertical Profile of Mud Density near the Bottom Boundary, Annual Journal of Coastal Engineering, JSCE, Vol.51, pp.986-990, 2004 (in Japanese)
- 9) Goda, Y.: Ports and Harbours (Second Edition), Easy-to-understand Civil Engineering Lecture, Shokokusha Publishing, p. 321, 1998
- 10) Horikawa, K.: New Edition, Coastal Engineering- Introduction to Offshore Engineering, Tokyo Univ. Press, 1991

- 11) Mogi, A.: Basic Lectures of Marine Science 7, Geology in Shallow Water, Shore line and surf zone, Tokyo Univ. Press, pp. 109-252, 1971
- 12) Toyoshima, O.: Coastal Engineering at construction site, Morikita Publishing, 1972
- 13) Sawaragi, T.: Littoral drift and coastal erosion, Disaster Prevention Series 3, Morikita Publishing, 1992
- 14) Noda, H. and H. Hashimoto: Littoral drift and shore protection facilities, New Series Civil Engineering 79, Giho-do Publishing, 1981
- 15) Honma, M. and K. Horikawa: Coast-environmental engineering, Tokyo Univ. Press, 1985
- 16) Sato, S.: Study related to port construction, Technical Note of PHRI, No. 5, 1962
- 17) Sonu, C. J.: Three-dimensional beach changes, Journal of Geology, Vol. 81, pp. 42–64, 1973
- 18) OZASA, H.: Field Investigation of Submarine Sand Banks and Large Sand Waves, Rept of PHRI Vol. 14 No. 2, pp. 3-46, 1975
- 19) Horikawa, K. T. Sunamura: Study of retreat of coastal cliff by aerial photographs, Proceedings of 14th Conference on Coastal Eng. JSCE, pp. 315-324, 1967
- 20) Horikawa, K. and M. Sunamura: Experimental study on erosion of sea cliff, Proceedings of 15th Conference on coastal Eng. JSCE, pp. 315-324, 1968
- 21) Horikawa, K. and T. Sunamura: Coastal erosion at Byobuga-ura, Chiba Prefecture (1), (2), & (3), Proceedings of on Coastal Eng. JSCE, Vol. 16 pp. 137–146, Vol. 17 pp. 289–296, Vol. 19 pp. 13–17, 1969, 1970, 1972
- 22) Bascom, W. N.: The relationship between sand size and beach – face slope, Transactions of AGU, Vol. 32 No. 6, pp. 866–874, 1951
- 23) KATO, K., N. TANAKA, H. KIMURA and M. AKAISHI: Movable-bed Model Experiments of a Large River-mouth and its Surroundings- On Deformation of Topography at the Yoshino River- Rept of PHRI Vol. 22 No. 2, pp. 3-87, 1983
- 24) Sato S. and N. Tanaka: Sand movement on horizontal bed, Proceedings of 9th Conference on Coastal Eng. JSCE, pp. 95-100, 1962
- 25) Sato, S. and N. Tanaka: Field investigation on sand drift at Port Kashima facing the Pacific Ocean, Proc. 10th Conf. on Coastal Eng., pp. 595-614, 1966
- 26) Savage, R. P.: Laboratory determination of littoral-transport rate, Proc. of ASCE., Vol. 88, WW2, 1962
- 27) U.S. Army Coastal Engineering Research Center: Shore Protection Manual, Vol. 1, Department of the Army Corps of Engineers, 1977
- 28) Komar, P. D.: Relative quantities of suspension versus bed-load transport on beaches, Journal of Sediment Petrology, Vol. 48, pp. 921–932, 1978
- 29) Sternberg, R. W., N. C. Shi and J. P. Dowing: Field observations of suspended transport in the nearshore zone, Proc. 19th Int. Conf. on Coastal Eng., pp. 1782–1798, 1984
- 30) Katoh, K., N. Tanaka, T. Kondoh, M. Akaishi and K. Terasaki: Field observation of local sand movement in the surf zone using fluorescent sand tracer (Second Report), Report of PHRI Vol. 24 No. 4, pp. 3–63, 1985
- 31) Katoh, K., N. Tanaka and I. Irie: Field observaion on suspended-load in the surf zone, Proc. of 19th Int. Conf. on Coastal Eng., pp. 1846–1862, 1984
- 32) Hino, M. K. Nadaoka and A. Omata: Organizational structure of turbulence and water particle motion in the surf zone, Proceedings of 31st Conference on Coastal Eng. JSCE, pp. 1-5, 1984
- 33) Kana, T.W.: Surf zone measurement of suspended sediment, Proc. of 16th Int. Conf. on Coastal Eng., pp. 1725–1741, 1978
- 34) Dean, R.G.: Heuristic models of sand transport in the surf zone, Proc. Conf. on Eng. Dynamics in the surf zone, pp. 208–214, 1973
- 35) Horikawa, K., T. Sunamura, H. Kondo and S. Okada: Discussion on 2-dimensional shore line change due to waves, Proceedings of 22nd Conference on Coastal Eng. JSCE, pp. 329-334, 1975
- 36) Kato, K. S. Yanagishima, H. Murakami and K. Suetsugu: Trial for modeling of short-term shore line change, Proceedings of 34th Conference on Coastal Eng. JSCE, pp. 297-301, 1987

- 37) Komar, P.D.: Beach process and sedimentation, Prentice-Hall, Inc., 1976
- 38) Kato, K., S. Yanagishima: Berm erosion due to infra-gravity waves, Jour. Of JSCE, No. 452/II-20, pp. 41-50, 1992
- 39) Kato K.: Shore protection by underground permeable layer, Journal of JSCE, February, pp. 18-21, 1996
- 40) Kuriyama, Y.: Long-term cross-shore movement of longshore bar and associated sediment transport, Jour. Of JSCE, No. 677, pp. 115-128, 2001
- 41) Tsuchiya, Y. and Y. Kawada: Wind brown sand transport rate law based on sand particle siltation. Proceedings of 19th Conference on Hydraulics, pp. 7-12, 1975
- 42) KURIYAMA, Y., T. NAKASHIMA, K. KAMIDOZONO and N. MOCHIZUKI: Field Measurements of the Effect of Vegetation on Beach Profile Change in the Region from a Backshore to the Foot of the Fore-dune and Modeling of Aeolian Sand Transport with Consideration of Vegetation, Rept of PHRI Vol. 40 No. 1, pp. 47-80, 2001
- 43) YANAGISHIMA, S.: Field Measurement of the Effect of Vegetation on Beach Profile Change In the Backshore, Technical Note of PHRI No. 1091, p. 35, 2004
- 44) IPCC fifth assessment report, <http://www.ipcc.ch/>, 2015
- 45) Mark A. Hemer, Yalin Fan, Nobuhito Mori, Alvaro Semedo and Xiaolan L. Wang (2013): Projected changes in wave climate from a multi-model ensemble, Nature Climate Change, Vol. 3
- 46) Banno, M. and Y. Kuriyama: Development of Shoreline Change Model Considering Time Heterogeneity and Tidal Impact and Prediction of Future Shoreline Position under Global Climate Change, Journals of JSCE Series B2 (Coastal Engineering), Vol.69 No.2, pp.I_541-I_545, 2013 (in Japanese)
- 47) Bruun,P.,1962. Sea level rise as a cause of shore erosion. Proc. Am. Soc. Civ. Eng., J. Waterways Harbors Div., 88:117-130
- 48) Bruun, P., 1983. Review of conditions for uses of the Bruun rule of erosion. Coastal Engineering, 7, pp. 77 -89
- 49) Shibutani, Y., M. Kuroiwa, K. Hayashi, K. Ikeda, N. Mori, Y. Matsubara and H. Mase: Long-term Beach Prediction and Impact Assessment of Climate Change on Contour Line Change, Journals of JSCE Series B2 (Coastal Engineering), Vol.70 No.2, pp.I_684-I_689, 2014 (in Japanese)
- 50) Saeki, H., T. Sato, T. Ono and K. Hamanaka: Experimental Study on scoring of foundation of sea walls, Proceedings of 32nd Conference on Coastal Eng. JSCE, pp. 440-444, 1985
- 51) Tanaka, N.: Transformation of sea bed and beach near port constructive in sandy beach, Proceedings of Lecture meeting of PHRI 1974, pp. 1-46,1974
- 52) Sato, S. and I. Irie: Variation of topography of sea-bed caused by the construction of breakwaters, Coastal Engineering in Japan, Vol. 13, pp. 141-152, 1970
- 53) IRIE, I., K. NADAOKA, T. KONDO and K. TERASAKI : Two Dimensional Seabed Scour in Front of Breakwaters by Standing Waves-A Study from the Standpoint of Bed load Movement- Report of PHRI Vol. 23 No. 1, pp. 3-52, 1984
- 54) Suzuki, K., S. Takahashi, T. Takano and K. Shimosako: Settlement Failure of Wave Dissipation Blocks in front of Caisson Type Breakwater due to Scouring under the Rubble Mound, Report of the Port and Airport Research Institute, Vol.41 No.1, pp.1-39, 2002 (in Japanese)
- 55) Suzuki, K. and S. Takahashi: Estimation of Scouring at the Bottom of Wave Dissipating Block Breakwater, Journals of Coastal Development Institute of Technology, No.12, pp.1-3, 2012 (in Japanese)
- 56) Takahashi, S., K. Suzuki, K. Tokubuchi, T. Okamura, K. Shimosako, K. Zen and H. Yamazaki: Hydraulic Model Experiments on the Settlement Failures of Caisson-type Seawalls, Report of the Port and Harbour Research Institute, Vol.35 No.2, pp.3-64, 1995 (in Japanese)
- 57) Takahashi, S., K. Suzuki and W.S. Park: Numerical Calculations on Wave Pressure Propagation into Backfill Rubbles of Caisson Type Seawall, Journals of JSCE Division B3 (Ocean Engineering), 2002 (in Japanese)
- 58) Kato, K.: Movable bed experiment and field observation, Monthly Magazine Marine Science, No. 169, pp. 417-423, 1984
- 59) Shimizu, T. and T. Takagi, K. Sato and M. Yamada: Mutual comparison of beach deformation models, Proceedings of Coastal Eng. JSCE Vol. 44, pp. 506-510, 1997

- 60) TANAKA, N. and K. NADAOKA: Development and Application of a Numerical Model for the Prediction of Shoreline Changes, Technical Note of PHRI No. 436, 1982
- 61) Watanabe, A.: Numerical simulation of beach change, Monthly Magazine Marine Science, Littoral Drift, Vol. 16 No. 7, pp. 409-416, 1984
- 62) OZASA, H. and A. H. BRAMPTON: Models for Predicting the Shoreline Evolution of Beaches Backed by Seawalls, Rept of PHRI Vol. 18 No. 4, pp. 77-103, 1979
- 63) Watanabe, A., Y. Maruyama, Y. Shimizu and T. Sakakiyama: Numerical model for the prediction of s-dimensional beach transformation due to the construction of structures, Proceedings of the 31st Conference on Coastal Eng. JSCE Vol. pp. 406-410, 1984
- 64) Bijker, E.W.: Longshore transport computations, J. Waterways, Harbors and Coastal Engineering Division, Vol. 97, No. 4, pp. 687-703, 1971
- 65) Bailard, J.A.: An energetics total load sediment transport model for a plane sloping beach, J. Geophys. Res., Vol. 82, No. C11, pp. 10938-10954, 1981
- 66) Kobayashi, H., T. Honda, S. Sato, A. Watanabe, M. Isobe and T. Ishii: A numerical model of three-dimensional beach deformation due to graded sediment transport under atilt waves, Jour. Of JSCE No. 740/II-64, pp. 157-169, 2003
- 67) Sawaragi, T. S. Ri, and I. Deguchi: Study on nearshore current around river mouth and model for topographic transformation, Proceedings of 31st Conference on Coastal Eng. JSCE Vol. pp. 411-415, 1984
- 68) Lesser, G.R., Roelvink, J.A., van Kester, J.A.T.M. and Stelling, G.S.: Development and validation of a three-dimensional morphological model, Coastal Eng., Vol. 51, pp. 883-915, 2004
- 69) Deguchi, I. and Sawaragi, T.: Calculation of the rate of net on-offshore sediment transport on the basis of flux concept, Proc. 19th Int. Conf. on Coastal Eng., ASCE, pp. 1325-1341, 1984
- 70) van Rijn, L.C.: Sediment transport: Part II, Suspended load transport, J. Hydraulic Eng., Vol. 11, pp. 1613-1641, 1984
- 71) van Rijn, L.C.: Principles of Sediment Transport in Rivers, Estuaries and Coastal Seas, Aqua Publications, Amsterdam, 1993
- 72) Murray, A. B. (2007): Reducing model complexity for explanation and prediction, Geomorphology, 90 (3), pp. 178-191
- 73) Yates, M. L., Guza, R. T. and O. Reilly W. C. (2009): Equilibrium shoreline response: Observation and modeling, Journal of Geophysical Research: Oceans, 114 (C9)
- 74) Banno, M., Y. Kuriyama and N. Hashimoto: Uncertainty Estimation of Equilibrium Beach Profile by Non-linear Mixed Effect Model with Long-term Measured Data, Journals of JSCE Series B2 (Coastal Engineering), Vol.70 No.2, pp.I_546-I_550, 2014 (in Japanese)
- 75) Vitousek, S., P. L. Barnard, P. Limber, L. Erikson, and B. Cole (2017), A model integrating longshore and cross-shore processes for predicting long-term shoreline response to climate change, J. Geophys. Res. Earth Surf., 122, 782-806, doi:10.1002/ 2016JF 004065.

8 Other Meteorology and Oceanology Items

8.1 Other Meteorology Items to be Considered

(1) General

The following meteorology items and effects on port facilities should be considered with regard to the performance verification of port facilities:

- ① Rain is a factor in determining the capacity of drainage facilities within the port and can interfere with cargo handling and other port operations.
- ② Fog interferes with ships' navigation and entry to and departure from the port. It can also decrease the usability of port facilities.
- ③ Snowfall may need to be considered with regard to its surcharge on port facilities.
- ④ Atmospheric temperature may affect the stress distribution on port facilities, creating temperature stress.

(2) Rain

Rain can generally be classified into a thunderstorm in which precipitation concentrates in a short time and a long-duration rain which is an indication of typhoon. When conducting a performance verification of drainage facilities, rainfall intensity shall generally be set for both cases where the outflow instantaneously increases and the efflux time is long. In the performance verification of sewage lines and others where the rainfall density concerns as in thunderstorms and others, Sherman's formula or Talbot's formula may be used:

Sherman's formula

$$R = \frac{a}{t^n} \quad (8.1.1)$$

Talbot's formula

$$R = \frac{a}{t + b} \quad (8.1.2)$$

where

R : rainfall intensity (mm/h)

t : rainfall duration (min)

a, b, n : constants

It is known that the relation between the maximum rainfall P and the rainfall duration can generally be expressed by $P = aTn^{0.1}$. Also, an experimental equation has been proposed which takes into consideration the type of rain and topography²⁾. The rainfall intensity in a scale of 1 hour or less is generally determined from an observed hourly precipitation by **equation (8.1.3)**.

$$R = 7.7R_0T^{0.5} \quad (8.1.3)$$

where

R : rainfall intensity in a target time scale (mm/h)

R_0 : rainfall intensity observed in an hour (mm/h); use a N -year probability rainfall for 60-min if available

T : target time scale less than 1 hour (min)

The maximum rainfall can be calculated using **equation (8.1.4)** when the total precipitation is massive as in typhoon or rain outflow from mountainous drainage basin is of concern.

$$P = 83D^{0.33} \quad (8.1.4)$$

where

P : maximum rainfall (mm)

D : rainfall duration (h)

(3) Fog

Fog interferes with ships' navigation and entry to and departure from the port. It also degrades the availability of port facilities. Although a few systematic investigations have been conducted on troubles caused by fog, a hearing survey example in the Seto Inland Sea and others has been reported³⁾.

(4) Snowfall

In districts where snowfall is expected, snowfall on the apron becomes live load as it is or hardened with rolling compaction by vehicles and others. **Part II, Chapter 10, 3.1 Live Load** may be referred to for more details.

(5) Atmospheric temperature

In the performance verification of statically indeterminate structure, consider the impact of temperature stress due to temperature change as an environmental action when needed.

8.2 Assessment of the Operating Rate of Construction Work Considering Meteorology and Oceanology

(English translation of this section from Japanese version is currently being prepared.)

[References]

- 1) Kawabata Y.: Hydro-meteorology, Chijinn Shokan Publishing, p. 33, 1961
- 2) Yamada, T., T. Hibino, T. Araki and M. Nakatsugawa: Statistical characteristics of rainfall in mountainous basins, Jour. JSCE No. 527, pp. 1-13, 1995
- 3) Sasa, K., Mizui, S. and Hibino, T.: A Basic Study on Difficulties of Ship Operation Under Restricted Visibility Due to Heavy Fog, Journal of Japan Institute of Navigation, Vol. 112, 2005

Chapter 3 Geotechnical Conditions

[Public Notice] (Geotechnical Conditions)

Article 13

Geotechnical conditions shall be set appropriately in terms of the soil's physical and mechanical properties based on the results of ground investigations and soil tests.

[Interpretation]

7. Setting of Natural Conditions

(5) **Items related to ground** (the Article 6 of the Ministerial Ordinance and the interpretation related to Articles 13 to 15 of the Public Notice)

① Geotechnical conditions

The various geotechnical conditions represent the geotechnical characteristics taken into consideration during performance verification of the facilities subjected to the technical standards. The geotechnical conditions shall be set by appropriately determining their reliability based on the results of ground investigations and soil tests carried out by appropriate methods.

② Ground investigation

Ground investigations for setting the geotechnical conditions shall appropriately take into consideration the structures, scale, and importance of the facilities subjected to the technical standards, as well as the properties of the ground close to the facilities' locations.

③ Soil tests

The soil tests for setting the geotechnical conditions shall be carried out using the methods capable of appropriately setting the geotechnical conditions considering performance verification of the facilities subjected to the technical standards.

1 Ground Investigations

1.1 Methods for Determining Geotechnical Conditions

- (1) The geotechnical conditions necessary for performance verification and construction planning include: the stratification conditions of ground, such as depths of the bearing strata, depths of the engineering foundation strata, thicknesses of weak strata; groundwater levels (residual water level); density (degree of compaction and relative density); physical characteristics; shear characteristics; consolidation characteristics; permeability; and liquefaction characteristics. Soil is strongly stress-dependent and greatly changes its mechanical characteristics over time in the case of consolidation or fluctuations in overburden, etc. Therefore, new ground investigations shall be planned and carried out when necessary depending on the situation. However, considering the limited ground investigations which can be actually implemented, it is necessary to proactively use previous information (including databases, etc.) obtained from document surveys. In this case, due consideration shall be given to confirming whether the fluctuations in overburden or progress of consolidation have changed the geotechnical conditions.

1.2 Positions, Intervals, and Depths of Ground Investigation Spots

- (1) The positions, intervals, and depths of ground investigation spots shall be determined in accordance with the stress distribution in the ground caused by the sizes and weights of object facilities, and the uniformity in ground stratification. However, in light of the need for due consideration of the construction costs and facilities' importance, it is not possible to categorically regulate the number of investigation spots and their depths. When determining the locations, intervals, and depths of investigation spots, the homogeneity or inhomogeneity of the ground is the most important aspect. Therefore, it is effective to conduct a preliminary check on the homogeneity or non-uniformity of the ground, with reference to the past investigation results, and the topography of land areas, or through geophysical exploration methods, such as sonic wave and surface wave exploration.

Although it is preferable not to determine target intervals of investigation spots mechanically to the extent possible, the target intervals and ranges of boring and sounding shown in **Table 1.2.1** can be used as references.

The ground investigation depths shall be enough to confirm strata with sufficient bearing capacity. Whether or not strata have sufficient bearing capacity depends on the types and scales of facilities and, therefore, cannot be categorically determined. As a guide, however, the ground investigations may be terminated after confirming: the strata which have an SPT-N value obtained through the standard penetration tests of 30 or more and thicknesses of at least several meters in the case of small-scale facilities or facilities having foundation structures other than end-bearing piles; or the strata which have an SPT-N value of 50 or more and thicknesses of at least several meters in the case of large-scale facilities expected to be supported by end-bearing piles. Also, the ground investigations for performance verification of seismic resistance shall be conducted until the strata having shear wave velocities of 300 m/s or more (engineering bedrock) are confirmed.

- (2) For details on ground investigation methods, **Reference (Part II), Chapter 1, 3 Ground Investigations and Tests, and Methods and Commentaries for Ground Investigation¹⁾** can be used as a reference.

Table 1.2.1 Target Intervals and Ranges of Boring and Sounding Investigation Spots

- ① In the case where the stratigraphical conditions are comparatively uniform both horizontally and vertically

(Units: m)

		Face line direction		Perpendicular to face line direction			
		Spacing layout		Spacing layout		Distance from face line (maximum)	
		Boring	Sounding	Boring	Sounding	Boring	Sounding
Preliminary survey	Wide area	300–500	100–300	50	25	50–100	
	Small area	50–100	20–50				
Detailed survey		50–100	20–50	20–30	10–15		

- ② When the stratigraphical conditions are complex

(Units: m)

		Face line direction		Perpendicular to face line direction			
		Spacing layout		Spacing layout		Distance from face line (maximum)	
		Boring	Sounding	Boring	Sounding	Boring	Sounding
Preliminary survey		50 or less	15–20	20–30	10–15	50–100	
Detailed survey		10–30	5–10	10–20	5–10		

Note) A sounding survey may or may not require a borehole.

The sounding surveys in the table are only those for which a borehole is not necessary. For sounding surveys that require a borehole, “the boring column” is applicable.

1.3 Selection of Investigation Methods

- (1) The investigation methods most suitable for investigation purposes shall be selected considering the scope of investigations, the facilities’ importance, and economic efficiency.
- (2) **Table 1.3.1** shows the investigation methods by investigation purposes and ground information obtainable through the methods.

Table 1.3.1 Investigation Methods by Investigation Purposes

Classification	Survey objective	Survey method	Survey details
Stratigraphical conditions	Confirmation of stratigraphical conditions	Boring Sounding Geophysical exploration	Foundation depth Thickness of weak strata Sequence of strata
Physical characteristics	Classification of soil properties	Undisturbed sampling (disturbed sampling is possible for all except γ_t , but pay attention to the discharge of fine grain fraction or particle crushing, etc.)	Wet unit weight γ_t Water content w Soil particle density ρ_s Particle size distribution Consistency w_L, w_P, I_P
(Hydraulic conductivity)	Hydraulic conductivity	Undisturbed sampling In-situ tests	Hydraulic conductivity k
Mechanical properties	Bearing capacity	Undisturbed sampling Sounding In situ tests	Undrained shear strength c_u
	Slope stability		Unconfined compressive strength q_u
	Earth pressure		Shear strength τ_f Cohesion c Angle of shear resistance ϕ Relative density D_r
	Consolidation characteristics	Undisturbed sampling	Compression index C_c Compression curve e -log p Coefficient of consolidation c_v Coefficient of volume compressibility m_v Coefficient of secondary consolidation C_a
	Compaction characteristics	Disturbed sampling also applicable In- situ tests	Maximum dry density ρ_{dmax} Optimum water content w_{opt} CBR
	Dynamic characteristics	Undisturbed sampling In- situ tests	Shear modulus G Attenuation coefficient h_p Liquefaction characteristics

(3) Types of ground investigation methods**① Collection and analyses of existing materials**

It is necessary to examine the outline of the ground properties of investigation areas through boring data, soil databases, records of groundwater levels, deformation of neighboring structures, records of ground settlement, and ground formation processes (geological information in the case of natural ground and development records in the case of artificial ground).

② Field surveys for geological and topographical conditions

Although the field surveys which are generally practiced for onshore ground investigations are not available for offshore ground investigations, the onshore field surveys in the areas close to offshore investigation spots are still important, even for offshore ground investigation, because offshore geology has close relation with onshore geology.

③ Geophysical explorations (elastic wave exploration, surface wave exploration, electric resistance)

Because geophysical explorations can be implemented on ground surfaces, they can be used to obtain information on the stratification conditions and groundwater levels in extensive areas. However, it is preferable to verify the soil properties and depths obtained through the geophysical explorations by comparing them to boring data to the extent possible.

④ Acoustic exploration

Acoustic exploration is effective to grasp offshore geology promptly. These technologies were originally developed to explore mineral resources like crude oil; therefore, they have been used for deep ground explorations. Owing to the improvement in sound sources, receivers, and processing systems, as well as

enhanced positioning accuracy with the use of GPSs, however, there has been considerable improvement in acoustic exploration accuracy. Still, there may be cases where the gases and gravel in ground cause acoustic waves to diffuse before reaching predetermined depths. Also, it shall be noted that the values obtained through acoustic exploration are not distances, but reflection time of compression waves. Thus, it is always necessary to combine acoustic exploration with boring or sounding, which enables depths to be measured reliably so as to confirm which reflecting layers obtained through the acoustic exploration correspond to which geological strata obtained through boring or sounding.

⑤ Boring

Boring is conducted to create soil profiles by getting information on stratification conditions and soil types through observing mud water from boreholes while drilling them. Also, the boreholes are used for sampling specimens and implementing sounding, such as the standard penetration test. To sample high quality specimens or obtain high quality sounding test results, it is necessary to implement boring so as not to disturb soil to the extent possible. For this purpose, boring is generally implemented with rotary type mechanical boring machines, which are considered to least disturbing to soil. When obtaining various constants necessary for performance verification, it is preferable to implement sampling for cohesive soil and the standard penetration test for sandy soil.

⑥ Sampling

When examining cohesive soil properties, some tests require undisturbed (less disturbed) specimens while others do not. When conducting mechanical tests to obtain shear strength and consolidation characteristics, it is preferable to use undisturbed specimens sampled with thin-walled samplers with fixed pistons. When such samplers are not available, undisturbed specimens can be obtained with rotary double tube samplers (Denison samplers) or rotary triple tube samplers. Sampling is to acquire less disturbed specimens which are used in laboratory tests as undisturbed specimens for obtaining the characteristic values of constants used in performance verification. The specimen collection device attached to the tip of equipment used for the standard penetration test is also called a sampler. However, there is no reason to use such a collection device for purposes other than soil classification. It is necessary to keep in mind that sampling is not just to collect soil, but to collect specimens subjected to soil tests.

⑦ Sounding

The methods for examining ground properties are classified into laboratory tests using specimens obtained through sampling and sounding (alternatively called in-situ tests) to obtain soil parameters with measuring devices directly inserted into, rotated inside, or pressed against the ground. Sounding is a collective term of methods which measure parameters (SPT-N values, tip resistance, pore water pressure, etc.) through in-situ tests and indirectly estimate soil parameters using the relational formula (empirical or theoretical formula) showing the relationships between the parameters and the soil parameters. Sounding is further classified into the tests using boreholes drilled to the depths where soil is tested in-situ, as is the case with the standard penetration test and the tests which can be implemented (without using boreholes) in a manner that directly inserts cone probes into ground, as is the case with the electric cone penetration test.

The comparisons of the characteristics of the laboratory tests and sounding are as follows.

(a) Disturbance

No matter how carefully specimens are sampled, they are inevitably subjected to disturbance due to stress release when exposed to atmospheric pressure. In contrast, sounding measuring parameters through in-situ tests are less likely to be affected by such disturbance.

(b) Boundary conditions

The triaxial test is a good example for easily understanding the difference in boundary conditions between laboratory tests and sounding. The boundary conditions of laboratory triaxial tests are clearly known, and the laboratory triaxial test, which can control drainage conditions, is advantageous in that soil shows different mechanical behavior depending on drainage conditions. In contrast, the boundary conditions of sounding, for example, stress, strain, and drainage conditions, are unclear and the sounding results require rarely theoretical but mostly empirical interpretations.

(c) Time and costs

Generally, laboratory tests take a long time and are expensive. In contrast, sounding, which makes measurement results readily available in-situ, can reduce costs. In addition to the above, there are many

laboratory test and sounding methods. Thus, it is necessary to select appropriate methods suitable for the types of ground, stratification conditions, and the types, as well as required accuracy, of object soil parameters.

[Reference]

- 1) The Japanese Geotechnical Society: Japanese Geotechnical Society Standards, Geotechnical and Geovironmental Investigation methods, 2013.

2 Geotechnical Properties

2.1 Estimation of Geotechnical Properties

(1) General

The design values of geotechnical properties used in performance verification are, in principle, estimated in accordance with the procedure¹⁾ shown in Fig. 2.1.1 following the **Design Principle for Foundation Structures based on the Performance Design Concept (JGS 4001)**. However, if there is a rational reason based on the characteristics of the ground investigations and the soil tests, derived values may be used as characteristic values. For example, in the case of measured SPT-N values through the standard penetration test, derived values can be used as characteristic values because there have been proposals of empirical and correlation equations, taking the variations in the measured values into consideration. Also, as with shear wave velocities measured by the geophysical logging, some measured values are obtained from evaluating the complex in-situ conditions and characteristics of the ground, and each measurement location has a different evaluation object. In these cases, derived values may also be used as characteristic values because statistical processing of plural measurement result is inappropriate.

Also, it is difficult to take into account the extent of individual influences of ground investigation or soil test methods on the variations of ground constants in each performance verification case. Thus, assuming that reliability of ground investigation or soil test methods appears in the form of data variations, characteristic values are subjected to corrections according to the variations. This approach simplifies the performance verification method, enabling partial factors (load resistance factors) to be set regardless of ground investigation and soil test methods. It shall be noted that the characteristic value to be set when the number of data is small or data has large variations is slightly different from the essential concept of making the average derived value a characteristic value, as stipulated in JGS 4001.

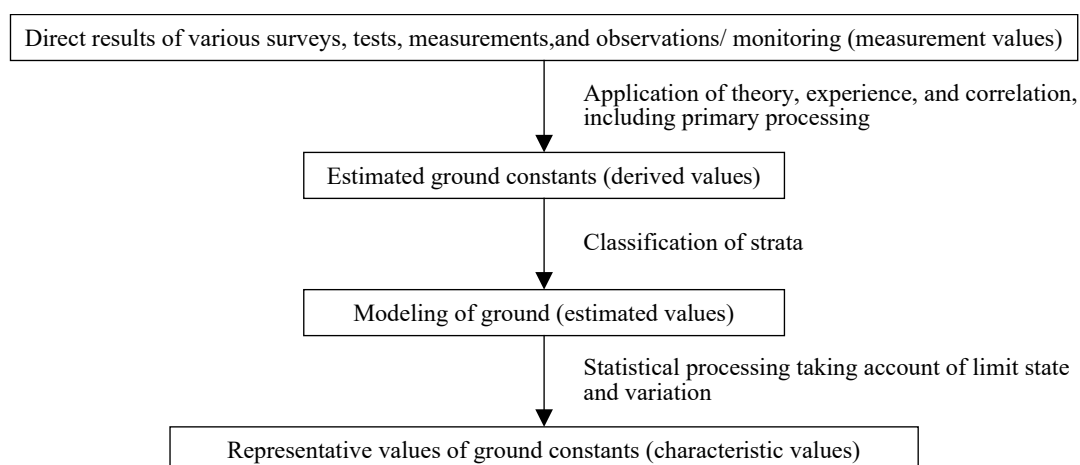


Fig. 2.1.1 Examples of the Procedure for Setting the Characteristic Values of Ground Constants

(2) Methods of estimating derived values

As described below, derived values can be obtained from measured ones through either method which: uses measured values directly as derived ones; applies primary processing to measured values; or converts measured values into different engineering quantities.

- ① The methods which use the measurement values directly as derived ones are, literally, direct ground constant measurements.
- ② The methods which apply primary processing to measured values include: area correction in shear tests; correction for the strain rates' effect on shear strength; and simple correction by multiplying measured values by coefficients. The primary processing also includes simple processing of test results such as calculating water contents w , wet density p_t , soil particle density p_s , and grain sizes; obtaining deformation moduli E from stress-strain relationships; and obtaining consolidation yield stress p_c from the e -log p relationship in compression curves.

- ③ The methods which convert measured values into different engineering quantities use theoretical or empirical formulas, or obtain fitting parameters, in accordance with theoretical formulas. The methods include: converting SPT-N values into angles of shear resistance ϕ using empirical formulas and obtaining consolidation coefficients c_v by fitting theoretical consolidation curves to settlement-time curves.

(3) Methods of setting characteristic values

① General

Characteristic values are set generally in accordance with the procedure shown in Fig. 2.1.2. When the number of derived values is large enough to be subjected to statistical processing, and the variations of the derived values are small, characteristic values can be calculated as the averages (expected) values of the derived ones in principle. Given that the number of the data of derived values n is 10 or more, and they have no significant variation with a coefficient of variation of less than 0.1, the statistical processing results of such data are considered to have a certain level of reliability, enabling their average (expected) values to be characteristic values. However, if there is an insufficient number of data on the derived values to carry out statistical processing, and the variation in the derived values is large, it is necessary to set characteristic values by correcting their average values (expected values) through the method shown below.

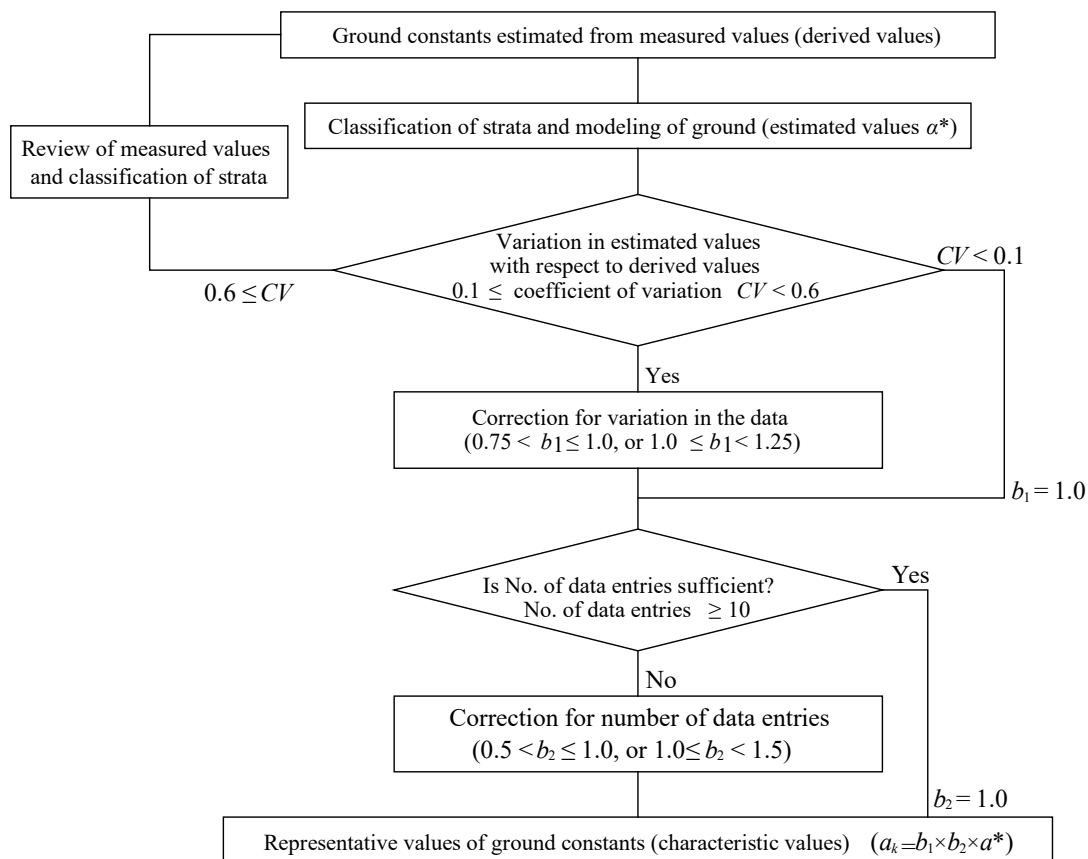


Fig. 2.1.2 Example of the Procedure for Setting the Characteristic Values of Ground Constants

② Correction of the average (expected) values of derived values

When the number of derived values is limited, or the variation in the derived values is large, the characteristic values shall be set not by simply and automatically obtaining the average (arithmetic average value) of the derived values but by appropriately taking into consideration the estimated error of the statistical average value. In this case, the following method may be used. Because characteristic values have such uncertain factors as errors in the ground investigations and soil tests, estimation errors in the derived values, and inhomogeneity in ground itself, it is desirable to determine characteristic values carefully, with due consideration of the ground investigation conditions (such as the types of survey equipment), soil test conditions (such as the types of test equipment and methods and condition of test specimen), and other soil information, such as stratal

organization. The method of correcting the average (expected) of the derived values described here is expected to be applied not only to the values for stability verification of facilities, but also to soil constants in general, including settlement prediction values. The method specified in **JGS 4001** is to set the characteristic values in accordance with confidence intervals, assuming that derived values show a normal distribution, if the standard deviation of the population is known, or a t -distribution if the standard deviation is unknown. However, unlike quality indices for factory products, simple statistical processing is difficult when dealing with geotechnical parameters because of errors attributable to ground investigation and soil test methods, estimation errors of derived values, and the distribution and variations in the derived values attributable to the inhomogeneity of ground itself as well as sedimentation conditions.

To obtain geotechnical parameters (the averages, corresponding to characteristic values, with statistical errors incorporated into them) for reliability design, it is necessary to collect a sufficiently large number of test results for statistical processing. Also, to reflect the soil investigation and soil test results in performance verification, it is necessary to model the distribution in the depth direction of the estimated values a^* of the geotechnical parameters (expressed by “ a ” here), for example: uniform distribution in the depth direction ($a^* = c_1$); linear distribution with estimated values increased in proportion to depth ($a^* = c_1z + c_2$); and quadratic distribution in the depth direction ($a^* = c_1z^2 + c_2z + c_3$). Here c_1 , c_2 , and c_3 are constants. At least 10 pieces of test data are required when a portion of ground is modeled to a certain depth and the model is subjected to statistical processing. The geotechnical parameters obtained through different soil tests (such as undrained shear strength by triaxial test and unconfined compression tests) have different reliability. Therefore, different partial factors (load resistance factors) shall be set for respective parameters; however, there is no way of knowing the degrees of difference in these partial factors. In contrast, it is well-known that the variation coefficients of these two tests results are significantly different. Based on this, the characteristic values are to be calculated not simply by making the arithmetic averages, but by multiplying the estimated values by the correction coefficients that take into account the variation of the derived values. This method is based on having sufficient test data for statistical processing. Therefore, when there is insufficient test data, it is necessary to further set the characteristic values on the safe side in a manner that multiplies the estimated values by the correction coefficients with respect to insufficient test data. In other words, the characteristic values are calculated either by **equation (2.1.1)** or **equation (2.1.2)**. Here, **equation (2.1.2)** is used when it is reasonable to examine the variations of, for example, consolidation yield stress p_c , consolidation coefficients c_v , volume compressibility coefficients m_v , etc. on logarithmic axes.

$$a_k = b_1 b_2 a^* \quad (2.1.1)$$

$$\log a_k = b_1 b_2 \log a^* = \log a^{*b_1 b_2} \quad (2.1.2)$$

where

- a_k : a representative value of a ground constant (characteristic value);
- b_1 : a correction coefficient with respect to the variation in the derived values;
- b_2 : a correction coefficient with respect to the number of data on derived values; and
- a^* : a model value of the ground constant (estimated value).

A specific correction method (correction coefficient setting method) is described below. When dealing with quantities considered to have balance between action and bearing sides in essence, as is the case with the unit weight of original ground in stability analyses, the correction coefficient values b_1 and b_2 can be set at 1.

③ Method of setting correction coefficients with respect to derived value variations

When examining the variation of test results a with the estimated geotechnical parameters, obtained by modeling the distribution of the test results expressed by a^* , it is convenient to use the standard deviation a/a^* , the normalization of a with a^* (called a coefficient of variation, or CV). Here, this is based on the major premise that a^* is uniformly distributed in a model stratum at its average value or distributed in a manner that enables the least square method to minimize errors. The CV s of the geotechnical parameters, obtained by sampling less disturbed specimens from uniform ground with a thin-walled tube sampler with a fixed piston, and carefully conducting variety of soil tests using the sampled specimens as undisturbed specimens, are 0.1 or less. In other words, test results inevitably vary at this level because even homogeneous ground has a certain

amount of inhomogeneity, and even carefully conducted soil tests are subjected to errors. Test results may have larger variations in cases where the ground is inhomogeneous, sampling causes large disturbance in specimens, soil test methods are conducted improperly, or the ground is modeled with inappropriate distribution of values in depth direction. In such cases, characteristic values need to be set on the safe side considering the effects of uncertain factors without applying estimation values a^* directly to the characteristic values.

Therefore, the correction coefficient b_1 with respect to the variations of the derived values are set in accordance with the CV s, defined as the standard deviations SD of (a/a^*) . When an object parameter a contributes to the bearing side (advantageous for design such as shear strength) in performance verification, the correction coefficient can be set at about $b_1 = 1 - (CV/2)$. When contributing to the action side (disadvantageous for design such as the unit weight of earth fill and compression indexes), the correction coefficient can be set at about $b_1 = 1 + (CV/2)$. Based on this concept, the values to be used in performance verification are calculated and summarized as shown in **Table 2.1.1**. The concept of the correction coefficient b_1 is to apply the derived values corresponding to the cumulative probability density of about 70% (called fractal values) to the characteristic values. If the CV s are 0.6 or higher, the test results are unreliable for performance verification. In such a case, the interpretation of test results shall be revised and, if necessary, the ground modeling shall be reexamined. There may be a case of redoing ground investigations.

Table 2.1.1 Values of Correction Coefficients

Coefficient of variation CV	Correction coefficient b_1	
	When it is necessary to correct the characteristic value to a value smaller than the derived values	When it is necessary to correct the characteristic value to a value larger than the derived values
$\geq 0, < 0.1$	1.00	1.00
$\geq 0.1, < 0.15$	0.95	1.05
$\geq 0.15, < 0.25$	0.90	1.10
$\geq 0.25, < 0.4$	0.85	1.15
$\geq 0.4, < 0.6$	0.75	1.25
≥ 0.6	Re-investigate the interpretation of the results or the modeling, or re-do the survey	

There are cases of examining the logarithmic distribution of test results when obtaining some geotechnical parameters, such as consolidation yield stress p_c , the consolidation coefficients c_v , and the volume compressibility coefficients m_v . When obtaining the characteristic values of these geotechnical parameters by conducting a large number of soil tests, assuming the object ground is uniform, it is reasonable to examine the variations on logarithmic axes because these geotechnical parameters show logarithmic normal distribution. That is, the CV can be expressed by the standard deviations SD of $\log a / \log a^*$ with respect to the geotechnical parameter a and, therefore, the values in **Table 2.1.1** can be used directly as the correction coefficient b_1 on the logarithmic axes. In the case of the angles of shear resistance ϕ , the variations of $\tan \phi$, not the variations of ϕ , should be examined by taking their mechanical significance into consideration. However, there is no need to consider CV when dealing with the angles of shear resistance of mound materials because the characteristic values to be used for performance verification have already been specified empirically, and the influences of the variations are already incorporated in these values. Here, the CV need to be applied to the characteristic values obtained from statistical processing of reported soil test results. In other words, **Table 2.1.1** does not show the required levels of variations that ground investigation and soil test results need to satisfy, but the values corresponding to the variation levels required when evaluating ground investigation and soil test results.

④ Method of setting correction coefficients with respect to the number of data on derived values

In ③ Method of setting correction coefficients with respect to derived value variations, the method is based on the availability of sufficient data to conduct statistical processing. However, if there is insufficient data for statistical processing, the correction coefficients b_2 with respect to the number of data on derived values shall be applied based on the concept that statistical results cannot have a certain degree of reliability unless the number of data is 10 or more. The characteristic values shall be corrected by $b_2 = \{1 \pm (0.5/n)\}$ when there is insufficient data. Here, in the formula of b_2 , the negative sign is used to correct the characteristic values of geotechnical parameters used in performance verification if they should be smaller than the derived values, and the positive sign is used to correct the characteristic values if they should be larger than the derived values. For

performance verification, there must be two or more data on derived values. However, even in the case where there is only one piece of data on a derived value, the data can still be used for performance verification provided that other parameters (for example SPT-N values or grain size distribution) are available and the distribution of the derived values can be modeled based on the correlation (limited to generally known correlation) between the derived values and the parameters. In such a case, b_1 and b_2 shall be set at 1 and 1 ± 0.5 respectively.

⑤ Method of setting characteristic values taking into consideration modes of the performance verification

Soil parameters with respect to consolidation and shear strength are not mutually independent. In performance verification, if these parameters are considered independent, the characteristic values can be obtained by taking the reliability of the respective parameters into consideration. However, the parameters with respect to consolidation need to be closely related to those with respect to shear strength. For example, the stability evaluation needs to consider the effect of consolidation on strength increases. In this case, in the process of obtaining characteristic values from derived values, the respective parameters must be correlated when modeling the distribution of soil test results and obtaining the estimated values. For example, given the relationship of $c_u = m \times \text{OCR} \times \sigma'_{v0}$ derived from the strength increase ratio of $m = c_u/p_c$ and the overconsolidation ratio of $\text{OCR} = p_c/\sigma'_{v0}$ where σ'_{v0} is an effective soil overburden pressure, p_c is consolidation yield stress, and c_u is undrained shear strength, the characteristic values are preferably set through the statistical processing of the variations based on the estimated geotechnical parameters consistent with the relationship.

2.2 Physical Property of Soil

2.2.1 Unit Weight of Soil

- (1) The unit weight of soil shall be obtained through laboratory tests by 1) following the **test method for bulk density of soils (JIS A 1225)** after collecting less disturbed specimens and preserving in-situ conditions; 2) directly through in-situ tests following the **test method for soil density by the sand replacement method (JIS A 1214)**; or 3) through indirect tests following the **test method for soil density using a nuclear gage (JGS 1614)**.
- (2) The unit weight normally means the weight per unit volume in air, including the wet unit weight and dry unit weight. Also, the unit weight in water (weight per unit volume from which buoyancy is deducted) is referred to as the submerged unit weight. To measure the unit weight, methods of collecting the less disturbed specimens of cohesive soil have been established, and it is possible to obtain specimens representing in-situ conditions. Therefore, the unit weight of cohesive soils can be obtained from laboratory tests. However, the unit weight of sandy soils or sand must be obtained directly in-situ. For the unit weight of sandy soil or sand, there are cases of obtaining it through in-situ density logging or RI cone penetration tests.

The wet unit weight is one of the indices indicating the soil's fundamental properties and is used to calculate soil stiffness, degrees of looseness, the weight of soil masses and void ratios.

① Wet unit weight

The wet unit weight is generally expressed by **equation (2.2.1)** as the sum of the weight of soil particles and the weight of water (seawater at sea bottoms) within the voids per unit volume.

$$\gamma_t = \rho_t g = \frac{\rho_s + \frac{S_r}{100} e \rho_w}{1 + e} g = \frac{1 + \frac{w}{100}}{1 + e} \rho_s g \quad (2.2.1)$$

where

- γ_t : wet unit weight (kN/m³);
- ρ_t : bulk density (t/m³);
- ρ_s : soil particle density (t/m³);
- e : a void ratio;
- S_r : the degree of saturation (%);
- w : a water content (%);
- ρ_w : the density of seawater (t/m³); and

g : gravitational acceleration (m/s^2).

The approximate values of the unit weight of soil in port and harbor areas in Japan are generally in the ranges shown in **Table 2.2.1** or in the ranges of the histogram shown in **Fig. 2.2.1**. As can be seen in **equation (2.2.1)**, the unit weight has a close relationship with moisture contents. The relationships between the unit weight and moisture contents are shown in **Fig. 2.2.2** and **2.2.3**.

Table 2.2.1 Unit Weight and Water Contents of Typical Soil

	Holocene clays	Pleistocene clays	Sandy soils
Wet unit weight γ_t (kN/m^3)	12–16	16–20	16–20
Dry unit weight γ_d (kN/m^3)	5–14	11–14	12–18
Water content w (%)	150–30	60–20	30–10

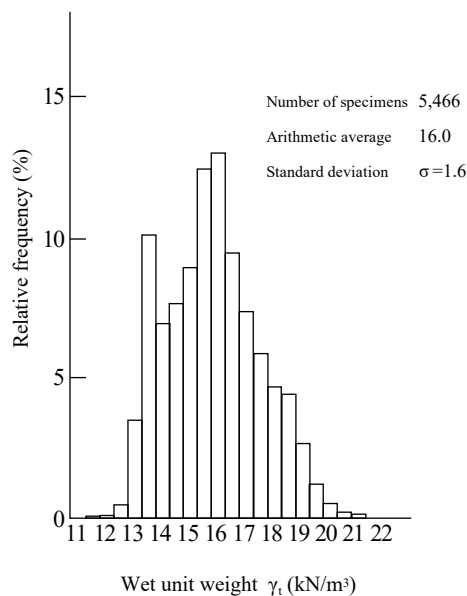


Fig. 2.2.1 Histogram of Wet Unit Weight²⁾

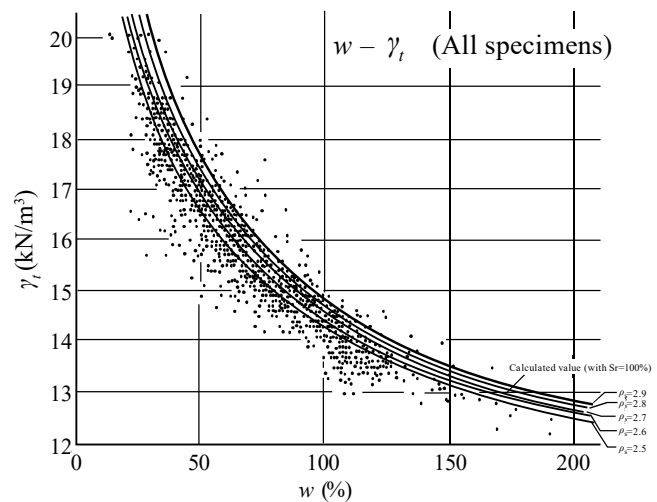


Fig. 2.2.2 Correlation Diagram between Wet Unit Weight and Moisture Contents³⁾

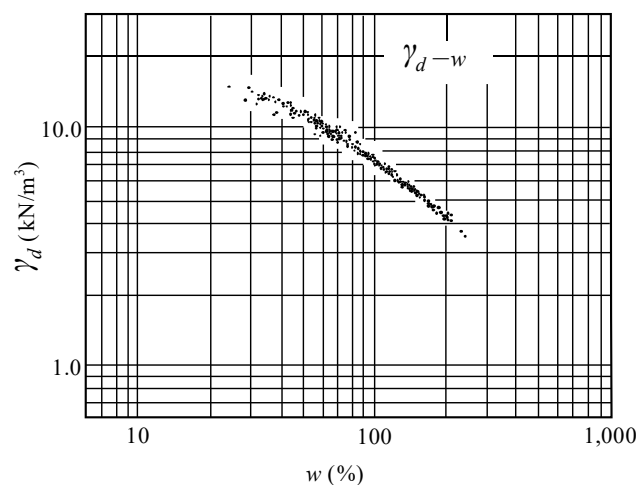


Fig 2.2.3 Correlation Diagram between Dry Unit Weight and Moisture Contents²⁾

② Dry unit weight

The dry unit weight considers only the weight of soil particles per unit volume of soil and is expressed by **equation (2.2.2)** which can be obtained by substituting 0 for w and S_r in **equation (2.2.2)**.

$$\gamma_d = \rho_d g = \frac{\rho_s g}{1 + e} \quad (2.2.2)$$

where

γ_d : dry unit weight (kN/m³); and

ρ_d : dry density (t/m³)

Also, the relationship between wet unit weight γ_t and dry unit weight γ_d is given by the following equation.

$$\gamma_d = \frac{\gamma_t}{1 + \frac{w}{100}} \quad (2.2.3)$$

③ Submerged unit weight

Given that the voids are fully saturated with water, the submerged unit weight can be expressed by **equation (2.2.4)** taking buoyancy into account.

$$\gamma' = \gamma_{sat} - \gamma_w = \frac{\rho_s - \rho_w}{1 + e} g \quad (2.2.4)$$

where

γ' : immersed unit weight (kN/m³);

γ_{sat} : saturated unit weight (kN/m³); and

γ_w : the unit weight of water (or seawater at sea bottom) (kN/m³).

Although the unit weight of water γ_w depends somewhat on salt concentrations and temperatures, correct values are known. Therefore, such dependency does not cause variations of the unit weight of water. Thus, when obtaining the characteristic values of saturated foundations, considering the variations in their unit weight, variations not in γ_{sat} but in γ' can be considered.

The histogram of the density ρ_s of soil particles is shown in **Fig. 2.2.4** for reference.

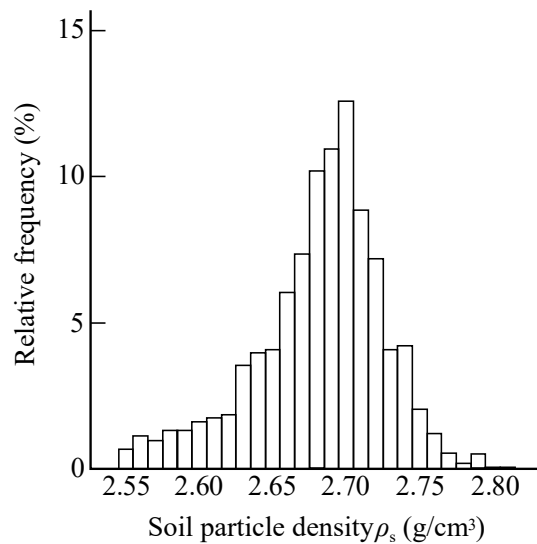


Fig. 2.2.4 Histogram of the Soil Particle Density

(3) Measurement of in-situ unit weight

The methods for directly obtaining the in-situ unit weight include those applicable only to the soil close to ground surfaces and those applicable to soil at deep depths. A simple method, specified in **JIS A 1214** the **test method for soil density by the sand replacement method** (the so called sand replacement method), is an example of the former methods. Also, the **test method for soil density using nuclear gage** specified in **JGS 1614** is an example of the latter methods.

① Sand replacement method

The sand replacement method is mainly used for measuring soil close to land surfaces to manage earth works, but it can be applied to the measurement at a certain depth where pits can be excavated. For the details of the sand replacement method, refer to **JIS A 1214**.

② Method using radioisotope (RI)

In recent years, RI has become available relatively easily. Although there are strict statutory regulations for using RI, such as the **Act on Prevention of Radiation Hazards due to Radioisotopes, etc.** and its related laws and ordinances, there have been many cases of measuring in-situ unit weight with γ -ray densitometers when it is difficult to obtain undisturbed specimens of sand and sandy soil. Also, there are no legal restrictions on using sealed radioactive sources with source intensities of 3.7 MBq (megabecquerel) or less.

As introduced in one of the standards of the Japanese Geotechnical Society, titled the **Test Method for Soil Density Using Nuclear Gauge (JGS 1614)**, there are two types of γ -ray densitometers to which RI has been applied: one is a surface type and the other is an insertion type. Just like the name implies, the surface type is suitable for measuring near the ground surface and is used to manage earth work, as is the case with the sand replacement method. The surface type is further classified into a back scattering system and a transmission system. The back scattering system had been used frequently soon after the development of γ -ray densitometers but, in recent years, the transmission system, which is advantageous in terms of accuracy, has become more popular. On the other hand, the insertion type is suitable for measuring the density distribution in the vertical direction or depth direction. For example, the insertion type is used to examine the density distribution in the depth direction in: foundation ground investigations; determining soil improvement effects through density measurement of replaced sand; and the density measurement of filling sand in caissons.

The RI method is advantageous in that it is nondestructive, capable of measuring in-situ density, and can be implemented with simple measurement operation. However, depending on the level of radiation danger associated with the intensity of radioactive sources, there are several regulations on RI equipment operation. Thus, the RI method cannot be implemented easily. In addition, in surveys associated with port construction, the type of γ -ray densitometer which has been used mainly is the insertion type, requiring access pipes to be inserted into ground. In this respect, measurement accuracy is affected by the materials, quality, and insertion conditions of the access pipes; in particular, the degree of disturbance of the soil around the access pipes when they are inserted and the adhesiveness between the access pipes and soil. Recently, a new type of RI equipment,

called the RI cone penetrometer, has been commercialized. The RI cone penetrometer incorporates RI in a cone probe, so measurements can be made with the cone probe inserted directly into the ground.

(4) Relative density

The degree of compaction (looseness) of sand can be expressed by the relative density defined by **equation (2.2.5)**.

$$D_r = \frac{e_{\max} - e}{e_{\max} - e_{\min}} = \frac{\rho_d - \rho_{d\min}}{\rho_{d\max} - \rho_{d\min}} \frac{\rho_{d\max}}{\rho_d} \quad (2.2.5)$$

where

D_r : relative density;

e_{\max} : the void ratio in the loosest state;

e_{\min} : the void ratio in the densest state;

e : the void ratio of a specimen in the present state;

$\rho_{d\min}$: dry density in the loosest state (g/cm³) or (t/m³);

$\rho_{d\max}$: dry density in the densest state (g/cm³) or (t/m³); and

ρ_d : dry density of a specimen in the present state (g/cm³) or (t/m³).

Sand density is greatly affected by the shapes and grain size compositions of particles. The typical parameters expressing sand density as absolute quantities are the unit weight and the void ratios calculated from it. However, the dominant parameter expressing sand's mechanical properties is the relative density D_r which shows the degree of compaction; in other words, the relative value within the void ratio range that object sand can possibly take. The values of e_{\max} , e_{\min} , $\rho_{d\min}$, and $\rho_{d\max}$ necessary for obtaining D_r can be measured in accordance with the **Test Method for Minimum and Maximum Densities of Sands (JIS A 1224)**.

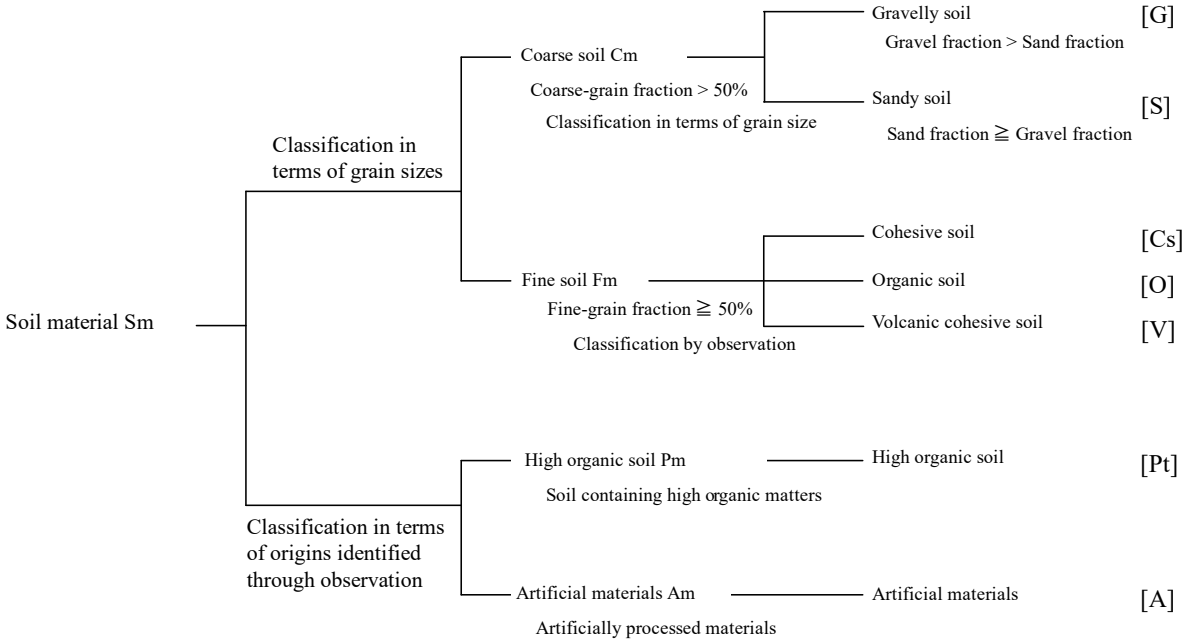
Because it is difficult to take undisturbed specimens of sand, there are many cases of indirectly obtaining the relative density through sounding (Refer to **2.3.4(4) Angle of shear resistance of sandy ground**).

2.2.2 Classification of Soil

- (1) Soil is classified in terms of the grading for coarse soil and the consistency, which represents the degrees of softness or hardness of soil affected by moisture contents, for fine soil in general case.
- (2) The mechanical properties of soil, such as strength and deformation, have close relationships with grading in the case of coarse soil and its consistency in the case of fine soil.
- (3) **Engineering classification method of subsoil materials (the Japanese unified soil classification system)**

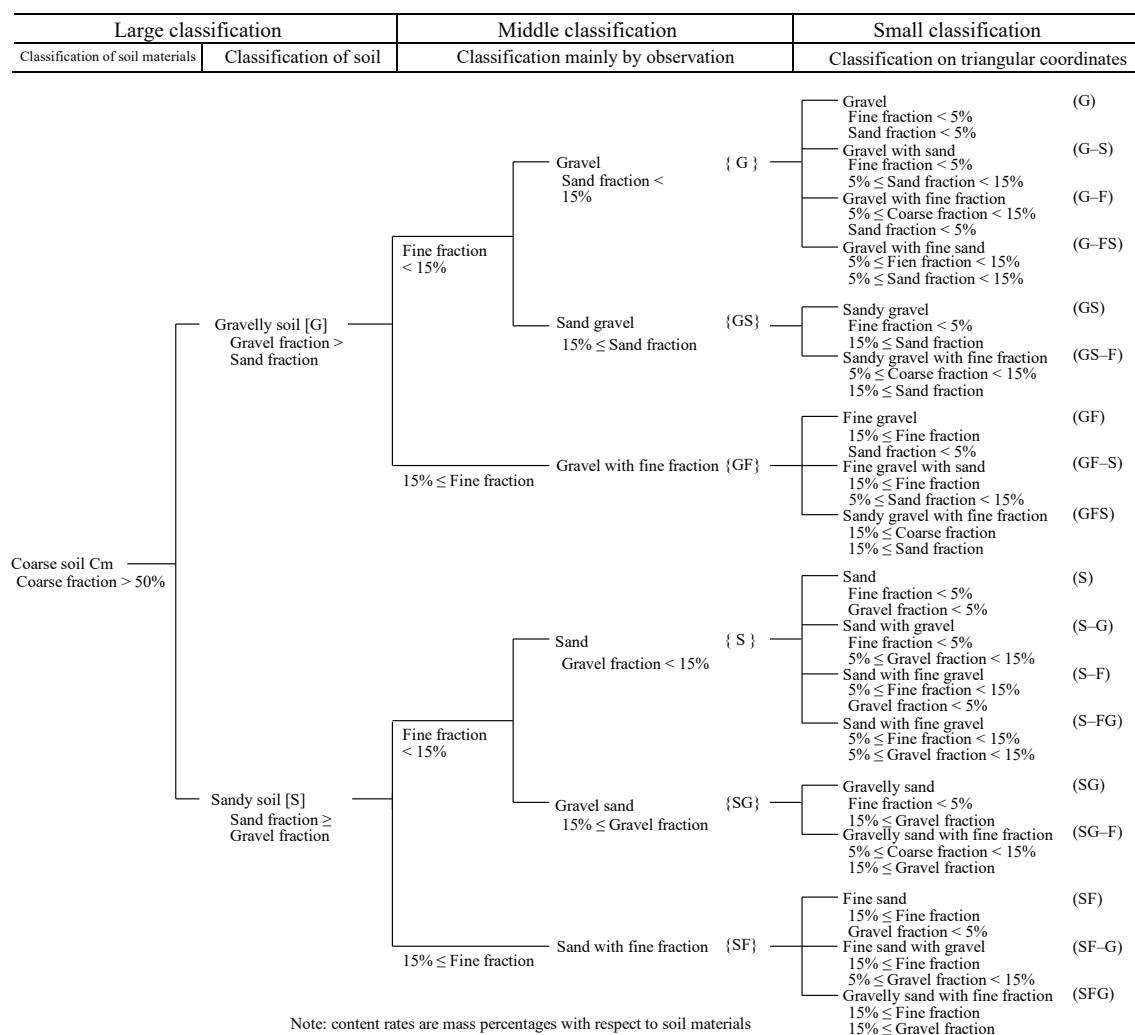
The methods for classifying soil and rock and expressing the classification results can conform to the **Engineering Classification Method for Subsoil Material Prescribed (JGS 0051)** (Japanese Unified Soil Classification System). The grain size classifications of subsoil materials and their nominal designations are shown in **Fig. 2.2.5**. Coarse soil consists primarily of the grain components having grain sizes in the range from 75 μm to 75 mm. Fine soil consists primarily of grain components having grain sizes smaller than 75 μm . **Fig. 2.2.6** and **Fig. 2.2.7** show the engineering soil classification system, and **Fig. 2.2.8** shows the plasticity chart used in the classification of fine soil.

(Note) The word "particle" is affixed when referring to a constituent particle belonging to a particular category; and the word "fraction" is affixed when referring to a component belonging to a particular category.

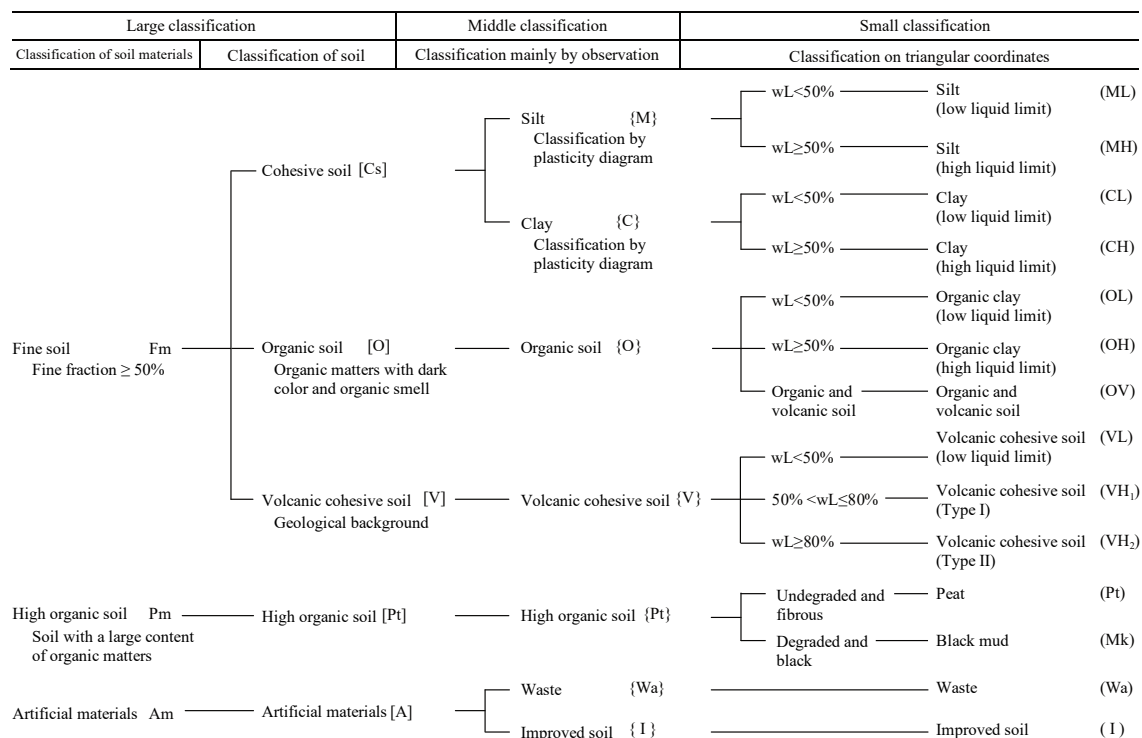


Note: content rates are mass percentages with respect to soil materials

Fig. 2.2.6 Engineering Classification of Subsoil Materials (Large Classification) (JGS 0051)



(a) Engineering Classification System of Coarse Soil



(b) Engineering Classification System of Major Fine Soil

Fig. 2.2.7 Engineering Classification Method for Subsoil Material (JGS 0051)

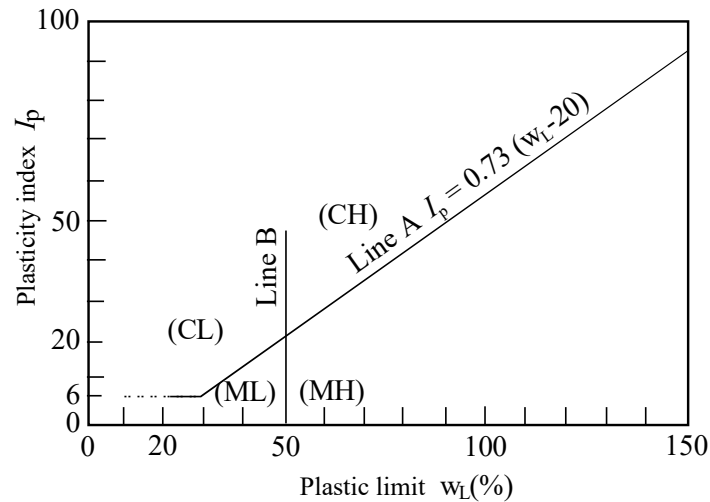


Fig. 2.2.8 Plasticity Chart Used for the Classification of Fine Soil (JGS 0051)

(4) Classification by grain size

Grain sizes have particularly close relationships with the engineering properties of coarse soil. The classification by grain size is to classify several types of soil particles constituting soil in terms of the content ratios of certain ranges of grain diameters. Generally, the content ratios of fine particles with grain sizes smaller than $75 \mu\text{m}$ are measured through the sedimentation analysis method, using hydrometers. Coarse particles with grain sizes of $75 \mu\text{m}$ or more are measured through the sieving analysis method. These measuring methods are specified in the **Test Method for Particle Size Distribution of Soils (JIS A 1204)**. The analysis results are expressed as grain diameter accumulation curves to obtain uniformity coefficients U_c , coefficients of curvature U'_c , and effective grain diameter D_{10} .

The uniformity coefficient U_c is the numerical expression of grain diameter distribution of sandy soil as shown in equation (2.2.6).

$$U_c = D_{60} / D_{10} \quad (2.2.6)$$

Where

U_c : an uniformity coefficient;

D_{60} : a grain diameter corresponding to 60% by mass passing (counting from smaller diameters) (mm); and

D_{10} : a grain diameter corresponding to 10% by mass passing (mm).

Large uniformity coefficients U_c mean that soil has wide and uniform grain size distribution, which is called “well graded.” In contrast, small uniformity coefficients U_c mean that soil has narrow grain size distribution with large concentrations of similarly sized particles, which is called “poorly graded.” In the Japanese Unified Soil Classification System, coarse soil with fine-grain contents lower than 5% is further classified into “well graded soil” and “poorly graded soil” in terms of U_c as follows.

Well graded soil: $10 \leq U_c$

poorly graded soil with classified grain distribution: $U_c < 10$

(5) Role of cohesive soil particles

Cohesive soil characteristics are the result of the activations of colloid particles with diameters of 1 to $2 \mu\text{m}$ or smaller and completely different from those of soil with larger particle diameters in terms of mineral textures and physicochemical properties. Cohesive soil has unique engineering properties obtained through the sedimentary environment formed together with coexisting materials (such as amorphous colloid and salts). Thus, when examining soil's engineering characteristics, it is necessary to focus on the qualitative and quantitative analyses with respect not to cohesive soil particles with diameters of $5 \mu\text{m}$ or smaller, but to colloid particles with diameters of $1 \mu\text{m}$ or smaller and coexisting materials. However, commonly used existing grain size tests have accuracy

problems for particles with diameters of 5 μm or smaller in terms of the appropriateness of dispersing particles and stabilizing dispersed particles, appropriateness of applying the Stokes' law to the sedimentation method, and errors associated with the hydrometer method.

In contrast, because the consistency tests show particle activation, including the influences of coexisting matters, for the purpose of the engineering classification of fine particles, it is rational to use a classification method based on the results of the consistency test, which can be carried out more easily than the grain size test.

(6) Relationship between consistency and engineering properties of cohesive soil

Consistency is one of the physical properties with which the engineering properties of cohesive soil have a close relationship. Consistency is generally expressed in the forms of liquid limit w_L or plastic limit w_p measured through the **Test Method for Liquid Limit and Plastic Limit of Soils (JIS A 1205)**; and plasticity index $I_p (= w_L - w_p)$ or liquidity index $I_L (= w_n - w_p)/I_p$ which can be obtained from those limits and natural water content w_n . For further information on the relationship between the engineering properties and consistency of cohesive soil, reference can be made to the literature by Ogawa and Matsumoto³⁾.

2.2.3 Coefficient of Permeability of Soil

- (1) When the seepage flow in completely saturated ground can be considered as a steady laminar flow, the coefficient of permeability can be calculated in accordance with the Darcy's law.
- (2) The coefficient of permeability k is calculated by **equation (2.2.7)** in accordance with the Darcy's law with the measured values of a cross-sectional area of soil A , a hydraulic gradient i and the volume of seepage flow in unit time q .

$$k = \frac{q}{iA} \quad (2.2.7)$$

where

k : the coefficient of permeability (cm/s) or (m/s);

q : the volume of water flow in a soil layer in unit time (cm^3/s) or (m^3/s);

i : a hydraulic gradient, $i = \frac{h}{L}$

h : a head loss (cm) or (m);

L : the length of a seepage path (cm) or (m); and

A : a cross-sectional area (cm^2) or (m^2).

The measurement methods for determining k include a laboratory permeability test of undisturbed soil specimens sampled from sites and an in-situ permeability test.

(3) Scope of application of the Darcy's law

Darcy's law needs to be applied to laminar flows which are defined by the critical Reynolds numbers R_e . That is, when effective diameters D_{10} are used, laminar flows need to have the critical Reynolds numbers in the range of $3 < R_e < 10$. This range is considered to correspond to the types of soil with grain sizes smaller than those of medium and coarse sand. It is expressed by the effective diameter D_{10} as shown in **Table 2.2.2**.⁴⁾

Table 2.2.2 Scope of Application of the Darcy's Law (D_{10} : Grain diameter corresponding to 10% by mass passing)

Material	Gravel			Sand gravel	Sand		Sandy soil, silt
	Large	Coarse	Medium		Coarse	Fine	
D_{10} (mm)	75	26.5	9.5	2.0	0.6	0.25	0.075–0.02
State of seepage flow	Normally disturbed flow in reality			Laminar flow when $i < 0.2$ to 0.3 for loose sand, and $i < 0.3$ to 0.5 for dense sand			Normally laminar flow with general values of i

(4) Laboratory permeability tests

There are two types of laboratory permeability tests: the constant head permeability test and the falling head permeability test. These tests can be conducted in accordance with the **Test Methods for Permeability of Saturated Soils (JIS A 1218)**. When conducting the laboratory permeability tests with undisturbed specimen's sampled in-situ, it is necessary to clarify the installation directions of specimens before measuring because natural soil has been deposited in layers, to some extent, and its permeability differs depending on the specimens' installation directions. In principle, undisturbed specimens are used for laboratory permeability tests but when it is difficult to obtain them (in the case of soil with low fine fraction contents), laboratory permeability tests can be conducted by necessity using disturbed specimens with different densities to obtain the permeability corresponding to the appropriate density. When using disturbed specimens which are subjected to compaction in a laboratory for adjusting density, there may be cases where the measured permeability largely differs from in-situ permeability because the in-situ skeleton structures of soil cannot be restored in these specimens.

(5) In-situ permeability test

Because laboratory test conditions are different from natural ones, in-situ tests are conducted when needed. The in-situ permeability test is conducted in a manner that installs one or two observation wells and measures ground water level fluctuations with water injected into or pumped out of one of the wells. The in-situ permeability test method can be conducted with reference to the **Method for Determining an Aquifer's Hydraulic Properties in Single Borehole (JGS 1314)**.

(6) Approximate values of the coefficients of permeability

Hazen figured out that coefficients of permeability of sand are correlated with effective diameters, and the coefficients of permeability k can be calculated by **equation (2.2.8)** in the case of the sand with relatively uniform density using the uniformity coefficient $U_c < 5$ and the effective diameter $D_{10} = 0.1$ to 0.3 mm.⁵⁾

$$k = CD_{10}^2 \quad (2.2.8)$$

where

k : a coefficient of permeability (cm/s) or (m/s);

C : a coefficient ($C = 100$ (1/cm/s)) or ($C = 10000$ (1/m/s)); and

D_{10} : a grain size called effective diameter corresponding to 10% by mass passing (cm)

Terzaghi argued that **equation (2.2.8)** can also be applied to cohesive soils by using $C=2$ (or 200) but it is necessary to carefully determine such applicability. The approximate values of the coefficients of permeability are listed in **Table 2.2.3**.⁵⁾

Table 2.2.3 Approximate Values of the Coefficient of Permeability⁵⁾

Type of soil layer	Sand layer	Silt layer	Cohesive layer
Coefficient of permeability	10^{-2} cm/s (10^{-4} m/s)	10^{-5} cm/s (10^{-7} m/s)	10^{-7} cm/s (10^{-9} m/s)

2.3 Mechanical Properties of Soil**2.3.1 Elastic Constants**

- (1) When analyzing soil as elastic materials, the elastic constants shall be appropriately set taking into consideration the fact that soil is material showing nonlinearity.
- (2) The elastic constants generally used when analyzing soil as elastic materials are the deformation moduli and Poisson's ratios. In addition to stress dependency, the deformation moduli depend strongly on strain. Therefore, when conducting elastic analyses of ground, it is necessary to appropriately set elastic moduli taking strain levels of object ground into consideration.

(3) Strain dependency of deformation moduli

The stress-strain relationship of soil shows strong nonlinearity. **Fig. 2.3.1** shows one example of the relationship between deformation moduli and strain of the Pleistocene cohesive soil in Osaka Bay, obtained through a monotonous loading triaxial test.⁶⁾ In the figure, NCs are the triaxial test results of specimens which are subjected to anisotropic consolidation to in-situ effective overburden pressure with K_{0NC} kept at 0.5. OCs are the triaxial test results of specimens which are subjected to consolidation to consolidation yield stress with K_{0NC} kept at 0.5, followed by unloading to the level of OCR of 1.2 with K_{0OC} kept at $K_{0NC}OCR^{\sin\phi}$ to reproduce consolidation history. Also, K_{0NC} is the coefficient of earth pressure at rest in a normal consolidation region, ϕ is the angle of shear resistance, and OCR is an overconsolidation ratio. As can be seen in the figure, the deformation moduli are almost constant at their maximum values in the range where strain levels are 10^{-5} or less (0.001% or less). The maximum value E_{max} in this case corresponds to the value measured in dynamic tests, such as the elastic wave exploration, and is called a dynamic elastic modulus. As the strain level increases, the shear modulus of elasticity decreases. The secant modulus E_{50} , obtained from conventional unconfined compression tests or triaxial compression tests, is considered the deformation moduli when the strain is in the order of 10^{-3} (0.1%). When conducting elastic analyses of soil, it is necessary to set elastic constants appropriate for the strain level of object ground.

(4) Measurement of deformation moduli through in-situ tests

In many cases, the deformation moduli are obtained through the following in-situ tests:

- ① In-situ elastic wave exploration;
- ② PS logging;
- ③ Surface wave exploration;
- ④ Seismic cone test;
- ⑤ Loading test inside borehole;
- ⑥ Plate loading test; and
- ⑦ CBR test.

When using deformation moduli obtained through these tests, it is necessary to give due consideration to the fact that respective in-situ tests are conducted with different strain levels of ground.

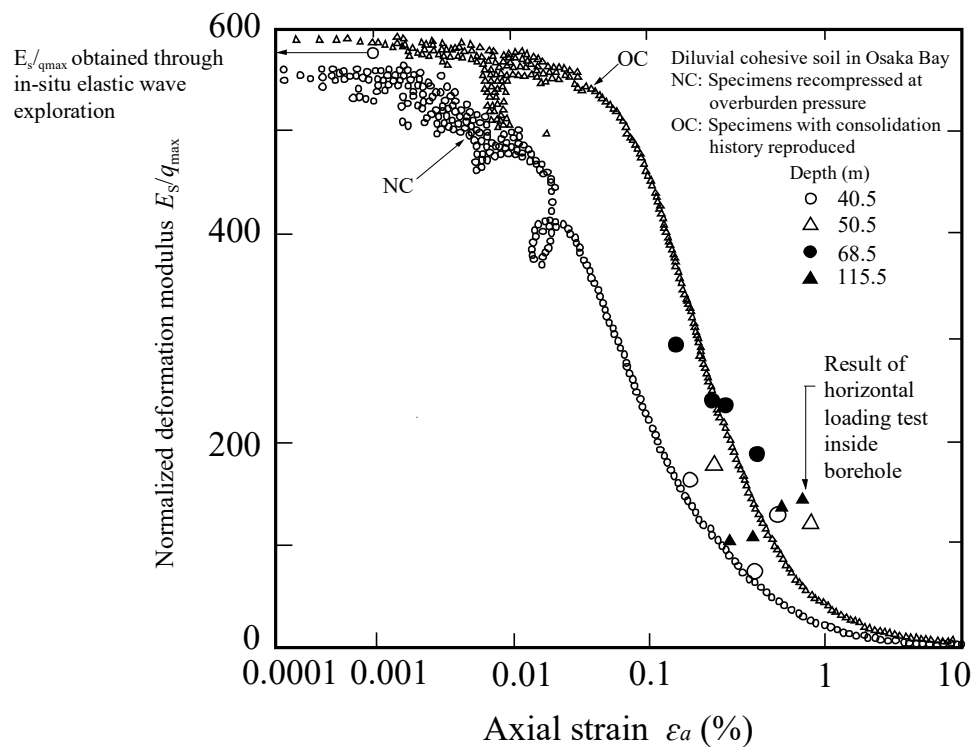


Fig. 2.3.1 Relationship between Strain and Elastic Moduli (Diluvial Cohesive Soil in Osaka Bay)⁶⁾

(5) Relationship between undrained shear strength and deformation moduli

For cohesive soil, the approximate values of initial tangent elastic moduli E_i , and secant elastic moduli E_{50} can be calculated by **equations (2.3.1) and (2.3.2)** respectively.⁷⁾

$$E_i = 210c_u \quad (2.3.1)$$

$$E_{50} = 180c_u \quad (2.3.2)$$

where

E_i : an initial tangent elastic modulus (kN/m²)

E_{50} : a secant elastic modulus (kN/m²)

c_u : undrained shear strength (kN/m²)

The above relationship between E_i and c_u is applicable only to the high-plasticity marine cohesive soil with well-developed structures.

(6) Poisson's ratio

Despite several proposals, there have been no established test methods for obtaining Poisson's ratio. In general, Poisson's ratio is set at around $\nu = 1/2$ for undrained saturated soil and $\nu = 1/3$ to $1/2$ for other soil.

2.3.2 Compression and Consolidation Characteristics

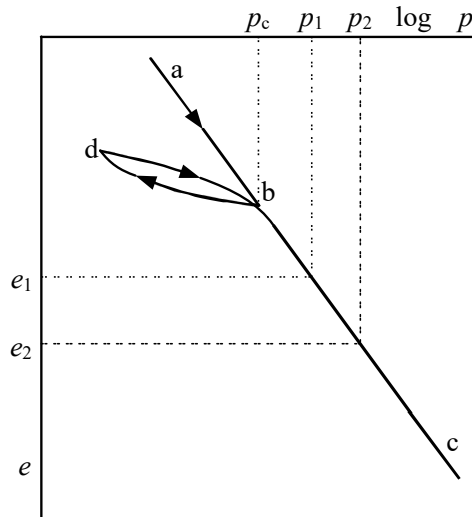
- (1) Soil compression characteristics and coefficients for estimating ground settlement due to consolidation can be calculated from the values obtained based on the **Test Method for One-dimensional Consolidation Properties of Soils Using Incremental Loading (JIS A 1217)**.
- (2) Compression is one of the soil characteristics which causes ground settlement, with soil particle structures compressed when the soil is subjected to one-dimensional loading. When voids among soil particles are saturated with pore water, the pore water needs to be drained, which will compress the soil particles due to loading. Highly permeable sandy soil shows compression immediately after loading with pore water smoothly drained. In contrast, cohesive soil ground has significantly low permeability, so compressive settlement occurs very slowly because it takes long time until the pore water is drained. The phenomenon in which cohesive soil ground shows gradual compressive settlement over time is called consolidation.

The consolidation characteristics of soil are used not only to calculate settlement due to loading but also for estimating the increase in shear strength in soil improvement work.

(3) Calculation of final consolidation settlement

When plotting consolidation pressure and void ratios at the end of consolidation with the consolidation pressure (applied for 24 hours) on a semi-logarithmic graph, a compression curve (so called e - $\log p$ curve) is obtained as illustrated in **Fig. 2.3.2**. The almost linear section a-b-c in the e - $\log p$ curve represents a loading process, and the consolidation states of soil on the linear section a-b-c are called normal consolidation states. When soil is subjected to unloading at point b in the e - $\log p$ curve and reaches equilibrium under reduced pressure, the relationship between the void ratios and stress of the soil follows the transition route b-d in the e - $\log p$ curve and, when the soil is subjected to reloading, the relationship follows the transition route d-b. The states expressed by the transition routes b-d and d-b are called the overconsolidation state. When conducting consolidation tests, the relationship between stress and void ratios of soil specimens shows the transition route d-b-c because they are initially in overconsolidation states. Then, a boundary point b can be identified from the elastic deformation section, represented by the transition route d-b, and the plastic deformation section, represented by the transition route b-c. The pressure corresponding to the point b is called consolidation yield stress p_c .

The relationship between void ratio e and pressure p in the linear section a-b-c (normal consolidation region) in **Fig. 2.3.2** is expressed by **equation (2.3.3)**.


 Fig. 2.3.2 e - $\log p$ Relationship in Consolidation

$$e_2 = e_1 - C_c \log_{10} \frac{p_2}{p_1} \quad (2.3.3)$$

Where, C_c is a non-dimensional parameter showing the inclination of the linear section a-b-c and is defined as the decrement of the void ratio in one logarithmic cycle.

The final settlement resulting from the consolidation loads can be obtained through three methods which respectively use: e - $\log p$ curves; C_c ; and the coefficients of volume compressibility m_v .

The decrease in void ratio Δe , when the pressure increases from in-situ effective overburden pressure σ'_{v0} to $(\sigma'_{v0} + \Delta p)$, can be obtained by directly reading the e - $\log p$ relationship available through consolidation tests. Otherwise, when allowing the consolidation settlement to be overestimated (the settlement in the overconsolidation region evaluated in the same manner as the settlement of normal consolidation region so as to be on the safe side), the final settlement may be calculated by **equation (2.3.4)** derived from **equation (2.3.3)**.

$$\Delta e = e_{\sigma'_{v0}} - e_{\sigma'_{v0} + \Delta p} = C_c \log_{10} \frac{\sigma'_{v0} + \Delta p}{\sigma'_{v0}} \quad (2.3.4)$$

When calculating the final settlement S through the method using the e - $\log p$ curves, the value of Δe either read directly from the e - $\log p$ curve or calculated by **equation (2.3.4)** is plugged into **equation (2.3.5)**.

$$S = h \frac{\Delta e}{1 + e_0} \quad (2.3.5)$$

where

h : the thickness of a stratum.

When calculating the final settlement S through the method using C_c , **equation (2.3.6)** can be used.

$$S = h \frac{C_c}{1 + e_0} \log_{10} \frac{\sigma'_{v0} + \Delta p}{\sigma'_{v0}} \quad (2.3.6)$$

Equation (2.3.6) corresponds to equation obtained by substituting **equation (2.3.4)** into **equation (2.3.5)**.

The coefficient of volume compressibility m_v can be used to estimate settlement because the amount of compression by the increment of a load is proportional to m_v . However, because the method for calculating the final settlement using m_v applies linear approximation to soil which has strong nonlinearity, the method is effective only for small increments in consolidation pressure Δp so that m_v can be assumed to be constant. In the case of the method using m_v , the final settlement S can be calculated by **equation (2.3.7)**.

$$S = m_v \Delta p h \quad (2.3.7)$$

where

m_v : the coefficient of volume compressibility when the consolidation load is $(\sqrt{\sigma'_{v0}(\sigma'_{v0} + \Delta p)})$

Generally, the value of m_v during consolidation decreases with the increase of effective overburden pressure p . Under the normal consolidation state, the relationship between p and m_v plotted on a double logarithmic graph is almost linear. The value of m_v to be used when calculating settlement by **equation (2.3.7)** shall be the mean value in the period when the effective overburden pressure of ground is changed from σ'_{v0} to $(\sigma'_{v0} + \Delta p)$. Normally, the value of m_v corresponding to the geometric mean of the effective overburden pressure $(\sqrt{\sigma'_{v0}(\sigma'_{v0} + \Delta p)})$

(4) Settlement rates

The following section describes the settlement rate analysis method based on Terzaghi's one-dimensional consolidation theory, one of the classical consolidation theories. When saturated cohesive soil is subjected to an increment in pressure Δp under undrained condition and excess pore water pressure Δu , equivalent to the increment in pressure Δp , is generated in the soil. The excess pore water pressure gradually dissipates as consolidation progresses with the gradual increase in the effective stress σ' in a manner that balances the sum of the increments of excess pore water pressure Δu and effective stress $\Delta \sigma'$ with the increment in pressure Δp as shown in **equation (2.3.8)**.

$$\Delta p = \Delta \sigma' + \Delta u \quad (2.3.8)$$

In the case of a cohesive stratum having a thickness of $h = (2H)$, placed in between upper and lower sand strata with large permeability, the distribution of $\Delta \sigma'$ and Δu in the depth direction when the cohesive stratum is subjected to the increment in consolidation pressure Δp is as shown in **Fig. 2.3.3**. That is, the state of the sand stratum when consolidation begins ($t = 0$) can be expressed by the line DC because of $\Delta u = \Delta p$ and $\Delta \sigma' = 0$, and when consolidation is completed, the state can be expressed by the line AB because of $\Delta u = 0$ and $\Delta \sigma' = \Delta p$. The curved line AEB shows the distribution of the excess pore water pressure after the lapse of t_1 since consolidation began. As can be seen in the figure, the portions in the cohesive soil stratum away from drainage layers have relatively slow consolidation rates.

The ratio of the increment in effective stress to the increment in consolidation pressure ($\Delta \sigma' / \Delta p$) at a certain depth z is called a degree of consolidation U_z and the average of the degree of consolidation at respective depths in the entire stratum is called an average degree of consolidation. In **Fig. 2.3.3**, the average consolidation rate can be expressed by the ratio of the area of AEBCD to that of ABCD.

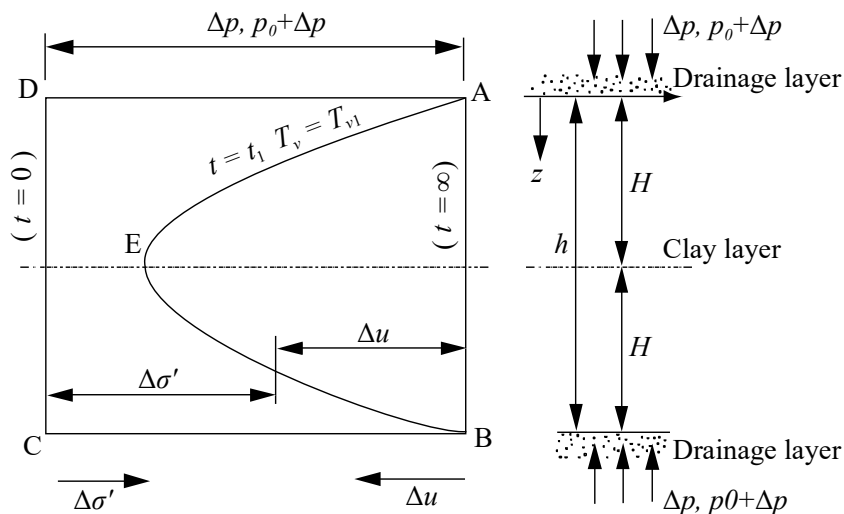


Fig. 2.3.3 Distribution of Pore Water Pressure in the Depth Direction

Consolidation progress in an entire cohesive soil stratum can be expressed by the magnitude of the average degree of consolidation U . A time factor T_v which is a non-dimensional quantity is used as the unit showing time. The relationship between the time factor T_v and actual time t can be expressed by **equation (2.3.9)**.

$$T_v = \frac{c_v t}{H^{*2}} \quad (2.3.9)$$

where

T_v : a time factor;

c_v : the coefficient of consolidation (cm²/day) or (m²/s);

t : time after the consolidation is started (day) or (s); and

H^* : the maximum flow distance of pore water (maximum drainage distance) (cm) or (m).

The consolidation coefficient c_v is a soil parameter showing the consolidation progress rate. In the case of a cohesive soil stratum with a thickness of $2H$ placed in between upper and lower drainage strata (called double drainage), H can be used as H^* in **equation (2.3.9)**. In the case of the cohesive soil stratum with only one drainage stratum placed one above or the other (called single drainage), $2H$ can be used as H^* in **equation (2.3.9)**. As indicated by the consolidation isochronous curve in **Fig. 2.3.4**, the degree of consolidation at each depth transitions along with the time factor. **Fig. 2.3.5** shows the relationship between the average degree of consolidation and time factors.

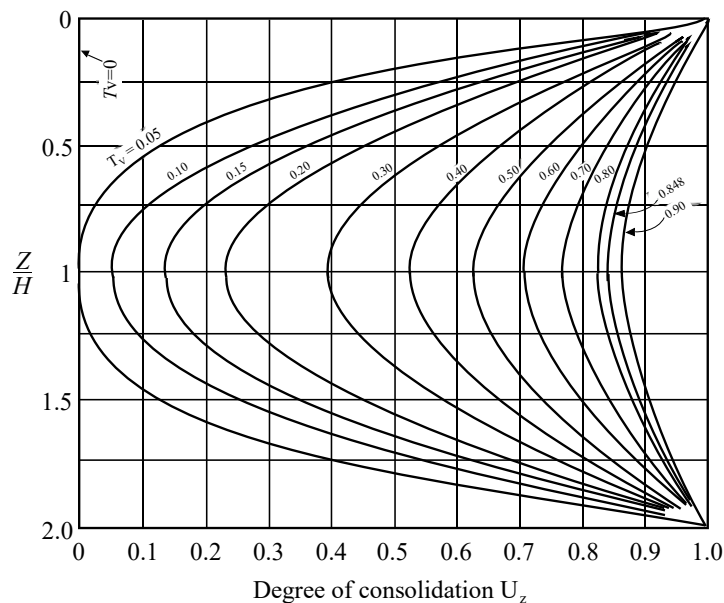


Fig. 2.3.4 Consolidation Isochronous Curve

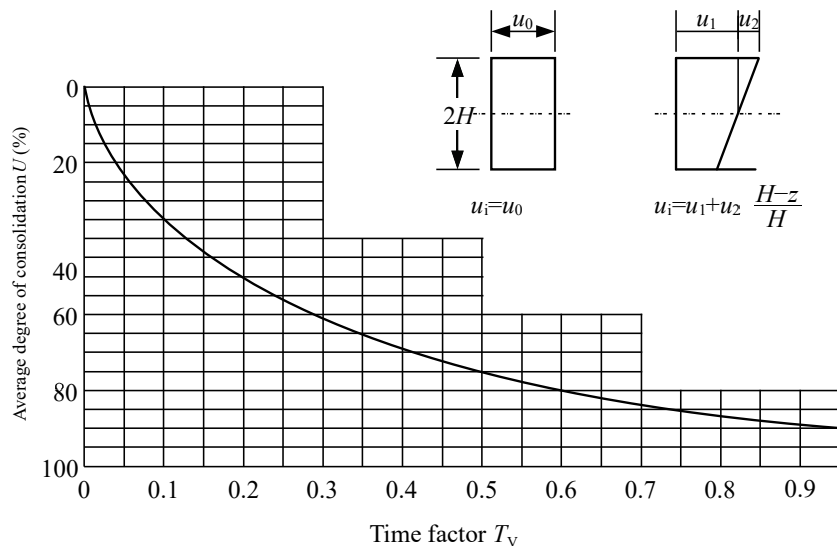


Fig. 2.3.5 Relationship between the Average Degree of Consolidation and Time Factors

Although Terzaghi's consolidation theory has been widely practiced as a simple analysis method, the theory cannot take into account the following four factors:

- ① the influence of the self-weight of cohesive soil layers;
- ② the inhomogeneity of the coefficients of consolidation and the compaction property of cohesive soil strata;
- ③ the secondary consolidation attributable to the viscosity of cohesive soil skeletons (not attributable to the dissipation of excess pore water pressure); and
- ④ consolidation phenomena in multi- dimension, namely two and three dimensions.

To analyze consolidation settlement with improved accuracy by considering the above factors, it is necessary to implement finite element analysis methods using an elasto-viscoplastic constitutive equation, which has also been widely practiced recently.

(5) Primary and secondary consolidation

According to the relationship between degree of consolidation, measured in consolidation tests, and time (corresponding to the relationship between settlement and time) which can be schematically shown in **Fig. 2.3.6**, the test results do not agree with a theoretical curve in the later consolidation stage. In the relationship between settlement and time, the process where U is up to 100% and test results almost agree with the consolidation theory. This is categorized as the primary consolidation. The process where U is larger than 100% and the test results do not agree with the consolidation theory is categorized as the secondary consolidation. Secondary consolidation is considered to be the creep phenomenon of soil and tends to have a linear relationship between settlement and the logarithm of elapsed time.

In the performance verification of port facilities, there are many cases where the consolidation pressure due to loading reaches several times the consolidation yield stress. In such conditions, the settlement due to the primary consolidation is significantly large, and settlement due to the secondary consolidation is relatively small, thereby allowing most performance verification to be carried out without special consideration to the settlement due to the secondary consolidation. Also, when the settlement is large, there may be cases where no secondary consolidation is apparently observed; the effects of the secondary consolidation are canceled out by the increased effects of buoyancy with the progress of settlement. However, performance verification shall be carried out considering the effects of the secondary consolidation in the following cases:

- ① when the effect of settlement over time on facilities after their construction is large; and
- ② when the consolidation pressure due to loading does not significantly exceed the consolidation yield stress of original ground and, therefore, the contribution of the secondary consolidation settlement to the entire settlement is not negligible, as is the case with the deep the pleistocene cohesive soil ground.

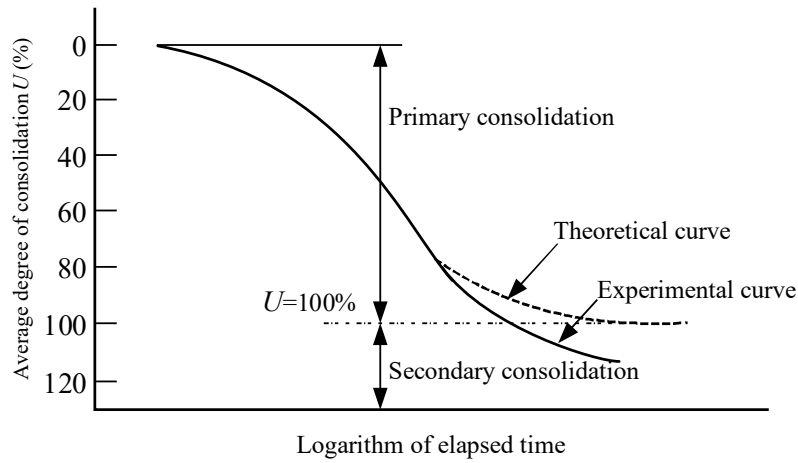


Fig. 2.3.6 Primary and Secondary Consolidation

The long-term consolidation settlement which occurs as residual settlement causes serious issues in design and maintenance when constructing a huge artificial island in a deep sea area or on the cohesive soil seabed. In such a case, a widely used method for estimating final settlement is to add secondary consolidation settlement calculated by using the secondary consolidation coefficient C_α to the completed primary consolidation settlement. However, this method has problems in that: the point to start the calculation of the secondary consolidation settlement is unclear; and the theoretical assumption of a continuous linear relationship between settlement and logarithm of elapsed time in the secondary consolidation cannot consider the actual relationship, which shows a convex-downward curve with the inclination getting gentler as time advances.

According to research on improving the prediction accuracy of long-term consolidation settlement⁸⁾, an isotach concept⁹⁾ focusing on the strain rate dependency of consolidation yield stress is considered an effective approach to continuously deal with the primary and secondary consolidation.

Focusing on viscoplastic strain ε_{vp} obtained by subtracting elastic strain ε_e from total strain ε , the method based on the isotach concept uses **equation (2.3.10)** to model the strain rate dependency of consolidation yield stress p'_c .

$$\ln \frac{p'_c - p'_{cL}}{p'_{cL}} = c_1 + c_2 \ln \dot{\varepsilon}_{vp} \quad (2.3.10)$$

In Equation, $\dot{\varepsilon}_{vp}$ is a viscoplastic strain rate, p'_{cL} , c_1 , and c_2 are constants called isotach parameters, and p'_c converges on the lower limit p'_{cL} when a strain rate reaches an infinitesimal value.

Fig. 2.3.7 shows the relationship of **equation (2.3.10)** normalized with the yield stress p'_{c0} corresponding to the strain rate of $1.0 \times 10^{-7} \text{s}^{-1}$ (equivalent to the strain rate after the lapse time of 24 hours in an incremental loading consolidation test). The isotach parameters of p'_{cL}/p'_{c0} and c_1 are set 0.7 and 0.935, respectively, to be applicable to a variety of cohesive soil. The other isotach parameter c_2 can be automatically determined by the following equation.

$$c_2 = \frac{\ln \frac{p'_c - p'_{cL}}{p'_{cL}} - c_1}{\ln \dot{\varepsilon}_{vp}} = \frac{\ln \frac{1 - 0.7}{0.7} - c_1}{\ln 1.0 \times 10^{-7}} \quad (2.3.11)$$

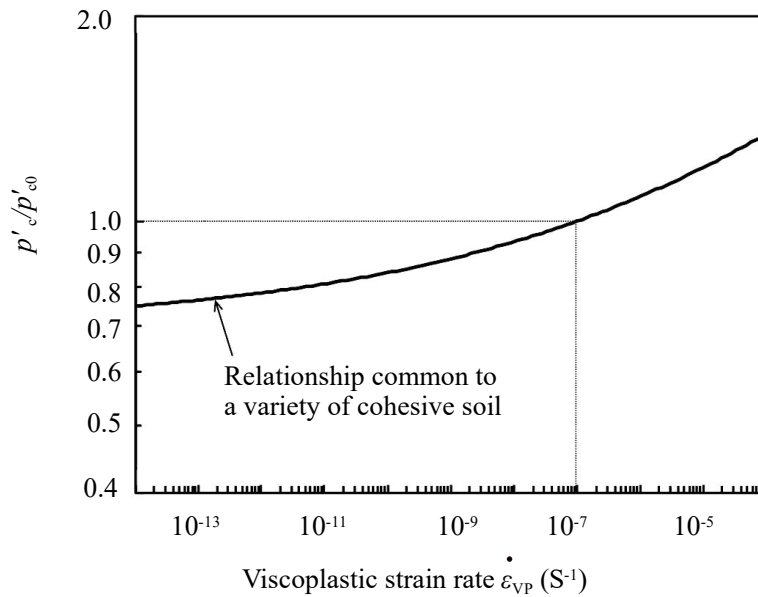


Fig. 2.3.7 Strain Rate Dependency of Consolidation Yield Stress⁸⁾

The consolidation settlement prediction method, taking a strain rate into consideration, can be explained using Fig. 2.3.8 assuming that consolidation pressure is increased from the effective overburden pressure σ'_{v0} to the in-situ consolidation pressure p'_1 after loading. The compression curve passing through the point D in the figure corresponds to that obtained through incremental loading consolidation tests. In the laboratory long-term consolidation tests, strain rates show the transit route of A-C-D-E. In contrast, in-situ strain rates show the transit route of A-B-E-F.

By additionally predicting an in-situ strain rate or setting an allowable long-term strain rate for the required performance of facilities, the settlement which corresponds to the strain rate, namely the strain increment ($\Delta\epsilon_{Field}$) as shown by the section D-E in the figure, can be calculated using equation (2.3.12). Furthermore, consolidation has a possibility to reach the point F in the figure and then the maximum possible settlement corresponding to the strain increment ($\Delta\epsilon_{ult}$) as shown by the section D-F can be calculated by equation (2.3.13).

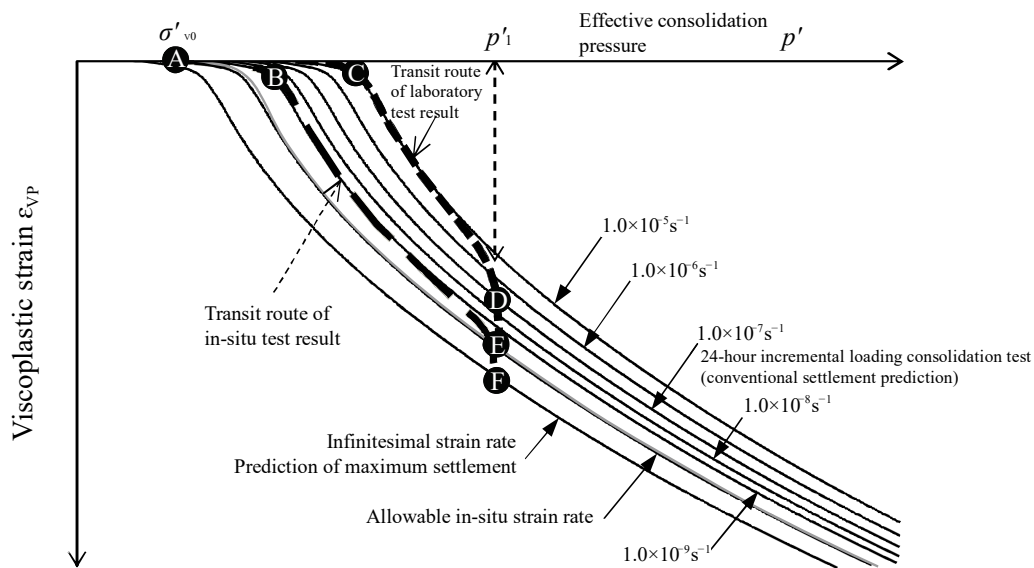


Fig. 2.3.8 Relationship between laboratory test results and in-situ settlement behavior⁸⁾

$$\Delta \varepsilon_{\text{Field}} = \frac{C_c}{1+e_0} \log \left[\frac{p'_{c0}}{p'_{cL}} \left\{ \frac{1}{1 + \exp(c_1 + c_2 \ln \dot{\varepsilon}_{\text{Field}})} \right\} \right] \quad (2.3.12)$$

$$\Delta \varepsilon_{\text{ult}} = \frac{C_c}{1+e_0} \log \frac{p'_{c0}}{p'_{cL}} \quad (2.3.13)$$

The relationships expressed by **equations (2.3.12) and (2.3.13)** are graphically illustrated in **Fig. 2.3.9** and **2.3.10** respectively.

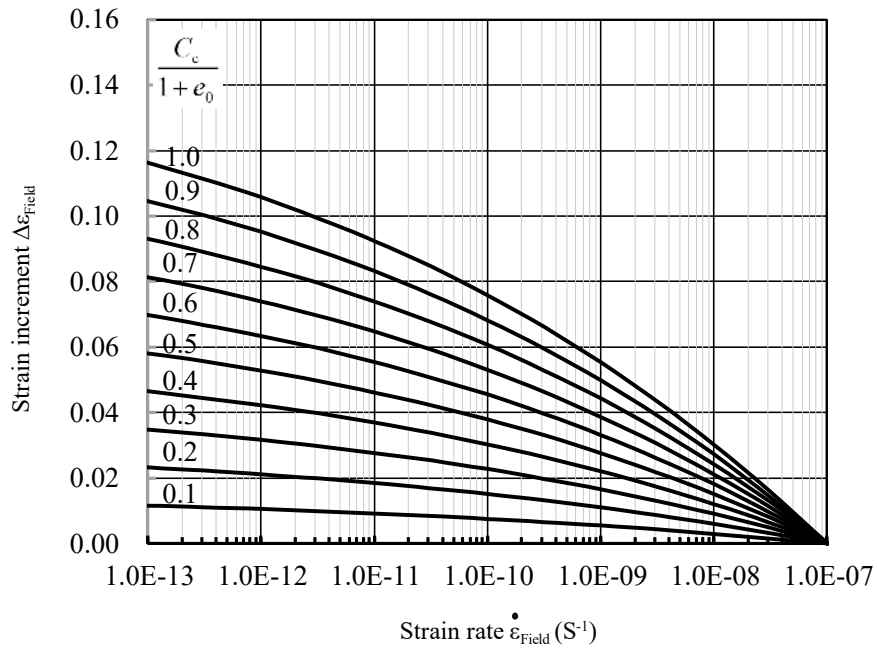


Fig. 2.3.9 Strain Increment Corresponding to In-situ Strain Rate
Strain Increment Additional to Strain Predicted from the Results of Incremental Loading Consolidation Test Result⁸⁾

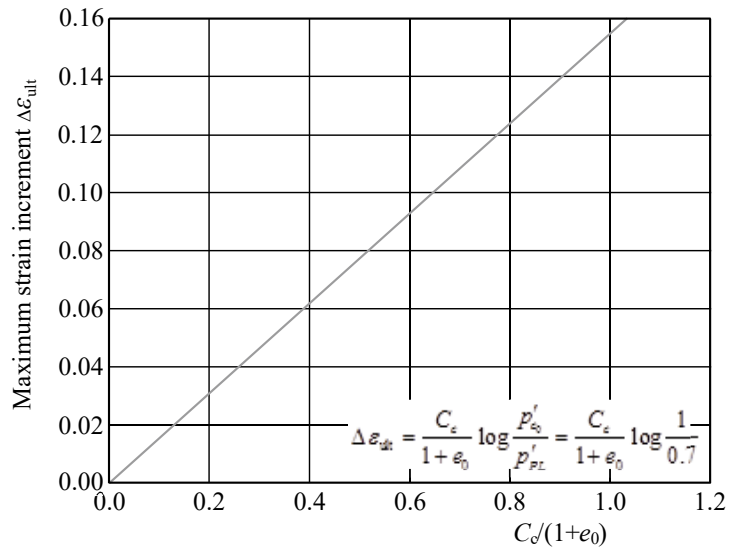


Fig. 2.3.10 Relationship Diagram between Maximum Strain Increment after Strain Rate reaches at $1 \times 10^{-7} \text{s}^{-1}$ and $C_c/(1 + e_0)$ ⁸⁾

(6) Consolidation settlement of very soft cohesive soil

In landfilling with dredged soil or disposing of sludge, a problem of consolidation settlement of extremely soft ground may be encountered. The consolidation theories applicable to these problems include Mikasa's¹⁰⁾ consolidation theory, which takes into account the effects of the changes in layer thicknesses during consolidation and the self-weight of cohesive soil strata. Closed solution of this theory on settlement and settlement rates cannot be found, the solution of which are obtained by a finite differential method.

When the reduced thickness of a stratum due to settlement is too large compared to the original thickness to ignore, normal consolidation settlement calculation methods are susceptible to large errors. For example, if the stratum thickness is reduced by 10 to 50%, the difference between the normal calculation method and the calculation method considering the effect of the change in stratum thickness is in the range of 3 to 30%. Also, the effect of self-weight on settlement is maximized when dredged soil is left on a landfill site. In such a case, the effect of self-weight is relatively reduced with the increased surcharge pressure. For example, the effect of self-weight on very soft strata becomes negligibly small when the surcharge pressure on the surface of a landfill site is about twice or more the self-weight of ground at the central depth of the very soft stratum.

A consolidation test method¹¹⁾ in which specimens are subjected to continuous displacement through constant strain rate loading has been standardized (**JIS A 1227**) to estimate the consolidation properties of very soft cohesive soil. Because of the ability to obtain continuous e - $\log p$ curves, the consolidation test method has a wide field of application and is effective, not only for testing consolidation properties of very soft cohesive soil, but also obtaining consolidation yield stress of cohesive soil, including that with a large aging effect, which shows abrupt settlement after reaching the consolidation yield. However, the e - $\log p$ curves are strongly affected by strain rates. The e - $\log p$ curves obtainable through the above consolidation test method, which generally uses high loading rates, are normally shifted toward a large consolidation pressure side compared to the e - $\log p$ curves obtainable through the **Incremental Loading Consolidation Test Specified (JIS A 1217)**. Therefore, it is preferable to set appropriate consolidation yield stress while being aware that the consolidation yield stress based on the consolidation test using a constant rate of strain tends to become larger, and combining the incremental loading consolidation test results.

(7) Correlation between compression and consolidation coefficients and physical properties

Consolidation tests require the longest testing time among all the soil tests. It is advantageous if consolidation properties become available with disturbed specimens and obtainable through physical tests, which can speedily produce test results through relatively simple operation. Skempton proposed **equation (2.3.14)**, which expresses a relationship between the compression index C_c and the liquid limit w_L .

$$C_c = 0.009(w_L - 10) \quad (2.3.14)$$

Equation (2.3.14) is applicable to cohesive soil re-molded and re-consolidated in laboratories or the young cohesive soil ground immediately after being reclaimed. However, it may underestimate the compression characteristics of naturally deposited cohesive soil.

Fig. 2.3.11 shows the results of surveying the similar relationship using marine cohesive soil in Japan. **Equation (2.3.15)** was also proposed as another relationship between C_c and w_L (%) in the figure.

$$C_c = 0.015(w_L - 19) \quad (2.3.15)$$

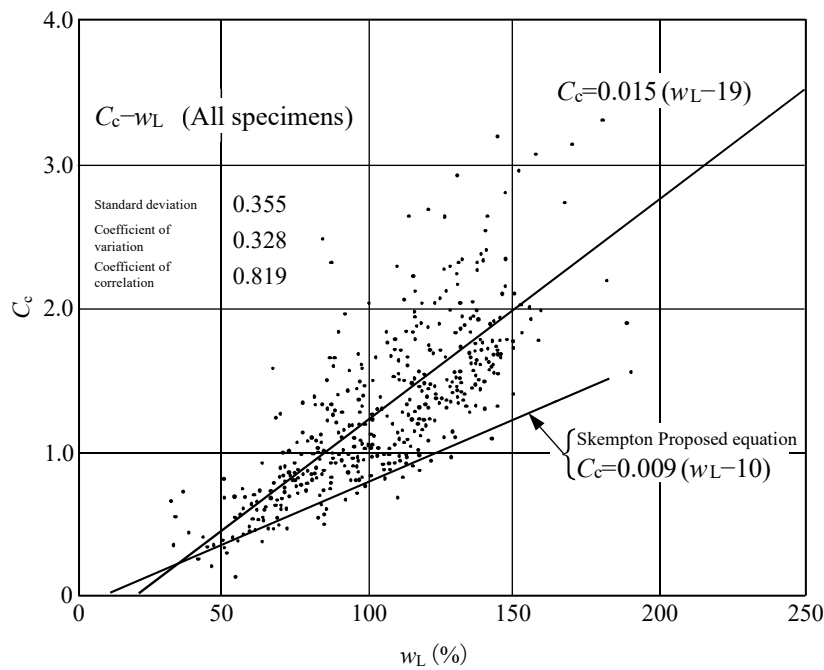


Fig. 2.3.11 Correlation between Compression Index and Liquid Limit¹²⁾

The reason why natural cohesive soil ground has larger compression index values than young cohesive soil ground is because natural cohesive soil structures, which have formed through the aging effects such as cementation in the sedimentation process over a long period of time, show high compressibility when destroyed with consolidation pressure exceeding consolidation yield stress.

Fig. 2.3.12 and **Fig. 2.3.13** show the relationship among the coefficients of consolidation c_v , coefficients of volume compressibility m_v , and liquid limits w_L which can be obtained through consolidation tests. The values of c_v are those measured when they are almost constant and consolidation processes are already in normal consolidation states. Because m_v linearly changes with respect to the increments in consolidation pressure p on double logarithmic graphs, **Fig. 2.3.13** shows cases when the values of p are 100 kN/m² and 1000 kN/m² respectively. Although respective relationships show large dispersions, they can be used to obtain approximate values of these coefficients from liquid limits.

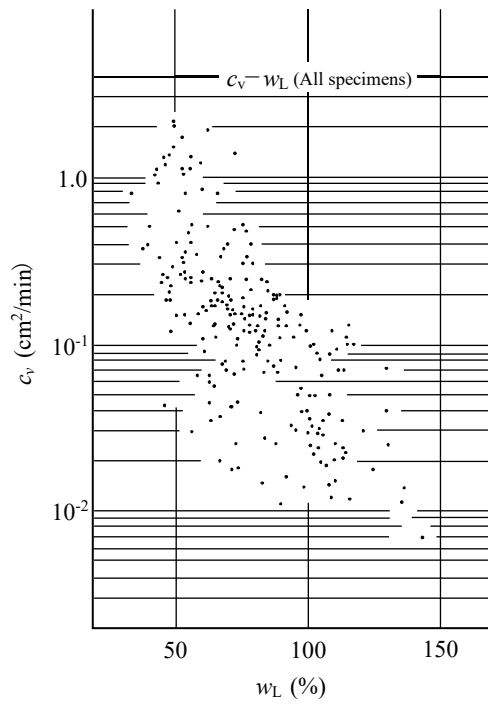


Fig. 2.3.12 Relationship between Coefficient of Consolidation c_v and Liquid Limit¹²⁾

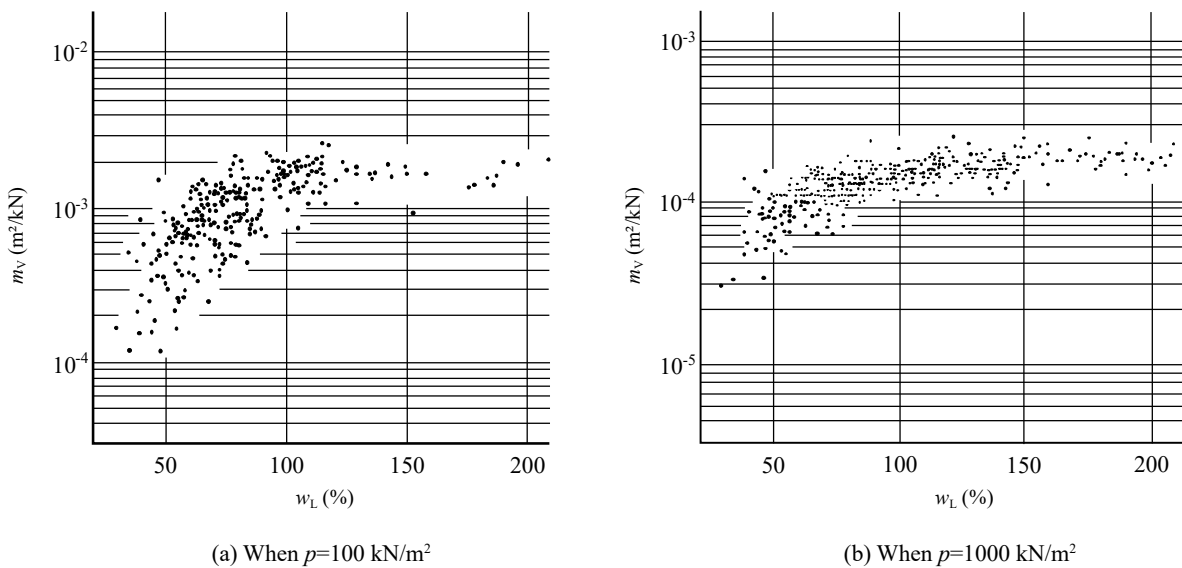


Fig. 2.3.13 Relationship between Coefficients of Volume Compressibility and Liquid Limit¹²⁾

2.3.3 Shear Characteristics

- (1) The shear strength of soil is generally set classifying soil into sandy soil and cohesive soil. Also, the shear strength of sandy and cohesive soil is set under drained and undrained conditions, respectively.
- (2) In general, the coefficient of permeability of sandy soil is 10^3 to 10^5 times larger than that of cohesive soil. In the case of sandy ground, pore water is considered to have been drained completely during construction. Thus, the shear strength of sandy ground is evaluated with the angles of shear resistance ϕ_D and cohesion c_D under the drained condition. Because c_D is negligibly small in general, the shear strength of sandy ground is evaluated with ϕ_D as the only strength parameter with c_D set at 0.

In contrast, because of low permeability, the shear strength of cohesive ground has been barely changed with the pore water undrained during construction. In the case of cohesive soil ground, the undrained shear strength before construction is used as the strength parameter.

If the ground has intermediate permeability, between that of sandy and cohesive ground, it shall be classified as either sandy or cohesive ground in accordance with the coefficients of permeability and construction conditions, and then shear strength shall be determined through appropriate test methods.

(3) Concept of shear strength

The shear strength of soil τ_f is generally expressed by the following equation.

$$\tau_f = c + \sigma \tan \phi \quad (2.3.16)$$

where

- τ_f : shear strength (kN/m²);
- c : cohesion (or apparent cohesion) (kN/m²);
- ϕ : the angle of shear resistance (or angle of internal friction) (°); and
- σ : normal stress on a shear surface (kN/m²).

When stress is applied to soil, both the effective stress and pore water pressure in the soil are changed. Given that σ , σ' and u denote the stress applied to the soil, the effective stress acting on the soil, and pore water pressure respectively, the following relationship can be established. Here, σ is called total stress as opposed to effective stress σ' .

$$\sigma = \sigma' + u \quad (2.3.17)$$

The strength parameters such as c and ϕ in **equation (2.3.16)** vary depending on the shear test conditions. Among shear test conditions, the drainage condition has the largest impact on strength parameters. Soil undergoes volume changes when being subjected to shear force (and such behavior of soil is called dilatancy). Thus, the shear strength of soil varies depending on the presence or absence of volume changes (absorption or discharge of water in the case of saturated soil). Generally, the drainage condition is classified into the following three categories, and different strength parameters are used in accordance with each condition:

- ① Unconsolidated and undrained condition (UU condition);
- ② Consolidated and undrained condition (CU condition); and
- ③ Consolidated and drained condition (CD condition).

Fig. 2.3.14 shows the schematic diagram of the results of direct shear tests conducted under different drainage conditions ①, ②, and ③ above.¹²⁾ The diagram shows the change in shear strength of the soil specimens subjected to first consolidation at p_0 under increased or reduced normal stress σ . As can be seen in the diagram, under the UU condition ①, shear strength is constant and independent of σ ; under the CU condition ②, shear strength linearly increases with the increase in σ in the range of $p_0 < \sigma$; and under the CD condition ③, shear strength is overall larger than that under conditions ① and ② because the consolidation and shear force causes reduced void ratios in soft cohesive soil and loose sand. However, when σ is significantly smaller than p_0 (at the critical value of normal stress indicated as σ^* in the diagram), the shear strength under the CD condition is smaller than the strength under the CU condition due to the swelling effect of soil specimens when subjected to shear force. The above relationships are summarized below in terms of the range of σ .

In the range of $p_0 < \sigma$ (namely a surcharge load is larger than the pre-consolidation pressure);
①<②<③

In the range of $\sigma^* < \sigma < p_0$ (namely a surcharge load is slightly smaller than the pre-consolidation pressure);
②<①<③ or ②<③<①

In the range $\sigma < \sigma^*$ (namely a surcharge load is significantly smaller than the pre-consolidation pressure);
③<②<①

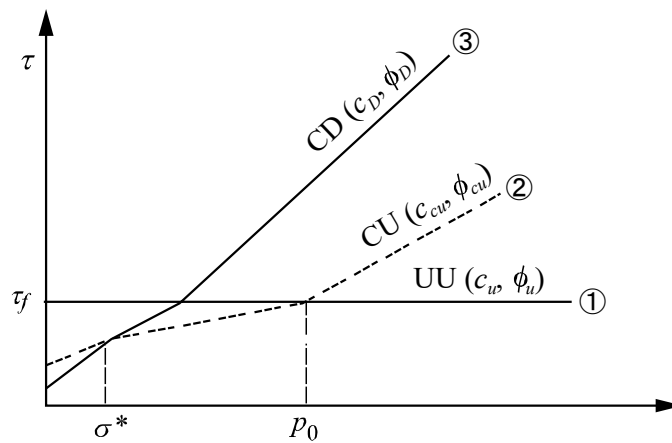


Fig. 2.3.14 Relationship between Drainage Conditions and Shear Strength¹³⁾

Considering that the shear strength under the most dangerous drainage condition should be used for ground performance verification, the following drainage conditions can be the determining factors of shear strength in respective cases.

(a) Case of rapid loading on cohesive soil ground:

Because shear strength increases as consolidation progresses over time, the ground is in the most dangerous condition immediately after loading, when almost all pore water is undrained (this is called a short-period stability problem). The shear strength τ_f to be used under such a drainage condition is the shear strength c_u which can be obtained through UU tests. The shear strength c_u is also called apparent cohesion, and the analysis using c_u is called $\phi_u = 0$ method. The situations to which the shear strength c_u is applied are the construction of revetments, breakwaters (without involving excavation), landfills, and earth fill on soft cohesive ground.

(b) Case of the ground with high permeability or very slow loading, allowing pore water to be drained completely during construction:

In this case, the strength of the ground is expected to increase with pore water drained while the loading is applied to it and ground performance verification is carried out with the strength parameter c_D or ϕ_D which can be obtained through CD tests. The situations to which c_D or ϕ_D is applied are the construction of revetments, breakwaters, landfills, and earth fill on sandy ground.

(c) Case of expecting strength increase by phased construction:

In phased construction, loading is divided into some phases and conducted stepwise. After each phase of loading, the ground is allowed to have a consolidation period long enough to increase its strength. The load of the next phase is small enough to reliably secure the safe loading operation. Because loading in each phase is implemented in a short period of time, drained condition cannot be applied to the staged construction; however, ground strength increases can be expected during consolidation periods. The shear strength to be used under such a drainage condition is the undrained shear strength c_u which can be obtained through CU tests.

(d) Case of the ground which has poor permeability and is subjected to a load reducing normal stress σ on a shear surface:

In this case, the ground gradually increases the level of danger along with the decrease in shear strength because the ground undergoes swelling due to reduction of the normal stress σ (this is called a long-period stability problem). As can be seen in Fig. 2.3.14, when the OCR is small (σ is slightly smaller than p_0), the undrained shear strength c_u is the smallest after swelling. In this case, the shear strength to be used is c_u taking the strength reduction due to swelling into consideration. The situations to which c_u is applied are earth retaining and excavation work in cohesive soil ground and the behavior of cohesive soil ground after the removal of preloading. In contrast, in the case of heavily overconsolidated ground with σ significantly smaller than p_0 , the CD shear strength is the smallest and, therefore, c_D or ϕ_D is the strength parameter to use in performance verification. The situations to which c_D or ϕ_D is applied are normally cut earth work and construction work in coastal areas involving the removal of preloading, such as deepening quaywalls and seabed dredging.

The strength parameters to be frequently used when examining the construction conditions of port facilities in the performance verification are: the undrained shear strength under the UU condition as described in (a) above (or the CU condition in (c) above when expecting strength increase through staged construction) for cohesive soil ground and the drained shear strength under the CD condition in (b) above for sandy soil ground. The calculation equations of respective shear strength are as follows.

1) Cohesive soil ground (with the sand content of less than 50%)

$$\tau = c_u \quad (2.3.18)$$

where

τ : shear strength (kN/m²); and
 c_u : undrained shear strength (kN/m²).

2) Sandy soil ground (with the sand content of 80% or more)

$$\tau = (\sigma - u) \tan \phi_D \quad (2.3.19)$$

where

τ : shear strength (kN/m²);
 σ : normal stress on a shear surface (kN/m²);
 u : in-situ steady hydraulic pressure (mainly static hydraulic pressure) (kN/m²); and
 ϕ_D : the angle of shear resistance under drained conditions (°).

Soil with 50 to 80% sand content shows properties intermediate between sandy and cohesive soil and, therefore, is called intermediate soil. Because evaluating the shear strength of intermediate soil is difficult compared to sandy or cohesive soil, the shear strength for such soil should be evaluated carefully by referring to the latest research results and the performance records of previous survey, design and construction. With respect to the intermediate soil that can be treated as cohesive soil, it is preferable to evaluate shear strength through triaxial CU tests, etc., rather than unconfined compression tests, which often significantly underestimate the shear strength. As described later, the shear strength shall be carefully set in the case where intermediate soil undergoes dilation when subjected to shear force.

(4) Shear strength of sand

Because sandy soil is highly permeable and considered to be under a completely drained condition, the shear strength of sand can be expressed by **equation (2.3.19)**. The angle of shear resistance under drained condition ϕ_D can be obtained through triaxial CD tests. Also, because the ϕ_D of sand gets larger with decrease in void ratio or increase in density, it is necessary to obtain accurate void ratios e_0 of ground in a manner that samples less disturbed specimens from the ground and conducts laboratory tests using such specimens as undisturbed ones. Although even sand will show slightly different ϕ_D values depending on shear conditions, the ϕ_D obtained through triaxial CD tests using undisturbed specimens preserving in-situ conditions under the confined pressure according to the design condition can be used as the characteristic value in stability analyses. However, when examining the bearing capacity problems of foundations susceptible to progressive fracture, bearing capacity may be overestimated if the ϕ_D obtained through triaxial CD tests is directly used as the characteristic value.

Generally, compared with the case of cohesive soil, sampling less disturbed sand specimens is technically difficult and also very expensive. Thus, there are many cases of obtaining the angles of shear resistance of sand ground not from laboratory test results but from the SPT-N values measured through the standard penetration tests. For equation to calculate ϕ_D from SPT-N values, refer to **Part II, Chapter 3, 2.3.4 (4) Angle of Shear Resistance of Sandy Ground**.

(5) Shear strength of cohesive soil

This section focuses on cohesive soil with a clay and silt content of 50% or more. There are several methods for determining the undrained shear strength c_u of cohesive soil as introduced below. It is necessary to select an appropriate strength determination method by comprehensively evaluating the performance records involving the object ground, ground properties, and the importance of facilities.

① q_u method:

In this method, the undrained shear strength c_u of cohesive soil for performance verification is calculated by the following equation, which uses unconfined compression strength q_u of undisturbed specimens.

$$c_u = q_u / 2 \quad (2.3.20)$$

The unconfined compression tests shall be conducted as specified in the **Method for Unconfined Compression Test of Soils (JIS A 1216)**. The unconfined compression tests are conducted mainly with high-plasticity cohesive soil. Because specimens are not subjected to confined pressure, test results are susceptible to the disturbance of specimens, and there may be the cases of getting significantly small strength. Unconfined compression tests are particularly difficult to apply to cohesive soil sampled from deep ground, such as the Pleistocene cohesive soil, which is hard and liable to crack. Also, the unconfined compression test shall not be considered applicable to intermediate soil with high sand contents because the test results show too small a shear strength with the effective stress in specimens of such soil easily released during the tests. Thus, in the case of intermediate soil, it is preferable to employ other shear tests where specimens are subjected to consolidation with confined pressure applied to them such as triaxial test or direct shear test.

② Method using the strength obtained through triaxial tests taking into consideration initial stress and anisotropy:

When analyzing the stability of embankment on cohesive soil ground with respect to circular slip failures, as shown in **Fig. 2.3.15**, because the soil immediately below the embankment is subjected to shear force due to increased vertical stress, the shear strength of the soil with respect to such shear force can be evaluated through triaxial undrained compression tests (compression shear tests under CU condition). Strictly speaking, there is a difference between shear strength under plane strain condition and axi-symmetric condition, and the former is slightly larger than the latter. In contrast, the shear force is generated on the soil at the end point of the slip circle, or at the foot of a slope, due to increased horizontal stress. Therefore, the shear strength of the soil with respect to such shear force can be evaluated through triaxial undrained extension tests (extension shear tests under CU condition). There is a difference between shearing conditions in the triaxial extension test and the circular slip failure, in addition to the difference between shear strength under plane strain condition and axi-symmetric condition. Horizontal stress increases in the circular slip failure of embankment, whereas axial force is reduction in the triaxial extension test. In the case of the soil at the bottom of the slip circle, which is subjected to almost horizontal shear force unlike in the case of soil subjected to deformation modes due to compression and extension force, the shear strength of the soil can be evaluated through a box shear test or simple shear test.

The undrained shear strength c_u^* to be used in the performance verification is generally calculated as the average of the shear strength c_{uc} and c_{ue} obtained through compression and extension tests, respectively, using the following equation.

$$c_u^* = \frac{c_{uc} + c_{ue}}{2} \quad (2.3.21)$$

The shear strength c_{us} obtained through box shear tests may be used as a characteristic value. In many cases of Japanese cohesive soil, the shear strength c_{ue} obtained through triaxial undrained extension tests is about 70% of the shear strength c_{uc} obtained through triaxial undrained compression tests.

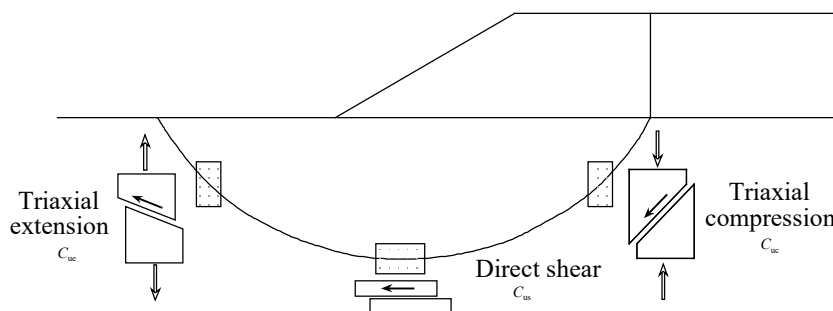


Fig. 2.3.15 Stability Problem and Strength Anisotropy of Earth Fill Constructed on Cohesive Soil Ground

Sampling inevitably causes specimens to have a certain level of disturbance despite continued efforts to minimize it. Although unconfined compression tests are considered unreliable, many performance verification methods have been empirically established based on the tests and persist without being replaced by other methods. Among the methods for determining undrained shear strength currently proposed, the **recompression method**¹⁴⁾ is considered the most reliable because it is capable of reducing the influence of disturbance of specimens on test results in a manner that allows the specimens to undergo consolidation with their in-situ stress states restored.

The triaxial recompression test shall be implemented in accordance with the standards established by the Japanese Geotechnical Society, titled the **Method for K_0 Consolidated-undrained Triaxial Compression (K_0 CUC) Test on Soils with Pore Water Pressure Measurements (JGS 0525)**, and the **Method for K_0 Consolidated-undrained Triaxial Extension (K_0 CUE) Test on Soils with Pore Water Pressure Measurements (JGS 0526)**. Soil elements are subject to vertical overburden effective stress σ'_{v0} , and horizontal earth pressure at rest σ'_{h0} ($=K_0\sigma'_{v0}$) *in-situ*. Sampled specimens have no total stress under atmospheric pressure, but do have a certain level of isotropic residual effective stress due to suction. The recompression method allows specimens to undergo consolidation with $\sigma'_1=\sigma'_{v0}$, $\sigma'_3=K_0\sigma'_{v0}$ in a triaxial test equipment (this process is called recompression), thereby enabling undrained shear tests to be conducted with their in-situ stress states restored. The effective overburden pressure σ'_{v0} can be calculated from the unit weight of sampled specimens. The problem here is how to obtain the coefficient of earth pressure at rest K_0 . Several methods have been proposed for obtaining it through in-situ tests. The coefficient can also be obtained through a laboratory test called the K_0 consolidation test (a consolidation test which controls the cell pressure σ_3 to avoid changing the cross-sectional areas of specimens when the axial pressure σ_1 or the axial strain ε_1 is increased). The values of K_0 obtained through this method are those in the normally consolidated state (expressed as K_{0NC} in many cases) and close to those of the soil in actual ground in pseudo-overconsolidated states due to the aging effect (the K_0 values of the soil in intensively overconsolidated states is much higher than the K_0 values obtained through the method). Japanese cohesive soil in a normally consolidated state generally has K_0 values in the range of 0.45 to 0.55.

The recompression method can also be implemented in the box shear tests. In this case, because shear rings can restrain the change in specimen diameters, the recompression method can be implemented by simply controlling consolidation pressure to the effective overburden pressure σ'_{v0} without paying special attention to K_0 values.

Although the values of undrained shear strength ($q_u/2$) obtained through unconfined compression tests have wide variations, their averages almost coincide with those of undrained shear strength (averages of c_{uc} and c_{ue}), obtained through triaxial compression and extension tests using the recompression methods which can restore in-situ stress states in specimens. The triaxial compression and extension tests using the recompression method, of which effective stress state of specimens and mechanical rationale are clearer, provide more reliable results than the unconfined compression tests. Thus, it is expected that triaxial tests from which results with small variations can be obtained are advantageous for performance verification based on **Part II, Chapter 3, 2.1 Estimation of Geotechnical Properties**. Also, in the case of intermediate soil, because the unconfined compression tests may lead to uneconomical design through underestimating undrained shear strength, the recompression method is preferable.

The recompression method is used mainly for obtaining in-situ undrained shear strength of naturally deposited cohesive soil. It can also be used to evaluate the undrained shear strength if specimens undergo consolidation considering the increment in in-situ stress due to loading.

When extension tests cannot be conducted, extension strength can be estimated from compressive strength using the ratio of undrained extension strength to undrained compressive strength as the anisotropy of shear strength c_{ue}/c_{uc} (about 0.7 in many cases of Japanese cohesive soil).

③ Method using strength obtained through box shear test:

This method uses the strength τ_{DS} obtained through box shear tests after undisturbed specimens of cohesive soil are subjected to one-dimensional consolidation with in-situ effective stress. The box shear tests can be conducted in accordance with the standards of the Japanese Geotechnical Society, titled the **Method for Consolidated Constant-volume Direct Box Shear Test on Soils (JGS 0560)**. The undrained shear strength, c_u , to be used in performance verification is given by the following equation:

$$c_u = 0.85\tau_{DS} \quad (2.3.22)$$

In this equation, 0.85 is a correction factor with respect to a shear rate effect. Thus, in this method, derivative values are obtained through primary processing of measured values.

④ **Method combining the strength obtained through unconfined compression tests and triaxial compression tests:**

The q_u method, which uses unconfined compression strength, has a problem with low reliability when evaluating soil with no past record because unconfined compression strength is susceptible to specimen disturbance when they are sampled. In order to solve the problem, in the method described in this section, strength is determined through evaluating quality of specimen in a manner that combines q_u and strength obtained from triaxial CU tests using undisturbed specimens. In this method, the specimens are subjected to first isotropic consolidation with in-situ mean effective stress (equivalent to $2\sigma'_{v0}/3$ when $K_0=0.5$) for two hours and then undrained compression through triaxial CU tests. The undrained shear strength, obtained through the above processes, is finally multiplied by 0.75 as empirical correction. That is, like the boxshear test, this method requires obtaining derivative values through primary processing of measured values. This triaxial test is also called a simplified triaxial test (simplified CU test) and has been used as an alternative to the triaxial test with the recompression method. Also, this method is used for natural ground and cannot be applied to unconsolidated ground such as ground just after reclamation. This method does not require measuring pore water pressure. For more details, see **references 15) and 16)**.

⑤ **Method for obtaining shear strength through in-situ vane shear test**

The vane shear test can be conducted in accordance with the standards of the Japanese Geotechnical Society, titled the **Method for Field Vane Shear Test (JGS 1411)**. The average values of the shear strength $c_{u(v)}$ obtained through the vane shear tests can be used for performance verification as the undrained shear strength c_u .¹⁷⁾ The in-situ vane shear test is advantageous in that it can be conducted by flexibly changing positions in survey areas and accurately measure the shear strength of cohesive soil, even when it is too soft to sample self-standing specimens for unconfined compression tests. Thus, the vane shear test is suitable for construction management of, for example, soil improvement work through the vertical drain method. Although the test method and principle are simple, it must be conducted with attention to friction on a rod, which may affect test results and, therefore, requires measures to calibrate the influence of friction on test results or to reduce friction. However, the vane shear test has rarely been used in actual port development works.

⑥ **Method for obtaining shear strength through electric cone penetration test:**

The electric cone penetration test can be conducted in accordance with the standards of the Japanese Geotechnical Society, titled the **Method for Electric Cone Penetration Test (JGS 1435)**. In the test, the following three parameters are measured: cone penetration resistance q_c ; skin friction f_s ; and pore water pressure u . Measurements of cone penetration resistance q_c are affected by the influence of pore water pressure and, therefore, reported as tip resistance q_t after the correction of such influence. In the case of cohesive soil, the shear strength c_u can be estimated by the following equation.

$$c_u = \frac{q_t - \sigma_{v0}}{N_{kt}} \quad (2.3.23)$$

In the equation, σ_{v0} is overburden pressure as total stress, and N_{kt} is a constant called cone coefficient. The values of the cone coefficient N_{kt} differ according to ground characteristics and are in the range of 8 to 16. It is necessary to preliminarily set an appropriate value of N_{kt} of object ground by comparing the calculated values to undrained shear strength additionally obtained through a reliable method, such as the triaxial recompression test with respect to undisturbed specimens.

In the electric cone penetration test, measuring at short intervals is conducted and provides practically continuous data in depth direction. Therefore, thin strata typical in heterogeneous ground can be detected. In contrast, in the case of gravelly ground, gravel which is hit by a cone may cause a test result to have excessively high tip resistance or may prevent the cone from penetrating further into the ground. New penetration equipment, which has been developed and commercialized recently, has a rotary boring mechanism so that equipment operation can be swiftly switched from cone penetration to rotary boring when a cone hits gravel or hard strata and switched back to cone penetration when rotary boring reaches a measurable depth.

In order to set a cone coefficient N_{kt} , it is necessary to implement either one of the methods described in ① to ④ requiring laboratory tests or the method described in ⑤ requiring direct in-situ measurement through the vane shear test. Also, there may be a necessity of additional surveys at many locations to interpolate the data between major survey points. The electric cone penetration test, which can be conducted easily, is considered to be effective in such a case.

These methods described in ① to ⑥ above have their distinctive characteristics and, therefore, it is necessary to select and implement the method appropriate for the purposes and object soil as needed.

The undrained shear strength c_u of cohesive soil is increased with the progress of consolidation. Also, the greater consolidation loads, the greater c_u after consolidation. Because the overburden pressure gets larger with increasing depth, the soil at deeper depth is subjected to larger consolidation pressure. Thus, the c_u of normally consolidated ground gets larger with increasing depth in general. Based on this, the c_u to be used in the performance verification can be normally given by the following equation.

$$c_u = c_{u0} + kz \quad (2.3.24)$$

where

c_u : the undrained shear strength at depth z from the surface of a cohesive stratum;

c_{u0} : the undrained shear strength on the surface of a cohesive soil stratum;

k : an increase rate of c_u at depth z ; and

z : the depth from the surface of a cohesive soil stratum.

(6) Increase in strength of cohesive soil due to consolidation

The undrained strength of cohesive soil increases with the progress of consolidation. Thus, in the soil improvement methods, such as the vertical drain method, which improves the strength of cohesive soil by accelerating pore water drainage due to consolidation, a strength increase ratio c_u/p by consolidation is an important parameter. Naturally deposited cohesive ground may be in a slightly overconsolidated state (actually pseudo-overconsolidated state as explained below) or, even in a normally consolidated state in terms of stress history, appear to be overconsolidated with consolidation yield stress p_c larger than effective overburden pressure σ'_{v0} due to aging effect. For this reason, by normalizing undrained shear strength c_u not by effective overburden pressure σ'_{v0} equivalent to consolidation pressure but by consolidation yield stress p_c ($m=c_u/p_c$), the strength increase ratio can be a parameter specific to cohesive soil. The larger the value of c_u/p_c , which is a soil property used when increasing soil strength through, for example, the vertical drain method, the higher the strength increase ratio will be, thereby enabling higher soil improvement effects to be achieved. Based on the performance records and existing survey results with respect to Japanese marine cohesive soil, the value of c_u/p_c lies in a range shown by the following equation regardless of its plasticity.

$$c_u/p_c = 0.2 \sim 0.25 \quad (2.3.25)$$

Considering that overconsolidation ratios OCR ($= p_c/\sigma'_{v0}$) of naturally deposited cohesive soil are generally in the range of 1.0 to 1.5, and the effective overburden pressure can be expressed by $\sigma'_{v0}=p_c/OCR$, the data (in Fig. 2.3.16)¹⁸⁾ exemplifies the credibility of equation (2.3.25).

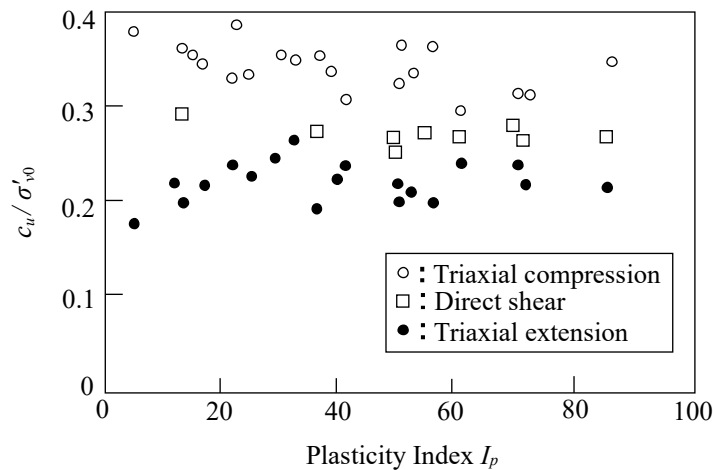


Fig. 2.3.16 Relationship between Plasticity Indexes and c_u/σ'_{v0} ¹⁸⁾

(7) Decrease in strength of cohesive soil due to swelling

When a load is partially removed after consolidation, cohesive soil undergoes swelling with time, thereby reducing the c_u . In addition, the time required for the swelling is considerably shorter than the time required for consolidation. The drainage condition in this case corresponds to the CD condition in an overconsolidated state, as described in **Part II, Chapter 3, 2.3.3 Shear Characteristics** and, therefore, the strength should be evaluated considering its reduction after swelling.¹⁹⁾ Examples of situations corresponding to this case are: removal of loads at the end of consolidation in soil improvement works, such as the vertical drain method or the preload method; excavation for earth retaining structures²⁰⁾; and dredging to deepen the sea bottom.

(8) Strength of intermediate soil

Soil with sand content of 50 to 80% is classified as intermediate soil with properties intermediate between sandy and cohesive soil.²¹⁾ The shear strength of intermediate soil is calculated assuming it as either sandy or cohesive soil, depending on the permeability and design conditions. In the case of intermediate soil with high sand content or coral gravel soil (limited to that with low coral gravel contents), it is preferable to devise test methods and compare the laboratory test results of the coefficients of permeability with those obtained through in-situ permeability tests or the electric cone penetration test.²²⁾ This is because consolidation tests have a high possibility of underestimating coefficients of permeability due to limited test conditions. When the coefficients of permeability determined through the methods described above are 1×10^{-4} cm/s (1×10^{-6} m/s) or more, the ground can be regarded permeable and the ϕ_D can be determined through the electric cone penetration test or triaxial CD test with $c_D=0$. According to previous research on Japanese intermediate soil, the values of ϕ_D are not less than 30° in many cases.^{23), 24), 25), 26)} and ²⁷⁾ However, there may be cases where the electric cone penetration test cannot be applied to the ground with gravel. For the ground surveys on the soil with coral gravel, refer to the **Survey and Design Manual of Coral Gravelly Soil**.

When the coefficients of permeability are not more than 1×10^{-4} cm/s (1×10^{-6} m/s), intermediate soil is considered cohesive in performance verification. However, because the influence of releasing confined pressure during sampling on less disturbed specimens is much greater in intermediate soil than in cohesive soil, the shear strength obtained through the unconfined compression test (q_u) method is underestimated. Although there have been proposed methods for obtaining shear strength by correcting the unconfined compressive strength of specimens with high sand contents using cohesive soil contents or plasticity indexes²⁸⁾, the triaxial test using the recompression method is preferably used to evaluate the shear strength of intermediate soil ground. Alternative methods equivalent to the triaxial test using the recompression method include comparing shear strength obtained through both unconfined compression and triaxial tests and using the strength obtained through the constant-volume box shear test.²⁹⁾

In contrast, the intermediate soil with high silt or coarse particle contents is likely to undergo dilation during shearing. Thus, in the triaxial CU test, such intermediate soil shows a strong tendency of strain hardening where shear strength is increased with the progress of shearing without expressing peak strength, thereby making it difficult to set shear strength. This is because negative excess pore water pressure is generated along with dilation. Since actual soil conditions do not correspond to the definite undrained conditions of triaxial tests, such negative

excess pore water pressure may be too large for soil to have under actual conditions and thereby causing overestimation of shear strength. Thus, as a measure to avoid the overestimation problem, there is a method for setting undrained shear strength with that obtained through the triaxial CD test as the upper limit.

2.3.4 SPT-N value Interpretation Methods

- (1) The angle of shear resistance of sandy soils can be calculated by the following equation from the values obtained through the standard penetration test.

$$\phi = 25 + 3.2 \sqrt{\frac{100N}{\sigma'_{v0} + 70}} \quad (2.3.26)$$

where

ϕ : the angle of shear resistance of sand ($^{\circ}$);

N : the SPT-N value obtained through the standard penetration test; and

σ'_{v0} : the effective overburden pressure at the depth where the standard penetration test is performed (kN/m^2).

- (2) SPT-N values have been associated with a wide variety of geotechnical properties so far. When using related equations of SPT-N values, it is necessary to confirm their scope of application by examining the backgrounds that led to the proposal and establishment of related equations and ground conditions. Many related equations, such as Dunham's equation, which has been commonly used for many years, calculate the ϕ directly from SPT-N values without considering effective overburden pressure σ'_{v0} . However, because the relative density D_r varies depending on the σ'_{v0} as can be seen in **Fig. 2.3.17**, it is necessary to consider the σ'_{v0} when calculating D_r from SPT-N values. This concept has been incorporated in the liquefaction determination,³⁰⁾ where liquefaction resistance of ground is examined with the equivalent SPT-N values (N_{65}) which are converted values under the effective overburden pressure is $\sigma'_{v0}=65 \text{ kN/m}^2$. It is also known that, even ground with identical ϕ , SPT-N values get larger with increasing effective overburden pressure. Therefore, the influence of the σ'_{v0} shall be taken into account when calculating ϕ from SPT-N values.

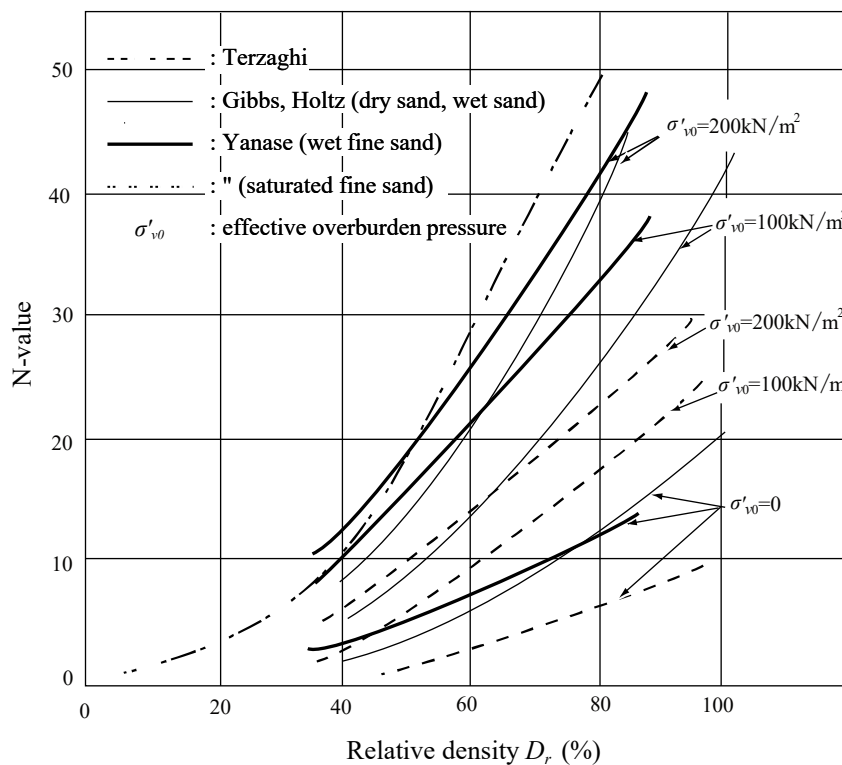


Fig. 2.3.17 Influence of Effective Overburden Pressure and Relative Density on SPT-N values³⁰⁾

(3) Factors affecting SPT-N values

Because the factors influencing SPT-N values mutually interact, methods for quantitatively correcting SPT-N values with respect to these factors have not yet been established. The factors and the extent of influences important to better understand SPT-N values are summarized below.

① Density

Particularly in the case of sandy ground, SPT-N values get larger with the increase in soil density (relative density).

② Water contents

Apart from well compacted fine sand and silty sand, the SPT-N values of saturated sand, dry sand, and wet sand get larger in this order.

③ Effective overburden pressure

SPT-N values get larger with the increase in effective overburden pressure σ'_{v0} .

④ Influence of groundwater

When groundwater levels fluctuate, effective overburden pressure and degrees of saturation vary and so do the SPT-N values.

⑤ Other influencing factors

SPT-N values vary depending on the shapes, grain size distributions, and mineral compositions of soil particles.

⑥ Influencing factors attributable to test methods

The self-weight of a boring rod increases as its length is extended with increasing depths. Thus, in the case of loose sand, SPT-N values tend to be lower than actual ones because the tip of the standard penetration test equipment sinks under the self-weight of the equipment. In contrast, in the case of dense sand, SPT-N values tend to be larger than actual ones because hammer impact efficiency is reduced by rod deflection or wobbling. In the standard penetration test, the SPT-N values to be measured differ depending on hammer dropping methods. To reduce the influence of the different hammer dropping methods on impact efficiency, the International Society for Soil Mechanics and Geotechnical Engineering has set an impact efficiency of 60% as the international standard. That is, SPT-N values shall be measured on the basis that 60% of the free falling energy of a hammer of 63.5 kg dropped from a predetermined height (76 cm) is transmitted to the tip of a rod.³¹⁾ For reference, the SPT-N values measured through the trigger method which is one of the hammer dropping methods and has an impact efficiency of about 80%. It is about 30% lower than those measured through the internationally standardized method.³¹⁾ Thus, caution shall be taken when referring to foreign literature and applying the information in the literature to domestic projects.

Recently, a new method using an automatic hammer dropping device has been promoted as substitute for the trigger method. The new method enables accurate tests to be conducted easily. When simply dropping a hammer with a rope hanging on a cone pulley, without using the automatic hammer dropping device or a trigger, the hammer connected to the rope is inevitably subjected to some resistance, preventing a complete free fall and thereby causing the number of hammer blows, namely SPT-N values, to be overestimated. It shall be particularly noted that overestimating SPT-N values results in the evaluation of bearing capacity and deformation moduli, as well as the determination of liquefaction, on the dangerous side.

(4) Angles of shear resistance of sandy ground

Angle of shear resistance ϕ is an important constant in performance verification of foundations, as is the case with undrained shear strength of cohesive soil. However, because the angle of shear resistance ϕ is affected by many interacting factors, even the same soil does not show constant value of ϕ . Thus, it is necessary to investigate sufficiently the background to establish performance verification methods, including the conditions on which the performance verification methods using ϕ were based.

The ground for deriving **equation (2.3.26)** is as follows. First, reference was made to **equation (2.3.27)** proposed by Meyerhof³²⁾ to express the relationship between SPT-N values and D_r . In this equation, D_r is in the unit of %.

$$D_r = 21 \sqrt{\frac{100N}{\sigma'_{v0} + 70}} \quad (2.3.27)$$

Equation (2.3.27) has been used in the **Specification for Highway Bridges (by the Japan Road Association)** when correcting SPT-N values with effective overburden pressure to examine liquefaction. Then, reference was additionally made to **equation (2.3.28)** proposed by Meyerhof⁽³³⁾ to express the relationship between D_r and ϕ_D .

$$\phi_D = 28 + 0.15D_r \quad (2.3.28)$$

On the basis of **equations (2.3.27) and (2.3.28)**, ϕ_D can be calculated from SPT-N values. However, the values of ϕ_D calculated by using these equations are slightly larger than those calculated using Dunham's equation. Thus, to be consistent with the Dunham's equation (in the case of well-graded angular particles), **equation (2.3.26)** where ϕ_D becomes 25° when SPT-N value is 0 was determined to be the equation to calculate ϕ_D from SPT-N values.

(5) SPT-N values in cohesive ground

Compared to sandy ground, SPT-N values of cohesive soil are too small to be used as a reliable parameter. According to past experience and test results, SPT-N values of cohesive soil are difficult to measure unless q_u is 100kN/m^2 or more. In the case of cohesive soil with q_u not more than 100 kN/m^2 , SPT-N values cannot be used to determine mechanical properties such as strength although implementing standard penetration tests still has significance in confirming whether or not object cohesive soil is soft through observing specimens taken by samplers, as is the case with preliminarily surveys; and determining the physical properties of object cohesive soil. In the case of the Pleistocene cohesive soil with high strength, repeated changes in deposition environments and stress history in the past have often caused such soil to have heterogeneous properties, even in identical strata, or to be in overconsolidation states regardless of effective overburden pressure. Therefore, there may be cases where slight differences in positions or depths cause significant differences in SPT-N values and ground properties. Also, sampling hard cohesive soil is technically difficult because hard cohesive soil specimens are easily cracked. In Japan, the strength of cohesive soil has been evaluated frequently using q_u values, but the q_u values are very easily affected by the quality of specimens. Thus, the relationships between q_u values and SPT-N values normally have large dispersion. The relationship between q_u values and SPT-N values which has been conventionally used is shown in **Fig. 2.3.18**.

Similar to rock ground, to be described in (6) below, the problem with hard cohesive soil is often not strength but other parameters, such as deformation moduli. These parameters have been associated with SPT-N values or q_u values based on past test results. Thus, it is necessary to interpret SPT-N values with due consideration of object facilities and the background of establishing empirical equations, without mechanically obtaining parameters using empirical equations associated with SPT-N values.

(6) SPT-N values of rock ground

The scope of application in which SPT-N values can be used reliably is sandy ground containing a small amount of gravel with the size of 10 mm or less. There is a risk of overestimating SPT-N values when the ground has higher gravel contents. Thus, SPT-N values are certainly too unreliable to be applied to rock ground. **Fig. 2.3.19** shows the relationship between SPT-N values and q_u values in the case of soft rock, called mudstone. As can be seen in the figure, no significant relationship cannot be found between them. When the object ground happens to be rock ground of this sort, and still measurement is required for deformation moduli and compressive strength with high accuracy, it is preferable to measure shear wave velocities or conduct horizontal loading test inside borehole or laboratory tests, using quality specimens without cracks.

(7) Interpretation of SPT-N values of the ground having SPT-N values of 50 or more

The analyses using SPT-N values have problems with dense sand and gravel, gravel, and rock ground. In ground of these types, penetration depths do not reach the predetermined 30 cm even after the number of hammer blows exceeds 50. Generally, in ground where SPT-N values exceed 50, the vibrations on rods and rebounds of hammers prevent proper penetration of samplers, thereby making accurate measurement of SPT-N values difficult. Therefore, SPT-N values are generally expressed by exact figures until 50 and, when exceeding 50, they are simply expressed by $N > 50$. However, because there are cases of overestimating SPT-N values when tips of samplers are clogged with gravel or rock fragments, estimating strength and deformation moduli on the basis of simply determined $N > 50$ has a risk of the overestimation of SPT-N values. Thus, it is necessary to determine $N > 50$ comprehensively by, for example, observing specimens in samplers.

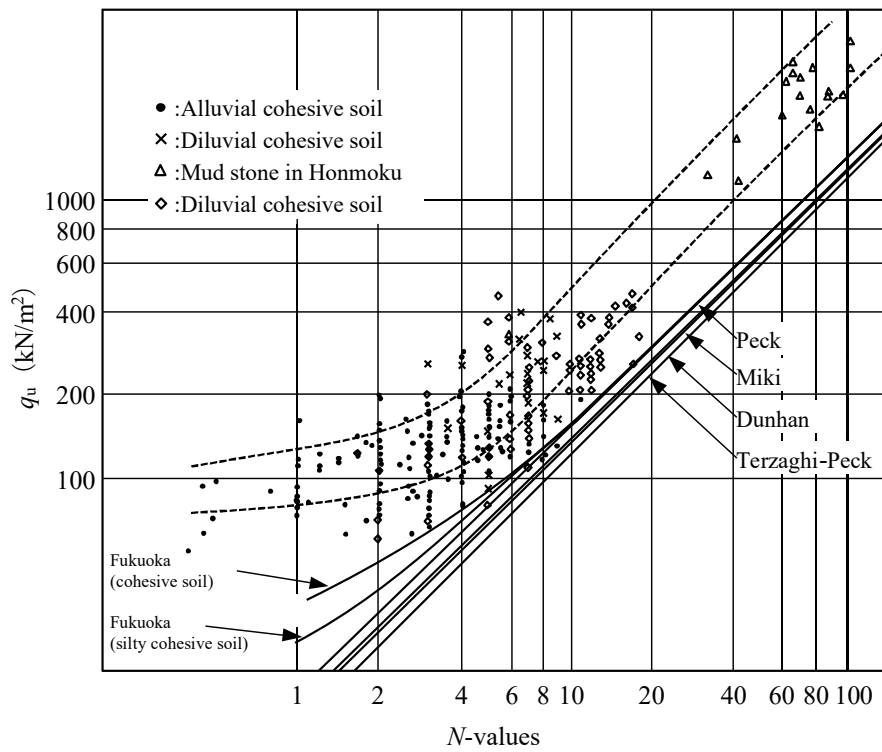


Fig. 2.3.18 Relationship between q_u Values and SPT-N values of Cohesive Soil

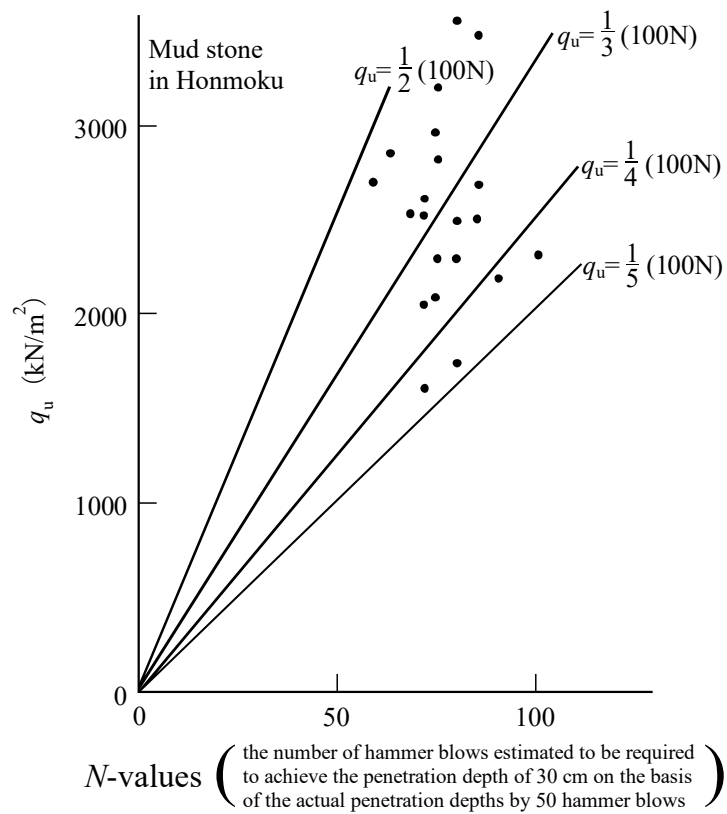


Fig. 2.3.19 Relationship between q_u Values and SPT-N values of Soft Rock

2.4 Dynamic Analyses

2.4.1 Dynamic Deformation Moduli

- (1) In seismic response analyses, it is necessary to set appropriate values of dynamic deformation moduli of soil which defines the relationship between the shear stress and shear strain of soil.
- (2) The performance verification methods with respect to seismic resistance can be broadly classified into static and dynamic performance verification methods. Static performance verification methods, represented by the seismic coefficient method, analyze the stability of ground and facilities through balancing force with actions, due to earthquake ground motions, applied to the ground and facilities as static inertia force. In contrast, dynamic performance verification methods analyze the stability of ground and facilities through calculating amplification ratios and amplified values of acceleration, velocities, and deformation with respect to the ground above foundations of facilities and the foundations themselves. As for the seismic response analysis methods, they are also classified as the time domain analysis method and the frequency domain analysis method. Both methods require the relationship between shear stress and shear strain of soil, which constitutes ground.

Normally the relationship between the shear stress and shear strain of soil subjected to dynamic loading is described separately by a skeleton curve and a hysteresis curve, as shown in **Fig. 2.4.1 (a)**. The skeleton curve shows remarkable nonlinearity as the shear strain amplitude becomes larger. Since the dynamic deformation moduli define the relationship between shear stress and shear strain, they shall be input appropriately when conducting seismic response analyses.

(3) Relationship between dynamic shear stress and shear strain of soil

There are many models introducing shear stress and shear strain curves of soil into analyses, including a hyperbolic model (Hardin-Dornevich model) and the Ramberg-Osgood model.³⁴⁾

(4) Methods for displaying deformation moduli in equivalent liner model

To reasonably estimate the behavior of ground during earthquakes, it is necessary to appropriately evaluate and model relationship nonlinearity between dynamic stress and strain of soil with respect to a wide range of shear strain amplitude. When replaced with an equivalent linear model, the relationship between dynamic stress and strain of soil is expressed by two parameters: shear moduli of elasticity and damping constants (which are alternatively called moduli of rigidity and damping ratios respectively). As shown in **Fig. 2.4.1 (b)**, the shear moduli of elasticity G and the damping constants h are defined by **equations (2.4.1)** and **(2.4.2)**, respectively, with respect to the shear strain amplitude. The scope of application of the equivalent linear model is considered up to strain levels of 10^{-3} . When strain levels exceed 10^{-3} , due consideration shall be given to interpreting the calculation results.

$$G = \frac{\tau}{\gamma} \quad (2.4.1)$$

$$h = \frac{\Delta W}{2\pi W} \quad (2.4.2)$$

where

- G : a shear modulus of elasticity (kN/m²);
- τ : shear stress amplitude (kN/m²);
- γ : shear strain amplitude;
- h : a damping constant;
- W : strain energy (kN/m²); and
- ΔW : damping energy (kN/m²).

The values of the shear modulus of elasticity G and the damping constant h , with respect to arbitrary shear strain amplitude γ , vary depending on the values of γ as shown by a G/G_0 - γ curve and a h - γ curve in **Fig. 2.4.2**. In the figure, G_0 is the shear modulus of elasticity corresponds to $\gamma=10^{-6}$.

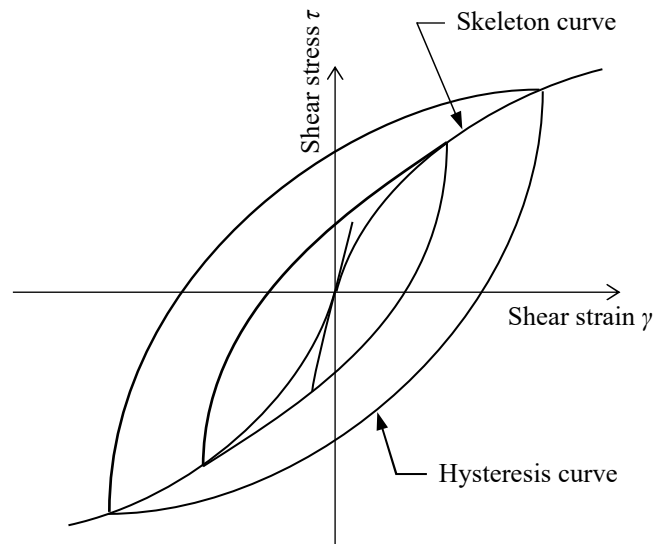


Fig. 2.4.1 (a) Stress-strain Curve

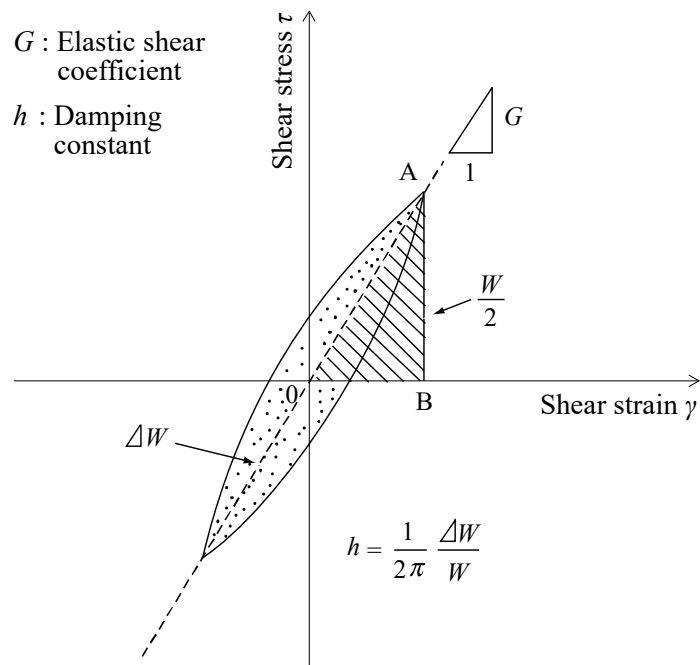


Fig. 2.4.1 (b) Shear Modulus of Elasticity and Damping Constant

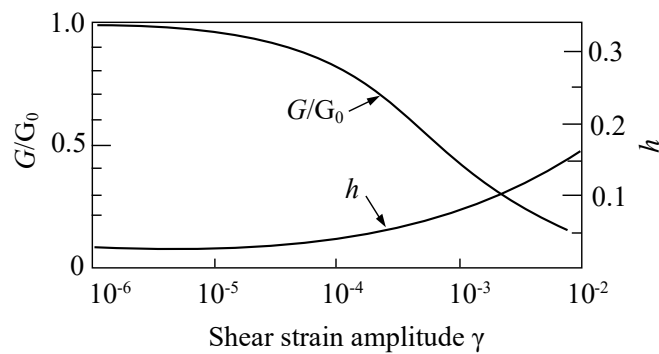


Fig. 2.4.2 Shear Modulus of Elasticity, Damping Constant and Shear Strain Amplitude

(5) Measurement of shear moduli of elasticity and damping constants

The shear moduli of elasticity and damping constants shall be obtained through laboratory tests, such as the cyclic triaxial test and in-situ tests using elastic waves such as the PS logging and the cross hole velocity methods. Laboratory tests require undisturbed specimens sampled in-situ and have a wide scope of applications in that they can be used for the measurement of the shear moduli of elasticity and damping constants corresponding to a wide range from shear strain amplitude of 10^{-6} to failure of specimens. They can also measure change of dynamic deformation moduli caused by construction of facilities. In the cyclic triaxial test, **equation (2.4.3)** can be used to obtain shear moduli of elasticity by assuming Poisson's ratios ν .

$$G = \frac{\sigma_a}{2\varepsilon_a(1+\nu)} \quad (2.4.3)$$

where

σ_a : axial stress amplitude (kN/m²); and

ε_a : axial strain amplitude.

The value of ν is 0.33 under a drained condition or 0.45 under an undrained condition.

The damping constants can be calculated by **equation (2.4.2)** with W and ΔW obtained from the stress-strain curve similar to **Fig. 2.4.1 (b)**.

Regarding the use of in-situ tests for the measurement of shear moduli of elasticity and damping constants, in-situ tests have been available only for shear moduli of elasticity corresponding to shear strain amplitude in the level of about 10^{-6} . In-situ tests capable of measuring both shear moduli of elasticity and damping constants in the range of wide shear strain amplitude has not been commercialized. However, in-situ tests can directly measure in-situ values directly. They are also useful in that their results can be referred to when correcting shear moduli of elasticity obtained through laboratory tests whose results are affected by specimen disturbance. The elastic constants of ground can be obtained by **equations (2.4.4)** to **(2.4.6)** using the elastic wave velocities measured through the elastic seismic exploration using boreholes.

$$G_0 = \rho V_s^2 = \frac{\gamma_t}{g} V_s^2 \quad (2.4.4)$$

$$E_0 = 2(1+\nu)G_0 \quad (2.4.5)$$

$$\nu = \frac{\left(\frac{V_p}{V_s}\right)^2 - 2}{2\left\{\left(\frac{V_p}{V_s}\right)^2 - 1\right\}} \quad (2.4.6)$$

where

V_p : a longitudinal wave velocity (m/s);

V_s : a transverse wave velocity (m/s);

G_0 : a shear modulus of elasticity (kN/m²);

E_0 : Young's modulus (kN/m²);

ν : Poisson's ratio;

ρ : density (t/m³);

γ_t : wet unit weight (kN/m³); and

g : gravitational acceleration (m/s²).

There are various items requiring attention when applying the elastic wave exploration to the soft seabed. These items include: methods for exciting and receiving elastic waves (longitudinal and transversal waves); accuracy in reading waveforms; and methods for protecting borehole walls.

(6) Simple estimation of shear moduli of elasticity and damping constants

In cases where it is difficult to directly measure the shear moduli of elasticity and the damping constants of soil through laboratory tests or in-situ tests, there are methods for estimating them from plasticity indexes, void ratios, unconfined compressive strength, and SPT-N value.³⁵⁾ However, it should be noted that the method for estimating them from SPT-N values produces large variations in estimation results, with a variation coefficient of about 0.2. For example, **Fig. 2.4.3** shows the study result of the estimation errors in measuring S wave velocities of Holocene sandy and cohesive soil based on the variations of SPT-N values and S wave velocities for respective types of ground measured by Imai.³⁶⁾ The horizontal axis shows the ratio of the S wave velocities converted from the SPT-N values to the actual velocities. In the case of the Holocene sandy soil, the average and standard deviations of the ratios of converted S wave velocities to actual ones are 1.12 and 0.29 respectively. In the case of the Holocene cohesive soil, the average and standard deviations are 0.95 and 0.32 respectively. The probability distribution of both cases is considered log-normal distribution.³⁷⁾

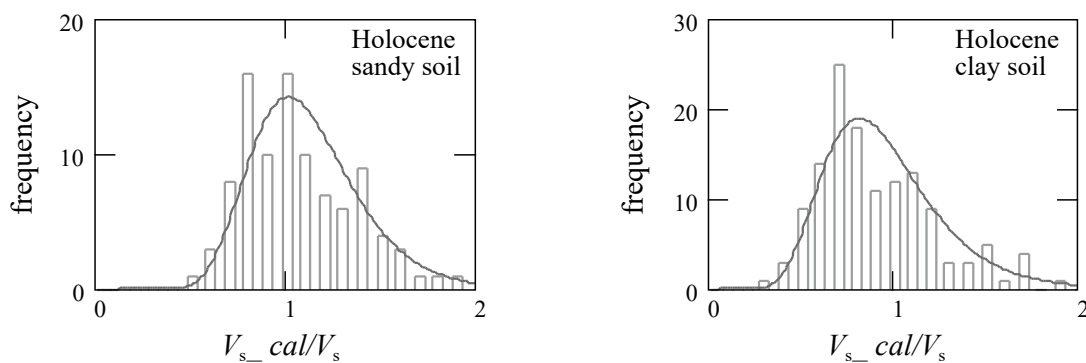


Fig. 2.4.3 Estimation Accuracy of S Wave Velocities³⁶⁾

2.4.2 Dynamic Strength Properties

- (1) The soil strength with respect to dynamic actions is normally determined through laboratory tests. In this case, it is necessary to set the characteristics of the actions and ground conditions appropriately.
- (2) The typical dynamic actions in ports and harbors are seismic movements and wave actions. The seismic movements are characterized by short periods and few cyclic repetitions. In contrast, the wave forces are characterized by long periods and many cyclic repetitions. These dynamic actions are generally converted into static actions, as in the seismic coefficient method; however, there are cases where they need to be analyzed as dynamic actions. Examples include predicting liquefaction during earthquake movements and examining reductions in the strength of foundation ground of structures subjected to wave actions based on dynamic strength properties obtained through cyclic triaxial tests. Depending on the purposes, the cyclic triaxial tests can be conducted with reference to the **Method for Cyclic Undrained Triaxial Test on Soils (JGS 0541)** and the **Method for Cyclic Triaxial Test to Determine Geomaterials' Deformation Properties (JGS 0542)**.

(3) Types of dynamic actions

The characteristic of dynamic actions distinctly different from those of static actions are twofold: ① dynamic actions have shorter durations; and ② dynamic actions are repetitive but static ones are not. Some dynamic actions, like earthquake movements, have both the above characteristics and others, like impulsive force of blasting which is a one-shot action with very short duration, have either of the above characteristics. Dynamic actions may also include those repetitive actions with relatively slow loading velocities, such as wave force in the board sense. **Fig. 2.4.4** shows the classifications of dynamic and static problems in terms of loading time and cyclic repetitions.³⁸⁾ According to **Fig. 2.4.4**, the general wave force based on the period of around 10 seconds is considered the problem positioned around the border between dynamic and static problems.

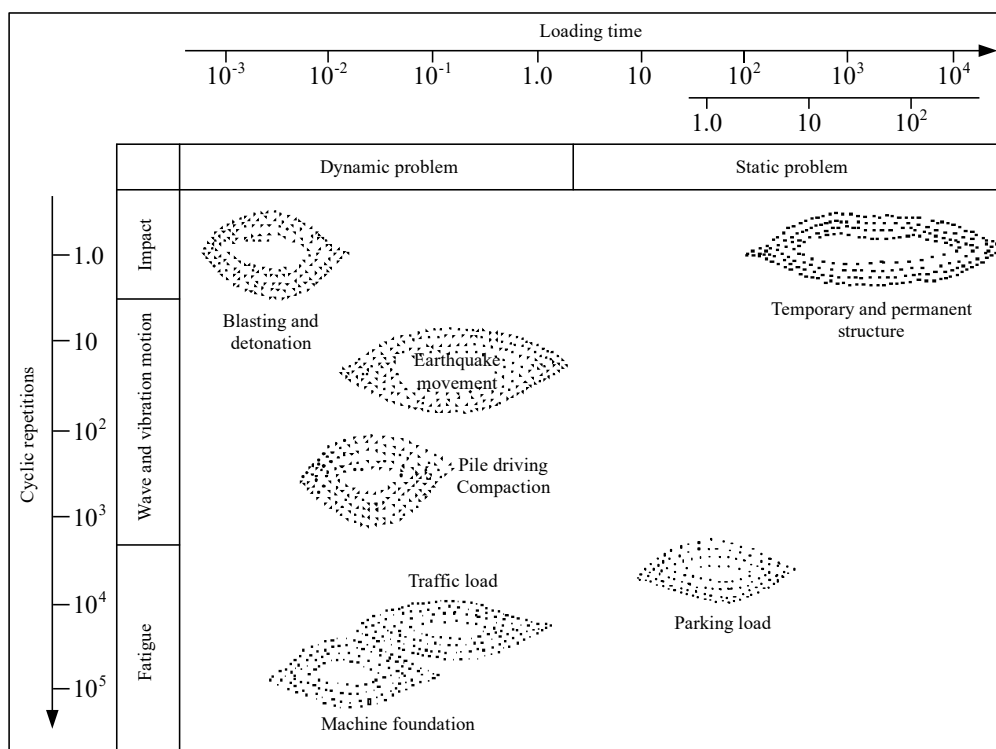


Fig. 2.4.4 Classification of Dynamic Problems in Terms of Loading Time and Recurrence Rates³⁸⁾

(4) Test methods

Laboratory dynamic tests include cyclic triaxial, cyclic simple shear, and torsional shear tests, and they have their own characteristics. Among them, the cyclic triaxial test has been used most heavily because it produces consistent test results less influenced by individual variations in test engineers' skills. When implementing laboratory dynamic tests, reference can be made to the **Method for Cyclic Undrained Triaxial Test on Soils (JGS 0541)**, the **Method for Cyclic Triaxial Test to Determine Geomaterials' Deformation Properties (JGS 0542)**, and the **Method for Cyclic Torsional Shear Test on Hollow Cylindrical Specimens to Determine Deformation Properties of Soils (JGS 0543)**.

Dynamic strength can be examined through laboratory and in-situ tests, and there have been many cases of using laboratory tests. Undisturbed specimens are used in principle except when examining the strength of landfilling materials, for which specimens prepared by remolding disturbed soil can be used. The cyclic shear strength of soil largely differs depending on the two characteristics (duration and cyclic repetitions) with respect to dynamic actions, even though physical properties and stress states of soil are identical; and drain conditions relative to the velocities of actions. Therefore, when soil strength with respect to dynamic actions is required, due consideration shall be given to the characteristics of dynamic actions and ground conditions.

Implementing laboratory tests also requires loading conditions where dynamic actions are replaced by appropriate loads. The characteristics of actions to be considered in such a case are: waveforms (amplitude and periods); cyclic repetitions; loading velocities; and irregularity in waveforms. Thus, it is preferable to set the loading conditions which can reproduce these characteristics as precisely as possible.

The shear strength of soil differs depending on drain conditions. When subjected to dynamic actions, such as earthquake ground motions, ground is in an undrained condition because the ground's drainage velocities are relatively smaller than loading velocities. Thus, laboratory tests for such ground shall be conducted under undrained conditions. Determining whether to examine soil strength with respect to wave force under drained or undrained condition depends on the wave characteristics and stratal organization. Thus, drain conditions shall be set to evaluate the strength and deformation on the safe side. In the case of cohesive soil, laboratory tests shall be implemented under undrained conditions.

(5) Application of test results

To obtain dynamic strength, laboratory tests do not directly apply dynamic actions to specimens but apply loading conditions in which dynamic actions are simplified, to some extent. Thus, due consideration shall be given to the

relationship between the test conditions and characteristics of dynamic actions, as well as ground conditions, when using the dynamic strength obtained through laboratory tests.

When applying cyclic triaxial test results to predict ground liquefaction during earthquakes, refer to prediction and determination of liquefaction in the **Handbook of Liquefaction Countermeasures for Reclaimed Areas** (revised edition).³⁹⁾

[References]

- 1) Watabe, Y., M. Tanaka, S. Sassa and Y. Kikuchi: New Determination Method of Soil Parameters for Performance Based Design, Report of the Port and Airport Research Institute, Vol.48 No.2, pp.123-143, 2009. (in Japanese)
- 2) Matsumoto, K. and F. Ogawa: Correlation of the Mechanical and Index Properties of Soils in Harbor Districts (First Report), Report of the Port and Harbour Research Institute, No.71, 1969. (in Japanese)
- 3) Ogawa, F. and K. Matsumoto: The Correlation of the Mechanical and Index Properties of Soils in Harbour Districts, Report of the Port and Harbour Research Institute, Vol. 17, No. 3, pp.3-89, 1978. (in Japanese)
- 4) Japanese Geotechnical Society: Japanese Geotechnical Society Standards, p.456, 2010. (in Japanese)
- 5) Terzaghi, K. and P.B. Peck.: Soil Mechanics in Engineering Practice, New York John Wiley and Sons Inc., p.44, 1948.
- 6) Mukabi, J.N., F. Tatsuoka, Y. Kohata, T. Tsuchida and N. Akino: Small strain stiffness of Pleistocene clays in triaxial compression, Proceedings of International Symposium on Prefailure Deformation Characteristics of Geomaterials, pp.189-195, 1994.
- 7) Nakase, A., M. Kobayashi and A. Kanechika: Undrained Shear Strength and Secant Modulus of Clays, Report of the Port and Harbour Research Institute, Vol. 11, No. 2, pp.243-259, 1972. (in Japanese)
- 8) Watabe, Y and T. Kaneko: Interpretation of Long-term Consolidation Behavior of Worldwide Clays on the basis of the Isotache Concept, Report of the Port and Airport Research Institute, Vol.54 No.1, pp.3-30, 2015. (in Japanese)
- 9) Šuklje, L.: The analysis of the consolidation process by the isotache method, Proceedings of the 4th International Conference on Soil Mechanics and Foundation Engineering, London, Vol.1, pp.200-206, 1957.
- 10) Mikasa, M.; Consolidation of soft clay, Kajima Publications, 1966. (in Japanese)
- 11) Umehara, Y.: Study on the consolidation characteristics of soils and consolidation test methods, Technical Note of the Port and Airport Research Institute, No.469, 1983. (in Japanese)
- 12) Ogawa, F. and K. Matsumoto: The Correlation of the Mechanical and Index Properties of Soils in Harbour Districts, Report of the Port and Harbour Research Institute, Vol. 17, No. 3, pp.3-89, 1978.
- 13) Japanese Geotechnical Society: Strength Parameters in Design- c , ϕ and N Values, Soil Mechanics and Foundation Engineering Library No.32, pp.15-68, 1988. (in Japanese)
- 14) Beere, T. and L. Bjerrum: Shear strength of normally consolidated clays, Proceedings of the 8th International Conference on Soil Mechanics and Foundation Engineering, pp.39-49, 1973.
- 15) Tsuchida, T., J. Mizukami, K. Oikawa and Y. Mori: New Method for Determining Undrained Strength of Clayey Ground by Means of Unconfined Compression Test and Triaxial Test, Report of the Port and Harbour Research Institute, Vol. 28, No. 3, pp.81-145, 1989. (in Japanese)
- 16) Tsuchida, T.: Study on Determination of Undrained Strength of Clayey Ground by Mean of Triaxial Test, Technical Note of the Port and Airport Research Institute, No. 688, 1990. (in Japanese)
- 17) Tanaka, H. and M. Tanaka: Determination of Undrained Shear Strength of Clayey Ground Measured by Vane Shear Tests, Report of the Port and Harbour Research Institute, Vol. 33, No. 4, pp.1-17, 1994. (in Japanese)
- 18) Hanzawa, H. and H. Tanaka: Normalized undrained strength of clay in the normally consolidated state and in the field, Soils and Foundations, Vol.32, No.1, pp.132-148, 1992.
- 19) Nakase, A., M. Kobayashi and M. Katsuno: Change in Shear Strength of Saturated Clays through Consolidation and Rebound, Report of the Port and Harbour Research Institute, Vol. 8 No. 4, pp.103-143, 1969. (in Japanese)
- 20) Tanaka, H.: Behavior of Braced Excavations in Soft Ground, Technical Note of the Port and Airport Research Institute, No. 734. (in Japanese)

- 21) Kurata, S. and T. Morishita: Study on engineering characteristics of Sand-clay mixed soil, Report of Transport Technical Research Institute, Vol. 11 No. 9, 1961. (in Japanese)
- 22) Tanaka, H., M. Sakakibara, K. Goto, K. Suzuki and K. Fukazawa: Properties of Japanese Normally Consolidated Marine Clays Obtained from Static Piezocone Penetration Test, Report of the Port and Harbour Research Institute, Vol. 31 No. 4, pp. 61-92, 1992. (in Japanese)
- 23) Kobayashi, M., T. Tsuchida and Y. Kamei: Intermediate soil -Sand or clay ?- Geotech-Note 2, Japanese Society of Soil Mechanics and Foundation, 1992. (in Japanese)
- 24) Tsuchida, T., M. Kobayashi, S. Ifuku and I. Fukuda: Engineering properties of coral soils in Japanese south western islands, Proceedings of the International Conference on Calcareous Sediments, Vol.1, pp.137-144, 1988.
- 25) Tsuchida, T: Consolidation, Compression and Permeability Properties of Intermediate Soil and Mixture Soil, Soil and Foundation, TSUCHI-TO-KISO, Vol. 41, No. 7, pp.5-10, 1993. (in Japanese)
- 26) Watabe, Y, T. Kaneko and S. Sassa: Mechanical properties of coral-graveled soil- a parametric study using reconstituted samples, Report of the Port and Airport Research Institute, Vol.55 No.2, pp.61-74, 2016. (in Japanese)
- 27) Watabe, Y., T. Kaneko and S. Sassa: Mechanical properties of coral-graveled soil- an integrated governing parameter for undisturbed samples, Report of the Port and Airport Research Institute, Vol.55 No.3, pp.3-19, 2016. (in Japanese)
- 28) Nakase, A., M. Katsuno and M. Kobayashi: Unconfined compression strength of soils of intermediate grading between sand and clay, Report of the Port and Harbour Research Institute, Vol. 11, No. 4, 1972. (in Japanese)
- 29) Tanaka, H., M. Tanaka, and T. Tsuchida: Strengthening characteristics of undisturbed intermediate soil, Jour. JSCE No.589/ III-42, pp.195-204, 1998. (in Japanese)
- 30) Iai, S., K. Koizumi and H. Tsuchida: Affiliation A New Criterion for Assessing Liquefaction Potential Using Grain Size Accumulation Curve and N-value, Report of the Port and Harbour Research Institute, Vol. 25, No. 3, pp.125-234, 1986. (in Japanese)
- 31) Iwasaki, T.: Problems related to Standard Penetration Test, Foundation, Vol. 18, No. 3, pp.40-48, 1990. (in Japanese)
- 32) Meyerhof, G.G.: Discussion on soil properties and their measurement, Discussion 2, Proceedings of the 4th International Conference on Soil Mechanics and Foundation Engineering, Vol.3, p.110, 1957.
- 33) Meyerhof, G.G.: Compaction of sands and bearing capacity of piles, Journal of the Soil Mechanics and Foundations Division, ASCE, Vol.85, No.SM6, pp.1-29, 1959.
- 34) Ishihara, K: Fundamentals of Soil Dynamics. Mechanics, Kajima Publishing, pp.7-34, 1976. (in Japanese)
- 35) Coastal Development Institute of Technology (CDIT): Handbook of Countermeasure against Liquefaction of Reclaimed Land (Revised Edition), CDIT, pp.60-77, 1997. (in Japanese)
- 36) Imai, T.: P- and S- wave velocities of the ground in Japan, Proceedings of the 9th International Conference on Soil Mechanics and Foundation Engineering, Vol.2, pp.257-260, 1977.
- 37) Nagao, T., Y. Kikuchi, M. Fujita, M. Suzuki and T. Sanuki: Reliability-based design method for pile-supported wharves against the level-one earthquake ground motion, Journal of Structural Engineering, Vol.A52, pp.201-208, 2006. (in Japanese)
- 38) Refer to Reference 34), pp.1-6
- 39) Refer to Reference 35), pp.114-136

3 Groundwater Levels and Seepage

(1) General

In the performance verification of port facilities, it is necessary to give proper consideration to the groundwater levels of sand coasts, seepage flow velocities, and seepage flow rates in permeable ground, or inside facilities, as needed.

(2) Groundwater levels in coastal areas

The depths of underground saltwater surfaces in coastal areas can be estimated by **equation (3.1.1)** (refer to **Fig. 3.1.1**).^{1), 2), and 3)}

$$h^2 = h_0^2 + \left(h_l^2 - h_0^2 \right) \frac{x}{L} \quad (3.1.1)$$

where

$$h_0 = \frac{\rho_1}{\rho_2 - \rho_1} \zeta_0, \quad h_l = \frac{\rho_1}{\rho_2 - \rho_1} \zeta_l$$

h : the depth below sea level of an interface between fresh and saltwater at a distance x (m);

h_0 : the depth below sea level of an interface between fresh and saltwater at $x = 0$ (m);

h_l : the depth below sea level of an interface between fresh and saltwater at $x = L$ (m);

ρ_1 : density of fresh water (g/cm^3);

ρ_2 : density of salt water (g/cm^3);

ζ_0 : the height from sea level of fresh water surface at a shoreline ($x = 0$) (m);

ζ_l : the height from sea level of fresh water surface at $x = L$ (m);

L : the distance from a shoreline ($x = 0$) to an observation point (m); and

x : the landward distance from a shoreline (m).

Equation (3.1.1) cannot be applied to the ground where impermeable strata exist close to ground surfaces or underground. In such cases, reference can be made to **reference 2)**. **References 3)** and **4)** can be used for tidal influences on groundwater in coastal areas. Also, for increases in groundwater levels and beach deformation due to run-up waves, refer to **Part II, Chapter 2, 7.4.9 Relationship between the Topographic Changes of Foreshore and Groundwater Levels**.

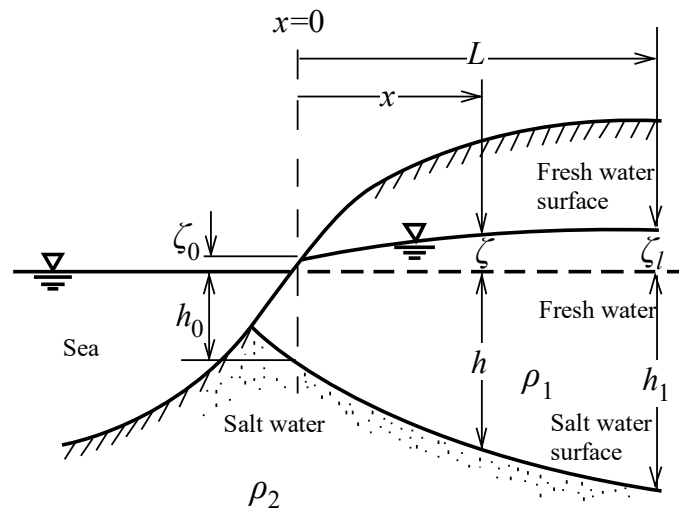


Fig. 3.1.1 Schematic Drawing of Groundwater in a Coastal Area

(3) Seepage flows inside foundations and facilities

① Equation to calculate permeating flow rates

In the case of steady laminar flows in permeable strata, the seepage flow rates can be calculated by Darcy's formula, as shown below.

$$q = kiA \quad (3.1.2)$$

where

q : the flow rate of water flowing in a permeable stratum per unit time (cm³/s);

k : a coefficient of permeability (cm/s);

i : a hydraulic gradient $i = \frac{h}{L}$

h : a head loss (cm);

L : the length of a seepage flow passage (cm); and

A : a cross-section area (cm²).

The formula applicability limit is governed by the grain sizes of soil particles, constituting permeable strata, and the Reynolds numbers related to seepage flow rates. However, considering there are no sufficiently united opinions about applicability, therefore, the calculation results should be verified with actual measurements.⁵⁾ For the details on the applicability and coefficient of permeability, reference can be made to **Part III, Chapter 3, 2.2.3 Coefficient of Permeability of Soil**.

② Seepage in permeable ground

The seepage flow rate in permeable ground can be obtained by drawing a flow net.

The flow net is a pattern of equipotential lines and flow lines, orthogonal to each other, drawn in a manner that can be locally seen as a square grid (refer to **Fig. 3.1.2**).⁶⁾ In the flow net, the flow rate in a flow tube between two flow lines next to each other is constant, and the head loss in each square is also constant. Thus, when a flow net, as shown in the figure, can be drawn in a flow field, a total flow rate can be calculated by **equation (3.1.3)**.

$$q = kh \frac{F}{N} \quad (3.1.3)$$

where

q : a seepage flow rate per unit width (cm³/s/cm);

k : the coefficient of permeability (cm/s);

h : a total water head difference (cm);

N : the number of segments on a flow line separated by equipotential lines; and

F : the number of segments on an equipotential line separated by flow lines.

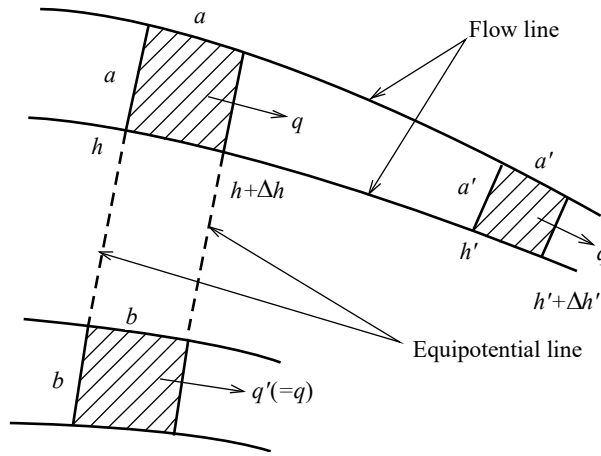


Fig. 3.1.2 Explanatory Diagram of a Flow Net

③ Seepage of sheet pile walls

Rates of seepage flow through the sheet pile walls are not determined only by the permeability of the walls; the dominant determination factor is the soil permeability behind the walls. Shoji et al.⁷⁾ conducted comprehensive seepage tests by varying conditions of tension applied to interlocking joints and sand filling in the joint section, and based on the test results, proposed an empirical equation (refer to **equation (3.1.4)**).

$$q = Kh^n \quad (3.1.4)$$

where

q : a seepage flow rate per unit length in the depth direction of an interlocking joint ($\text{cm}^3/\text{s}/\text{cm}$);

K : the coefficient of permeability at a joint section (cm^{2-n}/s);

h : the pressure head difference between upstream and downstream sides of an interlocking joint (cm);

n : a coefficient determined by the state of an interlocking joint;

$n \doteq 0.5$ when not filled with soil

$n \doteq 1.0$ when filled with soil

The value of K is set at 7.0×10^{-4} (cm/s) when sand is filled on both sides of a sheet pile with tensile force applied to an interlocking joint. However, because the calculation result of a seepage flow rate using this value was 30 times the actual measurement, the reason for such a large difference has been investigated. Thus, when using the equation, it is necessary to give due consideration to the differences between the states of the sheet pile walls used in tests vs. the actual sheet pile walls.

④ Seepage flows inside rubble mounds

The seepage flow rates inside rubble mounds for gravity type structures can be calculated by **equation (3.1.5)**.

$$q = UH$$

$$U = \sqrt{\frac{2gd}{\zeta} \frac{\Delta H}{\Delta S}} \quad (3.1.5)$$

where

q : a seepage flow rate per unit width ($\text{cm}^3/\text{s}/\text{cm}$);

U : an average flow velocity in the cross section of a rubble mound (cm/s);

H : the height of a permeable layer (cm);

d : a grain size of rubble (cm);

g : gravitational acceleration (cm/s^2);

$\frac{\Delta H}{\Delta S}$: hydraulic gradient; and
 ζ : a coefficient of resistance.

Equation (3.1.5) was established on the basis of the seepage tests using eight types of rubble samples with uniform grain sizes in the range of 5 to 100 mm. In the equation, the virtual flow length ΔS can be a distance obtained by adding 0.7 to 0.8 times the height of a permeable layer to the bottom width of a caisson. Also in the equation, the coefficient of resistance can be set in accordance with **Fig. 3.1.3** or set at $\zeta \approx 20$ when Reynolds number $Re (= Ud/v)$ is larger than 10^4 .

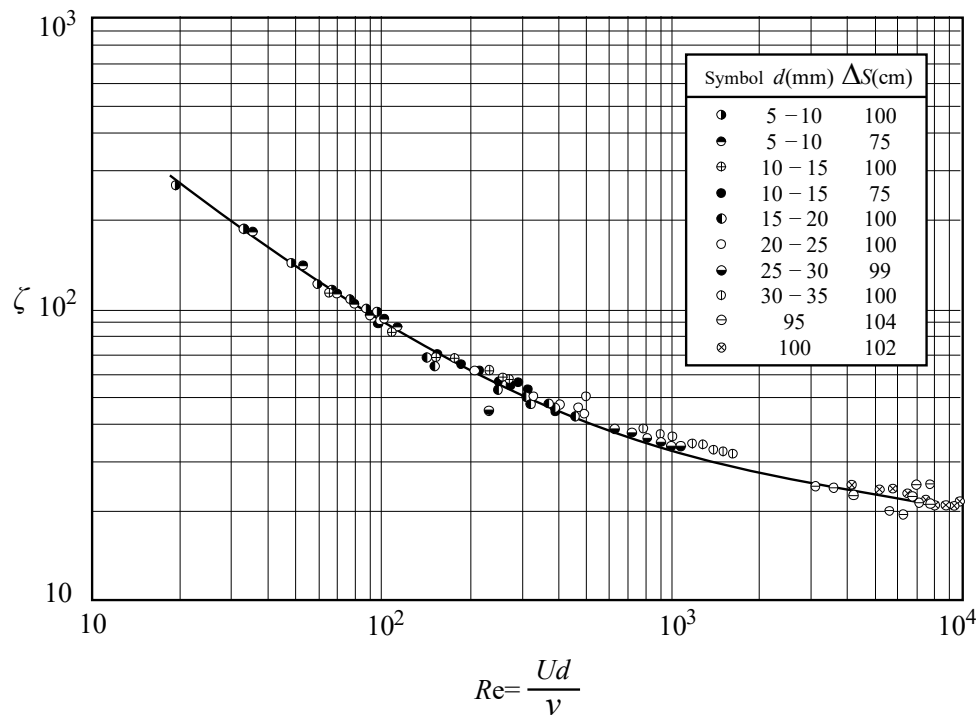


Fig. 3.1.3 Relationship between Coefficient of Resistance and Reynolds Number^{8) and 9)}

[References]

- 1) Todd, D.K.: Groundwater hydrology, John Wiley & Sons, Inc., 1963.
- 2) Japan Society of Civil Engineers: The Collection of Hydraulic Formulae (1985 Edition), 1985. (in Japanese)
- 3) Ishihara, T. and H. Honma: Applied Hydraulics (Vol.II), Maruzen, 1966. (in Japanese)
- 4) Sakai, G: Geohydrology, Asakura Publishing, 1965. (in Japanese)
- 5) Iwasa, Y.: Hydraulics, Asakura Publishing, p.226, 1965. (in Japanese)
- 6) Yamaguchi, H.: Soil Mechanics, Gihodo Shuppan, p.76, 1969. (in Japanese)
- 7) Shoji, Y., M. Kumeda and Y. Tomita: Experiments on Seepage through Interlocking Joints of Sheet Pile, Report of the Port and Harbour Research Institute, Vol.21 No.4, pp.41-82, 1982. (in Japanese)
- 8) Ministry of Transport, Second Port Development Bureau: Report on the experiment of water penetration over storm surge barrier using hydraulic model of Nagoya Port, First report, 1962. (in Japanese)
- 9) Ministry of Transport, Second Port Development Bureau: Report on the experiment of water penetration over storm surge barrier using hydraulic model of Nagoya Port, Second report, 1963. (in Japanese)

Chapter 4 Earth Pressures and Water Pressures

[Public Notice] (Earth Pressures and Water Pressures)

Article 14

- 1 Earth pressures shall be set appropriately based on ground conditions considering the structure of the facility, surcharge, action of earthquake ground motions, etc.
- 2 The residual water pressure shall be set appropriately considering the structure of the facility, surrounding ground conditions, tide levels, etc.
- 3 The dynamic water pressure shall be set appropriately considering the structure of the facility, action of earthquake ground motions, etc.

1 General

(1) Earth Pressure (Relating to Item 1 of the Public Notice Above)

In setting an earth pressure, proper consideration should be given to earth pressure state, namely, whether it is an active or a passive earth pressure as a result of the behavior of the facility concerned, and the design situation, depending on the type of soil quality, such as sandy or cohesive, and the structural characteristics of the facility concerned.

(2) Residual Water Pressure (Relating to Item 2 of the Public Notice Above)

The residual water pressure mentioned herein refers to the water pressure arising from the difference in the water level between the front and rear sides of a facility. This difference must be taken into account in setting the residual water pressure of the facility.

(3) Dynamic Water Pressure (Relating to Item 3 of the Public Notice Above)

In verifying the performance of facilities subject to the technical standards, proper consideration should be given, as required, to the effects of the dynamic water pressure.

(4) Other

In verifying the performance of facilities subject to the technical standards, buoyancy should be considered, as required, in addition to these settings.

2 Earth Pressure

2.1 General

Soil behavior varies with physical conditions, such as grain size, void ratio, and water content, and with stress history and boundary conditions, which also affect earth pressure. The earth pressures discussed in this chapter are those exerted by ordinary soil. The earth pressures exerted by improved soil and reinforced soil will require separate consideration. (For example, refer to **Part III, Chapter 2, 5.18 Active Earth Pressure of Geotechnical Materials Treated with Stabilizer**.) The earth pressure during an earthquake for the design mentioned herein is based on the seismic coefficient method concept and is different from the actual earth pressure generated, during an earthquake, due to dynamic interactions among structures, soil, and water. However, according to analyses of past damages due to earth pressures during earthquakes, the earth pressure discussed here can generally be used in performance verifications. The hydrostatic pressure and dynamic water pressure acting on a structure should be calculated separately.

2.2 Earth Pressures at Permanent State

2.2.1 Earth Pressures of Sandy Soil

- (1) The earth pressures of sandy soil acting on the retaining wall of a structure and the angle of the failure surface from the horizontal surface can be calculated by using the following equations (see **Fig. 2.2.1**):

- ① Active earth pressure and the angle of the failure surface from the horizontal surface

$$p_{ai} = K_{ai} \left[\sum_{j=1}^i \gamma_j h_j + \frac{\omega \cos \psi}{\cos(\psi - \beta)} \right] \cos \psi \quad (2.2.1)$$

$$\cot(\zeta_i - \beta) = -\tan(\phi_i + \delta + \psi - \beta) + \sec(\phi_i + \delta + \psi - \beta) \sqrt{\frac{\cos(\psi + \delta) \sin(\phi_i + \delta)}{\cos(\psi - \beta) \sin(\phi_i - \beta)}} \quad (2.2.2)$$

where

$$K_{ai} = \frac{\cos^2(\phi_i - \psi)}{\cos^2 \psi \cos(\delta + \psi) \left[1 + \sqrt{\frac{\sin(\phi_i + \delta) \sin(\phi_i - \beta)}{\cos(\delta + \psi) \cos(\psi - \beta)}} \right]^2}$$

② Passive earth pressure and the angle of the failure surface from the horizontal surface

$$p_{pi} = K_{pi} \left[\sum_{j=1}^i \gamma_j h_j + \frac{\omega \cos \psi}{\cos(\psi - \beta)} \right] \cos \psi \quad (2.2.3)$$

$$\cot(\zeta_i - \beta) = \tan(\phi_i - \delta - \psi + \beta) + \sec(\phi_i - \delta - \psi + \beta) \sqrt{\frac{\cos(\psi + \delta) \sin(\phi_i - \delta)}{\cos(\psi - \beta) \sin(\phi_i + \beta)}} \quad (2.2.4)$$

where

$$K_{pi} = \frac{\cos^2(\phi_i + \psi)}{\cos^2 \psi \cos(\delta + \psi) \left[1 - \sqrt{\frac{\sin(\phi_i - \delta) \sin(\phi_i + \beta)}{\cos(\delta + \psi) \cos(\psi - \beta)}} \right]^2}$$

with

p_{ai}, p_{pi} : active and passive earth pressures, respectively, acting on the retaining wall in the i -th soil layer (kN/m²)

ϕ_i : angle of shear resistance of the i -th soil layer (°)

γ_j : unit weight of soil in each soil layer (kN/m³)

h_j : thickness of each soil layer, or depth from the top of the i -th soil layer for which the earth pressure is being calculated to the earth pressure calculation level (m)

K_{ai}, K_{pi} : coefficients of active and passive earth pressures, respectively, in the i -th soil layer

ψ : angle of batter of the retaining wall from the vertical plane (°)

β : angle of the ground surface from the horizontal plane (°)

δ : angle of wall friction (°)

ζ_i : angle of the failure surface of the i -th soil layer from the horizontal plane (°)

ω : surcharge per unit area of the ground surface (kN/m²)

(2) The earth pressures at the permanent state are based on Coulomb's earth pressure theory.

(3) The earth pressure at rest as expressed by **equation (2.2.5)** may be used when there is little displacement due to the wall being confined.

$$p = K_0 \left(\sum_{j=1}^i \gamma_j h_j + \omega \right) \quad (2.2.5)$$

where

K_0 : coefficient of earth pressure at rest

(4) Angle of Shear Resistance of Soil

It is possible to use the results of soil tests and/or to estimate the angle of shear resistance of soil by using reliable estimation formulas. For the angle of shear resistance of backfilling material, refer to **Part II, Chapter 11, 5.3 Backfilling**.

(5) Angle of Wall Friction

The angle of wall friction normally has a value of $\pm 15^\circ$ – 20° . It can be estimated as one-half of the angle of shear resistance of backfilling material.

(6) Unit Weight of Soil

The wet unit weight γ_t should be used for soil above the residual water level and the submerged unit weight γ' be used for soil below the residual water level. For the unit weight of backfilling material, refer to **Part II, Chapter 11, 5.3 Backfilling**.

(7) Calculation Formula for the Resultant Force of Earth Pressure

The resultant force of earth pressure can be calculated at each layer. The objective force for the i -th layer can be calculated using **equation (2.2.6)**.

$$P_i = \frac{p_{iu} + p_{il}}{2} \frac{h_i}{\cos \psi'} \quad (2.2.6)$$

where

P_i : resultant force of earth pressure acting on the retaining wall in the i -th soil layer (kN/m)

p_{iu} : earth pressure acting on the retaining wall at the top level of the i -th soil layer (kN/m²)

p_{il} : earth pressure acting on the retaining wall at the bottom level of the i -th soil layer (kN/m²)

h_i : thickness of the i -th soil layer (m)

Moreover, the horizontal and vertical components of the resultant force of earth pressure can be calculated using **equations (2.2.7) and (2.2.8)**.

$$P_{ih} = P_i \cos(\psi' + \delta) \quad (2.2.7)$$

$$P_{iv} = P_i \sin(\psi' + \delta) \quad (2.2.8)$$

where

P_{ih} : horizontal component of the resultant force of earth pressure

P_{iv} : vertical component of the resultant force of earth pressure

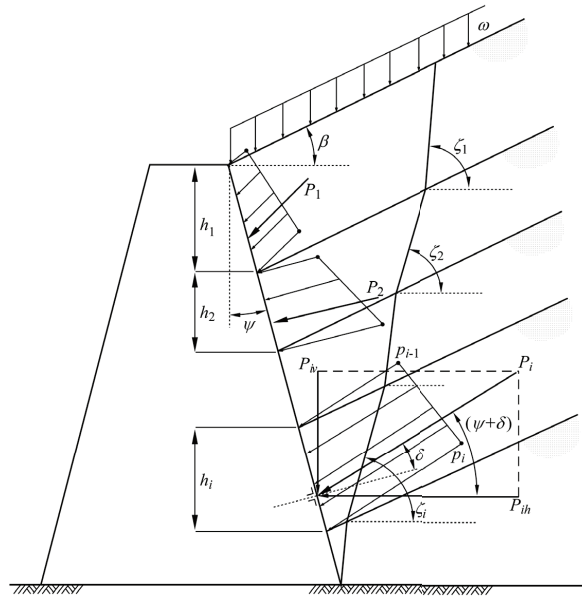


Fig. 2.2.1 Earth Pressures

2.2.2 Earth Pressures of Cohesive Soil

(1) The earth pressures of cohesive soil acting on the retaining wall of a structure can be calculated using **equations (2.2.9) and (2.2.10)**.

① Active earth pressure

$$p_{ai} = \sum_{j=1}^i \gamma_j h_j + \omega - 2c_u \quad (2.2.9)$$

② Passive earth pressure

$$p_{pi} = \sum_{j=1}^i \gamma_j h_j + \omega + 2c_u \quad (2.2.10)$$

where

p_{ai} : active earth pressure acting on the retaining wall in the i -th soil layer (kN/m²)

p_{pi} : passive earth pressure acting on the retaining wall in the i -th soil layer (kN/m²)

 γ_j : unit weight of soil in each soil layer (kN/m³)

h_j : thickness of each soil layer, or depth from the top of the i -th soil layer for which the earth pressure is being calculated to the earth pressure calculation level (m)

w : surcharge per unit area of the ground surface (kN/m²)

c_u : undrained shear strength of cohesive soil (kN/m²)

(2) The earth pressures of cohesive soil are complex. The equations above are based on expedient calculation methods and must be applied with care.

(3) The active earth pressure can be calculated using **equation (2.2.9)**. If the calculated earth pressure has a negative value (meaning that the soil is pulled), the pressure should be assumed to be zero in the calculations of the stability of the wall body.

(4) **Equation (2.2.5) in Part II, Chapter 4, 2.2.1 Earth Pressures of Sandy Soil** can be used for the earth pressure at rest.

(5) Undrained Shear Strength of Cohesive Soil

The undrained shear strength of cohesive soil should be determined using an appropriate method. For the calculation, refer to **Part II, Chapter 3, 2.3.3 Shear Characteristics**.

(6) Wall Friction

In case of cohesive soil, the wall friction force due to the cohesion between the soil and retaining wall should be ignored in principle.

(7) Unit Weight of Cohesive Soil

The unit weight of cohesive soil should be estimated by conducting a soil test. The wet unit weight γ_t should be used for soil above the residual water level and the submerged unit weight γ' be used for soil below the residual water level.

2.3 Earth Pressures during Earthquake

2.3.1 Earth Pressures of Sandy Soil

The earth pressures of sandy soil acting on the retaining wall of a structure during an earthquake and the angle of the failure surface from the horizontal surface can be calculated by using the following equations:

(1) Active Earth Pressure and the Angle of the Failure Surface from the Horizontal Surface

$$p_{ai} = K_{ai} \left[\sum_{j=1}^i \gamma_j h_j + \frac{\omega \cos \psi}{\cos(\psi - \beta)} \right] \cos \psi \quad (2.3.1)$$

$$\cot(\zeta_i - \beta) = -\tan(\phi_i + \delta + \psi - \beta) + \sec(\phi_i + \delta + \psi - \beta) \sqrt{\frac{\cos(\psi + \delta + \theta) \sin(\phi_i + \delta)}{\cos(\psi - \beta) \sin(\phi_i - \beta - \theta)}} \quad (2.3.2)$$

where

$$K_{ai} = \frac{\cos^2(\phi_i - \psi - \theta)}{\cos \theta \cos^2 \psi \cos(\delta + \psi + \theta) \left[1 + \sqrt{\frac{\sin(\phi_i + \delta) \sin(\phi_i - \beta - \theta)}{\cos(\delta + \psi + \theta) \cos(\psi - \beta)}} \right]^2}$$

(2) Passive Earth Pressure and the Angle of the Failure Surface from the Horizontal Surface

$$p_{pi} = K_{pi} \left[\sum_{j=1}^i \gamma_j h_j + \frac{\omega \cos \psi}{\cos(\psi - \beta)} \right] \cos \psi \quad (2.3.3)$$

$$\cot(\zeta_i - \beta) = \tan(\phi_i - \delta - \psi + \beta) + \sec(\phi_i - \delta - \psi + \beta) \sqrt{\frac{\cos(\psi + \delta - \theta) \sin(\phi_i - \delta)}{\cos(\psi - \beta) \sin(\phi_i + \beta - \theta)}} \quad (2.3.4)$$

where

$$K_{pi} = \frac{\cos^2(\phi_i + \psi - \theta)}{\cos \theta \cos^2 \psi \cos(\delta + \psi - \theta) \left[1 - \sqrt{\frac{\sin(\phi_i - \delta) \sin(\phi_i + \beta - \theta)}{\cos(\delta + \psi - \theta) \cos(\psi - \beta)}} \right]^2}$$

The notations p_{ai} , p_{pi} , K_{ai} , K_{pi} , ζ_i , ω , γ_i , h_i , ψ , β , δ , and ϕ_i are the same as those defined in equations (2.2.1) to (2.2.4) in **Part II, Chapter 4, 2.2.1 Earth Pressures of Sandy Soil** according to **Part II, Chapter 4, 2.2 Earth Pressures at Permanent State**. The composite seismic angle θ is defined as follows:

θ : composite seismic angle ($^\circ$) shown as follows:

(a) $\theta = \tan^{-1}k$

(b) $\theta = \tan^{-1}k'$

where

k and k' are as shown below:

k : seismic coefficient

k' : apparent seismic coefficient

- (3) The apparent seismic coefficient shall be in accordance with **Part II, Chapter 4, 2.3.3 Apparent Seismic Coefficient**.

- (4) The earth pressure during an earthquake is based on the theories proposed by Mononobe¹⁾ and Okabe²⁾.

- (5) Angle of Wall Friction

The angle of wall friction normally has a value of $\pm 15^\circ$ or less. It can be estimated as one-half of the angle of shear resistance ϕ of backfilling material.

- (6) Earth Pressure Below Residual Water Level

The earth pressure distribution above or below the residual water level can be determined respectively by using the seismic coefficient in air or the apparent seismic coefficient shown in **Part II, Chapter 4, 2.3.3 Apparent Seismic Coefficient** at each boundary plane.

- (7) Coefficient of Earth Pressure

The coefficient of earth pressure and the angle of the failure surface can be obtained from the diagrams in **Fig. 2.3.1**.

- (8) The earth pressure theory assumes that the soil and the pore water behave integrally. Thus, the equations mentioned above cannot be applied to liquefied soil. For liquefied soil, it is necessary to evaluate the seismic stability of the ground and structures with dynamic effective stress analysis or model tests.

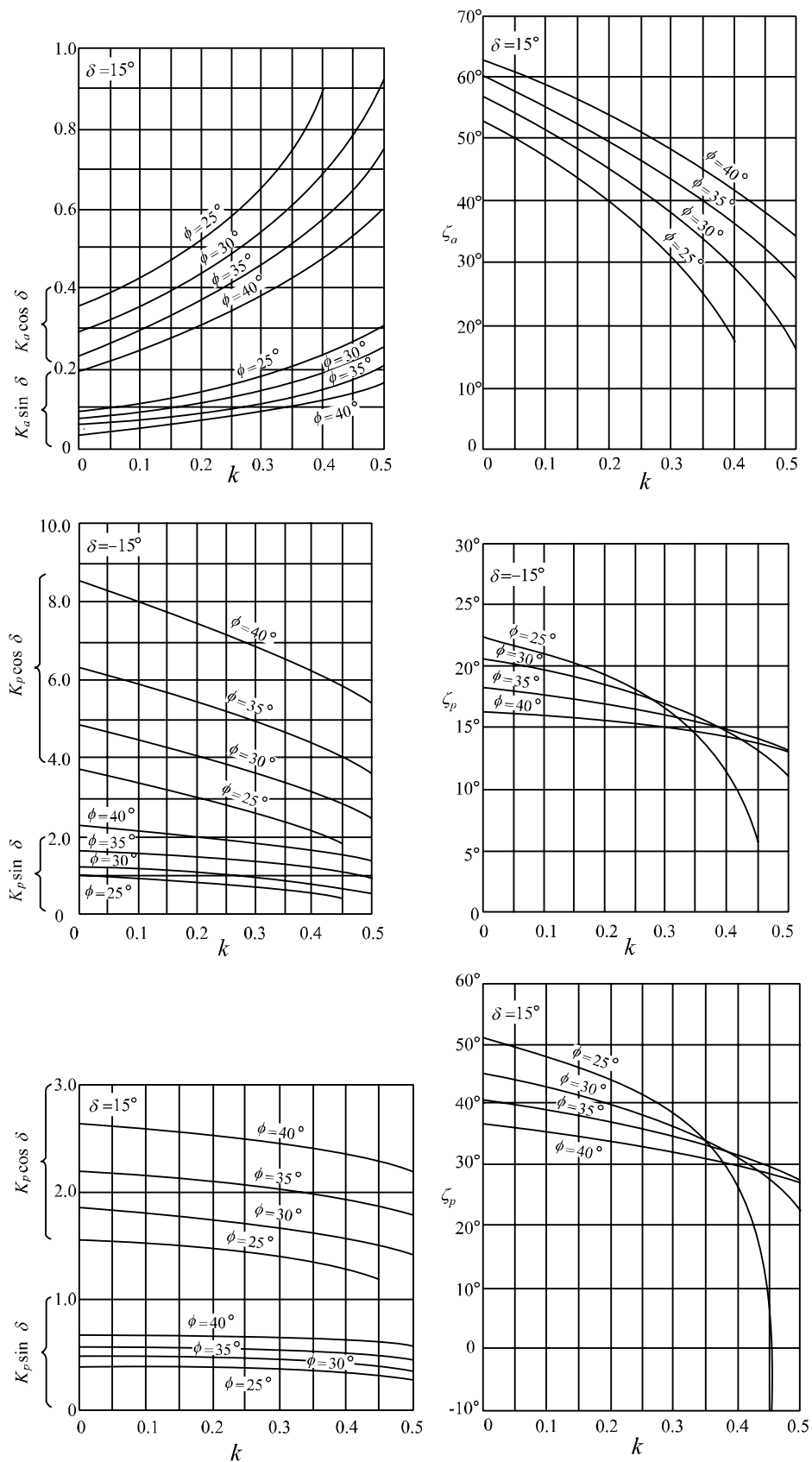


Fig. 2.3.1 Coefficient of Earth Pressure and Angle of Failure Surface

2.3.2 Earth Pressures of Cohesive Soil

The earth pressures of cohesive soil acting on the retaining wall of a structure during an earthquake and the angle of the failure surface from the horizontal surface can be calculated as follows:

(1) Active Earth Pressure during Earthquake

The active earth pressure shall be calculated using an appropriate earth pressure formula which takes the seismic coefficient into account so that the structural stability will be secured during an earthquake. Generally, the active earth pressure during an earthquake can be calculated using **equation (2.3.5)** and the angle of the failure surface from the horizontal surface using **equation (2.3.6)**.

$$p_{ai} = \frac{\left(\sum_{j=1}^i \gamma_j h_j + \omega \right) \sin(\zeta_a + \theta)}{\cos \theta \sin \zeta_a} - \frac{c_u}{\cos \zeta_a \sin \zeta_a} \quad (2.3.5)$$

$$\zeta_{ai} = \tan^{-1} \sqrt{1 - \left(\frac{\sum_{j=1}^i \gamma_j h_j + 2\omega}{2c_u} \right) \tan \theta} \quad (2.3.6)$$

where

- p_{ai} : active earth pressure (kN/m²)
- γ_j : unit weight of the soil (kN/m³)
- h_j : thickness of the soil layer
- ω : surcharge per unit area of the horizontal surface (kN/m²)
- c_u : undrained shear strength of cohesive soil (kN/m²)
- θ : composite seismic angle expressed as $\theta = \tan^{-1} k$ (°) or $\theta = \tan^{-1} k'$ (°)
- k : seismic coefficient
- k' : apparent seismic coefficient
- ζ_{ai} : angle of the failure surface from the horizontal surface (°)

(2) Passive Earth Pressure during Earthquake

The passive earth pressure shall be calculated using an appropriate earth pressure formula so that the structural stability will be secured during an earthquake.

There are many unknown factors concerning the method for determining the passive earth pressure of cohesive soil during an earthquake. Conventionally, however, **equation (2.2.10)** given in **2.2.2 Earth Pressures of Cohesive Soil** in this chapter for obtaining the earth pressure of cohesive soil is used in line with the methods for calculating earth pressures at permanent state. At present, **equation (2.2.10)** can be used as an expedient method.

- (3) The apparent seismic coefficient should be used to calculate the earth pressure of cohesive soil under the sea bottom during an earthquake. The apparent seismic coefficient can be set as zero when calculating the earth pressure at a depth of 10 m from the sea bottom or deeper. However, if the earth pressure at a depth of 10 m below the sea bottom becomes less than the earth pressure at the sea bottom, the latter should be applied.

2.3.3 Apparent Seismic Coefficient

- (1) The earth pressure acting on the soil below the water level during an earthquake can be calculated according to the procedures outlined in **Part II, Chapter 4, 2.3.1 Earth Pressures of Sandy Soil** and **Part II, Chapter 4, 2.3.2 Earth Pressures of Cohesive Soil** by using the apparent seismic coefficient which is determined from the following equation (see **Fig. 2.3.2**):

$$k' = \frac{2 \left(\sum \gamma_{ti} h_i + \sum \gamma_{satj} h_j + \omega \right) + \gamma_{sat} h}{2 \left\{ \sum \gamma_{ti} h_i + \sum (\gamma_{satj} - 10) h_j + \omega \right\} + (\gamma_{sat} - 10) h} k \quad (2.3.7)$$

where

k' : apparent seismic coefficient

γ_{ti} : unit weight of soil in the i -th soil layer above the residual water level (kN/m³)

h_i : thickness of the i -th soil layer above the residual water level (m)

γ_{satj} : saturated unit weight of soil in the j -th soil layer above the layer for which the earth pressure is being calculated below the residual water level (kN/m³)

h_j : thickness of the j -th soil layer above the layer for which the earth pressure is being calculated below the residual water level (m)

ω : surcharge per unit area of the ground surface (kN/m²)

γ_{sat} : saturated unit weight of soil in the soil layer for which the earth pressure is being calculated below the residual water level (kN/m³)

h : thickness of soil layer for which the earth pressure is being calculated below the residual water level (m)

If this soil layer continues, with no change in the soil property, down below the bottom of the retaining wall of the structure on which the earth pressure acts, the thickness of the portion below the bottom of the wall shall not be included in the thickness of the soil layer for which the earth pressure is being calculated.

k : seismic coefficient

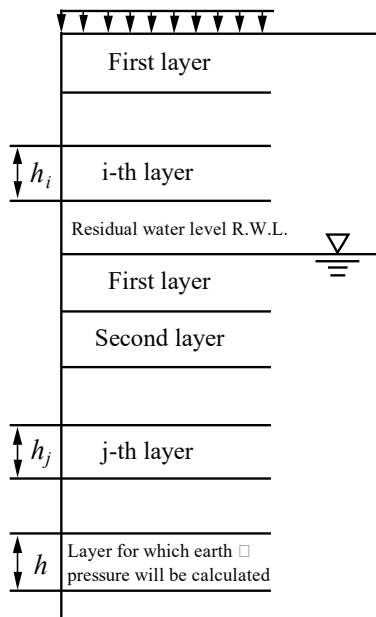


Fig. 2.3.2 Symbols for Apparent Seismic Coefficient

- (2) **Equation (2.3.7)**³ can be used to calculate the apparent seismic coefficient, which will also be used to calculate the earth pressure during an earthquake, as it can be applied to light-weight filling materials and other new materials and is believed to be the most rational method.
- (3) On the assumption that soil grains and water move in an integrated manner in soil under the water level during an earthquake, the force of the earthquake ground motion acting on the soil would be the product of the soil's saturated weight multiplied by the seismic coefficient. Moreover, since the soil under the water level is subject to buoyancy, the vertical force acting on the soil is the soil's underwater weight. Therefore, the resultant force on the soil under the water level during an earthquake would be different from that in the air. When calculating the earth pressure during an earthquake, the equation for determining the earth pressure during an earthquake for soil in the air can also be used for soil under water by applying the apparent seismic coefficient deduced from the composite seismic angle.

The vertical force acting on soil under water includes the weight of the soil layers above the layer for which the earth pressure is being calculated as well as the surcharge. Hence, the apparent seismic coefficient is affected by these factors.

[References]

- 1) Mononobe, N.: Seismic Civil Engineering, Riko-Tosho Publishing, 1952
- 2) Okabe, S.: General Theory on Earth Pressure and Seismic Stability of Retaining Wall and Dam, Journal of JSCE Vol. 10, No. 6, p. 1277, 1924
- 3) Arai, H. and T. Yokoi: Study on the characteristics of earthquake-resistance of sheet pile wall (Third Report), Proceedings of 3rd conference of PHRI, p. 103, 1965

3 Water Pressures

3.1 Residual Water Pressure

- (1) When mooring facilities or similar facilities have watertight structures or when backfilling materials and backfilling soil (hereinafter referred to in this paragraph as “backfilling”) have low permeability, there is a time delay in changes in the water level in the backfilling as opposed to the water level at the front, and the difference of water level appears. In performance verifications on mooring facilities or similar facilities, what needs to be checked is the condition where the water level in the backfilling is higher than that at the front, and that difference is at its greatest. The residual water pressure refers to the water pressure acting on the mooring facilities or similar facilities under this condition.

The magnitude of the residual water level difference varies depending on the permeability of the wall and its surrounding materials making up a mooring facility or a similar facility as well as the tidal range. The general values for the residual water level difference by structural type are shown in sections relating to performance verifications of the respective facilities. Values other than these general values can be used when determining the residual water level difference from surveys conducted on similar structures located nearby or from permeability checks carried out on the wall and its surrounding ground.

- (2) The characteristic value of the residual water pressure caused by the difference in water level between the front and rear sides of a facility can be calculated using the following equation (see **Fig. 3.1.1**):

- ① When y is less than h_w

$$p_{w_k} = \rho_w g y \quad (3.1.1)$$

- ② When y is equal to or greater than h_w

$$p_{w_k} = \rho_w g h_w \quad (3.1.2)$$

where

p_w : residual water pressure (kN/m²)

$\rho_w g$: unit weight of water (kN/m³)

y : depth of the soil layer from the residual water level at the back of the facility to the level for which the residual water pressure is being calculated (m)

h_w : water level difference between the residual water level at the back of the facility and the water level at the front of the facility when the former is higher than the latter (m)

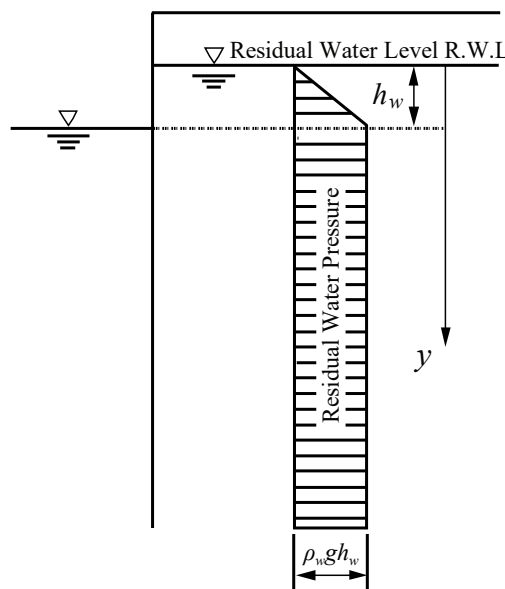


Fig. 3.1.1 Residual Water Pressure

- (3) The residual water level difference is determined taking into consideration whether the wall is well drained or poorly drained, as well as the tidal range. Normally, the height h_w will be 1/3–2/3 of the anterior tidal range.
- (4) After a facility is completed, the permeability of its wall and surrounding materials may diminish with time. Therefore, when the anterior tidal range is sizable, it would be preferable to take that into consideration in determining the residual water level difference.

3.2 Dynamic Water Pressure

- (1) Items (2) through (8) below should be followed when using performance verification equations that make use of the characteristic value of the dynamic water pressure, whereas item (9) should be followed in performing verifications that use techniques, such as the finite element method, for taking the effects of the dynamic water pressure into consideration.
- (2) Normally, methods based on the dynamic water pressure on steady oscillation¹⁾ are used for calculating the characteristic value of the dynamic water pressure. However, in view of the phase relationship of other actions, when a particular need arises, the dynamic water pressure on irregular oscillation should be calculated.

Also, if a liquid occupies spaces inside a facility, the dynamic pressure of the liquid must be taken into consideration. If the dynamic water pressure is acting on both sides of the facility, the sum of the resultant force of the dynamic water pressure becomes twofold. The dynamic water pressure need not be considered in the following cases:

- ① When performance verifications can be performed without taking the dynamic water pressure directly into consideration due to structural characteristics;
- ② When using verification methods that do not take the dynamic water pressure directly into account. This would require sufficient records of results.

More specifically, this would be in the following cases:

- (a) Dynamic water pressure of pore water in the caisson filling
 - (b) Dynamic water pressure of pore water in backfilling materials and backfilling soil of mooring quay walls or similar facilities
 - (c) Dynamic water pressure in designing reinforcement arrangement for caisson bottom slabs
- (3) The dynamic water pressure acting on a vertical wall of an underwater structure during an earthquake can be calculated using the following equation:

$$p_{dw} = \pm \frac{7}{8} k_h \rho_w g \sqrt{Hy} \quad (3.2.1)$$

where

- p_{dw} : dynamic water pressure (kN/m²)
 k_h : seismic coefficient
 $\rho_w g$: unit weight of water (kN/m³)
 y : depth of the dynamic water pressure calculation level from the still water level (m)
 H : depth of water (m)

The resultant force of the dynamic water pressure and its acting height can be calculated by using the following equation:

$$P_{dw} = \pm \frac{7}{12} k_h \rho_w g H^2$$

$$h_{dw} = \frac{3}{5} H \quad (3.2.2)$$

Here, P_{dw} and h_{dw} are the following values, and k_h , ρ_w , and H are equal to the values of k_h , ρ_w , and H in **equation (3.2.1)**, respectively.

P_{dw} : resultant force of dynamic water pressure (kN/m)

h_{dw} : depth of the acting point of the dynamic water pressure resultant force from the still water level (m)

- (4) In the case where water occupying a space in the shape of a cuboid is subject to an earthquake ground motion that causes vibrations in the direction parallel to one side of the cuboid, the dynamic water pressure acting on a wall surface perpendicular to the vibration direction can be calculated using the following equation in consideration of the shape of the cuboid (see **Fig. 3.1.2**):

$$p_{dw} = \pm \frac{7}{8} c k_h \rho_w g \sqrt{Hy} \quad (3.2.1) \text{Reference}$$

where

p_{dw} : dynamic water pressure (kN/m²)

k_h : seismic coefficient

$\rho_w g$: unit weight of water (kN/m³)

y : depth of the dynamic water pressure calculation level from the still water level (m)

H : depth of water (m)

L : length of the space occupied by water in the vibration direction (m)

c : correction factor

$$\text{When } \frac{L}{H} < 1.5, \quad c = \frac{L}{1.5H}$$

$$\text{When } \frac{L}{H} \geq 1.5, \quad c = 1.0$$

The dynamic water pressure acting on the bottom can be calculated using the following equation:

$$p_{dw} = \pm \frac{7}{8} c k_h \rho_w g H \frac{\cosh\left(\frac{\pi}{2} \frac{x}{H}\right) - \cosh\left(\frac{\pi}{2} \frac{L-x}{H}\right)}{1 - \cosh\left(\frac{\pi}{2} \frac{L}{H}\right)} \quad (3.2.3)$$

where

x : distance from the wall surface perpendicular to the vibration direction to the dynamic water pressure calculation point (m)

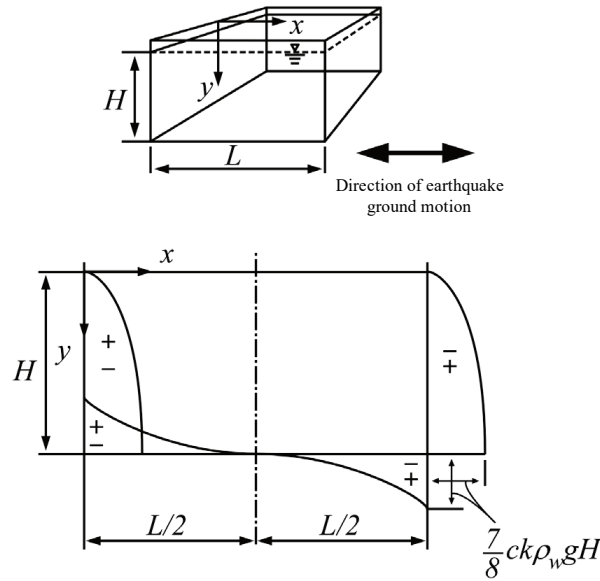


Fig. 3.1.2 Dynamic Water Pressure Exerted by Water in a Cuboid-Shaped Hollow

- (5) The action of the dynamic water pressure both in the front and the back of the wall is directed toward the sea.
- (6) When **equation (2.3.7) in Part II, Chapter 4, 2.3.3 Apparent Seismic Coefficient** is used for a structure, the dynamic water pressure acting on the front side of its wall should be directed seawards, while the dynamic water pressure on the rear side of the wall need not be considered.
- (7) Where the wall is inclined, the dynamic water pressure acting on that surface is smaller than that acting on a vertical wall. This is because the direction of the motion of water particles toward the wall surface is diverted diagonally upwards along the inclined surface. The dynamic water pressure in this case can be calculated using the method proposed by Zanger et al.²⁾.
- (8) The dynamic water pressure acting on a structure that has a complex shape due to an inclined and/or submerged wall can be determined by solving an equation of motion that takes into account the compressibility of water. An equation of motion of water particles in two dimensions is given by **equation (3.2.4)**.

$$\left. \begin{aligned} -\frac{\partial \sigma}{\partial x} &= \rho_w \frac{\partial^2 u}{\partial t^2} \\ -\frac{\partial \sigma}{\partial y} &= \rho_w \frac{\partial^2 v}{\partial t^2} \end{aligned} \right\} \quad (3.2.4)$$

where

- u : displacement of water particles in the x direction
 v : displacement of water particles in the y direction
 σ : dynamic water pressure
 ρ_w : density of water

When the bulk modulus of water is expressed as E_v , the relationship between the volumetric strain of water

$\left(\frac{\partial u}{\partial x} + \frac{\partial v}{\partial y} \right)$ and dynamic water pressure is given by the following equation:

$$\sigma = -E_v \left(\frac{\partial u}{\partial x} + \frac{\partial v}{\partial y} \right) \quad (3.2.5)$$

The dynamic water pressure under different conditions can be calculated by solving **equations (3.2.4) and (3.2.5)** under the boundary condition.

- (9) In the verification of deformation using a finite element method, such as the FLIP³⁾, the effects of the dynamic water pressure are generally considered in the form of an added mass matrix⁴⁾ in formulations. In this case, the solutions of the formulas are approximated on the assumption that the fluid is incompressible.
- (10) The dynamic water pressure acting on a steel pipe or similar structure in water is affected by the inertial force acting on water inside the pipe and the inertial force acting on nearby seawater (added mass) that behaves in an integrated manner with the steel pipe. For details, refer to **Part III, Chapter 5, 5.2.3 Actions**.

[References]

- 1) Westergaard, H. M.: Water Pressures on Dams during Earthquakes, Journal of ASCE. Transactions, No.1835, pp.418-472, 1933
- 2) Zanger, C. N.: Hydrodynamic Pressure on Dams due to Horizontal Earthquake, Proc. Exper. Stress Analysis, Vol.10, No.2, 1953
- 3) Iai, S., Matsunaga, Y. and Kameoka, T.: Strain space plasticity model for cyclic mobility, Soils and Foundation, Japanese Society of Soil Mechanics and Foundation Engineering, Vol.32, No.2, pp.1-15, 1992
- 4) Zienkiewicz, O. C.: The Finite Element Method, Third Edition, McGraw-Hill, 1977

Chapter 5 Ground Settlement, etc.

[Public Notice] (Ground Subsidence)

Article 15

Effects of ground subsidence shall be assessed using appropriate methods based on ground conditions considering the structures, the surcharge and surrounding situations of the facility.

1 Ground Settlement

Ground settlement includes immediate settlement, consolidation settlement, uneven settlement and lateral displacement. The effects of ground settlement should be evaluated based on ground conditions, appropriately considering the structures of the facilities concerned, surcharges, and seismic actions.

For the evaluation of ground settlement, see **part III, Chapter 2, 3.5 Settlement of Foundation**.

2 Crustal Deformations Due to an Earthquake

When a large earthquake occurs, the fault movement causes an elastic crustal deformation and may result in a permanent displacement of the ground in a large surrounding area. This is called a crustal deformation.

For the evaluation of a crustal deformation, see **Part II, Chapter 6, 2 Crustal Deformations**.

Chapter 6 Earthquakes

[Public Notice] (Earthquake Ground Motions)

Article 16

- 1 Level 1 earthquake ground motions shall be appropriately set in the form of probabilistic time histories based on the results of earthquake observations, taking into consideration the source, path and site effects.
- 2 Level 2 earthquake ground motions shall be appropriately set in the form of time histories based on the results of earthquake observations and the source parameters of scenario earthquakes, taking into consideration the source, path and site effects.

[Interpretation]

7. Setting of Natural Conditions

(6) Items related to Earthquakes (Article 6 of the Ministerial Ordinance and the interpretations related to Articles 16 and 17 of the Public Notice)

① The depth for setting earthquake ground motions

The time histories of Level 1 and Level 2 earthquake ground motions shall be specified at the engineering bedrock as defined in ②. If it is necessary to set earthquake ground motions at depths other than the engineering bedrock in the performance verification of facilities subjected to the technical standards, the earthquake ground motions at such depths shall be set through one-dimensional earthquake response analyses of the ground, etc. in which the design ground motion at the engineering bedrock is used as an input motion.

② Engineering bedrock

The engineering bedrock shall be the upper boundary of the layers that can be categorized as one of the following:

- bedrock;
- a sandy layer with standard penetration test values (*SPT-N* values) of 50 or more;
- a cohesive soil layer with an unconfined compression strength of 650 [kN/m²] or more; and
- a layer with a shear wave (S wave) velocity of 300 [m/s] or more.

③ Site effects

The site effects shall be appropriately evaluated taking into account the results of earthquake observations at the site of construction and/or in its vicinity.

④ Time histories of earthquake ground motions

In the performance verification of facilities subjected to the technical standards, Level 1 and Level 2 earthquake ground motions shall be appropriately set at the engineering bedrock in the form of acceleration, velocity or displacement time histories as needed, taking into account the results of earthquake observations and geotechnical properties at the site of construction.

⑤ Level 1 earthquake ground motions

a) Level 1 earthquake ground motions

Level 1 earthquake ground motions shall be set on the assumption that the earthquakes occur in the areas around the port under consideration in accordance with a stationary Poisson process, which means that these earthquakes occur randomly over time, regardless of the historical records. Thus, according to the above definition of Level 1 earthquake ground motions, even an earthquake such as the Nankai Trough earthquake, which is expected to occur in the near future based on the historical records, may not be considered in setting Level 1 earthquake ground motions if its average recurrence interval is longer, to some extent, than the return period of Level 1 earthquake ground motions.

b) Probabilistic time histories

Probabilistic time histories are the time histories of earthquake ground motions set through a probabilistic seismic hazard analysis which considers the probability of earthquake occurrence. The probabilistic time histories of Level 1 earthquake ground motions shall be set on the basis of uniform hazard Fourier spectra, in which any frequency components have identical return periods in order to appropriately consider the frequency content of earthquake ground motions.

⑥ Return period

The return period of the uniform hazard Fourier spectra for setting Level 1 earthquake ground motions shall be set at 75 years.

⑦ Level 2 earthquake ground motions

a) Level 2 earthquake ground motions

In setting Level 2 earthquake ground motions, scenario earthquakes shall be selected from the following six types of earthquakes, taking into account the peak amplitude, frequency content and duration of resultant ground motions and their potential effects on structures. The selection of the scenario earthquakes shall be based on a comprehensive evaluation of the survey results by government agencies such as the Central Disaster Management Council and the Headquarters for Earthquake Research Promotion, and of regional disaster prevention plans.

- i) Recurrence of past damaging earthquakes
- ii) Earthquakes caused by active faults
- iii) Other earthquakes expected from seismological and/or geological point of view
- iv) Scenario earthquakes hypothesized by government agencies such as the Central Disaster Management Council and the Headquarters for Earthquake Research Promotion
- v) Scenario earthquakes hypothesized by local governments
- vi) M6.5 earthquake just beneath the site

b) Source parameters

When setting Level 2 earthquake ground motions, outer and inner source parameters shall be appropriately set in accordance with the type of the scenario earthquake.

1 Earthquake Ground Motions

1.1 General

In general, earthquake ground motions are affected by three factors, namely, the source, path and site effects (**Fig. 1.1.1**). The source effects can be defined as the characteristics of seismic waves generated at the earthquake source as a result of a rupture process on the fault. The path effects can be defined as the attenuation and deformation of seismic waves during their propagation from the source to the upper boundary of the seismological bedrock below the site. The site effects can be defined as the influence of sediments above the seismological bedrock on the seismic waves. The seismological bedrock can be defined as the layers having a shear wave velocity greater than or equal to 3 km/s and it is often composed of granite in Japan. Among those effects, the influence of sediments above the seismological bedrock is so significant that it is important to accurately evaluate the site effects to estimate ground motions during future earthquakes at a construction site. Regarding the site effects, it has been increasingly recognized that, in addition to the influence of shallower sediments above the engineering bedrock, the influence of deeper sediments below the engineering bedrock is also significant¹⁾. In-situ earthquake observations and microtremor measurements can be a useful tool to evaluate the site effects. The existence of sediments affects not only the amplitude but also the temporal characteristics of earthquake ground motions. In the following, its effects on the amplitude will be called the “site amplification factors”. Its effects on earthquake ground motions in general will be simply referred to as the “site effects.”

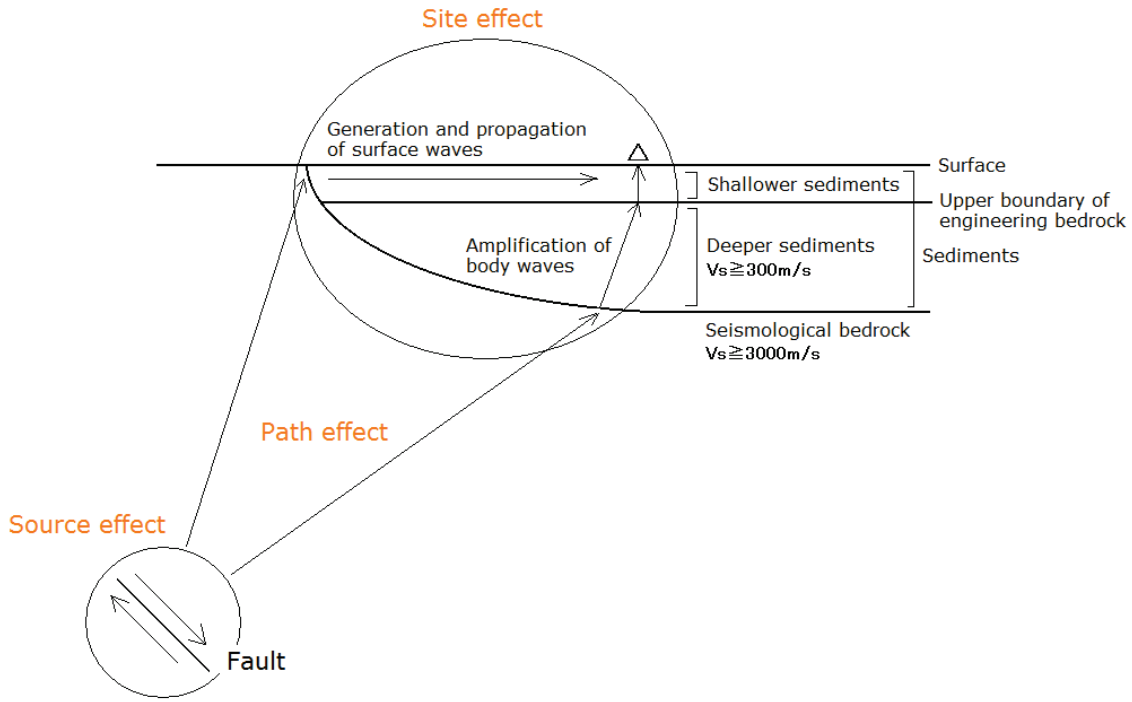


Fig. 1.1.1 Source, path and site effects

1.1.1 Source effects

(1) Omega-square model

The omega-square model²⁾ has been widely used to represent the source effects of earthquake ground motions. According to the omega-square model, the acceleration Fourier spectrum of a seismic wave radiated at the earthquake source, *i.e.*, the acceleration source spectrum can be represented as;

$$S(f) = C \frac{M_0}{4\pi\rho V_s^3} \frac{(2\pi f)^2}{1 + (f/f_c)^2}, \quad (1.1.1)$$

where

$S(f)$: Acceleration source spectrum

M_0 : Seismic moment

f : Frequency

f_c : Corner frequency

ρ : Density in the seismological bedrock

V_s : Shear wave velocity in the seismological bedrock

C : Constant (see **equation (1.3.5)**)

Fig. 1.1.2 shows the displacement, velocity and acceleration source spectra following the omega square model. **Equation (1.1.1)** and **Fig. 1.1.2** indicate that the acceleration source spectra following the omega square model are proportional to the squared frequency for frequencies below f_c and are constant for frequencies above f_c . Thus, f_c corresponds to the corner of the source spectrum.

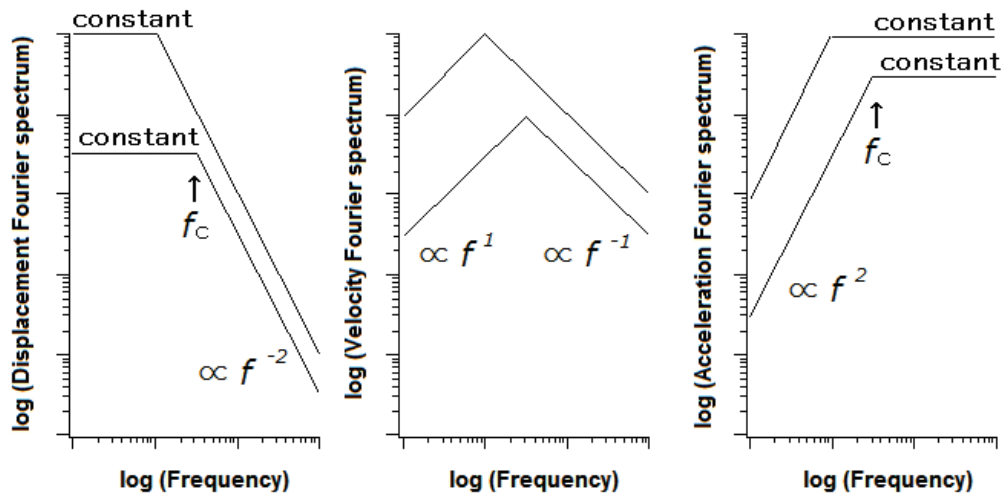


Fig. 1.1.2 Displacement, velocity and acceleration source spectra following the omega-square model

Seismic moment³⁾ M_0 is an indicator of the size of an earthquake. It is defined as follows:

$$M_0 = \mu A D_0, \quad (1.1.2)$$

where

μ : Shear modulus of rocks in the source region

A : Area of rupture along the fault

D_0 : Averaged final slip on the fault

On average, f_c is inversely proportional to $M_0^{1/3}$. Therefore, according to the omega-square model, the Fourier spectrum of a seismic wave radiated at the earthquake source is proportional to M_0 in the long period range, *i.e.*, in the low frequency range, while it is proportional to $M_0^{1/3}$ in the short period range, *i.e.*, in the high frequency range. Because M_0 is increased approximately by a factor of 30 for a unit increase in magnitude, the long and short period components of the seismic wave radiated at the earthquake source are increased approximately by a factor of 30 and 3, respectively, indicating that the long period components are more significantly increased than the short period components for a unit increase in magnitude. Therefore, when designing structures susceptible to long-period ground motions such as tall buildings, long bridges, oil tanks and base-isolated structures, it is important to pay attention especially to earthquakes with a great magnitude.

(2) Directivity

The source of a large earthquake is not just one point but a fault surface with finite dimension. Rupture starts at one point and propagates on the fault. Because the velocity of rupture propagation is more or less similar to the shear wave velocity in the source region, if the port is located in the direction of rupture propagation, seismic waves radiated at different parts on the fault arrive almost simultaneously, causing an intense ground motion. This effect is called the “forward directivity effect”. It has been suggested that the destructive ground motions in the City of Kobe during the 1995 Hyogo-ken Nanbu (Kobe) earthquake (M7.3) were partly caused by this effect as the rupture started below Akashi Strait and propagated toward the City of Kobe⁴⁾.

It has also been suggested that, in a region affected by the forward directivity effect, out of two horizontal components of ground motions, the component perpendicular to the strike of the fault tends to be stronger than the other component⁵⁾⁶⁾⁷⁾⁸⁾. When planning an important quay wall such as a high seismic resistant quay wall near an active fault, this tendency can be utilized to reduce potential damage to the quay wall by locating the facility in such a way that its face-line orientation be advantageous for coming strong motions; it is advantageous to orient its face line perpendicular to the strike of the fault⁹⁾¹⁰⁾. A high seismic resistant quay wall that was located at Maya Terminal in Kobe Port during the 1995 Hyogo-ken Nanbu earthquake could be mentioned as an example of a quay wall that avoided significant damage partly because of its orientation. Although many other quay walls in Kobe Port suffered large deformation of several meters, the quay wall at Maya Terminal suffered relatively slight

deformation of approximately 1 m partly because its face line was oriented perpendicular to the causative Rokko-Awaji fault system and it could avoid the action of strongest ground motions, although the reinforcement of the structure also contributed to the relatively slight damage.

(3) Asperity

It has been revealed that slip on the fault of a large earthquake is not uniform but heterogeneous. For crustal earthquakes, regions on the fault with significantly large slip are called the “asperities”. It is inevitable to consider the existence of asperities to explain intense ground motions such as those observed in the City of Kobe during the 1995 Hyogo-ken Nanbu earthquake⁴⁾. Two types of fault models have been used to represent slip heterogeneity on the fault, namely the “variable slip model” in which the slip is a continuous function on the fault and the “characterized source model” in which asperities are represented by rectangles. However, current knowledge tells us that, for a huge subduction earthquake, regions on the fault with large slip do not necessarily correspond to regions that generate strong ground motions¹¹⁾.

During subduction earthquakes such as the 2011 Tohoku earthquake, pulse-like ground motions with periods of one to several seconds have often been observed¹²⁾¹³⁾¹⁴⁾. The SPGA model¹²⁾¹³⁾ is a source model which is capable of fully reproducing the characteristics of ground motions of a subduction earthquake in the period range with engineering importance including those pulses. The model involves regions called “SPGAs (Strong-motion Pulse Generation Areas)”, each having a dimension of several kilometers.

1.1.2 Path effects

As for the path effects on the amplitude of earthquake ground motions, both geometrical spreading of body waves ($1/r$) and inelastic damping are commonly considered as follows:

$$P(f) = \frac{1}{r} \exp(-\pi f r / QV_s), \quad (1.1.3)$$

where

$P(f)$: Path effect

r : Source-to-site distance

Q : Quality factor

Quality factor is a quantity to represent the extent of inelastic damping in the propagation path due to scattering and the conversion of elastic energy into heat: greater quality factor implies smaller inelastic damping. It should be noted that, at greater distances from the source, the geometrical spreading term in the form of $1/r$ does not apply due to the existence of reverberating waves in the crust such as L_g waves¹⁵⁾.

1.1.3 Site effects

(1) Fundamental characteristics of site effects

The existence of sediments above the seismological bedrock (**Fig. 1.1.1**) has significant effects on the amplitude, frequency content and duration of earthquake ground motions. These effects are referred to as the “site effects.” The relationship between the subsurface structure and the site effects is summarized in **Fig. 1.1.3**.

- ① At the outcrop of the seismological bedrock or a layer equivalent to it, ground motions are relatively weak.
- ② If the sediments above the seismological bedrock are thin, predominantly short period ground motions are observed, because the natural period of the sediments is short.
- ③ If the sediments above the seismological bedrock are thick, predominantly long period ground motions are observed, because the natural period of the sediments is long.
- ④ If the sediments have a closed shape, long duration ground motions are observed, because the seismic waves are easily trapped and continue reverberation within the sediments.

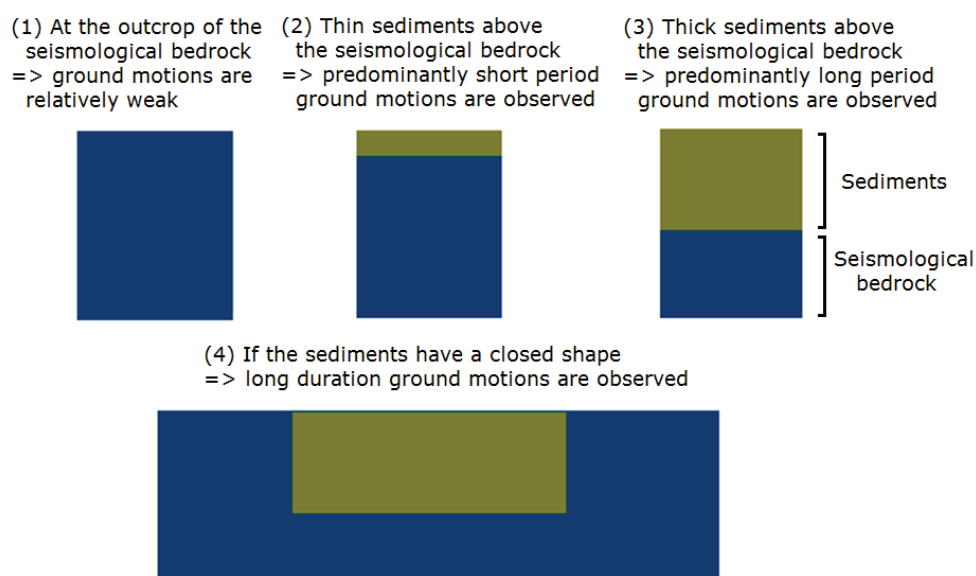


Fig. 1.1.3 Relationship between the subsurface structure and the characteristics of ground motions

There have been a lot of case histories in which earthquake ground motions were significantly affected by the existence of sediments. For example, it has been suggested that the “damage belt” in the City of Kobe during the 1995 Hyogo-ken Nanbu earthquake was generated partly because pulse-like ground motions with periods of 1-2 s were amplified by the sediments below the City of Kobe⁴⁾. Comparison of observed ground motions at strong motion stations around the Port of Sakai (**Fig. 1.1.4**) during the 2000 Tottori-ken Seibu earthquake (M7.3) revealed that peak ground velocities were four times greater for the two stations in the plains of Yumigahama Peninsula (Sakaiminato-G and JMA) than for the two stations in mountainous Shimane Peninsula (SMN001 and SMNH10) (**Fig. 1.1.5**). The difference can be attributed to the amplification of seismic waves due to the existence of sediments below Yumigahama Peninsula. The damage was also concentrated in the City of Sakaiminato in Yumigahama Peninsula. The existence of sediments has such significant effects on strong ground motions that it is fundamentally important to appropriately consider the site effects to evaluate strong ground motions during future large earthquakes. In this regard, in addition to the influence of shallower sediments above the engineering bedrock, it is also important to consider the influence of deeper sediments below the engineering bedrock¹⁾.

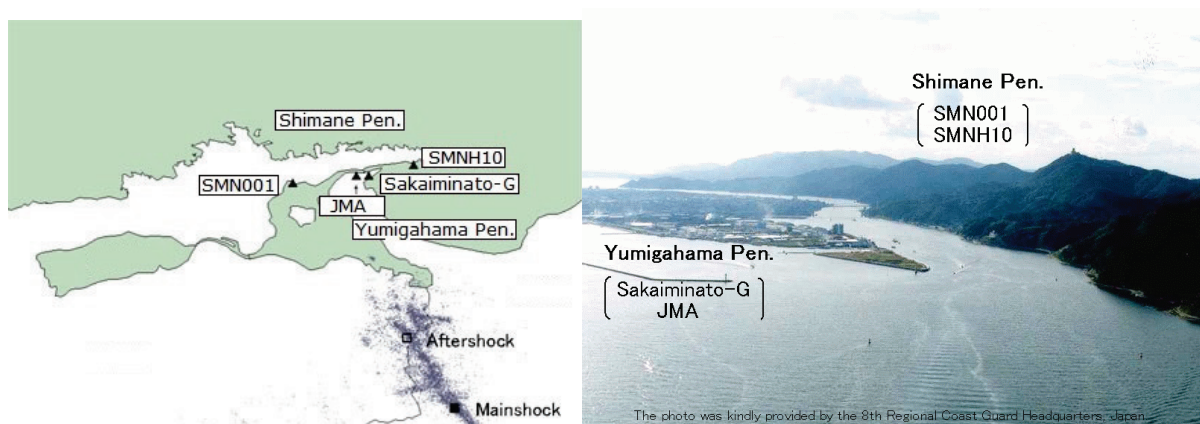


Fig. 1.1.4 Topography around the Port of Sakai and strong motion stations

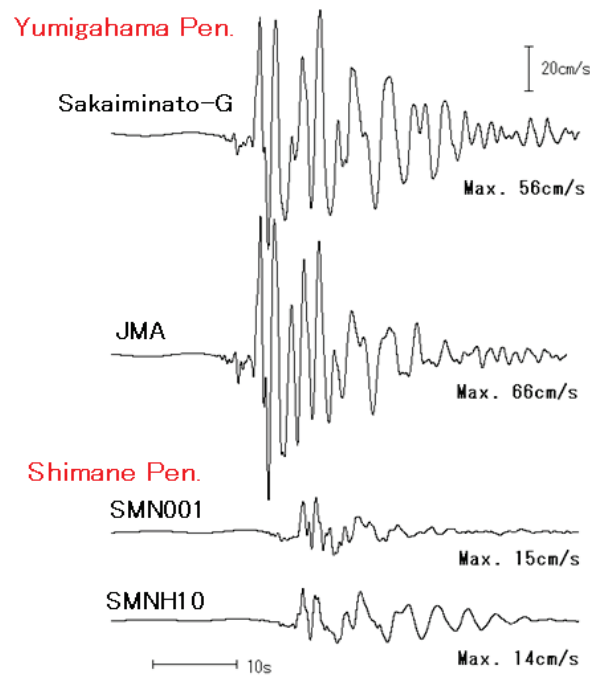


Fig. 1.1.5 Velocity waveforms for the fault-normal components observed around the Port of Sakai during the 2000 Tottori-ken Seibu earthquake

The frequency content of strong ground motions is also significantly affected by the existence of sediments. **Fig. 1.1.6** compares the Fourier spectra of past major strong motion records obtained at Hachinohe Port and Kansai International Airport. At Hachinohe Port, both of the Fourier spectra for the 1968 Tokachi-oki earthquake (M7.9) and the 1994 Sanriku-haruka-oki earthquake (M7.5) were characterized by a peak at the frequency of 0.4 Hz, *i.e.*, the period of 2.5 seconds. It has been revealed that this predominant period at Hachinohe Port is due to the subsurface geological structure below Hachinohe Port¹⁶⁾. On the other hand, at Kansai International Airport, both of the Fourier spectra for the 1995 Hyogo-ken Nanbu earthquake and the 2000 Tottori-ken Seibu earthquake were characterized by a peak at the frequency of 0.2 Hz, *i.e.*, the period of 5 seconds. The site-specific nature of the predominant period of ground motions can be attributed to the site effects. Knowing the predominant period of ground motions at a construction site can contribute to the safety of a structure by, for example, enabling the engineers to avoid resonance effects due to the coincidence of the natural period of the structure and the predominant period of ground motions.

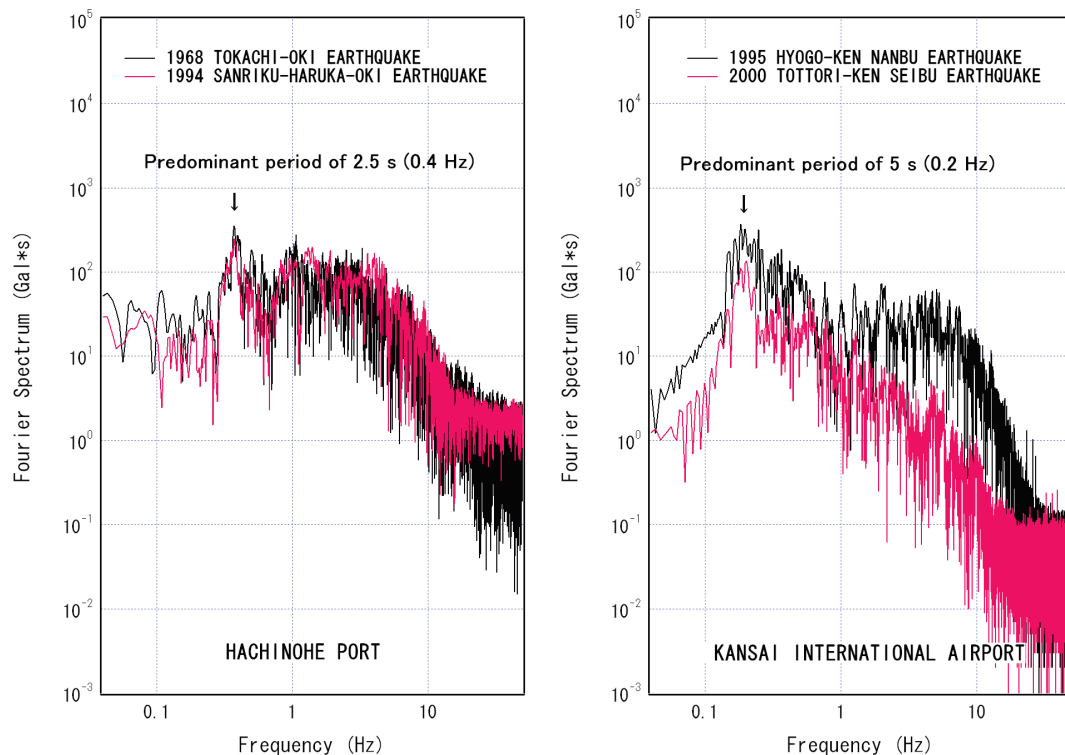


Fig. 1.1.6 Fourier spectra of past major strong motion records obtained at Hachinohe Port (NS component) and Kansai International Airport (Runway-normal component)

(2) Site effects all over Japan

The site effects can be most reliably evaluated by conducting earthquake observations. In Japanese ports and harbours, strong-motion observations have been conducted (**Fig. 1.1.7**). Strong-motion observations can be distinguished from other types of earthquake observations by the fact that they are conducted with instruments that are operable under severe earthquakes. Although the primary purpose of the Strong-Motion Earthquake Observation in Japanese Ports is to observe damaging ground motions due to severe earthquakes, weak-motion records daily obtained by the network can be used to evaluate site effects. The records obtained by the network can be downloaded from the website of the Ports and Harbours Bureau, Ministry of Land, Infrastructure, Transport and Tourism at <http://www.mlit.go.jp/kowan/kyosin/eq.htm>.

Nozu et al.¹⁷⁾ applied a kind of regression analysis known as the “generalized inversion” to a dataset composed of strong motion data from the Strong-Motion Earthquake Observation in Japanese Ports as well as K-NET¹⁸⁾ and KiK-net¹⁹⁾ and evaluated the site amplification factors at strong motion stations all over Japan at the ground surface with respect to the seismological bedrock. The results are available on a CD attached to their report¹⁷⁾ or at the PARI website at https://www.pari.go.jp/bsh/jbn-kzo/jbn-bsi/taisin/siteamplification_jpn.html. **Fig. 1.1.8** shows the strong motion stations for which the generalized inversion was applied¹⁷⁾.



Fig. 1.1.7 Strong-Motion Earthquake Observation in Japanese Ports

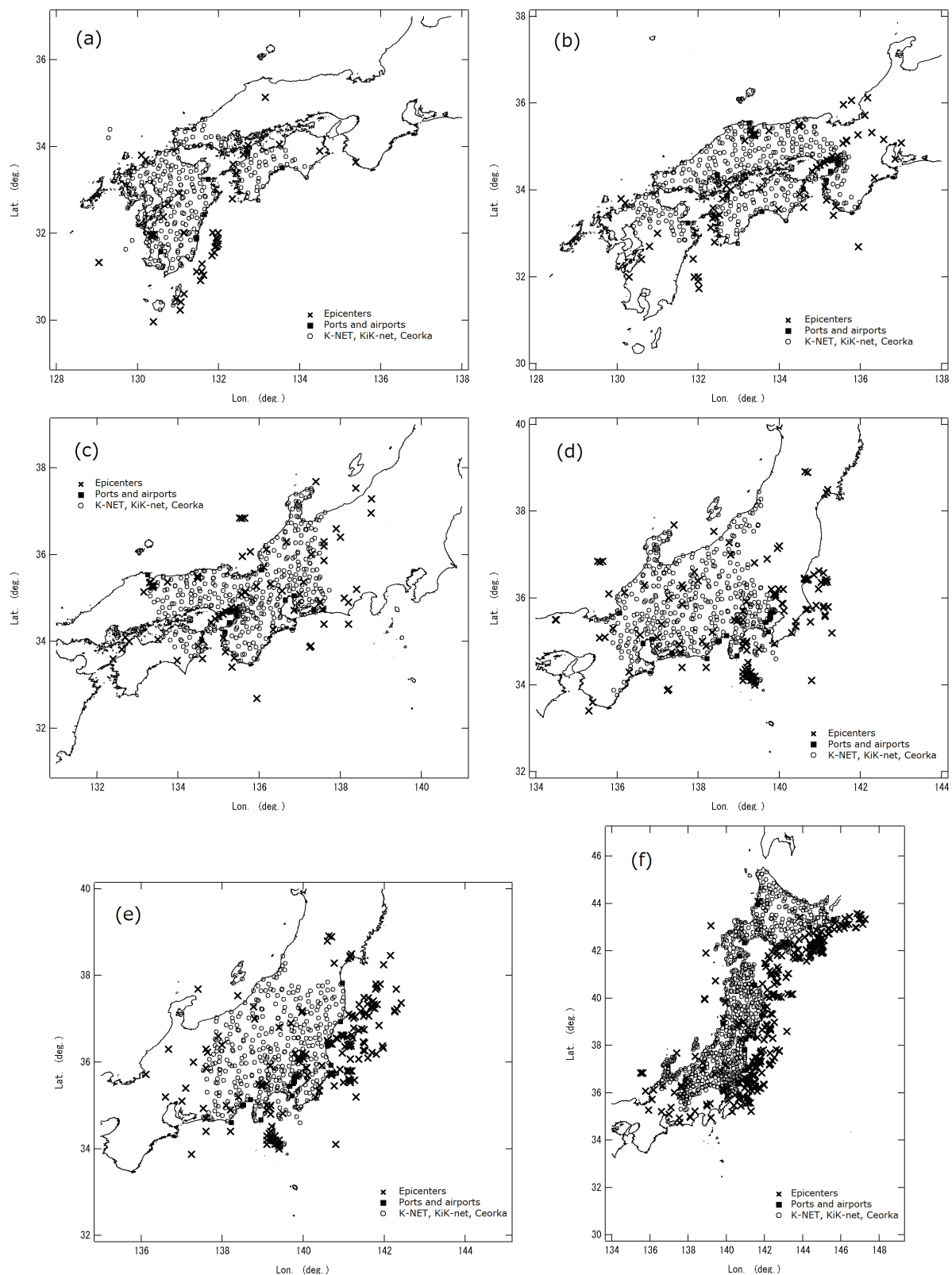


Fig. 1.1.8 Strong motion stations for which the generalized inversion was applied¹⁷⁾.

The inversion was separately applied to regions shown in (a) – (f).
Each panel shows the epicenters of the earthquakes and the strong motion stations.

Typical results from their report¹⁷⁾ are shown in **Fig. 1.1.9** and **Fig. 1.1.10**.

In the northern part of Chugoku District, Japan, alluvial plains are distributed around Lake Nakaumi and Lake Shinji, including cities like Yonago, Sakaiminato, Matsue and Izumo. The left panel of **Fig. 1.1.9** shows the strong motion stations located in the alluvial plains and in the mountains to the south of the plains. The right panel of **Fig. 1.1.9** shows the site amplification factors at those stations. At the stations located in the alluvial plains, namely, TTR008, SMN002, SMN005 and Sakaiminato-G, the site amplification factors include a peak exceeding 10 in the frequency range between 0.5 – 2 Hz, although the peak frequency depends on the site. On the other hand, at the stations located in the mountains, namely, TTR007, TTR009, SMN003, SMN004 and SMN016, the site amplification factors are around 1 – 2 in the frequency range below 1 Hz as shown by black lines in the right panel of **Fig. 1.1.9**, indicating that those stations are almost rock sites. Thus, the site amplification factors are significantly different between the plains and the mountains. At the stations located in the alluvial plains, the peak frequency depends on the site because of the difference of the thickness of the sediments below each site.

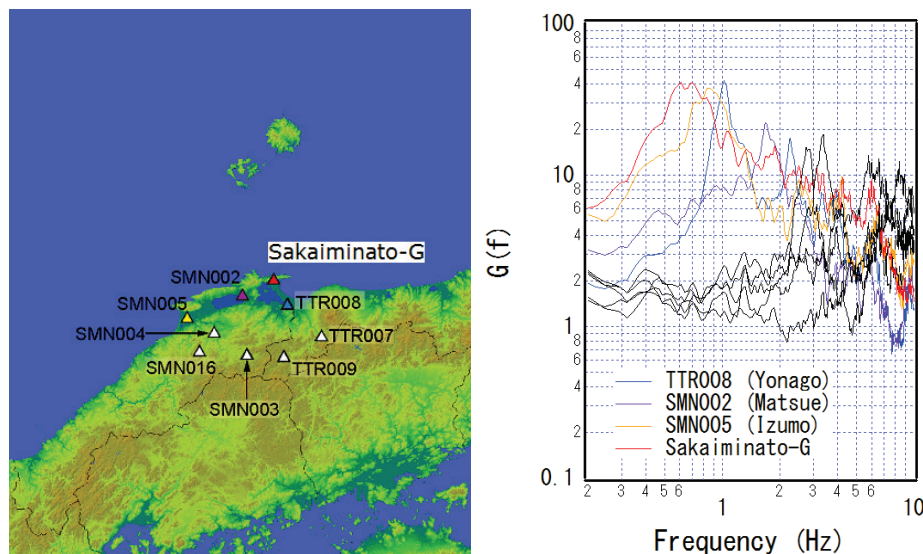


Fig. 1.1.9 Strong motion stations in the northern part of Chugoku District, Japan, and the site amplification factors at those stations

The left panel of **Fig. 1.1.10** shows the K-NET stations in Saitama Prefecture, Japan. The right panel of **Fig. 1.1.10** shows the site amplification factors at those stations. The site amplification factors are small at stations located in the mountains in the west such as SIT004, SIT005, SIT012 and SIT014 as shown by black lines, whereas the site amplification factors are large at stations located in the plains in the east such as SIT003, SIT008, SIT010 and SIT011 as shown by red lines. At SIT006 (Chichibu) located in a small basin surrounded by mountains, the site amplification factor is slightly larger than at the surrounding stations. Takemura²⁰⁾ suggested that significant damage corresponding to seismic intensity of 6 in the Japanese scale occurred in the east of Saitama Prefecture during the 1923 Great Kanto earthquake. The region that suffered significant damage almost coincides with the region with large site amplification factors in **Fig. 1.1.10**.

Regarding the site amplification factors at strong motions stations, in addition to the above report¹⁷⁾, there are other published reports for the site amplification factors in Nansei Islands²¹⁾ and Northern Hokkaido²²⁾, Japan.

Although strong motion stations look so densely located once plotted on a nationwide map as in **Fig. 1.1.8**, they are actually 20 – 30 km apart from each other. Therefore, the site amplification factor at a construction site cannot usually be revealed only by the existing strong motion networks. It is necessary to conduct in-situ earthquake observations and/or microtremor measurements to evaluate the site amplification factor. The details will be explained in **Part II, Chapter 6, 1.2.2 Evaluation of site amplification factors**.

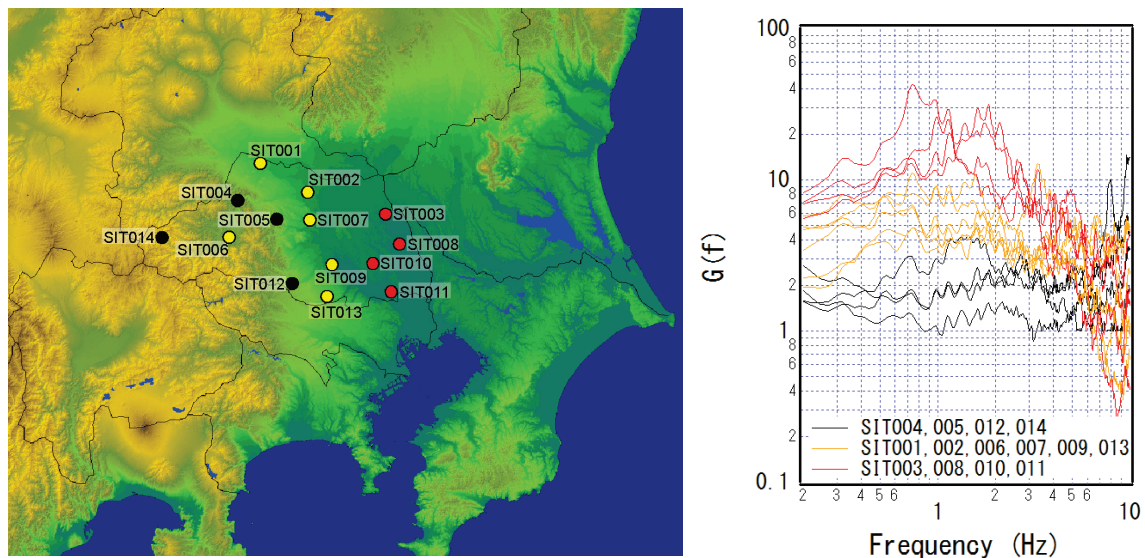


Fig. 1.1.10 K-NET stations in Saitama Prefecture, Japan, and the site amplification factors at those stations. (The red, yellow and black markers indicate strong motion stations with large, medium and small site amplification factors, respectively.)

1.1.4 Soil nonlinearity

In general, material properties of shallower sediments are dependent on their strain levels; under strong ground motions, the shear modulus decreases and the damping factor increases. These characteristics are called “soil nonlinearity”. Nonlinear behavior of the soil can be easily detected by taking the surface to borehole Fourier spectral ratios of strong and weak motion records. **Fig. 1.1.11** shows the surface to borehole Fourier spectral ratios for all the records in 2003 with M5.0 or greater at Kushiro Port. The Fourier spectra for the EW and NS components were smoothed with moving average and their compositions were plotted. The thick line is for the September 26, 2003, Tokachi-oki earthquake (M8.0). Except for the M8.0 earthquake, the spectral ratios always had peaks at 1 Hz and 3 Hz, whereas the peaks shifted to lower frequencies for the M8.0 event. This is a typical example of soil nonlinearity.

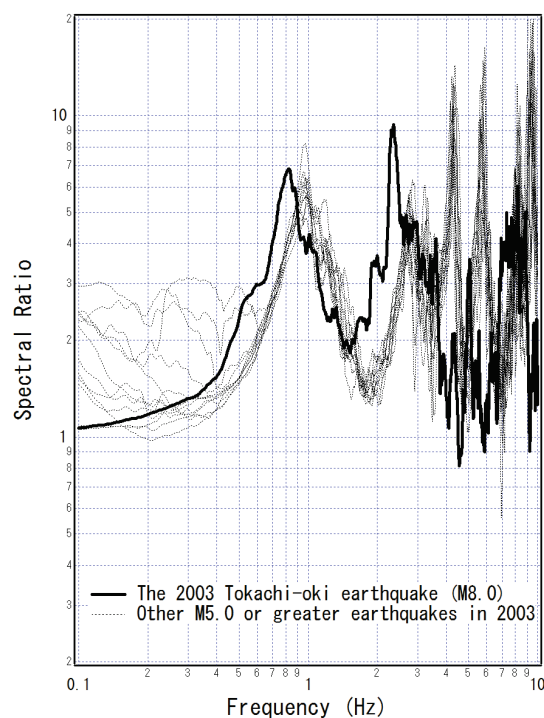


Fig. 1.1.11 Surface to borehole Fourier spectral ratios at Kushiro Port. All the records in 2003 with M5.0 or greater are plotted.

1.1.5 Spatial variation of earthquake ground motions

Spatial variation of earthquake ground motions can be an important issue to be considered in designing a long or a large structure such as a submerged tunnel or a buried pipeline. Horizontal heterogeneity of the ground within the dimension of a long or a large structure can cause spatial variation of earthquake ground motions. For a ground with less horizontal heterogeneity, horizontal wave propagation can be a major cause of spatial variation of earthquake ground motions. For details see **Part II, Chapter 6, 1.4 Spatial variation of earthquake ground motions for the performance verification of structures**.

1.2 Level-1 ground motions for the performance verification of structures

1.2.1 General

In general, level-1 ground motions are determined by means of a probabilistic seismic hazard analysis considering the source and path effects and the site amplification factor at the engineering bedrock with respect to the seismological bedrock. The ground motions to be determined are the so called “2E wave”²³⁾, which is the incident wave impinging at the surface of the engineering bedrock multiplied by 2.

Time history data of level-1 ground motions at major ports, etc. that were determined taking account of regional source and path effects are available at the website of the National Institute for Land and Infrastructure Management at <http://www.ysk.nilim.go.jp/kakubu/kouwan/sisetu/sisetu.html>. Detailed procedures for the determination can be found in Takenobu et al.²⁴⁾. In some cases, however, it cannot be guaranteed that the site amplification factor that was used to calculate a level-1 ground motion be equivalent to the site amplification factor at a construction site. In that case, it is necessary to confirm this equivalence by using microtremor measurements. The details will be explained in **Reference (Part II), Chapter 1, 4.2 Microtremor measurements at the construction site** and in its vicinity. If they are equivalent, the existing level-1 ground motion available at the website can be used without correction. If they are not equivalent, it is necessary to evaluate the site amplification factor at the construction site by means of earthquake observations (See **Part II, Chapter 6, 1.2.2 Evaluation of site amplification factors (1)**) and/or microtremor measurements (See **Part II, Chapter 6, 1.2.2 Evaluation of site amplification factors (2)**) and to correct the existing level-1 ground motion before it is used for the design (See **Part II, Chapter 6, 1.2.4 Correction of level-1 ground motions**).

If it is difficult to conduct in-situ earthquake observations and/or microtremor measurements because of, for example, insufficient period of construction, the site amplification factor at the construction site can be evaluated by using an empirical relation (See **Part II, Chapter 6, 1.2.2 Evaluation of site amplification factors (3)**) based on the site amplification factor at a nearby strong motion station. In that case, it is important to recognize that the accuracy of the level-1 ground motion will be significantly degraded compared to cases with site amplification factors based on earthquake observations and/or microtremor measurements.

For the detailed procedures of the performance verification of a structure, see the descriptions in **Part III** depending on the type of the structure.

1.2.2 Evaluation of site amplification factors

(1) Evaluation of site amplification factors based on earthquake observations

It is desirable to evaluate the site amplification factor at a construction site based on earthquake observations. First, it is efficient to consider the availability of the existing strong motion stations of the Strong-Motion Earthquake Observation in Japanese Ports (see **Part II, Chapter 6, 1.1.3 Site effects**), K-NET¹⁸⁾, KiK-net¹⁹⁾ and the network of seismic intensity meters by the JMA and local governments. For that purpose, it is necessary to conduct microtremor measurements at the construction site and a nearby strong motion station (**Fig. 1.2.1**). If the characteristics of microtremors are similar between the two locations, it is reasonable to assume that the dynamic characteristics of the ground are similar between the two locations. In that case the site amplification factor at the nearby strong motion station can be used for the construction site. Details can be found in **Reference (Part II), Chapter 1, 4.2 Microtremor measurements at the construction site** and in its vicinity.

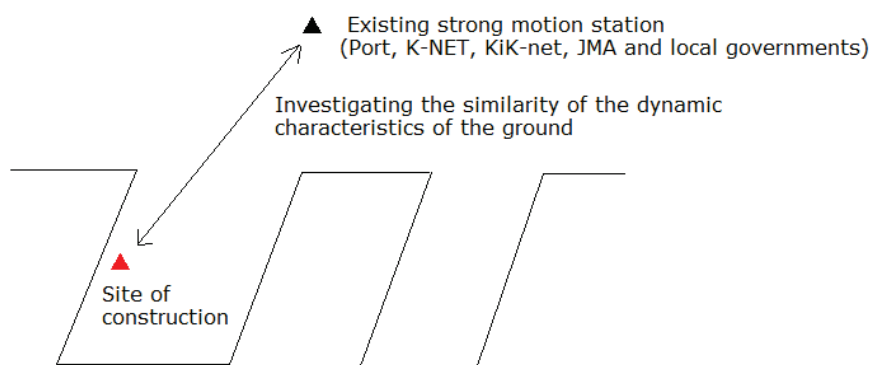


Fig. 1.2.1 Microtremor measurements at a construction site and a nearby strong motion station

However, if the results of the microtremor measurements indicate that the dynamic characteristics of the ground are different between the construction site and the nearby strong motion station, it is desirable to evaluate the site amplification factor at the construction site by means of in-situ earthquake observations, depending on the importance of the project. In that case, it is necessary to confirm that the dynamic characteristics of the ground are similar between the construction site and the site of the in-situ earthquake observations. Details of the evaluation of the site amplification factor by means of in-situ earthquake observations can be found in **Reference (Part II), Chapter 1, 4.3 Evaluation of site amplification factors based on in-situ earthquake observations.**

Once the site amplification factor at the ground surface with respect to the seismological bedrock is obtained based on earthquake observations, it can be divided by the transfer function between the engineering bedrock and the ground surface to obtain the site amplification factor at the engineering bedrock with respect to the seismological bedrock. For that purpose, the transfer function between the engineering bedrock and the ground surface can be evaluated based on geotechnical data at the observation site and the linear multiple reflection theory²³⁾²⁵⁾ (see **Part II, Chapter 6, 1.2.3 Earthquake response analysis of the ground**). For this analysis, the damping factor of approximately 3% can be used. This value was selected because it is slightly larger than the values obtained in laboratory tests (e.g., Zen et al.²⁶⁾) and it will result in conservative evaluation of the site amplification factor at the engineering bedrock with respect to the seismological bedrock.

(2) Evaluation of site amplification factors based on microtremor measurements

Microtremors can be defined as small vibrations of the ground under non-earthquake circumstances, which cannot usually be felt by human beings.

The horizontal to vertical spectral ratio of measured microtremors²⁷⁾, which is often called the “H/V spectrum”, is known to resemble the site amplification factor at the same site obtained from earthquake observations²⁸⁾. As an example, the microtremor H/V spectra obtained at the Port of Kochi and nearby strong motion stations are compared with the site amplification factors obtained from earthquake observations¹⁷⁾ in **Fig. 1.2.2**. The microtremor H/V spectra were calculated following the procedure described in **Reference (Part II), Chapter 1, 4.4 Evaluation of site amplification factors based on microtremor measurements**. At Kochi-G, the H/V spectrum has a clear peak at around 1.3 Hz, while the site amplification factor also has a peak almost at the same frequency. At KOC007, the H/V spectrum has a clear peak at around 1.6 Hz, while the site amplification factor also has a peak almost at the same frequency. At KOC005, the H/V spectrum does not have any clear peak, while the site amplification factor does not have any clear peak either. Thus, the microtremor H/V spectra capture the main features of the site amplification factors. A similar comparison is made for the Port of Wakayama and a nearby strong motion station in **Fig. 1.2.3**. Again, the microtremor H/V spectra capture the main features of the site amplification factors.

Thus, microtremor measurements can be a useful tool to reveal the major features of the site amplification factor at a construction site. Microtremor measurements can be used to answer such questions as “Is the amplification due to the existence of sediments anticipated at the construction site?” or “At which frequency does the amplification occur?”

On the other hand, following limitations are inherent in the evaluation of site amplification factors based on microtremor measurements. The first limitation concerns the height of the peak. As shown in **Fig. 1.2.2** and **Fig. 1.2.3**, peak frequencies are usually consistent between the microtremor H/V spectrum and the site amplification factor at the same site. However, there have been long discussions on the consistency of the peak heights. In fact, in

some cases, the peak heights are reversed between the microtremor H/V spectrum and the site amplification factor as shown in **Fig. 1.2.2** for Kochi-G and KOC007. The second limitation is that higher mode peaks appearing in the site amplification factors are often not present in the microtremor H/V spectra. In the above examples, the peak around 3.3 Hz for the site amplification factor at Kochi-G and the peak around 1.2 Hz for the site amplification factor at Wakayama-G are not visible in the microtremor H/V spectra.

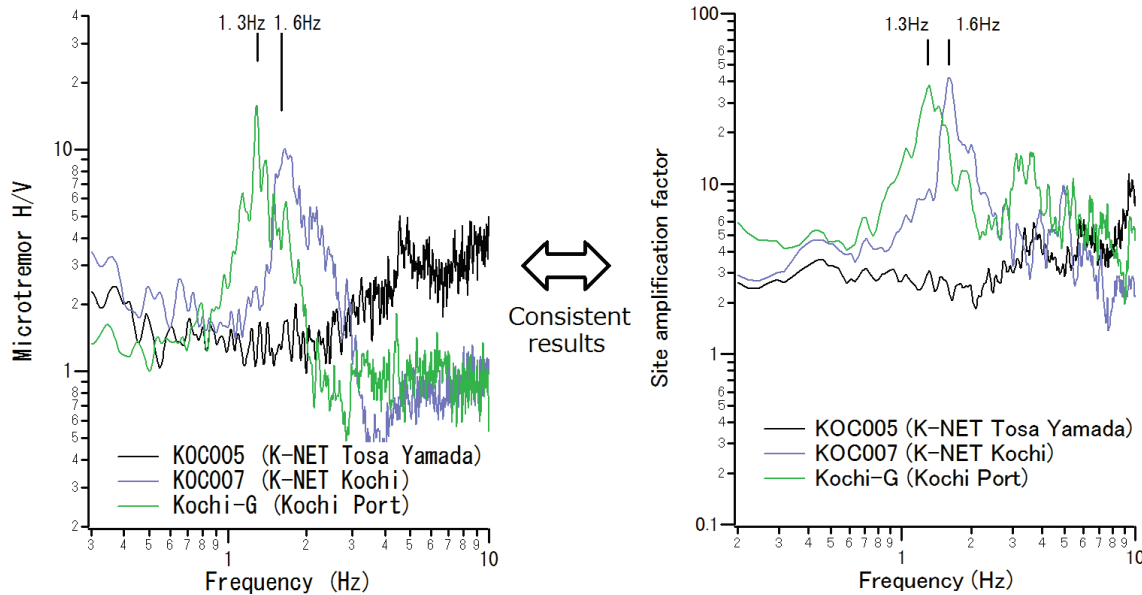


Fig. 1.2.2 Microtremor H/V spectra obtained at the Port of Kochi and nearby strong motion stations (left), compared with the site amplification factors obtained from earthquake observations¹⁷⁾ (right).

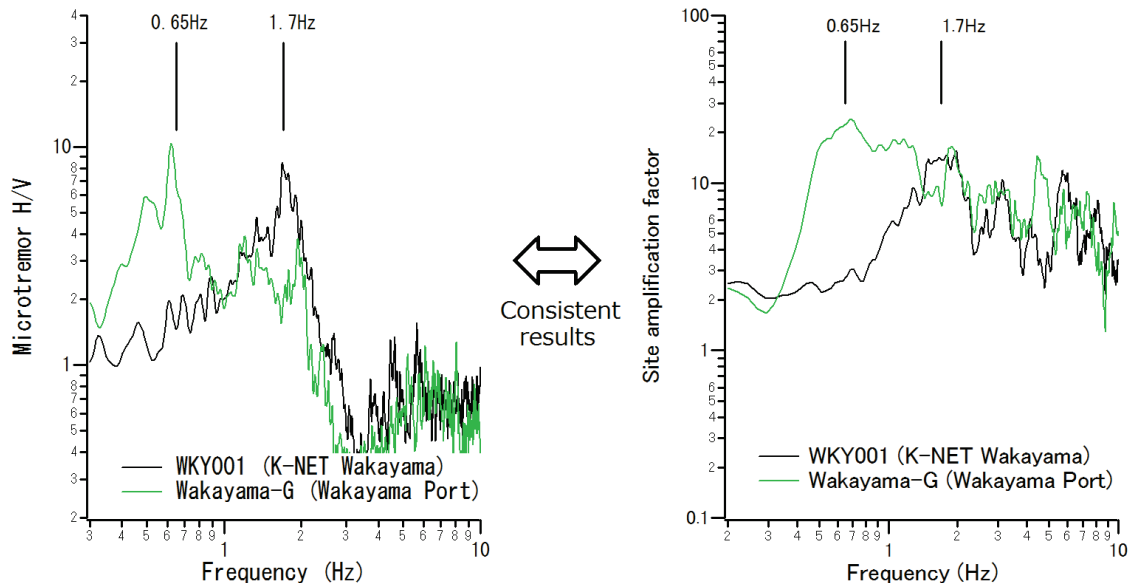


Fig. 1.2.3 Microtremor H/V spectra obtained at the Port of Wakayama and a nearby strong motion station (left), compared with the site amplification factors obtained from earthquake observations¹⁷⁾ (right).

Thus, uncertainties are inherent in the evaluation of site amplification factors based on microtremor measurements. Therefore, in the event of setting up design ground motions for a very important structure, it is desirable to evaluate the site amplification factor at the construction site based on earthquake observations. On the other hand, microtremor measurements are advantageous in setting up design ground motions for a number of facilities at the same time. Details of the evaluation of site amplification factors based on microtremor measurements can be found in **Reference (Part II), Chapter 1, 4.4 Evaluation of site amplification factors based on microtremor measurements.**

Once the site amplification factor at the ground surface with respect to the seismological bedrock is obtained based on microtremor measurements, the site amplification factor at the engineering bedrock with respect to the seismological bedrock can be obtained in a similar way as in the case of the site amplification factor at the ground surface evaluated based on earthquake observations (See **Part II, Chapter 6, 1.2.2 Evaluation of site amplification factors (1)**).

(3) Evaluation of site amplification factors without in-situ earthquake observations or microtremor measurements

An empirical relation¹⁷⁾ between the site amplification factors at a port and a nearby K-NET or KiK-net strong motion station can be used to evaluate the site amplification factor at a construction site, if the site amplification factor is to be evaluated without in-situ earthquake observations or microtremor measurements. In that case, however, it is important to recognize that the accuracy of the ground motions will be significantly degraded compared to cases with site amplification factors based on earthquake observations and/or microtremor measurements. Possible effects of this degradation on the evaluation of quay-wall deformation are described in Nagao et al.²⁹⁾. The empirical relation can be written as:

$$\begin{aligned} y &= A + Bx \\ y &= \log(GP(f)/GK(f)) \\ x &= \log GK(f), \end{aligned} \quad (1.2.1)$$

where

GP : Site amplification factor at the engineering bedrock w.r.t. the seismological bedrock at a port

GK : Site amplification factor at the engineering bedrock w.r.t. the seismological bedrock at a nearby K-NET or KiK-net station

The frequency-dependent coefficients A and B are shown in **Fig. 1.2.4**. These coefficients were determined taking into account the general tendency of the site amplification factors at a port and nearby K-NET or KiK-net strong motion stations averaged over Japan.

In general, site amplification factors at the engineering bedrock at a port, estimated from site amplification factors at nearby K-NET or KiK-net stations using the coefficients in **Fig. 1.2.4**, exhibit large values at frequencies lower than 1 Hz. This is a consequence of a tendency that the seismological bedrock is generally deeper for ports than for K-NET or KiK-net stations. Thus, the coefficients in **Fig. 1.2.4** are not suitable for estimating site amplification factors outside a port.

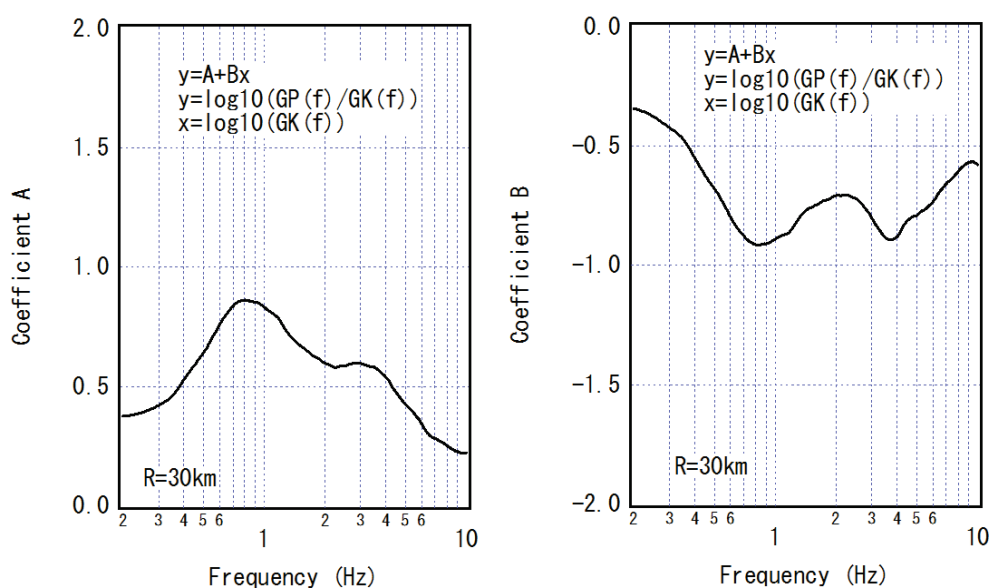


Fig. 1.2.4 Frequency-dependent coefficients A and B which specify the empirical relation between the site amplification factors at a port and a nearby K-NET or KiK-net strong motion station

1.2.3 Earthquake response analysis of the ground

In general, level-1 ground motions are specified in the form of so-called “2E wave” at the engineering bedrock, which is the incident wave impinging at the surface of the engineering bedrock multiplied by 2. Earthquake response analyses of the ground can be used to evaluate acceleration, velocity, displacement, shear stress and shear strain in the shallower sediments. Here, earthquake response analyses for this purpose will be described. Earthquake response analyses for the performance verification of facilities will be described in **Reference [Part III], Chapter 1, 2 Basic points of seismic response analyses**. While earthquake response analyses of the ground are usually conducted by appropriately modelling the shallower sediments above the engineering bedrock, there is a wide variation in the engineering bedrock itself in terms of its shear wave velocity; it is necessary to confirm that there is no significant difference in shear wave velocity between the layer regarded as the engineering bedrock in setting up the level-1 ground motion and the layer regarded as the engineering bedrock in the earthquake response analyses.

In the past, when earthquake response analyses were conducted for the prediction of liquefaction, the ground motions were converted to SMAC-B2 equivalent ground motions before they were used. This conversion is not necessary any more. In the past, existing strong motion records were adjusted to a specified PGA value and used for the earthquake response analyses. In that era, the specified PGA value was based on SMAC-B2 type accelerographs. This was the reason why the conversion into SMAC-B2 equivalent ground motions was necessary.

(1) Various earthquake response analyses of the ground

① Domain of analysis

There are one, two and three dimensional earthquake response analyses of the ground. In general, one dimensional analyses are used to calculate the response of horizontally layered natural or artificial deposits without a structure. For a horizontally layered ground often encountered in a coastal region, one dimensional analyses will give sufficiently accurate results.

In association with this, vertically travelling S waves are often considered in the earthquake response analyses of the ground. Because the shear wave velocities of the ground are generally small in the coastal regions, seismic rays become nearly vertical in the shallower sediments (**Fig. 1.1.1**). A similar tendency can also be found for surface waves: surface waves can also be considered as a superposition of elementary P and S waves in the shallower sediments and the rays of the elementary P and S waves also become nearly vertical near the surface. Thus, sufficiently accurate results can be obtained by simply considering vertically travelling S waves.

② Stress-strain relations

Earthquake response analyses of the ground can be categorized into equivalent linear analyses and purely nonlinear analyses from the viewpoint of how stress-strain relations are modelled. In the equivalent linear analyses, the dependence of the shear modulus and damping factor on the ground motion amplitude is considered (**Fig. 2.4.2 in Part II, Chapter 3, 2.4.1 Parameters for dynamic deformation**), while they are assumed to be constant during the action of a ground motion. Obviously this assumption does not represent the actual situations. However, this assumption was introduced for convenience because of the limited performance of the computers in the days when the equivalent linear analyses were developed. On the other hand, in the purely nonlinear analyses, time dependence of the shear modulus, etc., during the action of a ground motion is considered. While it is necessary to use purely nonlinear analyses to represent the actual situations as accurately as possible, it has been postulated that the equivalent linear analyses give reasonable results as long as the strain level is within a certain range. The equivalent linear analyses are applicable if the strain level is less than 0.5 – 1%, depending on the method³⁰⁾³¹⁾. If an equivalent linear analysis is used and a strain exceeding this level is obtained, then the analysis should be replaced by a purely nonlinear analysis.

In the equivalent linear analyses, following iterations are performed. First, at each step, the maximum shear strain at each layer (or at each element for two or three dimensional cases) is converted to the effective shear strain with the following equation:

$$\gamma_{eff} = \alpha \gamma_{max} , \quad (1.2.2)$$

where

γ_{max} : maximum shear strain

γ_{eff} : effective shear strain

α : a coefficient (typically 0.65)

Then, based on the effective shear strain, the shear modulus and damping factor are updated following the strain dependence shown in **Fig. 2.4.2 in Part II, Chapter 3, 2.4.1 Parameters for dynamic deformation** before going to the next step. The iteration is repeated until the shear modulus converges. SHAKE³²⁾ was the first computer program for the equivalent linear analysis of the ground. SHAKE has been widely used in practice partly because there was no competitive program for a while after SHAKE was initially developed. FLUSH³³⁾, which can be regarded as a two dimensional version of SHAKE, has also been widely used. However, in recent years, problems inherent in SHAKE have gradually been revealed by comparing the results of SHAKE with actual ground motion records, etc.³⁴⁾ One of the revealed shortcomings of SHAKE is its tendency to underestimate high frequency components. This in turn means that high frequencies tend to be overestimated when input ground motions at the engineering bedrock are to be estimated from surface records with SHAKE. In this regard, alternative programs such as FDEL³⁵⁾ and DYNEQ³⁶⁾ have been proposed, both of which can be regarded as improved versions of SHAKE. These programs mitigated the problem associated with high frequencies by introducing a frequency dependent effective strain instead of the effective strain defined in **equation (1.2.2)**.

Purely nonlinear analyses are applicable even when the strain level exceeds 0.5 – 1%. However, the accuracy of the results obviously depends on the appropriateness of the constitutive equations and model parameters. Various computer programs with various constitutive relations have been proposed for purely nonlinear analyses. It is important to use a computer program which successfully reproduced vertical array records with ground conditions and strain levels similar to the target problem³⁰⁾.

Purely nonlinear analyses can be further categorized into total stress analyses and effective stress analyses. When the ground is subject to the generation of excess pore water pressure, the effective stress is decreased, resulting in the change of the shear modulus and damping factor of the ground and, ultimately, in the change of the response characteristics of the ground. Effective stress analyses can handle these situations and directly calculate the excess pore water pressure. On the other hand, total stress analyses, which do not calculate the excess pore water pressure, cannot consider the change of the response characteristics of the ground due to the change in the effective stress. In a calculation case with the excess pore water pressure ratio exceeding 0.5, it is anticipated that the results of total stress analyses become unrealistic. Thus, it is necessary to perform effective stress analyses to accurately trace the actual phenomena.

FLIP³⁷⁾ is one of the computer programs for effective stress analyses. **Fig. 1.2.5** shows the application of FLIP ver.3.3 to the vertical array records at Port Island in Kobe Port during the 1995 Hyogo-ken Nanbu earthquake³⁸⁾. At Port Island, ground motions were observed at four different depths, at GL-83 m, GL-32 m, GL-16 m and the ground surface. In this analysis, the observed ground motion at GL-83 m was used as an input ground motion and ground motions at other depths, namely, GL-32 m, GL-16 m and the ground surface were calculated. The results accurately reproduced the recorded ground motions. Such results, together with other results pertaining to, for example, the 1993 Kushiro-oki earthquake³⁹⁾, indicate that FLIP is one of the programs that can generate reliable results as long as the model parameters are appropriately given.

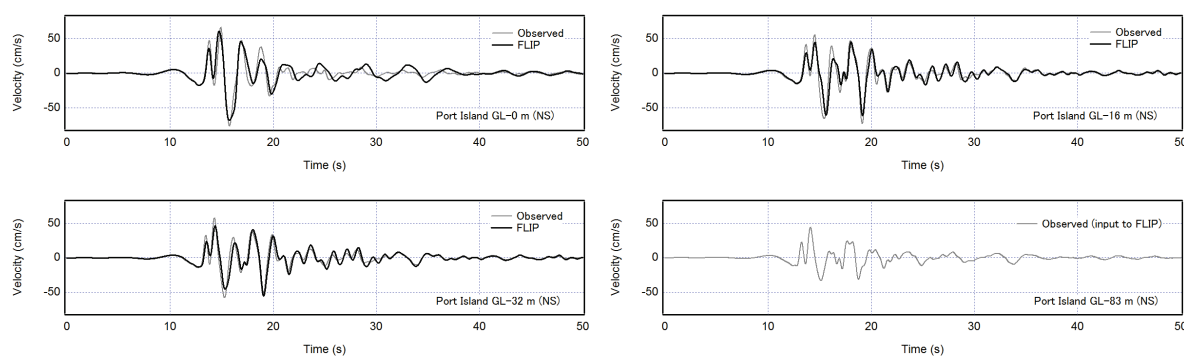


Fig. 1.2.5 Application of FLIP to the vertical array records at Port Island in Kobe Port during the 1995 Hyogo-ken Nanbu earthquake³⁸⁾

③ Numerical scheme

Earthquake response analyses of the ground can be based on the multiple reflection theory, the finite element method, or other numerical schemes.

In the earthquake response analyses of the ground based on the multiple reflection theory, a horizontally layered ground is assumed as shown in **Fig. 1.2.6**. An incident shear wave, impinging vertically at the bedrock, is assumed to propagate upward, repeatedly causing reflection and transmission at the boundaries of the layers. The amplitudes of upcoming and downgoing waves in each layer are determined so that the boundary conditions are satisfied. Details of the formulation can be found in, for example, Osaki²⁵⁾. In the earthquake response analyses based on the multiple reflection theory, the soil can only be modelled as a linear or an equivalent linear material. Calculations are usually performed in the frequency domain. SHAKE³²⁾, FDEL³⁵⁾ and DYNEQ³⁶⁾, among other programs, are based on the multiple reflection theory.

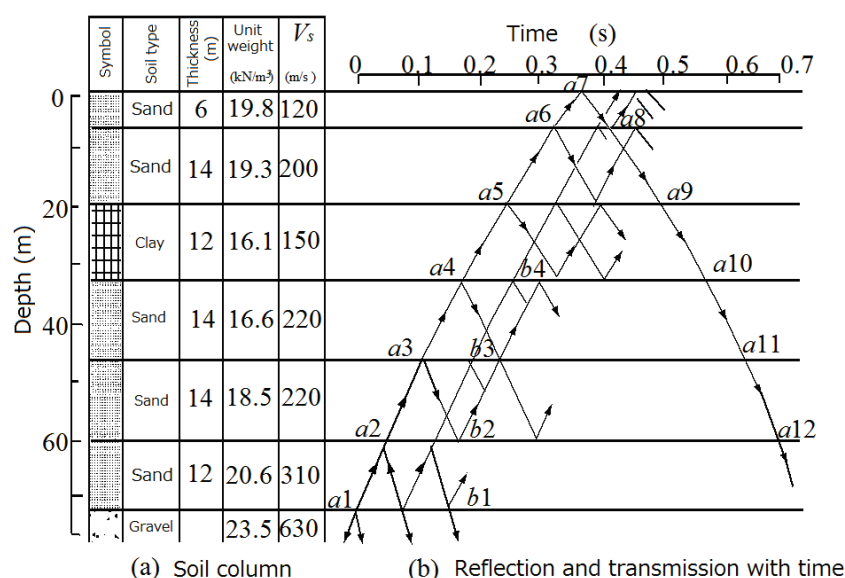


Fig. 1.2.6 Multiple reflection theory²³⁾

In the earthquake response analyses of the ground based on the finite element method, the ground is divided into a finite number of elements as shown in **Fig. 1.2.7** and the solution to the governing equation is obtained by replacing it with an algebraic equation in terms of displacements at nodal points. Obviously the application of the finite element method is not limited to geotechnical problems. The main advantage of the method is that it can be applicable to a ground with two or three dimensional variations in layer thickness and material properties. FLUSH³³⁾ and FLIP³⁷⁾, among other programs, are based on the finite element method. Calculations are performed either in the frequency domain or in the time domain, depending on the program.

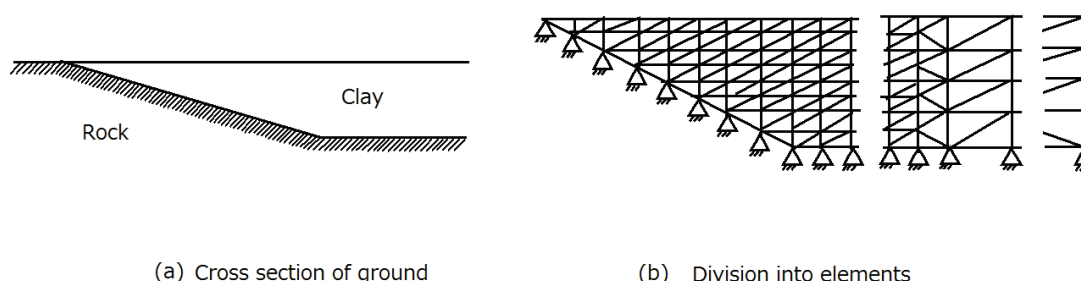


Fig. 1.2.7 Finite element method

(2) Modelling of the ground for earthquake response analyses

In the following section, the process of modelling the ground and determining model parameters will be described, with the emphasis on one dimensional analyses.

① General

To perform earthquake response analyses of the ground, the ground at a construction site should be divided into a stack of layers. Parameters such as the thickness, density and shear modulus at small strain are required for any kinds of analyses. In addition, for the equivalent linear analyses, the strain dependence of the shear modulus and damping factor should be specified. Parameters required for purely nonlinear analyses depend on how the stress-strain relation is modelled. In the case of FLIP, in addition to the above mentioned parameters, parameters such as the bulk modulus of the soil skeleton, the internal friction angle, the maximum damping factor and the parameters representing dilatancy should be specified. Among these parameters, the parameters representing dilatancy are only required for effective stress analyses.

② Modelling procedure

The engineering bedrock should be specified referring to the results of geotechnical investigations. There should be no significant difference in shear wave velocity between the layer regarded as the engineering bedrock in setting up design ground motions and the layer regarded as the engineering bedrock in the earthquake response analyses. The ground should be divided into a stack of layers, paying attention to the variation of soil type. Soils with different shear wave velocities, *SPT-N* values or q_u values should be assigned to different layers, even when the soil types are the same. Soils should be categorized into sand, clay or gravel. Actual soils are rarely composed of sand only or clay only. They are often combinations of gravel, sand, silt and clay with various percentages. Here, it is recommended that soils should be categorized as sandy soils if their fine fraction ($<75\mu$) is less than 20%. Otherwise, soils should be regarded as clayey soils. Stones that constitute mounds and backfills should be regarded as gravels.

In terms of the density, observed values should be used if undisturbed samples are available and their densities are known. If those values are not available, the values listed in **Table 1.2.1** can conveniently be used. It should be noted that the values listed in **Table 1.2.1** are only suitable for earthquake response analyses; they are not suitable for other analyses where the density can be a decisive factor.

Table 1.2.1 Typical values of density⁴⁰⁾

Soil type	Condition	Density (g/cm ³)
Clayey soil	Water content $\geq 60\%$	1.5
	Water content $< 60\%$	1.7
Sandy soil	Above water table	1.8
	Below water table	2.0
Mound / Backfill		2.0

The shear modulus at small strain ($\approx 10^{-6}$) can be determined from a shear wave velocity based on a PS logging as follows:

$$G_0 = \rho V_S^2, \quad (1.2.3)$$

where

G_0 : Shear modulus at small strain

ρ : Density

V_S : Shear wave velocity

If PS logging data is not available for a sandy soil, the following equation can be used to estimate the shear modulus at small strain from an *SPT-N* value:

$$G_0 = 14100 N^{0.68} \quad (\text{kN/m}^2). \quad (1.2.4)$$

It should be noted that the equation shows an averaged relation derived from data with significant scattering⁴¹⁾. For details, see also **Part II, Chapter 3, 2.4.1(6) Simplified evaluation of shear modulus and damping factor**.

For clayey soils, the following equation can be used to estimate the shear modulus at small strain from a q_u value obtained in an unconfined compression test:

$$G_0 = 170q_u. \quad (1.2.5)$$

In estimating the shear wave velocity of a soil which will be overlain by a caisson, for example, using an $SPT-N$ value, if the $SPT-N$ value is available only before construction, the $SPT-N$ value after construction can be estimated considering the increase in the effective overburden pressure due to a caisson or a mound.

$$N = \frac{(0.0041\sigma_v' + 0.7355)N_0 + 0.019(\sigma_v' - \sigma_{v0}')^B}{0.0041\sigma_{v0}' + 0.7355}, \quad (1.2.6)$$

where

N : $SPT-N$ value after construction

N_0 : $SPT-N$ value before construction

σ_v' : Effective overburden pressure after construction (kN/m²)

σ_{v0}' : Effective overburden pressure before construction (kN/m²)

If a soil will be subject to a change in the effective overburden pressure due to construction and PS logging data is only available before construction, the shear wave velocity after construction can be estimated from the shear wave velocity before construction considering the change in the effective overburden pressure using the following equation.

$$V_S = V_{S0} \left(\frac{\sigma_v'}{\sigma_{v0}'} \right)^B, \quad (1.2.7)$$

where

V_S : Shear wave velocity after construction

V_{S0} : Shear wave velocity before construction

σ_v' : Effective overburden pressure after construction (kN/m²)

σ_{v0}' : Effective overburden pressure before construction (kN/m²)

The value B can be 0.25 for a sandy soil or a clayey soil with $I_p < 30$. It can be 0.5 for a clayey soil with $I_p \geq 30$.

Less information is available regarding the shear wave velocities of a gravel mound or a gravel backfill because it is difficult to measure those quantities in-situ. For the shear wave velocities of a gravel mound or a gravel backfill of a large quay wall with the depth of approximately 10 m, the following values, estimated from an equation⁴²⁾ derived from the results of earthquake observations for a composite breakwater, can be used:

Shear wave velocity of a gravel mound: $V_S = 300$ m/s

Shear wave velocity of a gravel backfill: $V_S = 225$ m/s

On the other hand, in another application⁴³⁾, the shear wave velocity of 300 m/s for an effective confining pressure of 98 kN/m² was assumed both for a gravel mound and a gravel backfill.

If a caisson is assumed as part of the ground, the following value can be used as the shear wave velocity of a caisson.

Shear wave velocity of a caisson: $V_S = 2000$ m/s

It has been recognized that the shear modulus of a soil at small strain is proportional to some power of the effective confining pressure. Because the shear modulus and the shear wave velocity are related to each other through **equation (1.2.3)**, the above mentioned proportionality means that the shear wave velocity of a soil is proportional to some power of the effective confining pressure.

According to existing element test results²⁶⁾⁴⁴⁾, the proportionality can be given as follows:

- (a) For a clayey soil with $I_p \geq 30$, the shear modulus is proportional to the effective confining pressure.
- (b) For a sandy soil or a clayey soil with $I_p < 30$, the shear modulus is proportional to the effective confining pressure to the power of 0.5.

On the other hand, **Fig. 1.2.8** shows the result of a centrifuge test where centrifugal acceleration ranging from 10 G to 50 G was applied to a 24 cm thick ground with Toyoura sand to artificially vary the effective confining pressure⁴⁵⁾. **Fig. 1.2.8** shows the averaged shear wave velocity versus the effective confining pressure at the center of the sand layer. Fitted lines in the form of $V_s = K(\sigma_c')^a$ are also plotted. The averaged shear wave velocity increased with the increase of the centrifugal acceleration, indicating the dependence on the confining pressure. **Fig. 1.2.9** shows the shear wave velocity profiles estimated for the same specimens. The dotted lines indicate the curves with the assumption that the shear wave velocity is proportional to the effective confining pressure to the power of 0.25. Those curves were plotted so that they approach to the observed values for the central layer. For both cases, the shear wave velocity increased with depth and its dependence can be explained well with the assumption that the shear wave velocity is proportional to the effective confining pressure to the power of 0.25.

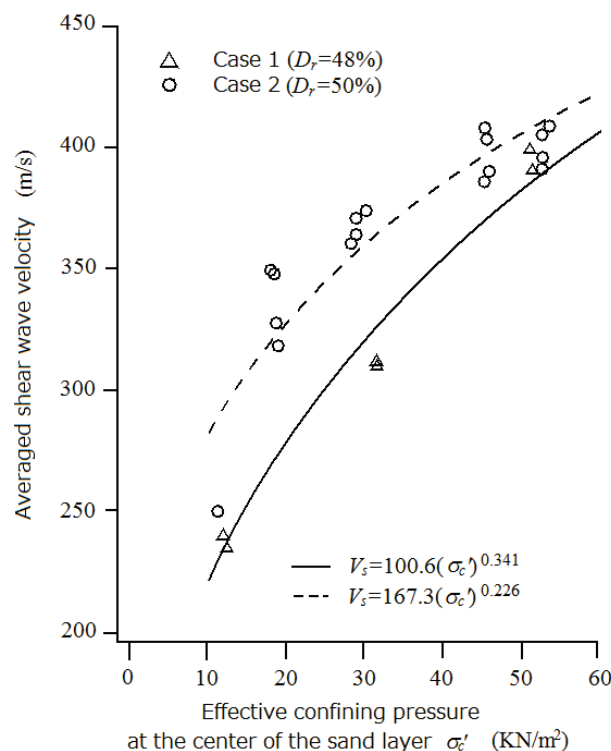


Fig. 1.2.8 Averaged shear wave velocity for a sand layer versus the effective confining pressure⁴⁵⁾

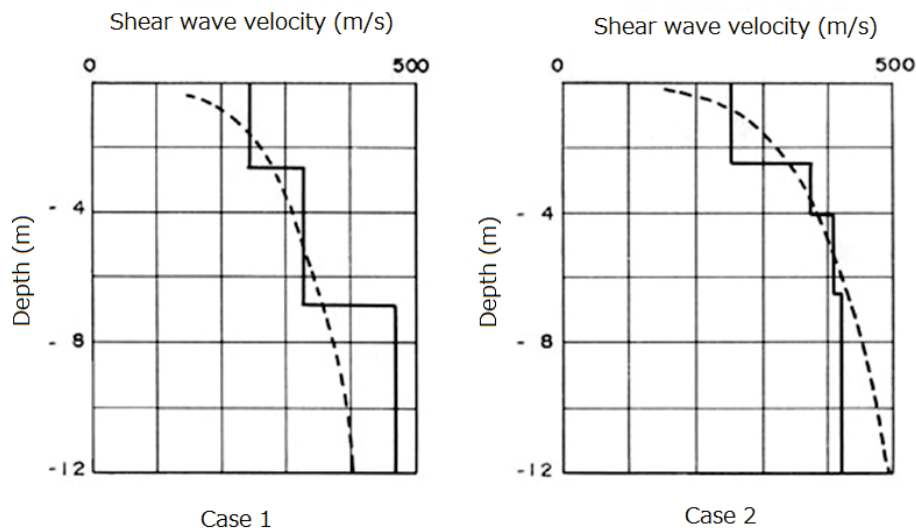


Fig. 1.2.9 Shear wave velocity profiles⁴⁵⁾

③ Strain dependence of shear modulus and damping factor

In general, the shear modulus is large and the damping factor is small at small strain. With the increase in strain, the former decreases and the latter increases (**Fig. 2.4.2 in Part II, Chapter 3, 2.4.1 Parameters for dynamic deformation**). The strain dependence of the shear modulus and damping factor could be dependent on the soil types and the confining pressure. Therefore, it is recommended to use strain dependent shear moduli and damping factors based on laboratory tests.

④ Parameters for purely nonlinear analyses

See Reference (Part III), Chapter 1, 2 Basic points of seismic response analyses for the determination of parameters for purely nonlinear analyses.

1.2.4 Correction of level-1 ground motions

If the site amplification factor that was used to calculate the existing level-1 ground motion available at the website of the National Institute for Land and Infrastructure Management at <http://www.ysk.nilim.go.jp/kakubu/kouwan/sisetu/sisetu.html> is not equivalent to the site amplification factor at a construction site, it is necessary to use the newly evaluated site amplification factor at the construction site by means of earthquake observations (See **Part II, Chapter 6, 1.2.2 Evaluation of site amplification factors (1)**) and/or microtremor measurements (See **Part II, Chapter 6, 1.2.2 Evaluation of site amplification factors (2)**) and to correct the existing level-1 ground motion before it is used for the design. The procedure can be as follows:

First, the existing level-1 ground motion at the engineering bedrock (a) should be obtained and transformed to an acceleration Fourier spectrum (b). Then, the site amplification factor at the same site at the engineering bedrock with respect to the seismological bedrock (c) should be obtained. By dividing (b) with (c), the acceleration Fourier spectrum of the level-1 ground motion at the seismological bedrock (d) can be obtained. Both (a) and (c) can be downloaded from the above mentioned website.

Then, the acceleration Fourier spectrum of the level-1 ground motion at the seismological bedrock (d) should be multiplied by the newly evaluated site amplification factor at the construction site at the engineering bedrock with respect to the seismological bedrock to obtain the acceleration Fourier spectrum of the level-1 ground motion at the construction site at the engineering bedrock.

Regarding waveform data to determine the phase characteristics of the level-1 ground motion, it is preferable to select the data from weak motion records at the construction site to take into account regional characteristics if the site amplification factor at the construction site has been evaluated by means of earthquake observations. If multiple weak motion records are available, it is preferable to select a record with average group delay time. The selected weak motion data should be converted to a “2E wave” at the engineering bedrock using geotechnical data at the site of earthquake observations and its phase characteristics should be used. If the site amplification factor at the construction site has been

evaluated by means of microtremor measurements, the phase characteristics of the original level-1 ground motion can be used.

The acceleration time history of the level-1 ground motion at the engineering bedrock can be evaluated by combining the acceleration Fourier spectrum of the level-1 ground motion at the engineering bedrock with the phase characteristics mentioned above and applying the inverse Fourier transform.

1.3 Level-2 ground motions for the performance verification of structures

1.3.1 General

Level-2 ground motions can be defined as the ground motion with greatest intensity among anticipated ground motions at a construction site. In general, Level-2 ground motions are determined based on strong motion simulations, taking into account the source and path effects and the site amplification factor at the engineering bedrock with respect to the seismological bedrock. Level-2 ground motions can be regarded as the “reference earthquake motions for safety during or after an earthquake” in ISO23469³¹⁾. The concept of “safety” in ISO23469 involves the ability for a critical facility to be operational for post-earthquake emergency transportation. Therefore, “safety” in ISO23469 has a slightly broader meaning than “safety” in **Part I, Chapter 1, 3.7 Performance requirements**. The ground motions to be determined are the so called “2E wave”²³⁾, which is the incident wave impinging at the surface of the engineering bedrock multiplied by 2. The procedure to determine level-2 ground motions can be as follows (**Fig. 1.3.1**):

- ① Selection of scenario earthquakes (**Part II, Chapter6, 1.3.2**)
- ② Determination of source parameters (**Part II, Chapter6, 1.3.3**)
- ③ Evaluation of site amplification factors (**Part II, Chapter6, 1.3.4**)
- ④ Simulation of strong ground motions (**Part II, Chapter6, 1.3.5**)

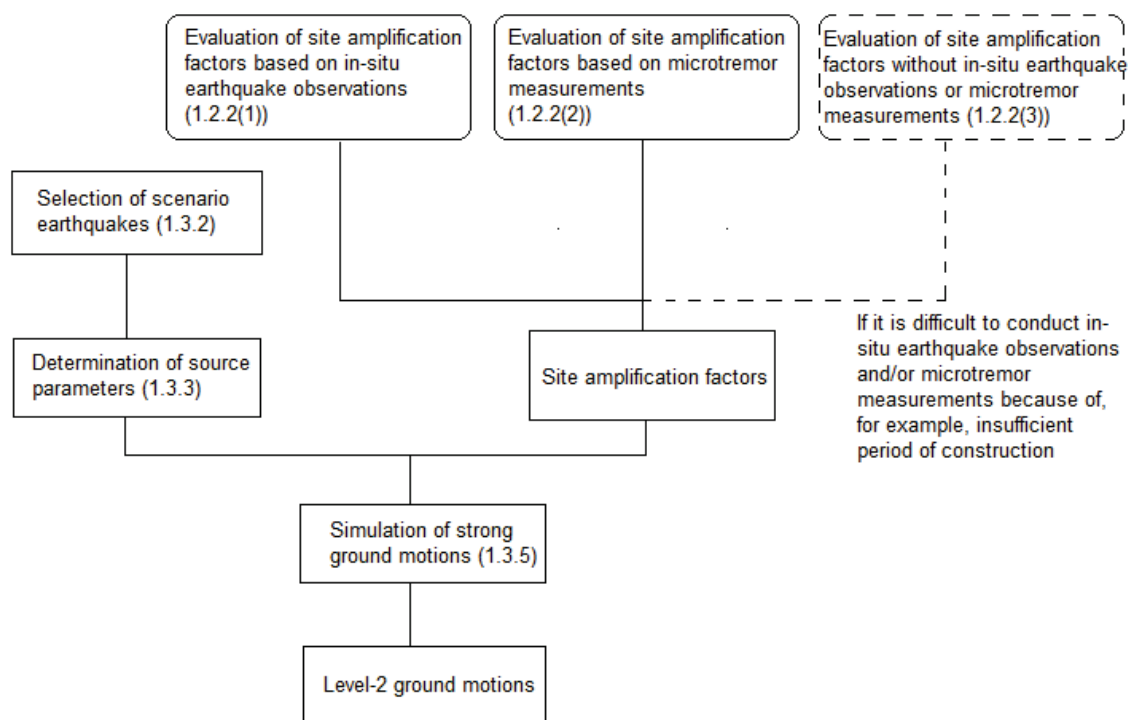


Fig. 1.3.1 Procedure to determine level-2 ground motions

It is desirable to evaluate the site amplification factor at a construction site by means of earthquake observations (See **Part II, Chapter 6, 1.2.2 Evaluation of site amplification factors (1)**). The site amplification factor at the construction site can also be evaluated by means of microtremor measurements (See **Part II, Chapter 6, 1.2.2**

Evaluation of site amplification factors (2)), however, it should be noted that uncertainties are inherent in the evaluation of site amplification factors based on microtremor measurements.

If it is difficult to conduct in-situ earthquake observations and/or microtremor measurements because of, for example, insufficient period of construction, the site amplification factor at the construction site can be evaluated by using an empirical relation (See **Part II, Chapter 6, “1.2.2 Evaluation of site amplification factors (3))** based on a site amplification factor at a nearby strong motion station. In that case, it is important to recognize that the accuracy of the ground motions will be significantly degraded compared to cases with site amplification factors based on earthquake observations and/or microtremor measurements.

The ground motion evaluated through the following procedure can be different from that evaluated by another organization for a similar earthquake scenario primarily because of the difference of the ways in which the site effects are evaluated. If the ground motion is to be evaluated for the performance verification of a port structure, the following procedure can be followed.

For the detailed procedures of the performance verification of a structure, see the descriptions in **Part III** depending on the type of the structure.

1.3.2 Selection of scenario earthquakes

In selecting scenario earthquakes to determine Level-2 ground motions, it is necessary to comprehensively consider information regarding past earthquakes and active faults. In particular, it is necessary to consider the latest information regarding active faults at the time of the performance verification of a facility. Chronological Scientific Tables⁴⁶⁾ and Materials for Comprehensive List of Destructive Earthquakes in Japan⁴⁷⁾ can be suggested as comprehensive documents regarding past earthquakes in Japan. Handbook of Earthquake Fault Parameters in Japan⁴⁸⁾ can be suggested as a comprehensive document regarding fault parameters of past major earthquakes in Japan. Active Faults in Japan⁴⁹⁾ and Digital Active Fault Map of Japan⁵⁰⁾ can be suggested as comprehensive documents regarding active faults in Japan. In addition to these documents, after the 1995 Hyogo-ken Nanbu earthquake, surveys on active faults have been actively conducted in Japan and their results have been published from the Headquarters for Earthquake Research Promotion or local governments. On the bases of those documents, following earthquakes should be considered.

- (a) Recurrence of past damaging earthquakes
- (b) Earthquakes caused by active faults
- (c) Other earthquakes expected from seismological and/or geological point of view
- (d) Scenario earthquakes hypothesized by government agencies such as the Central Disaster Management Council and the Headquarters for Earthquake Research Promotion
- (e) Scenario earthquakes hypothesized by local governments
- (f) M6.5 earthquake just beneath the site¹⁾

Some of the earthquakes (a) – (f) could overlap each other. From these earthquakes, earthquakes that could result in ground motions with greatest intensity at the port should be selected as the scenario earthquakes for calculating level-2 ground motions. However, it is sometimes difficult to decide which of these earthquakes could bring ground motions with greatest intensity at the port, especially when a smaller earthquake at a smaller distance and a greater earthquake at a greater distance are anticipated. In addition, because there are various aspects in ground motions such as amplitude, frequency content and duration, sometimes we can know which earthquake has the biggest effect on a facility only after ground motion simulations and earthquake response analyses are completed. Therefore, it is not reasonable to try to select only one earthquake at the initial stage. It is more reasonable to select multiple candidate earthquakes. In that case, among candidate level-2 ground motions, the ground motion that turns out to have the biggest effect on a facility as a result of earthquake response analyses should eventually be defined as the level-2 ground motion. If there are too many candidate earthquakes, a simple ground motion prediction equation can be used to reject earthquakes with obviously small effects. Regarding earthquakes in (d), the following websites are informative:

Central Disaster Management Council, Japan: <http://www.bousai.go.jp/kaigirep/chuobou/senmon/index.html>

Headquarters for Earthquake Research Promotion, Japan: http://www.jishin.go.jp/main/p_hyoka02.htm

An M6.5 earthquake just beneath the site is considered for the following reasons¹⁾: While active faults can be defined as the signs of surface fault traces of past earthquakes, surface fault traces do not appear for a relatively small earthquake, indicating that relatively small earthquakes can occur in a region without known active faults. Takemura⁵¹⁾ investigated the relation among the size of an earthquake, the frequency of the appearance of a surface fault trace and the damage

rank⁵²⁾ for $M \geq 5.8$ crustal earthquakes in 1885 – 1995 in Japan (**Fig. 1.3.2**). He found that, while $M \leq 6.5$ earthquakes seldom accompany surface fault traces, $M \geq 6.8$ earthquakes almost always accompany surface fault traces. He also noticed that there have been fewer earthquakes with $M 6.6$ and $M 6.7$ and suggested that, once an earthquake that could potentially be an $M 6.6$ or $M 6.7$ earthquake is initiated, it will break the shallower part of the crust, resulting in an $M \geq 6.8$ earthquake. Based on these reports, it has been suggested that an $M 6.5$ earthquake is suitable as a scenario earthquake in a region without known active faults.

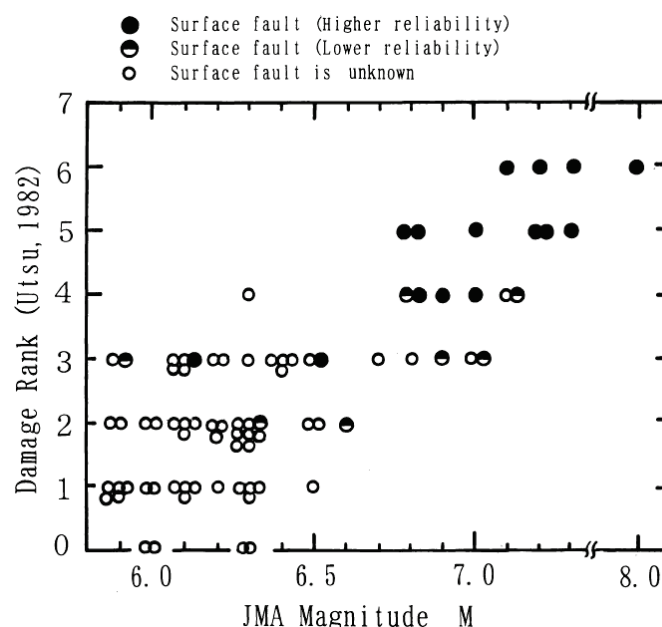


Fig. 1.3.2 Relation between the size of an earthquake and the frequency of the appearance of a surface fault trace⁵¹⁾

If a design tsunami and its preceding ground motion is to be specified and the performance of a structure is to be verified for this combination, the preceding ground motion could be different from a level-2 ground motion. Let us assume that an inland crustal earthquake and a subduction earthquake are anticipated at a port and the former is anticipated to result in a more intense ground motion. In this situation, it is not reasonable from an economic point of view to combine the former ground motion with a tsunami, because the inland crustal earthquake will not accompany a tsunami; a level-2 ground motion and a ground motion preceding a tsunami should be specified separately. The procedure to determine a level-2 ground motion, which will be described below, can be applied to determining a ground motion preceding a tsunami by replacing the scenario earthquake.

1.3.3 Determination of source parameters

The source parameters to be determined fall into three categories: the outer parameters, the inner parameters and additional parameters. The outer source parameters include the location of the fault, the strike of the fault, the dip of the fault, the length of the fault, the width of the fault and the seismic moment of the fault. The inner source parameters include the number of the asperities, the area of the asperities, the seismic moment of the asperities and the rise time of the asperities. The additional parameters include the rupture starting point, the rupture velocity and the rupture propagation pattern. The meanings of the source parameters are shown in **Fig. 1.3.3**. The source parameters should be determined either based on the standard procedure described below or based on independent detailed surveys.

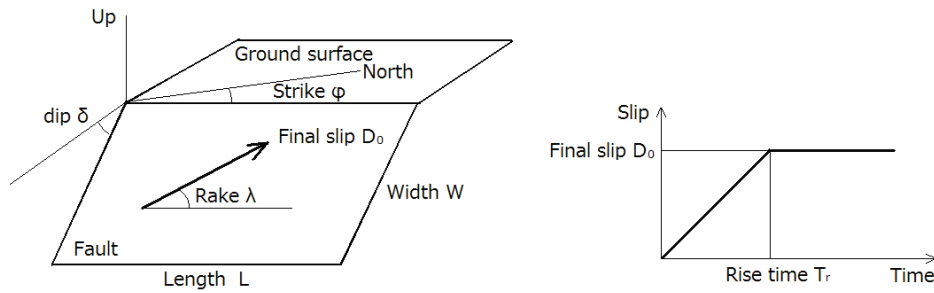


Fig. 1.3.3 Meanings of the source parameters

(1) Recurrence of past damaging earthquakes

If the recurrence of a past damaging earthquake is considered, it is preferable to effectively use the data regarding that particular past event, especially when a subduction earthquake is considered.

In terms of outer source parameters, the parameters for the past event can be used if they are known. Handbook of Earthquake Fault Parameters in Japan⁴⁸⁾ provides information regarding outer source parameters for past earthquakes. If one of the two outer parameters, namely, the seismic moment M_0 and the area of the fault S is known and the other is to be estimated, **equation (1.3.1)**⁵³⁾⁵⁴⁾ can be used:

$$S(\text{km}^2) = 1.88 \times 10^{-15} \times M_0^{2/3} (\text{dyne} \cdot \text{cm}). \quad (1.3.1)$$

Equation (1.3.1) implies that the average stress drop on the fault is 3 MPa once the equation is combined with Esherby's equation for a circular crack⁵⁵⁾.

In terms of the inner source parameters such as the location of the asperities, different strategies are required depending on the availability of the data. Inner source parameters of a past event can be used if they have been sufficiently studied based on waveform data. This applies for a case of considering the recurrence of the 1968 Tokachi-oki earthquake³⁸⁾ (M7.9) or the 1978 Miyagi-ken-oki earthquake³⁸⁾ (M7.4). For a past event for which waveform data is not available, if seismic intensity data is available based on historical documents, inner source parameters that have been determined to be consistent with the data can be used.

The additional source parameters such as the rupture starting point can be determined in a similar way as the inner source parameters.

When earthquakes caused by active faults are considered, it is generally difficult to rely on waveform data or seismic intensity data for a past event because recurrence intervals are generally long for earthquakes caused by active faults. As an exception to this, if the recurrence of the 1995 Hyogo-ken Nanbu earthquake is considered, the above idea can be applied, instead of the procedure described in **(2) Earthquakes caused by active faults**.

When subduction earthquakes are considered, the SPGA model can be used to fit to waveform data or seismic intensity data. As an example of the SPGA model, **Fig. 1.3.4** shows the SPGA model that was used to explain the waveform data of the 2011 Tohoku earthquake ($M_w 9.0$)¹²⁾¹³⁾⁵⁶⁾⁵⁷⁾.

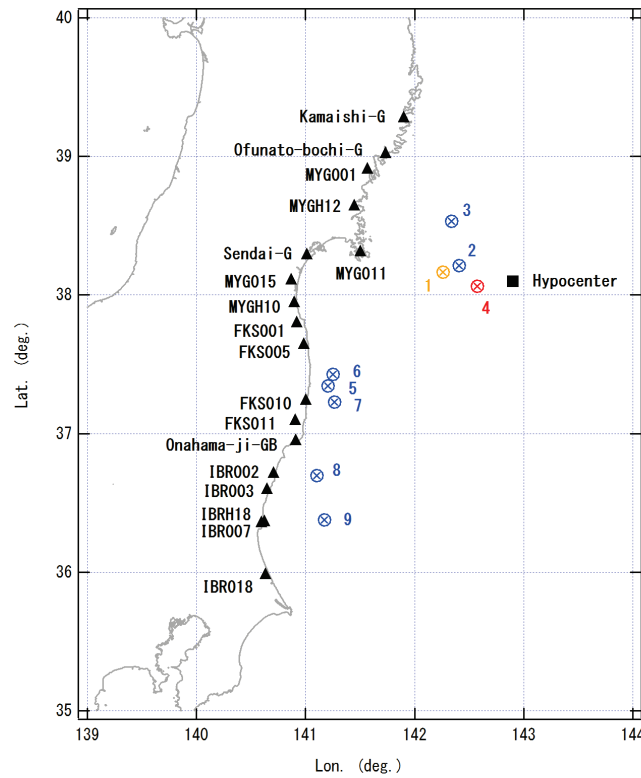


Fig. 1.3.4 SPGA model for the 2011 Tohoku earthquake¹²⁾¹³⁾⁵⁶⁾⁵⁷⁾

(2) Earthquakes caused by active faults

The outer source parameters of an earthquake caused by an active fault can be determined as follows: Based on geological and/or geomorphological investigations, the strike ϕ and dip δ of the fault should be determined. At the same time, the length of the fault or its segment should be determined and denoted as L . The dip δ can be 90° , 60° , 30° and 45° for a strike-slip fault, a high-angle reverse fault, a low-angle reverse fault and a reverse fault with no information on the dip angle, respectively, if there is no specific information to determine the dip angle. Because the fault width W of an earthquake caused by an active fault is restricted by the thickness H of the seismogenic layer in the upper crust, W can be determined by the following equation: $W=L$ if $L < H/\sin\delta$ and $W=H/\sin\delta$ if $L > H/\sin\delta$ ⁵⁴⁾⁵⁸⁾. The thickness of the seismogenic layer can be 20 km if there is no specific information to determine the thickness. The area of the fault S can be determined as the product of the length L and the width W . The seismic moment M_0 can be determined from the area of the fault S by using the following empirical relation⁵⁹⁾:

$$S(\text{km}^2) = 2.23 \times 10^{-15} \times M_0^{2/3} (\text{dyne} \cdot \text{cm}). \quad (1.3.2)$$

The inner source parameters of an earthquake caused by an active fault can be determined as follows: If an earthquake that involves the rupture of multiple faults or multiple fault segments is considered, the following procedure can be applied to each of the faults or fault segments. The combined area of the asperities can be 22% of the fault area⁵⁴⁾⁵⁸⁾⁵⁹⁾⁶⁰⁾⁶¹⁾. Generally one or two asperities are considered⁵⁴⁾. If an earthquake of $M \geq 7.0$ is considered, generally two asperities are considered. If two asperities are considered, the areas of the asperities can be 16% and 6% of the fault area for the larger and smaller of the asperities, respectively⁵⁴⁾⁶⁰⁾. It is preferable to consider square asperities whenever possible⁵⁴⁾⁵⁹⁾. The combined moment of the asperities can be 44% of the total moment of the earthquake⁵⁴⁾⁵⁹⁾⁶⁰⁾. If two asperities are considered, the moments of the asperities can be 36% and 8% of the total moment of the earthquake for the larger and smaller of the asperities, respectively⁵⁴⁾⁶⁰⁾. The rise time τ of an asperity can be determined from the width of the asperity W_a and the rupture velocity V_r with the following equation:

$$\tau = (W_a / V_r) / 4. \quad (1.3.3)$$

The locations of the asperities, together with the location of the rupture starting point, should be determined so that the rupture of one of the asperities propagates toward the port. This recommendation is based on the fact that especially intense ground motions are generally generated in the direction of the rupture propagation of an asperity

and that the significant damage during the 1995 Hyogo-ken Nanbu earthquake was partly caused by this effect⁴⁾. The locations of the asperities can be determined referring to **Fig. 1.3.5**. The depth of the asperity center can be 10 km. If two asperities are considered, it is preferable to avoid concentrating two asperities on one side of the fault.

Among the additional parameters, the rupture starting point can be determined referring to **Fig. 1.3.5**, together with the locations of the asperities. The rupture velocity can be 80% of the shear wave velocity in the source region⁵⁴⁾. The rupture can be assumed to propagate radially.

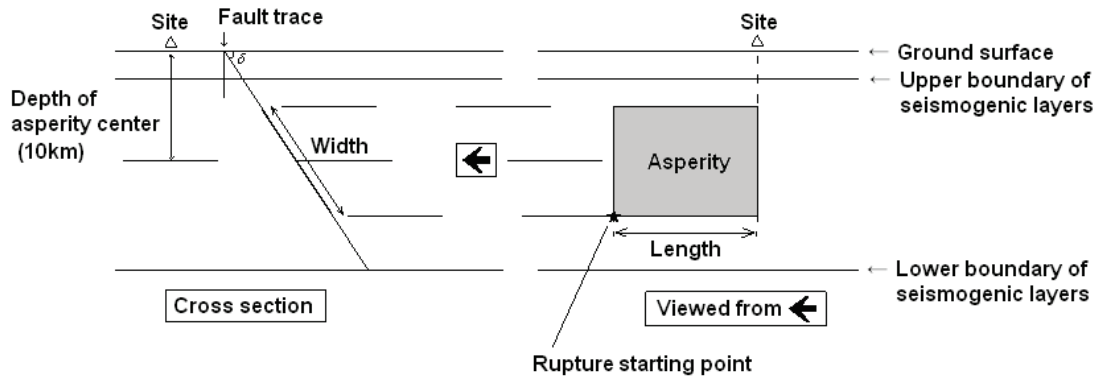


Fig. 1.3.5 Location of the asperity and the rupture starting point

(3) Huge subduction earthquakes greater than regional historical earthquakes

The occurrence of the 2011 Tohoku earthquake encouraged engineers to consider huge subduction earthquakes greater than regional historical earthquakes in various regions in Japan. In that case, the SPGA model¹²⁾¹³⁾⁵⁶⁾⁵⁷⁾, which shows excellent applicability to past huge subduction earthquakes including the 2011 Tohoku earthquake, can be used. If a huge subduction earthquake comparable to the 2011 Tohoku earthquake is considered, the inner source parameters of the SPGA model can be determined referring to the inner source parameters of the SPGA model for the 2011 Tohoku earthquake⁶²⁾⁶³⁾ (**Fig. 1.3.4**). If a huge subduction earthquake with a different size is considered, the inner source parameters of the SPGA model can be determined based on empirical relations¹²⁾¹³⁾. When a huge subduction earthquake greater than regional historical earthquakes is considered, the locations of the SPGAs cannot be constrained by seismic intensity data of historical earthquakes, leading to uncertainty in the locations of the SPGAs. Therefore, a lot of possible distributions of the SPGAs should be considered before selecting the locations⁶²⁾⁶³⁾. For example, if a huge subduction earthquake along the Nankai trough with $M_w 9.0$ is considered, among possible distributions of the SPGAs, it is reasonable to select a distribution that generates ground motions that are consistent on average with the seismic intensity distributions anticipated by the Cabinet Office⁶⁴⁾. Seismic intensity distributions calculated by SPGA models and those anticipated by the Cabinet Office were compared by Nozu et al.⁶⁵⁾.

(4) M6.5 earthquake just beneath the site

The seismic moment M_0 can be determined from the magnitude M with the following empirical relation⁶⁶⁾:

$$\log M_0 = 1.17M + 17.72(\text{dyne} \cdot \text{cm}). \quad (1.3.4)$$

The area of the fault S can be determined with **equation (1.3.2)**. The dip δ can be 90° . Then, the procedure described in **(2) Earthquakes caused by active faults** can be followed. Generally one asperity is considered.

1.3.4 Evaluation of site amplification factors

The site amplification factor at a construction site can be evaluated in a similar way as in the case of a level-1 ground motion as described in **Part II, Chapter 6, 1.2.2 Evaluation of site amplification factors**.

1.3.5 Simulation of strong ground motions

(1) General

Methods for the simulation of strong ground motions taking into account the source, path and site effects can be broadly categorized into theoretical methods and semi-empirical methods. In the theoretical methods, the media through which seismic waves are transmitted from the source to a port is modelled as an elastic body and the ground motions are calculated by solving elastic wave equations. In the empirical Green's function method⁽⁶⁷⁾⁽⁶⁸⁾⁽⁶⁹⁾, which is one of the semi-empirical methods, a recorded ground motion of a small event that shares the focal mechanism, that is, the strike, dip and rake angles and the propagation path with the anticipated large event is regarded as a Green's function and superposed to estimate the ground motion of the large event. In the stochastic Green's function method⁽⁷⁰⁾, which is also one of the semi-empirical methods, the ground motion of a small event is artificially generated and superposed. This method is applicable when there is no appropriate record of a small event. In addition to these methods, hybrid methods (*e.g.*, Kamae et al⁽⁷¹⁾) have also been proposed, in which low frequency components are calculated with a theoretical method and high frequency components are calculated with a semi-empirical method.

Among these methods, it has been shown that the theoretical methods can reproduce observed ground motions with high accuracy for frequencies lower than 1 Hz if they are applied to regions with sufficient information on subsurface structures (*e.g.*, Matsushima and Kawase⁽⁷²⁾). However, regions with sufficient information are quite limited in spite of efforts to collect information on subsurface structures (*e.g.*, Science and Technology Agency⁽⁷³⁾). On the other hand, in the empirical Green's function method that belongs to the semi-empirical methods, the site effects included in the Green's function will be naturally imposed on the results. In addition, within the framework of the stochastic Green's function method that belongs to the semi-empirical methods, it is possible to incorporate site amplification factors evaluated based on earthquake observations⁽³⁸⁾⁽⁷⁴⁾. This method will be referred to as the "corrected empirical Green's function method" in this article. In conclusion, in Japanese ports where strong motion records have been accumulated, it is preferable to use semi-empirical methods for the simulation of strong ground motions. In regions with sufficient information on subsurface structures, it is possible to use theoretical methods or hybrid methods, however, it is necessary to validate the appropriateness of the subsurface structure models using strong motion records before they are used.

It is meaningful to compare the results of strong motion simulations with strong motion records obtained in a similar condition. Comparing the results of strong motion simulations at a near-fault site of a crustal earthquake with, for example, near-fault records of the 1995 Hyogo-ken Nanbu earthquake or the 2004 Mid Niigata Prefecture earthquake will give some indications on the appropriateness of the results. However, because strong ground motions are strongly dependent on the source and site effects, the amplitude of a simulated ground motion can be different from those of past strong motion records depending on calculation conditions. If the amplitude of a simulated ground motion is significantly different from those of past strong motion records, it is preferable to investigate whether it is possible to reasonably explain the difference by considering the difference of the source and/or site effects. If it is possible, the result is acceptable. If it is not possible, it is necessary to check for mistakes in the input files, etc. Thus, comparison with past strong motion records is meaningful for preventing mistakes.

In comparing the results of strong motion simulations with past strong motion records, it is less meaningful to compare them in terms of peak ground accelerations. While peak ground accelerations are mostly affected by frequency components higher than 2 Hz, port facilities are less affected by frequency components higher than 2 Hz. Therefore, comparison in terms of peak ground accelerations does not make it possible to validate simulated ground motions in a frequency range that affects port facilities. In general, peak ground velocities are better indices than peak ground accelerations. Peak ground velocities in a range of 100 – 150 cm/s were observed at near-fault strong motion stations at the ground surface in sedimentary basins during the 1995 Hyogo-ken Nanbu earthquake and the 2004 Mid Niigata Prefecture earthquake.

(2) Corrected empirical Green's function method⁽³⁸⁾⁽⁷⁴⁾

In the corrected empirical Green's function method, the ground motion of a small event at a construction site is evaluated and called a "Green's function". Then the Green's functions are superposed to estimate the ground motion of a large earthquake. The details are as follows.

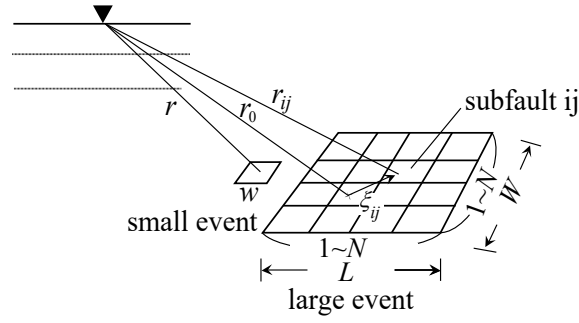


Fig. 1.3.6 Superposition of Green's functions. L and W are the length and width of an asperity, etc., respectively.

An asperity, etc. of a scenario earthquake is considered, which is shown as a “large event” in **Fig. 1.3.6**. The asperity is divided into $N \times N$ subfaults and a small earthquake that has the same area as one of the subfaults is considered, which is shown as a “small event” in **Fig. 1.3.6**. The Fourier amplitude spectrum of the Green's function at the ground surface is evaluated as the product of the source effect of the small event (**equation (1.3.5)**), the path effect (**equation (1.3.6)**) and the site amplification factor⁷⁵⁾:

$$S(f) = R_{\theta\phi} FS \cdot PRTITN \cdot \frac{M_{0e}}{4\pi\rho V_s^3} \frac{(2\pi f)^2}{1 + (f/f_c)^2} \quad (1.3.5)$$

$$P(f) = \frac{1}{r} \exp(-\pi f r / QV_s), \quad (1.3.6)$$

where

$S(f)$: Source effect

$P(f)$: Path effect

M_{0e} : Seismic *moment* of the small event

f_c : Corner *frequency* of the small event

ρ : Density in the *seismological* bedrock

V_s : Shear wave *velocity* in the seismological bedrock

$R_{\theta\phi}$: Radiation *coefficient*

FS : Coefficient *representing* amplification due to free surface (=2)

$PRTITN$: Coefficient representing partition of S wave energy into two horizontal components

r : hypocentral *distance* of the small event

Q : Quality factor

If an earthquake caused by an active fault is considered, values such as $\rho = 2.7 \text{ g/cm}^3$ and $V_s = 3.5 \text{ km/s}$ can be used. For $R_{\theta\phi}$, 0.63 can be used, which corresponds to the averaged value over all directions. $PRTITN$ can be 0.85 and 0.53 for the strike-normal and strike-parallel components, respectively, if an earthquake caused by an active fault is considered and the fault distance is less than 10 km. These suggestions are based on a report that, on average, the Fourier amplitude spectrum is approximately 1.6 times larger for the strike-normal component than for the strike-parallel component in the near-fault regions of large crustal earthquakes⁸⁾. $PRTITN$ can be 0.71 for any horizontal component if a scenario earthquake other than those caused by active faults is considered or if the fault distance is greater than 10 km, with the assumption that S wave energy is equally distributed into two horizontal components. In any case, $PRTITN$ should be determined in such a way that their squared sum is equal to 1.0. The standard values for $PRTITN$ are listed in **Table 1.3.1**.

Table 1.3.1 Standard values for *PRTITN*

	Near-fault sites	Other sites
Subduction earthquakes	0.71	0.71
Earthquakes caused by active faults	0.85 (strike-normal component) 0.53 (strike-parallel component)	0.71
M6.5 earthquake just beneath the site	0.71	0.71

The seismic moment of the small event M_{0e} can be calculated by dividing the seismic moment of the asperity, etc. by N^3 , where N is the number of discretization. The corner frequency of the small event f_c can be calculated by the following equation proposed by Brune⁷⁶⁾⁷⁷⁾.

$$f_c = \frac{0.66V_s}{\sqrt{S_e}}, \quad (1.3.7)$$

where

S_e : Area of the small event

Equation (1.3.7) is identical to **equation (36)** in the paper written by Brune⁷⁶⁾. Once **equation (1.3.7)** is combined with the equation for a circular crack by Esherby⁵⁵⁾, one obtains the well-known equation for expressing the corner frequency as a function of the seismic moment and the stress drop⁷⁵⁾. In **equation (1.3.6)**, the quality factor should be determined appropriately taking into account regional characteristics. Quality factors estimated for different regions include: $Q=114f^{0.92}$ for subduction earthquakes in eastern Japan⁷⁸⁾, $Q=152f^{0.38}$ for subduction earthquakes in western Japan⁷⁸⁾, $Q=166f^{0.76}$ for crustal earthquakes in eastern Japan⁷⁸⁾, $Q=63.8f^{1.00}$ for crustal earthquakes in the Kansai Region⁷⁹⁾ and $Q=104f^{0.63}$ for crustal earthquakes in Kagoshima and Kumamoto prefectures⁸⁰⁾.

The Green's function at the ground surface can be evaluated by combining the Fourier amplitude spectrum at the ground surface thus obtained with the phase characteristics of a weak motion record at the construction site or in its vicinity and applying the inverse Fourier transform³⁸⁾⁷⁴⁾. The procedure can be expressed as follows:

$$A(f) = S(f)P(f)G(f) \frac{O(f)}{|O(f)|_p}, \quad (1.3.8)$$

where

$A(f)$: Fourier transform of a Green's function at the ground surface (complex value)

$S(f)$: Source effect (real value)

$P(f)$: Path effect (real value)

$G(f)$: Site amplification factor at the ground surface with respect to the seismological bedrock (real value)

$O(f)$: Fourier transform of a weak motion record at a construction site or in its vicinity (complex value)

$|O(f)|_p$: Absolute value of $O(f)$, smoothed with a Parzen window with a band width of 0.05 Hz

It is preferable to use a weak motion record at a construction site with a similar incident angle to the scenario earthquake in **equation (1.3.8)** to consider the influence of sediments on the phase characteristics of earthquake ground motions more appropriately.

Before evaluating a Green's function at the ground surface with **equation (1.3.8)**, it is necessary to evaluate the site amplification factor $G(f)$. So far two approaches have been used to evaluate the site amplification factor: One approach is to isolate the "S wave portion" from an observed ground motion and to evaluate the site amplification factor for that portion⁸¹⁾. The other approach is to account not only for S waves but also for surface waves and to evaluate the site amplification factor based on Fourier spectra including the effects of later phases¹⁷⁾. Although both of these approaches are meaningful under certain conditions, the latter approach should be taken if it is intended to consider not only S waves but also surface waves in the simulation of strong ground motions. In particular, within the framework of the corrected empirical Green's function method, because the effects of S waves and surface

waves are inseparably included in a weak motion record to determine the phase characteristics of a Green's function, it is necessary to consider the effects of both waves in evaluating the Fourier amplitude spectrum.

The ground motion generated by the asperity, etc. can be calculated by superposing Green's functions at the ground surface with the following equation (**Fig. 1.3.6**)⁸²⁾. Through the process of the superposition, the forward directivity effects are considered, resulting in stronger predicted ground motions in the direction of rupture propagation:

$$U(t) = \sum_{i=1}^N \sum_{j=1}^N \left(r/r_{ij} \right) f(t) * u(t - t_{ij}) \quad (1.3.9)$$

$$f(t) = \delta(t) + \frac{1}{n' \left(1 - \frac{1}{e} \right)} \sum_{k=1}^{(N-1)n'} \left[e^{-(k-1)/(N-1)/n'} \delta \left\{ t - \frac{(k-1)\tau}{(N-1)n'} \right\} \right] \quad (1.3.10)$$

$$t_{ij} = \frac{r_{ij} - r_0}{V_S} + \frac{\xi_{ij}}{V_r}, \quad (1.3.11)$$

where

$U(t)$: Ground motion generated by the asperity, etc.

$u(t)$: Green's function at the ground surface

$f(t)$: Correction function for the difference of slip velocity time functions for the large and small events

r : hypocentral distance of the small event

r_{ij} : Distance from the ij subfault to the site

N : Number of discretization (Fig. 1.3.6)

τ : Rise time

n' : Integer to remove artificial periodicity that appears in the process of superposition

r_0 : Distance from the rupture starting point of the asperity, etc. to the site

ξ_{ij} : Distance from the rupture starting point of the asperity, etc. to the ij subfault

V_S : Shear wave velocity in the seismological bedrock

V_r : Rupture velocity

When two or more asperities, etc. are considered, the above mentioned process should be repeated for all the asperities, etc. and the resultant waveforms should be superposed to obtain the level-2 ground motion at the ground surface. The obtained ground motion, however, corresponds to a virtual situation where the shallower sediments above the engineering bedrock exhibit linear behavior. Finally, the level-2 ground motion at the engineering bedrock in the form of so-called "2E wave" can be evaluated by conducting earthquake response analyses of the shallow sediments. Contributions from the background region, *i.e.*, the region on the fault outside the asperities, etc., can be neglected if the strong motion simulation is aimed at generating ground motions for the performance verification of a typical port structure.

It should be noted that the level-2 ground motion at the ground surface that appears in the above process is often overestimated because it does not include the possible effects of soil nonlinearity for the shallower sediments during a large earthquake. If a realistic level-2 ground motion at the ground surface is required, it is generally obtained by nonlinear response analyses of the shallower sediments in which the level-2 ground motion at the engineering bedrock is used as an input motion.

So far, it has been assumed that a Green's function at the ground surface is used in **equation (1.3.9)**. However, a Green's function at the engineering bedrock in the form of "2E wave" can also be used in **equation (1.3.9)**. In that case, the level-2 ground motion at the engineering bedrock in the form of "2E wave" can be directly obtained. However, in that case, the site amplification factor at the engineering bedrock with respect to the seismological bedrock should be used in **equation (1.3.8)** and the weak motion record at the construction site or in its vicinity should be converted to a "2E wave" at the engineering bedrock before used in **equation (1.3.8)**.

Nozu et al.³⁸⁾ applied the above mentioned method to reproduce strong motion records during past large earthquakes. A FORTRAN program based on the method is available on a CD attached to their report³⁸⁾ or at the PARI website at https://www.pari.go.jp/bsh/jbn-kzo/jbn-bsi/taisin/sourcemodel/somodel_program.html.

(3) Empirical Green's function method

The empirical Green's function method assumes the existence of a weak motion record at a given site that recorded a small earthquake that occurred near the fault of a scenario earthquake. If such a record is available, it can be superposed to estimate the ground motion of the scenario earthquake at the site. The weak motion record is called the "empirical Green's function". The main advantage of the method is that the ground motion can be estimated accurately without explicitly evaluating the path and site effects, because those effects are naturally included in the weak motion record. However, the method cannot be applied if such a record is not available. In addition, the method requires more skills compared to the corrected empirical Green's function method as mentioned below:

Equations (1.3.9) – (1.3.11) for the corrected empirical Green's function method can almost be used for superposing empirical Green's functions, with the exception that **equation (1.3.9)** should be replaced by the following equation⁸²⁾ that includes the coefficient C to appropriately consider the characteristics of the small earthquake:

$$U(t) = \sum_{i=1}^N \sum_{j=1}^N \left(r/r_{ij} \right) f(t) * \left(Cu(t-t_{ij}) \right). \quad (1.3.12)$$

Parameters related to the superposition N and C should be determined so that

$$\begin{aligned} M_{0a}/M_{0e} &= CN^3 \\ S_a/S_e &= N^2, \end{aligned} \quad (1.3.13)$$

where

M_{0a} : Seismic moment of the asperity, etc.

M_{0e} : Seismic moment of the small event

S_a : Area of the asperity, etc.

S_e : Area of the small event

Equation (1.3.13) implies that it is inevitable to carefully evaluate the parameters of the small event in the application of the empirical Green's function method. For the seismic moment of the small event M_{0e} , moment tensor solutions⁸³⁾ such as those determined by the F-net of the National Research Institute for Earth Science and Disaster Resilience, Japan, can be referred. The area of the small event S_e can be determined from the corner frequency of the small event with **equation (1.3.7)**. The corner frequency of the small event can be determined by taking the spectral ratio of closely-located earthquakes with different size²⁾⁸⁴⁾.

Another issue to be carefully considered in the application of the empirical Green's function method is how to handle radiation coefficients. Theoretically speaking, radiation coefficients are dependent on the azimuth and the take-off angle⁸³⁾⁸⁵⁾. Therefore, a weak motion record at a construction site may correspond to a small radiation coefficient depending on the focal mechanism of the small event. In that case, superposing that record may lead to underestimation of the ground motion of a scenario earthquake. Thus, it is necessary to pay attention to the focal mechanism of the small event.

The points raised above imply that there are several issues to be carefully considered in the application of the empirical Green's function method, indicating that the empirical Green's function method requires more skills compared to the corrected empirical Green's function method.

1.3.6 Earthquake response analysis of the ground

Earthquake response analyses of the ground can be conducted referring to **Part II, Chapter 6, 1.2.3 Earthquake response analysis of the ground** with the exception that the analysis method should be selected carefully because the strain level tends to become large for a level-2 ground motion.

1.4 Spatial variation of earthquake ground motions for the performance verification of structures

(1) General

In designing a long or a large structure such as a buried pipeline or a submerged tunnel, one of the issues to be considered is that various parts of the structure will be subject to different ground motions.

“Spatial variation of earthquake ground motions” generally refers to lateral variation of earthquake ground motions. Spatial variation of earthquake ground motions can be induced by lateral variation in ground conditions, however, spatial variation of ground motions can be induced by other factors. When lateral variation in ground conditions is negligible, apparent propagation of seismic waves in a horizontal direction can cause phase difference of earthquake ground motions acting on various parts of a structure. In the following section, both of these issues will be addressed.

It should be noted that lateral variation of earthquake ground motions is not the only reason for the difference of earthquake ground motions acting on various parts of a structure. Structures with significant depth variation in the longitudinal direction such as submerged tunnels are more susceptible to vertical variation of earthquake ground motions, which should be appropriately taken into account in the design.

(2) If lateral variation in ground conditions is significant

Significant lateral variation in ground conditions within the dimension of a structure can cause spatial variation of earthquake ground motions. Therefore, lateral variation in ground conditions within the dimension of a structure should be evaluated appropriately. If it is significant, spatial variation of earthquake ground motions should be evaluated taking into account its effects. In this evaluation, it is preferable to consider the lateral variation not only in the shallower sediments but also in the deeper sediments below the engineering bedrock.

Spatial variation of earthquake ground motions induced by significant lateral variation in ground conditions can be most effectively evaluated by conducting array observations of earthquake ground motions and applying the method described in **Part II, Chapter 6, 1.3.5 Simulation of strong ground motions (2) and (3)** to evaluate strong ground motions at multiple locations. Numerical methods such as the finite element method or the finite difference method are also applicable if there is sufficient information on subsurface structures. If the method described in **Part II, Chapter 6, 1.3.5 Simulation of strong ground motions (2)** is to be used, care should be taken not to lose the physical meaning of the phase difference of predicted ground motions at multiple locations. The physical meaning of the phase difference could be lost when 1) random numbers are used for generating Green’s functions⁷⁵⁾ and different random numbers are assigned to different locations or 2) when weak motion records used in **equation (1.3.8)** for different locations have been triggered independently and cannot be aligned on the same time axis. For the former situation, it would be effective to use the same random numbers for different locations.

(3) If lateral variation in ground conditions is not significant

If lateral variation in ground conditions is not significant, the above mentioned procedure can also be applied, however, a simpler procedure³¹⁾ can be applied as follows:

When lateral variation in ground conditions is not significant, apparent propagation of seismic waves in a horizontal direction can be a major cause of the spatial variation of earthquake ground motions. The strain in the ground due to the apparent propagation of seismic waves $\varepsilon(\omega)$ is a function of the particle velocity $v(\omega)$ and the apparent propagation velocity of the seismic waves $c(\omega)$:

$$\varepsilon(\omega) = v(\omega)/c(\omega), \quad (1.4.1)$$

where ω is the angular frequency.

Because $\varepsilon(\omega)$ is a decreasing function of $c(\omega)$ as can be seen in **equation (1.4.1)**, using a smaller value of $c(\omega)$ leads to a more conservative design of a structure. Although both surface waves and obliquely incident S waves can cause apparent propagation of seismic waves in a horizontal direction, the phase velocity of the surface waves is smaller than that of the S waves for any angular frequency ω . Among surface waves, either fundamental-mode Love waves or fundamental-mode Rayleigh waves travel with the smallest phase velocity for any angular frequency ω . Therefore, it is most conservative to use the smaller of the phase velocities of fundamental-mode Love waves and fundamental-mode Rayleigh waves for $c(\omega)$.

In general, the phase velocity of surface waves is frequency-dependent. For example, **Fig. 1.4.1** shows the frequency dependent phase velocities of Love waves in a waterfront area of Tokyo. The theoretical phase velocities

(solid lines) were computed from the S-wave velocity structure model shown in **Table 1.4.1**. The solid rectangles in **Fig. 1.4.1** indicate the phase velocities obtained from array observations of earthquake ground motions at this particular site. The phase velocity of the fundamental-mode Love wave is approximately 400 m/s at the period of one second and approximately 750 m/s at the period of 3 seconds, indicating that the phase velocity is frequency dependent.

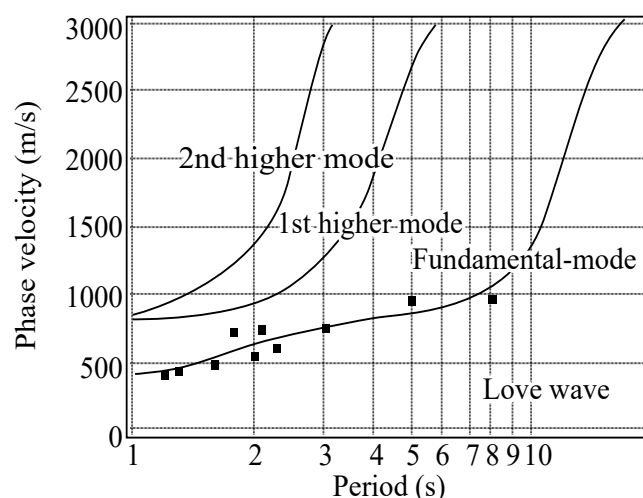


Fig. 1.4.1 Frequency dependent phase velocities of Love waves in a waterfront area of Tokyo⁸⁶⁾

Table 1.4.1 S-wave velocity structure model ⁸⁶⁾

Thickness (m)	S wave velocity (m/s)	Density (10^3 kg/m^3)
50	250	1.8
120	410	1.9
1580	800	1.9
1250	1200	2.1
3100	2600	2.6
—	3400	2.6

The *apparent velocity* is significantly site-specific. The values shown in **Fig. 1.4.1** cannot be used at an arbitrary site. The *apparent velocity* for the performance verification of a structure should be determined on a site-specific basis.

Earthquake ground motions evaluated by the method described in **Part II, Chapter 6, 1.2 Level-1 ground motions for the performance verification of structures** or **Part II, Chapter 6, 1.3 Level-2 ground motions for the performance verification of structures** generally involve different types of seismic waves such as surface waves and S waves. Ideally speaking, $c(\omega)$ for the performance verification should be determined based on the knowledge of the types of waves involved in the evaluated ground motions. In practice, however, it is not easy to specify the types of waves. Therefore, the smaller of the phase velocities of fundamental-mode Love waves and fundamental-mode Rayleigh waves can be used for $c(\omega)$ if it is intended to be sufficiently conservative. The phase velocities should be determined through in-situ array observations of earthquake ground motions or microtremors (see **Reference (Part II), Chapter 1, 3.8.4 Array observations of microtremors**).

However, earthquake ground motions involve various types of seismic waves other than fundamental-mode surface waves. It is necessary to consider the effects of those waves if it is intended to evaluate the strain in the ground more realistically. From such a point of view, a study was conducted to determine a more realistic value of the apparent velocity based on the results of earthquake observations in a sealed tunnel⁸⁷⁾. As a result, it was reported that the axial strain in the tunnel was well reproduced by assuming a seismic wave that travels with a velocity twice as large as the phase velocity of fundamental-model Love waves and intersects with the tunnel axis at 45° .

Considering a frequency dependent apparent velocity leads to a more rational design of a structure. However, a frequency independent apparent velocity is also used for simplicity. The apparent velocity along the tunnel axis obtained in the above mentioned study based on earthquake observations in a sealed tunnel⁸⁷⁾ was slightly larger than a frequency independent apparent velocity of 1 km/s.

Spatial variation of earthquake ground motions can be evaluated with considerations of a frequency dependent *apparent velocity* as follows:

Let $a_0(t)$ denote the time history of a ground motion evaluated through the process described in **Part II, Chapter 6, 1.2 Level-1 ground motions for the performance verification of structures** or **1.3 Level-2 ground motions for the performance verification of structures** at one representative point ($x=0, y=0$) at a specified depth in a horizontally layered ground. Let $c(\omega)$ denote the site-specific frequency-dependent phase velocity. Then the ground motion $a(t)$ at an arbitrary point (x,y) at the same depth can be specified as follows:

① Compute the Fourier transform of $a_0(t)$.

② Compute the Fourier transform of $a(t)$ as follows:

$$A(\omega) = A_0(\omega) \exp\{-i(k_x x + k_y y)\} \quad (1.4.2)$$

$$k_x = \{\omega/c(\omega)\} \cos \theta \quad (1.4.3)$$

$$k_y = \{\omega/c(\omega)\} \sin \theta, \quad (1.4.4)$$

where

$A_0(\omega)$: Fourier transform of $a_0(t)$

$A(\omega)$: Fourier transform of $a(t)$

θ : Angle between the positive- x direction and the propagation direction of the seismic wave

③ Compute the inverse Fourier transform of $A(\omega)$ to obtain $a(t)$.

[References]

- 1) Japan Society of Civil Engineers: Proposal and commentary on seismic design standards for infrastructures: the third proposal, 2000 (in Japanese).
- 2) Aki, K.: Scaling law of seismic spectrum, J. Geophys. Res., Vol.72, pp.1217-1231, 1967.
- 3) Aki, K.: Generation and propagation of G waves from the Niigata earthquake of June 16, 1964. 2. Estimation of earthquake moment, released energy, and stress-strain drop from G wave spectrum, Bulletin of the Earthquake Research Institute, Vol.44, pp.23-88, 1966.
- 4) Irikura, K.: Near-fault ground motions causing the Great Hanshin Earthquake Disaster, Annuals, Disaster Prevention Research Institute, Kyoto University, No.39A, pp.229-245, 1996 (in Japanese with English abstract).
- 5) Koketsu, K.: Damaging earthquakes in California and the Hyogo-ken Nanbu earthquake, Kagaku, Vol.66, No.2, pp.93-97, 1996 (in Japanese with English abstract).
- 6) Takemura, M., T. Moroi and K. Yashiro: Characteristics of strong ground motions as deduced from spatial distribution of damages due to the destructive inland earthquakes from 1891 to 1995 in Japan, Zisin, 2nd series, Vol.50, pp.485-505, 1998 (in Japanese with English abstract).
- 7) Somerville, P.G., N.F. Smith, R.W. Graves and N.A. Abrahamson: Modification of empirical strong ground motion attenuation relations to include the amplitude and duration effects of rupture directivity, Seismological Research Letters, Vol.68, pp.199-222, 1997.
- 8) Nozu, A., S. Iai and W.D. Iwan: A study on predominant direction of near-source ground motion and its application, Report of the Port and Harbour Research Institute, Vol.40, No.1, pp.107-167, 2001 (in Japanese with English abstract)
- 9) Nozu, A. and K. Ikeda: Planning high seismic resistant quay walls with considerations of predominant direction of near-fault ground motions, Kowan, Vol.78, No.9, pp.48-51, 2001 (in Japanese).

- 10) Ports and Harbours Bureau, Ministry of Land, Infrastructure and Transport and Port and Airport Research Institute: Handbook of Predominant Direction of Earthquake Ground Motions for Port Planning, CD-ROM, 2003 (in Japanese).
- 11) Lay, T., H. Kanamori, C.J. Ammon, K.D. Koper, A.R. Hutko, L. Ye, H. Yue and T.M. Rushing: Depth-varying rupture properties of subduction zone megathrust faults, *J. Geophys. Res.*, Vol.117, B04311, 2012.
- 12) Nozu, A., M. Yamada, T. Nagao and K. Irikura: Generation of strong motion pulses during huge subduction earthquakes and scaling of their generation areas, *Journal of Japan Association for Earthquake Engineering*, Vol.12, No.4, pp.209-228, 2012 (English translation is available in Vol.14, No.6).
- 13) Nozu, A. and T. Nagao: Strong motion pulse generation areas for huge subduction earthquakes: their scaling with overall earthquake size, *Technical Note of the Port and Airport Research Institute*, No.1257, 2012 (in Japanese with English abstract).
- 14) Kurahashi, S. and K. Irikura: Short-period source model of the 2011 M_w 9.0 off the Pacific coast of Tohoku earthquake, *Bull. Seism. Soc. Am.*, Vol.103, pp.1373-1393, 2013.
- 15) Street, R., R. Herrmann and O. Nuttli: Spectral characteristics of the L_g wave generated by central United States earthquakes, *Geophys. J. R. Astr. Soc.*, Vol.41, pp.51-63, 1975.
- 16) Kudo, K.: Progress of engineering seismology in Japan, specially related with strong motion prediction: An introduction to the series of reviews on strong motion seismology and engineering seismology, *Zisin*, 2nd series, Vol.46, pp.151-159, 1993 (in Japanese with English abstract).
- 17) Nozu, A. and T. Nagao: Site amplification factors for strong-motion sites in Japan based on spectral inversion technique, *Technical Note of the Port and Airport Research Institute*, No.1112, 2005 (in Japanese with English abstract).
- 18) Kinoshita, S.: Kyoshin Net (K-net), *Seim. Res. Lett.*, Vol. 69, pp.309-332, 1998.
- 19) Aoi, S., K. Obara, S. Hori, K. Kasahara and S. Okada: New strong-motion observation network: KiK-net, *EOS, Trans. Am. Geophys. Union*, Vol. 329, 2000.
- 20) Takemura, M.: Great Kanto Earthquake Disaster: Knowing Strong Ground Motions in Greater Tokyo, *Kajima Institute Publishing*, 2003 (in Japanese).
- 21) Nozu, A. and T. Sugano: Site amplification factors for strong-motion sites in Nansei Islands in Japan based on spectral inversion technique, *Technical Note of the Port and Airport Research Institute*, No.1149, 2007 (in Japanese with English abstract).
- 22) Nozu, A. and T. Sugano: Site amplification factors for strong-motion sites in Northern Hokkaido, Japan, based on spectral inversion technique, *Technical Note of the Port and Airport Research Institute*, No.1214, 2010 (in Japanese with English abstract).
- 23) Tsuchida, H. and S. Iai: *Earthquake Engineering for Practitioners*, Sankaido, 1991 (in Japanese).
- 24) Takenobu, M., A. Nozu, M. Miyata, Y. Sato and S. Asai: Comprehensive report for setting up level-1 earthquake ground motion with a probabilistic time history waveform for seismic design of port facilities, *Technical Note of National Institute for Land and Infrastructure Management*, No.812, 2014 (in Japanese with English abstract).
- 25) Osaki, Y.: *Introduction to Spectral Analysis of Earthquake Ground Motions: New Edition*, *Kajima Institute Publishing*, 2003 (in Japanese).
- 26) Zen, K., H. Yamazaki and Y. Umehara: Experimental study on shear modulus and damping ratio of natural deposits for seismic response analysis, *Report of the Port and Harbour Research Institute*, Vol.25, No.1, pp.41-113, 1987 (in Japanese with English abstract).
- 27) Nakamura, Y.: A method for dynamic characteristics estimation of subsurface layers using microtremor on the ground surface, *Report of the Railway Technical Research institute*, Vol.2, No.4, pp.18-27, 1988 (in Japanese with English abstract).
- 28) Nozu, A. and A. Wakai: Characteristics of ground motions at damaged ports during the 2011 Great East Japan Earthquake Disaster, *Technical Note of the Port and Airport Research Institute*, No.1244, 2011 (in Japanese with English abstract).
- 29) Nagao, T., N. Morishita and A. Nozu: Study on the effect of the site amplification factor on the evaluation of level-one earthquake ground motion, *Proceedings of Civil Engineering in the Ocean*, Vol.22, 2006 (in Japanese with English abstract).

- 30) Yoshida, N. and S. Iai: Nonlinear site response and its evaluation and prediction, The Effects of Surface Geology on Seismic Motion, Irikura, Kudo, Okada & Sasatani (eds), Balkema, 1998.
- 31) International Organization for Standardization: ISO23469, Bases for design of structures - Seismic actions for designing geotechnical works, 2005.
- 32) Shnabel, P.B., J. Lysmer and H.B. Seed: SHAKE, A computer program for earthquake response analysis of horizontally layered sites, Report No. EERC72-12, University of California at Berkeley, 1972.
- 33) Lysmer, J., T. Udaka, C.F. Tsai and H.B. Seed: FLUSH, A computer program of approximate 3-D analysis of soil-structure interaction problems, Report No. EERC75-30, University of California at Berkeley, 1975.
- 34) Yoshida, N.: Applicability of conventional computer code SHAKE to nonlinear problem, Proceedings of the Symposium on Amplification of Ground Shaking in Soft Ground, the Japan Society of Soil Mechanics and Foundation Engineering, Tokyo, pp.14-31, 1994 (in Japanese).
- 35) Sugito, M., H. Goda and T. Masuda: Frequency dependent equi-linearized technique for seismic response analysis of multi-layered ground, Journal of JSCE, No.493/III-27, pp.49-58, 1994 (in Japanese with English abstract).
- 36) Yoshida, N. and I. Suetomi: DYNEQ: A computer program for dynamic response analysis of level ground by equivalent linear method, Report of the Technical Institute, Sato Kogyo Co., Ltd., pp.61-70, 1996 (in Japanese).
- 37) Iai, S., Y. Matsunaga and T. Kameoka: Strain space plasticity model for cyclic mobility, Soils and Foundations, Vol.32, pp.1-15, 1992.
- 38) Nozu, A. and T. Sugano: Simulation of strong ground motions based on site-specific amplification and phase characteristics – Accounting for causality and multiple nonlinear effects –, Technical Note of the Port and Airport Research Institute, No.1173, 2008 (in Japanese with English abstract).
- 39) Iai, S., T. Morita, T. Kameoka, Y. Matsunaga and K. Abiko: Response of a dense sand deposit during 1993 Kushiro Oki earthquake, Soils and Foundations, Vol.35, pp.115-132, 1995.
- 40) Coastal Development Institute of Technology: Handbook on Liquefaction Remediation of Reclaimed Land, Revised Edition, 1997 (in Japanese).
- 41) Imai, T. and K. Tonouchi: Correlation of N value with S wave velocity and Shear Modulus, Proc. 2nd ESOPT, 1982.
- 42) Uwabe, T., H. Tsuchida and E. Kurata: Coupled hydrodynamic response analysis based on strong motion earthquake records of fill type breakwater in deep sea, Report of the Port and Harbour Research Institute, Vol.22, No.2, pp.289-326, 1983 (in Japanese with English abstract)
- 43) Ichii, K., S. Iai and T. Morita: Effective stress analysis of the mechanism of deformation in caisson type quay walls, Proceedings of the symposium on the Great Hanshin Awaji Earthquake Disaster, Japan Society of Civil Engineers, pp.397-404, 1996 (in Japanese with English abstract).
- 44) Kokusho, T., A. Sakurai and Y. Esashi : Development of dynamic triaxial tests from small to large strain and their application to sands, Proceedings of the 14th Japan National Conference on Soil Mechanics and Foundation Engineering, Sapporo, pp.513-516, 1979 (in Japanese).
- 45) Usui, H., M. Kazama and T. Inatomi: The influence of shear modulus of soils depended on confined pressure on the results of 1D equivalent linear seismic response analysis, Proceedings of the Symposium on Response of Soils and Geotechnical Structures during Earthquakes, the Japan Society of Soil Mechanics and Foundation Engineering, Tokyo, pp.219-224, 1989 (in Japanese).
- 46) National Astronomical Observatory of Japan (ed): Chronological Scientific Tables, 2017 (in Japanese).
- 47) Usami, T.: Materials for Comprehensive List of Destructive Earthquakes in Japan, [416]-2001, Latest Edition, University of Tokyo Press, 2003 (in Japanese).
- 48) Sato, R. (ed): Handbook of Earthquake Fault Parameters in Japan, Kajima Institute Publishing, 1989 (in Japanese).
- 49) The Research Group for Active Faults of Japan, Active Faults in Japan: Sheet Maps and Inventories, Revised Edition, University of Tokyo Press, 1991 (in Japanese).
- 50) Nakata, T. and T. Imaizumi, Digital Active Fault Map of Japan, University of Tokyo Press, 2000 (in Japanese).
- 51) Takemura, M.: Scaling law for Japanese intraplate earthquakes in special relations to the surface faults and the damages, Zisin, 2nd series, Vol.51, pp.211-228, 1998 (in Japanese with English abstract).

- 52) Utsu, T.: Catalog of large earthquakes in the region of Japan from 1885 through 1980, Bulletin of the Earthquake Research Institute, Vol.57, pp.401-463, 1982.
- 53) Kanamori, H. (ed): Physics of Earthquakes, Iwanami Shoten Publishers, 1991 (in Japanese).
- 54) Kataoka, S., T. Kusakabe, J. Murakoshi and K. Tamura: Study on a procedure for formulating level 2 earthquake motion based on scenario earthquakes, Research Report of National Institute for Land and Infrastructure Management, No.15, 2003 (in Japanese with English abstract).
- 55) Esherby, J.D.: The determination of the elastic field of an ellipsoidal inclusion and related problems, Proc. Roy. Soc. Lond., Ser. A 241, pp.376-396, 1957.
- 56) Nozu, A.: A super asperity model for the 2011 off the Pacific coast of Tohoku earthquake, Journal of Japan Association for Earthquake Engineering, Vol.12, No.2, pp.21-40, 2012 (English translation is available in Vol.14, No.6).
- 57) Nozu, A. and A. Wakai: A source model for the 2011 off the Pacific coast of Tohoku, Japan, earthquake to explain strong ground motions, Report of the Port and Airport Research Institute, Vol.51, No.1, pp.23-53, 2012 (in Japanese with English abstract).
- 58) Irikura, K.: Recipe for predicting strong ground motion from future large earthquake, Annuals, Disaster Prevention Research Institute, Kyoto University, No.47A, pp.25-46, 2004 (in Japanese with English abstract).
- 59) Somerville, P.G., K. Irikura, R. Graves, S. Sawada, D. Wald, N. Abrahamson, Y. Iwasaki, T. Kagawa, N. Smith and A. Kowada: Characterizing crustal earthquake slip models for the prediction of strong ground motion, Seismological Research Letters, Vol.70, pp.59-80, 1999.
- 60) Irikura, K. and H. Miyake: Prediction of strong ground motions for scenario earthquakes, Journal of Geography, Vol.110, No.6, pp.849-875, 2001 (in Japanese with English abstract).
- 61) Irikura, K. and H. Miyake: Source modelling for prediction of strong ground motions, Chikyu Monthly, No.37, pp.62-77, 2002 (in Japanese).
- 62) Nozu, A.: An example of strong motion evaluation for a scenario earthquake with M_w 9.0 along the Nankai trough with the SPGA model, Journal of JSCE, A1, Vol.69, No.4, pp.I_872-I_888, 2013 (in Japanese with English abstract).
- 63) Nozu, A. and A. Wakai: Application of SPGA model to strong motion estimation for a scenario earthquake with M_w 9.0 along the Nankai trough, Technical Note of the Port and Airport Research Institute, No.1271, 2013 (in Japanese with English abstract).
- 64) Investigation Team for Modelling of Huge Subduction Earthquake along the Nankai Trough, Cabinet Office, Japan: On the seismic intensity distribution and tsunami heights due to an anticipated huge subduction earthquake along the Nankai trough, 1st report, http://www.bousai.go.jp/jishin/nankai/model/pdf/1st_report.pdf, 2012 (in Japanese).
- 65) Nozu, A., A. Wakai and Y. Nagasaka: Strong motion simulation for the 2011 off the Pacific coast of Tohoku earthquake – With considerations of soil nonlinearity –, Technical Note of the Port and Airport Research Institute, No.1284, 2014 (in Japanese with English abstract).
- 66) Takemura, M.: Magnitude-seismic moment relations for the shallow earthquakes in and around Japan, Zisin, 2nd series, Vol.43, pp.257-265, 1990 (in Japanese with English abstract).
- 67) Irikura, K.: Prediction of strong acceleration motions using empirical Green's functions, Proc. 7th Japan Earthq. Eng. Symp., pp.151-156, 1986.
- 68) Takemura, M. and T. Ikeura: A semi-empirical method using a hybrid stochastic and deterministic fault models: Simulation of strong ground motions during large earthquakes, J. Phys. Earth, Vol.36, pp.89-106, 1988.
- 69) Dan, K., T. Watanabe and T. Tanaka: A semi-empirical method to synthesize earthquake ground motions based on approximate far-field shear-wave displacement, Journal of Structural and Construction Engineering, AIJ, No.396, pp.27-36, 1989.
- 70) Kamae, K., K. Irikura and Y. Fukuchi: Prediction of strong ground motion based on scaling law of earthquake by stochastic synthesis method, Journal of Structural and Construction Engineering, AIJ, No.430, pp.1-9, 1991 (in Japanese with English abstract).
- 71) Kamae, K., K. Irikura and A. Pitarka: A technique for simulating strong ground motion using hybrid Green's function, Bulletin of the Seismological Society of America, Vol.88, pp.357-367, 1998.

- 72) Matsushima, S. and H. Kawase: Multiple asperity source model of the Hyogo-ken Nanbu earthquake of 1995 and strong motion simulation in Kobe, *Journal of Structural and Construction Engineering, AIJ*, No.534, pp.33-40, 2000 (in Japanese with English abstract).
- 73) Science and Technology Agency, Japan: Proceedings of the 1st Symposium on Investigation Results of Subsurface Structure of Sedimentary Basins, 2000 (in Japanese).
- 74) Kowada, A., M. Tai, Y. Iwasaki and K. Irikura: Evaluation of horizontal and vertical strong ground motions using empirical site-specific amplification and phase characteristics, *Journal of Structural and Construction Engineering, AIJ*, No.514, pp.97-104, 1998 (in Japanese with English abstract).
- 75) Boore, D.M.: Stochastic simulation of high-frequency ground motions based on seismological models of the radiated spectra, *Bulletin of the Seismological Society of America*, Vol.73, pp.1865-1894, 1983.
- 76) Brune, J.N.: Tectonic stress and the spectra of seismic shear waves from earthquake, *J. Geophys. Res.*, Vol.75, pp.4997-5009, 1970.
- 77) Brune, J.N.: Correction, *J. Geophys. Res.*, Vol.76, p.5002, 1971.
- 78) Satoh, T. and Y. Tatsumi: Source, path and site effects for crustal and subduction earthquakes inferred from strong motion records in Japan, *Journal of Structural and Construction Engineering, AIJ*, No.556, pp.15-24, 2002 (in Japanese with English abstract).
- 79) Tsurugi, M., S. Sawada, M. Miyajima and M. Kitaura: Re-estimation of site amplification effects in Kansai region, *Journal of Structural Engineering*, Vol.48A, pp.577-586, 2002 (in Japanese with English abstract).
- 80) Kato, K.: Evaluation of source, path, and site amplification factors from the K-NET strong motion records of the 1997 Kagoshima-ken-hokuseibu earthquakes, *Journal of Structural and Construction Engineering, AIJ*, No.543, pp.61-68, 2001 (in Japanese with English abstract).
- 81) Iwata, T. and K. Irikura: Separation of source, propagation and site effects from observed S-waves, *Zisin*, 2nd series, Vol.39, pp.579-593, 1986 (in Japanese with English abstract).
- 82) Irikura, K., T. Kagawa and H. Sekiguchi: Revision of the empirical Green's function method by Irikura (1986), *Programme and Abstracts, The Seismological Society of Japan*, B25, 1997 (in Japanese).
- 83) Aki, K. and P.B. Richards: *Quantitative Seismology*, Second Edition, University Science Books, 2002.
- 84) Miyake, H., T. Iwata and K. Irikura: Source characterization for broadband ground-motion simulation: kinematic heterogeneous source model and strong motion generation area, *Bulletin of the Seismological Society of America*, Vol.93, pp.2531-2545, 2003.
- 85) The Research Group for Theoretical Ground Motions: *Earthquake Ground Motions – Synthesis and Analysis*, Kajima Institute Publishing, 1994 (in Japanese).
- 86) Nozu, A., T. Annaka, Y. Sato and T. Sugano: Characteristics of ground motions observed at Haneda Airport (First report) Characteristics of surface waves, *Technical Note of the Port and Airport Research Institute*, No.1022, 2002 (in Japanese with English abstract).
- 87) Nozu, A., H. Takahashi and T. Endoh: Apparent velocity of seismic waves traveling along shield tunnel evaluated based on earthquake observation, *Journal of JSCE, A1*, Vol.66, No.1, pp.61-72, 2010 (in Japanese with English abstract).

2 Crustal Deformations

When a large earthquake occurs, the fault movement causes an elastic crustal deformation and may result in a permanent displacement of the ground in a large surrounding area. This is called a crustal deformation.

The displacement can include horizontal and vertical components and the latter can be in the upward or downward directions depending on the direction of the fault movement and the relative location of the construction site with respect to the fault. In recent years, a subsidence of 1.2 m occurred in the Oshika Peninsula during the 2011 Tohoku earthquake¹⁾. During the 1707 Hoei earthquake, downtown Kochi suffered a subsidence of 2 m at maximum, while in Murotsu, an uplift of 1.8 m occurred and the port became unable to accommodate large ships²⁾.

Regarding crustal deformations due to an earthquake, the following issues should be considered upon necessity.

- ① If an uplift associated with a crustal deformation occurs at a port, a shortage can occur in the water depth of a high seismic resistant quay wall for emergency transport. Therefore, when a high seismic resistant quay wall for emergency transport is planned at a port where the occurrence of a huge subduction earthquake is anticipated, it is preferable to plan the quay wall so that it can maintain a sufficient water depth after the occurrence of the uplift by carefully examining the possibility and amount of the uplift. The same applies to related waterways and basins.
- ② If a subsidence associated with a crustal deformation occurs at a port, a shortage can occur in the height of a revetment or a coastal dike that constitutes part of countermeasures against a tsunami. In addition, an increase can occur in the tsunami force. Therefore, when those facilities are constructed at a port where the occurrence of a huge subduction earthquake is anticipated, it is preferable to plan those facilities so that they can maintain a sufficient height after the occurrence of the subsidence and to consider possible increase in the tsunami force due to the subsidence upon necessity, based on sufficient study on the possibility and amount of the subsidence.

Although the direction and amount of the permanent displacement associated with a crustal deformation can be calculated numerically considering the location and size of the anticipated earthquake, they can also be determined by referring to the amount of permanent displacements during large historical earthquakes in the region. For example, the amount of the uplift and subsidence during past great earthquakes along the Nankai trough is reported by Usami²⁾.

However, historical data is not always available at a given port. In addition, huge subduction earthquakes greater than regional historical earthquakes are considered in tsunami simulations more often than ever. Therefore, it is necessary to numerically calculate the permanent displacement associated with the crustal deformation if historical data is not available at the port under consideration or a huge subduction earthquake greater than regional historical earthquakes is considered. For this calculation, the analytical solution for the elastic deformation of a half space³⁾ is often used. A computer program for this calculation is provided by the National Research Institute for Earth Science and Disaster Resilience, Japan⁴⁾. It is important to make sure that the hypothesized slip distribution for the calculation of the permanent displacement is consistent with that assumed for the tsunami simulations. For anticipated great earthquakes along the Nankai trough, the direction and amount of the permanent displacements associated with a crustal deformation are also hypothesized by the Cabinet Office and are available for the design.

Permanent displacements associated with postseismic crustal deformations, which gradually occur for years after the occurrence of a great earthquake, can be in an opposite direction to those associated with coseismic crustal deformations, which occur at the moment of the earthquake. For example, in the Oshika Peninsula, in the five years following the 2011 Tohoku earthquake, an uplift equivalent to approximately 40% of the coseismic subsidence occurred⁵⁾. This tendency was due to the fact that, while the coseismic slip occurred relatively offshore, the postseismic slip occurred near the coast. It should be noted that the tendency can be significantly region dependent; it is not reasonable to assume the same tendency for different regions.

[References]

- 1) Geospatial Information Authority of Japan: Crustal deformations observed at continuously operating GNSS reference stations, Information regarding the 2011 Tohoku earthquake, <https://www.gsi.go.jp/chibankansi/chikakukansi40005.html>, 2011(in Japanese).
- 2) Usami, T.: Materials for Comprehensive List of Destructive Earthquakes in Japan, [416]-2001, Latest Edition, University of Tokyo Press, 2003 (in Japanese).
- 3) Okada, Y.: Surface deformation due to shear and tensile faults in a half-space, Bull. Seism. Soc. Am., Vol.75, pp.1135-1154, 1985.

- 4) National Research Institute for Earth Science and Disaster Resilience, Japan: Program to calculate deformation due to a fault model DC3D0/DC3D, http://www.bosai.go.jp/study/application/dc3d/DC3Dhtml_E.html.
- 5) Geospatial Information Authority of Japan: Observation results by the GEONET, Five years after the 2011 Tohoku earthquake, http://www.gsi.go.jp/kanshi/h23tohoku_5years.html, 2016 (in Japanese).

3 Seismic Actions

3.1 Modeling of Soil-structure System and Seismic Actions

In the following, various analysis methods for the performance verification of port structures against earthquakes and associated seismic actions will be explained.

First, the difference of “earthquake ground motions” and “seismic actions” will be explained based on the descriptions in ISO23469¹⁾. Earthquake ground motions can exist where there is no structure, however, seismic actions can only exist when there is a structure. For example, an inertia force acting on a deck of a pile-supported wharf, which is an example of a seismic action, can only exist when there is a deck. Similarly, a seismic earth pressure acting on a wall, which is also an example of a seismic action, can only exist when there is a wall.

According to ISO23469¹⁾, “seismic actions” can be differently defined for the same structure depending on the analysis method. For example, if a “caisson” is considered and its stability against sliding is examined as in **Fig.3.1.1 (a)**, the external forces acting on the caisson such as the inertia force, the seismic earth pressure and the hydrodynamic pressure can be defined as the seismic actions. However, if the response of a soil-structure system composed of a caisson, backfill soils, foundation soils and sea water is analyzed as in **Fig. 3.1.1 (b)**, the seismic earth pressure and the hydrodynamic pressure are not seismic actions; they are obtained as a result of the response analysis. In this case, the seismic actions are the earthquake ground motions specified at the bottom of the analysis domain. In both **Figs.3.1.1 (a)** and **(b)**, the analysis domain is shown by the shaded area and the “seismic actions” are defined at its boundary.

If part of a soil-structure system is considered as in **Fig. 3.1.1 (a)**, the analysis is called a simplified analysis. If the response of a whole system is considered as in **Fig.3.1.1 (b)**, the analysis is called a detailed analysis (**Table 3.1.1**). Each of these analyses involves static and dynamic analyses. As a result, analysis methods for the performance verification against earthquakes can be classified into $2 \times 2 = 4$ categories (**Table 3.1.1**). Among various analysis methods below, the seismic coefficient method, the modified seismic coefficient method and the seismic displacement method can be categorized as static simplified analyses. The earthquake response analyses of a soil-structure system such as the effective stress analyses can be categorized as dynamic detailed analyses.

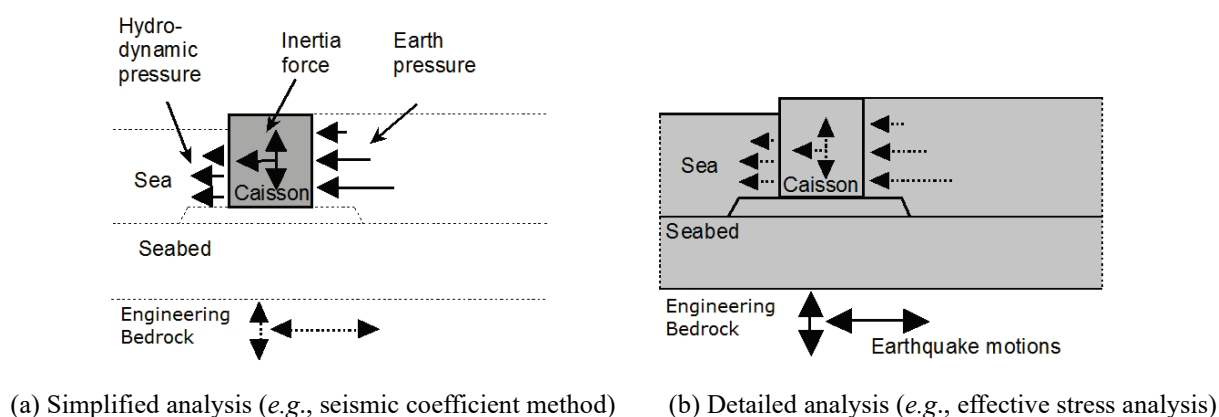


Fig. 3.1.1 Seismic actions in a simplified and detailed analysis

Table 3.1.1 Various analysis methods for the performance verification of port structures against earthquakes

	Simplified analysis	Detailed analysis
Static analysis	Static simplified analysis - Seismic coefficient method (3.2) - Modified seismic coefficient method (3.3) - Seismic displacement method (3.4)	Static detailed analysis - Static analysis of a soil-structure system
Dynamic analysis	Dynamic simplified analysis - Newmark method	Dynamic detailed analysis - Earthquake response analysis of a soil-structure system (3.5) (e.g., effective stress analysis)

3.2 Seismic Actions for Seismic Coefficient Method²⁾

Assume a rigid body on a rigid ground as shown in **Fig. 3.2.1**. Let m and $W (=mg)$ denote the mass and the weight of the rigid body, respectively, where g stands for the acceleration of gravity. When the ground moves with a rightward acceleration of α , the body will be subject to a leftward inertia force of $m\alpha$. In order for the rigid body not to slide, a friction force of $m\alpha$ should act at the bottom of the rigid body. If the static friction coefficient at the bottom is not sufficiently large, a sliding occurs and often results in a residual displacement, although the occurrence of the residual displacement could depend on the change of the acceleration afterwards. The occurrence of the sliding can be examined by applying a static force of $m\alpha$ on the rigid body. This is the basic idea of the seismic coefficient method.

The inertia force F applied in the seismic coefficient method can be written as follows:

$$F = (\alpha/g)W \quad (3.2.1)$$

By replacing α/g with k_h , one obtains the following expression:

$$F = k_h W \quad (3.2.2)$$

The equation implies that, if the weight is multiplied by the coefficient k_h , it yields the inertia force due to the earthquake ground motion. The coefficient k_h is called the “seismic coefficient”. The seismic coefficient determined for the performance verification of a structure is called the “seismic coefficient for performance verification”. The “seismic coefficient” is completely different from the “seismic intensity” announced by the Japan Meteorological Agency, although they are both pronounced in the same way as “shindo” in the Japanese language.

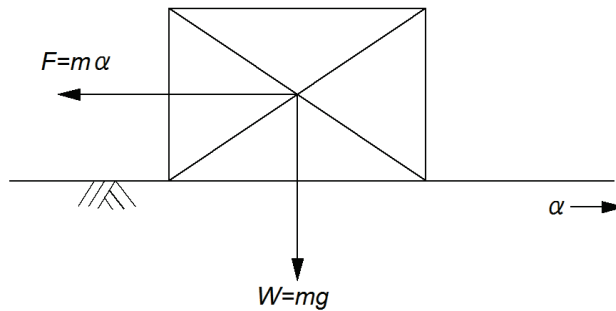


Fig. 3.2.1 Concept of seismic coefficient method

The seismic coefficient method was proposed in 1916 by Sano³⁾. According to the categorization in **Part II, Chapter 6, 3.1 Modeling of Soil-structure System and Seismic Actions**, the seismic coefficient method can be categorized as a static simplified analysis. The method has widely been used not only for port structures but also for other structures because, in the method, the problem of the seismic stability of a structure can be easily analyzed by replacing it with a problem of the equilibrium of static forces. For port structures, the method is used for the performance verification of gravity quay walls, sheet-pile quay walls, cell-type quay walls, etc. for level-1 ground motions. When the method is applied to a gravity quay wall, in addition to the inertia force on the wall, the seismic earth pressure and the hydrodynamic pressure should be considered as shown in **Fig.3.1.1 (a)**.

In the performance verification for a level-1 ground motion, if the ratio of the peak ground acceleration with respect to the acceleration of gravity is selected as the seismic coefficient, the value of the seismic coefficient will become much larger than the values usually used in the design. In fact, it is not necessary to directly adopt the ratio as the seismic coefficient. For example, if $\alpha = 215$ Gal, **equation (3.2.1)** yields $k = 0.22$. However, it is empirically known^{2,4)} that a ground motion exceeding 215 Gal does not necessarily cause a residual displacement to a quay wall designed with a seismic coefficient of 0.22. This is presumably due to the fact that, even if the quay wall is subject to a ground motion exceeding 215 Gal, as long as the duration of the action is short, it will not cause any visible residual displacement of the quay wall. The conversion method from the acceleration time history of a level-1 ground motion to the seismic coefficient for performance verification depends on the type of the structure. Details can be found in **Reference (Part III), Chapter 1, 1 Details of Seismic Coefficient for Performance Verification**.

The seismic coefficient method generally assumes that the backfill and foundation soils of a wall do not liquefy. The seismic earth pressures and the material properties of the foundation soils are given based on this assumption. Therefore, if the performance verification for a level-1 ground motion is conducted with the seismic coefficient method,

the possibility of liquefaction of the backfill and foundation soils should be assessed and, if the occurrence of liquefaction is anticipated, countermeasures against liquefaction should be taken (see **Part II, Chapter 7, Liquefaction**).

Because of the basic concept of the seismic coefficient method, it can assess the occurrence of the deformation of a structure following a few prescribed modes such as sliding, overturning and instability of the foundation soil based on the equilibrium of static forces, however, the method cannot estimate the amount of residual deformation once it occurs. Because of this limitation of the seismic coefficient method, it is not realistic to apply the seismic coefficient method to a level-2 ground motion. In general, for a very strong ground motion such as a level-2 ground motion, under the premise that certain amount of damage is inevitable, the performance of an infrastructure should be assessed considering the damage process⁵⁾⁶⁾. The same applies to a port facility such as a mooring facility; for a level-2 ground motion, under the premise that certain amount of residual deformation occurs, a facility should be designed so that the amount of deformation does not exceed a prescribed allowable value. To meet such requirements, instead of simplified analyses based on the seismic coefficient method, earthquake response analyses of a soil-structure system should be conducted as explained later.

3.3 Seismic Actions for Modified Seismic Coefficient Method²⁾

The seismic coefficient method assumes that the ground and the structure move together as shown in **Fig. 3.2.1**, however, in the case of a flexible structure, the acceleration of the structure α' does not coincide with that of the ground α as shown in **Fig. 3.3.1**. In this case, once the dynamic characteristics of the structure such as the natural period and the time history of the ground acceleration are given, the time history of the response acceleration can be calculated and, by applying a static force equivalent to the peak response acceleration multiplied by the mass m to the structure, the seismic design can be conducted by replacing actual dynamic phenomena with the equilibrium of static forces. The seismic coefficient method thus expanded to a flexible structure is called the “modified seismic coefficient method”. Once the time history of a ground acceleration is given, the time history of the response acceleration can be calculated for structures with various natural periods and the peak response acceleration can be plotted as a function of the natural period. This plot is called a “spectral acceleration”.

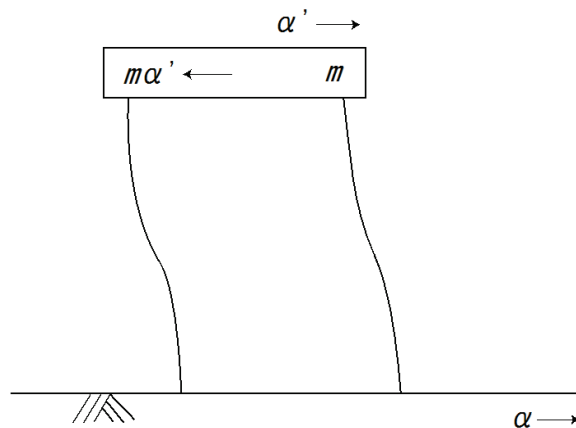


Fig. 3.3.1 Concept of modified seismic coefficient method

According to the categorization in **Part II, Chapter 6, 3.1 Modeling of soil-structure system and seismic actions**, the modified seismic coefficient method can be categorized as a static simplified analysis. In the modified seismic coefficient method, a linear restoring force is often assumed to calculate the response of the structure. However, when the structure is subject to a very strong ground motion, the restoring force of the structure shows a nonlinear behavior due to the yielding of its members. In that case, the response acceleration calculated by assuming a linear response becomes meaningless. Thus, the modified seismic coefficient method is not suitable for a very strong ground motion such as a level-2 ground motion.

3.4 Seismic actions for seismic displacement method²⁾

In designing a long structure with less apparent density and rigidity such as a buried pipeline or a submerged tunnel, the acceleration induced in the structure is less important in the design. Because of its less density and rigidity, its existence has little effects on the displacement of the surrounding ground; the displacement of the structure tends to be governed by the displacement of the ground. If the displacement of the ground is not uniform, strain is induced in the structure, which becomes an important issue in the design.

In the seismic displacement method, first, the displacement of the ground is calculated without considering the existence of the structure. Next, the displacement and stress of the structure are calculated by assuming that the displacement of the structure follows that of the ground. Thus, in contrast to the seismic coefficient method where a static force is applied to a structure as a seismic action, in the seismic displacement method, the displacement of the ground is applied to a structure as a seismic action. If the rigidity of the structure is slightly large, the assumption that the displacement of the structure follows that of the ground may lead to an error. In that case, the displacement of the ground is applied to a structure via springs. According to the categorization in **Part II, Chapter 6, 3.1 Modeling of Soil-structure System and Seismic Actions**, the seismic displacement method can be categorized as a static simplified analysis.

3.5 Seismic Actions for Earthquake Response Analysis of Soil-structure System

In each of the above mentioned methods, the actual phenomena are more or less simplified. However, earthquake response analyses are sometimes conducted aimed at examining a more realistic response of a soil-structure system. This type of analysis can be categorized as a dynamic detailed analysis according to the categorization in **Part II, Chapter 6, 3.1 Modeling of Soil-structure System and Seismic Actions**. Earthquake response analyses of a soil-structure system are often based on finite element analyses, especially on effective stress analyses as shown in **Fig. 3.5.1**. In this case, the seismic actions are the earthquake ground motions specified at the bottom of the analysis domain.

In general, the ground motion at the bottom of the analysis domain is the sum of the upcoming (E) and downgoing (F) waves. There are two methods to specify the ground motion at the bottom of the analysis domain: One is to specify the ground motion to be observed at the bottom of the analysis domain (E+F). The other is to specify the incident wave impinging at the bottom of the analysis domain multiplied by 2 (2E). In the event of reproducing actual damage in a past earthquake or reproducing the results of shake table tests, the observed ground motion at the bottom of the analysis domain including the effects of the upcoming and downgoing waves (E+F) may be available. In that case the E+F wave can be specified. However, in an earthquake response analysis of a soil-structure system for the performance verification of a structure, a 2E wave should be specified. If the analysis domain is just above the engineering bedrock, the ground motion obtained in **Part II, Chapter 6, 1 Earthquake Ground Motions** can be directly used. However, if the analysis domain is not in contact with the engineering bedrock, the ground motion defined at the engineering bedrock should be converted to a 2E wave just below the analysis domain by conducting an earthquake response analysis of the ground and used.

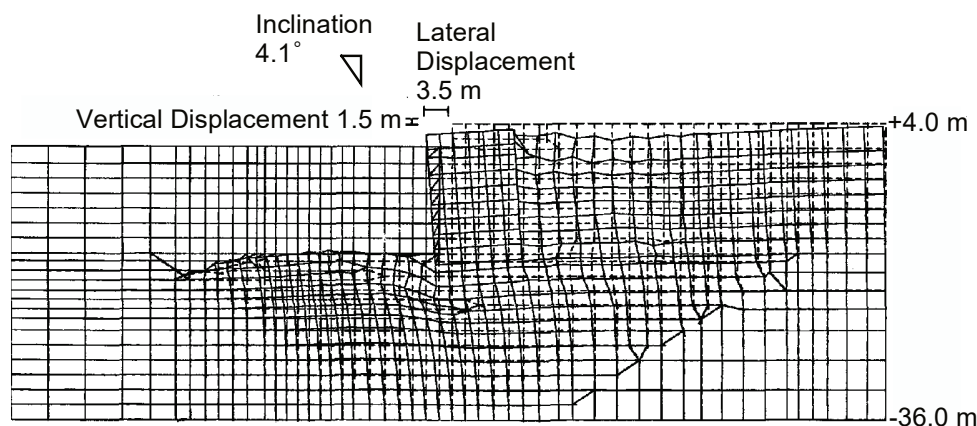


Fig. 3.5.1 Deformation of a gravity quay wall calculated by an effective stress analysis

[References]

- 1) International Organization for Standardization: ISO23469, Bases for design of structures - Seismic actions for designing geotechnical works, 2005.
- 2) Tsuchida, H. and S. Iai: Earthquake Engineering for Practitioners, Sankaido, 1991 (in Japanese).
- 3) Sano, R.: Earthquake resisting structure of houses, Reports of the Imperial Earthquake Investigation Committee, Vol.83, 1916 (in Japanese).
- 4) Noda, S., T. Uwabe and T. Chiba: Relation between seismic coefficient and ground acceleration for gravity quaywall, Report of the Port and Harbour Research Institute, Vol.14, No.4, pp.67-111, 1975 (in Japanese with English abstract).
- 5) Japan Society of Civil Engineers: Proposal on seismic design standards for infrastructures, 1996 (in Japanese).
- 6) Japan Society of Civil Engineers: Proposal and commentary on seismic design standards for infrastructures: the third proposal, 2000 (in Japanese).

Chapter 7 Ground Liquefaction

[Public Notice] (Ground Liquefaction)

Article 17

Ground liquefaction shall be assessed with appropriate methods based on ground conditions in consideration of the actions due to the earthquake ground motion.

[Interpretation]

7. Setting of Natural Conditions

(6) Subjects related to the earthquake (Article 6 of the Ministerial Ordinance and the interpretation related to Article 16 and 17 of the Public Notice)

⑧ Ground Liquefaction

a) Effects of Liquefaction in the Case of Level 1 Earthquake Ground Motions

For ground liquefaction in the case of Level 1 earthquake ground motions, measures against ground liquefaction are basically taken when liquefaction is predicted and assessed to occur by taking into account the effects of liquefaction on structures, surrounding situations of the target facilities, etc.

b) Effects of Liquefaction in the Case of Level 2 Earthquake Ground Motions

For the consideration of ground liquefaction in the case of Level 2 earthquake ground motions, the methods of taking measures against liquefaction and the necessity of their implementation are determined on the basis of a comprehensive consideration of the situations of the facilities surrounding the target facilities.

1 General

The subjects described in this chapter may refer to the *Handbook of Liquefaction Measures Works for Reclaimed Land* (Revised Edition).¹⁾

The following methods are basically for the consideration of ground liquefaction in the case of Level 1 earthquake ground motions. When liquefaction is predicted and assessed to occur by applying the following methods to the Level 1 earthquake ground motions, consider the effects on structures, and take the liquefaction countermeasure works in principle. The option to not perform liquefaction countermeasure works may be taken as long as there are strict restrictions in construction, such as the improvement of existing facilities. In that case, pay attention to the fact that the commonly used earth pressure formula, calculation equation for the modulus of subgrade reaction, bearing capacity formula, and others cannot be applied. Furthermore, the method of performance verification should be examined by considering the effect of liquefaction.

For the consideration of ground liquefaction in the case of Level 2 earthquake ground motions, careful consideration is needed because the equivalent linear analysis shown in **2(3)②** below may become an unsafe side evaluation for a certain ground composition when the strain level is high. Moreover, the methods of liquefaction countermeasure works and the necessity of their implementation shall be determined on the basis of a comprehensive consideration of the situations of the facilities surrounding the target facilities. Refer to the description on the performance verification of facilities in **[Action] Chapter 6 Earthquakes and Facilities**.

2 Prediction and Assessment of Liquefaction

- (1) The prediction and assessment of whether the ground is liquefied are generally performed by proper methods using grain sizes and *SPT-N* values or using the results of cyclic triaxial compression tests. **Figs. 2.1.1** and **2.1.2** show the basic prediction and assessment procedure of liquefaction and the prediction and assessment procedure with the grain size and *SPT-N* value.

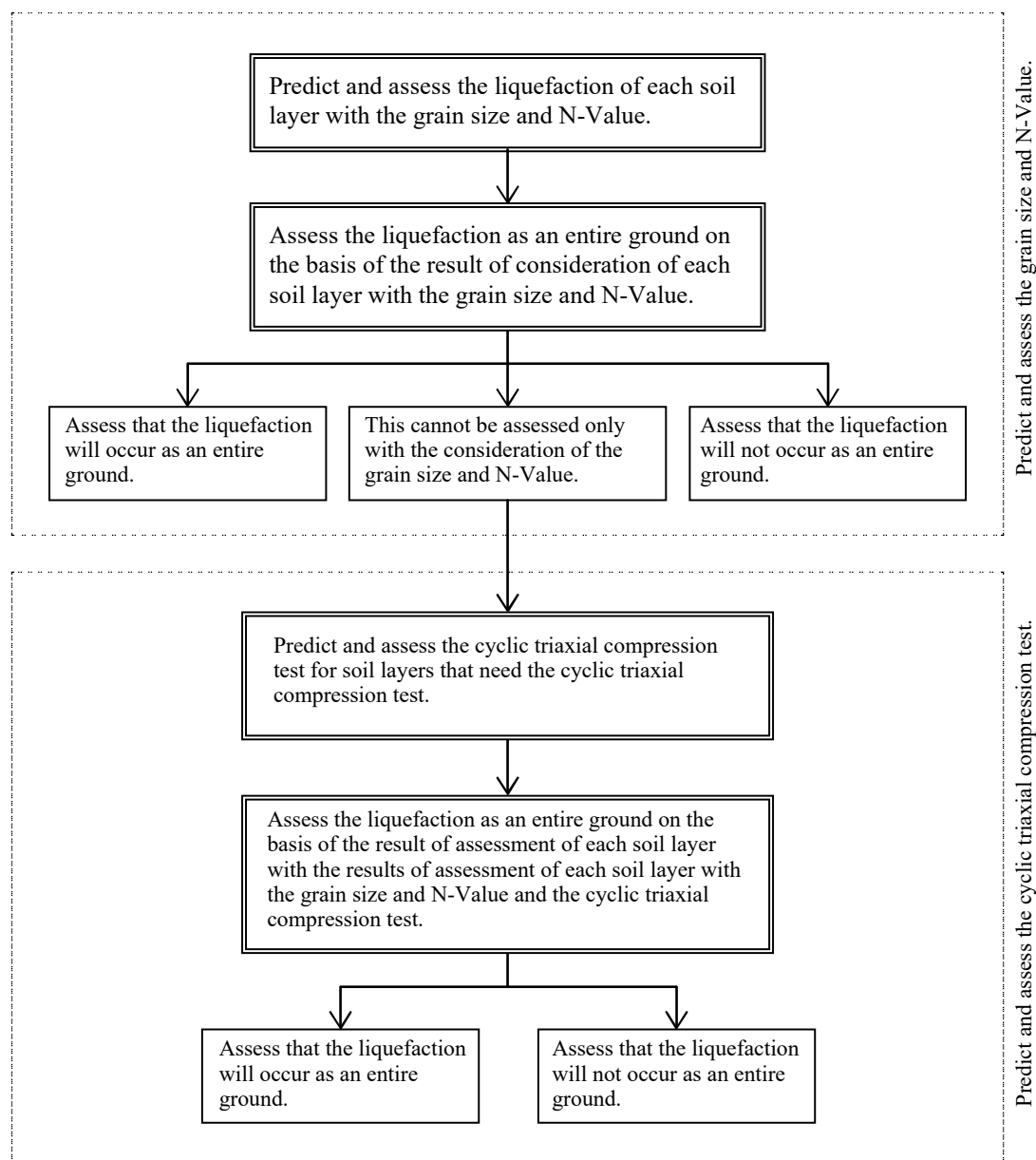


Fig. 2.1.1 Basic Prediction and Assessment of Liquefaction

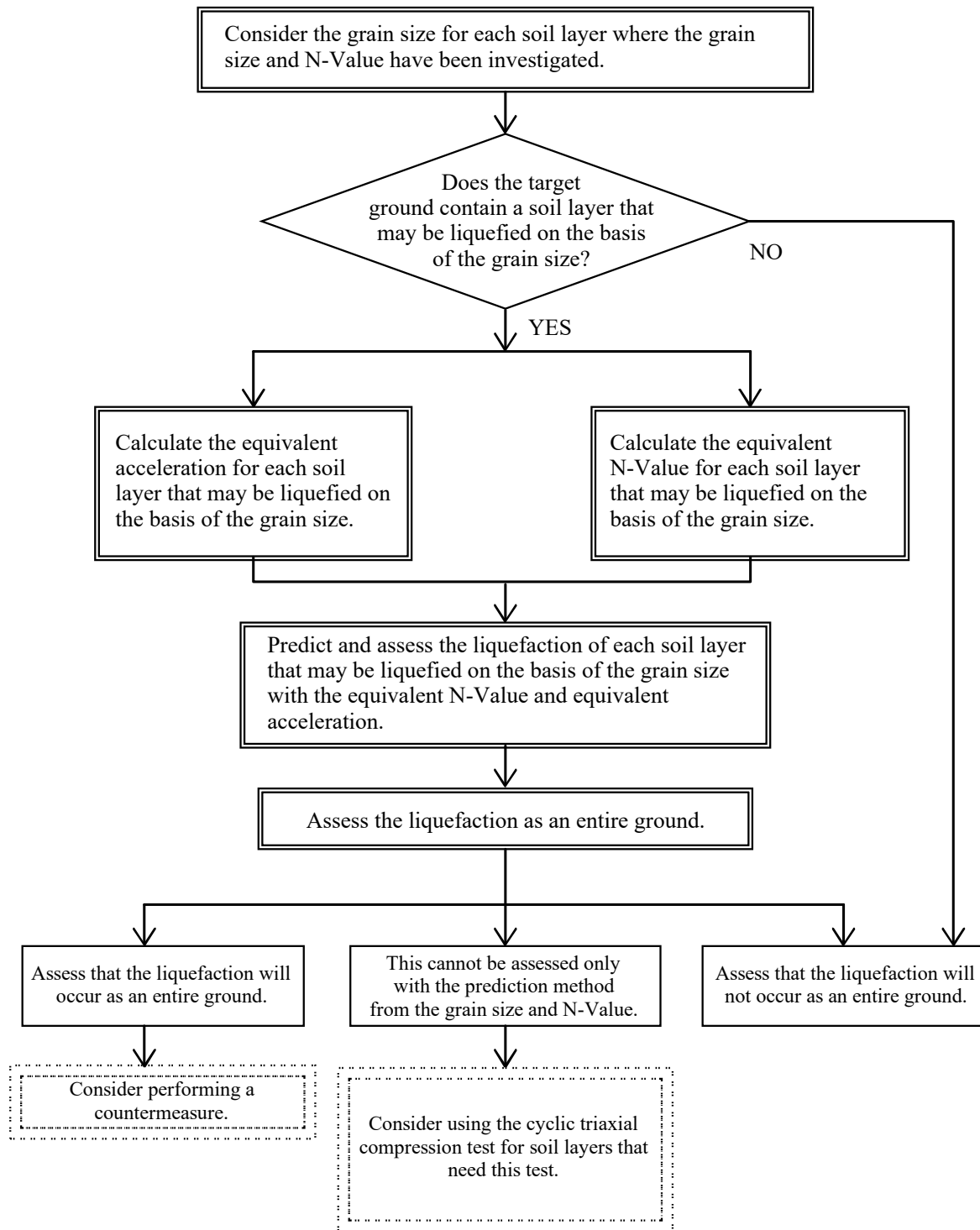


Fig. 2.1.2 Prediction and Assessment Procedure with the Grain Size and *SPT-N* value

(2) Types of Prediction and Assessment of Liquefaction

Liquefaction prediction and assessment methods include the method using grain sizes and *SPT-N* values or the method using the results of cyclic triaxial compression tests. The method using grain sizes and *SPT-N* values is simple and easy and can be generally used for predicting and judging liquefaction. The method using the results of cyclic triaxial compression tests is more detailed and can be used when the prediction and assessment using grain sizes and *SPT-N* values are difficult or when more detailed considerations are needed.

(3) Prediction and Assessment of Liquefaction Using Grain Size and *SPT-N* values²⁾

① Assessment based on grain size

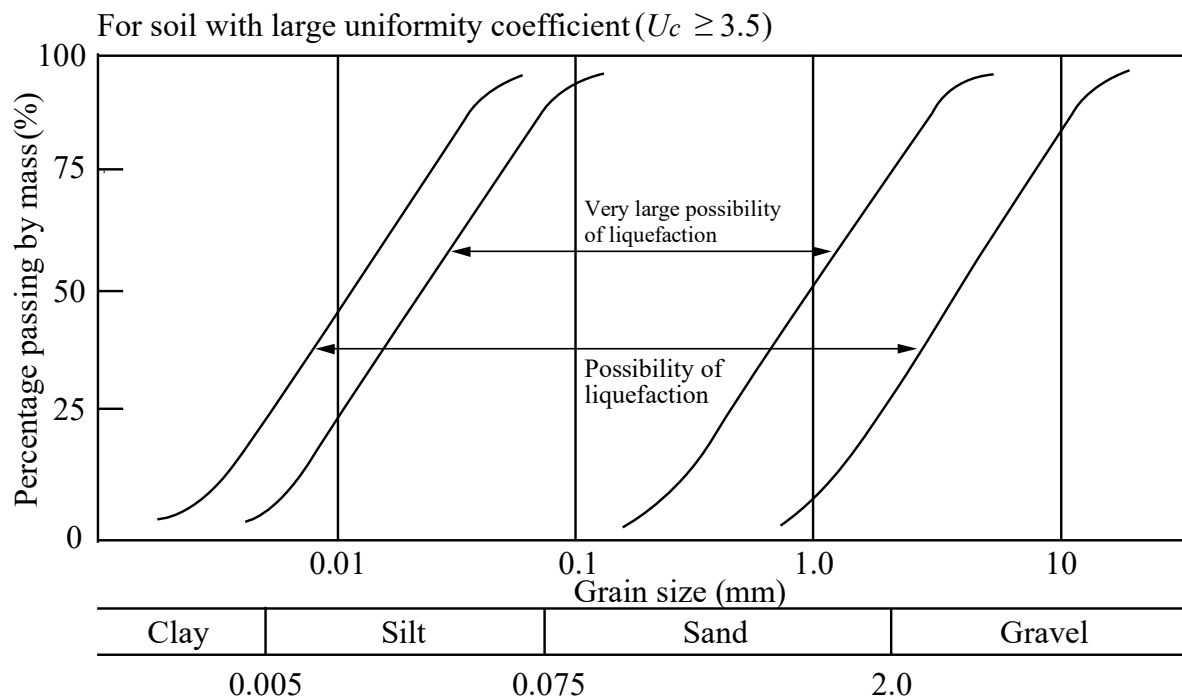


Fig. 2.1.3(a) Range of Possible Liquefaction ($U_c \geq 3.5$)

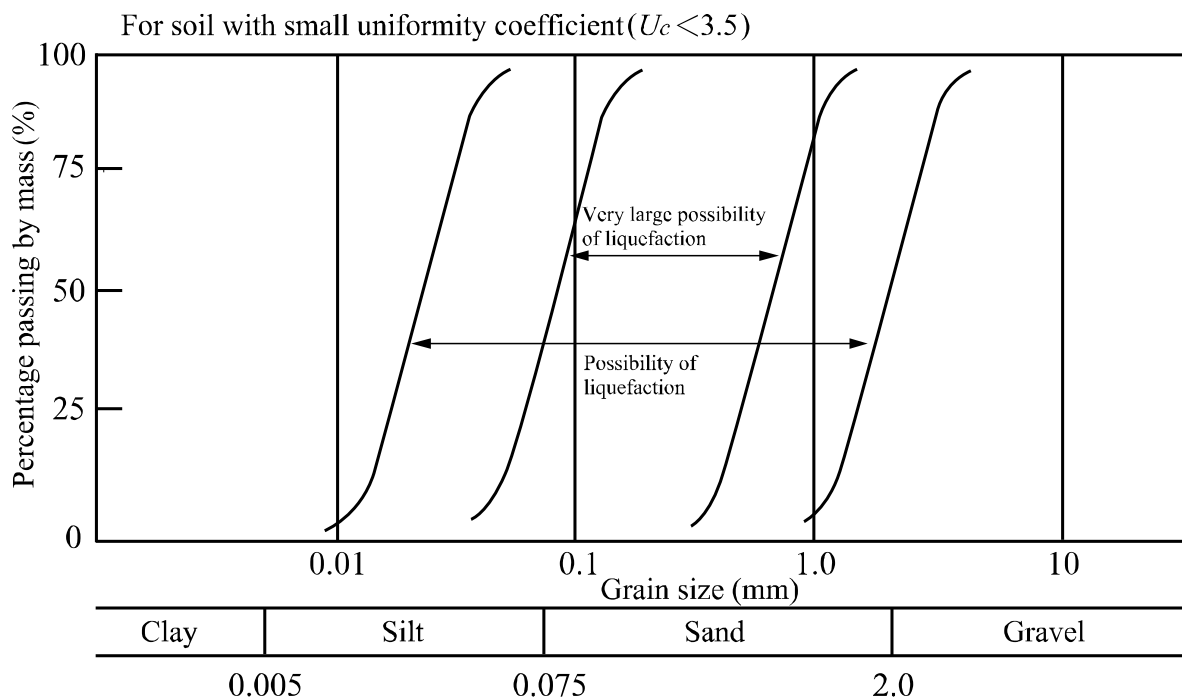


Fig. 2.1.3(b) Range of Possible Liquefaction ($U_c < 3.5$)

The soil shall be classified by grain size by using **Fig. 2.1.3**, which shall be used according to the multitude of the uniformity coefficient. The standard of the multitude of uniformity coefficient is $U_c = D_{60}/D_{10} = 3.5$, where U_c is the uniformity coefficient, D_{60} is the 60% diameter, and D_{10} is the effective diameter (10% diameter). Soil is assessed to not liquefy when its grain size accumulation curve is not included in the “possibility of liquefaction” range.

If the classification is difficult (for example, when the grain size accumulation curve spans the “possibility of liquefaction” range), proper countermeasures, such as the use of a prediction and assessment method via a cyclic triaxial compression test, is needed for soil with a large clay portion. For soil with a large gravel portion, the soil may be determined to not liquefy when the permeability factor is confirmed to be 3 cm/s or greater. When there are soil layers with poor permeability, such as clay or silt layers, on top of the target soil layer in this case, it should be treated as a type of soil that falls within the “possibility of liquefaction” range. A permeability test for the soil with a large coefficient of permeability of 3 cm/s shall be a special method.³⁾ A method of indirect estimation of a coefficient of permeability is available when the measurement of a coefficient of permeability is difficult.⁴⁾ However, when applying the indirect estimation method, careful consideration should be paid on the soil characteristics, such as content of fine particles.

② Prediction and assessment of liquefaction using equivalent *SPT-N* values and equivalent acceleration

For the soil layer with a grain size that falls within the range “possibility of liquefaction” shown in **Fig. 2.1.3**, further investigations should be based on the descriptions below.

(a) Equivalent *SPT-N* value

The equivalent *SPT-N* value should be calculated from **equation (2.1.1)**.

$$(N)_{65} = \frac{N - 0.019(\sigma_v' - 65)}{0.0041(\sigma_v' - 65) + 1.0} \quad (2.1.1)$$

where

$(N)_{65}$: equivalent *SPT-N* value

N : *SPT-N* value of the soil layer

σ_v' : effective overburden pressure of the soil layer (kN/m²)

(It should be noted that the effective overburden pressure used to calculate the equivalent *SPT-N* value should be calculated with respect to the ground elevation at the time of the standard penetration test.)

Fig. 2.1.4 shows the relationship given by **equation (2.1.1)**. When using **equation (2.1.7)**, the *SPT-N* values themselves of the soil layer are assumed to be equivalent *SPT-N* values.

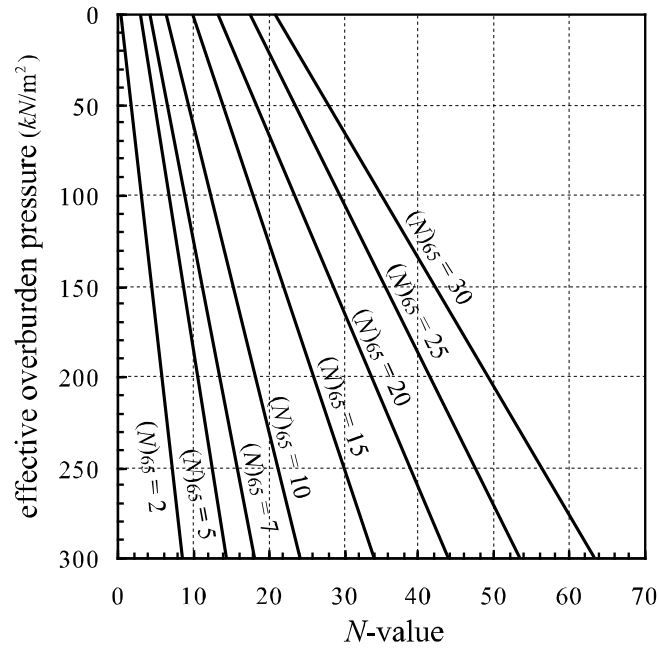


Fig. 2.1.4 Calculation Chart for an Equivalent *SPT-N* value

(The straight lines show the relationship between *SPT-N* values and effective overburden pressures when relative density and others are constant.)

(b) Equivalent acceleration

Equivalent accelerations are calculated from **equations (2.1.2) to (2.1.6)**. They are calculated for each soil layer by using the time history of the maximum shear stresses obtained from the seismic response calculation based on the equivalent linear analyses⁵⁾ of the ground.

$$\alpha_{eq} = 0.7 \cdot \frac{\tau_{max}}{\sigma_v'} \cdot g \cdot \frac{1}{c_\alpha} \quad (2.1.2)$$

$$c_\alpha = 5^{-d_1} \cdot n_{ef}^{d_1} \quad (2.1.3)$$

$$d_1 = 0.2 - 0.7 \cdot D_r \quad : \left(D_r \geq \frac{0.2}{0.7} \right) \quad (2.1.4)$$

$$d_1 = 0 \quad : \left(D_r < \frac{0.2}{0.7} \right) \quad (2.1.5)$$

$$D_r = 0.16 \cdot \sqrt{\frac{170 \cdot N}{70 + \sigma_v'}} \quad (2.1.6)$$

where

α_{eq} : equivalent acceleration (Gal)

τ_{max} : maximum shear stress (kN/m²)

g : gravitational acceleration (980 Gal)

c_α : wave correction coefficient⁶⁾⁻⁸⁾

(If the liquefaction is predicted and assessed by correcting the *SPT-N* value with the plasticity index described below, c_α shall be obtained by plugging in -0.3 for d_1 in **equation (2.1.3)**.)

d_1 : exponent of **equation (2.1.3)**

N_{ef} : effective number of waves ^{6)–8)}

(**Fig. 2.1.5** shows half of the number of wave crests, which is 60% or more of the maximum shear stresses in the time history of the shear stresses.)

N : *SPT-N* value

D_r : relative density

(If $D_r \leq 1.0$, this may be obtained from the *SPT-N* value and the effective overburden pressure at the time of *SPT-N* value measurement by using **equation (2.1.6)**.)

σ_v' : effective overburden pressure (kN/m²)

(Note that the effective overburden pressures used for calculating equivalent accelerations are obtained on the basis of the ground heights at the time of earthquakes, and the effective overburden pressures used for calculating relative densities are obtained on the basis of the ground heights at the time of the *SPT-N* value measurement.)

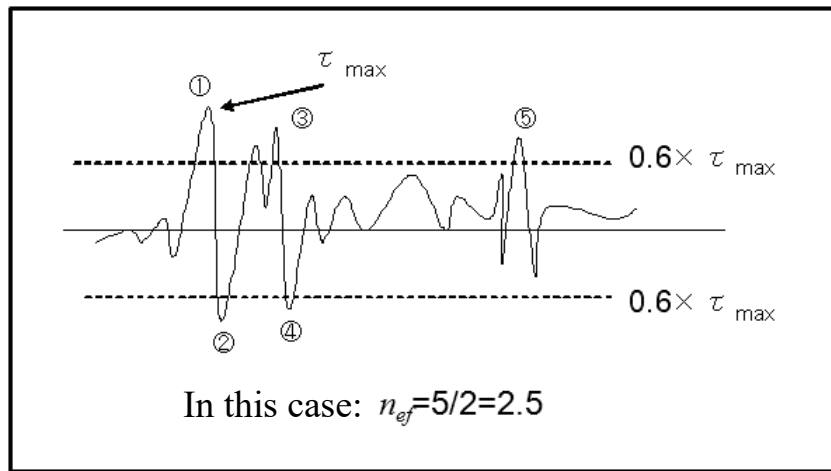


Fig. 2.1.5 Definition of the Effective Number of Waves N_{ef}

(c) Predictions and assessment using the equivalent *SPT-N* value and equivalent acceleration

It shall be assessed in which range (ranges I to IV in **Fig. 2.1.6**) the equivalent *SPT-N* value and equivalent acceleration of the target soil layer is contained.

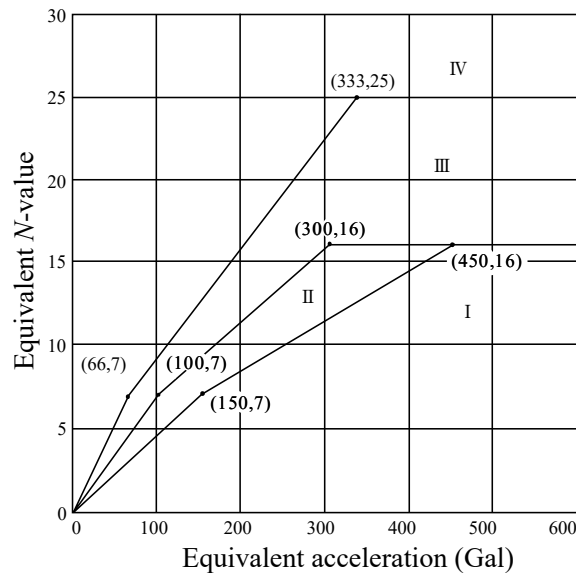


Fig. 2.1.6 Classification of Soil Layer with Equivalent *SPT-N* value and Equivalent Acceleration

③ **Correction of *SPT-N* values and prediction and assessment in cases with large fraction of fines content**

- (a) When the fines content, namely, grain size of 75 μm or less, is 5% or greater, the equivalent *SPT-N* value should be corrected, and the subject soil layer should be assessed to which range of I to IV in **Fig. 2.1.6** it falls into using the corrected equivalent *SPT-N* value. The correction of the equivalent *SPT-N* value is divided into the following three cases:
- 1) Case 1: when the plasticity index is less than 10 or cannot be determined or when the fines content is less than 15%
 - 2) Case 2: when the plasticity index is 10 or greater but less than 20, and the fines content is 15% or higher
 - 3) Case 3: when the plasticity index is 20 or greater, and the fines content is 15% or higher
- (b) Case 1: when the plasticity index is less than 10 or cannot be determined or when the fines content is less than 15%

The equivalent *SPT-N* value after correction should be set as $(N)_{65}/c_N$. The correction factor c_N is given in **Fig. 2.1.7**. The obtained equivalent *SPT-N* value after correction and the equivalent acceleration are used to determine the range in **Fig. 2.1.6**.

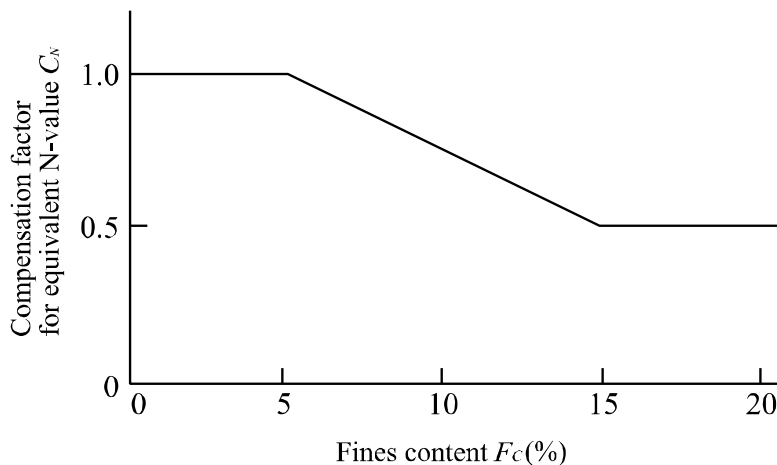


Fig. 2.1.7 Correction Factor of Equivalent *SPT-N* value Corresponding to Fines Content

- (c) Case 2: when the plasticity index is 10 or greater but less than 20, and the fines content is 15% or higher

The equivalent $SPT-N$ value after correction should be set as both $\{(N)_{65}/0.5\}$ and $\{N + \Delta N\}$, and the range should be determined according to the following situations, where ΔN is given by the following equation:

$$\Delta N = 8 + 0.4(I_p - 10) \quad (2.1.7)$$

- 1) When $\{N + \Delta N\}$ falls within range I, determine it to be in range I.
 - 2) When $\{N + \Delta N\}$ falls within range II, determine it to be in range II.
 - 3) When $\{N + \Delta N\}$ falls within range III or IV and when $\{(N)_{65}/0.5\}$ is within range I, II, or III, determine it to be in range III.
 - 4) When $\{N + \Delta N\}$ falls within range III or IV and when $\{(N)_{65}/0.5\}$ is within range IV, determine it to be in range IV.
- (d) Case 3: when the plasticity index is 20 or greater, and the fines content is 15% or higher

The equivalent $SPT-N$ value after correction should be set as $\{N + \Delta N\}$. The range should be determined according to the equivalent $SPT-N$ value after correction and the equivalent acceleration.

- (e) **Fig. 2.1.8** and **Table 2.1.1** show what was described in (b), (c), and (d) above in a figure and a table. **Table 2.1.1** shows a standard result of prediction by combining the prediction of the $SPT-N$ value corrected by the fines content and the prediction of the $SPT-N$ value corrected by the plasticity index.

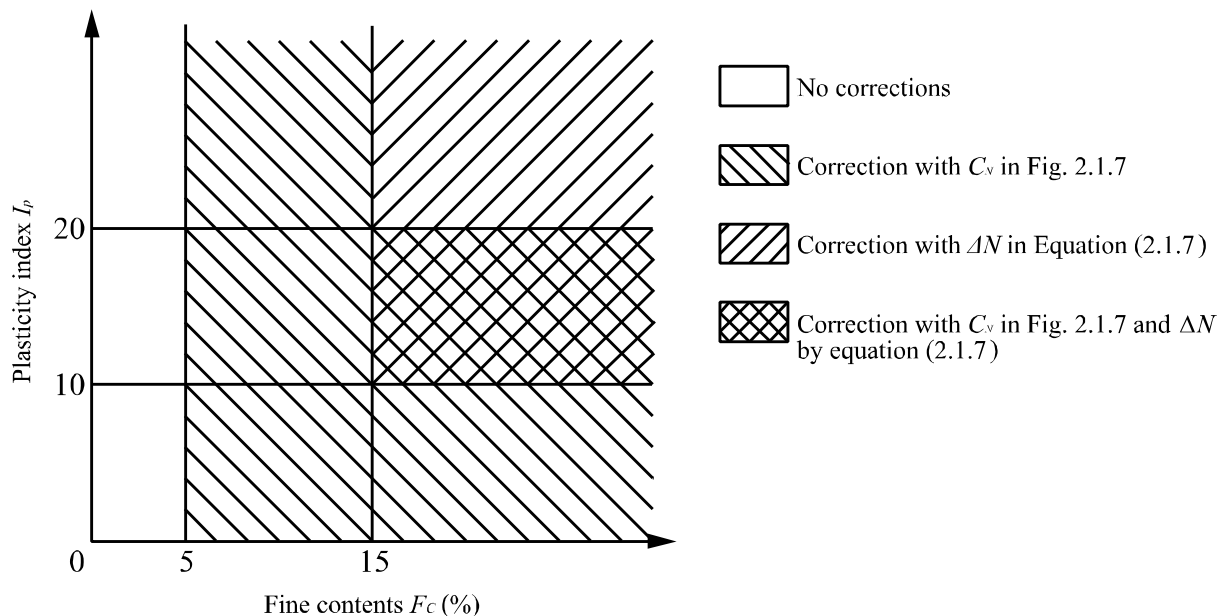


Fig. 2.1.8 $SPT-N$ value Correction Method and Relationship between Fines Content and Plasticity Index

Table 2.1.1(a) When the Plasticity Index Is Less than 10 or Cannot Be Obtained or When the Fines Content Is Less than 15%

		Correction with the fines content			
		I	II	III	IV
Correction with the plasticity index	—	I	II	III	IV
	—				
	—				
	—				

Table 2.1.1(b) When the Plasticity Index Is 10 or Greater but Less than 20 and
When the Fines Content Is 15% or Higher

		Correction with the fines content			
		I	II	III	IV
Correction with the plasticity index	I	I	II	III	IV
	II	II	II	II	II
	III	III	III	III	IV
	IV	III	III	III	IV

Table 2.1.1(c) When the Plasticity Index Is 20 or Greater and
When the Fines Content Is 15% or Higher

		Correction with the fines content			
		—	—	—	—
Correction with the plasticity index	I	I			
	II	II			
	III	III			
	IV	IV			

④ Prediction and assessment of liquefaction

The liquefaction shall be predicted and assessed for each soil layer by using **Table 2.1.2** according to the classification of I to IV soil layers in ② and ③. Given that liquefaction assessment also considers factors other than physical phenomena, such as the degree of safety anticipated for the target facilities, it is not possible to unambiguously set the assessments regarding each prediction result. **Table 2.1.2** shows the assessment that is considered standard for each result of the predictions.

In this table, the term “prediction of liquefaction” refers to the high or low possibility of liquefaction as a physical phenomenon. By contrast, the term “assessment of liquefaction” refers to the consideration of the high or low possibility of liquefaction and the determination of whether the target ground could liquefy. Therefore, it is necessary to consider factors other than physical phenomena, such as the degree of safety anticipated for the target facilities, when judging liquefaction.

Table 2.1.2 Prediction and Assessment of Liquefaction for Soil Layer According to Grain Size and *SPT-N* value

Range shown in Fig. 2.1.6	Prediction of liquefaction	Assessment of liquefaction
I	Possibility of liquefaction occurrence is very high	Liquefaction will occur
II	Possibility of liquefaction occurrence is high	Either to assess that liquefaction will occur or to conduct further evaluation based on cyclic triaxial compression tests.
III	Possibility of liquefaction is low	Either to assess that liquefaction will not occur or to conduct further evaluation based on cyclic triaxial compression tests. For a very important structure, either to assess that liquefaction will occur or to conduct further evaluation based upon cyclic triaxial tests.
IV	Possibility of liquefaction is very low	Liquefaction will not occur

(4) Application of Prediction and Assessment Methods of Liquefaction According to Grain Size and *SPT-N* values to Special Types of Soil

Special types of soil, such as shirasu, are known to have special characteristics that are different from common types of soil, on which the prediction and assessment methods with the grain size and *SPT-N* value are based. Therefore, it is preferable to conduct both of the predictions with the grain size and *SPT-N* value and with the cyclic

triaxial compression test at typical locations on a trial basis. Furthermore, confirm their consistency when applying the prediction and assessment methods with the grain size and *SPT-N* value.

(5) Prediction and Assessment Based on the Results of Cyclic Triaxial Compression Tests

- ① When it is not possible to predict and assess the occurrence of liquefaction of the subject ground from the results of grain size and *SPT-N* values, the prediction and assessment for ground liquefaction need to be made by conducting a seismic response calculation of the ground and cyclic triaxial compression tests on undisturbed soil samples.
- ② The proper consideration of the stress state in the ground, the irregularity of the actions caused by earthquake ground motions, and others is important in obtaining the results of the seismic response calculations of the ground and those of cyclic triaxial compression tests and in showing actual phenomena in the ground.

(6) Assessment of Overall Liquefaction of the Ground

In the assessment of overall ground liquefaction, the comprehensive decision should be made on the basis of the results of the assessment for each soil layer.

(7) Consideration for Continuous Earthquake Ground Motion

During continuous earthquake ground motion, such as the principal earthquake and aftershock, it should be noted that the sandy layer just below the clayey layer of the ground, particularly where cohesive soil interposes, may possibly liquefy during or after subsequent aftershocks depending on the ground composition even if it was predicted under the principal earthquake that there would be no liquefaction or the possibility of liquefaction was low. In this case, the occurrence of liquefaction can be predicted and assessed by linking this type of earthquake ground motion as a long-duration earthquake ground motion^{7) 8)} and by calculating the earthquake ground motion response.

(8) Worldwide use of the liquefaction prediction and assessment method

The liquefaction prediction and assessment method that is capable of considering the influence of the waveforms and durations of earthquakes has been generalized for overseas use⁸⁾. A unique feature of the new simplified method is its universality, allowing it to be applied to various types of liquefaction charts, facilitating more-rational liquefaction prediction and assessment worldwide. For details of the procedures, refer to Sassa and Yamazaki (2016)⁸⁾.

[References]

- 1) Coastal Development Institute of Technology (CDIT): Handbook of liquefaction of reclaimed land (Revised Edition), 1997 (in Japanese)
- 2) Yamazaki, H., K. Zen and F. Koike Study of the Liquefaction Prediction Based on the Grain Distribution and the SPT N-value, Technical Note of PHRI, No.914,1998 (in Japanese)
- 3) The Japan Geotechnical Society: Soil Testing Methods and Commentary, pp.271-288,2000 (in Japanese)
- 4) Japan Geotechnical Society: Geotechnical Engineering Handbook, pp.16-20,1999 (in Japanese)
- 5) Schnabel, P.B., Lysmer, J. and Seed, H.B.: SHAKE: A Computer Program for Earthquake Response Analysis of Horizontally Layered Sites” . Report No. UCB/EERC-72/12, Earthquake Engineering Research Center, University of California, Berkeley, 1972.
- 6) Yamazaki, H. and Emoto S.: Study on Liquefaction Prediction Method Considering Wave Forms of Seismic Motions, Report of the Port and Airport Research Institute, Vol. 49, No. 3, pp. 79-110, 2010 (in Japanese)
- 7) Sassa, S., Yamazaki, H. and Goto, Y.: A New Liquefaction Prediction and Assessment Method and Its Validation Considering Both Waveforms and Durations of Earthquakes, Journal of Japan Society of Civil Engineers, Ser. B3, Vol. 69, No. 2, pp. 143-148, 2013 (in Japanese)
- 8) Sassa, S. and Yamazaki, H.: Simplified Liquefaction Prediction and Assessment Method Considering Waveforms and Durations of Earthquakes, Journal of Geotechnical and Geoenvironmental Engineering, ASCE, DOI:10.1061/(ASCE) GT.1943-5606.0001597. 2016.

Chapter 8 Ships

[Public Notice] (Dimensions of Design Ships and Related Matters)

Article 18

- 1 The dimensions of design ships (hereinafter referred to as the ships used as the input data in the performance verification of the facilities subject to the technical standards) shall be set according to the methods prescribed respectively in the following items:
 - (1) In the case where design ships are identifiable, the dimensions of the design ships shall be used.
 - (2) In the case where design ships are unidentifiable, the dimensions shall be set appropriately based on the statistical analyses of the dimensions of ships in operation.
- 2 The actions from ship berthing, ship movements, and traction by ships shall be set according to the methods provided in the subsequent items in consideration of a single action or the combinations of two or more actions to be considered in the performance criteria and the performance verification of the facilities:
 - (1) The actions from ship berthing shall be set with appropriate methods in consideration of the dimensions of design ships, structures of the facilities, berthing methods, berthing velocities, etc.
 - (2) The actions from ship movements shall be set with appropriate methods in consideration of the dimensions of design ships, structures of the facilities, mooring methods, characteristics of mooring system, and the winds, waves, water currents, etc. acting on design ships.
 - (3) The actions from the traction by ships shall be set with appropriate methods in consideration of the dimensions of design ships, mooring methods, and the winds, waves, water currents, etc. acting on design ships.

[Interpretation]

7. Setting of Natural Conditions

- (7) **Items related to ships** (Article 6 of the Ministerial Ordinance and the interpretation related to Article 18 of the Public Notice)

① Principal dimension of design ships

Design ships are those, among the ships using the facilities concerned, assumed to have the most significant effects on the performance verification of the facilities. It shall be noted that design ships vary depending on the performance criteria to be applied even for the same facilities and that they are not always the ships with the largest gross tonnage.

② Actions due to ship berthing and traction by ships

(a) Actions caused by ship berthing

The actions caused by ship berthing on mooring facilities shall be properly considered. In setting the actions caused by ship berthing, ship berthing energy can be calculated using proper methods based on ship masses, ship berthing velocities, virtual mass factors, eccentricity factors, flexibility factors, and the berth configuration factors.

(b) Actions caused by ship movements

The actions caused by ship motions on mooring facilities shall be properly considered as needed. Proper methods to be considered are oscillation calculation, etc.

(c) Actions due to the traction by ships

The traction caused by ships on mooring facilities shall be properly considered as needed. The setting of the actions due to the traction by ships properly takes account of the actions caused by moored and berthed ships.

1 Principal Dimensions of Design Ships

1.1 Standard Values

- (1) Design ships are those, among the ships expected to use the facilities concerned, assumed to have the most significant effects on the performance verification of the facilities. Therefore, in the case where design ships are identifiable, their principal dimensions may be used.
- (2) In the cases, for example, public port facilities, where design ships are unidentifiable in advance, the values by ship type in **Table 1.1.1** may be used as the standard values of tonnages, lengths overall, lengths between perpendiculars, molded breadths, and full load drafts. The standard values in **Table 1.1.1** are prepared based on the statistical analysis of the dimensions of the existing ships with a coverage ratio of 75% for each tonnage category.¹⁾ With regard to the gross tonnage (GT), there are two different gross tonnages (GT): one is international gross tonnage and the other is domestic gross tonnage. Thus, types of the gross tonnages are specified in Items 4 to 9 of **Table 1.1.1**. In addition to gross tonnages, deadweight tonnages are also used in **Table 1.1.1** as the representative index expressing ship sizes for some types of ships. The principal dimensions used in the tables are schematically explained in **Fig. 1.1.1**. For the dimensions of the ships which are not shown in **Table 1.1.1**, such as patrol boats of the Japan Coast Guard, reference can be made to the **Manual for Disaster Prevention Base in Coastal Areas**.²⁾ and ³⁾

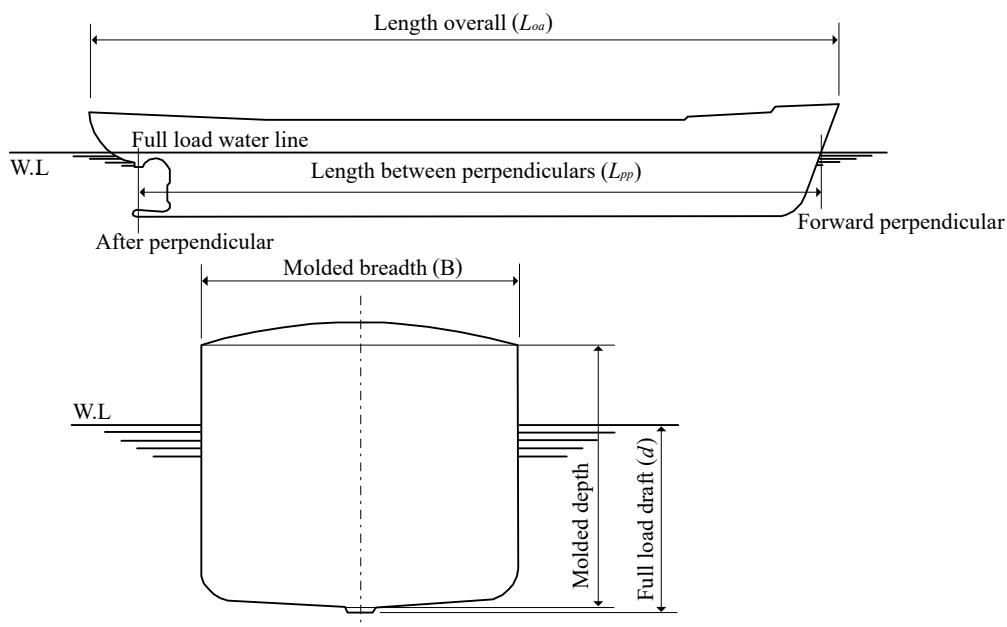


Fig. 1.1.1 Principal Dimensions of Ships

Table 1.1.1 Standard Values of the Principal Dimensions of Design Ships

1. General Cargo Ships

Deadweight tonnage DWT (ton)	Length overall L _{oa} (m)	Length between perpendiculars L _{pp} (m)	Molded breadth B (m)	Full load draft d (m)
1,000	63	57	10.4	3.7
2,000	77	71	12.8	4.6
3,000	87	81	14.3	5.3
5,000	102	95	16.6	6.2
6,000	108	100	17.5	6.5
10,000	125	118	20.3	7.7
12,000	132	125	21.4	8.1
15,000	142	134	22.8	8.7
18,000	149	141	24.0	9.2
30,000	174	166	27.9	10.8
40,000	190	181	30.3	11.8
50,000	203	195	32.3	12.6
55,000	209	200	32.3	13.0
70,000	225	216	32.3	14.0
90,000	242	234	38.2	15.1
120,000	264	256	41.5	16.6
150,000	282	274	44.3	17.7
200,000	308	300	48.1	19.4
250,000	328	319	56.2	20.8
300,000	333	324	57.3	22.0
400,000	361	353	65.0	23.1

2. Container Ships

Deadweight tonnage DWT (ton)	Length overall L _{oa} (m)	Length between perpendiculars L _{pp} (m)	Molded breadth B (m)	Full load draft d (m)	Reference: Container carrying capacity (TEU) ^{Note}
10,000	138	130	22.2	7.9	900 (50–1,345)
20,000	175	165	27.0	10.2	1,700 (648–1,808)
23,000	184	173	28.1	10.8	1,700 (1,400–2,259)
27,000	194	183	29.4	11.9	1,800 (1,356–2,268)
30,000	201	190	30.3	11.9	2,500 (1,728–3,535)
40,000	228	215	31.8	11.9	2,800 (1,700–4,370)
50,000	269	255	32.3	12.8	4,300 (2,496–5,752)
60,000	285	272	35.5	13.5	4,700 (2,815–7,030)
100,000	338	322	45.3	14.6	8,500 (5,541–10,622)
140,000	367	353	48.5	15.8	13,100 (6,600–15,000)
165,000	378	360	52.0	16.2	14,000 (11,000–15,550)
185,000	400	382	59.4	16.2	17,700 (15,908–19,200)
200,000	400	382	59.4	16.2	19,200 (17,608–21,413)

Note: The reference values for the container carrying capacity of each DWT class are median (approximate), minimum, and maximum values.

3. Tankers

Deadweight tonnage DWT (ton)	Length overall L_{oa} (m)	Length between perpendiculars L_{pp} (m)	Molded breadth B (m)	Full load draft d (m)
1,000	61	57	10.2	4.1
2,000	77	72	12.4	5.0
3,000	89	84	13.9	5.6
5,000	107	100	16.1	6.4
10,000	136	128	19.7	7.8
15,000	157	148	22.1	8.8
20,000	173	164	24.0	9.5
30,000	177	168	26.9	10.6
50,000	203	193	32.9	12.3
70,000	223	213	32.9	13.5
90,000	239	228	43.5	14.5
100,000	246	235	43.5	14.9
150,000	274	263	48.9	16.7
300,000	334	322	60.2	22.1

4. Roll-on Roll-off (RORO) Ships

4.1 RORO Ships (GT: Domestic gross tonnage)

Gross tonnage GT (ton)	Length overall L_{oa} (m)	Length between perpendiculars L_{pp} (m)	Molded breadth B (m)	Full load draft d (m)
3,000	120	110	19.0	5.6
5,000	141	131	22.2	6.2
10,000	171	161	27.4	7.0
15,000	171	161	30.3	7.6

4.2 RORO Ships (GT: International gross tonnage)

Gross tonnage GT (ton)	Length overall L_{oa} (m)	Length between perpendiculars L_{pp} (m)	Molded breadth B (m)	Full load draft d (m)
20,000	195	181	27.3	7.9
40,000	200	191	31.5	9.1
60,000	211	191	34.2	9.9

5. Pure Car Carrier (PCC) Ships

5.1 PCC Ships (GT: Domestic gross tonnage)

Gross tonnage GT (ton)	Length overall L_{oa} (m)	Length between perpendiculars L_{pp} (m)	Molded breadth B (m)	Full load draft d (m)
3,000	114	106	17.3	5.0
5,000	140	130	21.2	6.1
40,000	200	192	33.1	10.2

5.2 PCC Ships (GT: International gross tonnage)

Gross tonnage GT (ton)	Length overall L_{oa} (m)	Length between perpendiculars L_{pp} (m)	Molded breadth B (m)	Full load draft d (m)
12,000	147	136	24.0	6.5
20,000	162	151	26.3	7.0
30,000	175	164	28.3	7.5
40,000	184	174	31.4	9.2
60,000	201	192	33.3	10.2
70,000	230	220	33.3	10.9

6. Liquefied Petroleum Gas (LPG) Carriers (GT: International gross tonnage)

Gross tonnage GT (ton)	Length overall L_{oa} (m)	Length between perpendiculars L_{pp} (m)	Molded breadth B (m)	Full load draft d (m)
3,000	98	92	16.2	6.0
5,000	113	106	18.5	7.0
10,000	138	130	22.3	8.6
20,000	167	159	26.7	10.5
40,000	228	219	37.3	12.2
50,000	228	219	37.3	12.2

7. Liquefied Natural Gas (LNG) Carriers (GT: International gross tonnage)

Gross tonnage GT (ton)	Length overall L_{oa} (m)	Length between perpendiculars L_{pp} (m)	Molded breadth B (m)	Full load draft d (m)
20,000	168	159	26.8	8.0
30,000	192	183	30.6	8.9
50,000	228	217	36.0	10.1
80,000	267	255	41.9	11.5
100,000	287	275	45.0	12.2
130,000	314	301	48.9	13.1
160,000	345	333	54.6	13.8

8. Passenger Ships (GT: International gross tonnage)

Gross tonnage GT (ton)	Length overall L_{oa} (m)	Length between perpendiculars L_{pp} (m)	Molded breadth B (m)	Full load draft d (m)
3,000	94	81	16.5	4.2
5,000	112	96	18.5	4.8
10,000	143	122	21.8	5.7
20,000	183	155	25.5	6.4
30,000	211	178	28.0	6.9
50,000	252	213	32.3	7.6
70,000	284	239	32.3	8.0
100,000	294	270	35.6	8.4
130,000	325	297	38.5	8.8
160,000	345	311	41.0	9.1

9. Ferries (GT: Domestic gross tonnage)^{Note}

9.1 Intermediate and Short-Distance Ferries (Navigation Distances Less than 300 km)

Gross tonnage GT (ton)	Length overall L_{oa} (m)	Length between perpendiculars L_{pp} (m)	Molded breadth B (m)	Full load draft d (m)
400	55	46	11.6	2.8
700	67	58	13.2	3.3
1,000	76	67	14.4	3.6
3,000	112	104	18.6	4.7
7,000	152	145	22.6	5.8
10,000	172	167	24.6	6.4
13,000	189	186	26.1	6.8

9.2 Long-Distance Ferries (Navigation Distance Not Less than 300 km)

Gross tonnage GT (ton)	Length overall L_{oa} (m)	Length between perpendiculars L_{pp} (m)	Molded breadth B (m)	Full load draft d (m)
6,000	149	136	22.5	6.2
10,000	176	162	25.9	6.2
15,000	202	187	27.6	6.9
20,000	222	207	27.6	7.4

Note: In international ferries, the international gross tonnages can be converted to domestic gross tonnages by the following relational equation.⁴⁾

$$Y = 1.868X \quad (1.1.1)$$

where

Y : international gross tonnage

X : domestic gross tonnage

- (3) In these tables, the standard values of the principal dimensions of design ships are those for each tonnage category and obtained through statistical analyses, which has an overall coverage ratio of 75%.¹⁾ Thus, there may be some ships having larger dimensions than the standard values in the same tonnage categories in these tables and other

ships having smaller dimensions in a larger tonnage category than the standard values in a lower tonnage category in these tables.

- (4) The sources of the data used for establishing the tables of the principal dimensions of design ships are Lloyd's (Jan. 2017),⁵⁾ Clarkson (May 2017),⁶⁾ and the Register of Ships (2017).⁷⁾

(5) Tonnages

The definitions of various types of tonnages are as follows:

① Domestic gross tonnage

The gross tonnage based on the Act on Tonnage Measurement of Ships

② International gross tonnage

The gross tonnage based on the International Convention on Tonnage Measurement of Ships

③ Deadweight tonnage

The maximum weight, expressed in tons, of cargo that can be loaded on a ship

- (6) There are a certain number of container ships, which are called Panamax, and have unique dimensions, including molded breadths of about 32 m, because the navigable molded breadth of the Panama Canal was about 32 m until June 2016. When setting the dimensions of the container ships categorized as Under Panamax and Panamax, **Tables 1.1.2** and **1.1.3** can be used as references. For the dimensions of the large container ships which currently exist and are planned to be built, including very large container ships exceeding 200,000 DWT, **Table 1.1.4** can be used as a reference. For the dimensions of large passenger ships exceeding 220,000 GT, **Table 1.1.5** can be used as a reference.

Table 1.1.2 Principal Dimensions of Container Ships (Under Panamax)¹⁾

Deadweight tonnage DWT (ton)	Length overall L _{oa} (m)	Length between perpendiculars L _{pp} (m)	Molded breadth B (m)	Full load draft d (m)	Reference: Container carrying capacity (TEU) ^{Note}
10,000	138	129	22.2	7.8	900 (50 – 1,345)
20,000	176	165	26.9	10.2	1,700 (648 – 2,742)
30,000	202	191	30.2	11.8	2,500 (1,221 – 2,872)

Table 1.1.3 Principal Dimensions of Container Ships (Panamax)¹⁾

Deadweight tonnage DWT (ton)	Length overall L _{oa} (m)	Length between perpendiculars L _{pp} (m)	Molded breadth B (m)	Full load draft d (m)	Reference: Container carrying capacity (TEU) ^{Note}
30,000	196	186	32.2	11.3	2,600 (2,096 – 4,253)
40,000	232	219	32.2	12.1	3,100 (2,400 – 4,370)
50,000	264	248	32.2	12.8	4,300 (2,758 – 5,043)
60,000	293	275	32.2	13.3	4,600 (4,014 – 5,301)

Note: The reference values for the container carrying capacity of each DWT class are median (approximate), minimum, and maximum values.

Table 1.1.4 Principal Dimensions of Container Ships Exceeding 200,000 DWT in Operation and Planned to be Built^(5), 6) and 8)

Deadweight tonnage DWT (ton)	Length overall L _{oa} (m)	Length between perpendiculars L _{pp} (m)	Molded breadth B (m)	Full load draft d (m)	Reference: Container carrying capacity (TEU)	Existing or planned to be built
190,326	399.0	378.0	58.6	16.5	20,568	Planned to be built
191,570	399.9	383.0	58.8	16.0	21,413	Planned to be built
191,640	399.9	383.0	58.8	16.0	21,413	Planned to be built
191,688	399.9	383.0	58.8	16.0	21,413	Planned to be built
197,059	400.0	383.0	58.8	16.0	20,150	Planned to be built
197,106	400.0	383.0	58.8	16.0	20,150	Planned to be built
197,500	400.0	383.0	58.8	16.0	20,150	Existing
197,500	400.0	383.0	58.8	16.0	20,150	Planned to be built
199,744	400.0	388.0	59.0	16.0	18,691	Existing
200,000	*	*	*	*	22,000	Planned to be built
200,148	398.5	382.4	59.0	16.0	19,224	Existing
206,000	400.0	*	58.6	16.5	20,568	Existing
201,792	400.0	383.0	59.0	16.0	19,200	Existing
202,036	400.0	383.0	59.0	16.0	19,200	Existing
202,347	400.0	383.0	59.0	16.0	19,200	Existing
202,376	400.0	383.0	59.0	16.0	19,200	Existing
218,000	400.0	384.4	58.5	16.0	20,150	Planned to be built
230,000	400.0	*	59.0	*	20,600	Planned to be built
250,000	399.9	383.0	58.8	16.0	21,413	Existing
250,000	400.0	*	58.6	16.0	20,988	Planned to be built

Note: The values in the above table are based on Lloyd's data (Jan. 2017),⁵⁾ Clarkson's data (May 2017),⁶⁾ and Clarkson's data (Dec. 2017).⁸⁾ Also, the indications of existing and planned to be built are based on the data as of May 2017. In the case where there are two or more existing container ships or those planned to be built which have same DWT, the dimensions of the container ship having larger TEU is used in the table. The symbol * means that corresponding values are unknown.

Table 1.1.5 Principal Dimensions of Passenger Ships Exceeding 220,000 GT^(5), 6) and 8)

Gross tonnage GT (ton)	Length overall L _{oa} (m)	Length between perpendiculars L _{pp} (m)	Molded breadth B (m)	Full load draft d (m)	Existing or planned to be built
149,215	345.0	301.0	41.0	10.3	Existing
225,282	360.0	330.0	47.0	9.3	Existing
225,282	360.0	330.0	47.0	9.3	Existing
225,282	362.1	330.7	47.0	9.3	Planned to be built
226,963	362.1	331.0	47.0	9.3	Existing
227,000	362.1	330.7	47.0	9.3	Planned to be built

Note: The values in the above table are based on Lloyd's data (Jan. 2017),⁵⁾ Clarkson's data (May 2017),⁶⁾ and Clarkson's data (Dec. 2017).⁸⁾ Also, the indications of existing and planned to be built are based on the data as of May 2017.

1.2 Others

- (1) With regard to the small cargo ships, because there is the large variation on the data of the principal dimensions, reference can be made to **Table 1.2.1**, which shows reference values obtained by extracting data on the dimensions of small cargo ships with the coverage ratio of 75% in an object tonnage category.

Table 1.2.1 Reference Values of Principal Dimensions of Small Cargo Ships

Deadweight tonnage DWT (ton)	Length overall L _{oa} (m)	Length between perpendiculars L _{pp} (m)	Molded breadth B (m)	Full load draft d (m)
700	58	53	9.6	3.3

- (2) The heights of ships considerably differ even among the ships of identical types or tonnages. Thus, the performance verification of the bridges crossing water ways shall be carried out with due consideration to the heights of design ships from sea surfaces to the highest points. For the heights of ships, reference can be made to the study cases by Takahashi, etc.^{9) and 10)}

Particularly, there has been an increase in the number of large passenger ships calling at Japanese ports. Thus, for the purpose of showing a reference for determining whether or not large passenger ships can pass under bridges when they enter or leave ports, the correlation between the international gross tonnages (GT) and mast heights (air drafts), from sea surfaces to the highest points, of which data is obtained through hearing investigation, is shown in **Fig. 1.2.1**.¹⁾ And it shall be noted that the values obtainable by the regression expression and curve in **Fig. 1.2.1** are not standard ones but merely reference ones on the basis of 75% coverage ratio.

$$Mh = 2.2873 * GT^{0.2810} \quad (\text{Coverage ratio of 75\%})$$

Mh: Mast height (m)

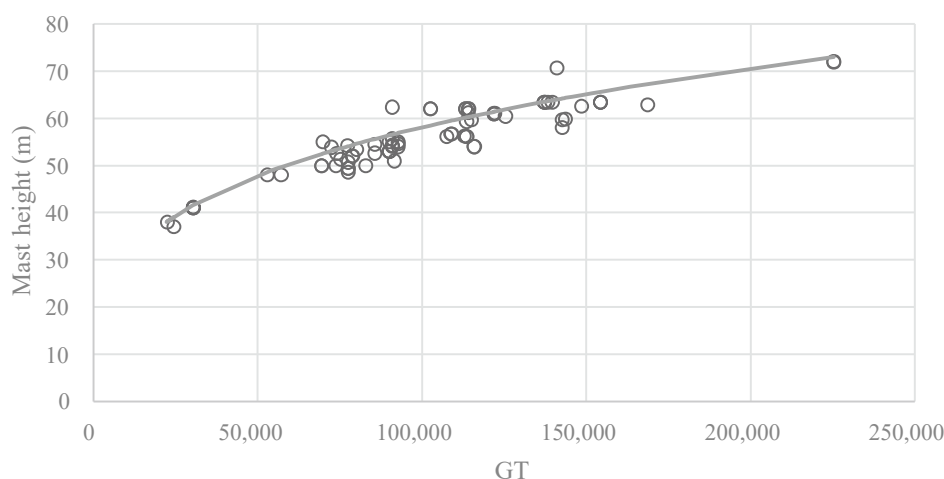


Fig. 1.2.1 Correlation between International Gross Tonnages and Mast Heights of Passenger Ships

- (3) In addition to the standard values of full load drafts of cargo ships in **Table 1.1.1**, a calculation method of the maximum drafts of large cargo ships (with approximate DWT exceeding 85,000) when their drafts are reduced (lightly loaded) is explained below.¹¹⁾
- ① The maximum drafts of ships when lightly loaded with no trims can be calculated by multiplying the full load drafts of design ships by corresponding draft ratios (*Cd*) (%). And the corresponding draft ratios (*Cd*) (%) are the ratios of the maximum drafts when ships are lightly loaded to the full load drafts provided that the ships have no trims and can be calculated by the following relational equation. In case of assuming trims when ships are in operation, the maximum drafts can be calculated by adding trims to the values obtained by multiplying the full load drafts by corresponding draft ratios (%).

$$Cd = 0.4724 \times e^{0.745 \times Lrw} \quad (1.2.1)$$

where

Cd : corresponding draft ratio (%)

Lrw : loading ratio on a weight basis (%)

- ② In a case where a loading ratio on a weight basis (Lrw) for the object ship in **equation 1.2.2** is unknown, the loading ratio on a weight basis (Lrw) can be calculated by using those on a volume basis (hereinafter referred to as the volume loading ratio (Lrv)) as shown in the following relational equation:

$$Lrw = (Hc \times Lrv \times Sg) / Dwm \quad (1.2.2)$$

where

Hc : hold capacity (m³)

Lrv : volume loading ratio (%)

Sg : specific gravity (ton/m³)

Dwm : maximum deadweight (ton)

- ③ When calculating the loading ratio on a weight basis (Lrw) in **equation 1.2.2** without knowing hold capacity (Hc) or specific gravity (Sg), respective unknown values can be set in the following ways.

- (a) When hold capacity (Hc) is unknown, it can be calculated by the following relational equation:

$$Hc = 1.1067 \times DWT \quad (1.2.3)$$

- (b) Setting of specific gravity

When specific gravity (Sg) is unknown, the values in **Table 1.2.2** can be referred. In the table, SF value has the same concept as specific gravity (Sg) and represents the capacity (ft³) per unit weight (L/T) of the cargo.

For typical large cargo ships, the corresponding draft ratios (Cd) can be selected from **Table 1.2.2**, which tabulates the calculation results of the corresponding draft ratios (Cd) according to respective volume loading ratios (Lrv) and specific gravity (Sg) so as to enable the corresponding draft ratios (Cd) to be simply obtained without using **equations (1.2.2)** and **(1.2.3)**.

Table 1.2.2 Specific Gravity and Corresponding Draft Ratios of Cargo Ships by Volume Loading Ratios, Cargoes, and Ship Sizes

Volume loading ratio of 40%

Specific gravity (Sg)	SF value	Cargo	Cd (Panamax)	Cd (Capesize)	Cd (VLOC)
2.72	13.00	Iron ore	—	—	—
2.35	15.00	Iron ore	—	—	—
2.08	17.00	Iron ore	0.95	0.95	0.95
0.88	40.00	Coal	0.63	0.64	0.64
0.84	42.00	Coal	0.63	0.63	0.63
0.78	45.00	Coal	0.61	0.61	0.62
0.75	47.00	Coal	0.61	0.61	0.61
0.71	50.00	Grain	0.60	0.60	0.60
0.68	52.00	Grain	0.59	0.59	0.59
0.64	55.00	Grain	0.59	0.59	0.59
0.62	57.00	Grain	0.58	0.58	0.58

Volume loading ratio of 50%

Specific gravity (Sg)	SF value	Cargo	Cd (Panamax)	Cd (Capesize)	Cd (VLOC)
2.72	13.00	Iron ore	—	—	—
2.35	15.00	Iron ore	—	—	—
2.08	17.00	Iron ore	—	—	—
0.88	40.00	Coal	0.68	0.68	0.69
0.84	42.00	Coal	0.67	0.67	0.67
0.78	45.00	Coal	0.66	0.66	0.66
0.75	47.00	Coal	0.65	0.65	0.65
0.71	50.00	Grain	0.63	0.64	0.64
0.68	52.00	Grain	0.63	0.63	0.63
0.64	55.00	Grain	0.62	0.62	0.62
0.62	57.00	Grain	0.61	0.61	0.61

Volume loading ratio of 60%

Specific gravity (Sg)	SF value	Cargo	Cd (Panamax)	Cd (Capesize)	Cd (VLOC)
2.72	13.00	Iron ore	—	—	—
2.35	15.00	Iron ore	—	—	—
2.08	17.00	Iron ore	—	—	—
0.88	40.00	Coal	0.74	0.74	0.74
0.84	42.00	Coal	0.72	0.72	0.72
0.78	45.00	Coal	0.70	0.70	0.70
0.75	47.00	Coal	0.69	0.69	0.69
0.71	50.00	Grain	0.67	0.67	0.68
0.68	52.00	Grain	0.66	0.66	0.67
0.64	55.00	Grain	0.65	0.65	0.65
0.62	57.00	Grain	0.64	0.65	0.65

Volume loading ratio of 70%

Specific gravity (Sg)	SF value	Cargo	Cd (Panamax)	Cd (Capesize)	Cd (VLOC)
2.72	13.00	Iron ore	—	—	—
2.35	15.00	Iron ore	—	—	—
2.08	17.00	Iron ore	—	—	—
0.88	40.00	Coal	0.79	0.79	0.80
0.84	42.00	Coal	0.77	0.77	0.78
0.78	45.00	Coal	0.75	0.75	0.75
0.75	47.00	Coal	0.73	0.73	0.74
0.71	50.00	Grain	0.71	0.72	0.72
0.68	52.00	Grain	0.70	0.70	0.71
0.64	55.00	Grain	0.69	0.69	0.69
0.62	57.00	Grain	0.68	0.68	0.68

Volume loading ratio of 80%

Specific gravity (Sg)	SF value	Cargo	Cd (Panamax)	Cd (Capesize)	Cd (VLOC)
2.72	13.00	Iron ore	—	—	—
2.35	15.00	Iron ore	—	—	—
2.08	17.00	Iron ore	—	—	—
0.88	40.00	Coal	0.85	0.85	0.86
0.84	42.00	Coal	0.83	0.83	0.83
0.78	45.00	Coal	0.80	0.80	0.80
0.75	47.00	Coal	0.78	0.78	0.78
0.71	50.00	Grain	0.76	0.76	0.76
0.68	52.00	Grain	0.74	0.75	0.75
0.64	55.00	Grain	0.73	0.73	0.73
0.62	57.00	Grain	0.72	0.72	0.72

Note: Corresponding draft ratios based on the data on actual ships (maximum deadweight tonnage, etc.) of 87,000 DWT in Panama Class, 170,000 DWT in Capesize Class, and 300,000 DWT in VLOC Class.

(4) For the maximum number of container rows on deck of container ships, **Fig. 1.2.2** can be used as a reference.¹⁾

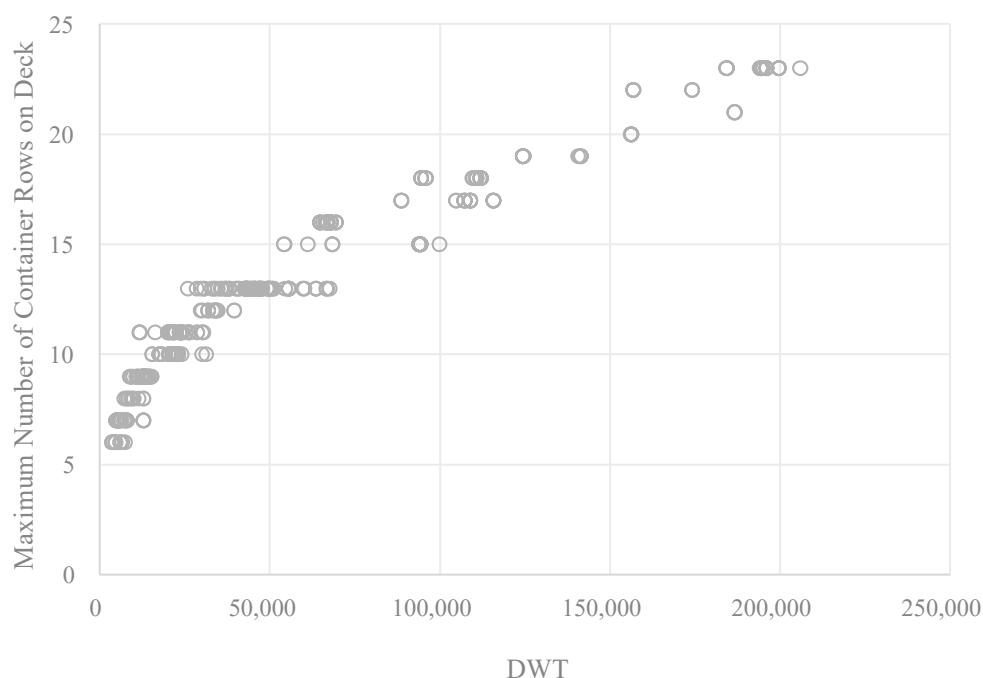


Fig. 1.2.2 Correlation between Deadweight Tonnages and Maximum Number of Container Rows on Deck in Container Ships

[References]

- 1) Iwasaki, K. and Yamagata, S.: Study On Ship Dimensions by Statistical Analysis, TECHNICAL NOTE of National Institute for Land and Infrastructure Management No.991, 2017
- 2) Ports and Harbours Bureau, MLIT: Manual for Disaster Prevention Base in Coastal Areas (Revised version), 2016
- 3) Akakura, Y. and Ono, K.: Analysis of the Dimensions of Emergency Relief Ships and Corresponding Berthing Facilities after Large-Scale Disaster- Examples of the Great East Japan Earthquake and the 2016 Kumamoto Earthquake -, TECHNICAL NOTE of National Institute for Land and Infrastructure Management No.942, 2017"
- 4) Koizumi, T., Suzuki, T. and Nagao, T.: Research on facilitation measures for expanding international ferry transport services in Asia, PROJECT RESEARCH REPORT of National Institute for Land and Infrastructure Management, 2015
- 5) Lloyd's Marine Intelligence Unite: LMIU Shipping Data (2017.1), 2017

- 6) Clarkson World Fleet Register: Clarkson Shipping Data, 2017 .5.
- 7) Japan Shipping Exchange, Inc.: The Annual “Register of Ships” (SENPAKU MEISAISHO)2017, 2017
- 8) Clarkson World Fleet Register: Clarkson Shipping Data, 2017 .12.
- 9) Takahashi, H. and Goto, A.: Study of ship Height by Statistical Analysis-Standard of Ship Height of Design Ship (Draft)-, RESEARCH REPORT of National Institute for Land and Infrastructure Management No.31, 2006
- 10) Takahashi, H. and Goto, A.: Study on Ship Height by Statistical Analysis-Standard of Ship Height of Design Ship (Draft)-, RESEARCH REPORT of National Institute for Land and Infrastructure Management No.33, 2007
- 11) Tanimoto, T. and Abe, M.: An Analysis on the Motions of Very Large Bulk Carrier under Reduced Draft, TECHNICAL NOTE of National Institute for Land and Infrastructure Management No.834, 2015

2 Actions Caused by Ships

2.1 General

2.1.1 Ship Berthing

- (1) The actions of berthing ships on mooring facilities shall be determined using appropriate methods by taking into account the dimensions of design ships, berthing methods and velocities, structures of mooring facilities, etc.
- (2) The performance verification of general mooring facilities shall take into account the berthing forces of ships as actions caused by ship berthing. In general, the berthing force of ships that acts on mooring facilities shall be calculated using the displacement-restoration characteristics of fenders on the basis of the berthing energy of ships.
- (3) The berthing force of ships is the dominant factor in the normal performance verification of general fender systems. Given that the berthing force is largely affected by the types of design ships and the berthing methods and velocities, the conditions of design ships shall be thoroughly examined in the performance verification.
- (4) Generally, the actions of ships rarely become dominant factors in the performance verification of mooring facilities. However, it shall be noted that the actions of ships may become dominant factors when designing the structure in the performance verification in the following cases: offshore berths wherein large tankers and large ore carriers are moored, piled piers designed with small seismic actions, and mooring facilities for ship refuge in the ports.

2.1.2 Ship Motions

- (1) The actions caused by moored ships on mooring facilities shall be determined using appropriate methods by taking into account the dimensions of design ships, structures of mooring facilities, mooring methods, characteristics of fenders and mooring ropes, and influences of winds, waves, and currents on design ships.
- (2) The actions caused by moored ships on mooring facilities shall include those caused by the motions of moored ships. The performance verification of general mooring facilities shall take into account the impact and tractive forces acting on mooring facilities owing to the motions of moored ships subjected to the wave forces, wind pressure forces, and fluid pressure forces of water currents. Particular attention is required for the influence of the actions of wave forces on ships in the cases of mooring facilities: in ports expecting the invasion of long-period waves, in the open sea or at port entrances similar to the case of offshore berths, and constructed for ship refuge in the ports.
- (3) The impact and tractive forces caused by the motions of moored ships can be generally calculated by using simulations of oscillation based on wave forces, wind pressure forces and fluid pressure forces of water currents, which act on ships, and characteristics of fenders and mooring ropes.
- (4) In the performance verification of general fender systems, it is preferable to take into account the impact force applied to them because of the motions of moored ships, in addition to the berthing force of ships, which is generally the dominant factor. In the case of mooring posts and bollards, the tractive force due to the motions of moored ships caused by wind pressure forces acting on ships is the dominant factor in the performance verification. The impact force due to the motions of moored ships is largely affected by the types of design ships, wave characteristics, and displacement-restoration characteristics of fenders. Furthermore, the tractive force due to the motions of moored ships is largely affected by the types and superstructures of design ships. Therefore, the performance verification of fenders shall be carried out by examining the conditions of design ships, wave characteristics, structures of mooring facilities, characteristics of fenders and mooring ropes, and others.

2.2 Actions Caused by Ship Berthing

(1) Berthing Energy of Ships

- ① The actions caused by ship berthing shall be calculated from the berthing energy of ships in general. The berthing energy of a ship can be calculated with **equation (2.2.1)** by using the mass of the ship, the berthing velocity of the ship, the virtual mass factor, the eccentricity factor, the flexibility factor, and the berth configuration factor. In the equation, the subscript k indicates the characteristic values.

$$E_{fk} = \frac{1}{2} M_{sk} V_{bk}^2 C_{mk} C_{ek} C_{sk} C_{ck} \quad (2.2.1)$$

where

- E_f : berthing energy of the ship (kJ)
- M_s : mass of the ship (t)
- V_b : berthing velocity of the ship (m/s)
- C_m : virtual mass factor
- C_e : eccentricity factor
- C_s : flexibility factor
- C_c : berth configuration factor

- ② In addition to the method in item ① above based on motion dynamics, there are other methods for obtaining the berthing energy of ships, including a statistical method, a method using hydraulic model tests, and a method based on hydrodynamic models.¹⁾ The method based on motion dynamics has been generally used because necessary data has not yet been accumulated and several constants needed for the calculations have not been fully elucidated for the other methods.
- ③ Given that a ship moves only in a lateral direction when berthing, the kinetic energy E_s (unit: kJ) of the ship is equal to $M_s V_b^2 / 2$. When a ship berths at a quaywall or a dolphin with fenders, the berthing energy E_f to be absorbed by each fender can be expressed by $E_s f$ by taking into consideration various influence factors, where $f = C_m C_e C_s C_c$.

(2) Mass of Ship

The mass of ships in the calculation equation of berthing energy is the full-load displacement tonnages expressing the displacement when ships are fully loaded in the unit of weight. **Equation (2.2.2)** can be used as relational equations between the characteristic values of the full-load displacement tonnage (DT) of the respective types of ships and deadweight tonnages (DWT) or gross tonnages (GT) of the ships. These relational equations are the regression equations obtained from statistical data on the relation of full-load displacement tonnages with deadweight tonnages or gross tonnages covering 75% of entire ships.²⁾ These relational equations are applicable in the range of tonnages shown in **Table 1.1.1**. In these relational equations, the subscript k indicates the characteristic values. When it is evident that ships are berthing at quaywalls in ballast, regression equations²⁾ can be used as references for the relational equations between the ballasted displacement tonnages of ships and their deadweight tonnages or gross tonnages. When the dimensions of design ships can be specified, including the displacement, when ships are fully loaded and in ballast, these specified values shall be used.

Cargo ships:	$DT_k = 2.920DWT^{0.924}$	
Container ships:	$DT_k = 1.634DWT^{0.986}$	
Tankers:	$DT_k = 1.688DWT^{0.976}$	
Roll-on roll-off (RORO) ships:	$DT_k = 8.728GT^{0.790}$	
Pure car carriers (PCC):	$DT_k = 1.946GT^{0.898}$	(2.2.2)
LPG carriers:	$DT_k = 4.268GT^{0.914}$	
LNG carriers:	$DT_k = 1.601GT^{0.970}$	
Passenger ships:	$DT_k = 2.730GT^{0.871}$	
Short-to-medium distance ferries (navigation distance of less than 300 km):	$DT_k = 4.980GT^{0.855}$	
Long distance ferries (navigation distance of 300 km or more):	$DT_k = 15.409GT^{0.735}$	

where

- DT : full-load displacement tonnage of the ship (ton)
- DWT : deadweight tonnage of the ship (ton)
- GT : gross tonnage of the ship (ton)

(3) Berthing Velocity

- ① The berthing velocities of ships shall be determined on the basis of actual measurements or the existing measurement data of berthing velocities by taking into consideration the types and loading conditions of design ships, locations and structures of mooring facilities, presence or absence of tugboat assistance and their sizes, and meteorological and oceanographical conditions.
- ② Large cargo ships and tankers berth at mooring facilities in a manner that temporarily stop at positions parallel to the mooring facilities at certain distances from them and then come alongside the mooring facilities with a few tugboats gently pushing them. If strong winds are blowing against mooring facilities, there may be cases wherein large cargo ships or tankers come alongside the mooring facilities with tugboats pulling them. When adopting the tugboat-assisted berthing method as mentioned above, the berthing velocities are normally set at approximately 10 to 15 cm/s on the basis of the existing performance records.
- ③ Special ships such as ferries, RORO ships, or small cargo ships may require berthing methods that are different from those used with large ships, e.g., berthing without the assistance of tugboats or approaching mooring facilities in the direction parallel to their normal lines when ships have ramps at their bows or sterns. Therefore, the berthing velocities of special ships should be carefully determined on the basis of actual measurements and others with particular focus on their berthing methods.
- ④ Considering that small ships, such as small cargo ships, berth at mooring facilities under their own power without tugboat assistance, it shall be noted that their berthing velocities are generally larger than those of large ships and may exceed 30 cm/s. Therefore, the berthing velocities of small ships should be carefully determined on the basis of actual measurements and others.
- ⑤ For the berthing velocities of medium and small ships, in anticipation of indiscreet berthing or berthing at mooring facilities subject to currents, it is necessary to determine the berthing velocities on the basis of the existing measurement data by taking into consideration the drift velocities of ships.
- ⑥ **Fig. 2.2.1** shows the relationship among ship maneuvering conditions, ship sizes, and berthing velocities established on the basis of the empirical data.³⁾ This figure suggests that larger berthing velocities should be set when ships berth at the mooring facilities that are not sheltered by breakwaters or when the sizes of design ships become smaller.

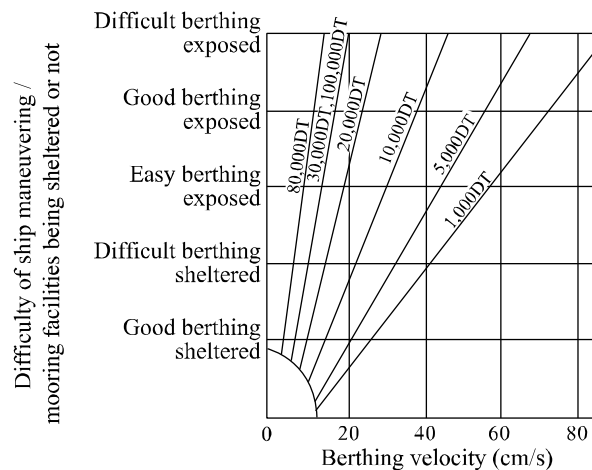


Fig. 2.2.1 Relationship among Ship Maneuvering Conditions, Ship Sizes, and Berthing Velocities³⁾

- ⑦ According to the study reports on berthing velocities,^{4) 5)} it has become clear that the loading conditions of ships largely affect berthing velocities, i.e., berthing velocities tend to decrease when ships are in a fully loaded state berth with small keel clearances and increase when ships are in a lightly loaded berth with large keel clearances.
- ⑧ The relationship between berthing velocities and ship sizes was studied using the measurement data collected in the previous studies on the berthing velocities of ships.⁶⁾ **Fig. 2.2.2** shows the relationship between the measurement values of berthing velocities and ship sizes for the respective types of ships. The figure shows that there is an overall trend of decreasing berthing velocities with increasing ship sizes and that berthing

velocities are approximately 20 cm/s at a maximum and are distributed widely from 5 to 15 cm/s with a large variance.

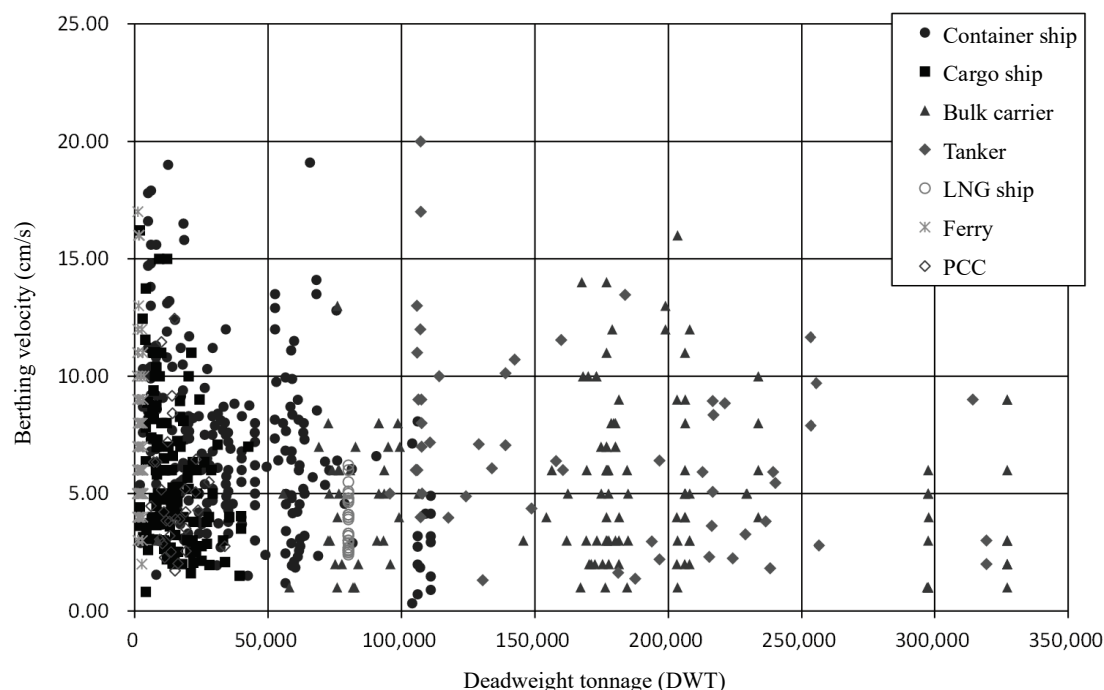


Fig. 2.2.2 Measurement Values of Berthing Velocities (by Ship Type)⁶⁾

Regarding the relationship between berthing velocities and ship sizes, the regression equations considering the coverage ratios were also proposed.⁶⁾ Fig. 2.2.3 shows the regression equations with different coverage ratios overlaid on the graph of the relationship between the measurement values of berthing velocities and ship sizes. The probability distribution of the berthing velocities of ships generally shows the logarithmic normal distribution, and the relationship between berthing velocities and ship sizes can be expressed by regression equations in the form of power functions.⁷⁾ It shall be noted that these regression equations show extremely large berthing velocities for small ships with the deadweight tonnages less than 10,000 tons.

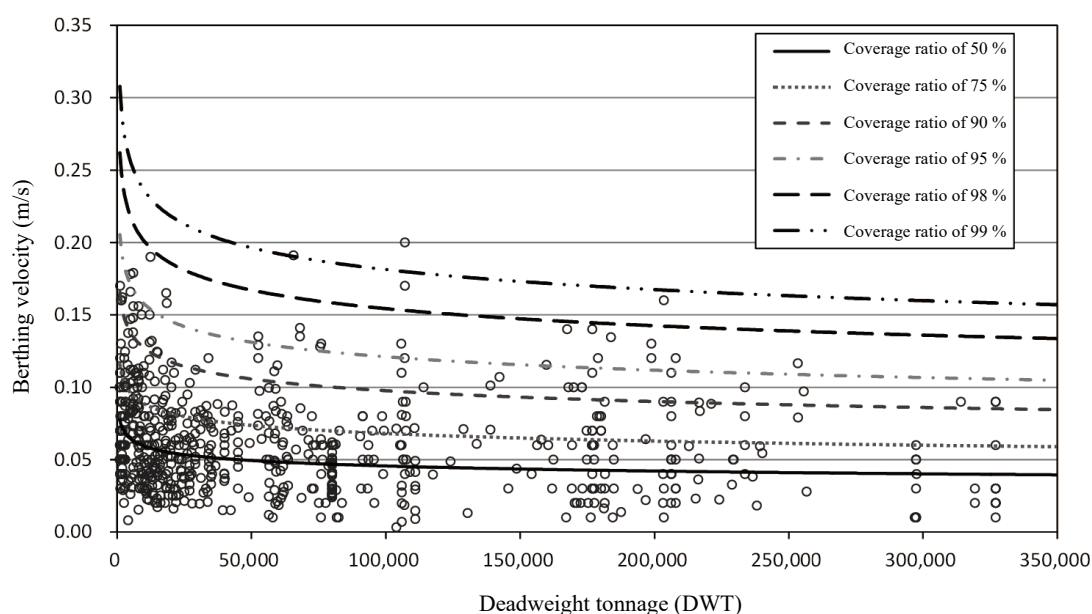


Fig. 2.2.3 Relationship between Measurement Values of Berthing Velocities of Ships and Regression Equations⁶⁾

(4) Virtual Mass Factor

- ① The virtual mass factor C_m can be calculated by the following equation:

$$C_m = 1 + \frac{\pi}{2C_b} \frac{d}{B} \quad (2.2.3)$$

$$C_b = \frac{\nabla}{L_{pp} B d} \quad (2.2.4)$$

where

C_m : virtual mass factor

C_b : block coefficient

∇ : displacement volume of the ship (m³)

L_{pp} : length between perpendiculars (m)

B : molded breadth (m)

d : full-load draft (m)

In the above equation, the values of the length between perpendiculars L_{pp} , molded breadth B , and full-load draft d should be those of design ships; however, the values listed in **Table 1.1.1** can be substituted for them when standard ships are used as design ships.

- ② When a ship berths, the velocities of not only the mass of the ship M_s but also the mass of the water body around the ship M_w are reduced simultaneously. Therefore, the inertia force due to the mass of the water body needs to be added to the motion of the ship. For this reason, the virtual mass factor can be defined by **equation (2.2.5)**.

$$C_m = \frac{M_s + M_w}{M_s} \quad (2.2.5)$$

where

C_m : virtual mass factor

M_s : mass of the ship (t)

M_w : mass of the water body around the ship (added mass) (t)

Ueda et al.⁸⁾ proposed **equation (2.2.3)** on the basis of the results of the hydraulic model tests and field measurements. The second term of the equation corresponds to M_w/M_s in **equation (2.2.5)**.

(5) Eccentricity Factor

- ① The eccentricity factors C_e can be calculated by the following equation:

$$C_e = \frac{1}{1 + \left(\frac{l}{r}\right)^2} \quad (2.2.6)$$

where

C_e : eccentricity factor

- l : distance measured from the ship's contact point to the center of gravity of the ship in the direction parallel to the normal line of the mooring facility (m)
- r : radius of rotation around the vertical axis passing through the center of gravity of the ship (m)

- ② During berthing, ships approach mooring facilities that are not perfectly alongside them. Therefore, ships start yawing in horizontal planes and rolling around their longitudinal axes when they come into contact with mooring facilities (fenders). As a result, the yawing and rolling partially consume the kinetic energy of the ships. Considering that the amount of energy consumed by rolling is negligibly smaller than that by yawing, **equation (2.2.6)** considers kinetic energy consumption only by yawing.
- ③ r/L_{pp} is a function of the block coefficient C_b and can be obtained from **Fig. 2.2.4.**⁹⁾ **Equation (2.2.7)**, which is a linear approximation of the curve in the figure, may also be used.

$$r = (0.19C_b + 0.11)L_{pp} \quad (2.2.7)$$

where

- r : radius of rotation (also called radius of gyration with the relationship of $I_z = M_s r^2$ with the moment of inertia I_z around the vertical axis of the ship)
- C_b : block coefficient
- L_{pp} : length between perpendiculars (m)

In the equation above, the values of the lengths between perpendiculars L_{pp} should be those of design ships; however, the values listed in **Table 1.1.1** can be substituted for them when standard ships are used as design ships.

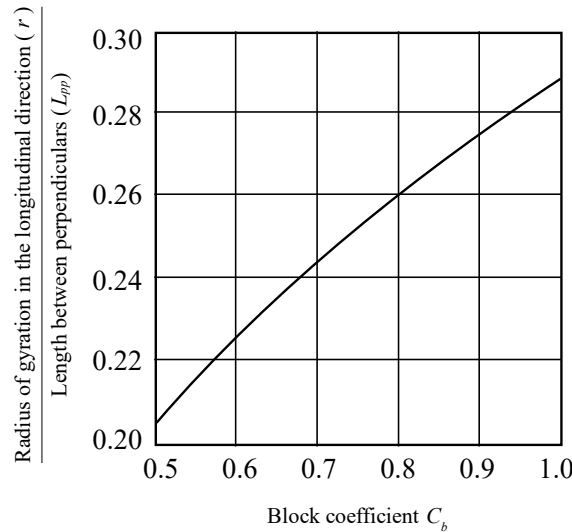
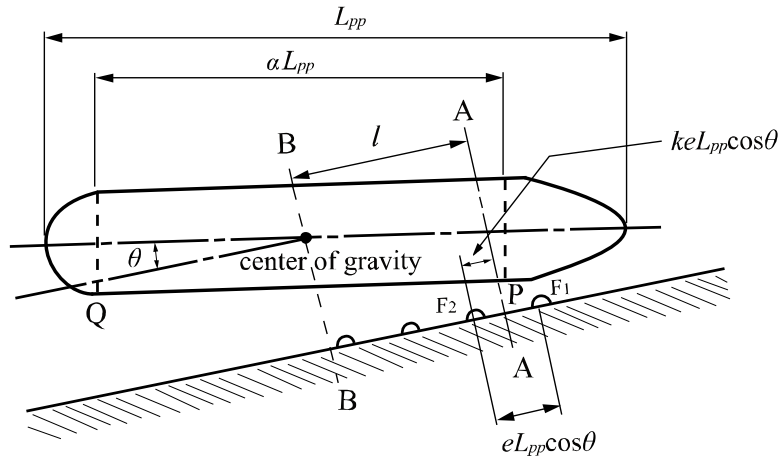


Fig. 2.2.4 Relationship between Radii of Gyration in the Longitudinal Direction and Block Coefficients⁹⁾

- ④ As shown in **Fig. 2.2.5**, when a ship comes closest to a mooring facility at point P and into contact with fenders F_1 and F_2 , the distance l measured from a point of contact to the center of gravity of the ship in the direction parallel to the mooring facility can be calculated by using **equation (2.2.8)** or **(2.2.9)**.¹⁰⁾ Here, the value of l needs to be L_1 when $k > 0.5$, L_2 when $k < 0.5$, and either L_1 or L_2 when $k = 0.5$ depending on which variable makes the value of C_e in **equation (2.2.6)** larger.


 Fig. 2.2.5 Schematic Illustration of Ship Berthing¹⁰⁾

$$L_1 = \{0.5\alpha + e(1-k)\}L_{pp} \cos \theta \quad (2.2.8)$$

$$L_2 = (0.5\alpha - ek)L_{pp} \cos \theta \quad (2.2.9)$$

where

- L_1 : distance measured from the point of contact to the center of gravity of the ship in the direction parallel to the mooring facility when the ship comes into contact with the fender F_1 (m)
- L_2 : distance measured from the point of contact to the center of gravity of the ship in the direction parallel to the mooring facility when the ship comes into contact with the fender F_2 (m)
- θ : berthing angle (generally set at around 0 to 10°)
- e : ratio of the interval of fenders measured in the longitudinal direction of the ship to the length between perpendiculars
- α : ratio of the length of the parallel side of the ship at the height of the point of contact with the fender to the length between perpendiculars (differs depending on the types of ships and block coefficients but is generally set at 1/3 to 1/2 or may be set at approximately 1/3 for ships with small breadths, such as container and passenger ships, or approximately 1/2 for ships with wide breadths, such as cargo ships and tankers)
- k : parameter representing the point between fenders F_1 and F_2 , where the ship comes closest to the mooring facility (set in the range of $0 < k < 1$ or may be set at 0.5 in general)

(6) Flexibility Factor

The flexibility factor C_s is the ratio of the berthing energy absorbed by the deformation of a ship hull to the berthing energy of the ship. Assuming that there is no energy absorption by the deformation of ship hull, the characteristic value of the flexibility factor C_{sk} can generally be set at 1.0.

(7) Berth Configuration Factor

The water mass compressed between a berthing ship and a mooring facility behaves like a cushion and produces an effect to decrease the kinetic energy of the ship to be finally absorbed by fenders. The berth configuration factor C_c needs to be determined by taking into account this effect. Furthermore, the behavior of water mass is considered to be affected by berthing angles, shapes of ship hulls, under-keel clearances (distances between ship bottoms and the seafloor), and berthing velocities. However, the characteristic value of the berth configuration factor C_{ck} can generally be set at 1.0.

2.3 Actions Caused by Ship Motions

(1) Motions of Moored Ship

- ① Generally, the actions caused by the motions of moored ships shall be obtained using motion calculations with appropriately setting wave forces, wind pressure forces, and fluid pressure forces of water currents.
- ② Ships that are moored at mooring facilities constructed in the open sea, close to port entrances, and in ports expecting the invasion of long-period waves or ships that are moored in rough weather are subjected to motions caused by the actions of waves, winds, and currents. In some cases, the kinetic energy of moored ships becomes larger than the berthing energy of ships. Therefore, the tractive force or impact force due to the motions of moored ships shall be examined in the performance verification of mooring posts, bollards or fenders.¹¹⁾ Particular attention is required in ports facing the open sea because it has been frequently reported that the slow drift oscillations of moored ships due to long-period waves cause difficulty with smooth cargo handling.^{12) 13)}
- ③ Generally, the motions of a moored ship shall be calculated using numerical simulation by taking into consideration the irregularity in the actions of waves, winds, and currents and the nonlinearity of the displacement-restoration characteristics of the mooring system consisting of mooring ropes and fenders. When numerical simulation is not available by necessity or when the ship is moored at a mooring system that can be considered almost symmetrical, the displacement and loads on the mooring system can be obtained with reference to the results of the frequency response analysis with respect to regular waves or the motion calculations of a floating body moored at a mooring system with bilinear displacement-restoration characteristics.¹⁴⁾
- ④ The wave forces acting on a ship consist of the wave-exciting force due to incident waves and the wave making resistance force accompanied by ship motions.¹⁵⁾ The wave-exciting force due to incident waves is the wave force calculated on the assumption that the motions of the ship are restrained. The wave making resistance force is the wave force acting on the ship when the ship undergoes a unit amplitude motion of respective motion components. The wave making resistance force can be expressed separately by using two terms proportional to the acceleration and velocity of ship motions. The former term can be expressed as an added mass when divided by the acceleration, and the latter term can be expressed as a damping coefficient when divided by the velocity.¹⁶⁾ In addition to the force mentioned above, the ship is subjected to nonlinear fluid force proportional to the square of wave heights (refer to **Part II, Chapter 2, 4.8 Actions on Floating Body and its Motions**).
- ⑤ The wave force acting on a ship with a block coefficient of 0.7 to 0.8, similar to the case for large tankers, can be obtained using a diffraction theory with the ship's hull approximated by an elliptical cylinder.¹⁷⁾
- ⑥ The wave force acting on a ship with a box-shaped cross-section, similar to the case for working crafts, can be obtained by approximating the ship's hull by a floating body with a rectangular cross-section or a rectangular solid.
- ⑦ For the actions caused by motions of moored ships, when conducting static motion calculations by taking into consideration wind pressure forces and the fluid pressure forces of water currents, **Reference 18)** can be used as a reference. It shall be noted that design ships are generally tankers in the reference.

(2) Wave Forces Acting on Ship

- ① The wave forces acting on moored ships shall be calculated using appropriate methods by taking into consideration the ship sizes and wave parameters.
- ② The wave force acting on a moored ship can be calculated using an appropriate method selected from the following: the strip method, the source distribution method, the boundary element method, or the finite element method. Among them, the strip method is the most frequently used method for ships.
- ③ **Wave forces based on the strip method**^{14) 15) 16) 19)}

(a) Wave force of regular waves acting on the ship

The wave force acting on a ship is given by the summation of the Froude-Kriloff force and the diffraction force.

(b) Froude-Kriloff force

The Froude-Kriloff force is the force derived from the waves passing through a ship. It is given by the summation of the force of the incident waves and the force of the reflected waves from the mooring facility.

(c) Diffraction force

The diffraction force acting on a ship is the force generated by the change in pressure field when incident waves are scattered by the ship. The diffraction force can be estimated by replacing this change in the pressure field with the radiation force (namely, the wave making resistance force when the ship moves at a certain velocity in still water) in a manner that causes the ship to have a relative movement. It is assumed that the certain velocity of the ship above is equal to the relative velocity of the ship to the water particles in the incident waves. This velocity is called the equivalent relative velocity.

(d) Force acting on the ship entirely

The wave force acting on a ship entirely can be obtained by integrating the Froude-Kriloff force and the diffraction force acting on a cross-section of the ship along the longitudinal direction from $x = -L_{pp}/2$ to $x = L_{pp}/2$ (where x is the positional coordinate in the longitudinal direction of the ship).

④ Wave forces based on diffraction theory¹⁷⁾

In cases wherein a ship with a wide breadth (with a block coefficients C_b of approximately 0.7 to 0.8) is considered to be moving in slight motions with no wave reflecting structures, such as mooring facilities located behind the ship, the wave force can be calculated by an equation¹⁷⁾ based on a diffraction theory with the ship's hull approximated by an elliptical cylinder.

- ⑤ When simply obtaining the wave force acting on a moored ship, it shall be obtained using an appropriate method in a manner that assumes the shape of the ship as a simplified one, such as a rectangular solid and refers to **Part II, Chapter 2, 6.4 Wave Force Acting on Structures Close to Water Surfaces** and **Part II, Chapter 2, 4.8 Actions on Floating Body and its Motions**.

(3) Wind Pressure Forces Acting on Ship

- ① The wind pressure forces acting on moored ships shall be determined by using appropriate calculation equations.
- ② It is preferable to determine the wind pressure forces acting on a moored ship by considering the temporal variability in wind velocity and the characteristics of wind drag coefficients dependent on the cross-sectional shape of the ship.
- ③ The wind pressure forces acting on a ship can be calculated with **equations (2.3.1) to (2.3.3)** by using wind drag coefficients C_X and C_Y in the X and Y directions, respectively, and wind pressure moment coefficient C_M around the midship section (the central section of the ship). The subscript k in the equations indicates the characteristic values.

$$R_{X_k} = \frac{1}{2} \rho_a U_k^2 A_T C_X \quad (2.3.1)$$

$$R_{Y_k} = \frac{1}{2} \rho_a U_k^2 A_L C_Y \quad (2.3.2)$$

$$R_{M_k} = \frac{1}{2} \rho_a U_k^2 A_L L_{pp} C_M \quad (2.3.3)$$

where

R_X : component of the resultant wind pressure force in the X direction (kN)

R_Y : component of the resultant wind pressure force in the Y direction (kN)

R_M : moment around the midship section of the resultant wind pressure force (kNm)

C_X : wind drag coefficient in the X direction (the bow direction of the ship)

C_Y : wind drag coefficient in the Y direction (the side direction of the ship)

C_M : wind pressure moment coefficient around the midship section

ρ_a : density of air ($\rho_a = 1.23 \times 10^{-3}$ (t/m³))

- U : wind velocity (m/s)
 A_T : above-water bow projected area of the ship (m²)
 A_L : above-water side projected area of the ship (m²)
 L_{pp} : length between perpendiculars (m)

- ④ It is preferable to determine wind drag coefficients C_X and C_Y and wind pressure moment coefficient C_M by using wind tunnel tests or water tank tests for specific ships. Alternatively, considering that these tests require large amounts of costs and time, respective coefficients can be obtained by using calculation equations^{21) 22)} on the basis of the existing wind tunnel test results²⁰⁾ or water tank test results.
 ⑤ The wind velocity U used in the equations shall be the maximum (10-minute average) wind velocity at the action points of wind pressure force.
 ⑥ The values of the above-water bow and side projected areas of ships are preferably those of design ships.
 ⑦ Considering that wind velocity fluctuates in terms of time and space, the motion calculation of a moored ship shall use the wind velocity of fluctuating wind. Some of the examples of fluctuating wind include the frequency spectra of the fluctuating wind in terms of the time proposed by Davenport²³⁾ and Hino.²⁴⁾ The frequency spectra proposed by Davenport and Hino are given by **equations (2.3.4) and (2.3.5)**, respectively.

$$\left. \begin{aligned} fS_u(f) &= 4K_r U_{10}^2 \frac{X^2}{(1+X^2)^{4/3}} \\ X &= \frac{1200f}{U_{10}} \end{aligned} \right\} \quad (2.3.4)$$

$$\left. \begin{aligned} S_u(f) &= 2.856 \frac{K_r U_{10}^2}{\beta} \left\{ 1 + \left(\frac{f}{\beta} \right)^2 \right\}^{-5/6} \\ \beta &= 1.169 \times 10^{-3} \frac{U_{10} \alpha}{\sqrt{K_r}} \left(\frac{z}{10} \right)^{2m\alpha-1} \end{aligned} \right\} \quad (2.3.5)$$

where

- $S_u(f)$: frequency spectrum (m²/s)
 U_{10} : average wind velocity at the standard height of 10 m (m/s)
 K_r : friction coefficient on the surface defined by the wind velocity at the standard height (appropriate value of K_r on the sea is 0.003)
 α : power exponent when the vertical distribution of wind velocity is expressed by the power law ($U \propto (z/10)^\alpha$)
 z : height above the ground or water surface (m)
 m : correction factor related to the stability of the atmosphere ($m = 2$ in the case of storms)

(4) Fluid Pressure Forces of Water Currents Acting on Ship

- ① The fluid pressure forces of water currents acting on ships shall be determined by using appropriate calculation equations.
 ② **Fluid pressure force of water currents from the bow**

The fluid pressure force generated between a ship and water currents from the bow can be calculated by **equation (2.3.6)**. In the equation, the subscript k indicates characteristic values.

$$R_{f_k} = 0.0014 S V_k^2 \quad (2.3.6)$$

where

- R_f : fluid pressure force of water currents from the bow (kN)
 S : hull area submerged below the draft line (m²)
 V : current velocity (m/s)

③ **Fluid pressure force of water currents from the side**

The fluid pressure force of water currents from the side can be calculated by **equation (2.3.7)**. In the equation, the subscript k indicates characteristic values.

$$R_k = 0.5 \rho_0 C V_k^2 B \quad (2.3.7)$$

where

- R : fluid pressure force of water currents from the side (kN)
 ρ_0 : density of seawater (t/m³)
 C : current pressure coefficient
 V : current velocity (m/s)
 B : projected area of the ship side below the draft line (m²)

- ④ The fluid pressure force of water currents can be divided into friction resistance and pressure resistance. The resistance against water currents from the bow and the side is considered to be mostly friction resistance and pressure resistance, respectively. However, it is difficult to strictly divide friction resistance from pressure resistance and examine them individually. **Equation (2.3.6)** is obtained by simplifying the Froude's formula in a manner that assigns 1.025 t/m³, 15°C and 0.14 to ρ_0 , t and λ in **equation (2.3.8)**. In the equation, the subscript k indicates characteristic values.

$$R_{f_k} = \rho_0 g \lambda \left\{ \frac{1 + 0.0043(15 - t)}{1000} \right\} S V_k^{1.825} \quad (2.3.8)$$

where

- R_f : fluid pressure force of water currents from the bow (kN)
 $\rho_0 g$: unit weight of seawater (kN/m³)
 t : temperature (°C)
 S : hull area submerged below the draft line (m²)
 V : current velocity (m/s)
 λ : coefficient (e.g., $\lambda = 0.14741$ for the ship with the total length of 30 m, and $\lambda = 0.13783$ for the ship with the total length of 250 m)

- ⑤ The current pressure coefficient C varies according to the relative current direction θ between a ship and water currents and can be determined with reference to the values obtained from **Fig. 2.3.1**.

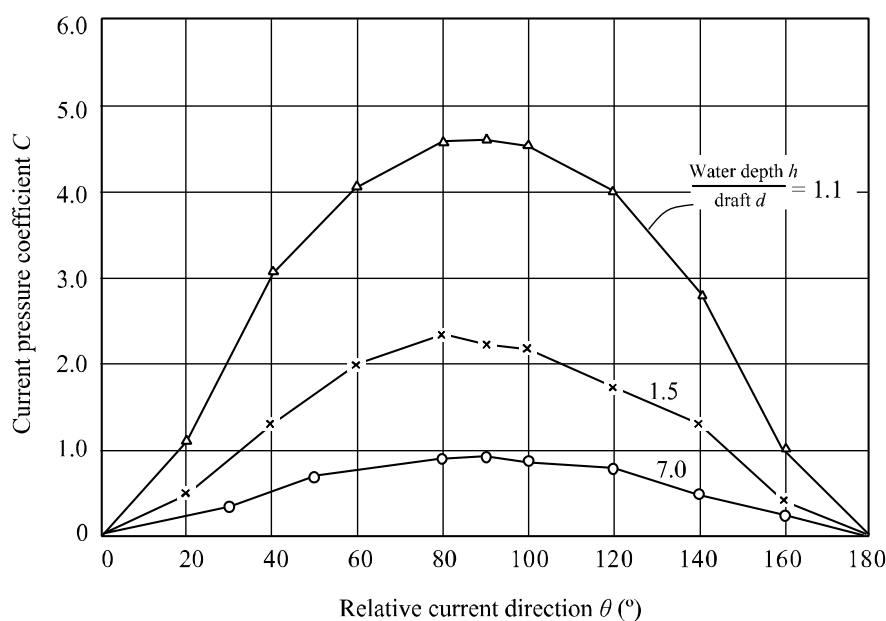


Fig. 2.3.1 Relationship between Current Pressure Coefficients and Relative Current Directions

(5) Characteristics of Mooring System

- ① The motion calculation of a moored ship shall be performed with appropriately modeled displacement-restoration characteristics of the mooring system consisting of mooring ropes and fenders.
- ② The displacement-restoration characteristics of the mooring system are nonlinear in general. Furthermore, there are cases of fenders with displacement-restoration characteristics that include hysteresis. Therefore, it is preferable to perform the motion calculation of a moored ship by using these appropriately modeled characteristics.²⁵⁾

2.4 Actions Caused by Traction of Ships

- (1) Generally, the values shown in **Table 2.4.1** shall be used as the standard values of tractive force by ships acting on mooring posts and bollards.²⁶⁾
- (2) In the case of bollards, they shall be generally subjected to the action of the tractive force by ships specified in item (1) in all directions.
- (3) In the case of mooring posts, they shall be generally subjected to the simultaneous actions of the tractive force by ships specified in item (1) in the horizontal direction and half the tractive force in the vertical direction.

Table 2.4.1 Standard Values of Tractive Force by Ships

GT of ship (ton)				Tractive force acting on a bollard (kN)	Tractive force acting on a mooring post (kN)
Over	200	and not more than	500	150	150
Over	500	and not more than	1,000	250	250
Over	1,000	and not more than	2,000	250	350
Over	2,000	and not more than	3,000	350	350
Over	3,000	and not more than	5,000	350	500
Over	5,000	and not more than	10,000	500	700
Over	10,000	and not more than	20,000	700	1,000
Over	20,000	and not more than	50,000	1,000	1,500
Over	50,000	and not more than	100,000	1,000	2,000

GT of ship (ton)	Tractive force acting on a bollard (kN)	Tractive force acting on a mooring post (kN)
Over 100,000 and not more than 120,000	1,500	2,000
Over 120,000 and not more than 150,000	1,500	2,000
Over 150,000 and not more than 170,000	2,000	2,000
Over 170,000 and not more than 200,000	2,000	2,000

- (4) Bollards are installed close to the face lines of mooring facilities, which are used to allow the mooring of ships and allow ships to come alongside or leave mooring facilities in calm weather. On the other hand, mooring posts are installed at or around both ends of mooring facilities away from their face lines, which are used to allow the mooring of ships in stormy weather.
- (5) For the layouts and names of mooring ropes used when mooring ships **Part III, Chapter 5, 2.1.1 Dimensions of Quaywalls** shall be referred to.
- (6) For the layouts and structures of mooring posts and bollards, **Part III, Chapter 5, 9.1 Mooring Posts, Bollards and Mooring Rings** shall be referred to.
- (7) When setting the tractive force of ships for which deadweight tonnages are normally used, similar to the case for cargo ships, the deadweight tonnages can be converted to the gross tonnages of design ships by using regression equations.²⁷⁾
- (8) It is preferable to calculate the tractive force acting on mooring posts and bollards by taking into consideration the forces caused by berthing ships, wind pressure forces acting on moored ships, and forces caused by the motions of ships,^{8) 14)} as needed on the basis of the breaking loads of mooring ropes mounted on design ships, the meteorological and oceanographical conditions of the locations where mooring facilities are constructed, and the dimensions of ships.
- (9) It is necessary to determine the following types of tractive force by taking into consideration the meteorological and oceanographical conditions, the structures of mooring facilities, and the existing records of the actual measurement of tractive force: the tractive force of ships with the gross tonnages not more than 200 tons or exceeding 200,000 tons (not shown in **Table 2.4.1**), the tractive force acting on the mooring facilities allowing ships to be moored in stormy weather, and the tractive force acting on the mooring facilities in water areas under severe meteorological and oceanographical conditions such as the open sea area.
- (10) The tractive force acting on bollards in **Table 2.4.1** is obtained by using the motion calculations of moored ships to allow the eight mooring ropes connected to bollards to safely moor cargo ships in ballast against winds with velocities up to 15 m/s blowing from the land side. Furthermore, the tractive force acting on mooring posts is obtained by using the motion calculations of moored ships to allow 10 mooring ropes to safely moor cargo ships in ballast against winds with velocities up to 30 m/s blowing from land sides; some of them are connected to mooring posts, whereas others are connected to bollards. The tractive force acting on bollards is also based on the condition that allows mooring ropes to be properly connected to bollards and mooring posts in storms and allows bollards to safely moored ships against winds with velocities of 30 m/s blowing from the land side. The tractive force acting on bollards corresponds to the breaking load of one or two mooring ropes specified in the **Rules for the Survey and Construction of Steel Ships; Guidance for the Survey and Construction of Steel Ships Part L (Equipment)**,²⁸⁾ and the tractive force acting on mooring posts corresponds to the breaking load of approximately two mooring ropes.
- (11) In the case of mooring facilities where ships are moored only in calm weather, half the values in **Table 2.4.1** can be used for the tractive force acting on bollards that are installed in the intermediate sections of the mooring facilities for spring lines and have no risk of being individually subjected to the tractive force of two mooring ropes or more. However, this provision cannot be applied to mooring facilities where ships using mooring ropes with large breaking loads, such as nylon ropes, are moored.
- (12) It is preferable to determine the tractive force of small ships with the gross tonnages of 200 tons or less by taking into consideration the dimensions of the ships, berthing situations, and structures of mooring facilities.²⁹⁾ However, for the tractive force to be used in the actual performance verification of bollards and mooring posts for mooring ships with the gross tonnages of 200 tons or less, 50 and 150 kN are used as the standard tractive forces acting on bollards and mooring posts, respectively.

- (13) Caution is required when calculating the tractive force of passenger ships, ferries, and container ships by using the values in **Table 2.4.1** because these types of ships have large wind pressure-receiving areas. When design ships can be specified, it is preferable to calculate the tractive force acting on mooring posts and bollards by using the wind pressure forces on the moored design ships and by taking into consideration their dimensions, mooring rope arrangement, breaking loads and others. For the wind pressure forces acting on moored ships, **Part II, Chapter 8, 2.3 Actions Caused by Ship Motions** shall be referred to.

[References]

- 1) PIANC: Report of the International Commission for Improving the Design of Fender Systems, Supplement to Bulletin, No.45, 1984.
- 2) Yoneyama, H.: Proposal of Regression Equations for Displacement Tonnage of Ships, Technical Note of PARI, No.1340, 2018. (in Japanese)
- 3) Baker, A. L. L.: The impact of ships when berthing, Proc. of the 18th International Navigation Congress (PIANC), Section II, Quest 2, pp.111-142, 1953.
- 4) Mizoguchi, M. and T. Nakayama: A Study on the Berthing Impact of the Ships, Technical Note of PHRI, No.170, 1973. (in Japanese)
- 5) Otani, H., S. Ueda, T. Ichikawa and K. Sugihara: A Study on the Berthing Impact of the Big Tanker, Technical Note of PHRI, No.176, 1974. (in Japanese)
- 6) Murakami, K., M. Takenobu, M. Miyata and H. Yoneyama: Fundamental Analysis on the Characteristics of Berthing Velocity of Ships for the Design of Port Facilities, Technical Note of NILIM, No.864, 2015. (in Japanese)
- 7) Ueda, S., R. Umemura, S. Shiraishi, S. Yamamoto, Y. Akakura and S. Yamase: Study on design of fenders of ship berthing by stochastic approach, Proceedings of Coastal Engineering, JSCE, Vol.47, pp.866-870, 2000. (in Japanese)
- 8) Ueda, S. and E. Ooi: On the Design of Fending Systems for Mooring Facilities in a Port, Technical Note of PHRI, No.596, 1987. (in Japanese)
- 9) Myers, J.: Handbook of Ocean and Underwater Engineering, McGraw-Hill, New York, 1969.
- 10) Japan Port Association: Examples of Design Calculation of Port Structures (Vol.1), pp.117-119, 1992. (in Japanese)
- 11) Ueda, S. and S. Shiraishi: On the Design of Fenders Based on the Ship Oscillations Moored to Quay Walls, Technical Note of PHRI, No.729, 1992. (in Japanese)
- 12) Shiraishi, S.: Low-Frequency Ship Motions Due to Long-Period Waves in Harbors, and Modifications to Mooring Systems That Inhibit Such Motions, Rept. of PHRI, Vol.37, No.4, pp.37-78, 1998.
- 13) Coastal Development Institute of Technology: Impact Evaluation Manual for Long-Period Waves in Ports, CDIT Library No.21, 2004. (in Japanese)
- 14) Ueda, S.: Analysis Method of Ship Motions Moored to Quay Walls and the Applications, Technical Note of PHRI, No.504, 1984. (in Japanese)
- 15) Motora, S., T. Koyama, M. Fujino and H. Maeda: (Revised Edition) Dynamics of Ships and Offshore Structures, Seizando-Shoten Publishing, pp.39-121, 1997. (in Japanese)
- 16) Ueda, S. and S. Shiraishi: Method and its Evaluation for Computation of Moored Ship's Motions, Rept. of PHRI, Vol.22, No.4, pp.181-218, 1983. (in Japanese)
- 17) Goda, Y., T. Takayama and T. Sasada: Theoretical and Experimental Investigation of Wave Forces on a Fixed Vessel Approximated with an Elliptic Cylinder, Rept. of PHRI, Vol.12, No.4, pp.23-74, 1973. (in Japanese)
- 18) Oil Companies International Marine Forum (OCIMF): Mooring Equipment Guidelines, 3rd Edition, Seamanship International Ltd, 2008.
- 19) Kobayashi, M., H. Yuasa, O. Kishimoto, M. Abe, Y. Kunitake, J. Narita, M. Hirano and Y. Sugimura: Theoretical calculation program for performance of seaworthiness of ships (Part 1, Theoretical equations), Technical Bulletin of Mitsui Shipbuilding, No.82, pp.18-34, 1973. (in Japanese)
- 20) Tsuji, T., K. Takaishi, S. Suga and T. Sato: Model Experiment on Wind Force on Ships, Rept. of National Ship Research Institute, Vol.7, No.5, pp.13-37, 1970. (in Japanese)

- 21) Isherwood, R. M.: Wind resistance of merchant ships, Bulletin of the Royal Institution of Naval Architects, pp.327-338, 1972.
- 22) Ueda, S., S. Shiraishi, K. Asano and H. Oshima: Proposal of Formula of Wind Force Coefficient and Evaluation of the Effect to Motions of Moored Ships, Technical Note of PHRI, No.760, 1993. (in Japanese)
- 23) Davenport, A. G.: Gust loading factors, Journal of the Structural Division, ASCE, Vol.93, Issue 3, pp.11-34, 1967.
- 24) Hino, M.: Relationship between the instantaneous peak values and the evaluation time- A theory on the gust factor, Journal of JSCE, Vol.117, pp.23-33, 1965. (in Japanese)
- 25) Coastal Development Institute of Technology: Technical Manual for Floating Structure, pp.37-55, 1991. (in Japanese)
- 26) Yoneyama, H.: Study on Tractive Forces of Ships Acting on Mooring Posts and Bollards, Technical Note of PARI, No.1341, 2018. (in Japanese)
- 27) Takahashi, H., A. Goto and M. Abe: Study on Ship Dimensions by Statistical Analysis - Standard of Main Dimensions of Design Ship (Draft) -, Research Report of NILIM, No.28, pp.116-118, 2006. (in Japanese)
- 28) Nippon Kaiji Kyokai (ClassNK): Rules for the Survey and Construction of Steel Ships; Guidance for the Survey and Construction of Steel Ships Part L (Equipment), 2017. (in Japanese)
- 29) Japan Fishing Port Association: Design Method for Shipping Port Facilities, 1984. (in Japanese)

Chapter 9 Environmental Actions

[Public Notice] (Environmental Actions)

Article 19

The effects of environmental actions shall be assessed with appropriate methods in consideration of the conditions to which the facilities are subjected such as the design service life, the material characteristics, the environmental conditions, the maintenance methods.

[Interpretation]

7. Setting of Environmental Conditions

(8) **Other Matters** (Article 6 of the Ministerial Ordinance and the interpretation related to Article 19 and 20 of the Public Notice)

① Environmental actions

When evaluating the effects of environmental actions, it is necessary to appropriately consider factors that cause the deterioration or change of properties of materials in structures by taking into account the design working life of the facility concerned, the material characteristics, the environmental conditions, the maintenance methods, and other conditions to which the facility is subjected. Considering that there are cases wherein multiple factors act together, it is also necessary to simultaneously consider multiple environmental actions depending on the circumstances.

If there is a possibility that environmental actions may cause the deterioration or a change in the properties of materials in a structure and make it difficult for the structure to achieve the required performance during its design working life, it is necessary to appropriately consider the effects of the environmental actions according to the circumstances. (Refer to **Part I, Chapter 2, 4 Maintenance of Facilities Subject to the Technical Standards.**) When evaluating the effects of environmental actions, it is necessary to appropriately consider the material characteristics, installation state of the facility, and other factors.

For the evaluation of environmental actions on steel, refer to **Part II, Chapter 11, 2.4 Corrosion Control of Steel** and **Part III, Chapter 2, 1.3.5 Corrosion Control Design of Steel**. For the evaluation of environmental actions on concrete, refer to **Part II, Chapter 11, 3.2 Concrete Quality and Performance Characteristics** and **Part III, Chapter 2, 1.2 Concrete**. For the evaluation of environmental actions on other materials, refer to **Part II, Chapter 11, 8 Other Materials**.

The main environmental actions include temperatures; moisture; substances that affect the progress of deterioration, such as chloride ions; and ultraviolet rays.

(1) Effects of environmental actions on reinforced concrete

① Overview

Regarding environmental actions on reinforced concrete, it is necessary to consider the factors that affect the change in the properties of concrete and the corrosion of internal steel members. Carbon dioxide and chloride ions affect steel corrosion, low temperatures affect frost damage, and sulfate ions affect chemical deterioration. Furthermore, temperature changes, water supply, and drying affect not only the abovementioned deterioration but also the temperature stress, cracking, shrinkage, alkali-aggregate reaction, and other phenomena of concrete.

② Evaluation of the effects of environmental actions on reinforced concrete

A deterioration phenomenon of concrete may be caused by not only a single factor but also combined factors. Therefore, when evaluating the effects of environmental actions on reinforced concrete, it is necessary to simultaneously consider two or more environmental actions depending on the circumstances.

For concrete port structures located in the ocean, it is common to consider the effects of chloride ions on steel corrosion in terms of the concentration of chloride ions on concrete surfaces (refer to **Part III, Chapter 2, 1.2.4 Examination of Change in Performance Over Time**).

(2) Effects of environmental actions on steel and its corrosion protection methods

① Overview

Regarding environmental actions on steel, it is necessary to consider factors that affect steel corrosion. The main factors include temperatures, flow velocities, waves, and water quality.

Steel corrosion protection methods include the cathodic protection method and coating method. Environmental actions on the cathodic protection method include temperatures, flow velocities, waves, and water quality, and those on the coating method include water quality, temperatures, and ultraviolet rays.

② Evaluation of the effects of environmental actions on steel and its corrosion protection methods

When evaluating the effects of environmental actions on steel, it is generally necessary to divide a steel corrosion environment into the part in the air over the sea, the splash zone, the tidal zone, the part in the seawater, and the part in the sea bottom soil depending on the installation state of the steel.

When evaluating environmental actions on the cathodic protection method, it is common to mainly consider the water quality and flow velocities. When evaluating environmental actions on the coating method, it is necessary to mainly consider the water quality, temperature, and ultraviolet ray intensity.

(3) Others

When evaluating the effects of environmental actions on materials other than concrete and steel, it is advisable to fully consider the special characteristics of facilities located in the ocean or in ports.

Chapter 10 Self-Weight and Surcharge

[Public Notice] (Self-weight and Surcharge)

Article 20

- 1 Self-weight shall be appropriately set based on the unit weight of each material.
- 2 Surcharge load shall be appropriately set in consideration of the assumed usage conditions, etc. of the facilities.

[Interpretation]

7. Setting of Environmental Conditions

(8) **Other Matters** (Article 6 of the Ministerial Ordinance and the interpretation related to Article 19 and 20 of the Public Notice))

② Self-weight and surcharge

When setting the self-weight and surcharge to be considered in the performance verifications of facilities subject to the technical standards, appropriate consideration shall be given to the preload, weight of construction equipment, and other loads applied during construction as needed.

1 General

(1) When verifying the performance of a port facility, its self-weight and surcharge shall be considered if necessary.

(2) Self-weight and surcharge are defined respectively as follows:

- ① Self-weight: This refers to the weight of the facility itself.
- ② Surcharge: The surcharge mentioned here is classified as static loads or live loads and refers to the actions of static loads, snow loads, train loads, vehicle loads, cargo-handling equipment loads, sidewalk live loads, and other loads. When setting the surcharge, it is necessary to appropriately consider the assumed usage conditions of the facility.

The characteristic value of surcharge shall be appropriately set by considering the usage conditions of the port facility, such as the type and volume of the cargo handled, and the handling methods.

(a) Static loads

Static loads are applied by general cargo and bulk cargo loaded on aprons, sheds, warehouses, and other facilities. In regions with heavy snowfall, snow that accumulated on an apron is also regarded a type of static load, namely, a snow load. For more information, refer to Article 86 of **the Order for Enforcement of the Building Standards Act** (Cabinet Order No. 156 of 2017).

(b) Live loads

The following dynamic loads shall be considered as live loads if necessary when verifying the performance of port facilities.

- 1) Train load
- 2) Vehicle load
- 3) Cargo-handling equipment load
- 4) Sidewalk live load

(3) The self-weight and surcharge to be considered in the performance verification of a port facility must be set with consideration given to the type of actions on the facility and its loading conditions. In particular, the self-weight and surcharge have large effects on the performance verification of the circular slip failure of quaywalls and the performance verification of beams and slabs of piled piers. Therefore, sufficient care should be taken when determining the types and sizes of self-weight and surcharge.

2 Self-weight

(1) Self-weight

In the performance verification of a facility to which the technical standards apply, the self-weight must be appropriately set on the basis of the unit weight of each material.

- (2) The values given in **Table 2.1.1**¹⁾ may be generally used as the characteristic values of the unit weights in the calculation of self-weight, except in cases wherein the unit weights can be specified in preliminary surveys or other methods.
- (3) The unit weights of stone, sand, gravel, and rubble depend on the stone quality, whereas the unit weights of materials other than metals, such as steel and aluminum, vary case by case. When using these materials, the characteristic values of unit weights must be determined with care.

Table 2.1.1 Characteristic Values of Unit Weights of Materials¹⁾

Material	Characteristic value of unit weight (kN/m ³)
Steel and cast steel	77.0
Cast iron	71.0
Aluminum	27.5
Reinforced concrete	24.0
Non-reinforced concrete	22.6
Timber	7.8
Asphalt concrete	22.6
Stone (granite)	26.0
Stone (sandstone)	25.0
Sand, gravel, and rubble (dry)	16.0
Sand, gravel, and rubble (wet)	18.0
Sand, gravel, and rubble (saturated)	20.0

[References]

- 1) Japan Port Association: Handbook of Construction of port facilities, p. 140, 1959

3 Surcharge

3.1 Static Load

(1) Static loads in permanent situations

- ① When determining the characteristic values of static loads in permanent situations, it is preferable to adequately consider factors such as cargo type handled, packing type, volume, handling methods, and loading time.
- ② Generally, in the performance verification of a facility such as an apron, a shed, or a warehouse, the mean value of the static load in an area of the facility is used. However, in the performance verification of a structural member, the static load on it is often used directly. The static load acting on an apron has a large effect on the stability verification of a mooring facility; therefore, it is necessary to consider it separately from the static loads on other facilities, such as sheds and warehouses. For an apron, the mean value of the static load per area is usually dependent on the scale of the mooring facility and the type of cargo handled, and the mean value may be determined by referring to verifications performed in the past. In the case of general-purpose wharves, the values from approximately 10 to 30 kN/m² are often used as the characteristic values of the static loads acting on aprons. For aprons wherein heavy cargo such as containers or steel is handled, it is preferable to determine the value of the static load on the basis of the study of usage conditions.
- ③ The characteristic values of unit weights for bulk cargo were obtained on the basis of surveys of past actual conditions, which are listed in **Table 3.1.1**.¹⁾

Table 3.1.1 Characteristic Values of Unit Weights for Bulk Cargo¹⁾

Type of cargo	Characteristic value of unit weight (kN/m ³)
Coke	4.9
Coal (lump)	8.8–9.8
Coal (fine)	9.8–11.0
Iron ore	20.0–29.0
Cement	15.0
Sand, gravel, and rubble	16.0–20.0

(2) Static loads during seismic ground motion

- ① It is preferable to determine the characteristic values of static loads during seismic ground motion in variable and accidental situations by adequately predicting whether static loads will act or not when the design seismic occurs in the future. The existence or nonexistence of a static load differs depending on the type of facility, such as sheds, warehouses, open storage yards, and aprons.
- ② For facilities such as sheds, warehouses, and open storage yards, static loads during seismic ground motion may be set according to their usage conditions. On the contrary, for facilities used as cargo-handling facilities, such as aprons, where cargo is only placed temporarily, static loads will vary considerably in terms of size and state depending on whether a ship on the berth is being loaded/unloaded. Moriya and Nagao²⁾ performed field measurements to study the moment-to-moment changes in the static load of bulk cargo that was loaded on an apron and evaluated the design value of the static load during seismic ground motion. According to their results, the design value of the static load during seismic ground motion is 0 kN/m² when it is calculated in accordance with **ISO 2394** and **Eurocodes**, but the adoption of 0 kN/m² as the design value of the static load during seismic ground motion results in the underestimation of the static load.²⁾ Therefore, it is preferable to calculate the static load during seismic ground motion by assuming the mean value of the static load in the permanent situation as the characteristic value and by multiplying this value by 0.5.

(3) Unevenly distributed static load

- ① When verifying the performance of the whole part of a facility, it is possible to calculate the characteristic value of a static load such as an apron, a shed, or a warehouse by substituting an unevenly distributed load with a uniformly distributed load in an area of the facility. However, when a large concentrated load acts on the facility, it should be considered as the concentrated load.

- ② Usually, it is unlikely that materials, such as cargo, are evenly loaded over the entire area. However, when steel is placed on timber pillows, it can be assumed that its weight acts as a line load. In this case, it is preferable to assume that the weight is a concentrated load, such as a line load or a point load.
- ③ When considering a given area, even though the mean value of the unevenly distributed load may fall within the value of the uniformly distributed load used as a substitute, it is necessary to take into account the case wherein the unevenly distributed load acts as a concentrated load. For example, in the case of a sheet pile quaywall, a dangerous situation may arise if a large concentrated load acts on the back of the quaywall. Similarly, in the case of a piled pier or a similar facility, if a concentrated load acts in the center of a slab, the slab may break. These possibilities should be considered when setting the static load.

(4) Snow load

- ① In snowy districts, snow that accumulated on an apron may compact under its own weight or be compacted and hardened by automobiles and the like depending on the amount of snowfall, and such snow acts as a static load. Therefore, it is preferable to set an appropriate snow load in line with the actual conditions.
- ② For a mooring facility where snow removal operations will be performed, it is often sufficient to determine the snow load on the basis of overnight snowfall. In this case, it is possible for engineers to determine the snow load appropriately by taking into consideration past snowfall records, general weather conditions during snowfall, snow quality, snow removal, and other conditions.
- ③ In most cases, the snow load is set as 1 kN/m^2 . This is equivalent to a snowfall of approximately 70 to 100 cm for dry or fresh powder snow.
- ④ **The Railway Structure Design Standards and Commentary³⁾** shows the relationship between normal snow conditions and the unit weight of snow as shown in **Table 3.1.2**.

Table 3.1.2 Snow Conditions and Characteristic Value of Unit Weight of Snow³⁾

Snow Condition	Characteristic Value of Unit Weight (kN/m^3)
Dry powder snow compressed under its own weight	1.2
Dry powered snow subject to wind pressure	1.7
Fairly wet snow compressed under its own weight	4.5
Very wet snow compressed under its own weight	8.5

3.2 Live Loads

(1) Train Load

The live loads caused by trains are based on the Technical Regulatory Standards on Japanese Railways.

- ① A train load shall be applied in such a way that induces the maximum effect on a facility or its members by taking into consideration the net weights, loaded weights, and axle arrangements of the trains or cars that are generally used for the line concerned. In doing so, the train load shall be applied as a full set of multiple loads in succession without dividing it into two or more separate sets.
- ② According to **the Railway Structure Design Standards and Commentary³⁾**, electric locomotives and diesel locomotives are mainly used for rail transport. In view of the extension of sections dedicated for electric railcar operations, EA-loads based on electric locomotives (**Fig. 3.2.1**) and M-loads based on modeled passenger trains, including electric railcars and diesel railcars (**Fig. 3.2.2**), are currently used as train loads for locomotives.

















	(kN)												(kN/m)	(kN)					
E-10	100	100	100	100	100	100	100	100	100	100	100	100	29	A-10	76	112	112	} Axle Load (kN)	
E-11	110	110	110	110	110	110	110	110	110	110	110	110	32	A-11	84	123	123		
E-12	120	120	120	120	120	120	120	120	120	120	120	120	35	A-12	92	134	134		
E-13	130	130	130	130	130	130	130	130	130	130	130	130	38	A-13	99	145	145		
E-14	140	140	140	140	140	140	140	140	140	140	140	140	41	A-14	107	156	156		
E-15	150	150	150	150	150	150	150	150	150	150	150	150	44	A-15	115	168	168		
E-16	160	160	160	160	160	160	160	160	160	160	160	160	47	A-16	122	179	179		
E-17	170	170	170	170	170	170	170	170	170	170	170	170	50	A-17	130	190	190		
																			
	2.8m	2.0	2.8	2.0	2.8	4.0		2.8	2.0	2.8	2.0	2.8	2.0			1.9m	2.0		Wheelbase (m)

Fig. 3.2.1 E-Loads and A-Loads in the EA-Load System³⁾

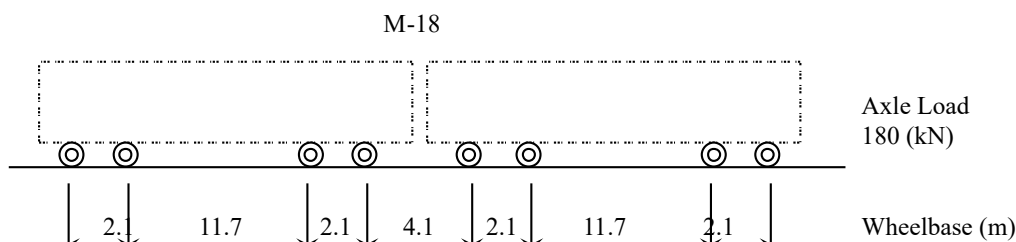


Fig. 3.2.2 M-Loads³⁾

(2) Vehicle Load

- ① For vehicle loads specified in the Appendix, refer to the **Highway Bridge Specifications and Commentary**.⁴⁾
- ② The **Highway Bridge Specifications and Commentary** specifies the vehicle loads. For port roads that are longer than 200 m, which are not subject to the **Highway Bridge Specifications and Commentary**, L-loads shall be set in consideration of the usage conditions of bridges.

(a) **Fig. 3.2.3** shows the T-loads.

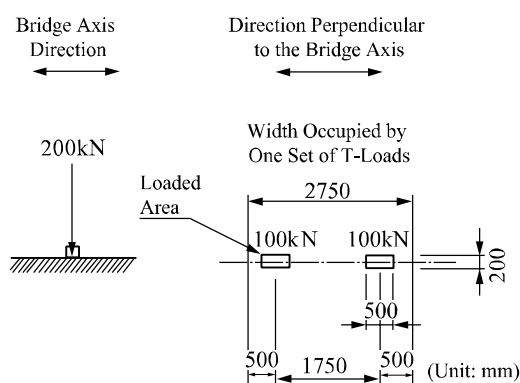


Fig. 3.2.3 T-Loads⁴⁾

(b) **Fig. 3.2.4** and **Table 3.2.1** show the L-loads for A-live loads and B-live loads.

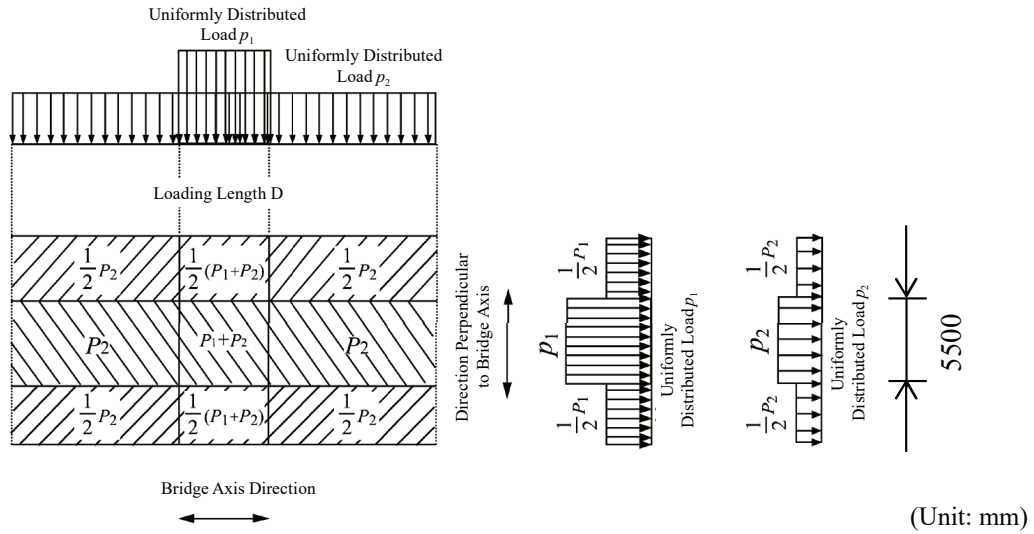


Fig. 3.2.4 L-Loads⁴⁾

Table 3.2.1 L-Loads⁴⁾

Load	Main Load (5.5 m wide)						Sub Load
	Uniformly Distributed Load p_1			Uniformly Distributed Load p_2			
	Loading Length D (m)	Load (kN/m ²)		Load (kN/m ²)			
		For Calculation of Bending Moment	For Calculation of Shearing	$L \leq 80$	$80 < L \leq 130$	$L > 130$	
A-live load	6	10	12	3.5	$4.3 - 0.01L$	3.0	50% of main load
B-live load	10						

Note) L: Span (m)

③ **Fig. 3.2.5** and **Table 3.2.2** show an example of a combination of a tractor and a trailer. They are based on a research by the Japan Association of Cargo-handling Machinery Systems and provide an example of the dimensions of tractors and trailers that are in practical use.

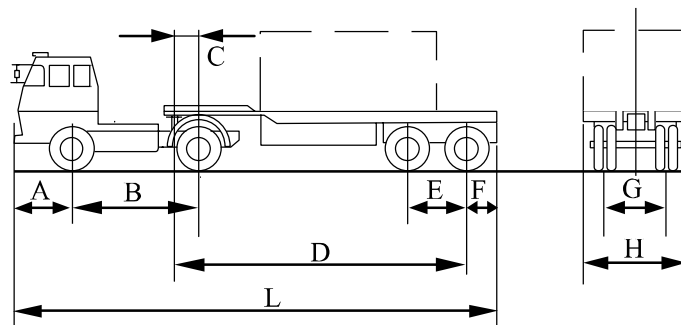


Fig. 3.2.5 Coupled Tractor and Trailer

Table 3.2.2 Example of Dimensions of Tractors and Trailers

	Dimensions									Maximum Load Capacity	Gross Vehicle Weight ^{*2,3}	Load Distribution When Loaded	
	Front Overhang	Maximum Tractor Wheelbase ^{*1}	Offset	Trailer Wheelbase ^{*1}	Tandem Wheelbase ^{*2}	Rear Overhang	Tread	Total Width	Overall Length			Fifth Wheel ^{*4}	Rear Wheel
Container Length	(A) m	(B) m	(C) m	(D) m	(E) m	(F) m	(G) m	(H) m	(L) m	t	t	kN	kN
20 ft (within the standard)	1.4	3.18	0.54	9.95	1.55	0.82	1.85	2.49	14.87	24.0	6.54 27.9	87.6	186.0
20 ft (fully loaded ISO container)	1.4	3.18	0.54	9.51	1.32×2	0.74	1.85	2.49	14.32	30.48	6.54 35.17	107.8	237.1
40 ft (within the standard)	1.4	3.18	0.54	9.66	1.55	2.29	1.85	2.49	16.03	24.0	6.54 27.47	87.1	182.3
40 ft (fully loaded ISO container)	1.4	3.18	0.54	9.52	1.32×2	1.99	1.85	2.49	15.60	30.48	6.54 35.12	107.5	236.9
20 ft/40 ft (within the standard)	1.4	3.18	0.54	9.53	1.55	2.44	1.85	2.49	16.01	23.6	6.54 27.8	87.6	185.1
20 ft/40 ft (fully loaded ISO container)	1.4	4.37	0.18	9.51	1.31 1.32×2	1.96	1.85	2.49	16.45	30.48	8.21 35.57	111.7	237.1

Notes: ^{*1} Maximum Tractor Wheelbase is the distance from the foremost axle to the rearmost axle, and Trailer Wheelbase is the distance from the center of the coupler to the rearmost axle.

^{*2} For Tandem Wheelbase and Gross Vehicle Weight, the numerical values in the upper and lower rows are for a tractor and a trailer, respectively.

^{*3} The Gross Vehicle Weight of a tractor is the sum of the tractor's vehicle weight and the weights of two occupants, and the Gross Vehicle Weight of a trailer is the sum of the trailer's vehicle weight and the maximum load capacity.

^{*4} Fifth Wheel refers to the coupling of a tractor and a trailer.

- ④ The international regulations concerning the dimensions and maximum gross mass of containers are indicated in **ISO 668:2005 (Table 3.2.3)**. The heights of vehicles are limited by the heights of aerial structures and traffic signals above roads. The Road Structure Ordinance specifies that the heights of aerial structures above roads shall not be lower than 4.5 m and that the total heights of vehicles shall not be higher than 3.8 m. However, for the transportation of high cube containers (with a height of 9 feet or 9 feet 6 inches), vehicles with a total height of up to 4.1 m are allowed to run only on designated roads (see **Fig. 3.2.6**).

Table 3.2.3 Standard Dimensions of Containers⁵⁾

Class	Length (L)				Width (W)				Height (H)				Maximum Gross Mass	
	mm	Allowance mm	ft in	Allowance in	mm	Allowance mm	ft	Allowance in	mm	Allowance mm	ft in	Allowance in	kg	Lb
1EEE ^{*3}	13,716	0 -10	45	0 -3/8	2,438	0 -5	8	0 -3/16	2,896	0	9 6	0	30,480	67,200
1EEE ^{*3}									2,591	-5	8 6	-3/16		
1AAA	12,192	0 -10	40	0 -3/8	2,438	0 -5	8	0 -3/16	2,896	0 -5	9 6 ^{*1}	0 -3/16	30,480 ^{*1}	67,200 ^{*1}
1AA									2,591 ^{*1}	0 -5	8 6 [*]	0 -3/16		
1A									2,438	0 -5	8	0 -3/16		
1AX									<2,534		<8			
1BBB ^{*2}	9,125	0 -10	29 11 1/4	0 -3/16	2,438	0 -5	8	0 -3/16	2,896 ^{*1}	0 -5	9 6 ^{*1}	0 -3/16	30,480 ^{*1}	56,000 ^{*1}
1BB									2,591 ^{*1}	0 -5	8 6 ^{*1}	0 -3/16		
1B									2,438	0 -5	8	0 -3/16		
1BX									<2,438		<8			

Class	Length (L)				Width (W)				Height (H)				Maximum Gross Mass	
	mm	Allowa nce mm	ft in	Allowa nce i in	mm	Allowa nce mm	ft	Allowa nce i in	mm	Allowa nce s mm	ft in	Allowa nce s in	kg	Lb
1CC ^{*2}	6,058	0 -6	19 10 1/2	0 -1.4	2,438	0 -58	8	0 -3/16	2,591 ^{*1}	0 -5	8 6 ^{*1}	0 -3/16	30,480 ^{*1}	52,900 ^{*1}
1C									2,438	0 -5	8	0 -3/16		
1CX									<2,438		<8			
1D	2,991	0 -5	9 9 3/4	0 -3/16	2,438	0 -5	8	0 -3/16	2,438	0 -5	8	0 -3/16	10,160 ^{*1}	22,400 ^{*1}
1DX									<2,438		<8			

Notes: ^{*1} Some countries regulate the overall height of a vehicle and a container.

^{*2} On September 15, 2005, the maximum gross mass was increased from 25,400 kg for Class 1BBB and 24,000 kg for Class 1CC to 30,480 kg.

^{*3} These classes were added on October 1, 2005.

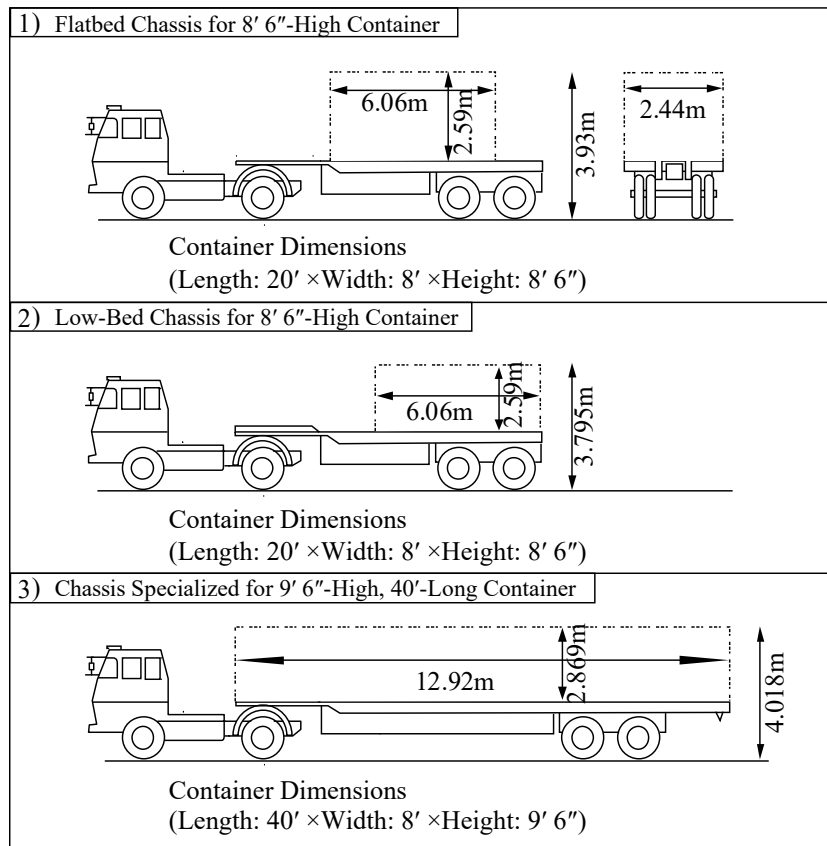


Fig. 3.2.6 Height of a Tractor Trailer Loaded with a Container

(3) Cargo Handling Equipment Load

① General

(a) Cargo handling equipment loads include the live loads of mobile cargo handling equipment, live loads of rail-mounted cargo handling equipment, and live loads of stationary cargo handling equipment, and their actions can generally be considered as follows:

- 1) As the characteristic value of a live load of mobile cargo handling equipment, the total weight, maximum wheel load, maximum outrigger load, or maximum crawler ground pressure of the mobile cargo-handling equipment that is expected to be used may be used.

- 2) As the characteristic value of a live load of rail-mounted cargo handling equipment, the maximum wheel load during an operation, during a heavy storm or during an seismic may be used. The wheel load has two components: vertical and horizontal.
 - 3) As the characteristic value of a live load of stationary cargo handling equipment, the maximum load may be used.
- (b) Cargo handling equipment continues to grow in size, and it is preferable to appropriately set the design conditions after fully studying the size of cargo handling equipment that is expected to be used in the facility concerned.

② Live Load of Rail-Mounted Cargo Handling Equipment

- (a) Rail-mounted cargo handling equipment includes container cranes, pneumatic unloaders, double-link level-luffing cranes, and double-link unloaders. In the case of large cargo handling equipment, such as portal bridge cranes and ore unloaders, it is necessary to appropriately consider factors such as the actions of seismic movement, wind loads, and impact loads during cargo-handling to perform the performance verification on the safe side.
- (b) **Fig. 3.2.7** and **Table 3.2.4** show examples⁶⁾ of rail-mounted cargo-handling equipment.

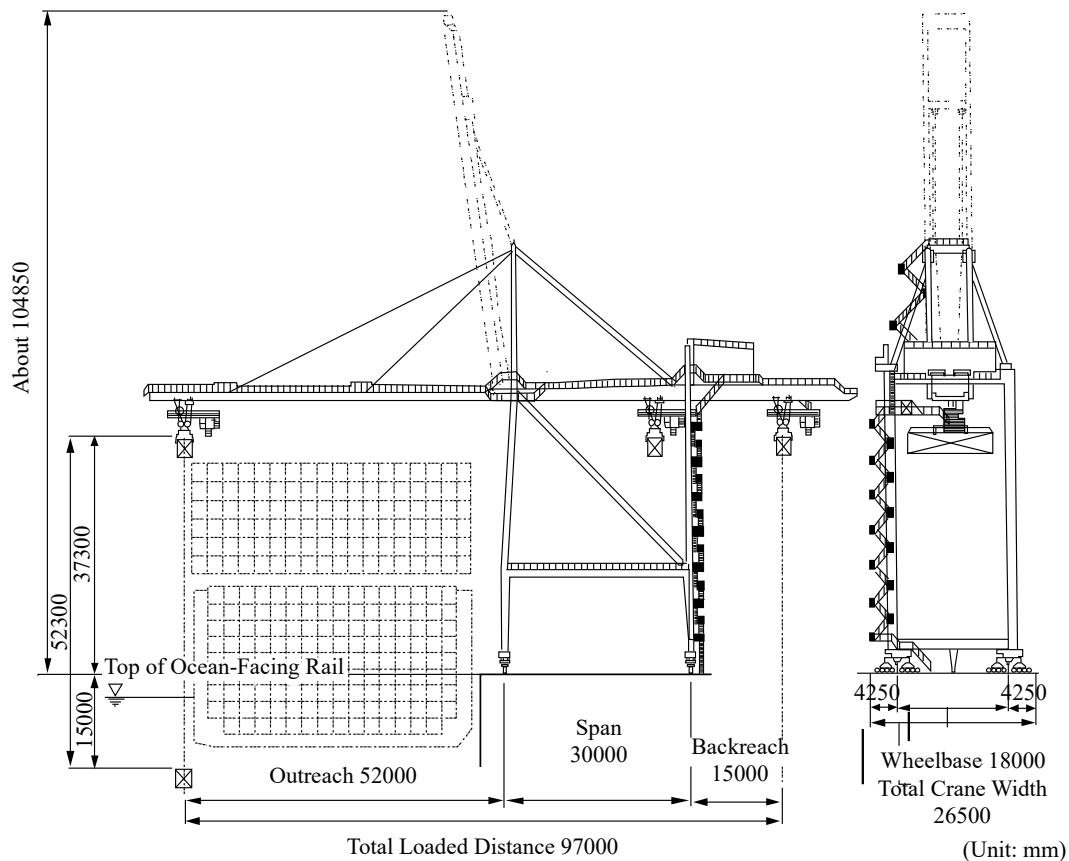


Fig. 3.2.7 Example of a Container Crane

Table 3.2.4 Examples of the Dimensions of Container Cranes

Machine Name	Handled Containers (ft)	Rated Load (kN)	Total Weight Equipped (kN)	Main Chassis Dimensions (m)						Maximum Wheel Load during Operation (kN/wheel)	Number of Wheels (Wheels/Corner)
				Outreach	Span	Backreach	Total Width	Total Height	Wheelbase		
A	20, 40	299	5,690	31.0	16.0	10.0	27.0	68.0	18.0	406	8
B	20, 40	299	6,151	31.0	16.0	9.0	28.0	72.0	18.0	314	8
C	20, 40	299	6,553	31.0	16.0	9.5	27.0	46.0	18.0	314	8
D	20, 40	299	6,229	40.0	16.0	11.0	27.0	80.5	18.0	343	8
E	20, 40	398	11,056	50.0	30.0	15.0	27.0	73.1	18.0	577	8
F	20, 40, 45	397	8,731	47.1	30.0	15.0	28.0	100.0	18.0	558	8
G	20, 40, 45	398	9,467	50.0	30.5	15.0	28.0	102.3	18.0	394	10
H	20, 40, 45	398	10,104	50.5	30.0	14.0	26.5	65.0	18.0	720	8
I	20, 40, 45	491	9,153	52.0	30.0	15.0	26.5	105.0	18.0	744	8
J	20, 40, 45	638	13,342	63.0	30.0	16.0	26.5	127.2	16.5	711	8

- (c) Automated Guided Vehicles (AGVs) are unmanned load carriers that were developed for various fields of physical distribution. AGVs refer to the unmanned load carriers used for automated and remote-controlled operations in container terminals. **Fig. 3.2.8** and **Table 3.2.5** show an example of the dimensions of an AGV.

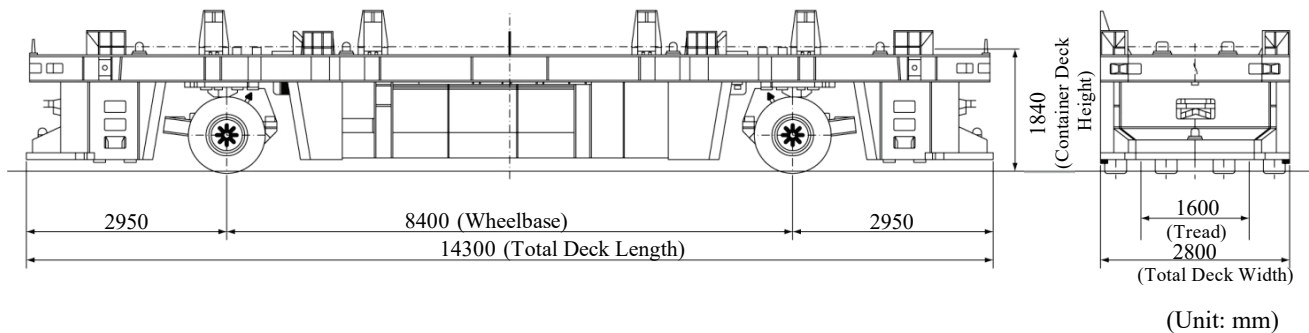

Fig. 3.2.8 Example of an AGV

Table 3.2.5 Example of the Dimensions of an AGV

Machine Name	Handled Containers (ft)	Rated Load (kN)	Total Weight Equipped (kN)	Main Chassis Dimensions (m)				Maximum Speed (km/h)	Positioning Accuracy (mm)
				Total Length	Total Width	Total Height	Wheel base		
A	20, 40, (45)	299	530	14.3	2.8	1.8	8.4	25	20

③ Live Load of Stationary Cargo Handling Equipment

Stationary cargo-handling equipment includes stationary jib cranes and stationary pneumatic unloaders.

④ Live Load of Mobile Cargo Handling Equipment

- (a) Mobile cargo handling equipment includes tire-mounted multipurpose jib cranes, rough-terrain cranes, all-terrain cranes, truck cranes, crawler cranes, container handling equipment including straddle carriers, transfer cranes, front-loading forklifts and side rollers, forklifts, and log loaders. Machines with outriggers, such as tire-mounted multipurpose jib cranes and truck cranes, cause relatively large concentrated loads; therefore, it is preferable to assume the most dangerous loading arrangement in the performance verification.

- (b) **Figs. 3.2.9 to 3.2.17** and **Tables 3.2.6 to 3.2.12** show examples⁶⁾ of mobile cargo-handling equipment.

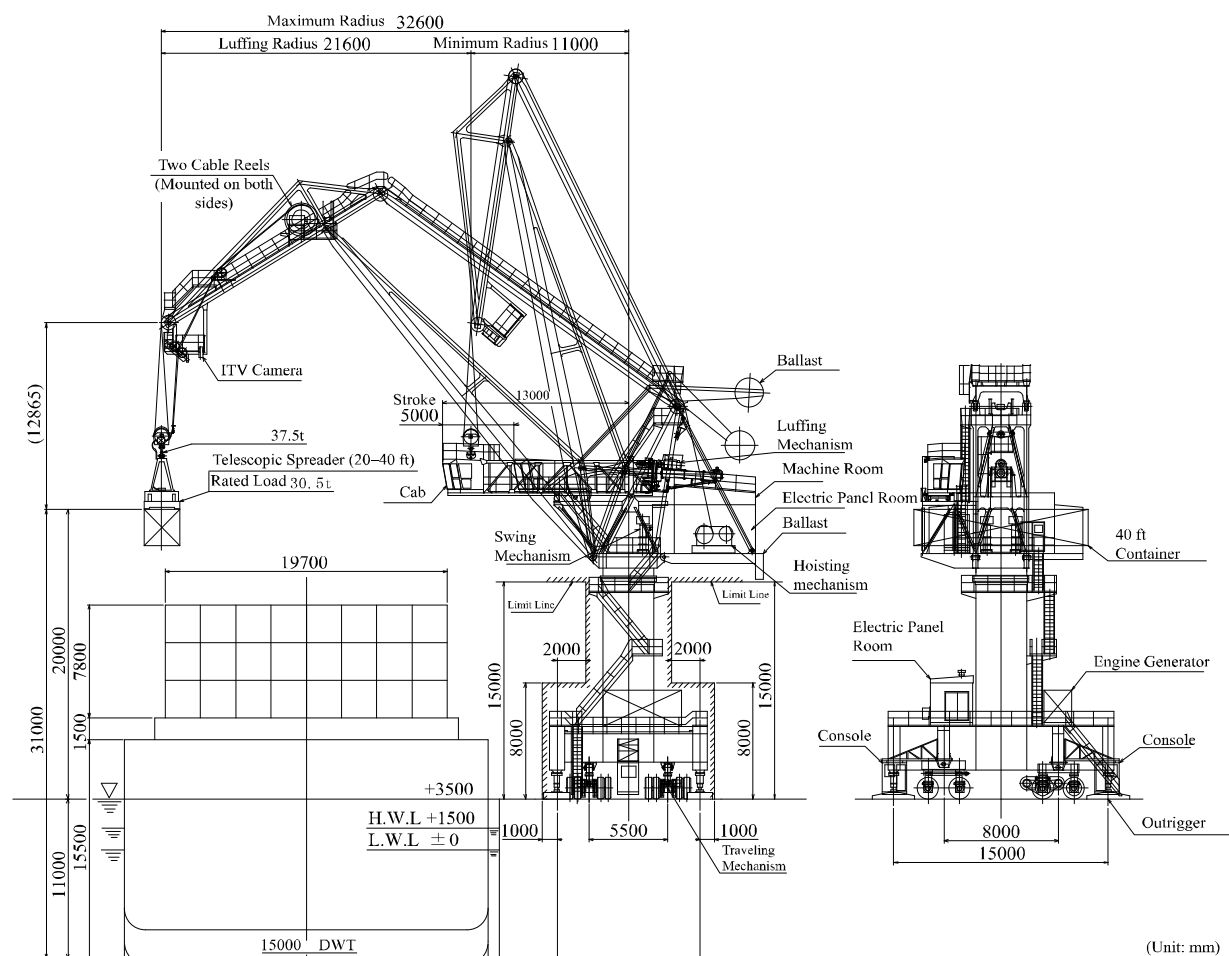


Fig. 3.2.9 Example of a Tire-Mounted Multipurpose Jib Crane

Table 3.2.6 Examples of the Dimensions of Tire-Mounted Multipurpose Jib Cranes

Type	Rated Load (kN)	Total Weight Equipped (kN)	Main Chassis Dimensions (m)					Maximum Wheel Load during Traveling (kN/wheel)	Maximum Ground Pressure during Operation*3 (kPa)
			Maximum Operating Radius	Total Width*1	Wheelbase	Wheel Track	Total Height*2		
Jib Crane	334	2,835	24.0	8.8	8.0	4.0	37.5	217	527
	335	3,875	30.0	11.0	25.2	3.5	48.0	255	174
	373	3,424	32.0	11.5	8.5	3.4	51.4	147	882
	392	3,630	34.0	12.0	9.7	4.3	59.5	320 (axle load)	280
Double-Link Level-Luffing Crane	334	3,983	30.0	13.0	15.0	5.0	42.5	142	358
	335	3,944	30.0	12.8	15.0	5.0	45.0	139	301
	338	4,169	28.0	11.7	10.0	4.5	39.0	294	314
	368	4,091	32.6	12.0	8.0	5.5	52.0	139	293

Notes: *1 Total Width is the total width of the traveling chassis.

*2 Total Height is the height of the top of the jib at the smallest operating radius.

*3 Maximum Ground Pressure during Operation is the outrigger ground pressure during operation.

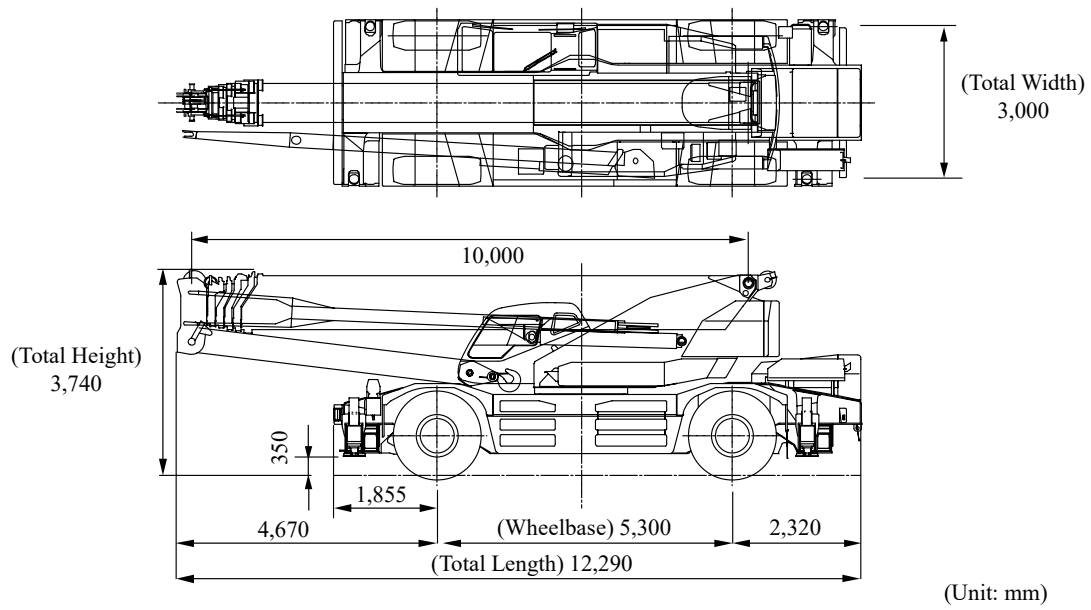


Fig. 3.2.10 Example of a Rough-Terrain Crane

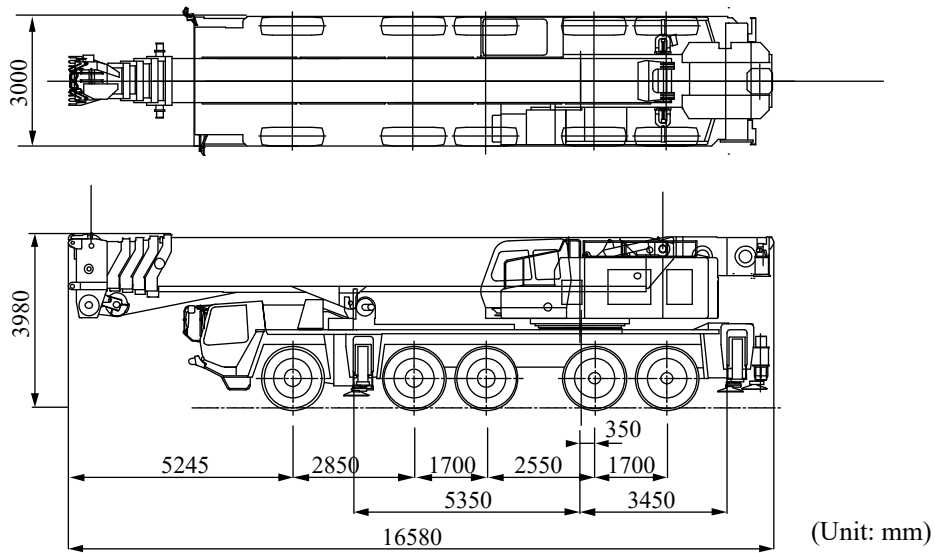


Fig. 3.2.11 Example of an All-Terrain Crane

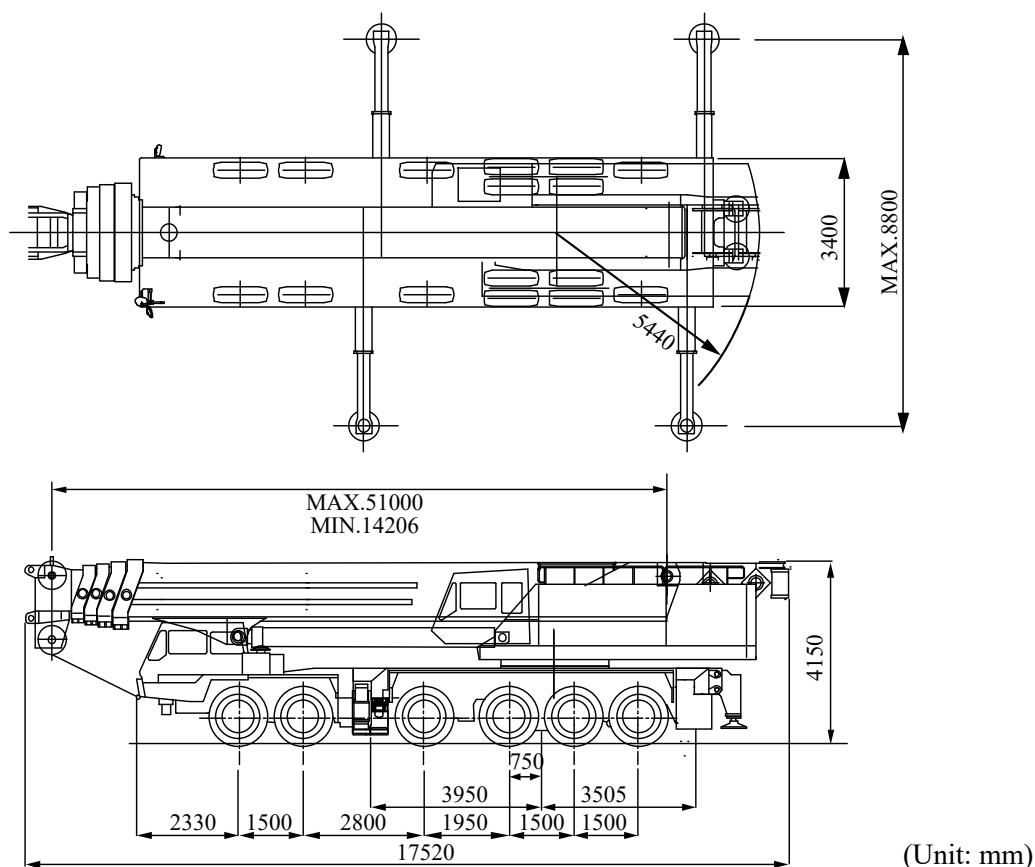


Fig. 3.2.12 Example of a Truck Crane

Table 3.2.7 Examples of the Dimensions of Rough-Terrain Cranes, All-Terrain Cranes, and Truck Cranes

Type	Maximum Lift Load (kN)	Total Weight Equipped (kN)	Main Chassis Dimensions* ¹ (m)					Maximum Axle Load* ² (kN)
			Total Length	Total Width	Total Height	Maximum Wheelbase	Wheel Track	
Rough-Terrain Crane	157	193	8.23	2.20	3.14	3.20	1.82	97.5
	245	260	11.21	2.62	3.45	3.65	2.17	131.2
	343	320	11.57	2.75	3.55	3.90	2.24	163.9
	491	371	11.85	2.96	3.71	4.85	2.38	185.3
	589	388	12.29	3.00	3.74	5.30	2.42	194.4
All-Terrain Crane	981	353	13.53	2.78	3.95	6.00	2.32	147.1
	1,570	858	16.58	3.00	3.98	8.80	2.56	171.6
	3,532	883	17.62	3.00	4.00	10.24	2.55	154.9
	3,924	1,236	18.29	3.00	4.10	11.30	2.56	179.5
	5,396	1,295	18.00	3.00	4.25	11.30	2.56	198.1
Truck Crane	1,177	929	15.38	3.40	4.00	7.38	2.76/2.52	392.8
	1,570	1,289	16.72	3.40	4.05	7.30	2.83/2.54	543.8
	3,532	1,118	17.52	3.40	4.34	9.25	2.83/2.54	297.7

 Notes: *¹ Main Chassis Dimensions are the dimensions when a crane is traveling in the premises.

 *² Maximum Axle Load is the maximum value of the axle loads when a crane is traveling in the premises.

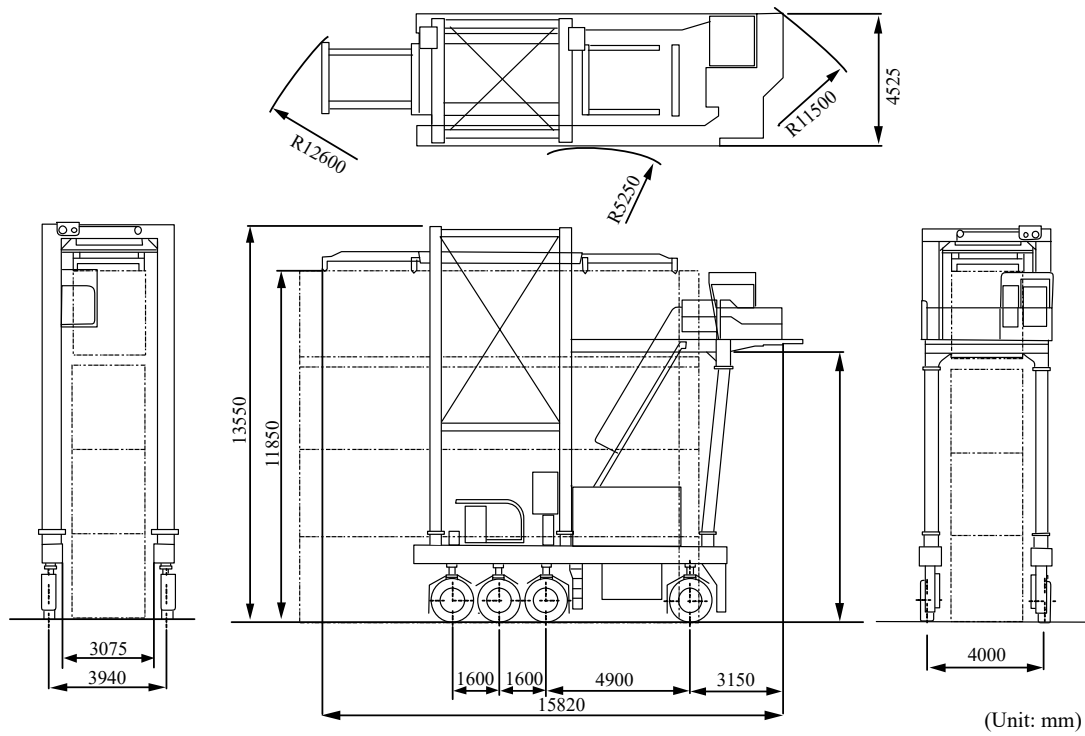


Fig. 3.2.13 Example of a Straddle Carrier

Table 3.2.8 Examples of the Dimensions of Straddle Carriers

Machine Name	Handled Containers (ft)	Rated Load (kN)	Total Weight Equipped (kN)	Main Chassis Dimensions (m)				Maximum Wheel Load during Operation (kN/wheel)
				Total Length* ¹	Total Width	Total Height	Wheel base	
A	20, 40	343	589	15.8	4.5	13.6	8.1	117
B	20, 40	392	579	12.2	5.3	12.6	7.4	122
C	20, 40, 45	343	579	17.4	4.5	13.7	8.0	124

Note: *¹ Total Length is the total length when a crane is handling a 40 ft container.

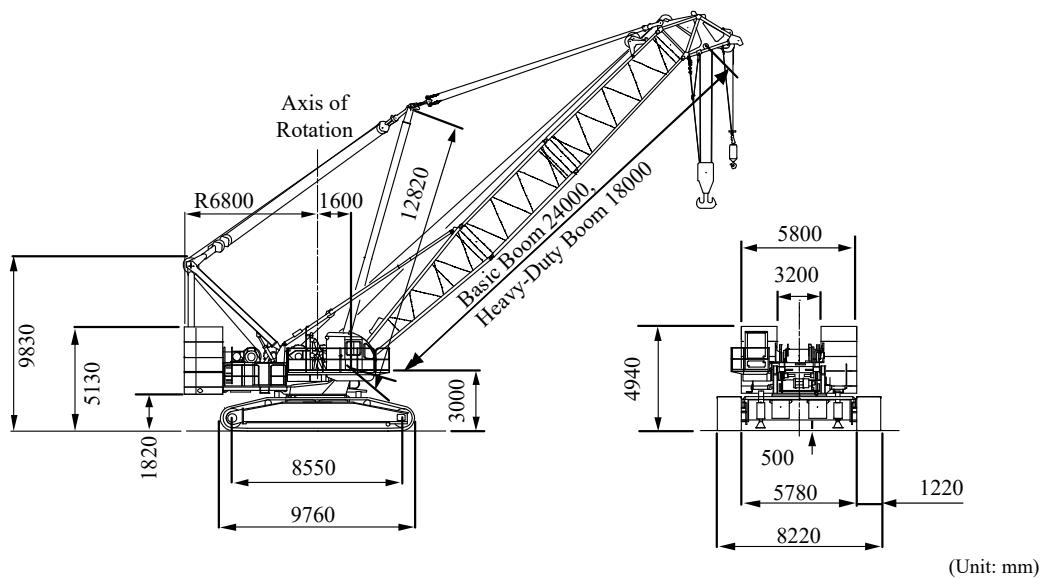


Fig. 3.2.14 Example of a Crawler Crane

Table 3.2.9 Example of the Dimensions of Crawler Cranes

Lift Load (kN)	Total Weight Equipped (kN)	Main Chassis Dimensions (m)				Crawler Ground Pressure (kPa)
		Total Height	Total Crawler Length	Total Crawler Width	Crawler Shoe Width	
294	324	4.72	4.49	3.30	0.76	54
441	441	5.12	5.40	4.30	0.76	60
491	481	5.25	5.57	4.35	0.76	61
687	697	6.18	5.99	4.83	0.80	80
785	850	6.56	6.32	4.90	0.90	86
883	834	6.64	6.40	4.90	0.85	91
981	1,197	7.92	7.88	6.17	0.92	90
1,472	1,579	8.49	8.49	7.07	1.07	89
1,962	1,893	8.49	9.18	7.07	1.07	103
2,943	2,786	9.83	9.76	8.22	1.22	127
3,434	2,884	7.82	10.14	8.79	1.29	120
4,415	3,826	10.12	11.51	9.50	1.50	122
7,848	11,674	—	14.68	12.80	2.00	127

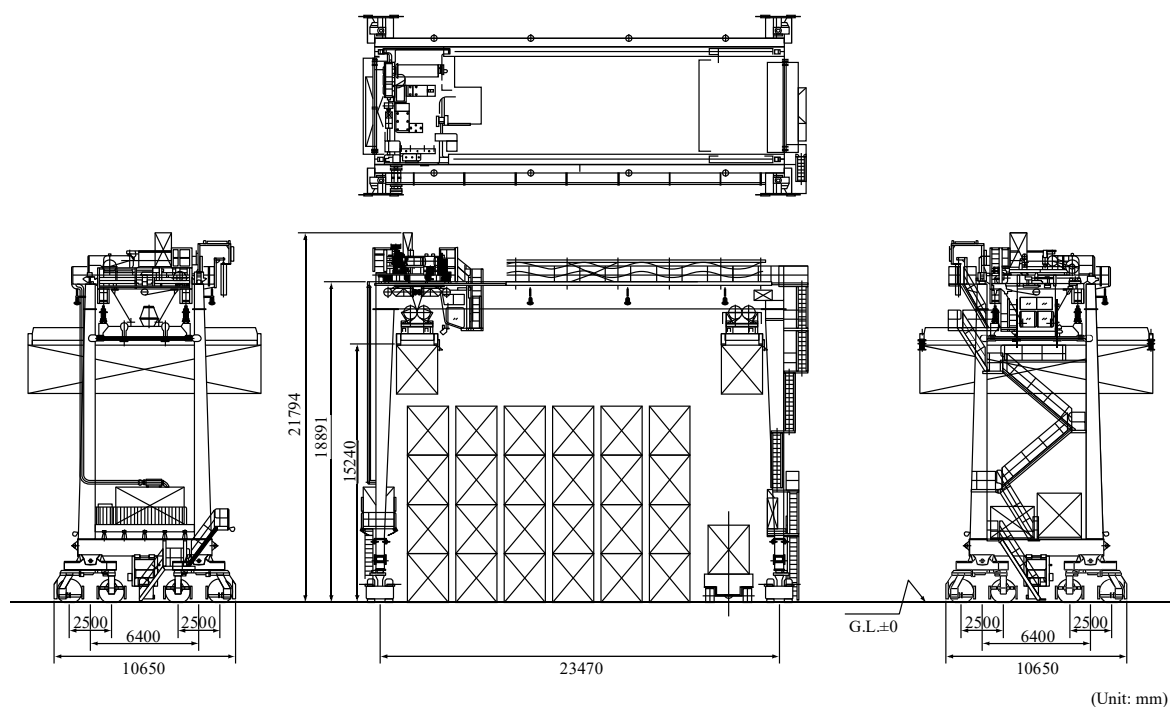

Fig. 3.2.15 Example of a Transfer Crane

Table 3.2.10 Examples of Dimensions of Transfer Cranes

Machine Name	Handled Containers (ft)	Rated Load (kN)	Total Weight Equipped (kN)	Main Chassis Dimensions (m)				Maximum Wheel Load during Operation (kN/wheel)	Number of Wheels (Wheels/ Corner)
				Total Length	Total Width	Total Height	Wheelbase		
A	20, 40	353	1,305	26.1	12.0	21.5	6.4	281	2
B	20, 40, 45	398	1,167	26.0	11.3	21.1	6.4	275	2
C	20, 40, 45	398	1,265	26.3	12.2	21.8	6.4	293	2
D	20, 40, 45	398	1,373	25.8	11.7	24.4	6.4	295	2
E	20, 40, 45	500	1,472	25.8	12.7	28.3	8.0	327	2
F	20, 40, 45	398	1,265	26.0	11.3	21.1	6.4	142	4
G	20, 40, 45	491	1,472	26.0	10.7	21.8	6.4	167	4

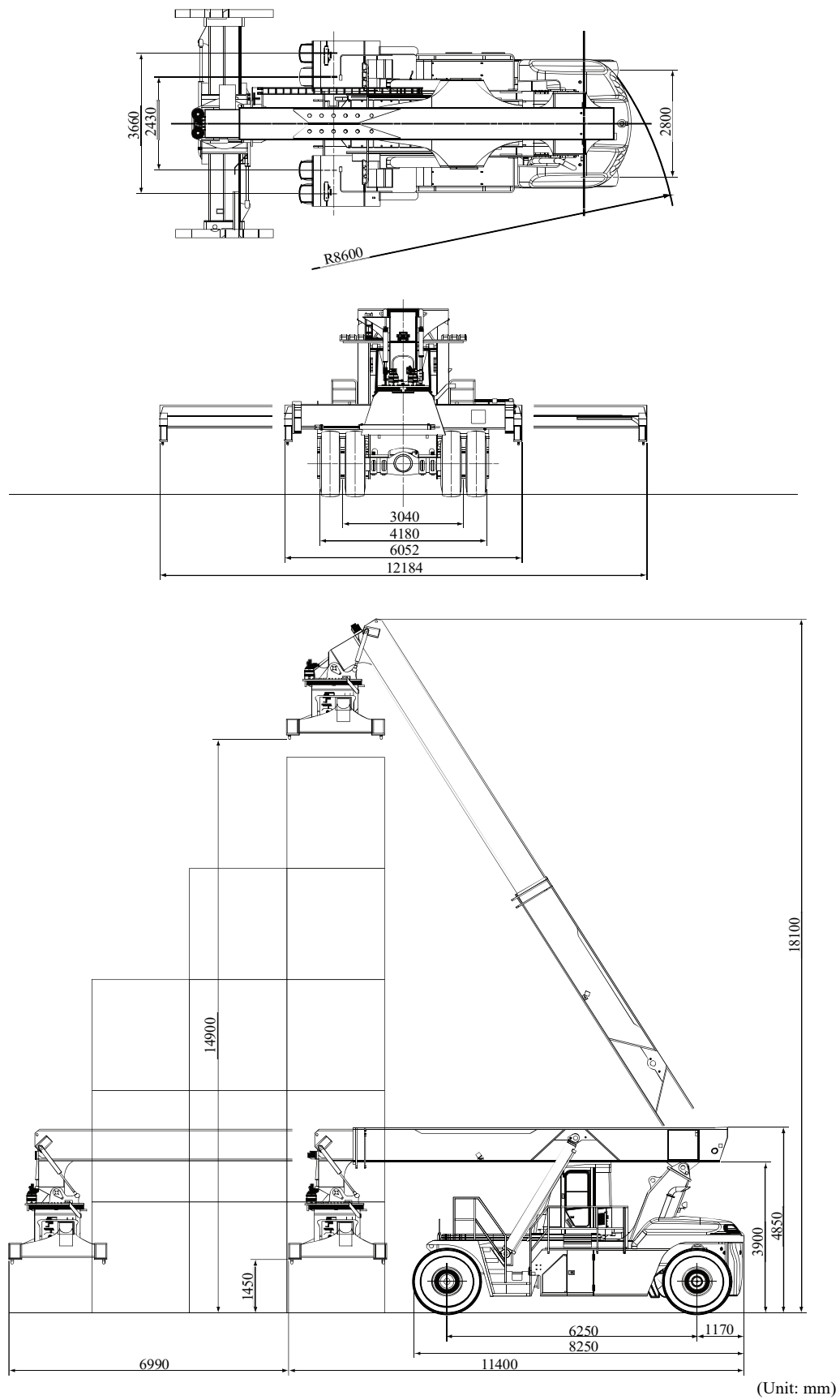


Fig. 3.2.16 Example of a Reach Stacker

Table 3.2.11 Examples of the Dimensions of Reach Stackers

Machine Name	Handled Containers (ft)	Rated Load (kN)	Total Weight Equipped (kN)	Main Chassis Dimensions (m)				Maximum Wheel Load during Operation (kN/wheel)	Number of Wheels (Wheels/Corner)
				Total Length	Total Width	Total Height	Wheelbase		
A	20, 40, 45	441	697	11.45	4.79	4.18	6.0	254.1	2
B	20, 40, 45	441	697	11.16	4.17	4.49	6.0	251	2

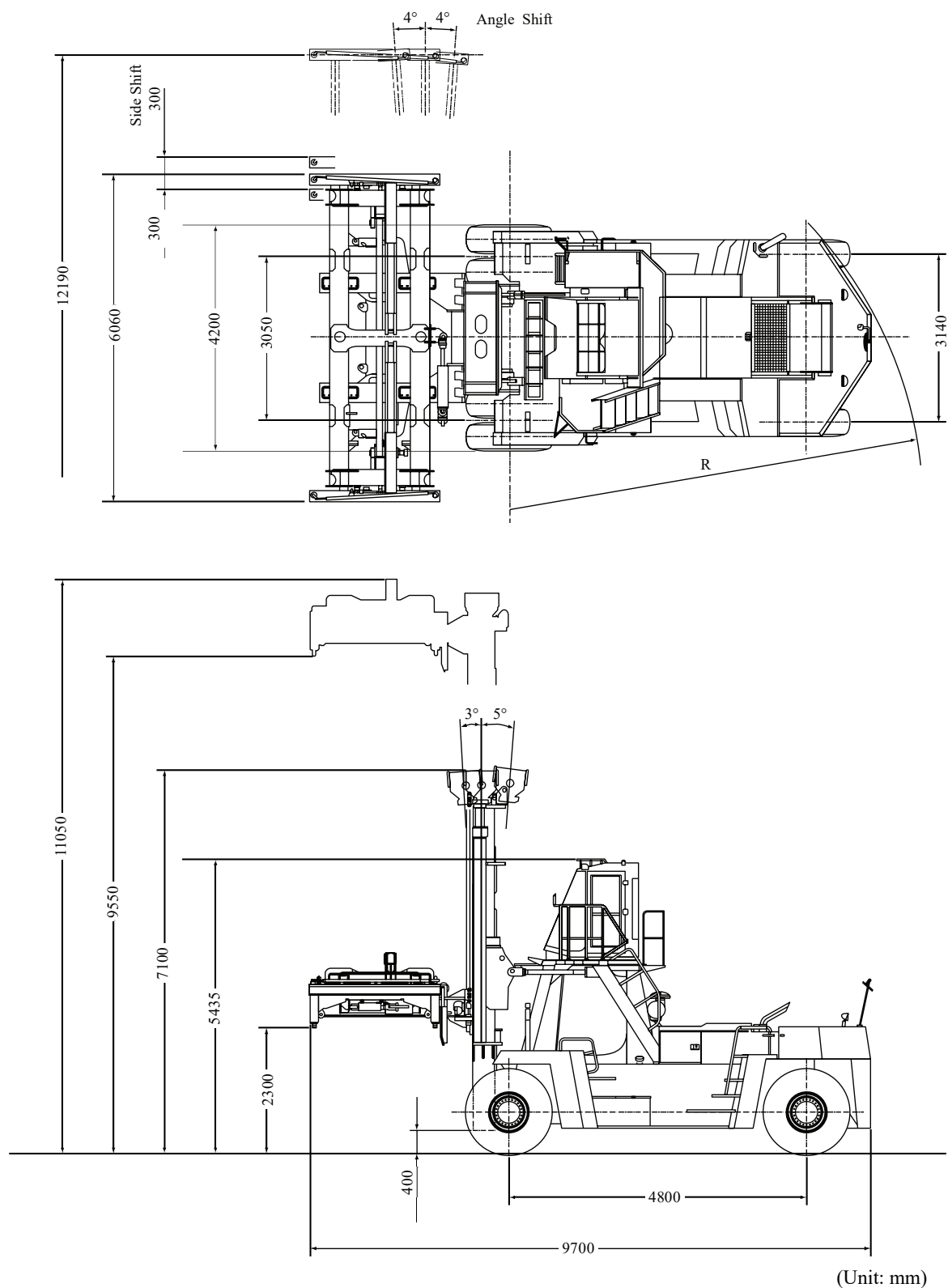


Fig. 3.2.17 Example of a Top Lift Container Handler

Table 3.2.12 Examples of the Dimensions of Top Lift Container Handlers

Machine Name	Handled Containers (ft)	Rated Load (kN)	Total Weight Equipped (kN)	Main Chassis Dimensions (m)				Maximum Wheel Load during Operation (kN/wheel)	Number of Wheels (Wheels/Corner)
				Total Length	Total Width	Total Height	Wheelbase		
A	20, 40, 45	343	643	10.4	4.2	8.3	5.5	226.1	2
B	20, 40, 45	343	667	15.8	4.5	13.9	4.8	223.4	2
C	20, 40, 45	314	670	10.89	6.1	10.7	5.5	-	2
D	20, 40, 45	343	715	17.4	4.5	18.7	5.5	-	2

(4) Sidewalk Live Load

The characteristic value of a sidewalk live load may usually be 5 kN/m^2 . However, it is preferable to appropriately set the characteristic values for special facilities by considering the usage conditions of the facilities.

[References]

- 1) Japan Port Association: Handbook of Construction of port facilities, pp. 303-304, 1959
- 2) Moriya Y. and T. Nagao: Earthquake loads of reliability design of mooring facilities, Proceedings of Offshore Development Vol. 19, pp. 713-718, 2003
- 3) Railway Technical Research Institute: Standard and commentary of design of railway structures—Concrete structures, Maruzen Publishing, pp. 58-59, 2004
- 4) Japan Road Association: Specifications for Highway Bridge Part I Common, pp.18-27, 2012
- 5) Japan Container Association: Containerization, No.291, p.15, 1996
- 6) Japan Association of Cargo-handling Machinery System: Handbook of port cargo-handling machinery system, 1996

Chapter 11 Materials

[Public Notice] (Fundamentals of Performance Verification)

Article 3 (excerpts)

- 2 The performance verification of the facilities subject to the Technical Standards shall be made, in principle, by executing the subsequent items, taking into consideration the situations that the facilities concerned will encounter during the design working life:
 - (1), (2) (omitted)
 - (3) Selection of materials and appropriate setting of their physical properties in consideration of their characteristics and environmental influences on them.

1 General

- (1) The materials to be used for port facilities shall be appropriately selected with consideration of actions, deterioration, designed working life, shapes, workability, economic efficiency, and impact on surrounding environments.
- (2) The materials to be used for buildings and railroad facilities are, respectively, subjected to the **Building Standards Act** (Act No. 201 of 1950), the **Technical Regulatory Standards on Japanese Railways** (Ordinance of the Ministry of Land, Infrastructure, Transport and Tourism No. 151 of 2001), the **Railway Construction Regulations** (Ordinance of the Ministry of Interior and Railways No. 1 of 1923), and orders related to these Acts and Ordinances.

(3) Selection of Materials

When selecting materials, give proper consideration to their quality and durability. The main materials for facilities subject to the Technical Standards include steel, concrete, bituminous materials, stone materials, wood materials, metal materials other than steel, plastic, rubber, paint materials, injection materials, landfill materials (including waste), and recyclable resource materials (for example, slag, coal ash, concrete mass, dredged soil, asphalt concrete mass). Also, those materials complying with Japanese Industrial Standards have the quality necessary to satisfy required performance of the facilities subject to the Technical Standards. The quality of those materials which do not comply with Japanese Industrial Standards, and those materials for which no Japanese Industrial Standards have been established, shall be verified through appropriate means such as material tests.

(4) Physical Properties of Materials

The physical properties of materials mean strength, unit weight, friction coefficient and others and shall be appropriately set on the basis of the standard values of Japanese Industrial Standards or quality data obtained through reliable tests. Also, the physical properties and cross-sectional specifications of materials shall be appropriately set considering the degradation of materials due to environmental actions.

2 Steel

2.1 General

- (1) Steel to be used for facilities subjected to the Technical Standards shall have the quality necessary to achieve the required performance for facilities. One example of materials satisfying such requirements is steel complying with Japanese Industrial Standard (JIS). In these Technical Standards and Commentaries, steel means carbon steel and, when referring to metal materials other than steel, respective individual names, such as stainless steel, titanium and aluminum, are used (Refer to **Part II, Chapter 11, 8.1 Metal Materials other than Steel**).

Tables 2.1.1 and **2.1.2** list steel which complies with JIS and has been used for port facilities relatively frequently.¹⁾ In addition to the types of steel listed in the tables, JIS has standardized many more steel materials.

- (2) In general, high-strength steel means structural steel with a tensile strength of 490 N/mm² or more. One of the important characteristics of high-strength steel is that a yield ratio (a ratio of yield strength to tensile strength) gets larger as the strength of steel is enhanced. Some types of high-strength steel, such as SM570, have had a problem with increased workload for preheating when used for welded members. The type of high-strength steel developed to solve this problem is the higher yield strength steel plates for bridges (SBHS steel), which has been used for Tokyo Gate Bridge.²⁾
- (3) The atmospheric corrosion-resisting steel is classified into Type W for use without painting and Type P for use with painting. In order to exhibit predetermined corrosion-resistant performance, the atmospheric corrosion-resisting steel needs to be used under proper environments. For example, when using Type W SMA without painting, pay attention to the applicable range in terms of the allowable amount of air-borne salt.³⁾ There have been cases of developing nickel-based and tin-based high atmospheric corrosion-resisting steel usable under a more severe splashed salt environment than SMA. Such types of steel have already been used for actual bridges.⁴⁾
- (4) Hat-shaped steel sheet piles, which have wider widths than conventional steel sheet piles, have been developed.⁵⁾ Because of the expanded widths per sheet, they are characterized by improved economic efficiency, workability, and structural reliability.

Table 2.1.1 Quality Standards of Steel (JIS)¹⁾

Type of steel	Standard		Symbol*1	Application
Structural steel	JIS G 3101	Rolled steels for general structure	SS400	Steel bar, shaped steel, steel plate, flat steel, steel strip
	JIS G 3106	Rolled steels for welded structure	SM400, SM490, SM490Y, SM520, SM570	Shaped steel, steel plate, flat steel, steel strip
	JIS G 3114	Hot-rolled atmospheric corrosion-resisting steels for welded structure	SMA400, SMA490, SMA570	Shaped steel, steel plate
	JIS G 3140	Higher yield strength steel plates for bridges	SBHS400, SBHS400W, SBHS500, SBHS500W, SBHS700, SBHS700W	Steel plate
	JIS G 3136	Rolled steels for building structure	SN400A, SN400B, SN400C, SN490B, SN490C	Steel plate, steel strip, shaped steel, flat steel
Steel pipe	JIS G 3444	Carbon steel tubes for general structure	STK400, STK490	
Steel pile	JIS A 5525	Steel pipe piles	SKK400, SKK490	
	JIS A 5526	Steel H piles	SHK400, SHK400M, SHK490M	
Steel sheet pile	JIS A 5528	Hot-rolled steel sheet piles	SY295, SY390	
	JIS A 5523	Weldable hot-rolled steel sheet piles*2	SYW295, SYW390, SYW430	
	JIS A 5530	Steel pipe sheet piles	SKY400, SKY490	
Cast and forged steel product	JIS G 3201	Carbon steel forgings for general use	SF490A, SF540A	Mooring post, chain, etc.
	JIS G 5101	Carbon steel castings	SC450	
	JIS G 4051	Carbon steels for machine structural use	S30CN,*3 S35CN*3	
	JIS G 5501	Gray iron castings	FC150, FC250	

Type of steel	Standard		Symbol*1	Application
Welding material	JIS Z 3211	Covered electrodes for mild steel, high tensile strength steel and low temperature service steel		Steel in general
	JIS Z 3214	Covered electrodes for atmospheric corrosion-resisting steel		Atmospheric corrosion-resisting steel
	JIS Z 3312	Solid wires for MAG and MIG welding of mild steel, high-strength steel and low temperature service steel		Steel in general
	JIS Z 3315	Solid wires for MAG and MIG welding of atmospheric corrosion-resisting steel		Atmospheric corrosion-resisting steel
	JIS Z 3313	Flux cored wires for gas shielded and self-shielded metal arc welding of mild steel, high-strength steel, and low temperature service steel		Steel in general
	JIS Z 3320	Flux cored wires for gas shielded and self-shielded metal arc welding of atmospheric corrosion resisting steel		Atmospheric corrosion-resisting steel
	JIS Z 3183	Classification for deposited metal of submerged arc welding for carbon steel and low alloy steel		Steel in general, atmospheric corrosion-resisting steel
	JIS Z 3351	Solid wires for submerged arc welding of carbon steel and low alloy steel		Steel in general, atmospheric corrosion-resisting steel
	JIS Z 3352	Fluxes for submerged arc welding		Steel in general, atmospheric corrosion-resisting steel
Joint material	JIS B 1180	Hexagon head bolts and hexagon head screws		
	JIS B 1181	Hexagon nuts and hexagon thin nuts		
	JIS B 1186	Sets of high-strength hexagon bolt, hexagon nut and plain washers for friction grip joints	F8T, F10T	
Wire	JIS G 3502	Piano wire rods	SWRS	Piano wire, oil tempered wire, PC steel, and stranded steel wire, wire rope
	JIS G 3506	High carbon steel wire rods	SWRH	Hard steel wire, oil tempered wire, PC hard steel wire, wire rope
	JIS G 3532	Low carbon steel wires	SWM	
	JIS G 3536	Steel wires and strands for prestressed concrete	SWPR1, SWPD1, SWPR2, SWPD3, SWPR7, SWPR19	
Bar	JIS G 3112	Steel bars for concrete reinforcement	SR235, SR295, SD295A, SD295B, SD345	
	JIS G 3117	Rerolled steel bars for concrete reinforcement	SRR235, SRR295, SDR235, SDR295, SDR345	
	JIS G 3109	Steel bars for prestressed concrete	Class A, Type 2; SBPR 785/1030 Class B, Type 1; SBPR 930/1080 Class B, Type 2; SBPR 930/1180 Class C, Type 1; SBPR 1080/1230	

Note:

*1: The symbols used for steel in JIS have suffixes. For example, JIS uses SM400A, SM400B, and SM400C for the classification of SM400 series. However, in the table above, these suffixes are omitted.

*2: There was a necessity of standardizing steel sheet piles having proper weldability to cope with the cases of breakage of welded sections on steel sheet piles caused by earthquakes. Thus, considering the importance of continued operation of the existing standards for steel sheet piles for the use which does not involve welding, particularly for temporary use, JIS A 5523 Weldable hot-rolled steel sheet piles was standardized separately from conventional JIS A 5528 Hot-rolled steel sheet piles.

*3: The materials standardized as S30C and S35C in JIS G 4051 are considered to be processed into the materials standardized as S30CN and S35CN respectively through normalizing so as to satisfy the mechanical properties specified in the explanatory attachment to JIS G 4051.

Table 2.1.2 Standardized Shapes of Steel (JIS)¹⁾

Type of steel		Standard	Material used
Structural steel	Steel bar	JIS G 3191	SS400
	Shaped steel	JIS G 3192	SS400, SM400, SM490, SM490Y, SM520, SM570, SMA400, SMA490, SMA570
	Steel plate and steel strip	JIS G 3193	SS400, SM400, SM490, SM490Y, SM520, SM570, SMA400, SMA490, SBHS400, SBHS500, SBHS700, SBHS400W, SBHS500W, SBHS700W
	Flat steel	JIS G 3194	SS400, SM400, SM490, SM490Y, SM520
Pile	Steel pipe piles	JIS A 5525	SKK400, SKK490
	H-shaped steel piles	JIS A 5526	SHK400, SHK400M, SHK490M
Sheet pile	Hot-rolled steel sheet piles	JIS A 5528	SY295, SY390
	Weldable hot-rolled steel sheet piles	JIS A 5523	SYW295, SYW390, SYW430
	Steel pile sheet piles	JIS A 5530	SKY400, SKY490
Joint material	Hexagon head bolts and hexagon head screws	JIS B 1180	
	Hexagon nuts and hexagon thin nuts	JIS B 1181	
	Sets of high-strength hexagon bolt, hexagon nut for friction grip joints	JIS B 1186	F8T, F10T
Reinforced concrete	Steel bars for concrete reinforcement	JIS G 3112	SR235, SR295, SD295, SD345
	Rerolled steel bars for concrete reinforcement	JIS G 3117	SRR235, SRR295, SDR235
Prestressed concrete	Steel wires and strands for prestressed concrete	JIS G 3536	SWPR, SWPD
	Steel bars for prestressed concrete	JIS G 3109	SBPR, SBPD
Mooring material	Wire ropes	JIS G 3525	SWRS, SWRH
	Flash butt welded anchor chain	JIS F 3303	
Wire mesh	Welded steel wire	JIS G 3551	WFP, WFR, WFI

- (5) When using rolled steel for general structures, rolled steel for welded structures, and hot-rolled atmospheric corrosion-resisting steels for welded structure, thicknesses can be selected with reference to **Fig. 2.1.1**.⁶⁾ When using steel with thicknesses less than 8 mm, it shall comply with the **Specifications and Commentary for Highway Bridges**.⁷⁾ The upper limits of thicknesses have been specified for respective steel grades in accordance with JIS standards because the steel to be used for members having large thicknesses requires a large additive amount of carbon to achieve the prescribed strength and increased carbon addition causes insufficient miniaturization of crystal grains during rolling and thereby aggravating notch brittleness.

Thickness (mm)		6	8	16	25	32	40	50	100
Steel grade	Steel for non-welded structure								
	SS400								
Steel for welded structure	SM400A								
	SM400B								
	SM400C								
	SM490A								
	SM490B								
	SM490C								
	SM490YA								
	SM490YB								
	SM520C								
	SM570								
	SMA400AW								
	SMA400BW								
	SMA400CW								
	SMA490AW								
	SMA490BW								
	SMA490CW								
	SMA570W								

 Fig. 2.1.1 Standards for Selecting Thicknesses by Steel Grades⁶⁾

- (6) The strength standards for PC steel wires and stranded steel wires are specified in **JIS G 3536** and the chemical compositions of steel are specified in **JIS G 3502 Piano wire rods**.
- (7) If the facilities have many welded sections (for example facilities with panel point structures), it is necessary to pay attention to chemical compositions and steel weldability. The steel grades generally used for welded members are: **JIS G 3106 Rolled steels for welded structure**; **JIS G 3114 Hot-rolled atmospheric corrosion-resisting steels for welded structure**; and **JIS G 3140 Higher yield strength steel plates for bridges**. In contrast, using SS400 specified in **JIS G 3101 Rolled steels for general structure** shall be limited to non-welded members.

2.2 Characteristic Values of Steel

- (1) The characteristic values of steel and cast steel required in the performance verification shall be appropriately set in consideration of strength characteristics.
- (2) **Characteristic Values of the Constants of Steel**

In general, the values in **Table 2.2.1** can be used for the Young's modulus, the shear modulus, Poisson's ratio, and the linear expansion coefficient of steel and cast steel.^{8) and 9)} For the constants of steel used for reinforced concrete and prestressed concrete, refer to the values in the **Standard Specification for Concrete Structures**.¹⁰⁾

 Table 2.2.1 Constants of Steel^{8) and 9)}

Young's modulus	E	2.0×10^5	N/mm ²
Shear modulus	G	7.7×10^4	N/mm ²
Poisson's ratio	ν	0.30	
Linear expansion coefficient	α	12×10^{-6}	1/°C

(3) Characteristic Values of Yield Stress

The characteristic values of yield stress of steel and cast steel shall be appropriately set on the basis of test results.

① Structural steel

- (a) In general, the values in **Table 2.2.2** can be used for characteristic values of yield stress of structural steel depending on the steel grades and thicknesses.¹¹⁾

Table 2.2.2 Characteristic Values of Yield Stress of Structural Steel¹¹⁾

Steel grade	Thickness mm	Tensile yield stress N/mm ²	Compressive yield stress N/mm ²	Shear yield stress* ¹ N/mm ²	Bearing yield stress (between steel plates) N/mm ²	Tensile strength N/mm ²
SS400	< 16	245 or more	245 or more	141	368	400 to 510
	16 to 40	235 or more	235 or more	136	353	
	40 to 100	215 or more	215 or more	124	323	
	100 <	205 or more	205 or more	118	308	
SM400 SMA400	< 16	245 or more	245 or more	141	368	400 to 510 (< 540)* ²
	16 to 40	235 or more	235 or more	136	353	
	40 to 75	215 or more	215 or more	124	323	
	75 to 100	215 or more	215 or more	124	323	
	100 to 160	205 or more	205 or more	118	308	
	160 to 200	195 or more	195 or more	113	293	
SM490	< 16	325 or more	325 or more	188	488	490 to 610
	16 to 40	315 or more	315 or more	182	473	
	40 to 75	295 or more	295 or more	170	443	
	75 to 100	295 or more	295 or more	170	443	
	100 to 160	285 or more	285 or more	165	428	
	160 to 200	275 or more	275 or more	159	413	
SM490Y SMA490	< 16	365 or more	365 or more	211	548	490 to 610
	16 to 40	355 or more	355 or more	205	533	
	40 to 75	335 or more	335 or more	193	503	
	75 to 100	325 or more	325 or more	188	488	
	100 to 160	305 or more	305 or more	176	458	
	160 to 200	295 or more	295 or more	170	443	
SM 520	< 16	365 or more	365 or more	211	548	520 to 640
	16 to 40	355 or more	355 or more	205	533	
	40 to 75	335 or more	335 or more	193	503	
	75 to 100	325 or more	325 or more	188	488	
SM570 SMA570	< 16	460 or more	460 or more	266	690	570 to 720
	16 to 40	450 or more	450 or more	260	675	
	40 to 75	430 or more	430 or more	248	645	
	75 to 100	420 or more	420 or more	242	630	
SBHS400 SBHS400W	6 to 100	400 or more	400 or more	231	600	490 to 610
SBHS500 SBS500W	6 to 100	500 or more	500 or more	289	750	570 to 720
SBHS700 SBHS700W	6 to 75	700 or more	700 or more	404	1050	780 to 930

*1: The von Mises yield criteria are applied to the calculation of shear yield stress.

*2: The figure within parentheses shows the value for SMA400.

- (b) When the contact mechanism between two steel surfaces is a flat surface against a flat surface (including cylindrical and curved surfaces close to plane ones), the bearing yield stress can be set at 50% more than the tensile yield stress. In the case of contact between a spherical (or cylindrical) steel surface and a plane steel surface on a very small area, the bearing yield stress can be calculated by the Hertz formula in the **Specifications and Commentary for Highway Bridges**¹²⁾ as needed.

② Characteristic values of steel piles and steel sheet piles

- (a) In general, the values in **Table 2.2.3** can be used for the characteristic values of the yield stress of steel piles and steel pipe sheet piles depending on the steel grades and the types of stress (for the reduction coefficients of axial compressive yield stress of steel piles, reference can be made to **Part III, Chapter 5**,

5.2.4 Performance Verification of Open-type Wharves on Vertical Piles).¹³⁾ There are cases of using high-strength steel equivalent to the grades of SM490Y, SM520, and SM570 for steel piles although the steel of these grades is not standardized by JIS.¹⁴⁾

Table 2.2.3 Characteristic Values of Yield Stress of Steel Piles and Steel Pipe Sheet Piles¹³⁾ (N/mm²)

Type of stress \ Steel grade	SKK400 SHK400 SHK400M SKY400	SKK490 SHK490M SKY490
Axial tensile stress (per net cross sectional area ^{*1)})	235	315
Bending tensile stress (per net cross sectional area ^{*1)})	235	315
Bending compressive stress (per total cross sectional area ^{*2)})	235	315
Shear stress (per total cross sectional area ^{*2)})	136	182

*1: A cross sectional area considering partial loss of areas such as bolt holes.

*2: A total cross sectional area without considering partial loss of areas.

- (b) The von Mises yield criteria are applied to the shear yield stress calculation.
- (c) When it is necessary to combine axial and shear stress, yield stress can be set with reference to the **Specifications and Commentary for Highway Bridges**.¹⁵⁾
- (d) Buckling strength varies, depending on the conditions of members subject to buckling and, therefore, shall be appropriately set in the verification of respective facilities.

③ Steel sheet piles

- (a) In general, the values in **Table 2.2.4** can be used for the characteristic values of the yield stress of steel sheet piles depending on the steel grades and the types of stress.¹⁶⁾

Table 2.2.4 Characteristic Values of Yield Stress of Steel Sheet Piles¹⁶⁾ (N/mm²)

Type of stress \ Steel grade	SY295 SYW295	SY390 SYW390	SYW430
Bending tensile stress (per net cross sectional area)	295	390	430
Bending compressive stress (per total cross sectional area)	295	390	430
Shear stress (per total cross sectional area)	170	225	248

- (b) The von Mises yield criteria are applied to the calculation of shear yield stress.

④ Cast and forged steel products

- (a) In general, the values in **Table 2.2.5** can be used for the characteristic values of the yield stress of cast and forged sheet products depending on the steel grades and the types of stress.¹⁷⁾

Table 2.2.5 Yield Stress of Cast and Forged Steel Products¹⁷⁾ (N/mm²)

Type of stress \ Type of steel	Forged steel		Cast steel	Steel for machine structure		Cast iron	
	SF490A	SF540A	SC450	S30CN	S35CN	FC150	FC250
Axial tensile stress (per net cross sectional area)	245	275	225	275	305	70	105
Axial compressive stress (per total cross sectional area)	245	275	225	275	305	140	210
Bending tensile stress (per net cross sectional area)	245	275	225	275	305	70	105
Bending compressive stress (per total cross sectional area)	245	275	225	275	305	140	210
Shear stress (per total cross sectional area)	141	159	130	159	178	54	88

- (b) The calculation method of bearing yield stress using the Hertz formula shall conform to the **Specifications and Commentary for Highway Bridges**¹⁸⁾ as needed.

⑤ **Yield stress of welding sections and joint materials**

- (a) In general, the values in **Table 2.2.6** can be used for the characteristic values of the yield stress of welding sections, depending on the steel grades and the types of stress. When joining steel members with different strengths, the values corresponding to the steel member with lower strength shall be used in general.

Table 2.2.6 Characteristic Values of Yield Stress of Welding Sections¹⁹⁾

(N/mm²)

Type of welding		Steel grade	SM400 SMA400	SM490	SM490Y SM520 SMA490	SM570 SMA570	SBHS400 SBHS400W	SBHS500 SBHS500W	SBHS700 SBHS700W
		Type of stress							
Shop welding	Full penetration groove welding	Compressive stress	235	315	355	450	400	500	700
		Tensile stress	235	315	355	450	400	500	700
		Shear stress	136	182	205	260	231	289	404
	Fillet welding, partial penetration groove welding	Shear stress	136	182	205	260	231	289	404
On-site welding		The same values as shop welding in principle.							

- (b) Considering the advancement of welding technologies and enhanced on-site construction management, as well as quality control, the same characteristic values of yield stress for shop welding can be applied to on-site welding, provided that on-site welding is executed by welders with appropriate skills under appropriate work environments, as stipulated in the **Specifications and Commentary for Highway Bridges**²⁰⁾ and the quality of on-site welding is controlled in the same level as that of shop welding through nondestructive tests and recording of work progresses. Basically, it is advisable to avoid underwater welding. Still, if underwater welding is to be executed by necessity, the characteristic yield stress values of the sections subjected to underwater welding shall be appropriately set, considering the possibility that welding quality largely fluctuates depending on work environments. When on-site construction management and quality control can be sufficiently implemented, the characteristic values for underwater welding can generally be 80% of those for shop welding.²¹⁾
- (c) For the characteristic values of yield stress of anchor bolts and pins, **Table 2.2.7** can be used as a reference. There have been many cases of using stainless steel for anchor bolts and pins (Refer to **Part II, Chapter 11, 8.1 Metal Materials other than Steel**).

Table 2.2.7 Characteristic Values of Yield Stress of Anchor Bolts and Pins (N/mm²)

Type	Steel grade	SS400	S35CN
	Type of stress		
Anchor bolt	Shear stress	100	133
Pin	Bending stress	320	438
	Shear stress	168	235
	Bearing stress	353	470

- (d) The anchor bolts specifications in this section are based on the assumption that they are being embedded in concrete. Considering the anchor bolt installation is likely to be problematic, and the strength of anchor bolts needs to be balanced with that of the supporting concrete, the design values of anchor bolts shall be calculated to have sufficient safety margins. Also, reference can be made to the **Recommendations for Design and Construction of Post-installed Anchors in Concrete**.²²⁾

- (e) Pins have no risk of being subjected to stress concentration because they do not require bolt holes, unlike steel plates and shaped steel, or do not normally require notches. Also, the verification items of pins are generally their resistance to shear and bearing stress, with no reduction in the limit values with respect to shear stress even if shear is accompanied by sliding. In consideration of these points, the values of shear yield stress for pins are larger than the values in **Tables 2.2.2 and 2.2.5**.
- (f) The yield stress characteristic values of finished bolts can be set with reference to the values in **Table 2.2.8**. The reference values of tensile stress in **Table 2.2.8** are the yield stress of hexagon head bolts specified in **JIS B 1180**. The mechanical properties of hexagon head bolts are specified for respective strength classifications in **JIS B 1051 Mechanical properties of fasteners made of carbon steel and alloy steel**. The values in the table below are those for the strength classifications of 4.6, 8.8 and 10.9.²³⁾

Table 2.2.8 Yield Stress of Finished Bolts²³⁾ (N/mm²)

Strength classification according to JIS B 1051	4.6	8.8	10.9
Type of stress			
Tensile stress	240	660	940
Shear stress	140	380	540
Bearing stress	360	990	1410

- (g) Studs reliably transfer cross sectional force from steel members (such as steel pipe piles and steel sheet piles) to reinforced concrete. The yield stress characteristic values of headed studs can be set with reference to the values in **Table 2.2.9**.²⁴⁾

Table 2.2.9 Shapes, Dimensions, and Mechanical Properties of Headed Studs²⁴⁾

Nominal designation	Nominal length	Shaft diameter	Head diameter	Head thickness (Minimum)	Yield point or 0.2% yield strength (N/mm ²)	Tensile strength (N/mm ²)	Elongation (%)
13	80, 100, 120	13	22	10	235	400 to 550	20% or more
16		16	29				
19		19	32				
22	80, 100, 130, 150	22	35				

2.3 Corrosion of Steel

2.3.1 General

The steel used for port facilities are generally under severe corrosive environments. Steel members are subjected to particularly severe local corrosion at the portions immediately below mean low water levels.

2.3.2 Corrosion of Steel

- (1) Steel undergoes corrosion due to the influences of surrounding environments. The corrosive environments for steel vary a great deal. In the port facility environments, where the pH values of seawater, fresh water, and soil are considered almost neutral, water and oxygen play important roles in steel corrosion. When steel is immersed in neutral water solution, there are numerous corrosion cells, comprising anodes and cathodes, formed on the steel surface.²⁵⁾ Generally, the chemical reactions, represented by **equations (2.3.1) and (2.3.2)**, progress at anodes and cathodes of corrosion cells in equivalent weight.



The dissolution of steel, represented by **equation (2.3.1)**, is called the anodic reaction of corrosion, and the reduction of oxygen, represented by **equation (2.3.2)**, is called cathodic reaction of corrosion. Then, the corrosion reaction of steel can be expressed by **equation (2.3.3)**.



$\text{Fe}(\text{OH})_2$ in **equation (2.3.3)** deposits on steel surface, undergoes further oxidation and dehydration syntheses, and finally turns into complex hydrated iron oxide which is called rust.

- (2) **Figure 2.3.1** shows typical corrosion distribution in the depth direction of a steel member installed in seawater.²⁶⁾ As can be seen in the figure, the portion of the steel positioned in a splash zone, with an ample supply of splashed seawater and oxygen, undergoes particularly severe corrosion. In the splash zone, the point immediately above the H.W.L. has the fastest corrosion rate.

In contrast, in the submerged portion of the steel, the point immediately below a tidal zone has the fastest corrosion rate. However, the corrosion rates in this portion vary significantly, depending on the environmental conditions and cross sectional shapes of long steel members. For steel sheet pile and steel pipe pile structures, the corrosion rates immediately below the M.L.W.L. are larger than those at other submerged portions and, in extreme cases, larger than those in splash zones. Such intensified local corrosion is called concentrated corrosion.

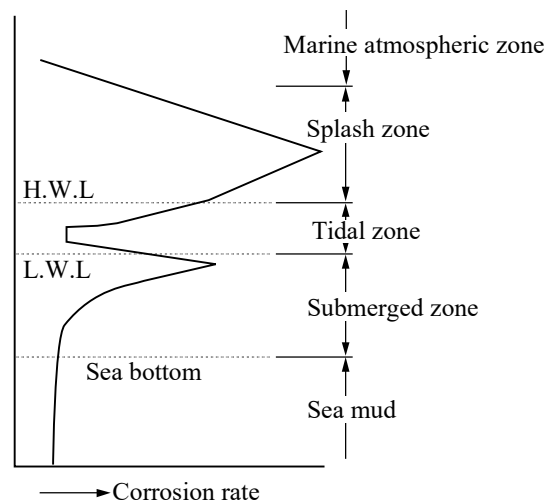


Fig. 2.3.1 Example of the Profile of the Reduction in Thickness of Steel Pipe Pile without Corrosion Protection²⁶⁾

2.3.3 Corrosion Rates of Steel

- (1) Steel corrosion rates vary depending on corrosion environment conditions. The corrosion rates of steel used for port facilities are largely affected by meteorological conditions in water areas, the salinity and pollution degrees of seawater, the presence or absence of the inflow of river water, and other aquatic environmental conditions.
- (2) **Table 2.3.1** shows the standard values of steel corrosion rates. These values are the averages obtained by summarizing the survey results of existing steel structures. Here, it shall be noted that the corrosion rates of concentrated corrosion may be significantly larger than those in **Table 2.3.1**.
- (3) The corrosion rates of steel in the ground are generally small. However, there may be cases where steel in the ground has large corrosion rates depending on the physical properties (grain sizes, moisture contents and soil resistivity) and chemical properties (pH, dissolved oxygen and the activity of microorganisms).
- (4) In closed spaces, such as inside steel pipe piles, steel is not considered to undergo corrosion because there is no oxygen supply.
- (5) Sand erosion is a phenomenon in which the movement of sand exposes bare steel surfaces by removing superficial rust layers, increasing the corrosion rates.²⁷⁾ There are cases of sand erosion on steel sheet piles constructed as sediment control groins, which caused the average corrosion rates of the portion of the steel sheet piles immediately above sand surfaces to increase to 1.25 to 2.39 mm per year.²⁸⁾ It is said that corrosion rates can be higher than the cases above when the sand surface level fluctuations are small and sand erosion is concentrated on the areas

immediately above sand surfaces. The application of cathodic protection to steel can control sand erosion progress.²⁷⁾

Table 2.3.1 Standard Values of Corrosion Rates of Steel²⁵⁾

Corrosive environment		Corrosion rate (mm/year)
Sea side	Above H.W.L.	0.3
	H.W.L. to 1 m below L.W.L.	0.1 to 0.3
	In seawater	0.1 to 0.2
	Sea mud	0.03
Land side	Above ground in the air	0.1
	Underground* ¹	
	a) Above residual water level	0.03
	b) Below residual water level	0.02

*1: Including the backside of steel sheet piles

2.4 Corrosion Protection of Steel

2.4.1 General

- (1) The corrosion protection countermeasures for steel shall be appropriately taken in a manner that implements either cathodic protection methods, protective coating methods or other corrosion protection methods. To design corrosion protection for steel, refer to **Part III, Chapter 2, 1.3.5 Corrosion Protection Design for Steel**.
- (2) For overall corrosion protection, refer to the **Manual for Corrosion Protection and Maintenance Work for Port Steel Facilities (2009 Edition)**.²¹⁾

2.4.2 Cathodic Protection Methods

- (1) Cathodic protection can be classified into a galvanic anode method and an impressed current method depending on energization systems.

In the galvanic anode method, anodes made of metal having negative potential with respect to steel, such as aluminum (Al), magnesium (Mg), or zinc (Zn), are connected to steel structures. The electric current generated due to the potential difference between the two types of metal is used as protective current. Almost all cathodic protection used for the port steel structures in Japan is the galvanic anode method, mainly because of easy maintenance. The performance of galvanic anode materials is summarized in **Table 2.4.1**. Aluminum alloy anodes are: the largest in electricity generation capacity per unit mass; excellent in economic efficiency; and suitable for the environments in seawater as well as sea bottom mud. Thus, aluminum alloy anodes are generally used for port steel structures.

In the impressed current method, protective current flows from external DC power sources to steel structures, with negative electrodes and counter electrodes connected to the steel structures and the positive terminals of power sources, respectively. Platinum based electrodes or oxide coating electrodes are typically used in seawater. Because the impressed current method enables output potential to be flexibly controlled, it can be applied to rapidly changing environments due to strong tides or inflow of river water and places requiring fine potential control.

Table 2.4.1 Comparison of Performance of Galvanic Anode Materials²⁹⁾

Characteristics		Al-Zn-In	Pure Zn, Zn alloy	Pure Mg-Mn	Mg-6Al-3Zn
Specific gravity		2.6 to 2.8	7.14	1.74	1.77
Closed circuit anode potential (V) (vs. S.C.E.)		-1.05	-1.00	-1.55	-1.45
Effective potential difference with respect to iron (V)		0.25	0.20	0.75	0.65
Theoretical effective electric quantity (A·h/kg)		2,700 to 2,900	820	2,200	2,210
In seawater with 1 mA/cm ² *1	Effective electric quantity (A·h/kg)	2,600	780	1,100	1,220
	Consumption (kg/A/year)	3.4	11.8	8.0	7.2
In soil with 0.03 mA/cm ² *1	Effective electric quantity (A·h/kg)	1,860*2	530	880	1,110
	Consumption (kg/A/year)	4.7	16.5	10.0	7.9
Applicable environment*3		In seawater and marine soil	In seawater	In land soil and fresh water	In land soil and fresh water

*1: The current density applied to test pieces of anode materials as specified in the **Laboratory test method of Galvanic Anodes for Cathodic Protection (JSCE S-9301)**, the standards of the Japan Society of Corrosion Engineering.

*2: The design value of 1,860 A·h/kg has been used as the electric power generation capacity (effective electric quantity) of aluminum alloy anodes for use in marine soil. Considering the possible fluctuation of the effective electric quantity and effective potential depending on the environment where aluminum alloy anodes are installed, verification tests to confirm the performance of these anodes have been conducted by authorities concerned. The test results will be available for use in the design of the aluminum alloy anodes to be installed in marine soil.

*3: It is preferable to select appropriate anodes through surveys and tests in the case of implementing the galvanic anode method in brackish water regions, and the regions with varying resistant ratios as well as strong tidal flows.

- (2) In the galvanic anode method, anodes are normally fixed to steel on-site with underwater welding. In some cases, for example, when jacket-type steel structures are assembled on shore, anodes are fixed to steel with shop welding.
- (3) There have been reports on the brittle fractures of galvanic anodes at the places where they were fixed to steel sheet pile wharves, using the steel sheet piles manufactured before relevant JIS was revised in 2000, by underwater welding when the steel sheet piles were subjected to excessive earth pressure with the ground at their back liquefied during earthquake ground motions.³⁰⁾ Based on these reports, the chemical compositions of steel sheet piles have been revised to ensure reliable underwater welding. When fixing anodes to steel sheet piles manufactured before the revised relevant JIS by underwater welding, the reliability of underwater welding performance can be improved by paying attention to the following points:³¹⁾
 - ① To avoid the degradation effect of abrupt heating and cooling in welding operation on steel sheet pile materials, welding shall be started and stopped at the positions not on steel sheet piles but on core bars of anodes.
 - ② To avoid material degradation due to temporary welding of anodes, the positions of temporary welding shall be limited to the areas for final welding.

2.4.3 Protective Coating Methods

(1) General

- ① Cathodic protection cannot be applied to the sections of port steel structures which are submerged in seawater only for a short period of time. Thus, it is preferable to apply coating methods to these sections.
- ② The following five types of protective coating methods are generally applied to port steel structures.
 - (a) Painting
 - (b) Organic coating
 - (c) Petrolatum coating
 - (d) Inorganic coating
 - (e) Metal coating
- ③ The coating methods protect objects from corrosion by isolating them from corrosive environmental factors. The scope of application of protective coating methods varies depending on the coating method. Some types are applied mainly to corrosion protection in tidal and splash zones, as well as marine atmospheres, and other types can be applied to corrosion protection, not only in tidal and splash zones, but also in seawater. The

protective coating methods applicable to corrosion protection in seawater are classified into those with or without the combined implementation with cathodic protection methods. Also, some protective coating methods are applicable only to new facilities and others are applicable to both new and existing facilities.

- ④ The corrosion protection performance of coating materials is affected by workmanship (particularly that of surface preparation). The purposes of surface preparation are: to remove substances on steel surfaces, such as rust, grease, and pollution harmful to adhesive and corrosion prevention properties of coating materials; and to provide surface roughness effective for insuring the initial adhesive strength of coating materials. Different coating materials require different types of surface preparation to ensure their corrosion prevention properties and service life.

Because steel surfaces after surface preparation are chemically active and undergo rapid oxidation, coating materials shall be applied to the steel surfaces immediately after surface preparation. Also, it is necessary to pay attention not to damage coated surfaces while applying coating materials.

(2) Painting

The painting is to apply paint to steel surfaces so as to form paint film on them when the paint is dried. The painting can prevent steel from corroding through its effect to isolate steel from corrosive environments and the effect of rust-proof colorants. Paint comprises resin, which is a main component of colorants and paint film, additive agents, and solvent. The painting has many advantages compared to other corrosion protection methods. For example, it can be implemented through simple application. Painting has long been used as the corrosion protection method of steel structures. Also, because the corrosion protection performance of paint has been improved, owing to the development of paint and painting technologies, many port steel structures have also used painting as corrosion protection methods.

The types of paint generally used for the painting are as follows.

- Marine painting (marine thick epoxy painting, marine epoxy glass flake painting, etc.)
- Other painting (fluorine resin painting, polyurethane resin painting, polyester resin painting, etc.)

(3) Organic coating

The organic coating is not advantageous in terms of workability, reparability, and construction costs because it requires larger film thicknesses than painting, which makes the organic coating highly durable. The organic coating has been used in particularly severe cases, such as corrosion protection in seawater, and tidal as well as splash zones, for which a high environmental isolation effect or extended service period of corrosion prevention is required.

The types of widely used organic coating are as follows.

① Heavy-duty corrosion protection coating (urethane elastomer coating, polyethylene coating)

Heavy-duty corrosion protection coating is applicable to steel pipe piles, steel sheet piles and steel pipe sheet piles in the factories having dedicated machines. The materials available for the heavy-duty corrosion protection coating are urethane elastomer and polyethylene. Applying the coating materials to steel products can be implemented through mass production systems under thorough quality control. The coating thicknesses are around 2 to 3 mm.

② Super high build coating

As is the case with the painting, the super thick film coating applies liquid materials to steel. The super thick film coating enables durable film having thickness of 1 to 3 mm which cannot be achieved by painting to be formed in a small number of applications. The super thick film coating can be applied to steel structures with complex shapes or large scale structures and is generally implemented in factories.

③ Underwater-cured resin coating

The underwater-cured resin coating is a method for coating steel, positioned in tidal and splash zones, using the materials capable of being applied to steel underwater. The major component of the material is hydraulic epoxy resin. The underwater-cured resin coating is classified into two types: one is a putty type which forms super thick film coating by manually applying putty like coating material to steel in the same as putty work; and the other is a paint type which applies liquid materials to steel with rubber pallets.

(4) Petrolatum Coating

The petrolatum coating coats steel surfaces with corrosion protection material using petrolatum, which is a type of petroleum wax separated from crude oil through reduced-pressure distillation. Coated steel surfaces are provided with protection covers to ensure long-term durability of corrosion protection film on the steel surfaces by protecting them from external forces, such as waves and impacts of floating objects. Depending on the types of materials used for protection covers, the petrolatum coating is largely classified into a resin protection cover method and an anticorrosion metal protection cover method.

Petrolatum corrosion protection materials are available in the forms of: nonwoven fabric tapes or sheets impregnated with petrolatum and corrosion inhibitor as an additive agent; paste of petrolatum as a primer; and tapes containing petrolatum paste. The petrolatum corrosion protection materials can control the progress of rust because: they have adherence and ductility, so as to attach firmly to steel surfaces; they can adhere a long period of time without being subjected to hardening or evaporation; their water-repellent property can isolate steel surfaces from moisture and air; and the corrosion inhibitor included in petrolatum paste forms an anticorrosive film on steel surfaces.

(5) Inorganic Coating

The inorganic coating, which has been used for port steel structures includes mortar, concrete, and electrodeposition coating. The inorganic coating has also been known as the corrosion protection methods implemented on-site.

① Mortar coating

The mortar coating is a corrosion protection method which coats the surfaces of steel structures with mortar to enable strong alkalinity of cement mortar to prevent seawater from corroding steel surfaces. There were cases where cement mortar had cracks, or was partially removed or washed off by severe waves and the impact of driftwood. Thus, in order to prevent cement mortar from significantly decreasing the corrosion protection function even in such cases, the mortar coating is basically provided with protection covers.

② Concrete coating

The concrete coating is a method to coat steel surfaces with reinforced concrete. The concrete coating is more resistant to external forces than the mortar coating and, therefore, advantageous in environments with risks of severe waves and impact from driftwood. Basically, the concrete coating does not require protection covers, which can enhance durability of the concrete coating.

③ Electrodeposition coating

The electrodeposition coating is to coat steel surfaces to be corrosion protection objects in a manner that: applies DC electricity from the electrodes installed in seawater to the steel surfaces to be negative electrodes; and deposits Ca^{2+} and Mg^{2+} in seawater on the steel surfaces as CaCO_3 and $\text{Mg}(\text{OH})_2$.

(6) Metal Coating

The metal coating is classified into a method which coats steel surfaces with molten metal through metal spraying or plating and a method which puts covering metal plates on steel surfaces. The latter method has excellent impact and abrasion resistance in that it can provide coated surfaces with larger mechanical strength than other coating methods. When using corrosion resistance metal for covering plates, the latter method is expected to improve long-term durability.

① Corrosion resistant metal covering

The corrosion resistant metal, which can be used for marine steel structures, includes titanium and seawater-resistant stainless. The corrosion resistant metal covering is implemented either by locally fixing thin corrosion resistant metal plates to steel surfaces by welding or covering steel surfaces with layers of corrosion resistant metal through hot rolling (called clad steel).

Titanium is highly resistant to pitting and crevice corrosion and is completely corrosion-free under a normal marine environment. However, because titanium produces brittle intermetallic compound when welded to steel, it cannot be directly welded to steel in a practical sense. Thus, thin-plate titanium clad steel has been used as corrosion protection coating in a manner that uses the titanium surfaces of the clad steel as corrosion protection coating with the steel members of the clad steel connected to steel structures.

The seawater-resistant stainless has larger contents of corrosion-resistant alloy elements, such as Cr, Ni, and Mo, than general stainless steel and, thereby, significantly improves corrosion resistance. Because the seawater-

resistant stainless can be directly welded to steel, the seawater-resistant stainless covering has been widely used for jacket structures with thin plates of seawater-resistant stainless steel locally welded to the structures.³²⁾ Recently, seawater-resistant stainless clad steel has been developed.

② Metal spraying and plating

The metal spraying and plating methods coat steel surfaces with molten metal. The types of corrosion resistance metal used in these methods are zinc, aluminum, and zinc-aluminum alloy.

In the metal spraying, metal sprayed film, with a sealing treatment, has been applied to the portion of steel surfaces exposed to the marine atmosphere with a primer coat preliminarily applied to them; in many cases, there has been no case of independently applying the metal spraying film with sealing treatment to steel surfaces.³³⁾

The metal plating has high corrosion resistance in the atmosphere but, as is the case with galvanization in particular, significantly poor durability under marine environments.³⁴⁾ Thus, it is necessary to select appropriate types of plates in consideration of use environments. The hot dip galvanized coating and hot dip aluminized coating have been specified in JIS (**JIS H 8641** and **JIS H 8642** respectively).

[References]

- 1) Japan Standard Association: JIS Handbook, Iron and Steel I, II, Japan Industrial Standards, 2002
- 2) Japan Society of Civil Engineers: Research Report on Utilization Technology of New High Performance Steel - Guideline for Design and Construction of SBHS500 (W), SBHS700 (W) (draft) -, pp.155-158, 2009.
- 3) Japan Road Association: Specifications and Commentary for Highway Bridges Vol. II, Steel Bridge, p. 141, 2017
- 4) National Institute for Land and Infrastructure Management, Japan Iron and Steel Federation, Japan Bridge Association: Research on Evaluation Technique of Applicable Condition for Weathering Steel Bridge (I) - Study about Evaluation Technique of Applicable Condition-, Technical Note of NILIM, No.777, 2014.
- 5) Akira, Y., Yamaji, T., Iwanami, M., Harata, N., Yoshizaki, N., Murase, M., Saito, I., Kamimura, T. and Kitamura, T.: , Fundamental study on durability of hat-type steel-sheet-pile protected by heavy duty coating, Technical Note of PARI, No.1230, 2011.
- 6) Refer to literature 3), p. 5, 2017
- 7) Refer to literature 3), pp. 69-70, 2017
- 8) Japan Road Association: Specifications and Commentary for Highway Bridges Vol. I, General, p. 126, 2017
- 9) Refer to literature 3), pp. 61-62, 2017
- 10) Japan Society of Civil Engineers: Standard Specifications for Concrete Structures, Design, 2018.
- 11) Refer to literature 3), pp. 10-11, 2017
- 12) Refer to literature 3), p. 46, 2017
- 13) Refer to literature 8), p. 151, 2018
- 14) Shiozaki, Y., Usami, S. and Ookubo, H.: Study on the Application of a High Strength Steel Pipe Pile (570N/mm² Grade) to PORT Structures, Annual Journal of Civil Engineering in the Ocean Vol.68, No.2, pp. I_366-I_371, 2012.
- 15) Refer to literature 3), pp. 65-138, 2017
- 16) Japan Standards Association: JIS Handbook, Iron and Steel II, Japan Industrial Standards, 2015
- 17) Refer to literature 8), p. 152, 2017
- 18) Refer to literature 3), p. 47, 2017
- 19) Refer to literature 3), p. 55, 2017
- 20) Refer to literature 3), pp. 527-569, 2017
- 21) Coastal Development Institute of Technology: Manual for corrosion protection and maintenance work for Port steel facilities, iron slug hydration hardener (revised Edition), 2009, p.320
- 22) Japan Society of Civil Engineers: Recommendations for Design and Construction of Post-installed Anchors in Concrete (Draft), CL.141, 2014.

- 23) Japan Standard Association: JIS Handbook, Screw Part I, Japan Standard, 2015
- 24) Refer to literature 21), pp. 299-300, 2009
- 25) Refer to literature 21), pp. 9-15, 2009
- 26) H.A. Humble: The cathodic protection of steel piling in seawater, Corrosion, Vol.5 No.9, p.292, 1949
- 27) Abe, M., Fukute, T, Shimizu, K. and Yamamoto, I.: Effect of cathodic corrosion protection against Sand erosion in wavy sea area., Proceeding of 42nd open forum on corrosion and corrosion protection, C-203, pp.371-374, 1995
- 28) C. W. Ross: Deterioration of steel sheet pile groins at Palm Beach, Florida, Corrosion, Vol.5 No.10, pp.339-342, 1949
- 29) Refer to literature 21), p. 70, 2009
- 30) Fukute, T., Abe, M., Hasegawa, H., and Matsuda, H.: A Study on Fractural Mechanism and Its Improvement for Underwater-Welded Steel Sheet Pile Structures, Rept. of PHRI Vol. 36, No. 2, pp. 43-68, 1997.
- 31) Japan Association of Cathodic Protection: Points of Attention in Underwater Welding of Steel Sheet Piles, 2018.
- 32) Kimura, F., Iwami, H., Sato, H. and Sekiguchi, T.: Welding Procedure in Haneda Airport Re-expansion Construction -Seawater Resistant Stainless Steel Coating-, Welding Technology, Vol.57, pp.53-57, 2009.
- 33) Gibo, M., Yogi, K. and Harada, M.: Durability Design for a Part of Main Sea Route in Irabu Bridge, The 65th JSCE Annual Meeting Proceedings, CS4-019, pp.37-38, 2010.
- 34) Research Group on Corrosion Protection Technology for Marine Steel Structures: Corrosion Protection Technology for Marine Steel Structures, Gihodo Shuppan, pp.114-117, 2010.

3 Concrete

3.1 Concrete Materials

- (1) The concrete materials to be used for port facilities shall have the quality necessary for achieving the required performance of the facilities. In principle, these concrete materials shall satisfy the quality specified in **JIS A 5308 Ready-mixed concrete**.

(2) Cement

The cement to be used for concrete shall comply with **JIS R 5210 Portland cement**, **JIS R 5211 Portland blast-furnace slag cement**, **JIS R 5212 Portland pozzolan cement**, and **JIS R 5213 Portland fly-ash cement**. The performance of the cement other than the above shall be confirmed through tests and past performance records.

Among the several types of cement, moderate-heat Portland cement, Portland blast-furnace cement, and Portland fly-ash cement are considered to have higher durability under marine environment than ordinary Portland cement. The concrete created using these types of cement has advantages of a large increment in long-term strength and reduced heat of hydration but has a disadvantage of low initial strength. Based on the viewpoint that the concrete created using type B Portland blast-furnace cement is more robust against corrosion of steel bars than the ordinary Portland cement,^{1) and 2)} it is preferable to use type B Portland blast-furnace cement. Therefore, it is necessary to pay special attention to initial curing when using these cements.

(3) Water

Mixing water shall be tap water or water complying with **JSCE-B 101 Qualities of Water for Concrete**.³⁾ For the reinforced concrete using ordinary steel bars, seawater cannot be used as mixing water. For plain concrete, seawater can be used only when clean fresh water is not easily available. There have been many studies on the use of seawater as mixing water for plain concrete^{1) and 4)} and cases of construction of plain concrete using seawater as mixing water.

It shall be noted that seawater tends to shorten the setting time of cement and causes the consistency of concrete to be lost in an early stage. Thus, when using seawater as mixing water, a retarder can be utilized as needed.

Also, the use of seawater as mixing water results in the increase of alkali ion concentration and pH values of fine pore solution in concrete, thereby enhancing the alkali-silica reaction (ASR). Thus, when using aggregate with a reactive property, it is necessary to take countermeasures to suppress the ASR.

(4) Admixtures

Fly-ash and ground granulated blast-furnace slag to be used for concrete as admixtures shall comply with **JIS A 6201 Fly ash for use in concrete** and **JIS A 6206 Ground granulated blast-furnace slag for concrete**, respectively. Both admixtures can improve the performance of concrete. When using fly-ash and ground granulated blast-furnace slag, reference can be made to the **Guide for Construction of Concrete Using Fly-ash**⁵⁾ and the **Guide for Design and Construction of Concrete Using Ground Granulated Blast-furnace Slag**, respectively.⁶⁾

Expansive additives to be used for concrete shall comply with **JIS A 6202 Expansive additive for concrete**. Expansive additives are used to control cracks due to the shrinkage of concrete. When using expansive additives, reference can be made to the **Guide for Design and Construction of Expansive Concrete**.⁷⁾

The performance of admixtures other than those mentioned above shall be confirmed through tests and past performance records.

(5) Chemical Admixture Agents

Those chemical admixture agents, such as AE agents, water-reducing agents, and high-performance AE water-reducing agents, shall comply with **JIS A 6204 Chemical admixtures for concrete**. When using the chemical admixture agents other than the above, their performance shall be confirmed through tests and past performance records to determine their availability.

In the case of the necessity to use cold-resistant agents when placing cold-weather concrete, reference can be made to the **Guide for Construction of Cold-Weather Concrete Using Cold-Resistant Agents**.⁸⁾

(6) Aggregate

Basically, the aggregate to be used for concrete shall meet the quality requirements specified in **Annex A of JIS A 5308 Ready-mixed concrete**. It is necessary to use aggregate which is clean, rigid, permanent, properly graded, and free from harmful substances, such as organic impurities and chloride in amounts exceeding the predetermined limits. It is also necessary to avoid the use of aggregate containing waste, mud, flakes of stone, and long and thin

stones or having water-absorbing and swelling properties. When using aggregate which does not comply with JIS (such as aggregate originated from coral), a preliminary examination is required to determine its availability.⁹⁾

(7) Reinforcing Materials

Steel bars to be used for concrete shall comply with **JIS G 3112 Steel bars for concrete reinforcement**.

The following types of steel bars are made of corrosion-resistant steel for the purpose of improving the durability of concrete members: a) epoxy-coated steel bars; b) stainless steel bars; and c) continuous fiber reinforcing materials. When using a), b), and c), reference can be made respectively to the **Guide for Design and Construction of Reinforced Concrete Using Epoxy-Coated Steel Bars [Revised Edition]**¹⁰⁾; the **Guide for Design and Construction of Concrete Structures Using Stainless Steel Bars**¹¹⁾; and the **Guide for Design and Construction of Concrete Structures Using Continuous Fiber Reinforcing Materials**.¹²⁾ The stainless steel bars to be used for concrete shall comply with **JIS G 4322 Stainless steel bars for concrete reinforcement**.

The steel materials to be used for prestressed concrete shall comply with **JIS G 3536 Steel wires and strands for prestressed concrete** and **JIS G 3109 Steel bars for prestressed concrete**. As is the case with steel bars for reinforced concrete, the types of steel materials for prestressed concrete include a) epoxy-coated steel materials and b) continuous fiber reinforcing materials. When using a) and b), reference can be made respectively to the **Guide for Design and Construction of Prestressed Concrete Using Epoxy-Coated Highly Functional PC Steel Materials**¹³⁾ and the **Guide for Design and Construction of Concrete Structures Using Continuous Fiber Reinforcing Materials**.¹²⁾

(8) Surface Protection Materials

There may be cases of application of surface protection materials to concrete surface for the purpose of protecting concrete from the infiltration of degrading factors, such as chloride ions. In such cases, reference can be made to the **Guide for Design and Construction of Surface Protection Work**¹⁴⁾ and the **Manual for Repairing Port Concrete Structures**.¹⁵⁾

(9) Cross-sectional Repair Materials

There are cases of repairing existing concrete structures (called cross-sectional repair method) in a manner that chips off deteriorated sections of concrete and restores exposed cross sections with new materials (cross-sectional repair materials). The main cross-sectional repair materials include polymer cement mortar. When applying the cross-sectional repair method to port concrete structures, reference can be made to the **Manual for Repairing Port Concrete Structures**.¹⁵⁾

(10) Chloride Ion Contents

To reduce the risk of corrosion of steel inside the concrete, the chloride ion contents in fresh concrete shall be no more than 0.30 kg/m³.

(11) Alkali -Silica Reaction Preventive Countermeasures

One of the following three countermeasures shall be appropriately selected as alkali -silica reaction preventive countermeasure:

① A countermeasure to control total alkali in concrete

The use of the types of cement in which total alkali contents are known, such as Portland cement, so as to ensure that total alkali contents are equal to or less than 3.0 kg/m³

② A countermeasure to use mixed cement effective in controlling the alkali-silica reaction

The use of the types of cement effective in controlling the alkali aggregate reaction, such as blast-furnace cement (Type B or C) or fly-ash cement (Type B or C)

③ A countermeasure to use aggregate confirmed safe for avoiding alkali-silica reaction

The use of aggregate confirmed to be harmless through the tests specified in **JIS A 1145 Method of test for alkali-silica reactivity of aggregates by chemical method** and **JIS A 1146 Method of test for alkali-silica reactivity of aggregates by mortar-bar method**.

3.2 Quality and Performance of Concrete

- (1) Concrete shall have uniform quality, workability suitable for concrete work, and properties to satisfy the required strength, durability, water tightness, crack resistance, and steel bar protection performance.
- (2) Concrete shall be resistant to deterioration caused by environmental actions, waves, and mechanical actions, such as impacts and abrasion due to drifting objects. The types of deterioration of concrete subjected to environmental actions are as follows:

① Freezing and thawing action

The progress of deterioration on concrete surface in the form of scaling and cracks when concrete is subjected to the repeated freezing and thawing actions involving the volume expansion with moisture inside concrete frozen and the water supply with frozen moisture inside concrete thawed.

② Deterioration due to the actions of salts in seawater

The sulfate ions in seawater react with calcium hydroxides and alumina (Al_2O_3) which are cement hydrates to form ettringite ($3\text{CaO} \cdot \text{Al}_2\text{O}_3 \cdot 3\text{CaSO}_4 \cdot \text{mH}_2\text{O}$). The pressure generated through volume expansion along with the above reaction causes crack on concrete. However, on the basis that the rate of sulfate ion penetration into concrete is lower than chloride ions and general seawater has a moderately low concentration of sulfate ions of about 2.6 g/L, it has become clear that the effect of the salts in seawater on the deterioration of concrete is not so high and the progress of deterioration of concrete is limited to superficial areas unless the quality of concrete is significantly low.¹⁶⁾

③ Leaching of calcium hydroxide

Because the calcium hydroxides in cement hydrates are soluble in seawater, the leaching of calcium hydroxides causes porosity and brittleness on concrete.

④ Deterioration due to the corrosion of steel bars

The existence of chloride ions on the surfaces of steel bars in concrete with ample supply of oxygen causes rust on the steel bars, and rusty steel bars, in turn, causes the deterioration of concrete in a manner that generates expansive pressure which develops cracks in concrete covering and allows cracked concrete to spall off. Such chloride ions are supplied to steel bars either: from external environments in the form of seawater or antifreezing agents; or along with the materials used when manufacturing fresh concrete.

⑤ Deterioration due to harmful aggregate reaction

In the case of concrete using reactive aggregate or cement with high alkalinity, harmful reaction between aggregate and cement may worsen abnormal cracks, cleavage, or swelling to a level that can result in partial or total destruction of concrete structures.

⑥ Deterioration due to the actions of waves and drifting objects

The impacts of waves and drifting objects aggravate the deterioration of concrete surfaces due to any of the above actions. Even sound concrete inevitably undergoes progressive abrasion due to continued actions of littoral drift.

(3) Characteristic values of concrete strength

- ① The characteristic values of concrete strength necessary for the performance verification shall be appropriately set through pertinent test results or by taking into consideration the types of concrete and natural and construction conditions of performance verification object facilities.
- ② For the characteristic values of concrete strength of ordinary concrete to be used in the performance verification of the main structural members of port facilities, it is usually preferable to use the values given in **Table 3.2.1** as standard values.

Table 3.2.1 Standard Characteristic Values of Concrete Strength of Ordinary Concrete

Concrete type	Characteristic value of concrete strength	
Plain concrete	Compressive	18 (N/mm ²)
Reinforced concrete	Compressive	24 (N/mm ²)
Concrete for apron pavement	Bending	4.5 (N/mm ²)

In the case of reinforced concrete with the maximum water-cement ratio set at 50% or less as the mix proportion condition of ordinary concrete in consideration of durability, 30 N/mm² can be used as the characteristic value of the compressive strength. In the case of plain concrete lids: having a risk of being subjected to wave impacts or floods in an early post-placement material ages; or to be constructed during cold months, 24 N/mm² can be used as the characteristic value of compressive strength. In the case of large-scale deformed plain concrete blocks with nominal weight in the range of 35 to 50 tons, the characteristic values of compressive strength can be set at 21 N/mm² or other values depending on individual situations.

- ③ The characteristic values of bond strength of ordinary concrete to be used in the performance verification of port facilities can be calculated using **equation (3.2.1)**.¹⁷⁾

$$f_{bok} = 0.28 f_{ck}'^{2/3} \quad (3.2.1)$$

where:

f_{bok} : characteristic value of bond strength of ordinary concrete (N/mm²)

f_{ck}' : characteristic value of compressive strength of ordinary concrete (N/mm²)

Equation (3.2.1) is applicable to deformed steel bars complying with **JIS G 3112 Steel bars for concrete reinforcement**. The characteristic values of plain bars can be 40% of the values calculated by **equation (3.2.1)** on the condition that the plain bars are provided with semicircular hooks at both ends.

- ④ The characteristic values of other types of concrete can follow the **Standard Specifications for Concrete Structures “Design.”**¹⁷⁾
- (4) The conditions for concrete mix proportion shall be appropriately set considering durability. Also, when setting the conditions, reference can be made to **Table 3.2.2**, which shows the standard conditions for concrete mix proportion by the type of structural members on the basis of the survey results of existing concrete structures in ports and the study outcomes and knowledge on the durability of concrete subjected to the actions of seawater. However, for the types of structural members, such as the superstructures of piled piers, having many cases of deterioration of the required performance due to chloride-induced corrosion in the past, proper conditions for mix proportion shall be set so as to achieve the required performance of facilities through examination on durability (the changes in performance over time). Such examination can be made with reference to **Part III, Chapter 2, 1.2.4 Examination on Change in Performance Over Time**.

Table 3.2.2 Reference Table of Conditions for Concrete Mix Proportion by the Type of Structural Members

Type	Example of the type of structural member	Condition for mix proportion		
		Maximum water-cement ratio (%)		Maximum dimension of coarse aggregate (mm)
		Region with frequent freezing and thawing actions	Region with temperatures rarely dropping below zero	
Plain concrete	Superstructure of breakwater, concrete lid, main block, deformed block (for wave dissipation or covering), foot protection block, packed concrete	65	65	40
	Superstructure of wharf, parapet, mooring post foundation (gravity type)	60		
Reinforced concrete	Mooring post foundation (pile type), parapet, superstructure of wharf ^{*1)}	60	65	20, 25, 40
	Superstructure of open-type piled pier ^{*2)}	—	—	—
	Caisson, well, cellular block, L-shaped block	50	50	20, 25, 40
	Wave-dissipating block	55	55	20, 25, 40
	Buttress, superstructure of anchor piles	60	60	20, 25, 40
Apron pavement		—	—	25 (20), ^{*3)} 40

*1) Excluding superstructure of open-type piled pier

- *2) Structural member with a risk of performance deterioration during design working life with steel bar corrosion due to chloride-induced corrosion
- *3) 25 mm for gravel and 20 mm for crushed stone

- (5) Concrete shall have consistency most suitable for individual work conditions. Also, AE concrete with air content normally set at 4.5% shall be used in principle unless otherwise required. The air contents shall be carefully set in cold areas and those areas with a risk of frost damage.
- (6) Recently, high-fluidity and medium-fluidity concrete has been developed, which has high fluidity and excellent material segregation resistance to achieve self-compaction performance by the combined use of appropriate admixtures.^{18) and 19)} The concrete with improved fluidity has facilitated concrete placement in the work items to which general concrete compaction methods cannot be applied, for example, concrete placement for members with dense arrangement of steel bars and spaces enclosed by steel shells. Also, it is preferable to apply the concrete with improved fluidity to wider scope in terms of structural types and construction conditions so as to take advantage of its beneficial effects to facilitate laborsaving and streamlining in concrete work and enhance the durability of concrete as a result of improved reliability of concrete placement.

(7) Construction Joints

There have been many cases of port facilities having concrete damage rising from construction joints.²⁰⁾ Thus, it is preferable to avoid construction joints to the extent possible. However, if construction joints are determined to be inevitable to alleviate the influence of the shrinkage of concrete or the reduction in workability, proper measures shall be taken. The use of epoxy resin to ensure concrete strength at construction joints is considered to be one of the measures; however, it shall be noted that epoxy resin is effective in enhancing the strength but not durability of construction joints.²¹⁾

(8) Curing

Concrete needs to be cured in a manner that maintains the temperature and humidity, for a certain period after placement, necessary for it to harden and to ensure the required quality.²²⁾ Generally, clean fresh water, such as tap water, is used for curing concrete, but the use of seawater for curing concrete, particularly the plain one, is proposed in literature 23).

Also, to prevent moisture from dissipating while curing, concrete may be covered with sheets or coated with film, or membrane curing agents may be applied to concrete.

(9) Surface Protection against Physical Actions

Those facilities subjected to severe physical actions, such as abrasion and impacts due to water flows with suspended sand particles and wave carrying gravel, shall be provided with surface protections in the form of shields made of appropriate materials or the increases in material cross sections or concrete cover of steel bars. The materials which can be used for shields include timber, high-quality stone, steel, or polymer materials, polymer-impregnated concrete, and ultra high strength fiberreinforced concrete. Some types of concrete formwork are left on concrete surfaces permanently as surface protections.

(10) Structural Types

It is known that there is a close relationship between structural types of facilities and susceptibility to chloride-induced corrosion. In terms of the types of structural members, beams and slabs are more susceptible to chloride-induced corrosion than columns and walls. Considering that the substances responsible for chloride-induced corrosion, such as chloride ions, oxygen, and water, infiltrate through concrete surfaces, the surface areas of members are preferably minimized to the extent possible. Or, it is also effective to select structural types which can be easily repaired, reinforced, or replaced on the assumption of inevitable degradation.

3.3 Underwater Concrete

The types of concrete to be placed underwater, for example, in marine construction are general underwater concrete and anti-washout underwater concrete. The characteristics of these types of concrete are described below.

3.3.1 General Underwater Concrete

- (1) General underwater concrete shall be placed and subjected to the performance verification in accordance with the **Standard Specifications for Concrete Structures**²²⁾ and the **Standard Specifications for Port and Harbor**

Works.²⁴⁾ For the underwater concrete work using casings, reference can be made to the **Maritime Underwater Concreting Method (Casing Method).**²⁵⁾

- (2) The points of caution when selecting mix proportion are as follows²²⁾: ① the strength of underwater concrete is basically set at 0.6 to 0.8 times that of the standard test pieces prepared on land; ② the standard water-cement ratio is 50% or less; ③ the standard unit cement content is 370 kg/m³ or more with the exception of 340 kg/m³ for the casing method mentioned in (1); and ④ the selection of mix proportion is based on past performance records in actual work environments (fluidity, strength, pumping capacity, etc.). Also, reference can be made to **References 26) to 29)** which summarize the past performance records.

3.3.2 Anti-washout Underwater Concrete

- (1) Anti-washout underwater concrete shall be placed and subjected to the performance verification in accordance with the **Standard Specifications for Concrete Structures**²²⁾ and the **Standard Specifications for Port and Harbor Works.**²⁴⁾ Also, reference can be made to the **Manual for Anti-washout Underwater Concrete (Design and Construction)**³⁰⁾ and the **Guideline for Design and Construction of Anti-washout Concrete in Underwater (Draft).**³¹⁾
- (2) The admixture agents used for anti-washout underwater concrete include anti-washout underwater admixture consisting primarily of cellulose or acrylic water-soluble polymer. In principle, the admixture agents shall comply with **JSCE-D104 Quality standards for anti-washout underwater admixture for concrete.**³⁾
- (3) The points of caution when selecting mix proportion are as follows²²⁾: ① the strength shall be set on the basis of the compressive strength of test pieces, prepared underwater in accordance with **JSCE-F 504 Method for underwater preparation of test pieces for compression tests for anti-washout underwater concrete,**³⁾ at the material age of 28 days; ② underwater segregation resistance shall be set on the basis of the degrees of underwater segregation or ratios of underwater strength to atmospheric strength; and ③ the selection of mix proportion is based on past performance records in actual work environments (fluidity, strength, pumping capacity, etc.).

3.4 Mass Concrete

The types of concrete for which cracks, generated by the increase in the temperature of concrete due to hydration heat of cement and succeeding decrease in the temperature, pose a major problem are required to be treated as mass concrete and provided with countermeasures accordingly.²²⁾ In the cases of port facilities, the footing sections of caissons, superstructures of breakwaters, and bridge piers may need to be treated as mass concrete depending on their cross-sectional dimensions.

When placing mass concrete, it is necessary to examine the countermeasures to suppress temperature cracks due to hydration heat of cement with due consideration to actual construction conditions. (For examination method, **Part III, Chapter 2, 1.2.5 Examination of Initial Cracks**, can be used as a reference, and the examples of examination are shown in **Reference 32).**)

It is particularly important to use appropriate cement selected by fully examining the characteristics of the available types of cements. Generally, it is preferable to use low-heat-generating cement, such as moderate-heat Portland cement, low-heat Portland cement, and Portland blast-furnace cement (low-heat type). Depending on the shapes and dimensions of structures, there may be cases where the use of expanding materials is effective in curbing temperature cracks.

3.5 Other Special Concrete

- (1) Infilled concrete can be used when placing concrete in closed spaces as is the case with immersed tunnel elements having composite structures. For the performance verification and construction of infilled concrete, reference can be made to the **Manual for Grout Concrete Construction with Vibrator.**³³⁾
- (2) For the performance verification and construction of prestressed concrete sheet piles (PC sheet piles), reference can be made to the **Technical Manual for PC Sheet Pile for Port Construction Work.**³⁴⁾
- (3) Other special types of concrete include high-strength concrete, lightweight concrete,^{35) to 37)} heavyweight concrete,³⁸⁾ and ³⁹⁾ high-fluidity concrete, moderate-fluidity concrete, expansive concrete, fiber-reinforced concrete,^{40) to 44)} continuous fiber-reinforced concrete, prepacked concrete, and spray concrete. For the performance verification and

construction of these special types of concrete, reference can be made to the **Standard Specifications for Concrete Structures, “Materials and Construction.”**²²⁾

3.6 Concrete Pile Materials

- (1) The physical values of concrete pile materials used in port facilities shall be appropriately set with due consideration to their characteristics. Generally, concrete piles are inferior to steel pile in terms of maintenance. It is particularly difficult to repair and reinforce concrete piles in comparison with steel piles if these concrete piles are installed in seawater or on the sea with the steel bars inside them subjected to aggravated corrosion.

(2) Precast Concrete Piles Molded by Centrifugal Force

Precast concrete piles molded by centrifugal force include RC piles which are reinforced concrete piles fabricated in factories; PC piles which are concrete piles with their tensile and bending capacity improved by applying tensile force to PC tendons (and they are classified into Types, A, B, and C, depending on the amount of effective prestress); and PHC piles which are PC piles made of high-strength concrete with standard design strength of 80 N/mm² or more. Recently, PHC piles have been the mainstream of precast concrete piles. In addition to the above, precast concrete piles include PRC piles which are PHC piles with the reinforcement of steel bars used to increase ductility and SC piles which are steel piles with high-strength concrete used as lining to achieve large bending and shear capacity. JIS standards corresponding to precast concrete piles are **JIS A 5372 Precast reinforced concrete products** for RC and SC piles and **JIS A 5373 Precast prestressed concrete products** for PC, PHC, and PRC piles.

When setting the characteristic values of concrete strength and yield strength of steel materials for precast concrete piles in the performance verification of port facilities, reference can be made to **JIS A 5372** and **JIS A 5373**. For PC steel bars, steels bars for PRC piles, and steel pipes for SC piles, reference can also be made to **JIS G 3137 Small diameter steel bars for prestressed concrete**, **JIS G 3112 Steel bars for concrete reinforcement**, and **JIS A 5525 Steel pipe piles**, respectively.

(3) Cast-in-Place Concrete Piles

Cast-in-place concrete piles are classified into two types, those with and those without outer shells. The feature of cast-in-place concrete piles is that they are constructed at the exact places underground where they are finally installed. Thus, unlike in the case of PRC piles, it is not necessary to pay attention to the influence of the impacts when piles are driven into the ground. However, different from the case of piles fabricated under a fully controlled condition on land, cast-in-place piles need to be constructed underground while being subjected to the influence of the neighboring piles under construction. Thus, it shall be noted that cast-in-place piles, particularly those without shells, have uncertainties about construction quality. For the details of cast-in-place piles, reference can be made to the **Specifications and Commentary for Highway Bridges Vol. IV, Substructures.**⁴⁵⁾

[References]

- 1) Fukute, T., Yamamoto, K. and Hamada, H.: A study of the durability of offshore concrete mixed with sea water, Report of PHRI, Vol.29, No. 3, 1990
- 2) Yamaji, T. Mohammed, T. U., Aoyama, T. and Hamada, H.: Effect of Exposure Environment and Cement Types on the Durability of Marine Concrete, Proceedings of the Japan Concrete Institute, Vol.23, No.2, pp.577-582, 2001.
- 3) Japan Society of Civil Engineers: Standard Specifications for Concrete Structures -2013, Test Methods and Specifications -JSCE Standards-, 2013.
- 4) Sakai, T., Takenaka, H., Tanaka, R., Koyama, H., Yamaji, T. and Kiyomiya, O. : Basic Properties of Self-compacting Concrete Using Seawater and Sea Sand, Concrete Journal, Vo.53, No.12, pp.1038-1045, 2015.
- 5) Japan Society of Civil Engineers: Recommendations for Construction of Concrete Using Fly Ash (Draft), 1999.
- 6) Japan Society of Civil Engineers: Recommendations for Design and Construction of Concrete Using Ground Granulated Blast-Furnace Slag, 2018.
- 7) Japan Society of Civil Engineers: Recommendations for Construction of Expansive Concrete (Draft), 1993.
- 8) Civil Engineering Research Institute for Cold Region (Edit): Recommendation for Construction of Cold Weather Concrete Using Frost-Resistant Accelerator (Draft), 1994.

- 9) Takenaka, H., Sakai, T., Yamaji, T. and Kiyomiya, O.: Basic Properties of Self-Compacting Concrete Using Seawater and Coral Aggregates, Proceedings of the Japan Concrete Institute, Vol.38, No.1, pp.1833-1838, 2016.
- 10) Japan Society of Civil Engineers: Recommendation for Design and Construction of Concrete Structures Using Epoxy-Coated Reinforcing Steel Bars (Revised Edition), 2003.
- 11) Japan Society of Civil Engineers: Recommendations for Design and Construction of Concrete Structures Using Stainless Steel Bars (Draft), 2008.
- 12) Japan Society of Civil Engineers: Recommendation for Design and Construction of Concrete Structures Using Continuous Fiber Reinforcing Materials (Draft), 1996.
- 13) Japan Society of Civil Engineers: Recommendations for Design and Construction of Prestressed Concrete Structures Using Advanced Prestressing Steel Coated by Epoxy Resin (Draft), 2010.
- 14) Japan Society of Civil Engineers: Recommendations for Concrete Repair and Surface Protection of Concrete Structures (Draft), 2005.
- 15) Coastal Institute of Technology: Manual for Repair of Port Concrete Structures, 2018.
- 16) Yamaji, T., Akira, T., Hamada, H. and Yamada, K.: Study On A Deterioration And Deterioration Indicator Of Concrete Under Marine Environments, Doboku Gakkai Ronbunshuu E, Vol. 66, No.1, pp.21-37, 2010.
- 17) Japan Society of Civil Engineers: Standard Specifications for Concrete Structures -2017, Design, 2017.
- 18) Fukude, T., Hamada, H., Miura, K., Sano, K., Moriwaki, A. and Hamazaki, K.: Applicability of super-workable concrete using viscous agent to densely reinforced concrete members, Rept. of PHRI Vol. 33 No. 2, pp. 231-257, 1994
- 19) Coastal Development Institute of Technology (CDIT): High-fluidity concrete Manual for port facilities, 1997
- 20) Seki, H., Onodera, Y. and Maruyama, H.: Deterioration of Plain Concrete for Coastal Structures Under Maritime Environments, Technical Note of PHRI No. 142, 1972
- 21) Otsuki, N., M. Harashige and H. Hamada: Test on the Effects of Joints on the Durability of Concrete in Marine Environment (after 10 years' exposure), Technical Note of PHRI No.606,1988
- 22) Japan Society of Civil Engineers: Standard Specifications for Concrete Structures -2017, Materials and Construction, 2017.
- 23) Japan Concrete Institute: JCI Technical Committee on the Use of Seawater in Concrete, pp.220-221, 2014.
- 24) Japan Port Association: Standard Specifications for Port Construction Work, Japan Port Association, 2017.
- 25) Cold Region Port and Harbor Engineering Research Center: Construction of Marine Underwater Concrete (Casing-system), 1993.
- 26) Seki, H.: Construction Examples of Underwater Concrete, Technical Note of PHRI, No.165, 1973.
- 27) Akatsuka, Y. and Seki, H.: Constructivity of Underwater Concrete, Kajima Institute Publishing CO., LTD., 1975.
- 28) Seki, H.: Underwater Concrete in Marine Structures, Concrete Journal, Vo.28, No.3, pp. 10-17, 1990.
- 29) Yasuda, O., Murase, K., Tokunaga, K., Nakazima, Y. and Kitahara, S.: Study for Improvement of Under Water Concreting at Marine Fields, Proceedings of Civil Engineering in the Ocean, Vol.8, pp.189-194, 1992.
- 30) Coastal Development Institute of Technology, The Japanese Institute of Technology on Fishing Ports, Grounds and Communities: Manual for design and construction of non-disjunction concrete in underwater (Draft), p.57, 1986.
- 31) JSCE: Guideline for design and construction of non-disjunction concrete in underwater (Draft), JSCE Concrete Library, No.67, 1991
- 32) Fukunishi, K. and Ono, K.: Construction of Tokyo Gate Bridge, Bridge and foundation engineering, Vol.45, No. 9, pp. 5-10, 2011.
- 33) Coastal Development Institute of Technology (CDIT): Manual for sealing concrete construction with vibrator (for immersed tunnel element of Steel and concrete sandwich structure), 2004
- 34) Coastal Development Institute of Technology: Technical Manual for PC sheet pile for port construction work, CDIT, 2000

- 35) Yokota, H., Yamada, M., Hamada, H., Yokozawa, K., Funahashi, M., Hara, N., Miwa, T., Okamoto, T., Tochigi, T. and Niwa, J.: Fundamental Study on the Application of Super-lightweight Concrete to Port Structures, Technical Note of PHRI, No.967, 2000.
- 36) Yokota, H., Funahashi, M., Yamada, M., Hada, N. and Niwa, J.: Shear Resisting Behavior of Super Lightweight Concrete Beams without Web Reinforcement, Rept. of PARI Vol. 40, No. 3, pp. 17-35, 2001.
- 37) Iwanami, M., Kato, E. and Yokota, H.: Experimental Study on Structural Performance and Constructivity of High Performance Light Weight Concrete, Technical Note of PARI, No.1138, 2006.
- 38) Kawabata, Y., Iwanami, M. and Kato, E.: Properties of Concrete with High Volume Slag Fine Aggregate, Technical Note of PARI, No.1232, 2011.
- 39) Kawabata, Y., Kato, E., Kawamura, N., Yamaji, T. and Iwanami, M., An Experimental Study on Applicability of Heavy Weight Concrete to Port Structures, Technical Note of PARI, No.1287, 2014.
- 40) Yokota, H., Ito, H., Iwanami, M. and Kato, E.: Structural Performance of Concrete Structures Reinforced by Short Fiber, Technical Note of PARI, No.1071, 2004.
- 41) Ito, H., Yokota, H. and Iwanami, M.: Study on Constructability of PVA Short Fiber Reinforced Concrete, Technical Note of PARI, No.1087, 2004.
- 42) Ito, H., Iwanami, M. and Yokota, H.: Evaluation on the Applicability of PVA Short Fiber Reinforced Concrete to Harbor Structures, Rept. of PARI Vol. 44, No. 3, pp. 3-37, 2005.
- 43) Iwanami, M., Shirane, Y., Yokota, H., Yamada, T. and Takehana, N.: Improvement of Impact Loading Resistance of Reinforced Concrete Members by Mixing PVA Short Fiber, Technical Note of PARI, No.1163, 2007.
- 44) Iwanami, M., Matsubayashi, T. and Kawabata, Y.: Structural Behavior of Reinforced Concrete Slabs Subjected to Repeated Impact Loads, Technical Note of PARI, No.1216, 2010.
- 45) Japan Road Association, : Specifications and commentary for Highway Bridges, Vol. IV, Substructures, pp.310-314, 2017.

4 Bituminous Materials

4.1 General

- (1) The bituminous materials to be used in port facilities shall have the following quality and properties necessary to achieve the required performance of the facilities: elasticity, viscosity, waterproof property, water resistance, durability, weather resistance, and others in accordance with the intended use. The bituminous materials include asphalt and asphalt emulsion.
- (2) The types of asphalt mainly used in port facilities are straight asphalt manufactured by distilling crude oil, blown asphalt manufactured through oxidative polymerization of straight asphalt, and polymer-modified asphalt manufactured by adding thermoplastic elastomer to straight asphalt so as to improve properties, such as antiflow resistance. In this section, asphalt means straight and blown asphalt as well as polymer-modified asphalt as the secondary product of straight asphalt unless otherwise noted.
- (3) Asphalt has rarely been used alone but is normally mixed with aggregate as asphalt mixtures for the use of asphalt concrete for pavement, asphalt mats, sand mastic, and asphalt stabilized material. The types and mix proportion of asphalt vary depending on the intended purposes. Thus, it is necessary to appropriately select materials satisfying predetermined purposes.
- (4) The performance of asphalt mixtures has been specified on the basis of appropriate material tests taking into consideration the intended purposes and construction methods. Generally, the standards of material tests have been specified so as to enable asphalt mixtures to have sufficient stability and durability to achieve predetermined purposes.
- (5) Asphalt emulsion is liquid manufactured by dispersing particulate asphalt in water containing an emulsifying agent. Asphalt emulsion enhances bonding strength through it breaks to water and asphalt. It is also used as a tack coat to improve adherence between the layers of asphalt mixtures for pavement and prime coat to protect the base course.
- (6) The Japanese Industrial Standards with respect to bituminous materials are **JIS K 2207 Petroleum Asphalts** and **JIS K 2208 Asphalt Emulsion**. In addition to JIS, the **Japan Emulsified Asphalt Association Standard (JEAAS-2011)**¹⁾ specifies the requirements for asphalt emulsion having high adherence.
- (7) **Tables 4.1.1 to 4.1.3** show the standard values of the quality of asphalt generally used in port facilities.

Table 4.1.1 Quality of Straight Asphalt (JIS K 2207)

Item		Type Unit	40 to 60	60 to 80	80 to 100
Penetration (25°C)		(1 for 0.1 mm)	More than 40 and less than 60	More than 60 and less than 80	More than 80 and less than 100
Softening point		°C	47.0 to 55.0	44.0 to 52.0	42.0 to 50.0
Elongation (15°C)		cm	10 or more		100 or more
Toluene soluble		mass%	99.0 or more		
Flash point		°C	260 or more		
Thin film heating	Mass change rate	mass%	0.6 or less		
	Residual penetration rate	%	58 or more	55 or more	50 or more
Penetration ratio after vaporization		%	110 or less		
Density (15°C)		g/cm ³	1.000 or more		

Note: The kinetic viscosity at 120°C, 150°C, and 180°C shall be indicated in test reports.

Table 4.1.2 Quality of Blown Asphalt (JIS K 2207)

Item	Type Unit	10 to 20	20 to 30	30 to 40
Penetration (25°C)	(1 for 0.1 mm)	More than 10 and less than 20	More than 20 and less than 30	More than 30 and less than 40
Softening point	°C	90.0 or more	80.0 or more	65.0 or more
Elongation (25°C)	cm	1 or more	2 or more	3 or more
Toluene soluble	mass%	98.5 or more		
Flash-point	°C	210 or more		
Change rate of vaporized mass	mass%	0.5 or less		
Penetration-index		2.5 or more		1.0 or more

Table 4.1.3 Quality Standards of Polymer-Modified Asphalt (JMAAS-01)²⁾

Item	Type	Type I	Type II	Type III		Type H	
	Added symbol			Type III-W	Type III-WF	Type H-F	Type H-F
Softening point	°C	50.0 or more	56.0 or more	70.0 or more		80.0 or more	
Elongation (7°C)	cm	30 or more	-	-		-	-
Elongation (15°C)	cm	-	30 or more	50 or more		50 or more	-
Toughness (25°C)	N·m	5.0 or more	8.0 or more	16 or more		20 or more	-
Tenacity (25°C)	N·m	2.5 or more	4.0 or more	-		-	-
Stripping area ratio of coarse aggregate	%	-	-	-	5 or less	-	-
Frath breaking point	°C	-	-	-	-12 or less	-	-12 or less
Bending work (-20°C)	kPa	-	-	-	-	-	400 or more
Bending stiffness (-20°C)	MPa	-	-	-	-	-	100 or less
Penetration rate (25°C)	1/10 mm	40 or more					
Mass change rate through thin film heating	%	0.6 or less					
Residual penetration after thin film heating	%	65 or more					
Flash point	°C	260 or more					
Density (15°C)	g/cm ³	to be added in test reports					
Optimum mixing temperature	°C	to be added in test reports					
Optimum compaction temperature	°C	to be added in test reports					

Definitions of added symbols: W for water resistance and F for flexibility

4.2 Asphalt Mats

4.2.1 General

- (1) Asphalt mats shall have appropriate structures satisfying the required strength, durability, and workability according to the intended use, the locations of use, and the hydrographic conditions of construction sites.
- (2) Asphalt mats are manufactured in a manner that embeds reinforcement materials and wire ropes for suspension in asphalt mixtures made by mixing asphalt, fillers (limestone powder), sand, and crushed stone and molding them into the form of mats (see **Fig. 4.2.1**).
- (3) There are several types of asphalt mats, including friction enhancement mats to increase sliding resistance of gravity-type structure bodies, scouring prevention mats to prevent structural foundations from scouring, and sand washing-out prevention mats to prevent foundation sand mounds and backfill sand from being washed out. When using asphalt mats, it is preferable to give due consideration to their quality, long-term durability, and workability

according to the intended use, the locations of use, and the hydrographic conditions of construction sites. Particularly in the special hydrographic conditions, such as cold and subtropical regions, as well as tidal zones, which are considered to be severe environmental conditions for asphalt mats in terms of long-term durability^{3),4)}, it is preferable to carefully examine the use of asphalt mats, including their applicability.

- (4) The strength and workability of asphalt mats vary depending on the mix proportion of asphalt mixtures and thickness as well as the sizes of reinforcement materials and mats. The mix proportion of asphalt mats can be determined with reference to **Part II, Chapter 11, 4.2.3 Mix Proportion**. Also, reinforcement materials are preferably determined on the basis of the results of the push-out test specified also in **4.2.3**.

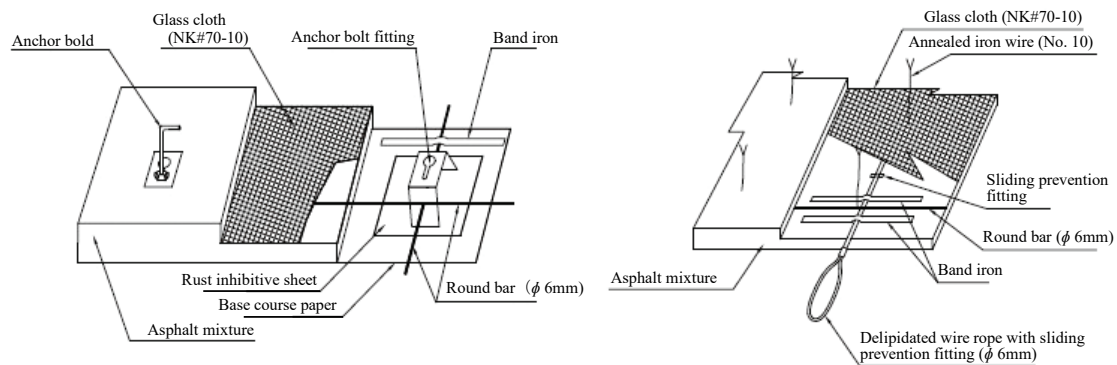


Fig. 4.2.1 Example of Structure of Friction Enhancement Mats
(Left: Anchor Bolt Method, Right: Annealed Iron Wire Method)

- (5) The thicknesses of asphalt mats can be determined in consideration of the intended use and the required strength and flexibility, provided, however, that the thicknesses of friction enhancement mats shall be determined, as a standard, by additionally taking into consideration residual thicknesses, strain amounts, and the amounts sinking into rubble mounds.
- (6) For the friction coefficients of friction enhancement mats, reference can be made to **Part II, Chapter 11, 9 Friction Coefficients**.

4.2.2 Materials

- (1) The materials for asphalt mats shall be appropriately selected so as to ensure the required strength and durability.
- (2) The following materials can be used for asphalt mats.

① Asphalt

Straight asphalt or blown asphalt which complies with **JIS K 2207 Petroleum Asphalts** or the mixture of straight and blown asphalt

② Sand

Clean sand with the maximum grain size of 2.5 mm with no inclusion of waste, mud, and organic matters

③ Fillers

Those fillers which comply with **JIS A 5008 Limestone Filler for Bituminous Paving Mixtures**

④ Crushed stone

Crushed stone which has grain sizes from 2.5 to 20 mm and complies with **JIS A 5001 Crushed Stone for Road Construction**

- (3) The straight or blown asphalt which complies with **JIS K 2207 Petroleum Asphalts** can be used for asphalt mats. However, because there are large differences in plastic fluidity and other properties between straight and blown asphalt and single use of either of the two types of asphalt cannot develop the required strength and poses a problem with workability, they are normally mixed so as to ensure the required properties of asphalt mats. In this case, the

needle penetration rates of 40 to 100 and 10 to 40 are generally used as standards to evaluate the availability of straight asphalt and blown asphalt, respectively.

- (4) Crushed stone is a coarse aggregate of asphalt mats and has an important influence on the strength of asphalt mats. Thus, crushed stone shall be of sufficiently high quality. Generally, the maximum grain size of crushed stone is preferably not more than 1/6 of the thicknesses of asphalt mats for the purpose of facilitating construction work; however, larger grain sizes are preferable when asphalt mats are subjected to large pressure as is the case with friction enhancement mats.
- (5) In addition to the materials described above, asphalt mats require reinforcement materials and wire ropes for suspension. Generally, glass cloth and glass fiber mesh tape are used as reinforcement materials.

4.2.3 Mix Proportion

- (1) The mix proportion of asphalt mats is generally determined through mix proportion tests to ensure the required strength and flexibility. Considering that friction enhancement mats and scouring/sand washing-out prevention mats have been used for a relatively long period and that extensive performance records exist^{5), 6)}, the values in **Table 4.2.1** can be used as the mix proportion of asphalt mats except in the case of special use conditions.

Table 4.2.1 Standard Mix Proportion of Asphalt Mats

Material	Ratio by weight (%)	
	Friction enhancement mat	Scouring/sand washing-out prevention mat
Asphalt	10 - 14	10 - 14
Dust	14 - 25	14 - 25
Fine aggregate	20 - 50	30 - 50
Coarse aggregate	30 - 50	25 - 40

Note: Dust means sand and fillers with grain sizes of 0.075 mm or less

Fine aggregate means crushed stone, sand and fillers with grain sizes of 0.075 to 2.5 mm.

Coarse aggregate means crushed stone with grain size of 2.5 mm or more.

- (2) The deformation property of asphalt mats is susceptible to temperature. Thus, it is preferable to use those unlikely to fluidize when constructed in summer and those capable of maintaining flexibility when constructed in winter.

(3) Performance Verification

- ① For friction enhancement mats and scouring/sand washing-out prevention mats, it is preferable to determine mix proportion through specific gravity tests of asphalt mixtures and bending as well as compression tests so as to ensure the required performance. In the case of sand washing-out prevention mats subjected to relative large local actions due to armor stones, mix proportion shall be determined, as a standard, through push-out tests of the mats in order to confirm the strength of the entire mats, including reinforcement materials.
- ② The performance verification of asphalt mats can be carried out in accordance with the **Reference 7)**. Generally, bending and compression tests shall be conducted at the temperature of 20°C and the loading rate of 20 mm/min, and push-out tests shall be conducted in a manner that uses loading test equipment, as shown in **Fig. 4.2.2**, where 30-cm-square test pieces of asphalt mixtures with reinforcement materials are subjected to the test at the temperature of 20°C and the loading rate of 50 mm/min.

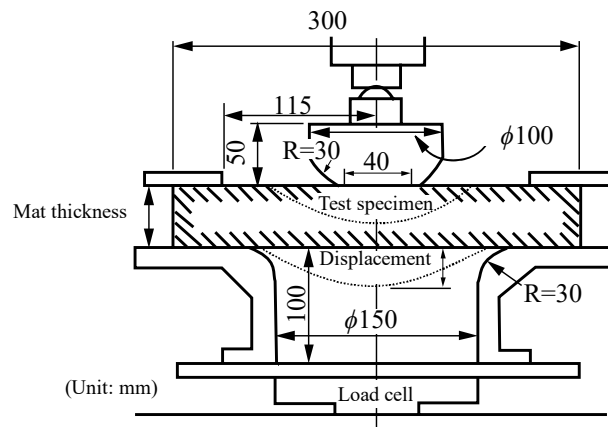


Fig. 4.2.2 Example of Push-Out Test Set-up

- ③ The required performance of asphalt mats is preferably set depending on the respective conditions. Table 4.2.2 shows the standard limit values for the respective test results.

Table 4.2.2 Determination Reference Values of the Test Results

Test item		Friction enhancement mat	Scouring/sand washing-out prevention mat	
			Normal mat	Reinforced mat
Tests for asphalt mixture	Specific gravity test	2.2 or more	2.2 or more	
	Bending test			
	Strength	2.0 N/mm ² or more	1.0 N/mm ² or more	
	Displacement	3 mm or more	3 mm or more	
Compression test		2.0 N/mm ² or more	1.0 N/mm ² or more	
Strength				
Push-out test				
Maximum load		—	8 kN or more	15 kN or more
Displacement		—	10 mm or more	30 mm or more

The types and applicability of scouring/sand washing-out prevention mats shall be determined on the basis of past performance records and meteorological as well as hydrographic conditions; however, there are cases of using normal mats and reinforced mats for armor blocks of less than 3 tons/unit and not less than 3 tons/unit, respectively.

4.3 Paving Materials

- (1) Paving materials can comply with **the Guideline for Pavement Design and Construction⁸⁾**, **the Handbook for Pavement Design⁹⁾**, and **the Handbook for Pavement Construction¹⁰⁾** except in the areas subjected to special actions.
- (2) Aprons are examples of areas subjected to special actions. Slightly different from general roads, the type of traffic on the paved areas of cargo handling facilities, particularly aprons, is mostly large vehicles with a large proportion of heavy equipment having large ground contact pressure. Also, the actions of large vehicles are rarely in a fast-moving state but mostly in a stationary or slow-moving state. Moreover, there are cases where the paved areas are partially used as yards to store cargoes to be loaded or unloaded. Thus, it is necessary to select paving materials for such paved areas with appropriate consideration to the characteristics of materials with reference to **Part III, Chapter 5, 9.18 Aprons**.
- (3) Guss asphalt has impervious and high deflection tracking properties and is, therefore, frequently used for steel floor and bridge deck pavement.

4.4 Sand Mastic

4.4.1 General

- (1) Sand mastic is an asphalt mixture manufactured by mixing and heating the mixture of asphalt, mineral fillers or additives, and sand. Sand mastic has almost no voids and does not necessitate compaction after injection.
- (2) When sand mastic kept in a certain high temperature state is poured over a rubble mound, it flows into the voids among rubble stones without undergoing material separation underwater. Because sand mastic can integrate a rubble mound as a whole by covering individual rubble stones, it prevents rubble stones from being dissipated or washed out. Thus, sand mastic can be effective when general rubble mounds cannot be constructed with rubble stones of predetermined sizes or such rubble stones are not economically available. Also, sand mastic can be injected into the joints between caissons so as to ensure water tightness or to prevent sand from being washed out and used as impervious materials for the revetments of waste disposal sites.
- (3) The performance verification of sand mastic shall be carried out with consideration to plastic flow due to the material characteristics of asphalt so as to ensure the stability.
- (4) Regarding the durability of sand mastic, in the case where it is used underwater with less influences of ultraviolet rays and oxygen, it is considered that sand mastic does not undergo the changes in physical properties as is the case with asphalt mats. As a reference for the use of sand mastic above water, there is a test report on sand mastic used for solidifying rubble mound for a breakwater, stating that specimens taken out from the tidal zone of the rubble mound showed sufficient durability with respect to strength and deflection following property even after the service period of 36 years⁽¹⁾.

4.4.2 Materials

- (1) The materials for sand mastic shall be appropriately selected so as to ensure the required strength and durability.
- (2) The examples of the materials for sand mastic are as follows:

① Asphalt

The asphalt for sand mastic to be used underwater can be the straight asphalt with the needle penetration rates of either 40 to 60, 60 to 80, or 80 to 100 as specified in **JIS K 2207 Petroleum Asphalts**.

② Sand

Clean sand with the maximum grain size of 2.5 mm with no inclusion of waste, mud, and organic matters.

③ Fillers

Those fillers which comply with **JIS A 5008 Limestone Filler for Bituminous Paving Mixtures**.

- (3) The asphalt for sand mastic to be used underwater^{(2),(3)} shall have sufficient fluidity because sand mastic is required to reliably flow into the voids among rubble stones when poured underwater over rubble mounds.
- (4) Generally, the fluidity of asphalt mixture becomes greater with the increase in the sizes of sand grains, thereby allowing a small quantity of asphalt to achieve the required fluidity at the increased risk of material separation. In contrast, although the fluidity is low, denser sand mastic becomes available with the decrease in the size of sand grains. Thus, in order to prevent material separation of asphalt mixtures, sand preferably has continuous grain size distribution and gentle grading curves.
- (5) When mixed with asphalt mixtures, fillers fill the voids among aggregate together with asphalt and function as binding materials which reduce the fluidity and increase viscosity and stability of asphalt mixtures. Asphalt generally adheres well to alkaline fillers. Thus, it is possible to use fillers made of limestone powder which shows mild alkalinity.

4.4.3 Mix Proportion

- (1) The mix proportion of sand mastic shall generally be determined through mix proportion tests suitable for confirming the required fluidity and strength taking into consideration construction and natural conditions.
- (2) The properties of sand mastic vary depending on mix proportion and the properties of materials. Also, the requirements for workability, strength, and flexibility of sand mastic vary depending on the locations of the construction sites and natural conditions.

(3) General

The values in **Table 4.4.1** are frequently used as the mix proportion of sand mastic to solidify rubble stones underwater.

Table 4.4.1 Standard Mix Proportion of Sand Mastic

Material	Proportion by weight (%)
Asphalt	16 - 20
Dust	18 - 25
Fine aggregate	55 - 66

Note: Dust refers to sand and fillers passing through a 0.075 mm sieve.

Fine aggregate refers to sand and fillers remaining on a 0.075 mm sieve.

(4) Performance Verification

The mix proportion of sand mastic for solidifying rubble stones is preferably determined so as to ensure the required performance through the following tests:

(a) Fluidity test

- 1) The time of flow of sand mastic used underwater shall be in the range of 10 to 60 s.
- 2) No visually identifiable material separation while flowing.

(b) Specific gravity test: 1.95 or more**(c) Bending test:** strength of 1.0 N/mm² or more and deflection amount of 5.0 mm or more**(d) Compression test:** 1.0 N/mm² or more

The tests of (c) and (d) above shall be conducted at the temperature of 10°C and the loading rate of 20 mm/min.

(5) Method for Calculating the Required Amount of Sand Mastic

The required amount of sand mastic used for a rubble layer can be calculated by **equation (4.4.1)**.

$$V = \alpha A(hv + d) \quad (4.4.1)$$

where:

- V : required amount of sand mastic (m³)
- A : area of a rubble layer into which sand mastic is injected (m²)
- h : thickness of a rubble layer into which sand mastic is injected (m)
- v : porosity of a rubble layer into which sand mastic is injected
- d : thickness of a sand mastic cover on a rubble layer (m)
- α : additional rate in consideration of the injection into a lower rubble layer (which varies depending on the size of the lower rubble layer and the fluidity of sand mastic but is generally set at 1.0 to 1.3)

(6) Points of caution in the performance verification

The points of caution when designing sand mastic are as follows:

- ① Careful attention is required when applying sand mastic to the locations with the risks of powerful impulsive wave pressure or damage due to drifting objects.
- ② Sand mastic shall not be used in locations where expected deflection is too large for sand mastic to follow as is the case with rapid or large-scale sedimentation.
- ③ The gradients of rubble surfaces to which sand mastic is applied are preferably 1:1.3 or less.

- ④ The sand mastic used at the tops and foots of slopes as well as edges of structures shall be provided with proper reinforcement.
- ⑤ The design working life of port facilities and the durability of the sand mastic asphalt should be fully taken into account.

[References]

- 1) Japan Emulsified Asphalt Association: Japan Emulsified Asphalt Association Standard (JEAAS), 2011
- 2) Japan modified asphalt association: Japan modified asphalt association standard (JMAAS-01), 2007.
- 3) Imoto, T., Y. Mizuno and K. Yano: Research on durability of asphalt mats employed in the gravity type port facilities, Proceedings of Offshore Development, JSCE, Vol. 5, pp. 119-124, 1989
- 4) Mizuno Y., M. Tokunaga, Y. Sugimoto, K. Murase and O. Yasuda: Development and study of asphalt mats for friction increase of gravity type of offshore structures in cold sea area, Proceedings of Offshore Development Vol. 8, pp. 171-176, 1992
- 5) Kataoka, S., K. Nishi, M. Yazima and O. Miura: Durability of asphalt mats placed under caisson for friction increase, Proceedings of 30th Conference on Coastal Eng, pp. 643-647, 1983
- 6) T.hamada,H.kitayama,A.oka,A.nakai,T. wakasugi:long term(30 years) durability of aspahlt mat in sea water, pp1001-1005, 2001.
- 7) Itakura, T. and T. Sugahara: Recent Development of Asphalt Utilization, Journal of Japanese Petroleum Institute Vol. 7, No. 8, p. 9, 1964
- 8) Japan Road Association: Guideline for pavement design and construction 2006.
- 9) Japan Road Association: Pavement design handbook 2006.
- 10) Japan Road Association: pavement construction handbook 2006.
- 11) S.Obuchi,H.Nakano,F.Hoshino: study on 36 year long term durability test of asphalt mastic, mainly co ncerning deformation following property;JSCE 2005
- 12) Study group for asphalt mixture for hydraulic structures: Asphalt mixture for hydraulic structures – materials, design and construction for field engineers –, Kajima Publishing, 1976
- 13) Kagawa, M. and T. Kubo: Experimental study on stability of rubles poured sand mastic, Proceedings of 12th Conference on Coastal Eng., JSCE, 1965

5 Stones

5.1 General

- (1) Stone materials shall be selected taking into consideration the required quality and performance suitable for the intended use and economic efficiency.
- (2) Generally, stone materials are used in large quantities for the construction of port facilities, such as breakwaters and wharves. Careful consideration shall be given to the selection of stone materials because they have large influences on the stability of facilities and construction period as well as costs.
- (3) **Table 5.1.1** summarizes the results of the research conducted by the Okinawa General Bureau of the Cabinet Office on the types and physical properties of major stone materials related to port development. It shall be noted that even stone materials of identical types may have large differences in physical properties depending on production areas and quarrying positions.

It is also necessary to pay attention to the possible difference between actual and designed unit weight of stone materials because unit weight fluctuates in accordance with the porosities which vary depending on the shapes and sizes of stone materials.

Table 5.1.1 Physical Properties of Stones

Rock classification	Stone type	Specific gravity (Apparent)	Water absorption rate (%)	Compression strength (N/mm ²)
Igneous rock	Granite	2.60 to 2.78	0.07 to 0.64	85 to 190
	Andesite	2.57 to 2.76	0.27 to 1.12	78 to 269
	Basalt	2.68 (true)	1.85	85
	Gabbro	2.91 (true)	0.21	177
	Peridotite	3.18	0.16	187
	Diabase	2.78 to 2.85	0.008 to 0.03	123 to 182
Sedimentary rock	Tuff	2.64	0.16	377
	Slate	2.65 to 2.74	0.08 to 1.37	59 to 185
	Sandstone	2.29 to 2.72	0.04 to 3.65	48 to 196
	Limestone	2.36 to 2.71	0.18 to 2.59	17 to 76
	Chert	2.64	0.14	119
Metamorphic rock	Hornfels	2.68	0.22	191

Note: (true) means true specific gravity. The values not in the form of ranges are averages.

5.2 Rubble for Foundation

- (1) The stones used as rubble for foundation shall be in proper shapes, not flat or slender and should be hard, dense, durable, and free from the risks of weathering and freezing damage.
- (2) Stone materials to be used shall be determined on the basis of the material quality confirmed through tests, availability, transportability, and costs.
- (3) The type of rocks classified as igneous rock is generally used for rubble foundations. However, aside from the portions of rubble foundations to which large loads are directly applied, such as the areas immediately below caissons, another type of rocks classified as sedimentary rock, such as tight sands, or artificial stone materials, such as hydration-hardened steel slag, can be used as rubble provided that they satisfy the required performance.
- (4) Shoji¹⁾ studied the shear characteristics of rubble for foundations by conducting large-scale triaxial compression tests on the basis of the actual use conditions of rubble stones in port construction works.
- (5) As a guide to determine strength constants without conducting large-scale triaxial tests, Minakami and Kobayashi²⁾ reported that rubble stones with unconfined compression strength of 30 N/mm² or more are expected to have apparent cohesion of 0.02 N/mm² and an angle of shear resistance of 35°.

5.3 Backfill Materials

- (1) Backfill materials shall be selected taking into consideration their properties, such as angles of shear resistance and unit weight.
- (2) Generally, the stone materials used for backfilling are rubble, unscreened gravel, cobblestone, and steel slag.
- (3) The values in **Table 5.3.1** can be used as the characteristic values for backfill materials.
- (4) In this section, rubble means the stone materials which are used in port-related works and comply with **JIS A 5006 Rubbles**.
- (5) The unscreened gravel means the mixtures of equal parts of sand and gravel.
- (6) Slope gradients are standard values of gradients of slopes of the backfill materials when they are naturally stabilized underwater during construction.
Generally, smaller values of gradients are used for the backfill areas with small influence of waves and larger values of gradients for the backfill areas with large influence of waves.
- (7) When using steel slag, careful examination is required because its quality varies depending on the production factories. For the details of steel slag, **Part II, Chapter 11, 7.2.2 Steel Slag**, can be used as a reference.
- (8) There are cases in which lightweight aggregates are used as backfill materials in order to reduce earth pressure.

Table 5.3.1 Characteristic Values of Backfill Materials

		Angle of shear resistance (°)	Unit weight		Slope gradient
			Above residual water level (kN/m ³)	Below residual water level Underwater effective weight (kN/m ³)	
Rubble	Ordinary type	40	18	10	1:1.2
	Brittle type	35	16	9	1:1.2
Unscreened gravel		30	18	10	1:2 – 1:3
Cobblestone		35	18	10	1:2 – 1:3

5.4 Armor Stones

- (1) Armor stones are subjected to severe meteorological actions and the abrasive action of sand carried by waves. Thus, as is the case with rubble for foundations, stone materials used for armor stones shall be hard, dense, large in specific gravity, durable, and free from weathering and freezing damage.
- (2) Stone materials to be used shall be determined on the basis of the material quality confirmed through tests, availability, transportability, and costs.
- (3) In addition to natural stone materials, artificial stone materials, such as hydration-hardened steel slag, have been used for armor stones.

5.5 Base Course Materials

- (1) Base course materials shall be selected taking into consideration the required bearing capacity, the ease of compaction, and durability.
- (2) Normally, granular materials, cement stabilized soil, or bituminous stabilized soil are used as base course materials. Granular materials include crushed stone, steel slag, unscreened gravel, pit gravel, unscreened crushed stone, crushed stone dust, and sand. These granular materials may be used independently or as mixtures with other types of granular materials.
- (3) Base courses disperse loaded weight applied on them and transfer dispersed load to subgrades. Generally, base courses are separated into lower and upper base courses. The lower base courses have relatively low bearing capacity and are constructed by inexpensive materials. In contrast, the upper base courses are constructed by high-quality materials with large bearing capacity. The specifications for the required bearing capacity and use materials

of base courses differ between concrete and asphalt pavement. For these requirements, Cement Concrete Pavement³⁾ and Essential Points of Asphalt Pavement⁴⁾ in **Part III, Chapter 5, 9.18 Aprons**, can be used as references.

[References]

- 1) Shoji, Y.: Study on Shearing Properties of Rubbles with Large Scale Triaxial Compression Test, Rept. of PHRI Vol. 22 No. 4, 1983
- 2) Minakami, J. and M. Kobayashi: Soil Strength Characteristics of Rubble by Large Scale Triaxial Compression Test, Technical Note of PHRI No. 699, p. 20, 1991
- 3) Japan Road Association: Cement Concrete Pavement, Maruzen Publishing, 1997
- 4) Japan Road Association: Essential Points of Asphalt Pavement, Maruzen Publishing, 1998

6 Timber

6.1 General

Timber installed below groundwater levels can maintain its long-term durability and was widely used for foundations of concrete structures in ports such as quaywalls and breakwaters until the 1960s. Some timber piles constructed at that time are still in use, even now. Also, recently, a log placing method was developed for using logs as ground improvement materials for underground storage of carbon dioxide as a countermeasure against global warming, and there have been increasing cases of using the method.^{1) and 2)}

The government, municipalities, business operators, and people are encouraged to promote the use of timber in the **Act on Promotion of Use of Wood in Public Buildings, etc.** (Act No. 36 of 2010) which was promulgated and put into effect on May 26, 2010. Owing to advanced wood fireproofing technologies, and the development of large cross sectional wooden structural members such as cross laminated timber (CLT), there has been widespread use of timber in public facilities, such as stadiums and school buildings. Timber has also been used for passenger terminal buildings, decks, and boardwalks in ports and airports, and the use of timber is expected to be further promoted in the future.

In contrast, it is difficult to apply timber to the undersea structural members, such as a pile of piled piers because, in such an environment, timber is subjected to feeding damage of marine borers, such as shipworms. Conventional conservation treatment through chemical injection has had problems because the chemical leaches into the environment and there is an unsustainable conservation effect. Recently however, conservation treatment technologies (thermal treatment, low-molecular phenol injection treatment, etc.) have been developed which can solve these problems^{3) and 4)} and enable the use of timber as undersea structural members in the future.

Compared with steel, concrete, and plastic materials, timber has the following characteristics. When using timber in port facilities, it is necessary to pay attention to these characteristics.

(1) Strength Performance

Timber density differs depending on species. Because timber species with high density have few voids in timber textures, they are likely to have high strength and Young's modulus. Also, timber has anisotropic strength performance, where the strength and Young's moduli, with respect to loads in the direction perpendicular to fibers (woodgrains), are significantly smaller than those with respect to loads in the direction parallel to fibers. In addition, in timber, the tensile strength is higher than the compressive strength; bending failure is started with compressive buckling; and moisture contents and loading duration have measurable influences on strength.

(2) Durability

Timber undergoes degradation such as discoloration, surface contamination, morphology changes, and strength reductions due to the actions of organisms (such as bacteria, insects, and marine borers) and meteorological factors (such as ultraviolet rays, rain, and temperature). The main degradation factors of timber vary greatly depending on usage environments and moisture contents.

(3) Environmental Characteristics

Trees grow in a manner that fixes carbon dioxide in the atmosphere using solar energy. Thus, timber is a material which releases little carbon dioxide into the atmosphere through its production. Also, using thinned wood can help preserve artificial forests. It shall be noted that using timber from natural forests has a risk of causing forest destruction.

(4) Others

Timber has: flammable nature; esthetic values of the woodgrain patterns with moderate irregularity and shading; fragrance with favorable physical and mental effects on people; moderate elasticity to reduce the chance of people getting injured when falling on timber members; low thermal conductivity, which produces warmth texture; and moderately large friction coefficients with almost no difference between static and kinetic friction coefficients, which makes walking easier.⁵⁾

6.2 Strength Performance

Setting the characteristic values of timber strength and verification of the bearing capacity of timber as structural members can be made based on the **Standard for Structural Design of Timber Structures**⁶⁾ (hereinafter referred to as the "Standard") or the **Recommendation for Limit State Design of Timber Structures (Draft)**⁷⁾ (hereinafter referred

to as the “**Recommendation (Draft)**”) of the Architectural Institute of Japan. The following items are of particular concern when timber is used for port facilities.

(1) Moisture Content

The dry base moisture content, calculated by $(\text{mass of water in timber}) / (\text{total dry mass of timber}) \times 100(\%)$, is normally used as the value expressing timber moisture content. The moisture in timber is separated into bound moisture and free moisture. The bound moisture is bound to cellulose in timber cell walls. In contrast, free moisture exists in intracellular spaces in the form of liquid. When timber has a moisture content of about 30% or less, it has no free moisture.

The strength of timber (compressive, tensile, bending, and shear strength) is affected, not by free moisture, but by bound moisture. As schematically illustrated in **Fig. 6.2.1**, timber shows a continuous decrease in its strength when moisture content is increased from totally dry to about 30% (fiber saturation point) as a result of the increase in bound moisture. In contrast, the strength is almost stabilized even when the moisture content is increased beyond the fiber saturation point as a result of the increase in free moisture. Under the meteorological conditions in Japan, the moisture content of timber reaches equilibrium at around 15%. Therefore, in the **Standard** and the **Recommendation (Draft)**, the standard strength characteristic values of timber are specified based on test results at the moisture content of 15%. Also, the **Standard** and the **Recommendation (Draft)** categorizes a constantly wet state as Usage Environment I, an intermittently wet state as Usage Environment II, and other states as Usage Environment III and requires the standard strength characteristic values of timber in the Usage Environments I and II to be reduced in a manner that multiplies them by the reduction coefficients of 0.7 and 0.8 respectively. Thus, when the wet states of timber structural members in port facilities fall under the categories of Usage Environments I and II, their standard strength characteristic values shall be reduced by using the reduction coefficients.

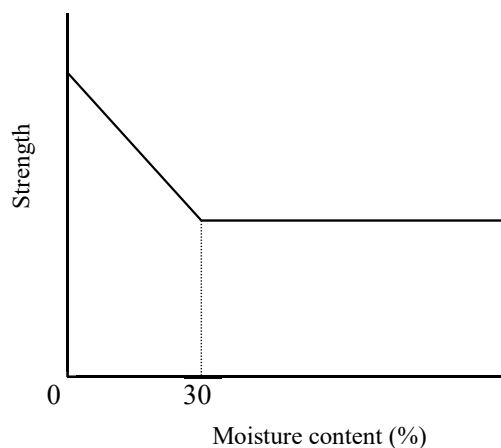


Fig. 6.2.1 Influence of Moisture Content on Timber Strength (Schematic Drawing)

Timber also undergoes dimensional changes (expansion or contraction) depending not on free moisture but on bound moisture. The timber dimensions are increased when the moisture content is increased from totally dry to about 30% (fiber saturation point) as a result of the increase in bound moisture. In contrast, the dimensions are almost stabilized even when the moisture content is increased beyond the fiber saturation point as a result of the increase in free moisture. The dimensional changes of timber are anisotropic in that the change rates are decreased in the order of tangential direction with respect to annual rings, radial direction with respect to annual rings and fiber direction with the approximate relative ratio of 1.0:0.5:0.1. In the case of Japanese cedar, the total expansion ratio from a totally dry point to a fiber saturation point reaches about 6% in the tangential direction with respect to annual rings. When timber is used in environments with possible fluctuations in moisture contents below fiber saturation points, it is necessary to design timber considering these dimensional changes.

The unit weight of timber largely varies depending on species and moisture contents. For example, the unit weight of Japanese cedar, Japanese red pine, and Japanese oak is about 0.38, 0.52, and 0.68 g/cm³, respectively, in an air-dried state (moisture content of 15%).⁸⁾ With a large amount of moisture in intracellular spaces, the unit weight of the undried logs immediately after logging and timber which has been used underwater may be more than twice the unit weight in an air-dried state. Although the unit weight of 0.8 g/cm³ (7.8 kN/m³) has been used conventionally

for timber in the design of port facilities, it is necessary to ensure that the design of port facilities is still on the safe side even after possible large fluctuations in actual unit weight of timber depending on the species and moisture contents.

(2) Loading Duration

According to the **Recommendation (Draft)**, loading duration has a relationship with loading duration influence coefficients, as shown in **Fig. 6.2.2**. The loading duration influence coefficients are: the coefficients to be multiplied by standard strength characteristic values when loading is expected to continue beyond 10 minutes, which is the standard material testing period; and introduced for the purpose of incorporating the influence of loading duration on material strength. It is also necessary for port facilities to reduce the standard strength characteristic values using the loading duration influence coefficients based on the assumption of the loading duration of respective temporary loads during construction and long-term loads after completion.

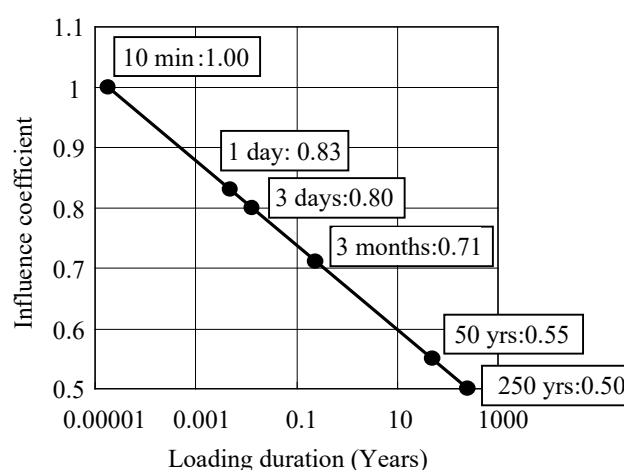


Fig. 6.2.2 Loading Duration Influence Coefficient⁷⁾

(3) Standard Strength Characteristic Values of Logs

With no fibers cut, logs are mechanically superior to lumber and suitable for use in port facilities in terms of economic efficiency and environmental friendliness. The **Standard** and the **Recommendation (Draft)** allow the standard strength characteristic values of general structural timber, or mechanically graded lumber, to be used as the standard strength characteristic values of logs.

6.3 Durability

The problems inherent in the use of timber are discoloration, surface contamination, morphology changes, and strength reductions. The degrees of importance of respective problems vary depending on the intended use of timber (required performance such as aesthetic property and strength).

(1) Degradation Factors

The main factors causing timber degradation are: living organisms (fungi, insects, marine borers, etc.), meteorological factors (ultraviolet rays, rain, temperature, etc.), and continuous loading. The main degradation factors of timber differ depending on the usage environments and moisture contents of timber as shown in **Table 6.3.1**. The three types of moisture states in the table are defined as follows: “Dry” means moisture contents, equal to or less than the fiber saturation point (about 30%), with no moisture in intracellular spaces; “Wet” means moisture contents, equal to or more than the fiber saturation point (about 30%), with moisture and oxygen in intracellular spaces; and “Saturated” means a state where intracellular spaces are almost filled with moisture and nearly empty of oxygen.

Table 6.3.1 Usage Environments and Degradation Factors

Usage environment		Example of application	Moisture state	Main degradation factor
Indoor		Residence	Dry	Insects harmful to dried wood
			Wet	Fungi and termites
Outdoor	In the air	Outdoor construction material	Dry	Meteorological factors and insects harmful to dried wood
			Wet	Fungi, termites, meteorological factors
	Underground	Pile	Wet	Fungi and termites
			Saturated	Bacteria, continuous loading
	In fresh water	River facility	Wet	Fungi
			Saturated	Bacteria, continuous loading
	Splash zone of seawater	Port facility	Wet	Meteorological factors
	Tidal zone and in the seawater	Port facility	Wet	Marine borers
			Saturated	Marine borers

① Fungi⁹⁾

Generally, the types of fungi that are timber degradation factors can be classified into mold and wood rotting fungi. Mold causes the discoloration and contamination of timber surfaces, thereby posing problems when aesthetic properties are important. In contrast, wood rotting fungi degrade cellulose and lignin, which are the main compositions of wood, thereby causing morphology changes and strength reductions.

Wood rotting fungi are classified into brown-rot fungi, white-rot fungi, and soft decay fungi. Wood rotting fungi do not develop in timber in a dry state with too little free moisture, or in a saturated state with too little oxygen, because they require intracellular moisture (free moisture) and oxygen to grow. Thus, timber piles installed underground below groundwater levels are not subjected to degradation due to wood rotting fungi, thereby maintaining long-term durability.^{10) and 11)}

② Bacteria

Bacteria and continuous loading can be timber degradation factors in a saturated state. Timber degradation due to bacteria progresses from the timber surfaces to the interiors at rates of 0.1 to 0.5 mm/year. There is a report saying that degradation is significantly slowed when bacteria reach heartwood (to be described later).¹²⁾

③ Insects⁹⁾

Termites (Japanese subterranean termites and formosan subterranean termites) and the insects harmful to dried wood (coleopteran such as *Lyctus brunneus*) can be degradation factors of timber.

④ Marine borers^{3), 13), 14), 15), 16), and 17)}

Those marine borers causing timber degradation are shipworms, which are mollusks, and *Limnoria* species, which are crustaceans.

Shipworms are bivalves. Once their larvae with diameters of around 0.3 mm attach to timber in seawater, they penetrate the timber by grinding it with their shells. They leave only small holes, with diameters of about 0.3 mm on the timber surfaces, but their nests inside timber have diameters about 7 mm and lengths of about 10 cm or more. Thus, shipworms may significantly reduce sectional areas and strength of timber within a couple of months. The larvae of shipworms in an adhesion period are considered mobile in the entire vertical range from sea surfaces to sea bottoms but stop activities when salinity becomes 0.6% or less. Broad-leaf trees, such as oaks, are more susceptible to damage from shipworms than needle-leaf trees, such as cedars and cypress, but pines, one of the needle-leaf trees, are susceptible and camphor trees, one of the broad-leaf trees, are not susceptible to damage from shipworms.

Limnoria are a species of crustaceans, about 3 mm long and 1 mm wide, which create nest holes close to the surface of timber in seawater. Once porous pile surface sections due to the nest holes are removed by waves, they create nest holes close to the newly exposed pile surfaces, thereby reducing timber volumes. Their activities are slower when the salinity is reduced to 1.6%, and they are mostly dead when the salinity is 0.6%.

The types of timber having low density with soft surfaces are susceptible to the damage due to Limnoria and needle-leaf trees are likely to be more susceptible than broad-leaf trees.

In brackish-water regions, such as river mouths, timber is susceptible to the damage due to Sphaeromidae¹⁸⁾ which is a species of crustaceans like Limnoria and has a length of about 5 to 15 mm.¹³⁾

⑤ Meteorological factors⁹⁾

The meteorological factors causing timber degradation are sunlight (mainly ultraviolet rays), temperature, precipitation, fallen snow, and winds. Timber undergoes ashy white discoloration and grain depression (reductions in cross sectional areas and mass) through the degradation of lignin, which is one of the main composition elements of timber due to ultraviolet rays and the eluviation of degraded lignin due to the action of precipitation. Also, timber is susceptible to minute cracks, due to alternative wetting and drying, and abrasion, due to earth and sand blown by winds. The degradation caused by these meteorological factors is called weathering. In the case of the fast-growing sections (sections of annual rings with lighter colors) of needle-leaf trees, the degradation rates due to weathering are considered to be about 5 to 6 mm in 100 years but are largely affected by regional and local meteorological conditions of the places where timber is used. The fast-growing sections are softer and more susceptible to the grain depression than slow-growing sections (sections of annular rings with darker colors) and, therefore, weathering causes timber surface to aggravate concavity and convexity along annular rings.

(2) Degradation Countermeasures

Degradation countermeasures include: the use of inherently highly durable timber, conservation treatments, coating and maintenance.

① Use of inherently highly durable timber

In most tree species, the peripheral sections close to the bark have lighter colors than the interior sections. The peripheral sections, with lighter colors, and the interior sections, with darker colors, are called sapwood and heartwood, respectively. The heartwood contains larger substances called extractives than sapwood. The extractives include phenols, terpenes, tannins, and other substances which are active in preventing enzyme actions of decay fungi, fill gaps inside timber, and protect cell walls. For example, Ipe (South America), teak (Southeast Asia), Lophira alata (Africa), and cypress pine (Australia) are the species considered unsusceptible to biological degradation because of the effects of special extractives. The use of these exotic species of inherently highly durable timber shall be contingent on avoiding deforestation and disruption of the ecosystem. For ensuring the avoidance of deforestation and disruption of the ecosystem, it is preferable to use the certification system supported by the international organizations, such as the Forest Stewardship Council or illegal logging information, provided by environmental NGOs. Also, it is dangerous to easily introduce exotic species with favorable performance records of durability because they may be vulnerable to the indigenous fungi in Japan.

② Conservation treatments

Timber impregnated with antiseptic insect repellent chemicals has been widely used as foundation material for housing and outdoor facilities. The detailed specifications of these chemicals can be found in **JIS K 1570 Wood Preservatives**. Conventionally, creosote oil and copper chromated arsenate (CCA) have been widely used; however, because they have posed health problems for workers and increased environmental loads in the drainage and waste management, they have been substituted with low toxic chemicals. These alternative chemicals are generally less effective than CCA, and their effects on marine borers have not been elucidated. The other conservation treatments besides chemicals include low-molecular phenol resin infusion treatment and thermal treatment.^{3) and 4)} When examining conservation treatments, it is necessary to evaluate the influences of treatments on environments through the life cycle, including production, use, and disposal based on precautionary principles.

③ Coating

Degradation countermeasures by coating have been experimentally implemented using FRP sheets, urethane resin, and polymer cement as coating materials.¹⁹⁾ Coating timber with screens having mesh sizes smaller than those of larvae of shipworms (about 0.3 mm) is confirmed effective against shipworms in on-site experiments in the sea.^{3) and 20)}

④ **Maintenance**^{21), 22) and 23)}

Maintenance is another degradation countermeasure for timber. For proper maintenance, inspections and diagnoses of timber degradation are important; therefore, it is necessary to examine inspection items and methods depending on the degrees of degradation.

The primary diagnoses of timber degradation shall include: visual identification of whether or not timber has discoloration, cracks, fruit bodies (mushrooms), and traces of insect damage with particular focus on the joint sections between timber and the ground or concrete members, as well as the portions of timber prone to rainwater accumulation; examination of whether timber surfaces slightly yield under pressure of a finger; examination of whether or not a sharp point, such as that of a screw driver, sinks into timber surfaces; identification of voids by tapping with a mallet; and photographing surface conditions with a digital camera and storage of image data.

The secondary diagnoses of timber degradation shall include quantitative evaluation of the degrees of degradation using the following on-site measuring devices: a Pilodyn (a device to measure a penetration depth of a pin shot into timber with given energy); a Resistograph (a device to measure torque required to screw a drill into timber at a constant rotation rate); an ultrasonic propagation velocity meter; a moisture content meter; and a driver with a force gauge.²⁴⁾

The tertiary diagnoses of timber degradation include determining degradation causes through: the inspection of the presence or absence of hyphae and degradation of cell walls by observing specimen collected in the field through a microscope; and separation and cultivation of the hyphae.

On the basis of these diagnoses, it is necessary to implement proper maintenance such as the replacement of members as needed.

[References]

- 1) Japan Society of Civil Engineers, Timber Engineering Committee: Introduction to timber engineering for civil engineers, 2017 (in Japanese)
- 2) Miwa, S., Numata, A., Murata, T., Matsuhashi, T., Naraoka, I.: Example of seismic reinforcement work by LP-LiC for fishing port quay, Proceedings of the 71st Annual Conference of the Japan Society of Civil Engineers, V-074, 2016 (in Japanese)
- 3) Yamada, M.: Experiments on marine borers' attacks on wood materials, their Protective methods and the weathering in coastal atmospheres, Technical Note of the Port and Airport Research Institute, No.1281, 2014 (in Japanese)
- 4) Nakamura, K., Nanbu, R., Yamada, M., Mori M., Uchikura K., Morita T., Kaneda T., Yoshida Y.: Marine exposure tests of various treated woods for the purpose of the wood use expansion in fishing port, Mokuzaï Hozon (Wood Protection), Vol.43, No.5, pp.258-269, 2017 (in Japanese)
- 5) Asano, I., Tsuzuki, K.: Some properties of wooden materials as floors, Mokuzaï Kogyo (Wood Industry), Vol.29, No.7, pp.310-313, 1974 (in Japanese)
- 6) Architectural Institute of Japan: Standard for structural design of timber structures, 4th edition, 2006 (in Japanese)
- 7) Architectural Institute of Japan: Recommendation for limit state design of timber structures (draft), 2003 (in Japanese)
- 8) Forestry and Forest Products Research Institute: Wood Industry Handbook, 4th edition, 2004 (in Japanese)
- 9) Japan Wood Protection Association: Introduction to wood protection sciences, 3rd edition, 2012 (in Japanese)
- 10) Japan Society of Civil Engineers, Timber Engineering Committee: Wood Use Library 005 - Examples of wood use in foundation of structures and historic changes of design method in Japan, 2012 (in Japanese)
- 11) Tomimatsu, Y., Numata, A., Hamada, M., Miwa, S., Motoyama, H.: Proposal of using wood in civil engineering field aiming for a sustainable society, Journal of Japan Society of Civil Engineers, F4, Vol.68, No.2, pp.80-91, 2012 (in Japanese)
- 12) Zelada-Tumialan, G., Konicki, W., Westover, P. and Vatovec, M.: Untreated submerged timber pile foundations, Part 1: Understanding biodegradation and compressive strength, STRUCTURE magazine, Dec. 2013, pp.9-11, 2013

- 13) Okada, K. edition: Shipworm damage and protection of wood and wooden vessels, Japan Society for the Promotion of Science, 1958 (in Japanese)
- 14) Tsunoda, K., Nishimoto, K.: Shipworm attack in the sea water log storage area and its prevention (3), Season of settlement, Mokuzai Kogyo (Wood Industry), Vol.35, No.4, pp.166-168, 1980 (in Japanese)
- 15) Yamada, M.: Durability test of untreated wood and wood-powder/plastic composite in marine environment (Part-2), Technical Note of the Port and Airport Research Institute, No.1117, 2006 (in Japanese)
- 16) Yamada, M.: Experiments on the marine borer attack and the atmospheric physical degradation of non-treated wood materials at Tokyo bay coast, Technical Note of the Port and Airport Research Institute, No.1208, 2010 (in Japanese)
- 17) Forestry and Forest Products Research Institute: Report of the research and development project for application in promoting new policy of agriculture, forestry and fisheries, Development of thinned wood utilization technology for frontier environment, Towards the creation of guidelines for utilization of thinned wood in the ground and the sea, 2013 (in Japanese)
- 18) Mimura, K., Hara, T., Kato, H., Honda, K., Nakauchi, T.: Study on the degradation factor of wood in brackish waters, Mokuzai Hozon (Wood Protection), Vol.43, No.1, pp.2-12, 2017 (in Japanese)
- 19) Sasaki, T., Hayashi, T., Araki, S., Ariyama, Y., Toyoda A., Takahashi K.: Construction of forest road bridge using CLT as deck slab, Proceedings of the 72nd Annual Conference of the Japan Society of Civil Engineers, V-572, 2017 (in Japanese)
- 20) Noda, R., Fujimoto, N., Murano, T.: Feasibility of using local wood as pilings for oyster cultivation, Proceedings of the 15th Symposium on Use of Wood for Civil Engineering, pp.60-65, 2016 (in Japanese)
- 21) Japan Wood Protection Association: Maintenance manual of wooden exterior structures, revised edition, 2008 (in Japanese)
- 22) Japan Wood Protection Association: Maintenance of wood materials and timber structures - Degradation diagnosis manual, 2014 (in Japanese)
- 23) Japan Wood Protection Association: Maintenance of wood materials and timber structures - Repair technical manual, 2014 (in Japanese)
- 24) Committee on the Guideline for Wooden Structures for Forest Conservation: Guideline for wooden structures for forest conservation (draft) (Design, construction and maintenance of durable wooden structures for forest conservation), 2016 (in Japanese)

7 Recyclable Materials

7.1 General

- (1) Recyclable materials shall be used with due consideration of the characteristics of materials and facilities.¹⁾
- (2) The use of recyclable materials described in this section is subjected to: the **Act on the Promotion of Effective Utilization of Resources** (Act No. 48 of 1991) (hereinafter referred to as the “**Recycle Act**”); the **Waste Management and Public Cleansing Act** (Act No. 137 of 1970) (hereinafter referred to as the “**Waste Management Act**”); the **Act on Prevention of Marine Pollution and Maritime Disaster** (Act No. 136 of 1970) (hereinafter referred to as the “**Marine Pollution Prevention Act**”); and the **Soil Contamination Countermeasures Act** (Act No. 53 of 2002).
- (3) The **Recycle Act** requires the government, municipalities, and ordering parties of construction works to promote respective countermeasures contributing to the effective use of limited resources and reduced waste generation.
- (4) Recyclable materials used in port construction include slag, coal ash, crushed concrete, dredged soil, and asphalt concrete mass. Most of these can be recycled as earth and stone materials, such as landfill materials, base course materials, soil improvement materials, and concrete aggregate.
- (5) When using slag, coal ash, crushed concrete, and asphalt concrete mass as recyclable materials, it is necessary to examine the applicability of the **Waste Management Act**, the **Marine Pollution Prevention Act**, and the **Soil Contamination Countermeasure Act**. Whether recyclable materials fall in the waste category cannot be objectively and essentially determined by their physical properties. Generally, when materials are useful and can be sold to others for value, they are not categorized as waste.
- (6) Effective use of recyclable materials is extremely important for developing a sustainable society. Because of the characteristics of using large quantities of materials, port and harbor construction works must contribute to environmental preservation and develop a sustainable society by reducing the use of natural resources through effectively using recyclable materials. Also, in compliance with the **Recycle Act**, which strongly recommends effective use of recyclable materials, it is necessary to proactively use materials generated through construction activities by taking advantage of their characteristics.

In contrast, recyclable materials shall be used with due consideration for ensuring environmental safety based on applicable laws and regulations.¹⁾ For the basic concept of environmentally conscious use of recyclable materials, the **Recycling Technology Guidelines for Harbor and Airport Construction and Maintenance (Revision)**¹⁾ can be used as a reference.

Disposing of construction and industrial by-products into the sea as waste (including the areas to be landfilled) shall be subjected to the standards for harmful substances, stipulated in the **Marine Pollution Prevention Act** and the **Waste Management Act**. Although the disposal of such by-products into the sea for their effective use shall not be subjected to the **Marine Pollution Prevention Act** and the **Waste Management Act**, the provisions in the **Reference 2)** can be used as references.

Also, the **References 3) to 6)** can be used as references on the required quality for recyclable materials described in this section to ensure environmental safety. As the precautions to ensure the environmental safety in terms of setting monitoring target values, such as pH during construction, the **References 7) and 8)** can also be used as references although they are not standards established exclusively for recyclable materials.

- (7) Some recyclable materials have relatively large fluctuations in their properties. Thus, it is necessary to examine whether such recyclable materials can fulfill their intended purposes by fully investigating, in advance, their physical and mechanical properties as well as availability (generation amounts).
- (8) When constructing facilities using recyclable materials, they shall be appropriately transported, stored, managed, and inspected depending on the material characteristics that are different from natural resources.
- (9) The facilities constructed using recyclable materials shall be appropriately maintained based on their material characteristics. Unlike natural resources, recyclable materials’ properties change over time. Thus, it is preferable to state the points of caution in maintenance plans to ensure proper implementation of maintenance. Also, when implementing repair, reinforcement, and improvement of these facilities, the types, quality, and quantities of recyclable materials used in these facilities shall be stated in the maintenance programs, considering the possible conditions to which recyclable materials may be exposed during the use of these facilities and recycled again as construction by-products.

- (10) When using recyclable materials exerts equivalent or superior marine environment improvement effects than using natural resources, these recyclable materials can be used to develop seaweed beds, shallow bottoms, mud flats, seabed cover, and artificial beaches.¹⁾ Examples of effective use of recyclable materials for marine environment improvement can be found in the verification tests on using recyclable materials for the foundations of marine organism habitats.^{9) to 13)} (**Reference Part I, Chapter 3, 3 Conservation and Restoration of Natural Environment**)

7.2 Slag

7.2.1 General

There are several types of slag, including iron and steel slag (blast furnace slag and steel slag), nonferrous slag (copper slag, ferronickel slag, zinc slag), and eco slag. The characteristics of respective types of slag are described below. Among them, blast furnace, electric furnace oxidized, ferronickel, copper, and eco slag have been standardized as concrete aggregate in JIS.^{1) and 14)}

7.2.2 Iron and Steel Slag

- (1) Iron and steel slag¹⁵⁾ are industrial by-products generated in large quantities from the steel industry and largely classified into blast furnace slag and steel slag. Blast furnace slag is generated from the pig iron manufacturing process (about 300 kg of slag from 1 ton of pig iron) and further classified into air-cooled blast furnace slag, produced through slow cooling by ambient air and spray of water, and granulated blast furnace slag, produced through quenching treatment with jets of pressurized water. Steel slag is generated from the process of manufacturing steel from pig iron and further classified into converter slag and electric furnace slag, depending on the types of steel furnaces (about 130 kg of slag from 1 ton of crude steel). For chemical compositions, physical properties, and use methods of iron and steel slag, the **Recycling Technology Guidelines for Harbor and Airport Construction and Maintenance (Revision)**¹⁾ can be used as a reference.
- (2) Air-cooled blast furnace slag is a granular material and has been used as road construction material.
- (3) Granulated blast furnace slag is a lightweight sandy material and has been used as a raw material of Portland blast furnace cement, a backfill material of port facilities and infill of sand compaction piles, taking advantage of its lightweight property. When using granulated blast furnace slag in port development works, the **Technical Manual for Granulated Blast Furnace Slag Utilization in Harbor and Airport Construction and Maintenance**¹⁶⁾ can be used as a reference. Also, when using granular blast furnace slag as a backfill material, reference shall be made to **Part III, Chapter 2, 5.7 Granulated Blast Furnace Slag Replacement Method**.
- (4) Steel slag is a granular material with larger particle density than sand and favorable grain size distribution. Steel slag undergoes swelling and disintegration when one of its components, free lime, reacts with water. Therefore, steel slag is normally used after being stabilized through an aging treatment with steam. In addition to the usage examples of steel slag as material for road construction and ground improvement, there are cases of using steel slag as material for sand compaction piles, taking advantage of the properties of steel slag with large shear resistance angles.¹⁷⁾ It has been known that, aside from the aging treatment, mixing steel slag with coal ash can be an efficient stabilization method to prevent steel slag from undergoing swelling and disintegration, and such steel slag has been used as concrete aggregate in the construction at Kashima Port.^{15) and 18)} In recent years, a method for using steel slag by mixing it with dredged soil (see **Part II, Chapter 11, 7.6 Dredged Soil**) has been developed. When using steel slag in port construction, the **Technical Manual for Steel Slag Utilization in Harbor and Airport Construction and Maintenance**²⁾ can be used as a reference.
- (5) There have been recent cases of using solidified steel slag through hydration as a civil engineering material of port structures, such as deformed blocks and foot protection blocks. For the details of such cases, the **Technical Manual for Utilizing Solidified Steel Slag through Hydration**¹⁹⁾ can be used as a reference.

7.2.3 Nonferrous Slag

Nonferrous slag is a material produced by solidifying molten slag, produced as by-products from the smelting process of metal materials other than iron (copper, ferronickel, and zinc in this section), through slow cooling or quenching with air or water. For nonferrous slag details, the **Recycling Technology Guidelines for Harbor and Airport Construction and Maintenance (Revision)**¹⁾ and the **Technical Manual for Nonferrous Slag Utilization in Harbor and Airport Construction**⁴⁾ can be used as references.

(1) Copper Slag

Copper slag is a sandy material produced by quenching molten slag with water, as is the case of granular blast furnace slag in a copper smelting process. Copper slag has larger grain density than sand and no hydraulic-setting properties. Although copper slag is likely to undergo grain crushing, it has a shear strength angle and permeability equivalent to sea sand. There have been the performance records of using copper slag as concrete aggregate, infill of caissons, and ground improvement material (such as sand compaction pile method).

(2) Ferronickel slag

Ferronickel slag is a material produced when manufacturing ferronickel, which is a raw material of stainless steel. Ferronickel slag has larger grain density than sand with no hydraulic-setting properties. Performance records exist on the use of ferronickel slag as concrete aggregate, infill of caissons, ground improvement material (such as sand compaction pile method), landfill material, and road paving material.

(3) Zinc slag

Zinc slag is a sandy material produced by quenching molten slag, in which iron and silica contents in a raw material are bound together with high pressure water in a zinc smelting process. Zinc slag has large density and almost no hydraulic-setting properties. There have been performance records of using zinc slag as infill of caissons.

7.2.4 Eco Slag

Eco slag is produced by solidifying molten slag into glassy or crystalline substances in a manner that cools molten inorganic substances and ash that remained after incinerating organic substances contained mainly in general waste (municipal solid waste) and sewage sludge at temperatures of 1200°C or higher. For the chemical compositions, physical properties and use methods of eco slag, the **Recycling Technology Guidelines for Harbor and Airport Construction and Maintenance (Revision)**¹⁾ can be used as a reference.

The use of solidified eco slag in port construction has been examined.²⁰⁾ Eco slag has undergone proper quality control and storage throughout its production process and, therefore, satisfies the standards for elution and contained amounts of harmful substances, specified by related notifications, when it is actually used. The type of eco slag produced by quenching molten slag with water is sandy grains and can be used as materials for concrete, ground improvement (sand compaction pile method), backfilling, infilling, and paving.¹⁾

7.3 Coal ash

- (1) Coal ash is generated when burning pulverized coal at coal-fired power plants. The properties of coal ash vary depending on the types of coal and combustion methods of boilers.
- (2) Coal ash is largely classified into fly ash and clinker ash, depending on the generation sites. Fly ash is collected from combustion gas of boilers through dust collectors. Clinker ash is produced by crushing coal ash welded at the bottoms of boilers.
- (3) Fly ash has grain size distribution similar to silt and pozzolanic activity, which is a hydraulic-setting property. Clinker ash has grain size distribution similar to sand, and its permeability also equivalent to sand. Both fly ash and clinker ash are characterized by their grain density, which is lower than sand.
- (4) Fly ash has been widely used as a raw material of cement and a mixture material of concrete. Also, it has been used as backfill, earth fill, and base course materials to take advantage of its lightweight and hydraulic-setting properties. In addition, there are cases of using fly ash as a ground improvement material in the deep mixing soil stabilization and surface stabilization of soft ground. In these cases, fly ash is normally used as a constituent material mixed with cement, water, and soil to produce solidified and crushed materials, solidified and granulated materials, slurry materials, coal ash plastic materials. For the properties of fly ash and respective coal ash mixing materials and their use methods, the **Recycling Technology Guidelines for Harbor and Airport Construction and Maintenance (Revision)**¹⁾ and the **Guidelines for Utilizing Coal Ash Mixing Materials in Harbor Construction**.³⁾ can be used as references.
- (5) Clinker ash, which is lightweight and permeable, has been used as materials for backfill and earth fill. It can also be used as a lower base course material for which performance equivalent to sand is required in road pavement work. For the properties and use methods of clinker ash, the **Recycling Technology Guidelines for Harbor and Airport Construction and Maintenance (Revision)**¹⁾ can be used as a reference.

7.4 Concrete Mass

- (1) Concrete mass is generated through concrete structure demolition. The iron materials, such as steel bars, are generally removed from concrete mass. **Table 7.4.1** summarizes main use forms of concrete mass. In the table, the utilization forms listed closer to the top require less energy for demolishing and recycling concrete mass.

Table 7.4.1 Utilization Forms of Concrete Mass

Utilization form		Typical application
As it is		Fish bed, paving stone
Block form of 20 to 40 cm		Stone material such as rubble
Crushed form	Coarse rubble	Stone material such as base course and backfill
	Coarse aggregate	Recycled coarse aggregate and base course material
	Fine aggregate	Recycled fine aggregate
Powder generated through demolition process		Ground improvement material, fillers

- (2) Concrete mass has been used mainly as a base course material for paving.²¹⁾ In addition, concrete mass has started to be used as a concrete aggregate substitute because of the increasing difficulty in getting good quality concrete aggregate.
- (3) The provisional concrete standards of recycled concrete mass to be used as aggregate for concrete, base course materials, and infill as well as backfill materials are specified in the **Provisional Quality Standards by Use for Recycling of Concrete By-products (Draft)** (Notification No. 88 of the Ministry of Construction on April 11, 1994). Recycled aggregate for concrete is subjected to the attachment of mortar, derived from concrete structures before demolition, and the quality of recycled aggregate, such as absorption and soundness, which varies depending on the degrees of such mortar adhesion and thereby largely affecting concrete properties. Recycled aggregate for concrete with high quality has been standardized in JIS (**JIS A 5021 Recycled aggregate for concrete-Class H**).¹⁾ In contrast, with respect to recycled aggregate for concrete with medium and low quality, JIS specifies the concrete quality using such aggregate (**JIS A 5022 Recycled aggregate concrete-Class M** and **JIS A 5023 Recycled concrete using recycled aggregate Class L**).¹⁾ Also, There have been studies on concrete performance using recycled aggregate under marine environments.^{22) and 23)}
- (4) It is difficult to show standard values of the material constants, such as angles of shear resistance, when the concrete mass is used as an earth and stone material because such values vary depending on the concrete mass to be generated. However, material constants can be set with reference to the **Reference 24)**, provided that the performance of concrete before demolition is equivalent to that shown in the reference.

7.5 Asphalt Concrete Mass

- (1) Asphalt concrete mass is asphalt debris generated when removing or scraping pavement. Many technical guides^{25) to 27)} have already been established for recycling asphalt concrete mass, promoting relatively wide use of recycled asphalt concrete mass. It has been used mainly in the field of pavement, and its use applications are roughly twofold: aggregate of asphalt pavement, such as surface base layers and stabilized base courses; and a granular base course material, such as recycled crusher-run and size controlled crush stone.
- (2) The asphalt concrete mass properties vary because it is collected from different construction sites in many cases.²¹⁾ Thus, variations of the quality of recycled asphalt mixtures are larger compared to new ones. It is necessary to prevent foreign matters from getting mixed in with recycled asphalt mixtures while being transported and stored.
- (3) Because aging causes asphalt to get harder, new asphalt and admixtures for recycled asphalt are generally added so that recycled asphalt can satisfy required needle penetration rates.
- (4) When using asphalt concrete mass for pavement, it is necessary to confirm that the asphalt concrete mass quality satisfies related standards which are listed in the **Recycling Technology Guidelines for Harbor and Airport Construction and Maintenance (Revision)**.¹⁾

- (5) When the recycled asphalt mixtures to be used as surface and base layers satisfy the requirements in related standards, they are considered to have the quality equivalent to the asphalt mixtures manufactured only with new raw materials. However, when problems associated with the use of facilities using recycle asphalt mixtures are identified in the past performance records and damage history, it is necessary to examine whether such recycled asphalt mixtures have equivalent quality to new ones through laboratory tests or test pavement. The wheel tracking test is one of the laboratory tests for examining fluidity and peeling resistance of asphalt.
- (6) Recycled asphalt concrete mass is considered available for a subgrade earth fill material. However, because sufficient information on applicable technologies has not been accumulated, it is necessary to confirm whether recycled asphalt concrete mass satisfies required performance, through laboratory tests and test construction, as needed.

7.6 Dredged Soil

- (1) Dredged soil has conventionally been used as a landfill material or disposed of at waste disposal sites in port areas in case no available landfill area is under construction at the time of dredging. In the port and offshore airport development, however, huge amounts of soil (ground materials) have been used constantly for backfilling quaywalls and revetments, filling reclamation land, improving soft ground, and developing shallow bottoms and mud flats (**Part III, Chapter 11, 3.6 Conservation of Natural Environment**), and sand covers (**Reference (Part I), Chapter 3, 3 Conservation and Restoration of Natural Environment**). Thus, increasing the percentage of dredged soil in the ground materials can be an extremely effective means of extending the service life of waste disposal sites and reducing construction costs.
- (2) Using sandy dredged soil as a landfill or backfill material causes filled ground to be statically stable but to undergo liquefaction easily when earthquake ground motions are applied to it, thereby requiring some sort of liquefaction countermeasures to be taken. Also, using cohesive dredged soil as a landfill or backfill material causes filled ground to be extremely soft with a high water content, thereby requiring ground improvement after the filling operation. One ground improvement method which has been used frequently in such cases is surface layer solidification followed by the installation of vertical drains to enhance consolidation.
- (3) In recent years, a method has been developed to solidify dredged cohesive soil and use it as a landfill or backfill material, and such a method has been implemented in a manner that uses a dedicated vessel where dredged soil is subjected to solidification before being used for landfill; solidifies dredged soil in a sand carrier, with a solidifier mixed with it, during the transport to a landfill site; and solidifies dredged soil in-situ with a solidifier mixed with it. In addition to cement-based solidified soil, converter steel slag-based solidified soil has been put into practical use. However, because the shear strength of solidified soil significantly varies depending on the additive amounts of solidifiers and the properties of dredged soil, it is necessary to solidify dredged soil appropriately, in accordance with intended use and use environments. For the details of converter steel slag-based solidified soil, reference can be made to the **Technical Manual for Calcia Modified Soil Utilization in Harbor, Airport and Coastal Construction**.²⁸⁾
- (4) The pneumatic flow mixing method is one of the solidification methods developed to implement a landfill economically and efficiently using dredged soil. The method enables transportation and kneading of dredged soil to be executed concurrently in a manner that injects solidifiers into pipes where dredged soil is pneumatically transported. It enhances the performance of a mixing device with the kneading effect of plug flows generated in the pipes when dredged soil is pneumatically transported in them. Many methods have been proposed for mixing dredged soil and solidifiers, including those which: make dredged soil and solidifiers pass through line mixers; add and mix powder solidifiers to and with dredged soil; make dredged soil with solidifiers preliminarily added to it pass through plural bent pipes to enhance a kneading effect; and directly inject slurry solidifier into the flows of cohesive dredged soil passing through transport pipes with plural solidifier slurry injection pipes arranged in them.
- (5) The lightweight treated soil method produces a lightweight landfill material, using dredged soil in a manner that slurries dredged soil by adjusting the moisture content to a liquid limit or higher and mixes it with a cement-based solidifier and a weight saving material, such as bubbles or expanded beads. The lightweight treated soil method has the following characteristics.
 - ① The method can effectively use dredged soil and develop stable ground, even undersea.
 - ② The method can adjust unit weight of soil to 10 to 12 kN/m³ to alleviate consolidation settlement of foundation ground, reduce earth pressure, and prevent soil from floating due to buoyancy.

- ③ The method can adjust unconfined compressive strength of soil to 200 to 600 kN/m² equivalent to hard cohesive soil.

Although the lightweight treated soil method's cost largely fluctuates depending on construction sizes, there has been a steady increase in the number of application cases since the first application to the earthquake disaster restoration works in Kobe Port. Other application cases include a large scale implementation at the upper sections of the shield tunnel under the apron of the international terminal and at the joint section of D runway in Haneda International Airport.

There is another method, which produces landfill material by dehydrating dredged soil with a dehydration plant, and has been applied, in a large scale, to the embankment material, raising the elevation of the offshore soil disposal site off Shin Moji Port.

7.7 Shells

7.7.1 General

Among shells, crushed oyster and scallop shells have been used as construction materials.

7.7.2 Oyster Shells

- (1) Oyster harvesting areas inevitably produce oyster shells in large quantities. Conventionally, they have been used mainly as cattle feed and fertilizers but, recently, there have been studies on using oyster shells as ground improvement materials (sand compaction pile method), developing shallow bottoms and mud flats, as well as sand covers.¹⁾
- (2) The characteristics of crushed oyster shells generally include: the angles of shear resistance equivalent to sand; specific gravity and density larger than sand; permeability larger than sand; CBR equivalent to sand; compaction property larger than sand; and grain size distribution equivalent to sand.^{29) to 31)}

7.7.3 Scallop Shells

- (1) There have been studies on the use of scallop shells, which are produced after scallops are subjected to external cleaning, boiling and shelling, as fine aggregate for concrete provided that they are appropriately crushed,^{32) to 34)} and ground improvement (sand compaction pile and sand drain methods) and road paving materials.
- (2) The characteristics of crushed scallop shells generally include: the angles of shear resistance equivalent to sand; specific gravity and density larger than sand; permeability larger than sand; compaction property larger than sand; and grain size distribution equivalent to sand.

[References]

- 1) MLIT: Recycling Technology Guidelines for Harbor and Airport Construction and Maintenance (Revision), 2018
- 2) Coastal Development Institute of Technology (CDIT), Technical Manual of steel manufacture slag for construction of port, airport and coast, 2015
- 3) Japan Coal Energy Center (JCOAL): Guidelines of the coal ash mix material for port construction, 2011
- 4) Coastal Development Institute of Technology: Technical Manual for Non-ferrous Slag Utilization in Port and airport construction, 2015.
- 5) Takahashi, K.: Utilization of Fly Ash and Steel Slug, Technical Note of PHRI, Technical Note of PHRI
- 6) Ministry of the Environment: Environmental Quality Standards for Water Pollution, 1971.12.28
- 7) Japan Fisheries Resource Conservation Association (JFRCA): Standard of fisheries water, 2012
- 8) MLIT: Technical Guideline of Dredged material as a resource for marine drop and utilization (Revision), 2013.7
- 9) PIANC: Biological Assessment Guidance for Dredged Material, PIANC EnviCom, Report of WG8, 56p., 2006.
- 10) PIANC: Dredged material as a resource, options and constraints, PIANC EnviCom, Report of WG14, 54p., 2009.

- 11) Furukawa, K.: Objectives for Conservation, Restoration and Creation of coastal environments and Recent Situation of Coastal Environment Management Methods, Japanese Association for Coastal Zone Studies, Vol. 20, No. 1, pp. 4-11, 2007.
- 12) Tsuruya, K., Nakagawa, M., Kiso, E. and Furukawa, K.: Water Tank Experiment on Applicability of Steelmaking Slag to Tidal Flat Materials, Proceedings of Coastal Engineering, JSCE, Vol. 52, pp. 986-990, 2005.
- 13) Waterfront Vitalization and Environment Research Center: Water Environment Improvement Technology in Closed Sea Area, Verification Test Result Report, 121p, 2010.
- 14) Kawabata, Y., Iwanami, M. and Kato, E.: Properties of Concrete with High Volume Slag Fine Aggregate, Technical Note of PARI, No.1232, 2011.
- 15) Nippon Slag Association: Characteristics and versatility of slag, 1996
- 16) Coastal development institute of technology: Technical manual for granulated blast furnace slag utilization in port and airport construction.2007. (in Japanese)
- 17) Matsuda, H., Nakagawa, M. and Shinozaki, H.:Effective use of construction and industrial by-products in geotechnical engineering, 9. Steel slag.JGS magazine (Tsuchi-to-Kiso), Vol.53, No.9, pp.40-47, 2005. (in Japanese)
- 18) Muraoka, T.: Report of test construction of Cellular type sea wall utilizing steel manufacture slag, Civil Engineering data, Vol. 51, No. 7, 1996
- 19) Coastal Development Institute of Technology: Technical Manual for iron slug hydration hardener (enlarged Edition), 200,
- 20) Coastal Development Institute of Technology: Handbook of utilization of Eco-Slug for port construction work, CDIT, 2006
- 21) Yokota, H. and S. Nakajima: Applicability of Recyclable Materials to Port and Harbour Construction, Technical Note of PHRI No.824,1996
- 22) Itou, M., T. Fukude, T. Yamaji and J. Tanaka: A Study on Applicability of Recycled Concrete to Marine Structures Vol. 37, No. 4, 1998
- 23) Hayakawa, K., Yamaji, T. and Hamada, H.: A Study on Durability of Recycled Concrete under Marine Environment, Rept. of PHRI Vol. 39, No. 2, 2000.
- 24) Mizukami, J., Y. Kikuchi and H. Yoshino: Characteristics of concrete debris as rubble in marine construction, Technical Note of PHRI No.906, 1998
- 25) Japan Road Association: Guidelines for Design and Construction of Pavement, 2006 (in Japanese)
- 26) Japan Road Association: Technical Guidelines for Road Surface Recycling Method (Draft), 1988 (in Japanese)
- 27) Japan Road Association: Technical Guidelines for Road Construction Method Using Recycled Basecourse (Draft), 1987 (in Japanese)
- 28) Coastal Development Institute of Technology: Technical Manual for the Use of Calcia Reformed Soil in Ports, Airports and Coasts, 2017 (in Japanese)
- 29) Hashidate, Y., Fukuda, S., Okumura, T. and Kobayashi, M.: Engineering Properties of Oister Shell-Sand Mixtures, 28th Proceedings of the Japan National Conference on Soil Mechanics and Foundation Engineering, pp.869-872, 1993.
- 30) Hashidate, Y., Fukuda, S., Okumura, T. and Kobayashi, M.: Engineering Properties of Oyster Shell-Sand Mixtures and Their Application to Sand Compaction Piles, 29th Proceedings of the Japan National Conference on Soil Mechanics and Foundation Engineering, pp.717-720, 1994.
- 31) Nishizuka, N.: Utilization of Oyster Shell in SCP Method, 11th Summary of Port Technical Report, pp.149-164, 1994.
- 32) Sendai Research and Engineering Office for Port and Airport, Tohoku Regional Development Bureau, MLIT: Application Guideline of Shell Concrete for Port Structure (draft), 2009.
- 33) Yamauchi, T., Kiyomiya, O., Takahashi, H. and Yamaji, T.: The Durability and the Proof Examination of the Concrete that Uses Scallop Shell as Fine Aggregate, Proceedings of the Japan Concrete Institute, Vol.30, No.2, pp.469-474, 2008.

- 34) Kiyomiya, O., Yamauchi, T. and Yokota, S.: Mechanical Properties of Concrete using Crushed Scallops, Proceedings of the Japan Concrete Institute, Vol.30, No.2, pp.475-480, 2008.h

8 Other Materials

8.1 Metal Materials other than Steel Product

- (1) When using metal materials other than steel (carbon steel) products, most suitable materials shall be selected taking into consideration use locations, purposes, environmental conditions, durability, and economic efficiency.
- (2) The metal materials other than steel (carbon steel) products used for the facilities subjected to the technical standards include stainless steel, aluminium, and titanium. The metal materials to be used for port facilities shall have quality necessary to achieve required performance of these facilities. The Japan Industrial Standards (JIS) are the typical examples of these metal materials satisfy such conditions.

① Stainless steel

Table 8.1.1 shows the types of stainless steel products, among those complying with JIS, generally used in civil engineering facilities.¹⁾ Stainless steel has been used mostly for corrosion prevention, but the corrosion resistance of stainless steel under marine environments significantly varies depending on the types of stainless steel. Thus, it is preferable to select appropriate types of stainless steel with reference to test results and past performance records. Additionally, when designing and constructing stainless steel structures, reference can be made to the **Guideline for the Design and Construction of Stainless Steel Civil Engineering Structures (Draft)**.¹⁾

The examples of stainless steel used in large quantity for facilities under marine environments include SUS 312L with high corrosion resistance in seawater used as the coating material for the jacket section of D runway in Haneda International Airport;²⁾ and SUS 304 N2, SUS 323L and SUS 821 L1 used for water gate facilities.

Recently, stainless steel has been used as concrete reinforcing bars (refer to **Part II, Chapter 11, 3.1 Concrete Materials**).

Table 8.1.1 Quality Standards for Stainless Steel Products¹⁾

Standard		Symbol	Application
JIS G 4303	Stainless steel bars	SUS304 (L), SUS316 (L), SUS304N2	General steel members
JIS G 4304	Hot-rolled stainless steel plate, sheet and strip	SUS304 (L), SUS316 (L), SUS821L1, SUS323L	General steel members
		SUS312L	Anticorrosion coating of steel structures
JIS G 4305	Cold-rolled stainless steel plate, sheet and strip	SUS304 (L), SUS316 (L), SUS821L1, SUS323L	General steel members
		SUS312L	Anticorrosion coating of steel structures
JIS G 4309	Stainless steel wires	SUS304 (L), SUS316 (L)	Ropes
JIS G 4317	Hot-formed stainless steel sections	SUS304 (L), SUS316 (L)	General steel members
JIS G 4321	Stainless steel for building structure	SUS304A, SUS316A, SUS304N2A	General steel members
JIS G 4322	Stainless steel bars for concrete reinforcement	SUS410-SD, SUS304-SD	Concrete reinforcing bars
JIS B 1054	Mechanical properties of corrosion-resistant stainless steel fasteners	A2-50 (equivalent to SUS304), A4-50 (equivalent to SUS316)	Fastener components (bolts)

② Aluminium

Aluminium and aluminium alloys have advantages in that they are light, with density of 2.65 to 2.80 kg/m³; high in corrosion and weather resistance; capable of being produced with strength and surface membranes depending on intended use; and excellent in workability. **Table 8.1.2** shows the types of aluminium materials, among those complying with JIS, generally used in civil engineering facilities. The examples of the facilities for which aluminium materials are used include water gates,³⁾ and ⁴⁾ land locks, tide gates, vehicle protection fences, intrusion prevention fences, lighting towers, inspection passages, guard rails, and bridge railings.

Also, aluminium alloys have been widely used as the anodes of the cathodic protection method by galvanic anodes (refer to **Part II, Chapter 11, 2 Steel Products**).

Table 8.1.2 Quality Standards for Aluminum Materials

Standard		Symbol	Application
JIS H 4000	Aluminum and aluminum alloy sheets, strips and plates	A5052P, A5083P, A3004P	Water gates, land locks, tide gates, lighting towers and roofs of facilities
JIS H 4100	Aluminum and aluminum alloy extruded shape	A5083S, A5052S, A6061S, A6063S, A6N01S	Water gates, land locks, tide gates, vehicle protection fences, bridge railings, intrusion protection fences, lighting towers, inspection passages and roofs of facilities
JIS H 8602	Combined coatings of anodic oxide and organic coatings on aluminum and aluminum alloys	A1, A2	Surface coating of aluminum and aluminum alloys

③ Titanium

Titanium has large strength-mass ratios. That is, titanium is strong (tensile strength of 350 to 520 N/mm²) for its weight (density of about 4.5 kg/m³). Titanium also has a high ability to bind oxygen and is easily passivated with an oxide layer (TiO₂) with a thickness of about a few dozen angstroms formed on its surface. Thus, titanium barely corrodes and shows extremely high resistance against pitting and crevice corrosion even undersea. Taking advantage of these properties, titanium has been used as material to prevent steel products from corrosion. **Table 8.1.3** shows the types of titanium materials, among those complying with JIS, used relatively frequently for port facilities. The examples of materials using titanium include titanium clad steel and protection covers for petrolatum coating.

Also, there are cases of using titanium meshes or grids as anode materials of the impressed current method as cathodic protection method to steel bars of reinforced concrete taking advantage of the fact that such anodes can stably function without undergoing material deterioration even after applying anode current to them for a long period of time.

Table 8.1.3 Quality Standards of Titanium Materials

Standard		Symbol	Application
JIS H 4600	Titanium and titanium alloys-sheets, plates and strips	TP270C	Titanium clad, protection covers for petrolatum coating
JIS H 4650	Titanium and titanium alloys-bars		

8.2 Fiber Reinforced Materials

The typical fiber reinforced materials are: 1) continuous-fiber reinforced materials using continuous fibers; and 2) short-fiber reinforced materials using short fibers mixed in cement-based materials. The raw materials frequently used for continuous-fiber reinforced materials are carbon, glass, and aramid fibers. The same raw materials are also used for producing for short-fiber reinforced materials but there are cases of using steel fibers instead of them.

(1) Continuous-fiber reinforced materials

Continuous-fiber reinforced materials have been used as steel bars and PC steel products for concrete taking advantage of their characteristics to be highly resistant against corrosion (refer to **Part II, Chapter 11, 3.1 Concrete Materials**).

Also, there are cases of using continuous-fiber reinforced materials as structural members. For example, FRP (Fiber Reinforced Plastic) is used for the scaffolds of inspecting facilities. When design and constructing structures using FRP, reference can be made to the **Standard Specifications for Hybrid Structures, Design**⁵⁾ and the **Standard Specifications for Hybrid Structures, Construction**.⁶⁾ There are cases of using FRP plates as embedded formwork for concrete and FRP sheets as reinforced materials of beam members and floor slabs.

(2) Short-fiber reinforced materials

Short-fiber reinforced materials are generally mixed in cement-based materials which are called fiber reinforced concrete. The characteristics of fiber reinforced concrete include high resistance against cracks and high ductility.⁷⁾

^{to 11)} When designing and constructing fiber reinforced concrete, reference can be made to the **Design Guidelines**

for Steel Fiber Reinforced Concrete Column Members (Draft)¹²⁾ and the Design and Construction Guidelines for Ultrahigh Strength Steel Fiber Reinforced Concrete (Draft).¹³⁾

8.3 Plastic and Rubber

- (1) When using plastic and rubber, appropriate types shall be selected taking into consideration the sections where plastic and rubber are used, intended use, environmental conditions, durability, and economic efficiency.
- (2) The followings are examples of the use of plastic and rubber products in port construction.^{14 and 15)}

① Geo-synthetics

The term geo-synthetics collectively denotes geo-textiles (permeable polymer sheet products) and geo-membranes which are the products having impermeable membrane-like structures. Geo-synthetics comprise geo-textiles, geo-membranes and geo-composites.

Geo-synthetics are largely separated into permeable and impermeable ones. The characteristic of respective geo-synthetics are as follows.¹⁶⁾

(a) Permeable geo-synthetics

Geo-woven is a woven cloth made of polyester in general and has textures of warp and weft threads perpendicular to each other.

Geo-nonwoven has a textile structure manufactured not by weaving but by making fibers adhere to or interlock with each other or both through mechanical or chemical means or other means using solvent media.

- 1) Long fiber: a material, represented by spunbond, which is made of extremely long fibers. It has a relatively thin thickness of 10 mm or less in general and the thickness cannot be adjusted easily.
- 2) Short fiber: a material, represented by felt, which is made of short fibers with lengths of 3 to 5 cm. It has a thickness of 10 mm or more and the thickness can be adjusted easily.

(b) Impermeable geo-synthetics

Impermeable geo-synthetics are represented by impermeable plates having impermeable membrane structures with soft vinyl chloride applied to woven cloth.

Also, the followings are the examples of applications of geo-synthetics in port construction

(a) Earth fill reinforcement countermeasure

When spreading quality soil over the ground filled with dredged cohesive soil, geo-synthetic sheets or nets are directly laid on the surfaces of the ground so as to construct a quality soil layer necessary to allow heavy equipment to travel on it while preventing the quality soil from sinking.¹⁷⁾ In the recent construction of earth fill on soft landfill areas, there have been many cases of using geo-synthetic nets.¹⁸⁾

(b) Sand washing-out and scouring prevention

When geo-synthetics are used as filter materials to prevent sand washing-out, sand invasion prevention geo-synthetic cloth is generally laid at the back of backfill stone or rubble mounds of quaywalls and on the entire bottom faces or a portion of the sections at the sea side of rubble mounds. Such sand invasion prevention geo-synthetic cloth is also used as a countermeasure to prevent scouring due to waves. For the details of sand washing-out and scouring prevention, reference can be made to **Part II, Chapter 2, 7.5 Sand Washing-out and Scouring**.

② Joint materials

The geo-synthetics used for construction joints of concrete structures include seal plates, joint plates, and joint-sealing materials. Seal plates are mostly made of vinyl chloride resin for which required quality has been standardized in **JIS K 6734 Plastics—Unplasticized poly (vinyl chloride) sheets**. Joint plates are mostly made of plastic foam such as vinyl chloride polyethylene, polyethylene. Joint-sealing materials are mostly elastic sealing compounds made of polysulfide, silicon, butyl rubber, or chloroprene rubber.

③ Fenders

The materials used for fenders are generally natural rubber or diene series synthetic rubber such as styrene-butadiene rubber. Rubber fenders shall be subjected to physical, static compression, and durability tests because

they need to deliver such physical performance as aging and ozone resistance, compression performance with respect to energy absorption and reaction force, and durability performance with respect to cyclic loads.¹⁹⁾ For the methods of these tests, reference shall be made to **Reference (Part II), Chapter 1, 5.7 Fenders**. The fenders to be selected in the performance verification shall be those which have ability to absorb berthing energy of ships when they come alongside berths. In selecting fenders, it shall be noted that the energy absorption performance of fenders is largely affected by their constituent materials and shapes. For the performance verification of fenders, **Part III, Chapter 5, 9.2 Fender Systems** can be used as a reference. When determining whether or not to replace (renew) rubber fenders through the evaluation of the degrees of aging degradation and damage in the course of maintaining rubber fenders, reference can be made to the **Guidelines for the Maintenance of Rubber Fenders (Revision)**.²⁰⁾

④ Seal Materials

Seal materials are used for the joints of sand discharge pipes and seal rubber gaskets of immersed tunnel elements.

⑤ Adhesives

There are adhesives made of several types of synthetic resin which have been used for joining bridge members or precast concrete slabs and repairing cracks on concrete.

⑥ Drain materials

There are two types of drain materials: one has a composite of a core made of especially hard core and a nonwoven filter; and the other has a porous unitary structure made of specially-treated polyvinyl chloride.²¹⁾

⑦ Joints and bearings

In bridges, rubber expansion joints, and single-layer or multi-layer rubber pad bearings have been used.

⑧ Ancillary facilities

FRP has also been used for floating facilities such as buoys and pontoons. FRP and rubber have been used for some types of ladders, handrails, and curb.

⑨ Expanded polystyrene

Taking advantage of its lightweight property, expanded polystyrene has been used as floats of buoys and pontoons; a part of civil engineering structures; civil engineering materials such as EPS blocks and expanded plastic beads. EPS blocks have been used as the countermeasures to reduce earth pressure, prevent settlement of earth fill constructed on soft ground, prevent ground surface from producing level differences, and facilitate foundation construction of temporary roads. Expanded plastic beads have been used as a material to produce lightweight backfill materials in a manner that mixes local soil with a solidifier such as cement so as to reduce settlement and earth pressure.²²⁾

- (3) The followings are the description of sand invasion prevention cloth and plates as well as rubber mats generally used in port facilities.

① Sand invasion prevention cloth

The types of cloth used for sand invasion prevention cloth preventing soil from mixing into backfill materials are plain-woven, multi-ply woven, high strength multi-ply woven, high elongation multi-ply woven, short fiber nonwoven, and long fiber nonwoven fabrics. When determining the types of cloth, it is preferable to give appropriate consideration to construction conditions including waves transmitting through mounds during construction, waves and winds in landfill areas, wearing due to the effect of ultraviolet rays, degradation, backfilling methods, residual water levels, the accuracy of the leveling work of backfill, and waves transmitting through mounds after construction. When laying sand invasion prevention cloth, it is necessary to ensure that neighboring sheets of cloth are arranged with enough allowance and sewn together with materials having strength and elasticity so as not to leave any gaps. The strength and elasticity of sewn sections between neighboring sheets of cloth shall be close to that of the cloth itself in both longitudinal and lateral directions. For the purpose of preventing sand invasion prevention cloth from floating and being worn by backfill stone, it is preferable to take preventive measures in a manner that puts sandbags, installs anchoring chains, and lays wire meshes over the cloth immediately after the laying of the cloth. In taking such preventive measures, it is also preferable to pay particular attention to ensure that the cloth is sufficiently covered without floatation at the

edges of the preventive counter measures where the cloth is vulnerable to wearing. For the pressure due to wave transmitting through mounds, **Part II, Chapter 2, 6 Wave Force** can be used as a reference.

The types of sand invasion prevention cloth laid under rubble mounds to prevent ground soil from being washed out shall be selected in consideration of such construction conditions as wave heights, tidal currents, and the sizes of rubbles.

Table 8.3.1 shows the minimum standards which have been applied to woven and nonwoven cloth so far. It is preferable to use the products in accordance with acting external force

Table 8.3.1 (a) Minimum Standards which have been Applied to Sand Invasion Prevention Cloth (Woven Cloth)

Type	Thickness	Tensile strength	Elongation	Mass	Remarks
Nonwoven cloth	4.2 mm or greater	880 N/5cm or greater	60% or greater	500 g/m ² or greater	JIS L 1908

Note: The thickness of 4.2 mm or greater is applied for the cloth under loading of 2 kN/m² according to JIS L 1908. With no loading, the thickness should be 5 mm or greater.

Table 8.3.1 (b) Minimum Standards which have been Applied to Sand Invasion Prevention Cloth (Nonwoven Cloth)

Type	Thickness	Tensile strength	Elongation	Mass
Woven cloth	0.47 mm or greater	4,080 N/5 cm or greater	15% or greater	JIS L 1908

② Sand invasion prevention plates

Sand invasion prevention plates to be used as scour prevention countermeasures and to be installed at vertical joints of caissons are made of flexible polyvinyl chloride or rubber. In order to prevent landfill soil from being washed out through the gaps between sand invasion prevention plates and joints, sand invasion prevention plates shall be provided with backfill so as to isolate landfill soil from the plates. Also, because the spaces inside joints are subjected to wave pressure, sand invasion prevention plates are preferably determined so as to prevent the plates from damage due to waves during their service period. For the wave pressure inside joints, **Part II, Chapter 2, 6 Wave Force** can be used as a reference.

Tables 8.3.2 and **8.3.3** show the minimum standards which have been applied to sand invasion prevention plates so far. It is preferable to use the products in accordance with acting external force.

Table 8.3.2 Minimum Standards which have been Applied to Sand Invasion Prevention Plates (Case of Flexible Vinyl Chloride Plates with a Thickness of 5 mm)

Test item	Contents of tests		Standard values
	Method	Tensile direction	
Tensile strength	Compliance with JIS K 6723 Test sample No. 1 type dumbbell	Lateral	740 N/cm or greater
Tear strength	Compliance with JIS K 6252 Test sample uncut angle shape	Longitudinal	250 N or greater
Elongation	Compliance with JIS K 6723 Test sample No. 1 type dumbbell	Lateral	180% or greater
Seawater resistance Tensile strength residual ratio	Compliance with JIS K 6773	Lateral	90% or greater
Seawater resistance Elongation residual ratio	Compliance with JIS K 6773	Lateral	90% or greater
Specific gravity	Compliance with JIS K 7112	—	1.2 - 1.5

Test item	Contents of tests		Standard values
	Method	Tensile direction	
Stripping strength	Compliance with JIS K 6256 Width 25×250 mm Strip-shaped sample	Longitudinal	30 N/cm or greater

Table 8.3.3 Minimum Standards which have been Applied to Sand Invasion Prevention Plates
(Case Rubber Plates)

Test item	Contents of tests		Standard value
	Method	Tensile direction	
Tensile strength	JIS K 6404-2	—	4,400 N/3 cm or greater

③ Rubber mats

The rubber mats used for increasing friction are twofold: one made of recycled rubber, and the other made of brand-new rubber. The rubber mats having quality shown in **Tables 8.3.4** and **8.3.5** have been used in many cases.

Table 8.3.4 Quality of Recycled Rubber

Test item			Performance	Test conditions/method
Physical tests	Before aging	Tensile strength	4.9 MPa or greater	JIS K 6251
		Tear strength	18 N/mm or greater	JIS K 6252
		Hardness	55–70 graduations	JIS K 6253
		Elongation	160% or greater	JIS K 6251
	After aging	Tensile strength	3.9 MPa or greater	JIS K 6251
		Tear strength	—	Aging tests are according to JIS K 6257
		Hardness	Within ± 8 of pre-aging value	JIS K 6253 Aging temperature 70°± 1°
		Elongation	140% or greater	JIS K 6251 Aging time 96 -2^0 hours

Table 8.3.5 Quality of Brand-new Rubber

Test item			Performance	Test conditions/method
Physical tests	Before aging	Tensile strength	9.8 MPa or greater	JIS K 6251
		Tear strength	25 N/mm or greater	JIS K 6252
		Hardness	70 ± 5 graduations	JIS K 6253
		Elongation	250% or greater	JIS K 6251
	After aging	Tensile strength	9.3 MPa and above	JIS K 6251
		Tear strength	—	Aging tests are according to JIS K 6257
		Hardness	Within ± 8 of pre-aging value	JIS K 6253 Aging temperature 70°± 1°
		Elongation	200% or greater	JIS K 6251 Aging time 96 -2^0 hours
	Compressive permanent strain		45% or less	JIS K 6262 Aging temperature 70°± 1° Aging time 24 -2^0 hours

8.4 Painting Materials

(1) Painting materials shall be selected taking into consideration the following items.

- ① The purposes of painting
- ② The properties and characteristics of painted surfaces
- ③ The performance and composition of painting materials
- ④ Economic efficiency
- ⑤ Maintenance

(2) Several types of painting materials are selectively used for the purposes of preventing rust and corrosion, protecting surfaces, resisting heat, enhancing aesthetic quality, and displaying information. Depending on the materials of the surfaces to be painted, the types of painting materials are classified into those for concrete, metal, and wood. It is necessary to select the painting materials most suitable for the purpose of the painting and the materials of the surfaces to be painted.

(3) Generally, two to three types of painting materials having different properties or performance are overlaid one above the other so as to allow them to collectively exert required performance. These roles of painting materials are classified into primer coat, base coat, middle coat, and top coat. It is necessary to select appropriate combinations of painting materials depending on the roles and purposes.

(4) When using painting materials for the purpose of preventing corrosion on port steel structures, reference can be made to **2.4.3 Coating Methods in this Chapter** and the **Manual for Corrosion Protection and Repair of Port Steel Structures**.²³⁾ When using painting materials for the purpose of preventing corrosion on port concrete structures, reference can be made to the **Guidelines for the Design and Construction of Surface Protection Methods (Draft)**.²⁴⁾ and the **Manual for the Repair of Port Concrete Structures**.²⁵⁾

(5) When selecting painting materials for the bridges categorized as port transportation facilities, reference can be made to the **Handbook for Steel Road Bridge Painting**.²⁶⁾ and the **Heavy-duty Coating**.²⁷⁾ for steel bridges and the **Guidelines for Chloride-induced Corrosion Countermeasures (Draft)**.²⁸⁾ for concrete bridges.

(6) When using painting materials for the purposes other than (4) and (5) above, the literatures introduced in these sections can be used as references.

(7) There are many variations in the colors of painting materials and the color is generally determined in consideration of intended use, aesthetic performance and economic efficiency.

(8) For traffic painting, there are following types of painting materials.

① Normal temperature drying type painting materials

They are the materials which are made of alkyd, vinyl, or acrylic resin and used for simple repairs because of low durability.

② High-temperature drying type painting materials

They are the materials which are made of special synthetic resin, heated before being sprayed over surfaces to be painted, excellent in workability due to quick-drying performance, high in abrasion resistance, and particularly suitable for cold regions.

③ Deposit type painting materials

They are the materials which are applied to surfaces to be painted in a hot and melted state and subjected to cooling and solidification after application, excellent in quick-drying performance, high in durability because of the availability of thick paint layers, and particularly suitable for urban districts.

④ Adhesive sheets

They are the painting sheets which are manufactured with vinyl resin as vehicle and pasted on surfaces to be painted.

8.5 Grout Materials

8.5.1 General

- (1) Grouting methods shall be appropriately selected in accordance with construction conditions and implemented with due consideration to surrounding environments.
- (2) The grouting methods are implemented for preventing groundwater flows, enhancing ground strength, and reinforcing the members such as caisson infill by filling gaps in bedrock, ground, in and around facilities, and coarse aggregate. Several types of grouting materials are available depending on the characteristics of grouting objects.

Grout materials are classified into following types in terms of raw materials as shown in **Fig. 8.5.1.**²⁹⁾

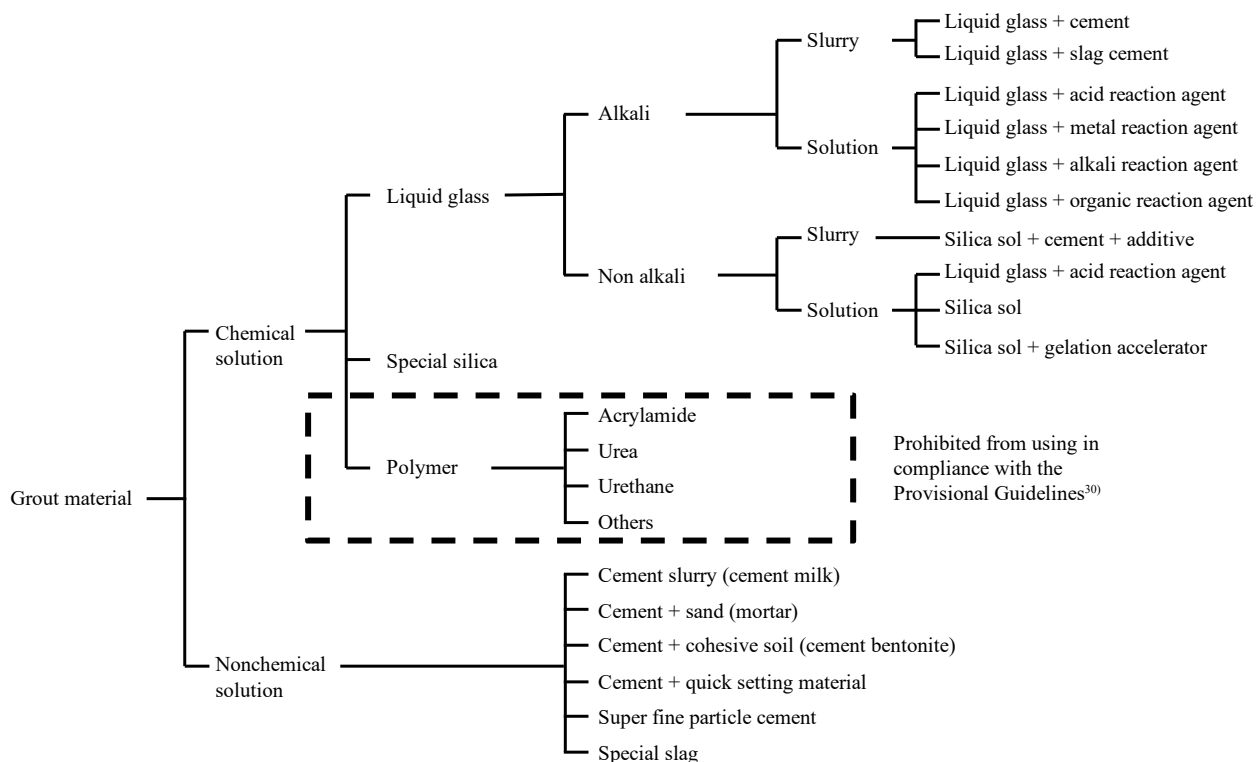


Fig. 8.5.1 Modification of Classification of Grout Materials ²⁹⁾

- (3) Because some types of grout materials are slightly toxic, it is necessary to pay particular attention to the influence of grout materials on the contamination of groundwater quality and associated human health when implementing chemical grouting methods with reference to the **Provisional Guidelines for the Implementation of Construction Works through Grouting Methods.**³⁰⁾

The essentials of the provisional guidelines are as follows.

- ① It is necessary to conduct preliminary soil, underground buried object and groundwater level surveys.
- ② The chemical solution shall be limited to liquid glass types (with silicate sodium as base resin) which do not contain deleterious substances or fluorine compounds except in the case of urgently cope with emergency during construction (the use of nonchemical solution is out of the scope of application of the provisional guidelines).
- ③ It is necessary to conduct on-site grouting tests.
- ④ It is necessary to prevent industrial accidents by paying particular attention to the safe execution of grouting operation and storage of chemicals and to take proper measures on the occurrence of abnormal situations

- ⑤ The drainage and sludge generated in drainage treatment facilities shall be treated in compliance with the standards and provisions in related laws and regulations. Also, surplus soil and remaining materials shall be disposed of in a manner that prevents the contamination of water quality and human health problems.
- ⑥ The quality of groundwater and public water shall be monitored so as to ensure that such quality is kept within the standards.

8.5.2 Properties of Grout Materials

- (1) Grout materials to be selected shall satisfy predetermined performance with respect to target ground.
- (2) The basic properties required for grout materials include permeability, filling and solidification performance, the strength of solidified materials, and water-imperviousness. Among them, the permeability largely affects the applicability of grout materials to grouting objects.

Grout materials can be classified into slurry types containing suspended components such as cement and slag and solution types containing no suspended components.^{29), 31) and 32)} In terms of gel time, grout materials are also classified into flash setting types and slow setting types. **Table 8.5.1** roughly summarizes the compatibility of the different types of chemicals with different types of object soil.³¹⁾

When comparing slurry type grout materials to solution ones, stabilized bodies by the slurry types grouting materials tend to have larger strength than those by the solution ones in the case of permeation grouting into the gaps among soil particles. In contrast, solution type grout materials have wider permeation areas of uniform stabilized bodies than slurry ones.³¹⁾ In recent years, however, there has been significant improvement in the permeability of slurry type grout materials through the advancement of atomization and the use of surface acting agents.^{33) and 34)}

Table 8.5.1 Soil and Grout Chemicals modification of 31)

Soil type	Slurry type		Solution type	
Gel time	Fast setting	Slow setting	Fast setting	Slow setting
Cohesive silt	○ (Cleave injection)	×	△ (Cleave injection)	×
Fine sand	×	△	△	○
Coarse sand	△	△	△	○
Gravel	△	○	○	△

○: Compatible, △: Compatible depending on conditions, ×: Not compatible

8.6 Waste as Landfill Materials

The disposal of waste as landfill materials is subjected to the provisions in the laws relevant to waste, i.e., the **Wastes Disposal and Public Cleansing Act** (Act No. 137 of 1970, hereinafter referred to as "**Waste Disposal Act**") and the **Act on Prevention of Marine Pollution and Maritime Disaster** (Act No. 136 of 1970, hereinafter referred to as the "**Marine Pollution Act**").

As summarized in **Table 8.6.1**, the applicability of the **Waste Disposal Act** and the **Marine Pollution Act** to the disposal of waste as landfill materials varies depending on the locations of waste generation, location of waste utilization and disposal methods.

Table 8.6.1 Applicability of the Laws Relevant to the Disposal of Waste

Location of disposal		Onshore	Sea area disposal		Ocean dumping
Disposal method		Ship or other facility than marine one	Ship or other facility than marine one	Ship or marine facility	Ship or marine facility
Location of generation	Onshore	Waste Disposal Act	Waste Disposal Act	Marine Pollution Act	Marine Pollution Act
	Offshore	Waste Disposal Act	Waste Disposal Act	Marine Pollution Act	Marine Pollution Act

Note) Marine facility means a structure constructed in the sea.

[References]

- 1) Japan Society of Steel Construction: Recommendations for Design and Construction of Civil Structure using Stainless steel (Draft), 2015.
- 2) Ishida, M., Sato, H., Sekiguchi, T., Noguchi, T. and Suzuki, N.: Haneda Airport Re-expansion Construction - Corrosion Protection for Jacket-type Steel Structure in the Piled-elevated Platform in the D-Runway -, Bousei Kanri, pp.13-19, Vol.51, No.11, 2007.
- 3) Japan Aluminium Association: Report of for Water Gate using Aluminum Alloy (Draft), 1979.
- 4) Japan Aluminium Association: Survey Report of Life Cycle Cost Calculation for Water Gate using Aluminum Alloy, 2004.
- 5) Japan Society of Civil Engineers: Standard Specifications for Hybrid Structures 2014, Design, 2015.
- 6) Japan Society of Civil Engineers: Standard Specifications for Hybrid Structures 2014, Construction, 2015.
- 7) Yokota, H., Ito, H., Iwanami, M. and Kato, E.: Structural Performance of Concrete Structures Reinforced by Short Fiber, Technical Note of PARI, No.1071, 2004.
- 8) Ito, H., Yokota, H. and Iwanami, M.: Study on Constructability of PVA Short Fiber Reinforced Concrete, Technical Note of PARI, No.1087, 2004.
- 9) Ito, H., Iwanami, M. and Yokota, H.: Evaluation on the Applicability of PVA Short Fiber Reinforced Concrete to Harbor Structures, Rept. of PARI Vol. 44, No. 3, pp. 3-37, 2005.
- 10) Iwanami, M., Shirane, Y., Yokota, H., Yamada, T. and Takehana, N.: Improvement of Impact Loading Resistance of Reinforced Concrete Members by Mixing PVA Short Fiber, Technical Note of PARI, No.1163, 2007.
- 11) Iwanami, M., Matsubayashi, T. and Kawabata, Y.: Structural Behavior of Reinforced Concrete Slabs Subjected to Repeated Impact Loads, Technical Note of PARI, No.1216, 2010.
- 12) Japan Society of Civil Engineers: Recommendations for Design and Construction of Column Member using Steel Fiber Reinforced Concrete (Draft), CL.97, 2004.
- 13) Japan Society of Civil Engineers: Recommendations for Design and Construction of Ultra High Strength Fiber Reinforced Concrete Structures (Draft), CL.113, 2004.
- 14) Japan Society of Civil Engineers: Handbook of Civil Engineering (4th edition), pp.143-146, pp.150-151, 1989.
- 15) Okada, K., S. Akashi and Materials for Civil Engineering (Revised Edition) People's Science, Kokumin-Kagaku Publishing, 1995
- 16) Industrial Technology Service Center: Compendium of reinforcing methods for slope and embankment, p174,1995
- 17) Industrial Technology Service Center: Compendium of practical measures for soft ground, pp.619-631,1993
- 18) Society of Soil Mechanics and Engineering Science, Handbook of Soil Mechanics, pp.1041-1043,1982
- 19) Ports and Harbours Bureau, MLIT: Standard Specifications for Port & Harbor Works, 2017. (in Japanese)
- 20) Coastal Development Institute of Technology: Guidelines for the Maintenance of Rubber Fender Systems (2nd Edition), CDIT Library No.2, 2019.
- 21) Kamon, M.: Plastic Board Drain Method, Foundation, Vol. 19, No.6, pp. 19-24, 1991
- 22) Kuraku, M: Characteristics of light weight embankment method and its applications, Foundation, Vol. 18 No.12,pp. 2-9,1990
- 23) Coastal Development Institute of Technology: Manual of corrosion protection and repair for port and harbour facilities (Revised Edition), 1997
- 24) Japan Society of Civil Engineers: Recommendations for Concrete Repair and Surface Protection of Concrete Structures (Draft), 2005.
- 25) Coastal Institute of Technology: Manual for Repair of Port Concrete Structures, 2018.
- 26) Japan Road Association: Handbook of Painting and corrosion protection of steel bridge, 2006
- 27) Japan Society of Steel Construction: Heavy Duty Coating, 2012.
- 28) Japan Road Association: Guideline and commentary of countermeasures against to salt damages for highway bridges (Draft), 1984

- 29) Editorial Committee of Civil Engineering of Construction Method: Civil Engineering of Construction Method 6th Edition, Industrial Research Institute Encyclopedia Publishing Center, pp.304-305
- 30) Tentative guidelines on constructions utilizing Chemical grouting method (Government Order), July 15, 1974 Safety Control Bureau, Ministry of Public Works, No.146, 1974
- 31) Japanese Geotechnical Society: Survey, Design and Construction of Ground Improvement-from individual houses to artificial island, pp.152-159, 2013 (in Japanese)
- 32) Editorial Committee of Comprehensive List of Practical Soft Ground Countermeasure Technologies: Comprehensive List of Practical Soft Ground Countermeasure Technologies for Civil and Architectural Engineers, Industrial Technology Service Center, p.808, 1993 (in Japanese)
- 33) Kumagai, K., K. Kaneko and J. Hironaka: Injection Material Using Ultrafine Slag Particles, Foundation Work, Vol.36 No.5, pp.34-36, 2008 (in Japanese)
- 34) Kanazawa, T: Ultrafine Cement Particle Effective for the Reinforcement of the Ground Difficult to be Improved through Conventional Slurry Injection Materials and for Spring Water Countermeasures, Foundation Work, Vol.43 No.10, pp.39-42, 2015 (in Japanese)

9 Friction Coefficients

- (1) Static friction coefficients can be used as the friction coefficients of materials used to calculate friction resistance against the sliding of facilities. In such a case, it is preferable to appropriately set the friction coefficients of materials in consideration of the characteristics of object facilities and materials.
- (2) The values listed in **Table 9.1.1** can generally be used as the characteristic values of static friction coefficients to be used in the performance verification of port facilities. It should be noted that the measurements of friction coefficients show large variations even when measurements are obtained through repeated tests under identical conditions. The values in **Table 9.1.1** have been conventionally used as empirically appropriate friction coefficients. For those cases which are not in the table, it is preferable to conduct tests to determine the values of friction coefficients.
- (3) The values in **Table 9.1.1** can be used only for the verification of stability of facilities with respect to sliding and cannot be used as friction coefficients in the examination of the bearing capacity of piles based on the skin friction between the outer peripheries of piles and soil; the verification of the stability of sloping breakwaters; the calculation of friction resistance when launching caissons through slip ways; and the calculation of earth pressure based on the angles of wall friction. In contrast, although the values in **Table 9.1.1** are static friction coefficients with respect to static actions, they can be used as the friction coefficients with respect to dynamic actions such as earthquake ground motions because no appropriate data on dynamic friction coefficient has been available.

Table 9.1.1 Characteristic Values of Static Friction Coefficients

Concrete and concrete	0.5
Concrete and bedrock	0.5
Underwater concrete and bedrock	0.7 to 0.8 ^{note 1)}
Concrete and rubbles	0.6
Rubbles and rubbles	0.8
Timber and timber	0.2 (wet) to 0.5 (dry)
Friction enhancement mat and rubbles	0.75

Note 1) In the case of friction between underwater concrete and bedrock, the friction coefficient can be 0.8 under standard conditions provided however that the value needs to be reduced to 0.7 depending on the severity of the brittleness or cracks of base rock or the movement of sand covering base rock.

Note 2) The friction coefficients in the performance verification of cellular blocks, reference can be made to **Part III, Chapter 5, 2.2 Gravity Type Wharves**.

- (4) For sliding and friction resistance, the **References 1) to 6)** can be used as references. Additionally, for the friction coefficients between the bottom faces of earth retaining walls (on land) and foundation ground, reference can be made to the **Guidelines for Road Earthwork, and Earth Retaining Walls**.⁷⁾

(5) Friction coefficients of friction enhancement mats

Generally, the materials for friction enhancement mats shall be selected with careful consideration to the test results of friction coefficients in addition to the durability of the materials to be used, the importance of facilities, hydrographic conditions and economic efficiency. As shown in **Table 9.1.1**, the friction coefficient of 0.75 can be used when bituminous or rubber materials are used for friction enhancement mats. In the case of cold regions, it is preferable to set friction coefficient through separate examinations. The above provisions shall not be applied to the cases of the friction coefficients to be individually verified for example through the tests on the basis of the design conditions and structural conditions of individual facilities.^{8) and 9)} For reference, the maximum friction coefficient between friction enhancement mats and rubbles is 0.8 in the past design. When using friction enhancement mats for mooring facilities, reference can be made to **Part III, Chapter 5, Mooring Facilities, 2.2.3 Performance Verification (3) ① (a)**.

(6) Friction coefficients of cast-in-place concrete

Among the values of static friction coefficients in **Table 9.1.1**, those related to concrete are considered to vary depending on whether the concrete is cast-in-place or precast. It is necessary to appropriately set the friction coefficients of cast-in-place concrete taking into consideration material properties and natural conditions.

(7) Sliding resistance between bedrock and prepacked concrete

There are cases of constructing mooring facilities or protective facilities for harbors on the seafloor through the prepacked concreted method. The resistance of these massive facilities against sliding is established as a result of complex mechanisms involving adhesion and friction resistance between bedrock and prepacked concrete and shear resistance of the bedrock and prepacked concrete due to the surface irregularity of the bedrock. In contrast, the sliding resistance of facilities is affected by the properties of base rock and the bottom sediment covering it at construction sites, the quality of injected mortar, the level of elaborate workmanship and the hydrographic conditions during construction. For convenience, after careful consideration of various aspects including the performance records of existing facilities,¹⁰⁾ the friction value for underwater concrete and bedrock in **Table 9.1.1** can be applied as the friction coefficient between bedrock and prepacked concrete. This provision can also be applied to other types of underwater concrete than prepacked concrete.

[References]

- 1) Morihira, M., T. Kihara and H. Horikawa: Friction coefficient of rubble mound of composite breakwater, Proceedings of 25th Conference on Coastal Eng., JSCE, pp.337-341, 1978 (in Japanese)
- 2) Morihira, M. and K. Adachi: Friction coefficient of rubble mound of composite breakwater (Second report), Proceedings of 26th Conference on Coastal Eng., JSCE, pp.446-450, 1979 (in Japanese)
- 3) Japan Society of Mechanical Engineers Edition: Handbook of mechanical Engineering (in Japanese)
- 4) Ishii, Y. and T. Ishiguro: Steel pile method. Giho-do Publishing, 1959 (in Japanese)
- 5) Yokoyama, Y.: Design and construction of steel piles, Sankai-do Publishing, 1963 (in Japanese)
- 6) Takenobu, M., Nishioka, S., Sato, T. and Miyata, M. A basic study of the level 1 reliability design method based on load and resistance factor approach, Technical Note of NILIM No.880, p.41, pp.62-63, 2015. (in Japanese)
- 7) Japan Road Association: Earth work for roads- guideline for construction of retaining wall, 2012 (in Japanese)
- 8) Kagawa, M.: Increase of friction coefficient of gravity structures, Proceedings of the 11th Conference on Coastal Eng. JSCE, 2012 (in Japanese)
- 9) Shinkai, E., O. Kiyomiya and Y. Kakizaki: friction coefficient of rubber mats for enlargement of friction, Proceedings of 52nd Conference of JSCE, pp.354-355, 1997 (in Japanese)
- 10) Onodera, Y. and Y. Aoki: A Study on the Coefficient of Friction between Prepacked Concrete and Bedrock, Technical Note of PHRI No.135, p. 8, 1972 (in Japanese)

